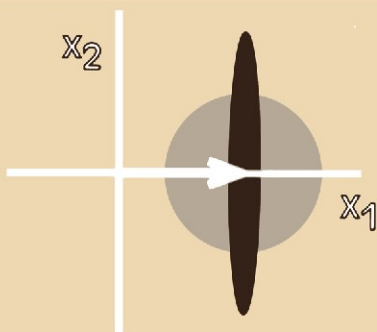


D.F. Walls_G.J. Milburn

Quantum Optics

SPRINGER
~~STUDY~~
EDITION



Springer

Quantum Optics

SPRINGER
STUDY
EDITION

D.F. Walls G.J. Milburn

Quantum Optics

With 98 Figures



Springer-Verlag
Berlin Heidelberg New York
London Paris Tokyo
Hong Kong Barcelona
Budapest

Professor D.F. WALLS, F.R.S.

University of Auckland
Private Bag 92019
Auckland
New Zealand

Dr. G.J. MILBURN

Physics Department
University of Queensland
St. Lucia QLD 4067
Australia

**First Edition 1994
Second Printing 1995**

ISBN-13: 978-3-540-58831-3

e-ISBN-13: 978-3-642-79504-6

DOI: 10.1007/978-3-642-79504-6

CIP data applied for

This work is subject to copyright. All rights are reserved, whether the whole or part of the material is concerned, specifically the rights of translation, reprinting, reuse of illustrations, recitation, broadcasting, reproduction on microfilm or in any other way, and storage in data banks. Duplication of this publication or parts thereof is permitted only under the provisions of the German Copyright Law of September 9, 1965, in its current version, and permission for use must always be obtained from Springer-Verlag. Violations are liable for prosecution under the German Copyright Law.

© Springer-Verlag Berlin Heidelberg 1994

The use of general descriptive names, registered names, trademarks, etc. in this publication does not imply, even in the absence of a specific statement, that such names are exempt from the relevant protective laws and regulations and therefore free for general use.

Typesetting: Macmillan India Ltd., Bangalore 25

SPIN: 10493491 54/3140/SPS – 5 4 3 2 1 0 – printed on acid-free paper

Preface

This text book originated out of a graduate course of lectures in Quantum Optics given at the University of Waikato and the University of Auckland. A broad range of material is covered in this book ranging from introductory concepts to current research topics. A pedagogic description of the techniques of quantum optics and their applications to physical systems is presented. Particular emphasis is given to systems where the theoretical predictions have been confirmed by experimental observation.

The material presented in this text could be covered in a two semester course. Alternatively the introductory material in Chaps. 1–6 and selected topics from the later chapters would be suitable for a one semester course. For example, for material involving the interaction of light with atoms Chaps. 10–13 would be appropriate, whereas for material on squeezed light Chaps. 7 and 8 are required. Chaps. 14–16 describe the interrelation of fundamental topics in quantum mechanics with quantum optics. The final chapter on atomic optics gives an introduction to this new and rapidly developing field.

One of us (D.F. Walls) would like to thank Roy Glauber and Hermann Haken for the wonderful introduction they gave me to this exciting field. We would also like to thank our students and colleagues at the Universities of Waikato, Auckland and Queensland who have contributed so much to the material in this book. In particular, Crispin Gardiner, Ken McNeil, Howard Carmichael, Peter Drummond, Margaret Reid, Shoukry Hassan, Matthew Collett, Sze Tan, Alistair Lane, Brian Kennedy, Craig Savage, Monika Marte, Murray Holland and Pippa Storey. Finally, we would like to thank all our friends and colleagues in Quantum Optics too numerous to name with whom we have shared in the excitement of the development of this field.

The completion of this book would not have been possible without the excellent work of Susanna van der Meer who performed the word processing through many iterations.

Auckland, New Zealand
St. Lucia, Australia
January 1994

D.F. WALLS
G.J. MILBURN

Contents

1. Introduction	1
2. Quantisation of the Electromagnetic Field	7
2.1 Field Quantisation.....	7
2.2 Fock or Number States.....	10
2.3 Coherent States	12
2.4 Squeezed States	15
2.5 Two-Photon Coherent States	18
2.6 Variance in the Electric Field	20
2.7 Multimode Squeezed States.....	22
2.8 Phase Properties of the Field.....	23
Exercises	26
3. Coherence Properties of the Electromagnetic Field	29
3.1 Field-Correlation Functions	29
3.2 Properties of the Correlation Functions	31
3.3 Correlation Functions and Optical Coherence	32
3.4 First-Order Optical Coherence	34
3.5 Coherent Field	38
3.6 Photon Correlation Measurements	39
3.7 Quantum Mechanical Fields.....	41
3.7.1 Squeezed States	42
3.7.2 Squeezed Vacuum.....	44
3.8 Phase-Dependent Correlation Functions	44
3.9 Photon Counting Measurements	46
3.9.1 Classical Theory	46
3.9.2 Constant Intensity	48
3.9.3 Fluctuating Intensity – Short-Time Limit	48
3.10 Quantum Mechanical Photon Count Distribution	51
3.10.1 Coherent Light	52
3.10.2 Chaotic Light	52
3.10.3 Photo-Electron Current Fluctuations	53
Exercises	55

4. Representations of the Electromagnetic Field	57
4.1 Expansion in Number States	57
4.2 Expansion in Coherent States	58
4.2.1 <i>P</i> Representation	58
a) Correlation Functions	60
b) Covariance Matrix	61
c) Characteristic Function	62
4.2.2 Wigner's Phase-Space Density	63
a) Coherent State	64
b) Squeezed State	64
c) Number State	64
4.2.3 <i>Q</i> Function	65
4.2.4 <i>R</i> Representation	66
4.2.5 Generalized <i>P</i> Representations	68
a) Number State	71
b) Squeezed State	71
4.2.6 Positive <i>P</i> Representation	71
Exercises	72
5. Quantum Phenomena in Simple Systems in Nonlinear Optics	73
5.1 Single-Mode Quantum Statistics	73
5.1.1 Degenerate Parametric Amplifier	73
5.1.2 Photon Statistics	75
5.1.3 Wigner Function	75
5.2 Two-Mode Quantum Correlations	77
5.2.1 Non-degenerate Parametric Amplifier	77
5.2.2 Squeezing	80
5.2.3 Quadrature Correlations and the Einstein– Podolsky– Rosen Paradox	81
5.2.4 Wigner Function	82
5.2.5 Reduced Density Operator	83
5.3 Quantum Limits to Amplification	85
5.4 Amplitude Squeezed State with Poisson Photon Number Statistics	86
Problems	89
6. Stochastic Methods	91
6.1 Master Equation	91
6.2 Equivalent c-Number Equations	98
6.2.1 Photon Number Representation	98
6.2.2 <i>P</i> Representation	99
6.2.3 Properties of Fokker– Planck Equations	101

6.2.4 Steady State Solutions – Potential Conditions	101
6.2.5 Time Dependent Solution	103
6.2.6 Q Representation	104
6.2.7 Wigner Function	106
6.2.8 Generalized P Representation	108
a) Complex P Representation	109
b) Positive P Representation	110
6.3 Stochastic Differential Equations	111
6.3.1 Use of the Positive P Representation	115
6.4 Linear Processes with Constant Diffusion	115
6.5 Two Time Correlation Functions in Quantum Markov Processes	117
6.5.1 Quantum Regression Theorem	118
6.6 Application to Systems with a P Representation	118
Exercises	119
7. Input–Output Formulation of Optical Cavities	121
7.1 Cavity Modes	121
7.2 Linear Systems	124
7.3 Two-Sided Cavity	126
7.4 Two Time Correlation Functions	127
7.5 Spectrum of Squeezing	129
7.6 Parametric Oscillator	129
7.7 Squeezing in the Total Field	132
7.8 Fokker–Planck Equation	132
Exercises	135
8. Generation and Applications of Squeezed Light	137
8.1 Parametric Oscillation and Second Harmonic Generation	137
8.1.1 Semi-classical Steady States and Stability Analysis	139
8.1.2 Parametric Oscillation	139
8.1.3 Second Harmonic Generation	140
8.1.4 Squeezing Spectrum	141
8.1.5 Parametric Oscillation	142
8.1.6 Experiments	143
8.2 Twin Beam Generation and Intensity Correlations	146
8.2.1 Second Harmonic Generation	150
8.2.2 Experiments	152
8.2.3 Dispersive Optical Bistability	153
8.3 Applications of Squeezed Light	158
8.3.1 Interferometric Detection of Gravitational Radiation	158

8.3.2 Sub-Shot-Noise Phase Measurements	172
Exercises	174
9. Nonlinear Quantum Dissipative Systems	177
9.1 Optical Parametric Oscillator: Complex P Function	177
9.2 Optical Parametric Oscillator: Positive P Function	182
9.3 Quantum Tunnelling Time	186
9.4 Dispersive Optical Bistability	191
9.5 Comment on the Use of the Q and Wigner Representations	193
Exercises	193
9.A Appendix	194
9.A.1 Evaluation of Moments for the Complex P function for Parametric Oscillation (9.17)	194
9.A.2 Evaluation of the Moments for the Complex P Function for Optical Bistability (9.48)	195
10. Interaction of Radiation with Atoms	197
10.1 Quantization of the Electron Wave Field	197
10.2 Interaction Between the Radiation Field and the Electron Wave Field	199
10.3 Interaction of a Two-Level Atom with a Single Mode Field	204
10.4 Quantum Collapses and Revivals	205
10.5 Spontaneous Decay of a Two-Level Atom	206
10.6 Decay of a Two-Level Atom in a Squeezed Vacuum	208
10.7 Phase Decay in a Two-Level System	210
Exercises	211
11. Resonance Fluorescence	213
11.1 Master Equation	213
11.2 Spectrum of the Fluorescent Light	217
11.3 Photon Correlations	221
11.4 Squeezing Spectrum	225
Exercises	228
12. Quantum Theory of the Laser	229
12.1 Master Equation	229
12.2 Photon Statistics	232
12.2.1 Spectrum of Intensity Fluctuations	233
12.3 Laser Linewidth	235
12.4 Regularly Pumped Laser	236

12.A Appendix: Derivation of the Single-Atom Increment	240
Exercises	244
13. Intracavity Atomic Systems	245
13.1 Optical Bistability	245
13.2 Nondegenerate Four Wave Mixing	252
13.3 Experimental Results	258
Exercises	259
14. Bell's Inequalities in Quantum Optics	261
14.1 The Einstein–Podolsky–Rosen (EPR) Argument	261
14.2 Bell Inequalities and the Aspect Experiment	262
14.3 Violations of Bell's Inequalities Using a Parametric Amplifier Source	268
14.4 One-Photon Interference	273
Exercises	279
15. Quantum Nondemolition Measurements	281
15.1 Concept of a QND measurement	282
15.2 Back Action Evasion	284
15.3 Criteria for a QND Measurement	284
15.4 The Beam Splitter	287
15.5 Ideal Quadrature QND Measurements	290
15.6 Experimental Realisation	291
15.7 A Photon Number QND Scheme	294
Exercises	296
16. Quantum Coherence and Measurement Theory	297
16.1 Quantum Coherence	297
16.2 The Effect of Fluctuations	303
16.3 Quantum Measurement Theory	306
16.4 Examples of Pointer Observables	310
16.5 Model of a Measurement	311
Exercises	313
17. Atomic Optics	315
17.1 Young's Interference with Path Detectors	316
17.1.1 The Feynman Light Microscope	319
17.2 Atomic Diffraction by a Standing Light Wave	321
17.3 Optical Stern–Gerlach Effect	325
17.4 Quantum Non-Demolition Measurement of the Photon Number by Atomic Beam Deflection	330

17.5 Measurement of Atomic Position	334
17.5.1 Atomic Focussing and Contractive States	337
Exercises	339
17.A Appendix	339
 References	341
 Subject Index	347

1. Introduction

The first indication of the quantum nature of light came in 1900 when M. Planck discovered he could account for the spectral distribution of thermal light by postulating that the energy of a harmonic oscillator is quantized. Further evidence was added by A. Einstein who showed in 1905 that the photoelectric effect could be explained by the hypothesis that the energy of a light beam was distributed in discrete bundles later known as photons.

Einstein also contributed to the understanding of the absorption and emission of light from atoms with his development of a phenomenological theory in 1917. This theory was later shown to be a natural consequence of the quantum theory of electromagnetic radiation.

Despite this early connection with quantum theory physical optics has developed more or less independently of quantum theory. The vast majority of physical-optics experiments can adequately be explained using classical theory of electromagnetic radiation based on Maxwell's equations. An early attempt to find quantum effects in an optical interference experiment by G.I. Taylor in 1909 gave a negative result. Taylor's experiment was an attempt to repeat T. Young's famous two slit experiment with one photon incident on the slits. The classical explanation based on the interference of electric field amplitudes and the quantum explanation based on the interference of the probability amplitudes for the photon to pass through either slit coincide in this experiment. Interference experiments of Young's type do not distinguish between the predictions of classical theory and quantum theory. It is only in higher-order interference experiments involving the interference of intensities that differences between the predictions of classical and quantum theory appear. In such an experiment two electric fields are detected on a photomultiplier and their intensities are allowed to interfere. Whereas classical theory treats the interference of intensities, in quantum theory the interference is still at the level of probability amplitudes. This is one of the most important differences between quantum theory and classical theory.

The first experiment in intensity interferometry was the famous experiment of R. Hanbury Brown and R.Q. Twiss. This experiment studied the correlation in the photo-current fluctuations from two detectors. Later experiments were photon counting experiments, and the correlations between photon numbers were studied.

The Hanbury–Brown–Twiss experiment observed an enhancement in the two-time intensity correlation function of short time delays for a thermal light

source known as photon bunching. This was a consequence of the large intensity fluctuations in the thermal source. Such photon bunching phenomena may be adequately explained using a classical theory with a fluctuating electric field amplitude. For a perfectly amplitude stabilized light field such as an ideal laser operating well above threshold there is no photon bunching. A photon counting experiment where the number of photons arriving in an interval T are counted, shows that there is still a randomness in the photon arrivals. The photon-number distribution for an ideal laser is Poissonian. For thermal light a super-Poissonian photocount distribution results.

While the above results may be derived from both classical and quantum theory, the quantum theory makes additional unique predictions. This was first elucidated by R.J. Glauber in his quantum formulation of optical coherence theory in 1963. One such prediction is photon antibunching where the initial slope of the two-time correlation function is positive. This corresponds to greater than average separations between the photon arrivals or photon antibunching. The photocount statistics may also be sub-Poissonian. A classical theory of fluctuating field amplitudes would require negative probabilities in order to give photon antibunching. In the quantum picture it is easy to visualize photon arrivals more regular than Poissonian.

It was not, however, until 1975 when H.J. Carmichael and D.F. Walls predicted that light generated in resonance fluorescence from a two-level atom would exhibit photon antibunching that a physically accessible system exhibiting nonclassical behaviour was identified. Photon antibunching was observed during the next year in this system in an experiment by H.J. Kimble, M. Dagenais and L. Mandel. This was the first nonclassical effect observed in optics and ushered in a new era in quantum optics.

The experiments of Kimble et al. used an atomic beam and hence the photon antibunching was convolved with the atomic number fluctuations in the beam. With developments in ion-trap technology it is now possible to trap a single ion for several minutes. H. Walther and coworkers in Munich have studied resonance fluorescence from a single atom in a trap. They have observed both photon antibunching and sub-Poissonian statistics in this system.

In the 1960's improvements in photon counting techniques proceeded in tandem with the development of new laser light sources. Light from incoherent (thermal) and coherent (laser) sources could now be distinguished by their photon counting properties. The groups of F.T. Arecchi in Milan, L. Mandel in Rochester and R.E. Pike in Malvern measured the photocount statistics of the laser. They showed that the photocount statistics went from super-Poissonian below threshold to Poissonian far above threshold. Concurrently, the quantum theory of the laser was being developed by H. Haken in Stuttgart, M.O. Scully and W. Lamb at Yale, and M. Lax and W.H. Louisell in New Jersey. In these theories both the atomic variables and the electromagnetic field were quantized. The result of these calculations were that the laser functioned as an essentially classical device. In fact H. Risken showed that it could be modelled by a van der Pol oscillator.

It is only quite recently that the role the noise in the pumping process plays in obscuring the quantum aspects of the laser has been understood. If the noise in the pumping process can be suppressed the output of the laser may exhibit sub-Poissonian statistics. In other words, the intensity fluctuations may be reduced below the shot-noise level characteristic of normal lasers. Y. Yamamoto in Tokyo has pioneered experimental developments in the area of semiconductor lasers with suppressed pump noise. In a high impedance constant current driven semiconductor laser the fluctuations in the pumping electrons are reduced below Poissonian. This results in the photon statistics of the emitted photons being sub-Poissonian.

It took another nine years after the observation of photon antibunching for another prediction of the quantum theory of light to be observed – squeezing of quantum fluctuations. The electric field for a nearly monochromatic plane wave may be decomposed into two quadrature components with the time dependence $\cos \omega t$ and $\sin \omega t$, respectively. In a coherent state, the closest quantum counterpart to a classical field, the fluctuations in the two quadratures are equal and minimize the uncertainty product given by Heisenberg's uncertainty relation. The quantum fluctuations in a coherent state are equal to the zero-point vacuum fluctuations and are randomly distributed in phase. In a squeezed state the quantum fluctuations are no longer independent of phase. One quadrature phase may have reduced quantum fluctuations at the expense of increased quantum fluctuations in the other quadrature phase such that the product of the fluctuations still obeys Heisenberg's uncertainty relation.

Squeezed states offer the possibility of beating the quantum limit in optical measurements by making phase-sensitive measurements which utilize only the quadrature with reduced quantum fluctuations. The generation of squeezed states requires a nonlinear phase-dependent interaction. The first observation of squeezed states was achieved by R.E. Slusher in 1985 at the AT&T Bell Laboratories in four-wave mixing in atomic sodium. This was soon followed by demonstrations of squeezing in an optical parametric oscillator by H.J. Kimble and by four-wave mixing in optical fibres by M.D. Levenson.

Squeezing-like photon antibunching is a consequence of the quantization of the light field. The usefulness of squeezed light was demonstrated in experiments in optical interferometry by Kimble and Slusher. Following the original suggestion of C.M. Caves at Caltech they injected squeezed light into the empty port of an interferometer. By choosing the phase of the squeezed light so that the quantum fluctuations entering the empty port were reduced below the vacuum level they observed an enhanced visibility of the interference fringes.

In the nonlinear process of parametric down conversion a high frequency photon splits into two photons with frequencies such that their sum equals that of the high-energy photon. The two photons (photon twins) produced in this process possess quantum correlations and have identical intensity fluctuations. This may be exploited in experiments where the intensity fluctuations in the difference photocurrent for the two beams is measured. The intensity difference fluctuations in the twin beams have been shown to be considerably below the

shot-noise level in experiments by E. Giacobino in Paris and P. Kumar in Evanston.

The twin beams may also be used in absorption measurements where the sample is placed in one of the beams and the other beam is used as a reference. The driving laser is tuned so that the frequency of the twin beams matches the frequency at which the sample absorbs. When the twin beams are detected and the photocurrents are subtracted, the presence of even very weak absorption can be seen because of the small quantum noise in the difference current.

The photon pairs generated in parametric down conversion also carry quantum correlations of the Einstein–Podolsky–Rosen type. Intensity correlation experiments to test Bell inequalities were designed using a correlated pair of photons. The initial experiments by A. Aspect in Paris utilized a two photon cascade to generate the correlated photons, however, recent experiments have used parametric down conversion. These experiments have consistently given results in agreement with the predictions of quantum theory and in violation of classical predictions. At the basis of the difference between the two theories is the interference of probability amplitudes which is characteristic of quantum mechanics. In these intensity interference experiments as opposed to interference experiments of the Young's type the two theories yield different predictions. This was strikingly demonstrated in an intensity interference experiment which has only one incident photon but has phase-sensitive detection. In this experiment proposed by S.M. Tan, D.F. Walls and M.J. Collett a single photon may take either path to two homodyne detectors. Nonlocal quantum correlations between the two detectors occur, which are a consequence of the interference of the probability amplitudes for the photon to take either path.

The major advances made in quantum optics, in particular the ability to generate and detect light with less quantum fluctuations than the vacuum, makes optics a fertile testing ground for quantum measurement theory. The idea of quantum non-demolition measurements arose in the context of how to detect the change in position of a free mass acted on by a force such as a gravitational wave. However, the concept is general. Basically one wishes to measure the value of an observable without disturbing it so that subsequent measurements can be made with equal accuracy as the first. Demonstrations of quantum non-demolition measurements have been achieved in optics. In experiments by M.D. Levenson and P. Grangier two electromagnetic-field modes have been coupled via a nonlinear interaction. A measurement of the amplitude quadrature of one mode (the probe) allows one to infer the value of the amplitude quadrature of the other mode (the signal) without disturbing it. This quantum non-demolition measurement allows one to evade the back action noise of the measurement by shunting the noise into the phase quadrature which is undetected.

The techniques developed in quantum optics include quantum treatments of dissipation. Dissipation has been shown to play a crucial role in the destruction of quantum coherence, which has profound implications for quantum measurement theory. The difficulties in generating a macroscopic superposition of

quantum states (Schrödinger's cat) is due to the fragility of such states to the presence of even small dissipation. Several schemes to generate these superposition states in optics have been proposed but to date there has been no experimental manifestation.

Matter-wave interferometry is a well established field, for example, electron and neutron interferometry. More recently, however, such effects have been demonstrated with atoms. Interferometry with atoms offers the advantage of greater mass and therefore greater sensitivity for measurements of changes of gravitational potentials. Using techniques of laser cooling the de Broglie wavelength of atoms may be increased. With slow atoms the passage time in the interferometer is increased thus leading to an increase in sensitivity. Atoms also have internal degrees of freedom which may be used to tag which path an atom took. Thus demonstrations of the principle of complementarity using a double-slit interference experiment with which path detectors may be realized with atoms.

Atoms may be diffracted from the periodic potential structure of a standing light wave. A new field of atomic optics is rapidly emerging. In atomic optics the role of the light and atoms are reversed. Optical elements such as mirrors and beam splitters consist of light fields which reflect and split atomic beams. The transmission of an atom by a standing light wave may be state selective (the optical Stern-Gerlach effect) and this property may be used as a beam splitter. The scattering of an atom by a standing light wave may depend on the photon statistics of the light. Hence, measuring the final momentum distribution of the atoms may give information on the photon statistics of the light field. Thus atomic optics may extend the range of quantum measurements possible with quantum optical techniques. For example, the position an atom passes through a standing light wave may be determined by measuring the phase shift it imparts to the light.

The field of quantum optics now occupies a central position involving the interaction of atoms with the electromagnetic field. It covers a wide range of topics ranging from fundamental tests of quantum theory to the development of new laser-light sources. In this text we introduce the analytic techniques of quantum optics. These techniques are applied to a number of illustrative examples. While the main emphasis of the book is theoretical, descriptions of the experiments which have played a central role in the development of quantum optics are included.

A summary of the topics included in this text book is given as follows:

A familiarity with non-relativistic quantum mechanics is assumed. As we will be concerned with the quantum properties of light and its interaction with atoms, the electromagnetic field is quantised in the second chapter. Commonly used basis states for the field, the number states, the coherent states, and the squeezed state are introduced and their properties discussed. A definition of optical coherence is given via a set of field correlation functions in Chap. 3. Various representations for the electromagnetic field are introduced in Chap. 4 using the number states and the coherent states as a basis.

In Chap. 5 we present a number of simple models which illustrate some of the quantum correlation phenomena we discuss in later chapters. In Chap. 6 a rather lengthy description is given of the quantum theory of damping and the stochastic methods which may be employed to treat problems with damping. In Chap. 7 we present the input–output formulation of interactions in optical cavities. This theory plays a central role in the study of squeezed light generation. In Chap. 8 the input–output theory is applied to several systems in nonlinear optics, which produce squeezed light. Comparison with experiments is included. Applications of squeezed light in the field of optical interferometry are given. Potential use of squeezed light in gravitational wave interferometry is discussed.

In Chap. 9 two examples are given where the steady state quantum statistics of a field generated via a nonlinear optical interaction may be found exactly. In the case of parametric subharmonic generation the quantum tunnelling time between two states of a superposition is calculated.

In Chap. 10 we introduce atoms for the first time. The atomic energy levels are quantised and the interaction Hamiltonian between a two-level atom and the electromagnetic field derived. The spontaneous decay of an excited atom into a vacuum is treated. The modification of the atomic decay when the vacuum is squeezed, is also studied. In Chap. 11 we treat the classic problem of resonance fluorescence from a coherently driven atom. The resonance fluorescence spectrum is derived as is the photon antibunching of the emitted light. A comparison of theory with experimental results is given.

In Chap. 12 the quantum theory of the laser is developed including the theory of pump-noise-suppressed lasers, which give a sub-Poissonian output. In Chap. 13 a full quantum treatment is presented of optical bistability and four-wave mixing. Both systems involve the interaction of an ensemble of two-level atoms with a cavity field. The generation of squeezed light from these systems is analysed. Fundamental questions in quantum mechanics are addressed in Chap. 14. Experimental tests of the Bell inequalities in optics are described. In Chap. 15 quantum non-demolition measurements in optical systems are analysed. Further fundamentals of quantum coherence and the quantum measurement theory are discussed in Chap. 16.

In Chap. 17 an introduction to the newly emerging field of atomic optics is given.

2. Quantisation of the Electromagnetic Field

The study of the quantum features of light requires the quantisation of the electromagnetic field. In this chapter we quantise the field and introduce three possible sets of basis states, namely, the Fock or number states, the coherent states and the squeezed states. The properties of these states are discussed. The phase operator and the associated phase states are also introduced.

2.1 Field Quantisation

The major emphasis of this text is concerned with the uniquely quantum-mechanical properties of the electromagnetic field, which are not present in a classical treatment. As such we shall begin immediately by quantizing the electromagnetic field. We shall make use of an expansion of the vector potential for the electromagnetic field in terms of cavity modes. The problem then reduces to the quantization of the harmonic oscillator corresponding to each individual cavity mode.

We shall also introduce states of the electromagnetic field appropriate to the description of optical fields. The first set of states we introduce are the number states corresponding to having a definite number of photons in the field. It turns out that it is extremely difficult to create experimentally a number state of the field, though fields containing a very small number of photons have been generated. A more typical optical field will involve a superposition of number states. One such field is the coherent state of the field which has the minimum uncertainty in amplitude and phase allowed by the uncertainty principle, and hence is the closest possible quantum mechanical state to a classical field. It also possesses a high degree of optical coherence as will be discussed in Chap. 3, hence the name coherent state. The coherent state plays a fundamental role in quantum optics and has a practical significance in that a highly stabilized laser operating well above threshold generates a coherent state.

A rather more exotic set of states of the electromagnetic field are the squeezed states. These are also minimum-uncertainty states but unlike the coherent states the quantum noise is not uniformly distributed in phase. Squeezed states may have less noise in one quadrature than the vacuum. As a consequence the noise in the other quadrature is increased. We introduce the

basic properties of squeezed states in this chapter. In Chap. 8 we describe ways to generate squeezed states and their applications.

While states of definite photon number are readily defined as eigenstates of the number operator a corresponding description of states of definite phase is more difficult. This is due to the problems involved in constructing a Hermitian phase operator to describe a bounded physical quantity like phase. How this problem may be resolved together with the properties of phase states is discussed in the final section of this chapter.

A convenient starting point for the quantisation of the electromagnetic field is the classical field equations. The free electromagnetic field obeys the source free Maxwell equations.

$$\nabla \cdot \mathbf{B} = 0 , \quad (2.1a)$$

$$\nabla \times \mathbf{E} = - \frac{\partial \mathbf{B}}{\partial t} , \quad (2.1b)$$

$$\nabla \cdot \mathbf{D} = 0 , \quad (2.1c)$$

$$\nabla \times \mathbf{H} = \frac{\partial \mathbf{D}}{\partial t} , \quad (2.1d)$$

where $\mathbf{B} = \mu_0 \mathbf{H}$, $\mathbf{D} = \epsilon_0 \mathbf{E}$, μ_0 and ϵ_0 being the magnetic permeability and electric permittivity of free space, and $\mu_0 \epsilon_0 = c^{-2}$. Maxwell's equations are gauge invariant when no sources are present. A convenient choice of gauge for problems in quantum optics is the Coulomb gauge. In the Coulomb gauge both \mathbf{B} and \mathbf{E} may be determined from a vector potential $\mathbf{A}(\mathbf{r}, t)$ as follows

$$\mathbf{B} = \nabla \times \mathbf{A} , \quad (2.2a)$$

$$\mathbf{E} = - \frac{\partial \mathbf{A}}{\partial t} , \quad (2.2b)$$

with the Coulomb gauge condition

$$\nabla \cdot \mathbf{A} = 0 . \quad (2.3)$$

Substituting (2.2a) into (2.1d) we find that $\mathbf{A}(\mathbf{r}, t)$ satisfies the wave equation

$$\nabla^2 \mathbf{A}(\mathbf{r}, t) = \frac{1}{c^2} \frac{\partial^2 \mathbf{A}(\mathbf{r}, t)}{\partial t^2} . \quad (2.4)$$

We separate the vector potential into two complex terms

$$\mathbf{A}(\mathbf{r}, t) = \mathbf{A}^{(+)}(\mathbf{r}, t) + \mathbf{A}^{(-)}(\mathbf{r}, t) , \quad (2.5)$$

where $\mathbf{A}^{(+)}(\mathbf{r}, t)$ contains all amplitudes which vary as $e^{-i\omega t}$ for $\omega > 0$ and $\mathbf{A}^{(-)}(\mathbf{r}, t)$ contains all amplitudes which vary as $e^{i\omega t}$ and $\mathbf{A}^{(-)} = (\mathbf{A}^{(+)})^*$.

It is more convenient to deal with a discrete set of variables rather than the whole continuum. We shall therefore describe the field restricted to a certain

volume of space and expand the vector potential in terms of a discrete set of orthogonal mode functions:

$$\mathbf{A}^{(+)}(\mathbf{r}, t) = \sum_k c_k \mathbf{u}_k(\mathbf{r}) e^{-i\omega_k t}, \quad (2.6)$$

where the Fourier coefficients c_k are constant for a free field. The set of vector mode functions $\mathbf{u}_k(\mathbf{r})$ which correspond to the frequency ω_k will satisfy the wave equation

$$\left(\nabla^2 + \frac{\omega_k^2}{c^2} \right) \mathbf{u}_k(\mathbf{r}) = 0 \quad (2.7)$$

provided the volume contains no refracting material. The mode functions are also required to satisfy the transversality condition,

$$\nabla \cdot \mathbf{u}_k(\mathbf{r}) = 0. \quad (2.8)$$

The mode functions form a complete orthonormal set

$$\int_V \mathbf{u}_k^*(\mathbf{r}) \mathbf{u}_{k'}(\mathbf{r}) d\mathbf{r} = \delta_{kk'} . \quad (2.9)$$

The mode functions depend on the boundary conditions of the physical volume under consideration, e.g., periodic boundary conditions corresponding to travelling-wave modes or conditions appropriate to reflecting walls which lead to standing waves. E.g., the plane wave mode functions appropriate to a cubical volume of side L may be written as

$$\mathbf{u}_k(\mathbf{r}) = L^{-3/2} \hat{\mathbf{e}}^{(\lambda)} \exp(i\mathbf{k} \cdot \mathbf{r}) \quad (2.10)$$

where $\hat{\mathbf{e}}^{(\lambda)}$ is the unit polarization vector. The mode index k describes several discrete variables, the polarisation index ($\lambda = 1, 2$) and the three Cartesian components of the propagation vector \mathbf{k} . Each component of the wave vector \mathbf{k} takes the values

$$k_x = \frac{2\pi n_x}{L}, \quad k_y = \frac{2\pi n_y}{L}, \quad k_z = \frac{2\pi n_z}{L}, \quad n_x, n_y, n_z = 0, \pm 1, \pm 2, \dots \quad (2.11)$$

The polarization vector $\hat{\mathbf{e}}^{(\lambda)}$ is required to be perpendicular to \mathbf{k} by the transversality condition (2.8).

The vector potential may now be written in the form

$$\mathbf{A}(\mathbf{r}, t) = \sum_k \left(\frac{\hbar}{2\omega_k \epsilon_0} \right)^{1/2} [a_k \mathbf{u}_k(\mathbf{r}) e^{-i\omega_k t} + a_k^\dagger \mathbf{u}_k^*(\mathbf{r}) e^{i\omega_k t}] . \quad (2.12)$$

The corresponding form for the electric field is

$$\mathbf{E}(\mathbf{r}, t) = i \sum_k \left(\frac{\hbar \omega_k}{2\epsilon_0} \right)^{1/2} [a_k \mathbf{u}_k(\mathbf{r}) e^{-i\omega_k t} - a_k^\dagger \mathbf{u}_k^*(\mathbf{r}) e^{i\omega_k t}] . \quad (2.13)$$

The normalization factors have been chosen such that the amplitudes a_k and a_k^\dagger are dimensionless.

In classical electromagnetic theory these Fourier amplitudes are complex numbers. Quantisation of the electromagnetic field is accomplished by choosing a_k and a_k^\dagger to be mutually adjoint operators. Since photons are bosons the appropriate commutation relations to choose for the operators a_k and a_k^\dagger are the boson commutation relations

$$[a_k, a_{k'}] = [a_k^\dagger, a_{k'}^\dagger] = 0, \quad [a_k, a_{k'}^\dagger] = \delta_{kk'} . \quad (2.14)$$

The dynamical behaviour of the electric-field amplitudes may then be described by an ensemble of independent harmonic oscillators obeying the above commutation relations. The quantum states of each mode may now be discussed independently of one another. The state in each mode may be described by a state vector $|\Psi\rangle_k$ of the Hilbert space appropriate to that mode. The states of the entire field are then defined in the tensor product space of the Hilbert spaces for all of the modes.

The Hamiltonian for the electromagnetic field is given by

$$H = \frac{1}{2} \int (\varepsilon_0 E^2 + \mu_0 H^2) d\mathbf{r} . \quad (2.15)$$

Substituting (2.13) for \mathbf{E} and the equivalent expression for \mathbf{H} and making use of the conditions (2.8) and (2.9), the Hamiltonian may be reduced to the form

$$H = \sum_k \hbar\omega_k (a_k^\dagger a_k + \frac{1}{2}) . \quad (2.16)$$

This represents the sum of the number of photons in each mode multiplied by the energy of a photon in that mode, plus $\frac{1}{2}\hbar\omega_k$ representing the energy of the vacuum fluctuations in each mode. We shall now consider three possible representations of the electromagnetic field.

2.2 Fock or Number States

The Hamiltonian (2.15) has the eigenvalues $\hbar\omega_k(n_k + \frac{1}{2})$ where n_k is an integer ($n_k = 0, 1, 2, \dots, \infty$). The eigenstates are written as $|n_k\rangle$ and are known as number or Fock states. They are eigenstates of the number operator $N_k = a_k^\dagger a_k$

$$a_k^\dagger a_k |n_k\rangle = n_k |n_k\rangle . \quad (2.17)$$

The ground state of the oscillator (or vacuum state of the field mode) is defined by

$$a_k |0\rangle = 0 . \quad (2.18)$$

From (2.16 and 18) we see that the energy of the ground state is given by

$$\langle 0 | H | 0 \rangle = \frac{1}{2} \sum_k \hbar \omega_k . \quad (2.19)$$

Since there is no upper bound to the frequencies in the sum over electromagnetic field modes, the energy of the ground state is infinite, a conceptual difficulty of quantized radiation field theory. However, since practical experiments measure a change in the total energy of the electromagnetic field the infinite zero-point energy does not lead to any divergence in practice. Further discussions on this point may be found in [2.1]. a_k and a_k^\dagger are raising and lowering operators for the harmonic oscillator ladder of eigenstates. In terms of photons they represent the annihilation and creation of a photon with the wave vector \mathbf{k} and a polarisation $\hat{\epsilon}_k$. Hence the terminology, annihilation and creation operators. Application of the creation and annihilation operators to the number states yield

$$a_k | n_k \rangle = n_k^{1/2} | n_k - 1 \rangle, \quad a_k^\dagger | n_k \rangle = (n_k + 1)^{1/2} | n_k + 1 \rangle . \quad (2.20)$$

The state vectors for the higher excited states may be obtained from the vacuum by successive application of the creation operator

$$| n_k \rangle = \frac{(a_k^\dagger)^{n_k}}{(n_k!)^{1/2}} | 0 \rangle, \quad n_k = 0, 1, 2 \dots . \quad (2.21)$$

The number states are orthogonal

$$\langle n_k | m_k \rangle = \delta_{mn} , \quad (2.22)$$

and complete

$$\sum_{n_k=0}^{\infty} | n_k \rangle \langle n_k | = 1 . \quad (2.23)$$

Since the norm of these eigenvectors is finite, they form a complete set of basis vectors for a Hilbert space.

While the number states form a useful representation for high-energy photons, e.g. γ rays where the number of photons is very small, they are not the most suitable representation for optical fields where the total number of photons is large. Experimental difficulties have prevented the generation of photon number states with more than a small number of photons. Most optical fields are either a superposition of number states (pure state) or a mixture of number states (mixed state). Despite this the number states of the electromagnetic field have been used as a basis for several problems in quantum optics including some laser theories.

2.3 Coherent States

A more appropriate basis for many optical fields are the coherent states [2.2]. The coherent states have an indefinite number of photons which allows them to have a more precisely defined phase than a number state where the phase is completely random. The product of the uncertainty in amplitude and phase for a coherent state is the minimum allowed by the uncertainty principle. In this sense they are the closest quantum mechanical states to a classical description of the field. We shall outline the basic properties of the coherent states below. These states are most easily generated using the unitary displacement operator

$$D(\alpha) = \exp(\alpha a^\dagger - \alpha^* a) , \quad (2.24)$$

where α is an arbitrary complex number.

Using the operator theorem [2.2]

$$e^{A+B} = e^A e^B e^{-[A, B]/2} , \quad (2.25)$$

which holds when

$$[A, [A, B]] = [B, [A, B]] = 0 ,$$

we can write $D(\alpha)$ as

$$D(\alpha) = e^{-|\alpha|^2/2} e^{\alpha a^\dagger} e^{-\alpha^* a} . \quad (2.26)$$

The displacement operator $D(\alpha)$ has the following properties

$$\begin{aligned} D^\dagger(\alpha) &= D^{-1}(\alpha) = D(-\alpha), & D^\dagger(\alpha)aD(\alpha) &= a + \alpha , \\ D^\dagger(\alpha)a^\dagger D(\alpha) &= a^\dagger + \alpha^* . \end{aligned} \quad (2.27)$$

The coherent state $|\alpha\rangle$ is generated by operating with $D(\alpha)$ on the vacuum state

$$|\alpha\rangle = D(\alpha)|0\rangle . \quad (2.28)$$

The coherent states are eigenstates of the annihilation operator a . This may be proved as follows:

$$D^\dagger(\alpha)a|\alpha\rangle = D^\dagger(\alpha)aD(\alpha)|0\rangle = (a + \alpha)|0\rangle = \alpha|0\rangle . \quad (2.29)$$

Multiplying both sides by $D(\alpha)$ we arrive at the eigenvalue equation

$$a|\alpha\rangle = \alpha|\alpha\rangle . \quad (2.30)$$

Since a is a non-Hermitian operator its eigenvalues α are complex.

Another useful property which follows using (2.25) is

$$D(\alpha + \beta) = D(\alpha)D(\beta) \exp(-i \operatorname{Im}\{\alpha\beta^*\}) . \quad (2.31)$$

The coherent states contain an indefinite number of photons. This may be made apparent by considering an expansion of the coherent states in the number-states basis.

Taking the scalar product of both sides of (2.30) with $\langle n |$ we find the recursion relation

$$(n+1)^{1/2} \langle n+1 | \alpha \rangle = \alpha \langle n | \alpha \rangle . \quad (2.32)$$

It follows that

$$\langle n | \alpha \rangle = \frac{\alpha^n}{(n!)^{1/2}} \langle 0 | \alpha \rangle . \quad (2.33)$$

We may expand $|\alpha\rangle$ in terms of the number states $|n\rangle$ with expansion coefficients $\langle n | \alpha \rangle$ as follows

$$|\alpha\rangle = \sum |n\rangle \langle n | \alpha \rangle = \langle 0 | \alpha \rangle \sum_n \frac{\alpha^n}{(n!)^{1/2}} |n\rangle . \quad (2.34)$$

The squared length of the vector $|\alpha\rangle$ is thus

$$|\langle \alpha | \alpha \rangle|^2 = |\langle 0 | \alpha \rangle|^2 \sum_n \frac{|\alpha|^{2n}}{n!} = |\langle 0 | \alpha \rangle|^2 e^{|\alpha|^2} . \quad (2.35)$$

It is easily seen that

$$\begin{aligned} \langle 0 | \alpha \rangle &= \langle 0 | D(\alpha) | 0 \rangle \\ &= e^{-|\alpha|^2/2} . \end{aligned} \quad (2.36)$$

Thus $|\langle \alpha | \alpha \rangle|^2 = 1$ and the coherent states are normalized.

The coherent state may then be expanded in terms of the number states as

$$|\alpha\rangle = e^{-|\alpha|^2/2} \sum \frac{\alpha^n}{(n!)^{1/2}} |n\rangle . \quad (2.37)$$

We note that the probability distribution of photons in a coherent state is a Poisson distribution

$$P(n) = |\langle n | \alpha \rangle|^2 = \frac{|\alpha|^{2n} e^{-|\alpha|^2}}{n!} , \quad (2.38)$$

where $|\alpha|^2$ is the mean number of photons ($\bar{n} = \langle \alpha | a^\dagger a | \alpha \rangle = |\alpha|^2$).

The scalar product of two coherent states is

$$\langle \beta | \alpha \rangle = \langle 0 | D^\dagger(\beta) D(\alpha) | 0 \rangle . \quad (2.39)$$

Using (2.26) this becomes

$$\langle \beta | \alpha \rangle = \exp [-\frac{1}{2}(|\alpha|^2 + |\beta|^2) + \alpha \beta^*] . \quad (2.40)$$

The absolute magnitude of the scalar product is

$$|\langle \beta | \alpha \rangle|^2 = e^{-|\alpha-\beta|^2} . \quad (2.41)$$

Thus the coherent states are not orthogonal although two states $|\alpha\rangle$ and $|\beta\rangle$ become approximately orthogonal in the limit $|\alpha - \beta| \gg 1$. The coherent states

form a two-dimensional continuum of states and are, in fact, overcomplete. The completeness relation

$$\frac{1}{\pi} \int |\alpha\rangle \langle \alpha| d^2\alpha = 1 , \quad (2.42)$$

may be proved as follows.

We use the expansion (2.37) to give

$$\int |\alpha\rangle \langle \alpha| \frac{d^2\alpha}{\pi} = \sum_{n=0}^{\infty} \sum_{m=0}^{\infty} \frac{|n\rangle \langle m|}{\pi \sqrt{n!m!}} \int e^{-|\alpha|^2} \alpha^{*m} \alpha^n d^2\alpha . \quad (2.43)$$

Changing to polar coordinates this becomes

$$\int |\alpha\rangle \langle \alpha| \frac{d^2\alpha}{\pi} = \sum_{n,m=0}^{\infty} \frac{|n\rangle \langle m|}{\pi \sqrt{n!m!}} \int_0^{\infty} r dr e^{-r^2} r^{n+m} \int_0^{2\pi} d\theta e^{i(n-m)\theta} . \quad (2.44)$$

Using

$$\int_0^{2\pi} d\theta e^{i(n-m)\theta} = 2\pi \delta_{nm} , \quad (2.45)$$

we have

$$\int |\alpha\rangle \langle \alpha| \frac{d^2\alpha}{\pi} = \sum_{n=0}^{\infty} \frac{|n\rangle \langle n|}{n!} \int_0^{\infty} d\varepsilon e^{-\varepsilon} \varepsilon^n , \quad (2.46)$$

where we let $\varepsilon = r^2$. The integral equals $n!$. Hence we have

$$\int |\alpha\rangle \langle \alpha| \frac{d^2\alpha}{\pi} = \sum_{n=0}^{\infty} |n\rangle \langle n| = 1 , \quad (2.47)$$

following from the completeness relation for the number states.

An alternative proof of the completeness of the coherent states may be given as follows. Using the relation [2.3]

$$e^{\zeta B} A e^{-\zeta B} = A + \zeta [B, A] + \frac{\zeta^2}{2!} [B, [B, A]] + \dots , \quad (2.48)$$

it is easy to see that all the operators A such that

$$D^\dagger(\alpha) A D(\alpha) = A \quad (2.49)$$

are proportional to the identity.

We consider

$$A = \int d^2\alpha |\alpha\rangle\langle\alpha|$$

then

$$D^\dagger(\beta) \int d^2\alpha |\alpha\rangle\langle\alpha| D(\beta) = \int d^2\alpha |\alpha - \beta\rangle\langle\alpha - \beta| = \int d^2\alpha |\alpha\rangle\langle\alpha|. \quad (2.50)$$

Then using the above result we conclude that

$$\int d^2\alpha |\alpha\rangle\langle\alpha| \propto I. \quad (2.51)$$

The constant of proportionality is easily seen to be π .

The coherent states have a physical significance in that the field generated by a highly stabilized laser operating well above threshold is a coherent state. They form a useful basis for expanding the optical field in problems in laser physics and nonlinear optics. The coherence properties of light fields and the significance of the coherent states will be discussed in Chap. 3.

2.4 Squeezed States

A general class of minimum-uncertainty states are known as *squeezed states*. In general, a squeezed state may have less noise in one quadrature than a coherent state. To satisfy the requirements of a minimum-uncertainty state the noise in the other quadrature is greater than that of a coherent state. The coherent states are a particular member of this more general class of minimum uncertainty states with equal noise in both quadratures. We shall begin our discussion by defining a family of minimum-uncertainty states. Let us calculate the variances for the position and momentum operators for the harmonic oscillator

$$q = \sqrt{\frac{\hbar}{2\omega}}(a + a^\dagger), \quad p = i\sqrt{\frac{\hbar\omega}{2}}(a - a^\dagger). \quad (2.52)$$

The variances are defined by

$$V(A) = (\Delta A)^2 = \langle A^2 \rangle - \langle A \rangle^2. \quad (2.53)$$

In a coherent state we obtain

$$(\Delta q)_{coh}^2 = \frac{\hbar}{2\omega}, \quad (\Delta p)_{coh}^2 = \frac{\hbar\omega}{2}. \quad (2.54)$$

Thus the product of the uncertainties is a minimum

$$(\Delta p \Delta q)_{coh} = \frac{\hbar}{2}. \quad (2.55)$$

Thus, there exists a sense in which the description of the state of an oscillator by a coherent state represents as close an approach to classical localisation as

possible. We shall consider the properties of a single-mode field. We may write the annihilation operator a as a linear combination of two Hermitian operators

$$a = \frac{X_1 + iX_2}{2} . \quad (2.56)$$

X_1 and X_2 , the real and imaginary parts of the complex amplitude, give dimensionless amplitudes for the modes' two quadrature phases. They obey the following commutation relation

$$[X_1, X_2] = 2i . \quad (2.57)$$

The corresponding uncertainty principle is

$$\Delta X_1 \Delta X_2 \geq 1 . \quad (2.58)$$

This relation with the equals sign defines a family of minimum-uncertainty states. The coherent states are a particular minimum-uncertainty state with

$$\Delta X_1 = \Delta X_2 = 1 . \quad (2.59)$$

The coherent state $|\alpha\rangle$ has the mean complex amplitude α and it is a minimum-uncertainty state for X_1 and X_2 , with equal uncertainties in the two quadrature phases. A coherent state may be represented by an "error circle" in a complex amplitude plane whose axes are X_1 and X_2 (Fig. 2.1a). The centre of the error circle lies at $\frac{1}{2}\langle X_1 + iX_2 \rangle = \alpha$ and the radius $\Delta X_1 = \Delta X_2 = 1$ accounts for the uncertainties in X_1 and X_2 .

There is obviously a whole family of minimum-uncertainty states defined by $\Delta X_1 \Delta X_2 = 1$. If we plot ΔX_1 against ΔX_2 the minimum-uncertainty states lie on a hyperbola (Fig. 2.2). Only points lying to the right of this hyperbola correspond to physical states. The coherent state with $\Delta X_1 = \Delta X_2$ is a special case of a more general class of states which may have reduced uncertainty in one quadrature at the expense of increased uncertainty in the other ($\Delta X_1 < 1 < \Delta X_2$). These states correspond to the shaded region in Fig. 2.2. Such states we shall call *squeezed states* [2.4]. They may be generated by using the unitary squeeze operator [2.5]

$$S(\varepsilon) = \exp(1/2\varepsilon^* a^2 - 1/2\varepsilon a^{\dagger 2}) , \quad (2.60)$$

where $\varepsilon = r e^{2i\phi}$.

Note the squeeze operator obeys the relations

$$S^\dagger(\varepsilon) = S^{-1}(\varepsilon) = S(-\varepsilon) , \quad (2.61)$$

and has the following useful transformation properties

$$S^\dagger(\varepsilon)aS(\varepsilon) = a \cosh r - a^\dagger e^{-2i\phi} \sinh r ,$$

$$S^\dagger(\varepsilon)a^\dagger S(\varepsilon) = a^\dagger \cosh r - a e^{2i\phi} \sinh r , \quad (2.62)$$

$$S^\dagger(\varepsilon)(Y_1 + iY_2)S(\varepsilon) = Y_1 e^{-r} + i Y_2 e^r ,$$

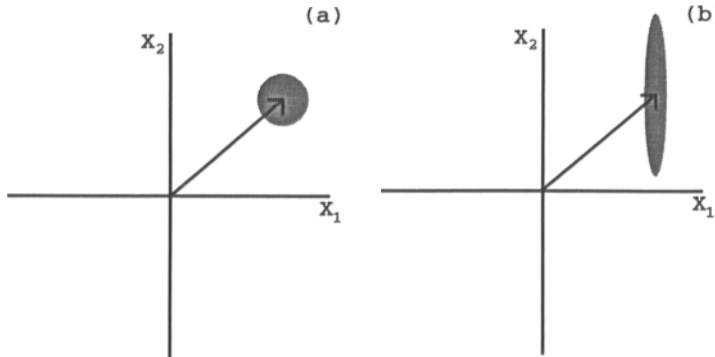


Fig. 2.1. Phase-space plot showing the uncertainty in (a) a coherent state $|\alpha\rangle$, and (b) a squeezed state $|\alpha, r\rangle$

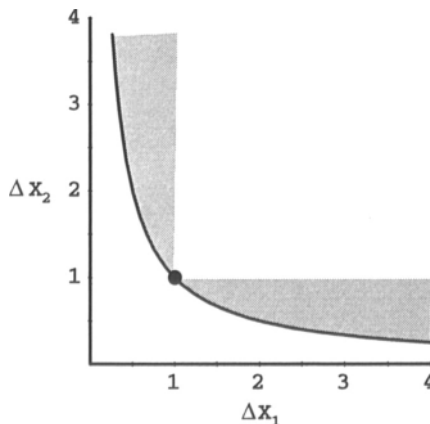


Fig. 2.2. Plot of ΔX_1 versus ΔX_2 for the minimum-uncertainty states. The dot marks a coherent state while the shaded region corresponds to the squeezed states

where

$$Y_1 + iY_2 = (X_1 + iX_2)e^{-i\phi} \quad (2.63)$$

is a rotated complex amplitude. The squeeze operator attenuates one component of the (rotated) complex amplitude, and it amplifies the other component. The degree of attenuation and amplification is determined by $r = |\epsilon|$, which will be called the *squeeze factor*. The squeezed state $|\alpha, \epsilon\rangle$ is obtained by first squeezing the vacuum and then displacing it

$$|\alpha, \epsilon\rangle = D(\alpha)S(\epsilon)|0\rangle . \quad (2.64)$$

A squeezed state has the following expectation values and variances

$$\begin{aligned}\langle X_1 + iX_2 \rangle &= \langle Y_1 + iY_2 \rangle e^{i\phi} = 2\alpha , \\ \Delta Y_1 &= e^{-r}, \quad \Delta Y_2 = e^r , \\ \langle N \rangle &= |\alpha|^2 + \sinh^2 r , \\ (\Delta N)^2 &= |\alpha \cosh r - \alpha^* e^{2i\phi} \sinh r|^2 + 2 \cosh^2 r \sinh^2 r .\end{aligned}\tag{2.65}$$

Thus the squeezed state has unequal uncertainties for Y_1 and Y_2 as seen in the error ellipse shown in Fig. 2.1b. The principal axes of the ellipse lie along the Y_1 and Y_2 axes, and the principal radii are ΔY_1 and ΔY_2 . A more rigorous definition of these error ellipses as contours of the Wigner function is given in Chap. 3.

2.5 Two-Photon Coherent States

We may define squeezed states in an alternative but equivalent way [2.6]. As this definition is sometimes used in the literature we include it for completeness.

Consider the operator

$$b = \mu a + v a^\dagger \tag{2.66}$$

where

$$|\mu|^2 - |v|^2 = 1 .$$

Then b obeys the commutation relation

$$[b, b^\dagger] = 1 . \tag{2.67}$$

We may write (2.66) as

$$b = U a U^\dagger \tag{2.68}$$

where U is a unitary operator. The eigenstates of b have been called *two-photon coherent states* and are closely related to the squeezed states.

The eigenvalue equation may be written as

$$b|\beta\rangle_g = \beta|\beta\rangle_g . \tag{2.69}$$

From (2.68) it follows that

$$|\beta\rangle_g = U|\beta\rangle \tag{2.70}$$

where $|\beta\rangle$ are the eigenstates of a .

The properties of $|\beta\rangle_g$ may be proved to parallel those of the coherent states. The state $|\beta\rangle_g$ may be obtained by operating on the vacuum

$$|\beta\rangle_g = D_g(\beta)|0\rangle_g \tag{2.71}$$

with the displacement operator

$$D_g(\beta) = e^{\beta b^\dagger - \beta^* b} \quad (2.72)$$

and $|0\rangle_g = U|0\rangle$. The two-photon coherent states are complete

$$\int |\beta\rangle_g \langle\beta| \frac{d^2\beta}{\pi} = 1 \quad (2.73)$$

and their scalar product is

$$_g\langle\beta|\beta'\rangle_g = \exp(\beta^*\beta' - \frac{1}{2}|\beta|^2 - \frac{1}{2}|\beta'|^2) . \quad (2.74)$$

We now consider the relation between the two-photon coherent states and the squeezed states as previously defined. We first note that

$$U \equiv S(\varepsilon)$$

with $\mu = \cosh r$ and $v = e^{2i\phi} \sinh r$. Thus

$$|0\rangle_g \equiv |0, \varepsilon\rangle \quad (2.75)$$

with the above relations between (μ, v) and (r, θ) . Using this result in (2.71) and rewriting the displacement operator, $D_g(\beta)$, in terms of a and a^\dagger we find

$$|\beta\rangle_g = D(\alpha)S(\varepsilon)|0\rangle = |\alpha, \varepsilon\rangle \quad (2.76)$$

where

$$\alpha = \mu\beta - v\beta^* .$$

Thus we have found the equivalent squeezed state for the given two-photon coherent state.

Finally, we note that the two-photon coherent state $|\beta\rangle_g$ may be written as

$$|\beta\rangle_g = S(\varepsilon)D(\beta)|0\rangle .$$

Thus the two-photon coherent state is generated by first displacing the vacuum state, then squeezing. This is the opposite procedure to that which defines the squeezed state $|\alpha, \varepsilon\rangle$. The two procedures yield the same state if the displacement parameters α and β are related as discussed above.

The completeness relation for the two-photon coherent states may be employed to derive the completeness relation for the squeezed states. Using the above results we have

$$\int \frac{d^2\beta}{\pi} |\beta \cosh r - \beta^* e^{2i\phi} \sinh r, \varepsilon\rangle \langle\beta \cosh r - \beta^* e^{2i\phi} \sinh r, \varepsilon| = 1 . \quad (2.77)$$

The change of variable

$$\alpha = \beta \cosh r - \beta^* e^{2i\phi} \sinh r \quad (2.78)$$

leaves the measure invariant, that is $d^2\alpha = d^2\beta$. Thus

$$\int \frac{d^2\alpha}{\pi} |\alpha, \varepsilon\rangle \langle \alpha, \varepsilon| = 1 . \quad (2.79)$$

2.6 Variance in the Electric Field

The electric field for a single mode may be written in terms of the operators X_1 and X_2 as

$$E(\mathbf{r}, t) = \frac{1}{\sqrt{L^3}} \left(\frac{\hbar\omega}{2\varepsilon_0} \right)^{1/2} [X_1 \sin(\omega t - \mathbf{k} \cdot \mathbf{r}) - X_2 \cos(\omega t - \mathbf{k} \cdot \mathbf{r})] . \quad (2.80)$$

The variance in the electric field is given by

$$V(E(\mathbf{r}, t)) = K \{ V(X_1) \sin^2(\omega t - \mathbf{k} \cdot \mathbf{r}) + V(X_2) \cos^2(\omega t - \mathbf{k} \cdot \mathbf{r}) \\ - \sin[2(\omega t - \mathbf{k} \cdot \mathbf{r})] V(X_1, X_2) \} \quad (2.81)$$

where

$$K = \frac{1}{L^3} \left(\frac{2\hbar\omega}{\varepsilon_0} \right) ,$$

$$V(X_1, X_2) = \frac{\langle (X_1 X_2) + (X_2 X_1) \rangle}{2} - \langle X_1 \rangle \langle X_2 \rangle .$$

For a minimum-uncertainty state

$$V(X_1, X_2) = 0 . \quad (2.82)$$

Hence (2.81) reduces to

$$V(E(\mathbf{r}, t)) = K [V(X_1) \sin^2(\omega t - \mathbf{k} \cdot \mathbf{r}) + V(X_2) \cos^2(\omega t - \mathbf{k} \cdot \mathbf{r})] . \quad (2.83)$$

The mean and uncertainty of the electric field is exhibited in Figs. 2.3a–c where the line is thickened about a mean sinusoidal curve to represent the uncertainty in the electric field.

The variance of the electric field for a coherent state is a constant with time (Fig. 2.3a). This is due to the fact that while the coherent-state-error circle rotates about the origin at frequency ω , it has a constant projection on the axis defining the electric field. Whereas for a squeezed state the rotation of the error ellipse leads to a variance that oscillates with frequency 2ω . In Fig. 2.3b the coherent excitation appears in the quadrature that has reduced noise. In Fig. 2.3c the coherent excitation appears in the quadrature with increased noise. This situation corresponds to the phase states discussed in [2.7] and in the final section of this chapter.

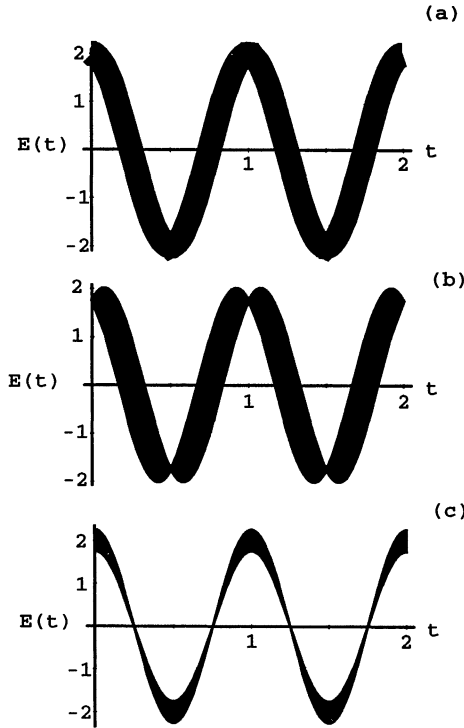


Fig. 2.3. Plot of the electric field versus time showing schematically the uncertainty in phase and amplitude for (a) a coherent state, (b) a squeezed state with reduced amplitude fluctuations, and (c) a squeezed state with reduced phase fluctuations

The squeezed state $|\alpha, r\rangle$ has the photon number distribution [2.6]

$$P(n) = (n! \mu)^{-1} \left(\frac{v}{2\mu} \right)^n \left| H_n \left(\frac{\beta}{\sqrt{2\mu v}} \right) \right|^2 e^{-|\beta|^2 + \frac{v}{2\mu} \beta^2 + \frac{v^*}{2\mu} \beta^{*2}} \quad (2.84)$$

where

$$v = \sinh r e^{2i\phi}, \quad \mu = \cosh r, \quad \beta = \mu\alpha + v\alpha^* .$$

$H_n(x)$ are Hermite polynomials.

The photon number distribution for a squeezed state may be broader or narrower than a Poissonian depending on whether the reduced fluctuations occur in the phase (X_2) or amplitude (X_1) component of the field. This is illustrated in Fig. 2.4a where we plot $P(n)$ for $r = 0$, $r > 0$, and $r < 0$. Note, a squeezed vacuum ($\alpha = 0$) contains only even numbers of photons since $H_n(0) = 0$ for n odd.

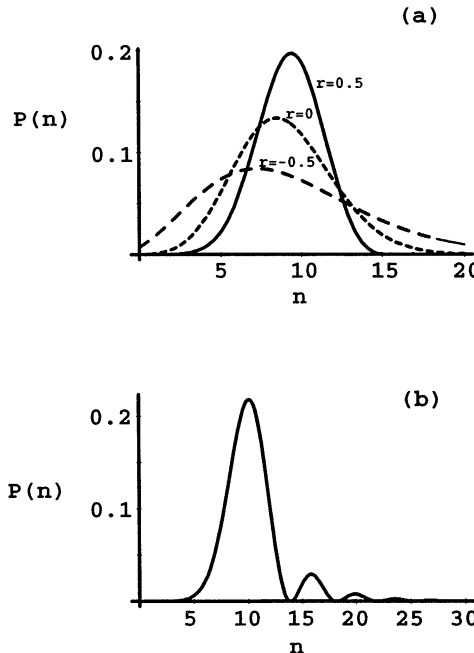


Fig. 2.4. Photon number distribution for a squeezed state $|\alpha, r\rangle$: (a) $\alpha = 3$, $r = 0, 0.5, -0.5$, (b) $\alpha = 3$, $r = 1.0$

For larger values of the squeeze parameter r , the photon number distribution exhibits oscillations, as depicted in Fig. 2.4b. These oscillations have been interpreted as interference in phase space [2.8].

2.7 Multimode Squeezed States

Multimode squeezed states are important since several devices produce light which is correlated at the two frequencies ω_+ and ω_- . Usually these frequencies are symmetrically placed either side of a carrier frequency. The squeezing exists not in the single modes but in the correlated state formed by the two modes.

A two-mode squeezed state may be defined by [2.9]

$$|\alpha_+, \alpha_-\rangle = D_+(\alpha_+)D_-(\alpha_-)S(G)|0\rangle \quad (2.85)$$

where the displacement operator is

$$D_{\pm}(\alpha) = \exp(\alpha a_{\pm}^{\dagger} - \alpha^* a_{\pm}) , \quad (2.86)$$

and the unitary two-mode squeeze operator is

$$S(G) = \exp(G^* a_+ a_- - G a_+^\dagger a_-^\dagger) . \quad (2.87)$$

The squeezing operator transforms the annihilation operators as

$$S^\dagger(G) a_\pm S(G) = a_\pm \cosh r - a_\mp^\dagger e^{i\theta} \sinh r , \quad (2.88)$$

where $G = r e^{i\theta}$.

This gives for the following expectation values

$$\begin{aligned} \langle a_+ \rangle &= \alpha_+, & \langle a_- \rangle &= \alpha_-, \\ \langle a_\pm^\dagger a_\pm \rangle &= |\alpha_\pm|^2 + \sinh^2 r, & \langle a_\pm^\dagger a_\mp^\dagger \rangle &= \alpha_\pm^* \alpha_\mp, \\ \langle a_\pm a_\pm \rangle &= \alpha_\pm^2, & \langle a_+ a_- \rangle &= \langle a_- a_+ \rangle = \alpha_+ \alpha_- - e^{i\theta} \sinh r \cosh r . \end{aligned} \quad (2.89)$$

The quadrature operator X is generalized in the two-mode case to

$$X = \frac{1}{\sqrt{2}}(a_+ + a_+^\dagger + a_- + a_-^\dagger) . \quad (2.90)$$

As will be seen in Chap. 5, this definition is a particular case of a more general definition. It corresponds to the degenerate situation in which the frequencies of the two modes are equal.

The mean and variance of X in a two-mode squeezed state is

$$\begin{aligned} \langle X \rangle &= 2(\text{Re}\{\alpha_+\} + \text{Re}\{\alpha_-\}) , \\ V(X) &= \left(e^{-2r} \cos^2 \frac{\theta}{2} + e^{2r} \sin^2 \frac{\theta}{2} \right) . \end{aligned} \quad (2.91)$$

These results for two-mode squeezed states will be used in the analyses of nondegenerate parametric oscillation given in Chaps. 4 and 6.

2.8 Phase Properties of the Field

The definition of an Hermitian phase operator corresponding to the physical phase of the field has long been a problem. Initial attempts by P. Dirac led to a non-Hermitian operator with incorrect commutation relations. Many of these difficulties were made quite explicit in the work of *Susskind* and *Glogower* [2.10]. Recently, *Pegg* and *Barnett* [2.11] showed how to construct an Hermitian phase operator, the eigenstates of which, in an appropriate limit, generate the correct phase statistics for arbitrary states. We will first discuss the *Susskind–Glogower* (SG) phase operator.

Let a be the annihilation operator for a harmonic oscillator, representing a single field mode. In analogy with the classical polar decomposition of a complex amplitude we define the SG phase operator,

$$e^{i\phi} = (aa^\dagger)^{-1/2}a . \quad (2.92)$$

The operator $e^{i\phi}$ has the number state expansion

$$e^{i\phi} = \sum_{n=0}^{\infty} |n\rangle\langle n+1| \quad (2.93)$$

and eigenstates $|e^{i\phi}\rangle$ like

$$|e^{i\phi}\rangle = \sum_{n=0}^{\infty} e^{in\phi} |n\rangle \quad \text{for } -\pi < \phi \leq \pi . \quad (2.94)$$

It is easy to see from (2.93) that $e^{i\phi}$ is not unitary,

$$[e^{i\phi}, (e^{i\phi})^\dagger] = |0\rangle\langle 0| . \quad (2.95)$$

An equivalent statement is that the SG phase operator is not Hermitian. As an immediate consequence the eigenstates $|e^{i\phi}\rangle$ are not orthogonal. In many ways this is similar to the non-orthogonal eigenstates of the annihilation operator a , i.e. the coherent states. None-the-less these states do provide a resolution of identity

$$\int_{-\pi}^{\pi} d\phi |e^{i\phi}\rangle\langle e^{i\phi}| = 2\pi . \quad (2.96)$$

The phase distribution over the window $-\pi < \phi \leq \pi$ for any state $|\psi\rangle$ is then defined by

$$P(\phi) = \frac{1}{2\pi} |\langle e^{i\phi} | \psi \rangle|^2 . \quad (2.97)$$

The normalisation integral is

$$\int_{-\pi}^{\pi} P(\phi) d\phi = 1 . \quad (2.98)$$

The question arises; does this distribution correspond to the statistics of any physical phase measurement? At the present time there does not appear to be an answer. However, there are theoretical grounds [2.12] for believing that $P(\phi)$ is the correct distribution for optimal phase measurements. If this is accepted then the fact that the SG phase operator is not Hermitian is nothing to be concerned about. However, as we now show, one can define an Hermitian phase operator,

the measurement statistics of which converge, in an appropriate limit, to the phase distribution of (2.97) [2.13].

Consider the state $|\phi_0\rangle$ defined on a finite subspace of the oscillator Hilbert space by

$$|\phi_0\rangle = (s+1)^{-1/2} \sum_{n=0}^s e^{in\phi_0} |n\rangle . \quad (2.99)$$

It is easy to demonstrate that the states $|\phi\rangle$ with the values of ϕ differing from ϕ_0 by integer multiples of $2\pi/(s+1)$ are orthogonal. Explicitly, these states are

$$|\phi_m\rangle = \exp\left(i \frac{a^\dagger a m 2\pi}{s+1}\right) |\phi_0\rangle; \quad m = 0, 1, \dots, s , \quad (2.100)$$

with

$$\phi_m = \phi_0 + \frac{2\pi m}{s+1} .$$

Thus $\phi_0 \leq \phi_m < \phi_0 + 2\pi$. In fact, these states form a complete orthonormal set on the truncated $(s+1)$ dimensional Hilbert space. We now construct the *Pegg–Barnett (PB) Hermitian phase operator*

$$\hat{\phi} = \sum_{m=0}^s \phi_m |\phi_m\rangle \langle \phi_m| . \quad (2.101)$$

For states restricted to the truncated Hilbert space the measurement statistics of ϕ are given by the discrete distribution

$$P_m = |\langle \phi_m | \psi \rangle_s|^2 \quad (2.102)$$

where $|\psi\rangle_s$ is any vector of the truncated space.

It would seem natural now to take the limit $s \rightarrow \infty$ and recover an Hermitian phase operator on the full Hilbert space. However, in this limit the PB phase operator does not converge to an Hermitian phase operator, but the distribution in (2.102) does converge to the SG phase distribution in (2.97). To see this, choose $\phi_0 = 0$.

Then

$$P_m = (s+1)^{-1} \left| \sum_{n=0}^s \exp\left(-i \frac{nm 2\pi}{s+1}\right) \psi_n \right|^2 \quad (2.103)$$

where $\psi_n = \langle n | \psi \rangle_s$.

As ϕ_m are uniformly distributed over 2π we define the probability density by

$$P(\phi) = \lim_{s \rightarrow \infty} \left[\left(\frac{2\pi}{s+1} \right)^{-1} P_m \right] = \frac{1}{2\pi} \left| \sum_{n=0}^{\infty} e^{in\phi} \psi_n \right|^2 \quad (2.104)$$

where

$$\phi = \lim_{s \rightarrow \infty} \frac{2\pi m}{s+1}, \quad (2.105)$$

and ψ_n is the number state coefficient for any Hilbert space state. This convergence in distribution ensures that the moments of the PB Hermitian phase operator converge, as $s \rightarrow \infty$, to the moments of the phase probability density.

The phase distribution provides a useful insight into the structure of fluctuations in quantum states. For example, in the number state $|n\rangle$, the mean and variance of the phase distribution are given by

$$\langle \phi \rangle = \phi_0 + \pi, \quad (2.106)$$

and

$$V(\phi) = \frac{2}{3}\pi, \quad (2.107)$$

respectively. These results are characteristic of a state with random phase. In the case of a coherent state $|re^{i\phi}\rangle$ with $r \gg 1$, we find

$$\langle \phi \rangle = \phi, \quad (2.108)$$

$$V(\phi) = \frac{1}{4\bar{n}}, \quad (2.109)$$

where $\bar{n} = \langle a^\dagger a \rangle = r^2$ is the mean photon number. Not surprisingly a coherent state has well defined phase in the limit of large amplitude.

Exercises

2.1 If $|X_1\rangle$ is an eigenstate for the operator X_1 find $\langle X_1|\psi\rangle$ in the cases
(a) $|\psi\rangle = |\alpha\rangle$; (b) $|\psi\rangle = |\alpha, r\rangle$.

2.2 Prove that if $|\psi\rangle$ is a minimum-uncertainty state for the operators X_1 and X_2 , then $V(X_1, X_2) = 0$.

2.3 Show that the squeeze operator

$$S(r, \phi) = \exp \left[\frac{r}{2} (e^{-2i\phi} a^2 - e^{2i\phi} a^{\dagger 2}) \right]$$

may be put in the normally ordered form

$$S(r, \phi) = (\cosh r)^{-1/2} \exp\left(-\frac{\Gamma}{2} a^{\dagger 2}\right) \exp[-\ln(\cosh r)a^\dagger a] \exp\left(\frac{\Gamma^*}{2} a^2\right)$$

where $\Gamma = e^{2i\phi} \tanh r$.

2.4 Evaluate the mean and variance for the phase operator in the squeezed state $|\alpha, r\rangle$ with α real. Show that for $|r| \gg |\alpha|$ this state has either enhanced or diminished phase uncertainty compared to a coherent state.

3. Coherence Properties of the Electromagnetic Field

In this chapter correlation functions for the electromagnetic field are introduced from which a definition of optical coherence may be formulated. It is shown that the coherent states possess n^{th} -order optical coherence. Photon-correlation measurements and the phenomena of photon bunching and antibunching are described. Phase-dependent correlation functions which are accessible via homodyne measurements are introduced. The theory of photon counting measurements is given.

3.1 Field-Correlation Functions

We shall now consider the detection of an electromagnetic field. A large-scale macroscopic device is complicated, hence, we shall study a simple device, an ideal photon counter. The most common devices in practice involve a transition where a photon is absorbed. This has important consequences since this type of counter is insensitive to spontaneous emission. A complete theory of detection of light requires a knowledge of the interaction of light with atoms. We shall postpone this until a study of the interaction of light with atoms is made in Chap. 10. At this stage we shall assume we have an ideal detector working on an absorption mechanism which is sensitive to the field $E^{(+)}(\mathbf{r}, t)$ at the space-time point (\mathbf{r}, t) . We follow the treatment of *Glauber* [3.1].

The transition probability of the detector for absorbing a photon at position \mathbf{r} and time t is proportional to

$$T_{if} = |\langle f | E^{(+)}(\mathbf{r}, t) | i \rangle|^2 \quad (3.1)$$

if $|i\rangle$ and $|f\rangle$ are the initial and final states of the field. We do not, in fact, measure the final state of the field but only the total counting rate. To obtain the total count rate we must sum over all states of the field which may be reached from the initial state by an absorption process. We can extend the sum over a complete set of final states since the states which cannot be reached (e.g., states $|f\rangle$ which differ from $|i\rangle$ by two or more photons) will not contribute to the result since they are orthogonal to $E^{(+)}(\mathbf{r}, t)|i\rangle$. The total counting rate or

average field intensity is

$$\begin{aligned} I(\mathbf{r}, t) &= \sum_f T_{fi} = \sum_f \langle i | E^{(-)}(\mathbf{r}, t) | f \rangle \langle f | E^{(+)}(\mathbf{r}, t) | i \rangle \\ &= \langle i | E^{(-)}(\mathbf{r}, t) E^{(+)}(\mathbf{r}, t) | i \rangle , \end{aligned} \quad (3.2)$$

where we have used the completeness relation

$$\sum_f |f\rangle\langle f| = 1 . \quad (3.3)$$

The above result assumes that the field is in a pure state $|i\rangle$. The result may be easily generalized to a statistical mixture state by averaging over initial states with the probability P_i , i.e.,

$$I(\mathbf{r}, t) = \sum_i P_i \langle i | E^{(-)}(\mathbf{r}, t) E^{(+)}(\mathbf{r}, t) | i \rangle . \quad (3.4)$$

This may be written as

$$I(\mathbf{r}, t) = \text{Tr}\{\rho E^{(-)}(\mathbf{r}, t) E^{(+)}(\mathbf{r}, t)\} , \quad (3.5)$$

where ρ is the density operator defined by

$$\rho = \sum_i P_i |i\rangle\langle i| . \quad (3.6)$$

If the field is initially in the vacuum state

$$\rho = |0\rangle\langle 0| , \quad (3.7)$$

then the intensity is

$$I(\mathbf{r}, t) = \langle 0 | E^{(-)} E^{(+)} | 0 \rangle = 0 . \quad (3.8)$$

The normal ordering of the operators (that is, all annihilation operators are to the right of all creation operators) yields zero intensity for the vacuum. This is a consequence of our choice of an absorption mechanism for the detector. Had we chosen a detector working on a stimulated emission principle, problems would arise with vacuum fluctuations. More generally the correlation between the field at the space-time point $x = (\mathbf{r}, t)$ and the field at the space-time point $x' = (\mathbf{r}, t')$ may be written as the correlation function

$$G^{(1)}(x, x') = \text{Tr}\{\rho E^{(-)}(x) E^{(+)}(x')\} . \quad (3.9)$$

The first-order correlation function of the radiation field is sufficient to account for classical interference experiments. To describe experiments involving intensity correlations such as the Hanbury-Brown and Twiss experiment, it is necessary to define higher-order correlation functions. We define the n^{th} -order correlation function of the electromagnetic field as

$$\begin{aligned} G^{(n)}(x_1 \dots x_n, x_{n+1} \dots x_{2n}) &= \text{Tr}\{\rho E^{(-)}(x_1) \dots E^{(-)}(x_n) \\ &\quad \times E^{(+)}(x_{n+1}) \dots E^{(+)}(x_{2n})\} . \end{aligned} \quad (3.10)$$

Such an expression follows from a consideration of an n -atom photon detector [3.1]. The n -fold delayed coincidence rate is

$$W^{(n)}(t_1 \dots t_n) = s^n G^{(n)}(r_1 t_1 \dots r_n t_n, r_n t_n \dots r_1 t_1) , \quad (3.11)$$

where s is the sensitivity of the detector.

3.2 Properties of the Correlation Functions

A number of interesting inequalities can be derived from the general expression

$$\text{Tr}\{\rho A^\dagger A\} \geq 0 , \quad (3.12)$$

which follows from the non-negative character of $A^\dagger A$ for any linear operator A .

Thus choosing $A = E^{(+)}(x)$ gives

$$G^{(1)}(x, x) \geq 0 . \quad (3.13)$$

In general, taking

$$A = E^{(+)}(x_n) \dots E^{(+)}(x_1) \quad (3.14)$$

yields

$$G^{(n)}(x_1 \dots x_n, x_n \dots x_1) \geq 0 \quad (3.15)$$

Choosing

$$A = \sum_{j=1}^n \lambda_j E^{(+)}(x_j) , \quad (3.16)$$

where λ_j are an arbitrary set of complex numbers gives

$$\sum_{ij} \lambda_i^* \lambda_j G^{(1)}(x_i, x_j) \geq 0 . \quad (3.17)$$

Thus the set of correlation functions $G^{(1)}(x_i, x_j)$ forms a matrix of coefficients for a positive definite quadratic form. Such a matrix has a positive determinant, i.e.,

$$\det[G^{(1)}(x_i, x_j)] \geq 0 . \quad (3.18)$$

For $n = 1$, this is simply (3.13). For $n = 2$ we find

$$G^{(1)}(x_1, x_1) G^{(1)}(x_2, x_2) \geq |G^{(1)}(x_1, x_2)|^2 \quad (3.19)$$

which is a simple generalisation of the Schwarz inequality.

Choosing

$$A = \lambda_1 E^{(+)}(x_1) \dots E^{(+)}(x_n) + \lambda_2 E^{(+)}(x_{n+1}) \dots E^{(+)}(x_{2n}) , \quad (3.20)$$

we find the general relation

$$\begin{aligned} G^{(n)}(x_1 \dots x_n, x_n \dots x_1) G^{(n)}(x_{n+1} \dots x_{2n}, x_{2n} \dots x_{n+1}) \\ \geq |G^{(n)}(x_1 \dots x_n, x_{n+1} \dots x_{2n})|^2 . \end{aligned} \quad (3.21)$$

For two beams we may take

$$A = \lambda_1 E_1^{(+)}(x) E_1^{(+)}(x') + \lambda_2 E_2^{(+)}(x) E_2^{(+)}(x') , \quad (3.22)$$

with $x \equiv (\mathbf{r}, 0)$ and $x' \equiv (\mathbf{r}, t)$. The Cauchy–Schwartz inequality then becomes

$$G_{11}^{(2)}(0) G_{22}^{(2)}(0) \geq [G_{12}^{(2)}(t)]^2 , \quad (3.23)$$

where

$$G_{ij}^{(2)}(t) = \text{Tr} \{ \rho E_i^{(-)}(x) E_i^{(-)}(x') E_j^{(+)}(x') E_j^{(+)}(x) \} ; \quad (3.24)$$

we have noted explicitly that $G_{ii}^{(2)}$ is time independent.

An inequality closely related to (3.23) may be derived by choosing

$$A = \lambda_1 E_1^{(-)}(x) E_1^{(+)}(x) + \lambda_2 E_2^{(-)}(x) E_2^{(+)}(x) . \quad (3.25)$$

This gives

$$\begin{aligned} & |\langle E_1^{(-)}(x) E_1^{(+)}(x) E_2^{(+)}(x) E_2^{(-)}(x) \rangle|^2 \\ & \leq \langle [E_1^{(-)}(x) E_1^{(+)}(x)]^2 \rangle \langle [E_2^{(-)}(x) E_2^{(+)}(x)]^2 \rangle . \end{aligned} \quad (3.26)$$

This inequality will be used in Chap. 5.

3.3 Correlation Functions and Optical Coherence

Classical optical interference experiments correspond to a measurement of the first-order correlation function. We shall consider Young's interference experiment as a measurement of the first-order correlation function of the field and show how a definition of first-order optical coherence arises from considerations of the fringe visibility.

A schematic sketch of Young's interference experiment is depicted in Fig. 3.1. The field incident on the screen at position \mathbf{r} and time t is the superposition of the fields at the two pin holes

$$E^{(+)}(\mathbf{r}, t) = E_1^{(+)}(\mathbf{r}, t) + E_2^{(+)}(\mathbf{r}, t) \quad (3.27)$$

where $E_i^{(+)}(\mathbf{r}, t)$ is the field produced by pinhole i at the screen with

$$E_i^{(+)}(\mathbf{r}, t) = E_i^{(+)}\left(\mathbf{r}_i, t - \frac{s_i}{c}\right) \left(\frac{1}{s_i}\right) e^{i(k - \frac{\omega}{c})s_i} \quad (3.28)$$

where $s_i = |\mathbf{r}_i - \mathbf{r}|$

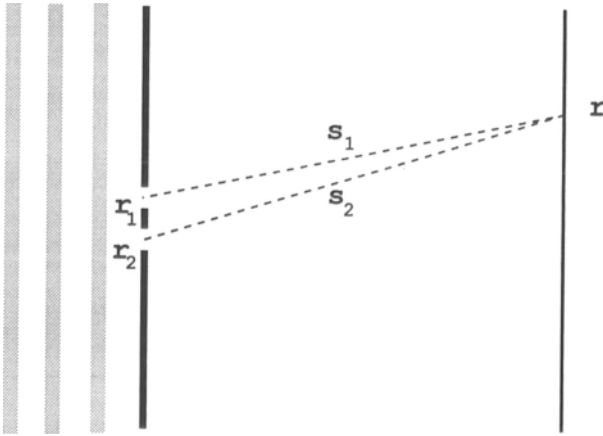


Fig. 3.1. Schematic representation of Young's interference experiment

and $E_i^{(+)}(\mathbf{r}_i, t - s_i/c)$ is the field at the i^{th} pinhole and for a spherical wave

$$k - \frac{\omega}{c} = 0 .$$

Therefore (3.27) becomes

$$E^{(+)}(\mathbf{r}, t) = \frac{E_1^{(+)}\left(\mathbf{r}_1, t - \frac{s_1}{c}\right)}{s_1} + \frac{E_2^{(+)}\left(\mathbf{r}_2, t - \frac{s_2}{c}\right)}{s_2} . \quad (3.29)$$

For $s_1 \approx s_2 \approx R$, we have

$$E^{(+)}(\mathbf{r}, t) = \frac{1}{R} [E_1^{(+)}(x_1) + E_2^{(+)}(x_2)] \quad (3.30)$$

where

$$x_1 = \left(\mathbf{r}_1, t - \frac{s_1}{c} \right), \quad x_2 = \left(\mathbf{r}_2, t - \frac{s_2}{c} \right) .$$

The intensity observed on the screen is proportional to

$$I = \text{Tr}\{\rho E^{(-)}(\mathbf{r}, t) E^{(+)}(\mathbf{r}, t)\} . \quad (3.31)$$

Using (3.27) we find

$$I = G^{(1)}(x_1, x_1) + G^{(1)}(x_2, x_2) + 2\text{Re}\{G^{(1)}(x_1, x_2)\} \quad (3.32)$$

where the R^{-2} factor is absorbed into a normalisation constant.

The first two terms on the right-hand side are the intensities from each pinhole in the absence of the other. The third term is the interference term. The

correlation function for $x_1 \neq x_2$, in general takes on complex values. Writing this as

$$G^{(1)}(x_1, x_2) = |G^{(1)}(x_1, x_2)| e^{i\Psi(x_1, x_2)}, \quad (3.33)$$

we find

$$I = G^{(1)}(x_1, x_1) + G^{(1)}(x_2, x_2) + 2|G^{(1)}(x_1, x_2)| \cos \Psi(x_1, x_2). \quad (3.34)$$

The interference fringes arise from the oscillations of the cosine term. The envelope of the fringes is described by the correlation function $G^{(1)}(x_1, x_2)$.

3.4 First-Order Optical Coherence

The idea of coherence in optics was first associated with the possibility of producing interference fringes when two fields are superposed. The highest degree of optical coherence was associated with a field which exhibits fringes with maximum visibility. If $G^{(1)}(x_1, x_2)$ was zero there would be no fringes and the fields are then described as incoherent. Thus the larger $G^{(1)}(x_1, x_2)$ the more coherent the field. The magnitude of $|G^{(1)}(x_1, x_2)|$ is limited by the relation

$$|G^{(1)}(x_1, x_2)| \leq [G^{(1)}(x_1, x_1)G^{(1)}(x_2, x_2)]^{1/2}. \quad (3.35)$$

The best possible fringe contrast is given by the equality sign. Thus the necessary condition for full coherence is

$$|G^{(1)}(x_1, x_2)| = [G^{(1)}(x_1, x_1)G^{(1)}(x_2, x_2)]^{1/2}. \quad (3.36)$$

Introducing the normalized correlation function

$$g^{(1)}(x_1, x_2) = \frac{G^{(1)}(x_1, x_2)}{[G^{(1)}(x_1, x_1)G^{(1)}(x_2, x_2)]^{1/2}}, \quad (3.37)$$

the condition (3.36) becomes

$$|g^{(1)}(x_1, x_2)| = 1 \quad (3.38)$$

or

$$g^{(1)}(x_1, x_2) = e^{i\Psi(x_1, x_2)}.$$

The visibility of the fringes is given by

$$v = \frac{I_{\max} - I_{\min}}{I_{\max} + I_{\min}}. \quad (3.39)$$

Using (3.27 and 3.31) for the intensity we may write v as

$$\begin{aligned} v &= \left| \frac{G^{(1)}(x_1, x_2)}{(G^{(1)}(x_1, x_1)G^{(1)}(x_2, x_2))^{1/2}} \right| \frac{2(I_1 I_2)^{1/2}}{I_1 + I_2} \\ &= |g^{(1)}| \frac{2(I_1 I_2)^{1/2}}{I_1 + I_2}. \end{aligned} \quad (3.40)$$

If the fields incident on each pinhole have equal intensities the fringe visibility is equal to $|g^{(1)}|$. Thus the condition for first-order optical coherence $|g^{(1)}| = 1$ corresponds to the condition for maximum fringe visibility.

A more general definition of first-order coherence of the field $E(x)$ is that the first-order correlation function factorizes

$$G^{(1)}(x_1, x_2) = \varepsilon^{(-)}(x_1)\varepsilon^{(+)}(x_2). \quad (3.41)$$

It is readily seen that this is equivalent to the condition for first-order optical coherence given by (3.38). It is clear that for a field in a left eigenstate of the operator $E^{(+)}(x)$ this factorization holds. The coherent states are an example of such a field. It is precisely this coherence property of the coherent states which led to their names.

We may generalize (3.41) to give the condition for n th optical coherence. This requires that the n th order correlation function factorizes:

$$G^{(n)}(x_1 \dots x_n, x_{n+1}, \dots, x_{2n}) = \varepsilon^{(-)}(x_1) \dots \varepsilon^{(-)}(x_n)\varepsilon^{(+)}(x_{n+1}) \dots \varepsilon^{(+)}(x_{2n}). \quad (3.42)$$

Again the coherent states possess n^{th} -order optical coherence.

Photon interference experiments of the kind typified by Young's interference experiment and Michelson's interferometer played a central role in early discussions of the dual wave and corpuscular nature of light. These experiments basically detect the interference pattern resulting from the superposition of two components of a light beam. Classical theory based on the wave nature of light readily explained the observed interference pattern. The quantum-mechanical explanation is based on the interference of the probability amplitudes for the photon to take either of two paths. We shall demonstrate how interference occurs even for a one photon field. For full details of the classical theory and experimental arrangements the reader is referred to the classic text of *Born and Wolf* [3.2].

We consider an interference experiment of the type performed by Young which consists of light from a monochromatic point source S incident on a screen possessing two pinholes P_1 and P_2 which are equidistant from S (see Fig. 3.1).

The pinholes act as secondary monochromatic point sources which are in phase and the beams from them are superimposed on a screen at position r and time t . In this region an interference pattern is formed.

To avoid calculating the diffraction pattern for the pinhole, we assume their dimensions are of the order of the wavelength of light in which case they

effectively act as sources for single modes of spherical radiation in keeping with Huygen's principle. The appropriate mode functions for spherical radiation are

$$\mathbf{u}_k(\mathbf{r}) = \left(\frac{1}{4\pi L} \right)^{1/2} \frac{e^{ik \cdot r}}{r} \hat{\mathbf{e}}_k , \quad (3.43)$$

where L is the radius of the normalization volume, and $\hat{\mathbf{e}}_k$ is the unit polarization vector.

The field detected on the screen at position \mathbf{r} and time t is then the sum of the two spherical modes emitted by the two pinholes

$$E^{(+)}(\mathbf{r}, t) = f(\mathbf{r}, t)(a_1 e^{ikr_1} + a_2 e^{iks_2}) , \quad (3.44)$$

with

$$f(\mathbf{r}, t) = i \left(\frac{\hbar\omega}{2} \right)^{1/2} \frac{\hat{\mathbf{e}}_k}{(4\pi L)^{1/2}} \frac{1}{R} e^{-i\omega t} ,$$

where s_1 and s_2 are the distances of the pinholes P_1 and P_2 to the point on the screen, and we have set $s_1 \approx s_2 = R$ in the denominator of the mode functions. Substituting (3.43) into (3.2) for the intensity we find

$$I(\mathbf{r}, t) = \eta [\text{Tr}\{\rho a_1^\dagger a_1\} + \text{Tr}\{\rho a_2^\dagger a_2\} + 2|\text{Tr}\{\rho a_1^\dagger a_2\}| \cos \Phi] . \quad (3.45)$$

where

$$\text{Tr}\{\rho a_1^\dagger a_2\} = |\text{Tr}\{\rho a_1^\dagger a_2\}| e^{i\phi} ,$$

$$\eta = |f(\mathbf{r}, t)|^2 ,$$

$$\Phi = k(s_1 - s_2) + \phi .$$

This expression exhibits the typical interference fringes with the maximum of intensity occurring at

$$k(s_1 - s_2) + \phi = n2\pi , \quad (3.46)$$

with n an integer.

The maximum intensity of the fringes falls off as one moves the point of observation further from the central line by the R^{-2} factor in $|f(\mathbf{r}, t)|^2$.

We shall evaluate the intensity for fields which may be generated by a single-mode excitation and hence have first-order coherence. A general representation of such a field is

$$|\psi\rangle = f(b^\dagger)|0\rangle , \quad (3.47)$$

where $|0\rangle$ denotes the vacuum state of the radiation field and b^\dagger is the creation operator for a single mode of the radiation field. The operator b^\dagger may be expressed as a linear combination of a_1^\dagger and a_2^\dagger as follows

$$b^\dagger = -\frac{1}{\sqrt{2}}(a_1^\dagger + a_2^\dagger) , \quad (3.48)$$

where we have assumed equal intensities through each slit. We shall now consider as a special case the field with only one photon incident on the pinholes, i.e.,

$$|1 \text{ photon}\rangle = b^\dagger |0\rangle = \frac{1}{\sqrt{2}} (|1,0\rangle + |0,1\rangle) , \quad (3.49)$$

where the notation used for the eigenkets $|n_1, n_2\rangle$ implies that there are n_1 photons present in mode k_1 and n_2 photons present in mode k_2 . This state of the field reflects the fact that we don't know which pinhole the photon goes through.

From (3.45) this yields the following expression for the mean intensity on the screen

$$I(r, t) = \eta(1 + \cos \Phi) . \quad (3.50)$$

It is clear from this equation that an interference pattern may be built up from a succession of one-photon interference fringes.

The quantum explanation for the interference pattern was first put forward by *Dirac* [3.3] in his classic text on quantum mechanics. There he argued that the observed intensity pattern results from interference between the probability amplitudes of a single photon to take either of two possible paths. The crux of the quantum mechanical explanation is that the wavefunction gives information about the probability of one photon being in a particular place and not the probable number of photons in that place. *Dirac* pointed out that the interference between the two beams does not arise because photons of one beam sometimes annihilate photons from the other, and sometimes combine to produce four photons. "This would contradict the conservation of energy. The new theory which connects the wave functions with probabilities for one photon gets over the difficulty by making each photon go partly into each of two components. Each photon then interferes only with itself. Interference between two different photons never occurs". We stress that the above-quoted statement of *Dirac* was only intended to apply to experiments of the Young's type where the interference pattern is revealed by detecting single photons. It was not intended to apply to experiments of the type where correlations between different photons are measured.

A very early experiment to test if interference would result from a single photon was performed by *Taylor* [3.4] in 1905. In this experiment the intensity of the source was so low that on average only one photon was incident on the slits at a time. The photons were detected on a photographic plate so that the detection time was very large. Interference fringes were observed in this experiment. This experiment did not definitively show that the interference fringes resulted from a single photon since the statistical distribution of photons meant that sometimes two photons could be incident on the slits. A definitive experiment was conducted by *Grangier et al.* [3.5] using a two-photon cascade as

a source. A coincidence technique which detected one photon of the pair enabled them to prepare a one photon source.

We now consider the interference patterns produced by other choices of a field.

3.5 Coherent Field

We consider a coherent field as generated by an ideal laser incident on the pinholes. The wavefunction for this coherent field is

$$|\text{coherent field}\rangle = |\alpha_1, \alpha_2\rangle = |\alpha_1\rangle|\alpha_2\rangle . \quad (3.51)$$

Since this wavefunction is a product state, it may well represent two independent light beams. This particular product may, however, be generated by a single-mode excitation in the following manner:

$$\begin{aligned} |\alpha_1\rangle|\alpha_2\rangle &= \exp(\alpha b^\dagger - \alpha^* b)|0\rangle \\ &= \exp\frac{1}{\sqrt{2}}(\alpha a_1^\dagger - \alpha^* a_1)\exp\frac{1}{\sqrt{2}}(\alpha a_2^\dagger - \alpha^* a_2)|0\rangle \\ &= \left| \frac{\alpha}{\sqrt{2}} \right\rangle \left| \frac{\alpha}{\sqrt{2}} \right\rangle . \end{aligned} \quad (3.52)$$

The intensity pattern produced by this coherent field is

$$I(\mathbf{r}, t) = \eta(|\alpha|^2 + |\alpha|^2 \cos \phi) . \quad (3.53)$$

The above example demonstrates the possibility of obtaining interference between independent light beams. Experimentally, this requires that the phase relation between the two beams be slowly varying or else the fringe pattern will be washed out. Such experiments have been performed by *Pfleegor* and *Mandel* [3.6]. Interference between independent light beams is, however, only possible for certain states of the radiation field, for example, the coherent states as demonstrated above. Interference is not generally obtained from independent light beams, as we shall demonstrate in the following example. We consider the two independent light beams to be Fock states, that is, described by the wavefunction

$$|\psi\rangle = |n_1\rangle|n_2\rangle . \quad (3.54)$$

This yields a zero correlation function and consequently no fringes are obtained.

The analysis we performed leading to (3.50) bears out *Dirac's* argument that the interference fringes may be produced by a series of one photon experiments. However, Young's interference fringes may perfectly well be explained by the interference of classical waves. Experiments of this kind which measure the first-order correlation functions of the electromagnetic field do not distinguish between the quantum and classical theories of light.

3.6 Photon Correlation Measurements

The first experiment performed outside the domain of one photon optics was the intensity correlation experiment of *Hanbury-Brown* and *Twiss* [3.7]. Although the original experiment involved the analogue correlation of photocurrents, later experiments used photon counters and digital correlations and were truly photon correlation measurements. In essence these experiments measure the joint photocount probability of detecting the arrival of a photon at time t and another photon at time $t + \tau$. This may be written as an intensity or photon-number correlation function. Using the quantum detection theory developed by *Glauber*, the measured quantity is the normally ordered correlation function

$$\begin{aligned} G^{(2)}(\tau) &= \langle E^{(-)}(t)E^{(-)}(t + \tau)E^{(+)}(t + \tau)E^{(+)}(t) \rangle \\ &= \langle : I(t)I(t + \tau) : \rangle \\ &\propto \langle : n(t)n(t + \tau) : \rangle \end{aligned} \quad (3.55)$$

where $: :$ indicates normal ordering, $I(t)$ is the intensity for analogue measurements and $n(t)$ is the photon number in photon counting experiments. It is useful to introduce the normalized second-order correlation function defined by

$$g^{(2)}(\tau) = \frac{G^{(2)}(\tau)}{|G^{(1)}(0)|^2}. \quad (3.56)$$

We shall evaluate $g^{(2)}(\tau)$ for certain classes of field. For a field which possesses second-order coherence

$$G^{(2)}(\tau) = \varepsilon^{(-)}(t)\varepsilon^{(-)}(t + \tau)\varepsilon^{(+)}(t + \tau)\varepsilon^{(+)}(t) = [G^{(1)}(0)]^2. \quad (3.57)$$

Hence $g^{(2)}(\tau) = 1$.

For a fluctuating classical field we may introduce a probability distribution $P(\varepsilon)$ describing the probability of the field $E^{(+)}(\varepsilon, t)$ having the amplitude ε where

$$E^{(+)}(\varepsilon, t) = -\left(i\frac{\hbar\omega}{2\varepsilon_0 V}\right)^{1/2} \varepsilon e^{-i\omega t}.$$

For a multimode field we have a multivariate probability distribution $P(\{\varepsilon_k\})$. The second-order correlation function $G^{(2)}(\tau)$ may be written as

$$G^{(2)}(\tau) = \int P(\{\varepsilon_k\}) E^{(-)}(\varepsilon_k, t) E^{(-)}(\varepsilon_k, t + \tau) E^{(+)}(\varepsilon_k, t + \tau) E^{(+)}(\varepsilon_k, t) d^2\{\varepsilon_k\}. \quad (3.58)$$

For zero time delay $\tau = 0$ we may write for a single-mode field

$$g^{(2)}(0) = 1 + \frac{\int P(\varepsilon)(|\varepsilon|^2 - \langle |\varepsilon|^2 \rangle)^2 d^2\varepsilon}{\langle |\varepsilon|^2 \rangle^2}. \quad (3.59)$$

For classical fields the probability distribution $P(\varepsilon)$ is positive, hence $g^{(2)}(0) \geq 1$.

For a field obeying Gaussian statistics with zero mean amplitude

$$\begin{aligned} & \langle E^{(-)}(\varepsilon, t)E^{(-)}(\varepsilon, t + \tau)E^{(+)}(\varepsilon, t)E^{(+)}(\varepsilon, t + \tau) \rangle \\ &= \langle E^{(-)}(\varepsilon, t)E^{(-)}(\varepsilon, t + \tau) \rangle \langle E^{(+)}(\varepsilon, t + \tau)E^{(+)}(\varepsilon, t) \rangle \\ &+ \langle E^{(-)}(\varepsilon, t)E^{(+)}(\varepsilon, t) \rangle \langle E^{(-)}(\varepsilon, t + \tau)E^{(+)}(\varepsilon, t + \tau) \rangle \\ &+ \langle E^{(-)}(\varepsilon, t)E^{(+)}(\varepsilon, t + \tau) \rangle \langle E^{(-)}(\varepsilon, t + \tau)E^{(+)}(\varepsilon, t) \rangle . \end{aligned} \quad (3.60)$$

For fields with no phase-dependent fluctuations the first term may be neglected. Then

$$G^{(2)}(\tau) = G^{(1)}(0)^2 + |G^{(1)}(\tau)|^2 . \quad (3.61)$$

Hence the normalized second-order correlation function is

$$g^{(2)}(\tau) = 1 + |g^{(1)}(\tau)|^2 . \quad (3.62)$$

Now $G^{(1)}(\tau)$ is the Fourier transform of the spectrum of the field

$$S(\omega) = \int_{-\infty}^{\infty} d\tau e^{-i\omega\tau} G^{(1)}(\tau) . \quad (3.63)$$

Hence for a field with a Lorentzian spectrum

$$g^{(2)}(\tau) = 1 + e^{-\gamma\tau} \quad (3.64)$$

and for a field with a Gaussian spectrum

$$g^{(2)}(\tau) = 1 + e^{-\gamma^2\tau^2} , \quad (3.65)$$

where γ is the spectral linewidth.

For values of $\tau \gg \tau_c$ the correlation time of the light, the correlation function factorizes and $g^{(2)}(\tau) \rightarrow 1$. The increased value of $g^{(2)}(\tau)$ for $\tau < \tau_c$ for chaotic light over coherent light [$g^{(2)}(0)_{\text{chaotic}} = 2g^{(2)}(0)_{\text{coh}}$] is due to the increased intensity fluctuations in the chaotic light field. There is a high probability that the photon which triggers the counter occurs during a high intensity fluctuation and hence a high probability that a second photon will be detected arbitrarily soon. This effect known as photon bunching was first detected by *Hanbury-Brown* and *Twiss*. Later experiments [3.8] showed excellent agreement with the theoretical predictions for chaotic and coherent light (Fig. 3.2). We note that the above analysis does not rely on any quantisation of the electromagnetic field but may be deduced from a purely classical analysis of the electromagnetic field with fluctuating amplitudes for the modes.

Measurement of the second-order correlation function of light with Gaussian statistics has formed the basis of photon correlation spectroscopy [3.10]. Photon correlation spectroscopy may be used to measure very narrow linewidths ($1-10^8$ Hz) which are outside the range of conventional spectrometers. The second-order correlation function $g^2(\tau)$ is measured using electronic

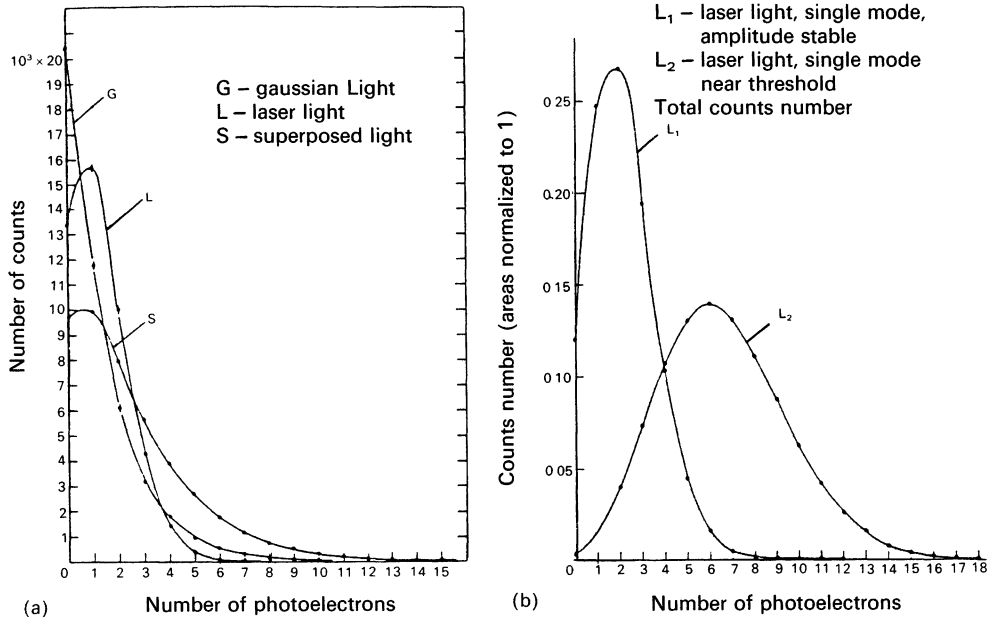


Fig. 3.2. Measured photo-count statistics for (a) Gaussian, laser and superposed fields. Measuring time of a single sample: 10 μ s. Coherence time of the Gaussian field; 40 μ s. (b) Two laser fields. Measuring time of a single sample: 10 μ s

correlators and the linewidth extracted using (3.64 or 3.65). This has found application, for example, in the measurement of the diffusion coefficient of macromolecules where the scattered light has Gaussian statistics. The linewidth of the scattered light contains information on the diffusion coefficient of the macromolecule. This technique has been applied to determine the size of biological molecules such as viruses as well as in studying turbulent flows.

3.7 Quantum Mechanical Fields

We shall now evaluate the second-order correlation function for some quantum-mechanical fields. We shall restrict our attention to a single-mode field and calculate $g^{(2)}(0)$ and the variance in the photon number $V(n)$

$$g^{(2)}(0) = \frac{\langle a^\dagger a^\dagger a a \rangle}{\langle a^\dagger a \rangle^2} = 1 + \frac{V(n) - \bar{n}}{\bar{n}^2}, \quad (3.66)$$

where $V(n) = \langle (a^\dagger a)^2 \rangle - \langle a^\dagger a \rangle^2$.

Coherent State

For a coherent state

$$\rho = |\alpha\rangle\langle\alpha|, \quad g^{(2)}(0) = 1 \quad (3.67)$$

and $V(n) = \bar{n}$ for a Poisson distribution in photon number.

Number state

$$\rho = |n\rangle\langle n|, \quad g^{(2)}(0) = 1 - \frac{1}{n}, \quad n > 2. \quad (3.68)$$

A number state has zero variance in the photon number ($V(n) = 0$). If $g^{(2)}(\tau) < g^{(2)}(0)$ there is a tendency for photons to arrive in pairs. This situation is referred to as *photon bunching*. The converse situation, $g^{(2)}(\tau) > g^{(2)}(0)$ is called *antibunching*. As noted above, however, $g^{(2)}(\tau) \rightarrow 1$ on a sufficiently long time scale. Thus a field for which $g^{(2)}(0) < 1$ will always exhibit antibunching on some time scale. A value of $g^{(2)}(0)$ less than unity could not have been predicted by a classical analysis. Eq. (3.59) always predicts $g^{(2)}(0) \geq 1$. To obtain a $g^{(2)}(0) < 1$ would require the field to have elements of negative probability, which is forbidden for a true probability distribution. This effect known as photon antibunching is a feature peculiar to the quantum mechanical nature of the electromagnetic field.

A distinction should be maintained between photon antibunching and sub-Poissonian statistics, although the two phenomena are closely related. For Poisson statistics the variance of the photon number is equal to the mean. Thus a measure of sub-Poissonian statistics is provided by the quantity $V(N) - \langle N \rangle$. For a stationary field one may show that [3.14].

$$V(N) - \langle N \rangle = \frac{\langle N \rangle^2}{T^2} \int_{-T}^T d\tau (T - |\tau|) [g^{(2)}(\tau) - 1], \quad (3.69)$$

where T is the counting time interval. If $g^{(2)}(\tau) = 1$ the field exhibits Poisson statistics. Certainly a field for which $g^{(2)}(\tau) < 1$ for all τ will exhibit sub-Poissonian statistics. However, it is possible to specify fields for which $g^{(2)}(\tau) > g^{(2)}(0)$ but which exhibit super-Poissonian statistics over some time interval.

3.7.1 Squeezed State

We consider a squeezed state $|\alpha, r\rangle$ with r defined as positive (Fig. 3.3). We align our axes such that the X_1 direction is parallel to the minor axis of the error ellipse. The direction (1) is referred to as the direction of squeezing and the direction (2) as the direction of coherent excitation. We then define α by

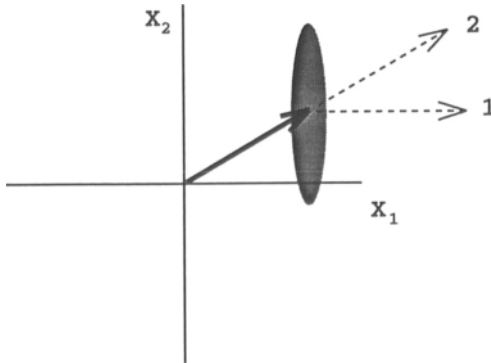


Fig. 3.3. A phase convention for squeezed states. Direction 1 is the direction of squeezing, direction 2 is the direction of coherent excitation. The error ellipse is aligned so that the squeezing direction is parallel to the X_1 direction.

$2\alpha = \langle X_1 \rangle + i\langle X_2 \rangle$ with $\theta = \tan^{-1}(\langle X_2 \rangle / \langle X_1 \rangle)$. The variance in the photon number for this squeezed state is

$$\frac{V(n) - \bar{n}}{\bar{n}^2} = \frac{|\alpha|^2(\cosh 2r - \sinh 2r \cos 2\theta - 1) + \sinh^2 r \cosh 2r}{(|\alpha|^2 + \sinh^2 r)^2} . \quad (3.70)$$

When $\theta = \pi/2$, that is the squeezing is out of phase with the complex amplitude

$$V(n) = |\alpha|^2 e^{2r} + 2 \sinh^2 r \cosh^2 r . \quad (3.71)$$

Thus this state with increased amplitude fluctuations has super-Poissonian statistics as expected.

When $\theta = 0$, that is the squeezing is in phase with the complex amplitude

$$V(n) = |\alpha|^2 e^{-2r} + 2 \sinh^2 r \cosh^2 r . \quad (3.72)$$

The first term corresponds to the reduction in number fluctuations in the original Poisson distribution. The second term is due to the fluctuations of the additional photons in the squeezed vacuum.

When $|\alpha|^2 \gg 2 \sinh^2 r \cosh^2 r$ this is an amplitude squeezed state with sub-Poissonian photon statistics. The maximum reduction in photon number fluctuations one can get in an amplitude squeezed state may be estimated as follows: For $r \geq 1$

$$V(n) \approx |\alpha|^2 e^{-2r} + \frac{1}{8} e^{4r} . \quad (3.73)$$

The minimum value of $V(n)$ occurs for $e^{6r} = 4|\alpha|^2$ which corresponds to $V_{\min}(n) \approx 0.94|\alpha|^{4/3}$. Diagrams depicting squeezed states with reduced amplitude and reduced phase fluctuations are shown in Fig. 3.4.

In Chap. 5 we will discuss a nonlinear interaction which produces a state with Poisson distribution in photon number, but can also exhibit amplitude squeezing.

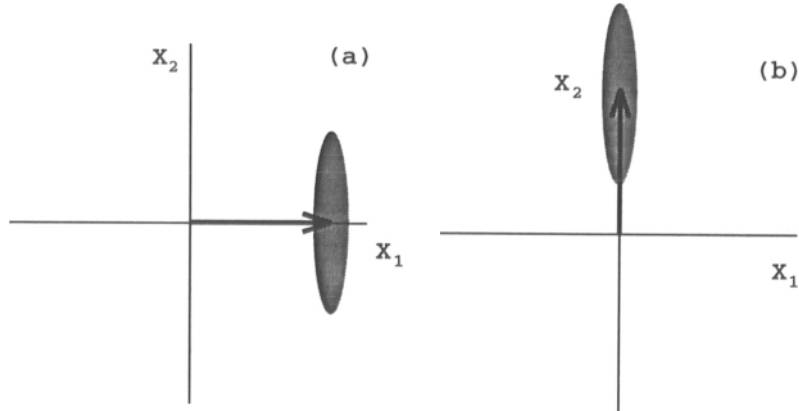


Fig. 3.4. Phase-space of amplitude and phase squeezed states. (a) The quadrature carrying the coherent excitation is squeezed ($\theta = 0$). (b) The quadrature out of phase with the coherent excitation is squeezed ($\theta = \pi/2$)

3.7.2 Squeezed Vacuum

For a squeezed vacuum $\alpha = 0$

$$V(n) = \bar{n}(1 + \cosh 2r) . \quad (3.74)$$

Hence a squeezed vacuum always exhibits super-Poissonian statistics.

We may compare the characteristics of a squeezed state with that of a number state. A number state has reduced photon number fluctuations but has complete uncertainty in phase. Thus a number state will not show any squeezing. For a number state

$$\Delta X_1^2 = \Delta X_2^2 = 2n + 1 . \quad (3.75)$$

A number state may be represented in an (X_1, X_2) phase space plot as an annulus with radius \sqrt{n} and width = 1.

3.8 Phase-Dependent Correlation Functions

The even-ordered correlation functions such as the second-order correlation function $G^{(n,n)}(x)$ contain no phase information and are a measure of the fluctuations in the photon number. The odd-ordered correlation functions $G^{(n,m)}$ ($x_1 \dots x_n, x_{n+1} \dots x_{n+m}$) with $n \neq m$ will contain information about the phase fluctuations of the electromagnetic field. The variances in the quadrature phases ΔX_1^2 and ΔX_2^2 are given by measurements of this type.

A number of schemes to make quadrature phase measurements have been discussed by *Yuen and Shapiro* [3.12].

These schemes involve homodyning the signal field with a reference signal known as the local oscillator before photodetection. Homodyning with a reference signal of fixed phase gives the phase sensitivity necessary to yield the quadrature variances.

Consider two fields $E_1(\mathbf{r}, t)$ and $E_2(\mathbf{r}, t)$ of the same frequency, combined on a beam splitter with transmittivity η , as shown in Fig. 3.5. This configuration is essentially identical to the single field quadrature homodyne detection scheme discussed by *Yuen and Shapiro*.

We expand the two incident fields into the usual positive and negative frequency components

$$E_1(\mathbf{r}, t) = i \left(\frac{\hbar\omega}{2V\varepsilon_0} \right)^{1/2} (ae^{i(k \cdot \mathbf{r} - \omega t)} - a^\dagger e^{-i(k \cdot \mathbf{r} - \omega t)}) , \quad (3.76)$$

$$E_2(\mathbf{r}, t) = i \left(\frac{\hbar\omega}{2V\varepsilon_0} \right)^{1/2} (be^{i(k \cdot \mathbf{r} - \omega t)} - b^\dagger e^{-i(k \cdot \mathbf{r} - \omega t)}) , \quad (3.77)$$

where a, b are boson operators which characterise the two modes E_1 and E_2 , respectively. Both fields are taken to have the same sense of polarization, and are phase locked.

The total field after combination is given by

$$E_T(\mathbf{r}, t) = i \left(\frac{\hbar\omega}{2V\varepsilon_0} \right)^{1/2} (ce^{i(k \cdot \mathbf{r} - \omega t)} - c^\dagger e^{-i(k \cdot \mathbf{r} - \omega t)}) , \quad (3.78)$$

where

$$c = \sqrt{\eta}a + i\sqrt{1-\eta}b . \quad (3.79)$$

We have included a 90° phase shift between the reflected and transmitted beams at the beam splitter.

The photon detector, of course, responds to the moments of $c^\dagger c$. We thus define the number operator $\hat{N} = c^\dagger c$.

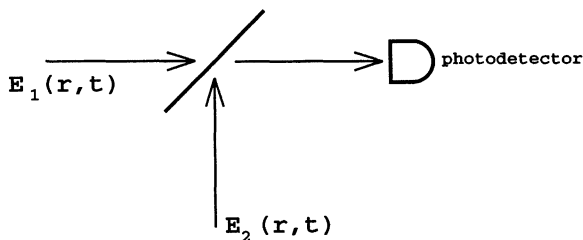


Fig. 3.5. Schematic representation of homodyne detection of squeezed states

The mean photo-electron current in the detector is proportional to $\langle c^\dagger c \rangle$ which is given by

$$\langle c^\dagger c \rangle = \eta \langle a^\dagger a \rangle + (1 - \eta) \langle b^\dagger b \rangle - i\sqrt{\eta(1 - \eta)} (\langle a \rangle \langle b^\dagger \rangle - \langle a^\dagger \rangle \langle b \rangle). \quad (3.80)$$

Let us take the field E_2 to be the local oscillator and assume it to be in a coherent state of large amplitude β . Then we may neglect the first term in (3.80) and write $\langle c^\dagger c \rangle$ in the form

$$\langle c^\dagger c \rangle \approx (1 - \eta) |\beta|^2 + |\beta| \sqrt{\eta(1 - \eta)} \langle X_{\theta + \pi/2} \rangle, \quad (3.81)$$

where

$$X_\theta \equiv a e^{-i\theta} + a^\dagger e^{i\theta}, \quad (3.82)$$

and θ is the phase of β . We see that when the contribution from the reflected local-oscillator intensity level is subtracted, the mean photo-current in the detector is proportional to the mean quadrature phase amplitude of the signal field defined with respect to the local oscillator phase. If we change θ through $\pi/2$ we can determine the mean amplitude of the two canonically conjugate quadrature phase operators.

We now turn to a consideration of the fluctuations in the photo-current. The rms fluctuation current is determined by the variance of $c^\dagger c$. For an intense local oscillator in a coherent state this variance is

$$V(n_c) \approx (1 - \eta)^2 |\beta|^2 + |\beta|^2 \eta (1 - \eta) V(X_{\theta + \pi/2}). \quad (3.83)$$

The first term here represents reflected local oscillator intensity fluctuations. If this term is subtracted out, the photo-current fluctuations are determined by the variances in $X_{\theta + \pi/2}$, the measured quadrature phase operator. To subtract out the contribution of the reflected local oscillator field balanced homodyne detection may be used. In this scheme the output from both ports of the beam splitter is directed to a photodetector and the resulting currents combined with appropriate phase shifts before subsequent analysis. Balanced homodyne detection realises a direct measurement of the signal field quadrature phase operators [3.12]. Alternatively, the contribution from the local oscillator intensity fluctuations may be reduced by making the transmittivity $\eta \approx 1$, in which case the dominant contribution to $V(n_c)$ comes from the second term in (3.83).

3.9 Photon Counting Measurements

3.9.1 Classical Theory

Consider radiation of intensity $I(t)$ falling on a photo-electric counter. The probability that a count occurs in a time dt is given by

$$\Delta p(t) = \alpha I(t) dt. \quad (3.84)$$

The parameter α is a measure of the sensitivity of the detector, and depends on the area of the detector and the spectral range of the incident light. Suppose initially there are no random fluctuations in the intensity $I(t)$. Now $1 - \Delta p(t')$ represents the probability that no counts occur in the time interval dt' at t' . Then assuming the independence of photocounts in different time intervals the joint probability that no counts occur in an entire interval t to $t + T$ is given by the product

$$\begin{aligned} \prod_t^{t+T} [1 - \Delta p(t')] &\approx \prod_t^{t+T} \exp[-\Delta p(t')] \\ &= \exp \left[- \sum_t^{t+T} \Delta p(t') \right] \\ &= \exp \left[- \int_t^{t+T} dp(t') \right]. \end{aligned} \quad (3.85)$$

Thus the probability for no counts in the interval t to $t + T$ is

$$P_0(T+t, t) = \exp \left[-\alpha \int_t^{t+T} I(t') dt' \right]. \quad (3.86)$$

The probability $P_1(T+t, t)$ that one count occurs between t and $t + T$ is

$$\sum_{t''} dp(t'') \prod_t^{t+T} [1 - \Delta p(t')] \rightarrow \int_t^{t+T} dp(t'') \exp \left[- \int_t^{t+T} dp(t') \right]. \quad (3.87)$$

Hence

$$P_1(T+t, t) = \left[\alpha \int_t^{t+T} I(t') dt' \right] \exp \left[-\alpha \int_t^{t+T} I(t') dt' \right]. \quad (3.88)$$

Following this reasoning the probability for n counts in the interval t to $t + T$ is

$$P_n(t, T) = \frac{1}{n!} [\alpha T \bar{I}(t, T)]^n \exp[-\alpha T \bar{I}(t, T)], \quad (3.89)$$

where

$$\bar{I}(t, T) = \frac{1}{T} \int_t^{t+T} I(t') dt'$$

is the mean intensity during the counting interval.

Now since $\bar{I}(t, T)$ may vary from one counting interval to the next, $P_n(T)$ is a time average of $P_n(t, T)$ over a large number of different starting times

$$\begin{aligned} P_n(T) &= \langle P_n(t, T) \rangle \\ &= \left\langle \frac{[\alpha \bar{I}(t, T) T]^n}{n!} \exp[-\alpha \bar{I}(t, T) T] \right\rangle. \end{aligned} \quad (3.90)$$

This formula was first derived by *Mandel* [3.13].

We note a useful generating function for the photon-counting distribution is

$$Q(\lambda, T) = \sum_{n=0}^{\infty} (1 - \lambda)^n P_n(T). \quad (3.91)$$

The factorial moments of the photon counting distribution may be obtained as follows:

$$\begin{aligned} \overline{n(n-1) \dots (n-k)} &= \sum_{n=0}^{\infty} n(n-1) \dots (n-k) P_n(T) \\ &= (-1)^k \left. \frac{\partial^k}{\partial \lambda^k} Q(\lambda, T) \right|_{\lambda=0}. \end{aligned} \quad (3.92)$$

We shall now consider some important cases of the photon counting formula (3.89).

3.9.2 Constant Intensity

In the simplest case of a constant intensity $\bar{I}(t, T)$ is independent of t and T , hence

$$\bar{I}(t, T) = I. \quad (3.93)$$

In this case the averaging over a fluctuating intensity $I(t)$ is unnecessary and

$$P_n(T) = \frac{\bar{n}^n}{n!} \exp(-\bar{n}), \quad (3.94)$$

where

$$\bar{n} = \alpha IT.$$

This is a Poisson distribution for which the variance $V(n) = \bar{n}$.

3.9.3 Fluctuating Intensity–Short-Time Limit

When the intensity is fluctuating, Eq. (3.89) can be simplified in the limit where the counting time T is short compared to the coherence time τ_c over which the

intensity changes. If, during the interval T , $I(t)$ remains reasonably constant then

$$\bar{I}(t, T) = \bar{I}(t) . \quad (3.95)$$

With ergodic hypothesis for a stationary light source we may convert the time average in (3.90) into an ensemble average over the distribution $p(\bar{I}(t))$.

The photon counting formula may then be written

$$P_n(T) = \int_0^{\infty} \frac{[\alpha \bar{I}(t) T]^n}{n!} e^{-\alpha \bar{I}(t) T} p(\bar{I}(t)) d\bar{I}(t) . \quad (3.96)$$

In the following we replace $\bar{I}(t)$ by the stochastic variable I for ease of notation. The mean photon count is

$$\begin{aligned} \bar{n} &= \sum_{n=0}^{\infty} n P_n(T) = \int_0^{\infty} \sum_{n=0}^{\infty} n \frac{(\alpha I T)^n}{n!} e^{-\alpha I T} p(I) dI \\ &= \int_0^{\infty} \alpha T I p(I) dI = \alpha T \langle I \rangle . \end{aligned} \quad (3.97)$$

Defining moments of intensity as

$$\langle I^n \rangle = \int_0^{\infty} I^n p(I) dI , \quad (3.98)$$

we find for the mean square count

$$\begin{aligned} \overline{n^2} &= \sum_{n=0}^{\infty} n^2 P_n(T) = \int_0^{\infty} (\alpha^2 T^2 I^2 + \alpha T I) p(I) dI \\ &= \alpha^2 T^2 \langle I^2 \rangle + \alpha T \langle I \rangle . \end{aligned} \quad (3.99)$$

Thus the variance is

$$V(n) = \overline{n^2} - \bar{n}^2 = \alpha T \langle I \rangle + \alpha^2 T^2 (\langle I^2 \rangle - \langle I \rangle^2) . \quad (3.100)$$

We note that this is always greater than the mean unless $p(I)$ is a Dirac delta function $\delta(I - I_0)$. This is true for classical fields. For certain quantum mechanical fields we shall see that it is possible to obtain $V(n) < \bar{n}$.

A thermal light field has the following probability distribution for its intensity

$$p(I) = \frac{1}{I_0} \exp\left(\frac{-I}{I_0}\right), \quad (3.101)$$

with moments

$$\langle I^n \rangle = n! I_0^n .$$

The mean and variance of the photocount distribution are

$$\bar{n} = \alpha T I_0, \quad V(n) = \bar{n}(1 + \bar{n}) . \quad (3.102)$$

The photon-counting distribution is

$$\begin{aligned} P_n(T) &= \frac{(\alpha T)^n}{I_0 n!} \int_0^\infty I^n \exp\left[-I\left(\alpha T + \frac{1}{I_0}\right)\right] dI \\ &= \frac{(\alpha T)^n}{I_0 n!} \left(\alpha T + \frac{1}{I_0}\right)^{-(n+1)} \int_0^\infty x^n e^{-x} dx \quad n! \\ &= \frac{1}{(1 + \bar{n})} \left(\frac{\bar{n}}{1 + \bar{n}}\right)^n . \end{aligned} \quad (3.103)$$

This power-law distribution for thermal light has been verified in photon-counting experiments. Experiments have also shown that the photon count distribution of highly stabilized lasers is approximated by a Poisson distribution [3.8, 9].

We conclude with a comment on the form assumed by $\bar{I}(t, T)$ if the depletion of the signal field by the detection process is taken into account. Then

$$I(t) = I_0 e^{-\lambda t}, \quad (3.104)$$

where λ is the rate of photon absorption. Then

$$\bar{I}(t, T) = \frac{I_0}{T} \int_t^{t+T} e^{-\lambda t'} dt', \quad (3.105)$$

Thus

$$\bar{I}(\tau, T) = \frac{I(t)}{\lambda T} (1 - e^{-\lambda T}). \quad (3.106)$$

We note that for short counting times this has the same form as (3.95).

3.10 Quantum Mechanical Photon Count Distribution

The photon count distribution for a quantum mechanical field may be written in a formally similar way to the classical expression [3.15]

$$P_n(T) = \left\langle : \frac{[\alpha \bar{I}(T) T]^n}{n!} \exp [-\alpha \bar{I}(T) T] : \right\rangle \quad (3.107)$$

where

$$\begin{aligned} \bar{I}(T) &= \frac{1}{T} \int_0^T I(t) dt \\ &= \frac{1}{T} \int_0^T E^{(-)}(\mathbf{r}, t) E^{(+)}(\mathbf{r}, t) dt \end{aligned} \quad (3.108)$$

and $: :$ denotes normal ordering of the operators. We shall demonstrate the use of this formula for a single-mode field, in which case (3.107) may be written as

$$P_n(T) = \text{Tr} \left(\rho : \frac{[\mu(T) a^\dagger a]^n}{n!} \exp [-a^\dagger a \mu(T)] : \right) \quad (3.109)$$

where $\mu(T)$ is the probability for detecting one photon in time T from a one photon field. The explicit form of $\mu(T)$ depends on the physical situation, e.g., $\mu(T) = \lambda T$ for an open system and $\mu(T) = (1 - e^{-\lambda T})$ for a closed system.

The photon count distribution may be related to the diagonal matrix elements $P_n = \langle n | \rho | n \rangle$ of ρ by

$$P_m(T) = \sum_n P_n \frac{[\mu(T)]^m}{m!} \left\langle n \left| \sum_{l=0}^{\infty} \frac{\mu(T)^l}{l!} a^{\dagger m+l} a^{m+l} \right| n \right\rangle. \quad (3.110)$$

This gives

$$P_m(T) = \sum_{n=m}^{\infty} P_n \sum_{l=0}^{n-m} (-1)^l \frac{\mu(T)^l}{l!} \frac{n!}{(n-m-l)!}. \quad (3.111)$$

The l summation is equivalent to a binomial expansion and we may write [3.16]

$$P_m(T) = \sum_{n=m}^{\infty} P_n \binom{n}{m} [\mu(T)]^m [1 - \mu(T)]^{n-m} \quad (3.112)$$

where

$$\binom{n}{m} = \frac{n!}{m!(n-m)!}.$$

This distribution is known as the *Bernoulli distribution*.

The photo-count distribution $P_n(T)$ is only the same as P_n in the case of unit quantum efficiency

$$P_m(T) = P_m, \quad \mu(T) = 1 . \quad (3.113)$$

In practice, quantum efficiencies are less than unity and the photon-count distribution is only indirectly related to P_n .

The following results may be proved:

3.10.1 Coherent Light

$$P_n = \frac{\bar{n}^n}{n!} \exp(-\bar{n}) , \quad (3.114)$$

$$P_m(T) = \frac{[\mu(T)\bar{n}]^m}{m!} \exp[-\mu(T)\bar{n}] . \quad (3.115)$$

3.10.2 Chaotic Light

$$P_n = \frac{(\bar{n})^n}{(1 + \bar{n})^{1+n}} , \quad (3.116)$$

$$P_m(T) = \frac{[\mu(T)\bar{n}]^m}{[1 + \mu(T)\bar{n}]^{1+m}} . \quad (3.117)$$

These results agree with those obtained by semiclassical methods, see (3.94 and 3.103). In these cases P_n and $P_m(T)$ have the same mathematical form with the mean number \bar{m} of counted photons related to the mean number \bar{n} of photons in the mode by $\bar{m} = \mu(T)\bar{n}$. No such simple relation holds in general.

For example, for a photon number state, P_n is a delta function δ_{nn_0} but the photo-count distribution $P_m(T)$ is non zero for all $m \leq n_0$. However the normalized second order factorial moments are the same in all cases.

For a single-mode field

$$\sum m(m-1) \frac{P_m(T)}{\bar{m}^2} = \sum_n n(n-1) \frac{P_n}{\bar{n}^2} = g^{(2)}(0) . \quad (3.118)$$

Thus the second-order correlation function $g^{(2)}(0)$ is directly obtainable from the photo-count distribution without any dependence on the quantum efficiency $\mu(T)$. For a multimode field a more complicated relation holds.

3.10.3 Photo-Electron Current Fluctuations

We now consider how the photon number statistics determines the statistics of the observed photo-electron current. Each individual photon detection produces a small current pulse, the observed current over a counting interval from $t - T$ to t is then due to the accumulated electrical pulses over this interval. Thus we write

$$i(t) = \int_{t-T}^t F(t') dn(t') . \quad (3.119)$$

Here $F(t')$ is a response function which determines the current resulting from each photon detection event. We assume $F(t')$ is flat, i.e. independent of t ,

$$F(t') = \frac{Ge}{T} , \quad (3.120)$$

where e is the electronic charge and G is a gain factor. Then the photo-electron current is given by

$$i(t) = \frac{Ge}{T} n , \quad (3.121)$$

where n is the total number of photon detection events over the counting interval. The mean current is then given by

$$\overline{i(t)} = \frac{Ge}{T} \sum_{n=0}^{\infty} n P_n(T; t) , \quad (3.122)$$

where $P_n(T, t)$ is given by (3.89) with

$$\overline{I}(t, T) = \frac{1}{T} \int_{t-T}^t dt' E^{(-)}(t') E^{(+)}(t') . \quad (3.123)$$

Thus

$$\overline{i(t)} = (\alpha Ge) \langle : \overline{I}(t, T) : \rangle . \quad (3.124)$$

The current power spectrum is directly related to the statistical properties of the current by

$$S(\omega) = \frac{1}{\pi} \sum_0^{\infty} d\tau \cos(\omega\tau) \overline{i(0) i(\tau)} . \quad (3.125)$$

The two-time correlation function is determined by joint emission probabilities for photo-electrons which are generalisations of the single photon result in

(3.84). Explicit expressions were given by *Carmichael* [3.17]. The result is, with the definitions of (3.120).

$$\overline{i(0)i(\tau)} = (\alpha Ge)^2 [\langle : \bar{I}(T, 0) \bar{I}(T, \tau) : \rangle + \theta(T - \tau) \langle : \bar{I}(\tau - T, 0) : \rangle] \quad (3.126)$$

where $\theta(x)$ is zero for $x \leq 0$ and unity otherwise. For multiple time correlations $::$ also signifies time ordering (time arguments increasing to the left in products of annihilation operators). In the case of constant intensity

$$\begin{aligned} \overline{i(0)i(\tau)} &= (\alpha \zeta Ge)^2 [\langle a^\dagger(0) a^\dagger(\tau) a(\tau) a(0) \rangle] \\ &\quad + (Ge)^2 \alpha \zeta \left[\theta(T - \tau) \frac{(T - \tau)}{T^2} \langle a^\dagger(0) a(0) \rangle \right] \end{aligned} \quad (3.127)$$

where ζ is a scale factor that converts the intensity operator into a photon-flux operator. For plane waves it is given by

$$\zeta = \frac{\epsilon_0 c A}{\hbar \omega c} \quad (3.128)$$

where A is the transverse area of the field over which the field is measured, and ω_c the frequency of the field. Using the following result for the delta function

$$\int_0^\infty dt' f(t') \delta(t') = \frac{1}{2} f(0), \quad (3.129)$$

one may show that

$$\lim_{T \rightarrow 0} \frac{\theta(T - t')}{T^2} (T - t) = \delta(t). \quad (3.130)$$

Then in the limit of broad-band detector response ($T \rightarrow 0$)

$$\overline{(i(0)i(\tau))} = (\alpha Ge \zeta)^2 \langle a^\dagger(0) a^\dagger(\tau) a(\tau) a(0) \rangle + (Ge)^2 \alpha \zeta \langle a^\dagger(0) a(0) \rangle \delta(t) \quad (3.131)$$

The last term in this expression is the *shot noise* contribution to the current.

It is more convenient to write this expression directly in terms of the normally-ordered correlation function

$$\langle : I(0), I(\tau) : \rangle \equiv \zeta^2 [\langle a^\dagger(0) a^\dagger(\tau) a(\tau) a(0) \rangle - \langle a^\dagger(0) a(0) \rangle^2]. \quad (3.132)$$

Then

$$\begin{aligned} \overline{(i(0)i(\tau))} &= (\alpha Ge \zeta)^2 \langle a^\dagger(0) a(0) \rangle^2 + \alpha \zeta (Ge)^2 \langle a^\dagger(0) a(0) \rangle \delta(t) \\ &\quad + (\alpha Ge)^2 \langle : I(0), I(\tau) : \rangle. \end{aligned} \quad (3.133)$$

The first term is a dc term and does not contribute to the spectrum. The second term is the shot-noise contribution. The final term represents intensity fluctuations, which for a coherent field is zero.

Exercises

3.1 Calculate the mean intensity at the screen when the two slits of a Young's interference experiment are illuminated by the two photon state $(b^\dagger)^2 |0\rangle / \sqrt{2}$ where $b = (a_1 + a_2) / \sqrt{2}$ and a_i is the annihilation operator for the mode radiated by slit i .

3.2 Consider a single-mode field prepared in a linear superposition of two coherent states $|\chi\rangle = N(|\alpha_1\rangle + |\alpha_2\rangle)$ where N is the normalisation constant and $|\alpha_1| = |\alpha_2|$. Show that $g^{(2)}(0)$ for such a state is zero when α_1 and α_2 are $\pi/2$ out of phase, and diverges when α_1 and α_2 are π out of phase.

3.3 In balanced homodyne detection the measured photocurrent is determined by the moments of the photon number difference at the two output ports of the beam splitter. Show that the variance of the photon-number difference for a 50/50 beam splitter is

$$V(n_-) = |\beta|^2 V(X_{\theta+\pi/2})$$

where $|\beta|^2$ is the intensity of the local oscillator. Thus the local oscillator intensity fluctuations do not contribute.

3.4 Show that the probability to detect m photons with unit quantum efficiency in a field which has been transmitted by a beam splitter of transmittivity μ , is given by

$$P_m(\mu) = \sum_{n=m}^{\infty} P_n \binom{n}{m} \mu^m (1-\mu)^{n-m}$$

where P_n is the photon number distribution for the field before passing through the beam splitter.

3.5 A beam splitter transforms incoming mode operators a_i, b_i to the outgoing operators a_0, b_0 where

$$a_0 = \sqrt{\eta}a_i + i\sqrt{1-\eta}b_i, \quad b_0 = \sqrt{\eta}b_i - i\sqrt{1-\eta}a_i .$$

(a) Show that such a transformation may be generated by the unitary operator

$$T = \exp[-i\theta(a^\dagger b + ab^\dagger)], \quad \eta = \cos^2 \Theta .$$

(b) Thus show that if the incoming state is a coherent state $|\alpha_i\rangle \otimes |\beta_i\rangle$, the outgoing state is also a coherent state with

$$\alpha_0 = \sqrt{\eta}\alpha_i + i\sqrt{1-\eta}\beta_i, \quad \beta_0 = \sqrt{\eta}\beta_i - i\sqrt{1-\eta}\alpha_i .$$

4. Representations of the Electromagnetic Field

A full description of the electromagnetic field requires a quantum statistical treatment. The electromagnetic field has an infinite number of modes and each mode requires a statistical description in terms of its allowed quantum states. However, as the modes are described by independent Hilbert spaces, we may form the statistical description of the entire field as the product of the distribution function for each mode. This enables us to confine our description to a single mode without loss of generality.

In this chapter we introduce a number of possible representations for the density operator of the electromagnetic field. One representation is to expand the density operator in terms of the number states. Alternatively the coherent states allow a number of possible representations via the P function, the Wigner function and the Q function.

4.1 Expansion in Number States

The number or Fock states form a complete set, hence a general expansion of ρ is

$$\rho = \sum C_{nm} |n\rangle\langle m| . \quad (4.1)$$

The expansion coefficients C_{nm} are complex and there is an infinite number of them. This makes the general expansion rather less useful, particularly for problems where the phase-dependent properties of the electromagnetic field are important and hence the full expansion is necessary. However, in certain cases where only the photon number distribution is of interest the reduced expansion

$$\rho = \sum P_n |n\rangle\langle n| , \quad (4.2)$$

may be used. Here P_n is a probability distribution giving the probability of having n photons in the mode. This is not a general representation for all fields but may prove useful for certain fields. For example, a chaotic field, which has

no phase information, has the distribution

$$P_n = \frac{1}{(1 + \bar{n})} \left(\frac{\bar{n}}{1 + \bar{n}} \right)^n, \quad (4.3)$$

where \bar{n} is the mean number of photons. This is derived by maximising the entropy

$$S = -\text{Tr}\{\rho \ln \rho\}, \quad (4.4)$$

subject to the constraint $\text{Tr}\{\rho a^\dagger a\} = \bar{n}$, and is just the usual Planck distribution for black-body radiation with

$$\bar{n} = \frac{1}{e^{\hbar\omega/kT} - 1}. \quad (4.5)$$

The second-order correlation function $g^2(0)$ may be written according to (3.66)

$$g^2(0) = 1 + \frac{V(n) - \bar{n}}{\bar{n}^2}, \quad (4.6)$$

where $V(n)$ is the variance of the distribution function P_n . Hence, for the power-law distribution $V(n) = \bar{n}^2 + \bar{n}$ we find $g^{(2)}(0) = 2$. For a field with a Poisson distribution of photons

$$P_n = \frac{e^{-\bar{n}}}{n!} \bar{n}^n \quad (4.7)$$

the variance $V(n) = \bar{n}$, hence $g^{(2)}(0) = 1$.

A coherent state has a Poisson distribution of photons. However, a measurement of $g^{(2)}(0)$ would not distinguish between a coherent state and a field prepared from an incoherent mixture with a Poisson distribution. In order to distinguish between these two fields a phase-dependent measurement such as a measurement of $\Delta X_1, \Delta X_2$ would need to be made.

4.2 Expansion in Coherent States

4.2.1 P Representation

The coherent states $|\alpha\rangle$ form a complete set of states, in fact, an overcomplete set of states. They may therefore be used as a basis set despite the fact that they are non-orthogonal. The following diagonal representation in terms of coherent states was introduced independently by *Glauber* [4.1] and *Sudarshan* [4.2]

$$\rho = \int P(\alpha) |\alpha\rangle \langle \alpha| d^2\alpha, \quad (4.8)$$

where $d^2\alpha = d(\text{Re}\{\alpha\})d(\text{Im}\{\alpha\})$. It has found wide-spread application in quantum optics.

Now it might be imagined that the function $P(\alpha)$ is analogous to a probability distribution for the values of α . However, in general this is not the case since the projection operator $|\alpha\rangle\langle\alpha|$ is on to non-orthogonal states, and hence $P(\alpha)$ cannot be interpreted as a genuine probability distribution. We may note that the coherent states $|\alpha\rangle$ and $|\alpha'\rangle$ are approximately orthogonal for $|\alpha - \alpha'| \gg 1$, see (2.41). Hence, if $P(\alpha)$ is slowly varying over such large ranges of the parameter there is an approximate sense in which $P(\alpha)$ may be interpreted with a classical description. There are, however, certain quantum states of the radiation field where $P(\alpha)$ may take on negative values or become highly singular. For these fields there is no classical description and $P(\alpha)$ clearly cannot be interpreted as a classical probability distribution. Let us now consider examples of fields which may be described by the P representation:

(i) Coherent state

If

$$\rho = |\alpha_0\rangle\langle\alpha_0| , \quad (4.9)$$

then

$$P(\alpha) = \delta^{(2)}(\alpha - \alpha_0) . \quad (4.10)$$

(ii) Chaotic state

For a chaotic state it follows from the central limit theorem that $P(\alpha)$ is a Gaussian

$$P(\alpha) = \frac{1}{\pi\bar{n}} e^{-|\alpha|^2/\bar{n}} . \quad (4.11)$$

That this is equivalent to the result for P_n is clear if we take matrix elements

$$P_n = \langle n|\rho|n\rangle = \int P(\alpha) |\langle n|\alpha\rangle|^2 d^2\alpha = \frac{1}{\pi\bar{n}} \int e^{-|\alpha|^2/\bar{n}} \frac{|\alpha|^{2n}}{n!} e^{-|\alpha|^2} d^2\alpha . \quad (4.12)$$

Using the identity

$$\pi^{-1} (l! m!)^{-1/2} \int \exp(-C|\alpha|^2) \alpha^l (\alpha^*)^m d^2\alpha = \delta_{lm} C^{-(m+1)} , \quad (4.13)$$

which holds for $C > 0$ and choosing

$$C = \frac{1 + \bar{n}}{\bar{n}}$$

we find

$$P_n = \frac{1}{1 + \bar{n}} \left(\frac{\bar{n}}{1 + \bar{n}} \right)^n . \quad (4.14)$$

For a mixture of a coherent and a chaotic state the P function is

$$P(\alpha) = \frac{1}{\pi\bar{n}} e^{-|\alpha - \alpha_0|^2/\bar{n}}, \quad (4.15)$$

which may be derived using the following convolution property of $P(\alpha)$. Consider a field produced by two independent sources. The first source acting constructs the field

$$\rho_1 = \int P_1(\alpha_1) |\alpha_1\rangle \langle \alpha_1| d^2\alpha_1. \quad (4.16)$$

Acting alone the second source would produce the field

$$\rho_2 = \int P_2(\alpha_2) |\alpha_2\rangle \langle \alpha_2| d^2\alpha_2 = \int P_2(\alpha_2) D(\alpha_2) |0\rangle \langle 0| D^{-1}(\alpha_2) d^2\alpha_2. \quad (4.17)$$

The second source acting after the first field generates the field

$$\begin{aligned} \rho &= \int P_2(\alpha_2) D(\alpha_2) \rho_1 D^{-1}(\alpha_2) d^2\alpha_2 \\ &= \int P_2(\alpha_2) P_1(\alpha_1) |\alpha_1 + \alpha_2\rangle \langle \alpha_1 + \alpha_2| d^2\alpha_1 d^2\alpha_2. \end{aligned} \quad (4.18)$$

The weight function $P(\alpha)$ for the superposed excitations is therefore

$$\begin{aligned} P(\alpha) &= \int \delta^2(\alpha - \alpha_1 - \alpha_2) P_1(\alpha_1) P_2(\alpha_2) d^2\alpha_1 d^2\alpha_2 \\ &= \int P_1(\alpha - \alpha') P_2(\alpha') d^2\alpha'. \end{aligned} \quad (4.19)$$

We see that the distribution function for the superposition of two fields is the convolution of the distribution functions for each field.

a) Correlation Functions

The $P(\alpha)$ representation is convenient for evaluating normally-ordered products of operators, for example

$$\langle a^{\dagger n} a^m \rangle = \int P(\alpha) \alpha^{*n} \alpha^m d^2\alpha. \quad (4.20)$$

This reduces the taking of quantum mechanical expectation values to a form similar to classical averaging.

Let us express the second-order correlation function in terms of $P(\alpha)$

$$g^{(2)}(0) = 1 + \frac{\int P(\alpha) [(|\alpha|^2) - \langle |\alpha|^2 \rangle]^2 d^2\alpha}{[\int P(\alpha) |\alpha|^2 d^2\alpha]^2}. \quad (4.21)$$

This looks functionally identical to the expression for classical fields. However, the argument that $g^{(2)}(0)$ must be greater than or equal to unity no longer holds since for certain fields as we have mentioned $P(\alpha)$ may take on negative values and allow for a $g^{(2)}(0) < 1$, that is, photon antibunching.

A similar result may be derived for the squeezing. We may write the variances in X_1 and X_2 as

$$\begin{aligned}\Delta X_1^2 &= \{1 + \int P(\alpha)[(\alpha + \alpha^*) - (\langle \alpha \rangle + \langle \alpha^* \rangle)]^2 d^2\alpha\}, \\ \Delta X_2^2 &= \left\{1 + \int P(\alpha) \left[\left(\frac{\alpha - \alpha^*}{i} \right) - \left(\frac{\langle \alpha \rangle - \langle \alpha^* \rangle}{i} \right) \right]^2 d^2\alpha\right\}. \quad (4.22)\end{aligned}$$

The condition for squeezing $\Delta X_1^2 < 1$, requires that $P(\alpha)$ takes on a negative value along either the real or imaginary axis in the complex plane, but not both simultaneously. Thus squeezing and antibunching are phenomena which are the exclusive property of quantum fields and may not be generated by classical fields. Some ambiguity may arise in the case of squeezing which only has significance for quantum fields. If a classical field is assumed from the outset arbitrary squeezing may occur in either quadrature or both simultaneously.

Quantised fields for which $P(\alpha)$ is a positive function do not exhibit quantum properties such as photon antibunching and squeezing. Such fields may be simulated by a classical description which treats the complex field amplitude ε as a stochastic random variable with the probability distribution $P(\varepsilon)$ and hence may be considered as quasiclassical. Coherent and chaotic fields are familiar examples of fields with a positive P representation. Quantum fields exhibiting antibunching and/or squeezing cannot be described in classical terms. For such fields the P representation may be negative and highly singular. The coherent state has a P representation which is a delta function, defining the boundary between quantum and classical behaviour. For fields exhibiting quantum behaviour such as a number state $|n\rangle$ or squeezed state $|\alpha, \varepsilon\rangle$ no representation for $P(\alpha)$ in terms of tempered distributions exists. Though representations in terms of generalised functions do exist [4.3], such representations are highly singular, for example, derivatives of delta functions. We shall therefore look for alternative representations to describe such quantum fields.

b) Covariance Matrix

Gaussian processes which arise, for example, in linearized fluctuation theory may be characterized by a covariance matrix. A covariance matrix may be defined by

$$C(a, a^\dagger) = \begin{pmatrix} \langle a^2 \rangle - \langle a \rangle^2 & \frac{1}{2} \langle aa^\dagger + a^\dagger a \rangle - \langle a^\dagger \rangle \langle a \rangle \\ \frac{1}{2} \langle aa^\dagger + a^\dagger a \rangle - \langle a^\dagger \rangle \langle a \rangle & \langle a^{\dagger 2} \rangle - \langle a^\dagger \rangle^2 \end{pmatrix}. \quad (4.23)$$

One may also introduce a correlation matrix $C(X_1, X_2)$ for the quadrature phase operators X_1 and X_2 :

$$C(X_1, X_2)_{p,q} = \frac{1}{2} \langle X_p X_q + X_q X_p \rangle - \langle X_p \rangle \langle X_q \rangle \quad (p, q = 1, 2). \quad (4.24)$$

These two correlation matrices are related by

$$C(X_1, X_2) = \Omega C(a, a^\dagger) \Omega^T \quad (4.25)$$

where

$$\Omega = \begin{pmatrix} 1 & 1 \\ -i & i \end{pmatrix}.$$

The covariance matrix $C_p(\alpha, \alpha^*)$ defined by the moments of α and α^* over $P(\alpha, \alpha^*)$ is related to the covariance matrix $C(a, a^\dagger)$ by

$$C(a, a^\dagger) = C_p(\alpha, \alpha^*) + \frac{1}{2} \begin{pmatrix} 0 & 1 \\ 1 & 0 \end{pmatrix}. \quad (4.26)$$

The distribution can be written in terms of the real variables

$$x_1 = \alpha + \alpha^*, \quad x_2 = \frac{1}{i}(\alpha - \alpha^*)$$

for which the covariance matrix relation is

$$C(X_1, X_2) = C_p(x_1, x_2) + I. \quad (4.27)$$

c) Characteristic Function

In practice, it proves useful to evaluate the P function through a characteristic function.

The density operator ρ is uniquely determined by its characteristic function

$$\chi(\eta) = \text{Tr} \{ \rho e^{\eta a^\dagger - \eta^* a} \}.$$

We may also define normally and antinormally ordered characteristic functions

$$\chi_N(\eta) = \text{Tr} \{ \rho e^{\eta a^\dagger} e^{-\eta^* a} \}, \quad (4.28)$$

$$\chi_A(\eta) = \text{Tr} \{ \rho e^{-\eta^* a} e^{\eta a^\dagger} \}. \quad (4.29)$$

Using the relation (2.25) the characteristic functions are related by

$$\chi(\eta) = \chi_N(\eta) \exp(-\frac{1}{2}|\eta|^2). \quad (4.30)$$

If the density operator ρ has a P representation, then $\chi_N(\eta)$ is given by

$$\chi_N(\eta) = \int \langle \alpha | e^{\eta a^\dagger} e^{-\eta^* a} | \alpha \rangle P(\alpha) d^2\alpha = \int e^{\eta \alpha^* - \eta^* \alpha} P(\alpha) d^2\alpha. \quad (4.31)$$

Writing η and α in terms of their real and imaginary parts we find that (4.31) expresses $\chi_N(\eta)$ as a two-dimensional Fourier transform of $P(\alpha)$. The solution for $P(\alpha)$ is the inverse Fourier transform

$$P(\alpha) = \frac{1}{\pi^2} \int e^{z\eta^* - \alpha^* \eta} \chi_N(\eta) d^2\eta. \quad (4.32)$$

Thus the criterion for the existence of a P representation is the existence of a Fourier transform for the normally-ordered characteristic function $\chi_N(\eta)$.

4.2.2 Wigner's Phase-Space Density

The first quasi-probability distribution was introduced into quantum mechanics by *Wigner* [4.4]. The Wigner function may be defined as the Fourier transform of the symmetrically ordered characteristic function $\chi(\eta)$

$$W(\alpha) = \frac{1}{\pi^2} \int \exp(\eta^* \alpha - \eta \alpha^*) \chi(\eta) d^2 \eta . \quad (4.33)$$

The Wigner distribution always exists but is not necessarily positive.

The relationship between the Wigner distribution and the $P(\alpha)$ distribution may be obtained via the characteristic functions. Using (4.30) we may express the Wigner function as

$$\begin{aligned} W(\alpha) &= \frac{1}{\pi^2} \int \exp(\eta^* \alpha - \eta \alpha^*) \chi_N(\eta) e^{-1/2 |\eta|^2} d^2 \eta \\ &= \frac{1}{\pi^2} \int \text{Tr}\{\rho e^{\eta(a^\dagger - \alpha^*)} e^{-\eta^*(a - \alpha)}\} e^{-1/2 |\eta|^2} d^2 \eta \\ &= \frac{1}{\pi^2} \int P(\beta) \exp[\eta(\beta^* - \alpha^*) - \eta^*(\beta - \alpha) - \frac{1}{2} |\eta|^2] d^2 \eta d^2 \beta . \end{aligned} \quad (4.34)$$

Substituting $\varepsilon = \eta/\sqrt{2}$ leads to

$$W(\alpha) = \frac{2}{\pi^2} \int P(\beta) \exp[\sqrt{2}\varepsilon(\beta^* - \alpha^*) - \sqrt{2}\varepsilon^*(\beta - \alpha) - |\varepsilon|^2] d^2 \varepsilon d^2 \beta . \quad (4.35)$$

The integral may be evaluated using the identity

$$\frac{1}{\pi} \int d^2 \eta \exp(-\lambda|\eta|^2 + \mu\eta + v\eta^*) = \frac{1}{\lambda} \exp\left(\frac{\mu v}{\lambda}\right) \quad (4.36)$$

which holds for $\text{Re}\{\lambda\} > 0$ and arbitrary μ, v . This gives

$$W(\alpha) = \frac{2}{\pi} \int P(\beta) \exp(-2|\beta - \alpha|^2) d^2 \beta . \quad (4.37)$$

That is, the Wigner function is a Gaussian convolution of the P function.

The covariance matrix $C_w(\alpha, \alpha^*)$ defined by the moments of α and α^* over $W(\alpha, \alpha^*)$ is related to the covariance matrix $C(a, a^\dagger)$ defined by (4.23) by

$$C(a, a^\dagger) = C_w(\alpha, \alpha^*) . \quad (4.38)$$

The error areas discussed in Chap. 2 may rigorously be derived as contours of the Wigner function. We shall now study the Wigner functions for several states of this radiation field and their corresponding contours.

For certain states of the radiation field the Wigner function may be written in the Gaussian form

$$W(x_1, x_2) = N \exp(-\frac{1}{2}Q) \quad (4.39)$$

where Q is the quadratic form

$$Q = (\mathbf{x} - \mathbf{a})^T A^{-1} (\mathbf{x} - \mathbf{a}) \quad (4.40)$$

and N is the normalization. A contour of the Wigner function is the curve $Q = 1$. We choose to work in the phase space where x_1 and x_2 are the c-number variables corresponding to the quadrature phase amplitudes X_1 and X_2 .

a) Coherent State

For a coherent state $|\alpha\rangle = |\frac{1}{2}(X_1 + iX_2)\rangle$ the Wigner function is

$$W(x'_1, x'_2) = \frac{2}{\pi} \exp\left[-\frac{1}{2}(x'^2_1 + x'^2_2)\right] \quad (4.41)$$

where $x'_i = x_i - X_i$. The contour of the Wigner function given by $Q = 1$ is

$$x'^2_1 + x'^2_2 = 1. \quad (4.42)$$

Thus the error area is a circle with radius 1 centred on the point (X_1, X_2) (Fig. 2.1a).

b) Squeezed State

The Wigner function for a squeezed state is

$$W(x') = \frac{2}{\pi} \exp\left[-\frac{1}{2}(x'^2_1 e^{-2r} + x'^2_2 e^{2r})\right]. \quad (4.43)$$

The contour of the Wigner function given by $Q = 1$ is

$$\frac{x'^2_1}{e^{2r}} + \frac{x'^2_2}{e^{-2r}} = 1 \quad (4.44)$$

which is an ellipse with the length of the major and minor axes given by e^r and e^{-r} , respectively (Fig. 2.1b).

c) Number State

The Wigner function for a number state $|n\rangle$ is

$$W(x_1, x_2) = \frac{2}{\pi} (-1)^n L_n(4r^2) e^{-2r^2} \quad (4.45)$$

where $r^2 = x_1^2 + x_2^2$, and $L_n(x)$ is the Laguerre polynomial. This Wigner function is clearly negative.

The Wigner function gives direct symmetrically-ordered moments such as those arising in the calculation of the variances of quadrature phases.

4.2.3 Q Function

An alternative function is the diagonal matrix elements of the density operator in a pure coherent state

$$Q(\alpha) = \frac{\langle \alpha | \rho | \alpha \rangle}{\pi} \geq 0 . \quad (4.46)$$

This is clearly a non-negative function since the density operator is a positive operator. It is also a bounded function

$$Q(\alpha) < \frac{1}{\pi} .$$

Writing the distribution in terms of the real variables

$$x_1 = \alpha + \alpha^*, \quad x_2 = -i(\alpha - \alpha^*)$$

the covariance matrix relation is

$$C(X_1, X_2) = C_Q(x_1, x_2) - I .$$

The Q function may be expressed as the Fourier transform of the anti-normally-ordered characteristic function $\chi_A(\eta)$

$$\chi_A(\eta) = \text{Tr}\{\rho e^{-\eta^* a} e^{\eta a^\dagger}\} = \int \frac{d^2\alpha}{\pi} \langle \alpha | e^{\eta a^\dagger} \rho e^{-\eta^* a} | \alpha \rangle = \int e^{\eta \alpha^* - \eta^* \alpha} Q(\alpha) d^2\alpha . \quad (4.47)$$

Thus $Q(\alpha)$ is the inverse Fourier transform

$$Q(\alpha) = \frac{1}{\pi^2} \int e^{\alpha \eta^* - \alpha^* \eta} \chi_A(\eta) d^2\eta . \quad (4.48)$$

The relation between the $P(\alpha)$ and the $Q(\alpha)$ follows from

$$Q(\alpha) = \frac{\langle \alpha | \rho | \alpha \rangle}{\pi} = \frac{1}{\pi} \int P(\beta) |\langle \alpha | \beta \rangle|^2 d^2\beta = \frac{1}{\pi} \int P(\beta) e^{-|\alpha - \beta|^2} d^2\beta . \quad (4.49)$$

That is, the Q function like the Wigner function is a Gaussian convolution of the P function. However, it is convoluted with a Gaussian which has $\sqrt{2}$ times the width of the Wigner function which accounts for the rather more well-behaved properties.

The Q function is convenient for evaluating anti-normally-ordered moments

$$\langle a^n a^{\dagger m} \rangle = \int \alpha^n \alpha^{*m} Q(\alpha, \alpha^*) d^2\alpha . \quad (4.50)$$

The covariance matrix $C_Q(\alpha, \alpha^*)$ defined by the moments of α and α^* over $Q(\alpha, \alpha^*)$ is related to the covariance matrix $C(a, a^\dagger)$ defined by (4.23) by

$$C(a, a^\dagger) = C_Q(\alpha, \alpha^*) - \frac{1}{2} \begin{pmatrix} 0 & 1 \\ 1 & 0 \end{pmatrix}. \quad (4.51)$$

The Q function has the advantage of existing for states where no P function exists and unlike the Wigner or P function is always positive. The Q functions for a coherent state and a number state are easily obtained.

For a coherent state $|\beta\rangle$ the Q function is

$$Q(\alpha) = \frac{|\langle\alpha|\beta\rangle|^2}{\pi} = \frac{e^{-|\alpha-\beta|^2}}{\pi}. \quad (4.52)$$

For a number state $|n\rangle$ the Q function is

$$Q(\alpha) = \frac{|\langle\alpha|n\rangle|^2}{\pi} = \frac{|\alpha|^{2n} e^{-|\alpha|^2}}{\pi n!}. \quad (4.53)$$

The Q function for a squeezed state $|\alpha, r\rangle$ is defined as

$$Q(\beta, \beta^*) = \frac{1}{\pi} |\langle\beta|D(\alpha)S(r)|0\rangle|^2. \quad (4.54)$$

This is a multivariate Gaussian distribution and may be written in terms of the quadrature phase variables x_1 and x_2 as

$$Q(x_1, x_2) = \frac{1}{4\pi^2 \cosh r} \exp[-\frac{1}{2}(\mathbf{x} - \mathbf{x}_0)^T C^{-1}(\mathbf{x} - \mathbf{x}_0)] \quad (4.55)$$

where

$$\mathbf{x}_0 = 2(\operatorname{Re}\{\alpha\}, \operatorname{Im}\{\alpha\}) ,$$

$$\mathbf{x} = (x_1, x_2) ,$$

$$C = \begin{pmatrix} e^{-2r} + 1 & 0 \\ 0 & e^{2r} + 1 \end{pmatrix} .$$

The Q function for a squeezed state is shown in Fig. 4.1.

4.2.4 R Representation

Any density operator ρ may be represented in a unique way by means of a function of two complex variables $R(\alpha^*, \beta)$ which is analytic throughout the finite α^* and β planes. The function R is given explicitly as

$$R(\alpha^*, \beta) = \langle\alpha|\rho|\beta\rangle \exp[(|\alpha|^2 + |\beta|^2)/2]. \quad (4.56)$$

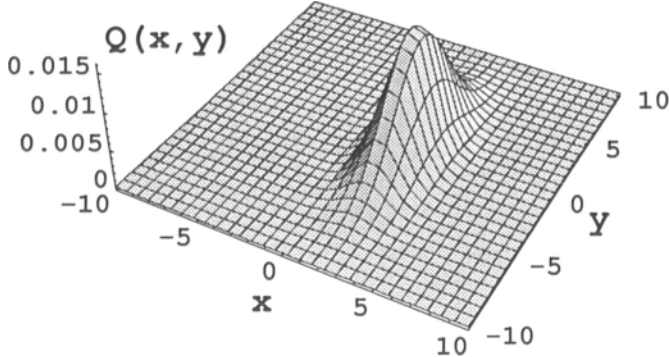


Fig. 4.1 Q function for a squeezed state with coherent amplitude $\alpha = 2.0$, $r = 1.0$

We may express the density operator in terms of $R(\alpha^*, \beta)$

$$\rho = \frac{1}{\pi^2} \int |\alpha\rangle R(\alpha^*, \beta) \langle \beta| e^{-(|\alpha|^2 + |\beta|^2)/2} d^2\alpha d^2\beta . \quad (4.57)$$

The normalization condition

$$\text{Tr}\{\rho\} = 1$$

implies

$$\int \langle \gamma | \alpha \rangle \langle \alpha | \rho | \beta \rangle \langle \beta | \gamma \rangle \frac{d^2\alpha}{\pi} \frac{d^2\beta}{\pi} \frac{d^2\gamma}{\pi} = 1 . \quad (4.58)$$

Interchanging the scalar products and performing the integrations over β and γ we arrive at the result

$$\frac{1}{\pi} \int \langle \alpha | \rho | \alpha \rangle d^2\alpha = 1 \quad (4.59)$$

which gives the normalization condition on R

$$\frac{1}{\pi} \int R(\alpha^*, \alpha) e^{-|\alpha|^2} d^2\alpha = 1 . \quad (4.60)$$

The function $R(\alpha^*, \beta)$ is analytic in α^* and β (and therefore non-singular) and is by definition non-positive. It has a normalization that includes a Gaussian weight factor. For these reasons it cannot have a Fokker–Planck equation or any direct interpretation as a quasiprobability. Nevertheless, the existence of this representation does demonstrate that a calculation of normally-ordered observables for any ρ is possible with a non-singular representation.

4.2.5 Generalized P Representations

Another representation which like the R representation uses an expansion in non-diagonal coherent state projection operators was suggested by *Drummond* and *Gardiner* [4.5]. The representation is defined as follows

$$\rho = \int_D \Lambda(\alpha, \beta) P(\alpha, \beta) d\mu(\alpha, \beta) \quad (4.61)$$

where

$$\Lambda(\alpha, \beta) = \frac{|\alpha\rangle\langle\beta^*|}{\langle\beta^*|\alpha\rangle}$$

and $d\mu(\alpha, \beta)$ is the integration measure which may be chosen to define different classes of possible representations and D is the domain of integration. The projection operator $\Lambda(\alpha, \beta)$ is analytic in α and β . It is clear that the normalization condition on ρ leads to the following normalization condition on $P(\alpha, \beta)$

$$\int_D P(\alpha, \beta) d\mu(\alpha, \beta) = 1 . \quad (4.62)$$

Thus, the $P(\alpha, \beta)$ is normalisable and we shall see in Chap. 6 that it gives rise to Fokker–Planck equations. The definition given by (4.61) leads to different representations depending on the integration measure.

Useful choices of integration measure are

1. Glauber–Sudarshan P Representation

$$d\mu(\alpha, \beta) = \delta^2(\alpha^* - \beta) d^2\alpha d^2\beta . \quad (4.63)$$

This measure corresponds to the diagonal Glauber–Sudarshan P representation defined in (4.8).

2. Complex P Representation

$$d\mu(\alpha, \beta) = d\alpha d\beta . \quad (4.64)$$

Here (α, β) are treated as complex variables which are to be integrated on individual contours C, C' . The conditions for the existence of this representation are discussed in the appendix. This particular representation may take on complex values so in no sense can it have any physical interpretation as a probability distribution. However, as we shall see it is an extremely useful representation giving exact results for certain problems and physical observables such as all the single time correlation functions.

We shall now give some examples of the complex P representation.

(a) Coherent State $|\gamma_0\rangle$

Consider a density operator with an expansion in coherent states as

$$\rho = \iint_{DD'} \rho(\alpha, \beta) |\alpha\rangle \langle \beta^*| d^2\alpha d^2\beta . \quad (4.65)$$

Using the residue theorem

$$\rho = -\frac{1}{4\pi^2} \iint_{DD'} \rho(\alpha, \beta) \langle \beta^* | \alpha \rangle \left[\iint_{CC'} \frac{\Lambda(\alpha', \beta') d\alpha' d\beta'}{(\alpha - \alpha')(\beta - \beta')} \right] d^2\alpha d^2\beta . \quad (4.66)$$

Exchanging the order of integration we see the complex P function is

$$P(\alpha, \beta) = -\frac{1}{4\pi^2} \iint_{DD'} \rho(\alpha', \beta') \langle \beta'^* | \alpha' \rangle \frac{d^2\alpha' d^2\beta'}{(\alpha - \alpha')(\beta - \beta')} . \quad (4.67)$$

Thus for a coherent state $|\gamma_0\rangle$

$$P(\alpha, \beta) = -\frac{1}{4\pi^2(\alpha - \gamma_0)(\beta - \gamma_0^*)} . \quad (4.68)$$

Examples of complex P functions for nonclassical fields where the Glauber–Sudarshan P function would be highly singular are given below.

(b) Number State $|n\rangle$

$$P(\alpha, \beta) = -\frac{1}{4\pi^2} e^{\alpha\beta} \frac{n!}{(\alpha\beta)^{n+1}} . \quad (4.69)$$

This may be proved as follows. Using

$$\langle \alpha | \beta \rangle = e^{\alpha^* \beta - |\alpha|^2/2 - |\beta|^2/2} \quad (4.70)$$

and

$$|\alpha\rangle = \sum \frac{e^{-|\alpha|^2/2} \alpha^n |n\rangle}{n!^{1/2}} , \quad (4.71)$$

we may write ρ as

$$\rho = \int P(\alpha, \beta) \sum \frac{|n'\rangle \langle m'|}{(n'!)^{1/2} (m'!)^{1/2}} e^{-\alpha\beta} (\alpha^{n'} \beta^{m'}) d\alpha d\beta . \quad (4.72)$$

Substituting (4.69) for $P(\alpha, \beta)$

$$\rho = -\frac{1}{4\pi^2} \sum \frac{(n!)^2}{(n'!)^{1/2} (m'!)^{1/2}} \int \alpha^{-(n+1-n')} \beta^{-(n+1-m')} |n'\rangle \langle m'| d\alpha d\beta . \quad (4.73)$$

Choosing any contour of integration encircling the origin and using Cauchy's theorem

$$\begin{aligned} \frac{1}{2\pi i} \oint dz z^n &= 0 \quad \text{if } n \geq 0 , \\ &= 1 \quad \text{if } n = -1 , \\ &= 0 \quad \text{if } n < -1 . \end{aligned} \tag{4.74}$$

We find

$$\rho = |n\rangle\langle n| .$$

(c) Squeezed State $|\gamma, r\rangle$

The complex P representation for a squeezed state is

$$P(\alpha, \beta) = N \exp\{(\alpha - \gamma)(\beta - \gamma^*) + \coth r[(\alpha - \gamma)^2 + (\beta - \gamma^*)^2]\} . \tag{4.75}$$

This may be normalized by integrating along the imaginary axis for r real. The resulting normalization for this choice of contour is

$$N = -\frac{1}{2\pi \sinh r} .$$

As an example of the use of the complex P representation we shall consider the photon counting formula given by (3.107). Using the diagonal coherent-state representation for ρ we may write the photon counting probability $P_m(T)$ as

$$P_m(T) = \int d^2z P(z) \frac{(|z|^2 \mu(T))^m}{m!} \exp[-|z|^2 \mu(T)] . \tag{4.76}$$

An appealing feature of this equation is that $P_m(T)$ is given by an averaged Poisson distribution with $P(z)$ in the role of a probability distribution over the complex field amplitude. It is a close analogue of the classical expression (3.96). We know however that $P(z)$ is not a true probability distribution and may take on negative values, and this may cause some anxiety over the validity of (4.76). In such cases we may consider a simple generalization of (4.76) by using the complex P representation for ρ . The photocount probability is then given by

$$P_m(T) = \int_{CC'} dz dz' P(z, z') \frac{(zz' \mu(T))^m}{m!} \exp[-zz' \mu(T)] . \tag{4.77}$$

We shall demonstrate the use of this formula to calculate $P_m(T)$ for states for which no well behaved diagonal P distribution exists.

a) *Number State*

For a number state with density operator $\rho = |n\rangle\langle n|$ we have

$$P(z, z') = -\frac{1}{4\pi^2} \exp(zz') n! (zz')^{-n-1} \quad (4.78)$$

and the contours C and C' enclose the origin. Substituting (4.77) for $m > n$ the integrand contains no poles and $P_m(T) = 0$, while for $m < n$ poles of order $n - m + 1$ contribute in each integration and we obtain the result of (3.112)

$$P_m(T) = \sum_{n=m}^{\infty} \binom{n}{m} [\mu(T)]^m [1 - \mu(T)]^{n-m} . \quad (4.79)$$

b) *Squeezed State*

For a squeezed state with density operator $\rho = |\gamma, r\rangle\langle \gamma, r|$ where γ and r are taken to be real, we have

$$\begin{aligned} P(z, z') = & -\frac{1}{2\pi} (\sinh r)^{-1} \exp \{ (z - \gamma)(z' - \gamma) + \coth r [(z - \gamma)^2 \\ & + (z' - \gamma)^2] \} \end{aligned} \quad (4.80)$$

and the contours C and C' are along the imaginary axes in z and z' space, respectively. Performing the integration in (4.77) gives the formula, see (3.112),

$$P_m(T) = \sum_{n=m}^{\infty} \binom{n}{m} [\mu(T)]^m [1 - \mu(T)]^{n-m} P_n \quad (4.81)$$

with

$$P_n = (n! \cosh r)^{-1} \exp [-\gamma^2 e^{2r} (1 + \tanh r)] (\tanh r)^n H_n^2 \left(\frac{\gamma e^r}{\sqrt{\sinh 2r}} \right)$$

where the $H_n(x)$ are Hermite polynomials. This agrees with the result of a derivation using the number state representation (3.109) when we recognise that $P_n = |\langle n | \gamma, r \rangle|^2$.

4.2.6 Positive P Representation

The integration measure is chosen as

$$d\mu(\alpha, \beta) = d^2\alpha d^2\beta . \quad (4.82)$$

This representation allows α, β to vary independently over the whole complex plane. It was proved in [4.5] that $P(\alpha, \beta)$ always exists for a physical density operator and can always be chosen positive. For this reason we call it the

positive P representation. $P(\alpha, \beta)$ has all the mathematical properties of a genuine probability. It may also have an interpretation as a probability distribution [4.6]. It proves a most useful representation, in particular, for problems where the Fokker–Planck equation in other representations may have a non-positive definite diffusion matrix. It may be shown that provided any Fokker–Planck equation exists for the time development in the Glauber–Sudarshan representation, a corresponding Fokker–Planck equation exists with a positive semi-definite diffusion coefficient for the positive P representation.

Exercises

4.1 Show that if a field with the P representation $P_i(\alpha)$ is incident on a 50/50 beam splitter the output field has a P representation given by $P_0(\alpha) = 2P_i(\sqrt{2}\alpha)$.

4.2 Show that the Wigner function may be written, in terms of the matrix elements of ρ in the eigenstates of X_1 , as

$$W(\alpha_1, \alpha_2) = \frac{1}{4\pi} \int_{-\infty}^{\infty} dx_1 \exp\left(\frac{i x_1 \alpha_2}{2}\right) \langle \alpha_1 + x_1 | \rho | \alpha_1 - x_1 \rangle$$

where $\alpha_1 = \alpha + \alpha^*$ and $\alpha_2 = -i(\alpha - \alpha^*)$.

4.3 The complex P representation for a number state $|n\rangle$ is

$$P(\alpha, \beta) = -\frac{1}{4\pi^2} e^{\alpha\beta} \frac{n!}{(\alpha\beta)^{n+1}} .$$

Show that

$$\langle a^\dagger a \rangle = \oint d\alpha d\beta \alpha\beta P(\alpha, \beta) = n .$$

4.4 Use the complex P representation for a squeezed state $|\gamma, r\rangle$ with γ and r both real, to show that the photon number distribution for such a state is

$$P_n = (n! \cosh r)^{-1} \exp[-\gamma^2 e^{2r}(1 + \tanh r)] (\tanh r)^n H_n^2 \left(\frac{\gamma e^r}{\sqrt{\sinh 2r}} \right) .$$

5. Quantum Phenomena in Simple Systems in Nonlinear Optics

In this chapter we will analyse some simple processes in nonlinear optics where analytic solutions are possible. This will serve to illustrate how the formalism developed in the preceding chapters may be applied. In addition, the simple examples chosen illustrate many of the quantum phenomena studied in more complex systems in later chapters.

This chapter will serve as an introduction to how quantum phenomena such as photon antibunching, squeezing and violation of certain classical inequalities may occur in nonlinear optical systems. In addition, we include an introduction to quantum limits to amplification.

5.1 Single-Mode Quantum Statistics

A single-mode field is the simplest example of a quantum field. However, a number of quantum features such as photon antibunching and squeezing may occur in a single-mode field. To illustrate these phenomena we consider the degenerate parametric amplifier which displays interesting quantum behaviour.

5.1.1 Degenerate Parametric Amplifier

One of the simplest interactions in nonlinear optics is where a photon of frequency 2ω splits into two photons each with frequency ω . This process known as parametric down conversion may occur in a medium with a second-order nonlinear susceptibility $\chi^{(2)}$. A detailed discussion on nonlinear optical interactions is left until Chap. 9.

We shall make use of the process of parametric down conversion to describe a parametric amplifier. In a parametric amplifier a signal at frequency ω is amplified by pumping a crystal with a $\chi^{(2)}$ nonlinearity at frequency 2ω . We consider a simple model where the pump mode at frequency 2ω is classical and the signal mode at frequency ω is described by the annihilation operator a . The Hamiltonian describing the interaction is

$$\mathcal{H} = \hbar\omega a^\dagger a - i\hbar \frac{\chi}{2} (a^2 e^{2i\omega t} - a^{\dagger 2} e^{-2i\omega t}), \quad (5.1)$$

where χ is a constant proportional to the second-order nonlinear susceptibility and the amplitude of the pump. If we work in the interaction picture we have the time-independent Hamiltonian

$$\mathcal{H}_1 = -i\hbar \frac{\chi}{2} (a^2 - a^{\dagger 2}) . \quad (5.2)$$

The Heisenberg equations of motion are

$$\frac{da}{dt} = \frac{1}{i\hbar} [a, \mathcal{H}_1] = \chi a^{\dagger}, \quad \frac{da^{\dagger}}{dt} = \frac{1}{i\hbar} [a^{\dagger}, \mathcal{H}_1] = \chi a . \quad (5.3)$$

The interaction picture can be viewed equivalently as transforming to a frame rotating at frequency ω .

These equations have the solution

$$a(t) = a(0) \cosh \chi t + a^{\dagger}(0) \sinh \chi t , \quad (5.4)$$

which has the form of a generator of the squeezing transformation, see (2.60). As such we expect the light produced by parametric amplification to be squeezed. This can immediately be seen by introducing the two quadrature phase amplitudes

$$X_1 = a + a^{\dagger}, \quad X_2 = \frac{a - a^{\dagger}}{i} \quad (5.5, 6)$$

which diagonalize equations (5.2 and 5.3)

$$\frac{dX_1}{dt} = +\chi X_1, \quad \frac{dX_2}{dt} = -\chi X_2 . \quad (5.7, 8)$$

These equations demonstrate that the parametric amplifier is a phase-sensitive amplifier which amplifies one quadrature and attenuates the other:

$$X_1(t) = e^{\chi t} X_1(0) , \quad (5.9)$$

$$X_2(t) = e^{-\chi t} X_2(0) . \quad (5.10)$$

The parametric amplifier also reduces the noise in the X_2 quadrature and increases the noise in the X_1 quadrature. The variances $V(X_i, t)$ satisfy the relations

$$V(X_1, t) = e^{2\chi t} V(X_1, 0) , \quad (5.11)$$

$$V(X_2, t) = e^{-2\chi t} V(X_2, 0) . \quad (5.12)$$

For initial vacuum or coherent states $V(X_i, 0) = 1$, hence

$$V(X_1, t) = e^{2\chi t} ,$$

$$V(X_2, t) = e^{-2\chi t} , \quad (5.13)$$

and the product of the variances satisfies the minimum uncertainty relation $V(X_1) V(X_2) = 1$. Thus the deamplified quadrature has less quantum noise than

the vacuum level. The amount of squeezing or noise reduction is proportional to the strength of the nonlinearity, the amplitude of the pump and the interaction time.

5.1.2 Photon Statistics

We shall next consider the photon statistics of the light produced by the parametric amplifier. First we analyse the light produced from an initial vacuum state. The intensity correlation function $g^{(2)}(0)$ in this case is

$$\begin{aligned} g^{(2)}(0) &= \frac{\langle a^\dagger(t)a^\dagger(t)a(t)a(t) \rangle}{\langle a^\dagger(t)a(t) \rangle^2} \\ &= 1 + \frac{\cosh 2\chi t}{\sinh^2 \chi t}. \end{aligned} \quad (5.14)$$

This indicates that the squeezed light generated from an initial vacuum exhibits photon bunching ($g^{(2)}(0) > 1$). This is expected for a squeezed vacuum which must contain correlated pairs of photons.

For an initial coherent state $|\alpha\rangle$ we find the mean photon number

$$\langle a^\dagger(t)a(t) \rangle = |\alpha|^2 (\cosh 2\chi t + \cos 2\theta \sinh 2\chi t) + \sinh^2 \chi t, \quad (5.15)$$

where we have used $\alpha = |\alpha|e^{i\theta}$, and the intensity correlation function

$$g^{(2)}(0) \approx 1 + \frac{1}{|\alpha|^2 e^{-2\chi t}} (e^{-2\chi t} - 1), \quad \theta = \frac{\pi}{4}, \quad (5.16)$$

where $|\alpha|^2$ is large compared with $\sinh^2 \chi t$ and $\sinh \chi t \cosh \chi t$.

Thus under these conditions the photon statistics of the output light is antibunched. We see that a parametric amplifier evolving from an initial coherent state $|i|\alpha\rangle$ evolves towards an amplitude squeezed state with a coherent amplitude of $|\alpha|e^{-\chi t}$. This reduction in amplitude is due to the dynamic contraction in the X_2 direction described by (5.10) (Fig. 5.1).

5.1.3 Wigner Function

The full photon statistics of the light generated in parametric amplification may be calculated via a quasi-probability distribution. While we could choose to calculate the P function we would find that it would become singular due to the quantum correlations which build up during the amplification process. Therefore we shall calculate the Wigner distribution which is a nonsingular positive function for this problem.

The Wigner function describing the state of the parametric oscillator at any time t may now be calculated via the symmetrically ordered characteristic function,

$$\chi(\eta, t) = \text{Tr} \{ \rho(0) e^{\eta a^\dagger(t) - \eta^* a(t)} \}. \quad (5.17)$$

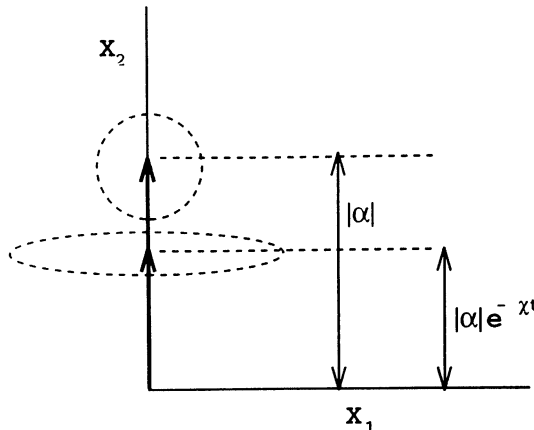


Fig. 5.1. Schematic representation of the evolution of an initial coherent state undergoing parametric amplification

Let us take the initial state to be the coherent state $\rho(0) = |\alpha_0\rangle\langle\alpha_0|$. Then substituting (5.4) into (5.17) we find

$$\chi(\eta, t) = \exp \left[\eta \alpha_0^*(t) - \eta^* \alpha_0(t) - \frac{|\eta|^2}{2} \cosh 2\chi t + \frac{1}{4}(\eta^2 + \eta^{*2}) \sinh 2\chi t \right], \quad (5.18)$$

where

$$\alpha_0(t) = \alpha_0 \cosh 2\chi t + \alpha_0^* \sinh 2\chi t. \quad (5.19)$$

This may be written as

$$\chi(\eta, t) = \exp [\eta^T \cdot a_0^*(t) + \frac{1}{2} \eta^T \Lambda \eta], \quad (5.20)$$

$$\eta^T = (\eta, -\eta^*), \quad (5.21)$$

$$a_0^T(t) = (\alpha_0(t), \alpha_0^*(t)) \quad (5.22)$$

and

$$\Lambda = \frac{1}{2} \begin{pmatrix} \sinh 2\chi t & \cosh 2\chi t \\ \cosh 2\chi t & \sinh 2\chi t \end{pmatrix}. \quad (5.23)$$

The Wigner function is then given by the Fourier transform of $\chi(\eta, t)$, see (4.33). Using (4.36) the result is

$$W(\alpha, t) = \frac{2}{\pi} \exp \left\{ \frac{1}{2} [\alpha - a_0(t)]^T C_\alpha^{-1} [\alpha - a_0(t)] \right\}, \quad (5.24)$$

where $a^T = (\alpha, \alpha^*)$. This is a two variable Gaussian with mean $a_0(t)$ and covariance matrix $C_\alpha = \Lambda$. In terms of the real variables $x_1 = \alpha + \alpha^*$.

$x_2 = -i(\alpha - \alpha^*)$ (corresponding to the quadrature phase operators), the Wigner function becomes

$$W(x_1, x_2) = \frac{1}{2\pi} \exp \left\{ -\frac{1}{2} [\mathbf{x} - \mathbf{x}_0(t)] C_x^{-1} [\mathbf{x} - \mathbf{x}_0(t)] \right\}, \quad (5.25)$$

where

$$C_x = \begin{pmatrix} e^{2xt} & 0 \\ 0 & e^{-2xt} \end{pmatrix}. \quad (5.26)$$

Thus the Wigner function is a two-dimensional Gaussian with the variance in fluctuations in the quadratures X_1 and X_2 given by the major and minor axes of the elliptic contours.

5.2 Two-Mode Quantum Correlations

In two-mode systems there are a richer variety of quantum phenomena since there exists the possibility of quantum correlations between the modes. These correlations may give rise to two mode squeezing such, as described by (2.85). There may also exist intensity and phase correlations between the modes. A simple system which displays many of the above features is the non-degenerate parametric amplifier [5.1].

5.2.1 Non-degenerate Parametric Amplifier

The non-degenerate parametric amplifier is a simple generalization of the degenerate parametric amplifier considered in the previous section. In this case the classical pump mode at frequency 2ω interacts in a nonlinear optical medium with two modes at frequency ω_1 and ω_2 . These frequencies sum to the pump frequency, $2\omega = \omega_1 + \omega_2$. It is conventional to designate one mode as the signal and the other as the idler.

The Hamiltonian describing this system is

$$\mathcal{H} = \hbar\omega_1 a_1^\dagger a_1 + \hbar\omega_2 a_2^\dagger a_2 + i\hbar\chi(a_1^\dagger a_2^\dagger e^{-2i\omega t} - a_1 a_2 e^{2i\omega t}), \quad (5.27)$$

where $a_1(a_2)$ is the annihilation operator for the signal (idler) mode. The coupling constant χ is proportional to the second-order susceptibility of the medium and to the amplitude of the pump.

The Heisenberg equations of motion in the interaction picture are

$$\frac{da_1}{dt} = \chi a_2^\dagger, \quad (5.28)$$

$$\frac{da_2^\dagger}{dt} = \chi a_1. \quad (5.29)$$

The solutions to these equations are

$$a_1(t) = a_1 \cosh \chi t + a_2^\dagger \sinh \chi t , \quad (5.30)$$

$$a_2(t) = a_2 \cosh \chi t + a_1^\dagger \sinh \chi t . \quad (5.31)$$

If the system starts in an initial coherent state $|\alpha_1\rangle, |\alpha_2\rangle$, the mean photon number in mode one after time t is

$$\begin{aligned} \langle n_1(t) \rangle &= \langle \alpha_1, \alpha_2 | a_1^\dagger(t) a_1(t) | \alpha_1, \alpha_2 \rangle \\ &= |\alpha_1 \cosh \chi t + \alpha_2^* \sinh \chi t|^2 + \sinh^2 \chi t . \end{aligned} \quad (5.32)$$

The last term in this equation represents the amplification of vacuum fluctuations since if the system initially starts in the vacuum ($\alpha_1 = \alpha_2 = 0$) a number of photons given by $\sinh^2 \chi t$ will be generated after a time t .

The intensity correlation functions of this system exhibit interesting quantum features. With a two-mode system we may consider cross correlations between the two modes. We shall show that quantum correlations may exist which violate classical inequalities.

Consider the moment $\langle a_1^\dagger a_1 a_2^\dagger a_2 \rangle$. We may express this moment in terms of the Glauber–Sudarshan P function as follows:

$$\langle a_1^\dagger a_1 a_2^\dagger a_2 \rangle = \int d^2\alpha_1 \int d^2\alpha_2 |\alpha_1|^2 |\alpha_2|^2 P(\alpha_1, \alpha_2) . \quad (5.33)$$

If a positive P function exists the right-hand side of this equation is the classical intensity correlation function for two fields with the fluctuating complex amplitudes α_1 and α_2 . It follows from the Hölder inequality that

$$\begin{aligned} \int d^2\alpha_1 d^2\alpha_2 |\alpha_1|^2 |\alpha_2|^2 P(\alpha_1, \alpha_2) &\leq [\int d^2\alpha_1 d^2\alpha_2 |\alpha_1|^4 P(\alpha_1, \alpha_2)]^{1/2} \\ &\times [\int d^2\alpha_1 d^2\alpha_2 |\alpha_2|^4 P(\alpha_1, \alpha_2)]^{1/2} . \end{aligned} \quad (5.34)$$

Re-expressed in terms of operators this inequality implies

$$\langle a_1^\dagger a_1 a_2^\dagger a_2 \rangle \leq [\langle (a_1^\dagger)^2 a_1^2 \rangle \langle (a_2^\dagger)^2 a_2^2 \rangle]^{1/2} , \quad (5.35)$$

a result known as the *Cauchy–Schwarz inequality*. If the two modes are symmetric as for the non-degenerate parametric amplifier this inequality implies

$$\langle a_1^\dagger a_1 a_2^\dagger a_2 \rangle \leq \langle (a_1^\dagger)^2 a_1^2 \rangle . \quad (5.36)$$

Because we have assumed a positive P function this is a weak inequality and there exists certain quantum fields which will violate it.

It is more usual to express the Cauchy–Schwarz inequality in terms of the second-order intensity correlation functions defined for a single-mode field in (3.63). The two-mode intensity correlation function is defined by

$$g_{12}^{(2)}(0) = \frac{\langle a_1^\dagger a_1 a_2^\dagger a_2 \rangle}{\langle a_1^\dagger a_1 \rangle \langle a_2^\dagger a_2 \rangle} . \quad (5.37)$$

This definition together with

$$g_i^{(2)}(0) = \frac{\langle a_i^\dagger a_i^\dagger a_i a_i \rangle}{\langle a_i^\dagger a_i \rangle^2} \quad (5.38)$$

enables one to write the Cauchy–Schwarz inequality as

$$[g_{12}^{(2)}(0)]^2 \leq g_1^{(2)}(0)g_2^{(2)}(0) . \quad (5.39)$$

A stronger inequality may be derived for quantum fields when a Glauber–Sudarshan P representation does not exist. The appropriate inequality for two non-commuting operators is, see (3.26),

$$\langle a_1^\dagger a_1 a_2^\dagger a_2 \rangle^2 \leq \langle (a_1^\dagger a_1)^2 \rangle \langle (a_2^\dagger a_2)^2 \rangle . \quad (5.40)$$

For symmetrical systems this implies

$$\langle a_1^\dagger a_1 a_2^\dagger a_2 \rangle \leq \langle (a_1^\dagger)^2 a_1^2 \rangle + \langle a_1^\dagger a_1 \rangle \quad (5.41)$$

or

$$g_{12}^{(2)}(0) \leq g_1^{(2)}(0) + \frac{1}{\langle a_1^\dagger a_1 \rangle} . \quad (5.42)$$

We now show that the non-degenerate parametric amplifier if initially in the ground state leads to a maximum violation of the Cauchy–Schwarz inequality (5.39), as is consistent with the inequality (5.42). That is, the correlations built up in the parametric amplifier are the maximum allowed by quantum mechanics.

In this system the following conservation law is easily seen to hold,

$$n_1(t) - n_2(t) = n_1(0) - n_2(0) , \quad (5.43)$$

where $n_i(t) \equiv a_i^\dagger(t)a_i(t)$. This conservation law has been exploited to give squeezing in the photon number difference in a parametric amplifier as will be described in Chap. 8. Using this relation the intensity correlation function may be written

$$\langle n_1(t)n_2(t) \rangle = \langle n_1(t)^2 \rangle + \langle n_1(t)[n_2(0) - n_1(0)] \rangle . \quad (5.44)$$

If the system is in the vacuum state the last term is zero, thus

$$\langle n_1(t)n_2(t) \rangle = \langle a_1^\dagger(t)a_1^\dagger(t)a_1(t)a_1(t) \rangle + \langle a_1^\dagger(t)a_1(t) \rangle , \quad (5.45)$$

which corresponds to the maximum violation of the Cauchy–Schwarz inequality allowed by quantum mechanics.

Thus the non-degenerate parametric amplifier exhibits quantum mechanical correlations which violate certain classical inequalities. These quantum correlations may be further exploited to give squeezing and states similar to those discussed in the EPR paradox, as will be described in the following subsections.

5.2.2 Squeezing

In the interaction picture the unitary operator for time evolution of the non-degenerate parametric amplifier is

$$U(t) = \exp [\chi t (a_1^\dagger a_2^\dagger - a_1 a_2)] . \quad (5.46)$$

Comparison with (2.87) shows that $U(t)$ is the unitary two mode squeeze operator $S(G)$ where $G = -\chi t$.

The squeezing will be defined with respect to quadrature phase amplitudes of the oscillation at the local-oscillator frequency and a phase θ [5.2]. In an experiment the signal and idler beams are mixed with a local oscillator in a homodyne detection scheme.

Ignoring the local oscillator field the total field consists of two modes with frequencies $\omega \pm \varepsilon$ symmetrically displaced from the local oscillator frequency ω :

$$\begin{aligned} E(t) = & \frac{1}{\sqrt{2}} [a_1(t)e^{-i(\omega-\varepsilon)t} + a_2 e^{-i(\omega+\varepsilon)t} + a_1^\dagger(t)e^{i(\omega-\varepsilon)t} \\ & + a_2^\dagger(t)e^{i(\omega+\varepsilon)t}] . \end{aligned} \quad (5.47)$$

The factor $1/\sqrt{2}$ has been inserted to give a convenient definition of the vacuum level. This may be written as

$$E(t) = X_\theta(t) \cos(\omega t + \theta) + X_{\theta+\pi/2}(t) \sin(\omega t + \theta) \quad (5.48)$$

and the quadrature phase amplitudes are given by

$$\begin{aligned} X_\theta &= \frac{1}{\sqrt{2}} [a_1(t)e^{i(\theta+\varepsilon t)} + a_2^\dagger(t)e^{-i(\theta-\varepsilon t)} + \text{h.c.}] , \\ X_{\theta+\pi/2} &= \frac{-i}{\sqrt{2}} [a_1(t)e^{i(\theta+\varepsilon t)} + a_2^\dagger(t)e^{-i(\theta-\varepsilon t)} - \text{h.c.}] . \end{aligned} \quad (5.49)$$

It is clear from the form of (5.48 and 5.49) that the squeezing signal will be found at frequency ε after mixing with a local oscillator at the frequency ω .

If the system starts in the vacuum state, the variance in $X_\theta(t)$ is expressed by

$$V(X_\theta) = \cosh 2\chi t + \cos 2\theta \sinh 2\chi t . \quad (5.50)$$

Thus, if $\theta = 0$,

$$V(X_0(t)) = e^{2\chi t} \quad (5.51)$$

while, if $\theta = \pi/2$,

$$V(X_{\pi/2}(t)) = e^{-2\chi t} . \quad (5.52)$$

Changing the phase of the local oscillator, θ , by $\pi/2$ enables one to move from enhanced to diminished, i.e. squeezed, quadrature phase fluctuations. We note that the squeezing in the non-degenerate parametric amplifier is due to the quantum correlations which build up in the signal and idler modes. The individual signal and idler modes are not squeezed.

5.2.3 Quadrature Correlations and the Einstein–Podolsky–Rosen Paradox

The non-degenerate parametric amplifier can also be used to prepare states similar to those discussed in the Einstein–Podolsky–Rosen (EPR) paradox [5.3]. In the original treatment two systems are prepared in a correlated state. One of two canonically conjugate variables is measured on one system and the correlation is such that the value for a physical variable in the second system may be inferred with certainty.

To see how this behaviour is manifested in the non-degenerate parametric amplifier we first define two sets, one for each mode, of canonically conjugate variables, i.e.,

$$X_i^\theta = a_i e^{i\theta} + a_i^\dagger e^{-i\theta} \quad (i = 1, 2) . \quad (5.53)$$

The variables X_i^θ and $X_i^{\theta + \pi/2}$ obey the commutation relation

$$[X_i^\theta, X_i^{\theta + \pi/2}] = -2i \quad (5.54)$$

and are thus directly analogous to the position and momentum operators discussed in the original EPR paper.

To measure the degree of correlation between the two modes in terms of these operators, we consider the quantity

$$V(\theta, \phi) \equiv \frac{1}{2} \langle (X_1^\theta - X_2^\phi)^2 \rangle . \quad (5.55)$$

If $V(\theta, \phi) = 0$ then X_1^θ is perfectly correlated with X_2^ϕ . This means a measurement of X_1^θ can be used to infer a value of X_2^ϕ with certainty. To appreciate why such a correlation should occur in the non-degenerate parametric amplifier, we can write the interaction Hamiltonian directly in terms of the defined canonical variables,

$$\begin{aligned} \mathcal{H}_1 = & -2\hbar\chi \sin(\theta + \phi)(X_1^\theta X_2^\phi - X_1^{\theta + \pi/2} X_2^{\phi + \pi/2}) \\ & - 2\hbar\chi \cos(\theta + \phi)(X_1^{\theta + \pi/2} X_2^\phi + X_1^\theta X_2^{\phi + \pi/2}) . \end{aligned} \quad (5.56)$$

The Heisenberg equation of motion for X_1^θ is then

$$\dot{X}_1^\theta = -4\chi[X_2^\phi \cos(\theta + \phi) - X_2^{\phi + \pi/2} \sin(\theta + \phi)] \quad (5.57)$$

and we see that X_1^θ is coupled solely to X_2^ϕ when $\theta + \phi = 0$.

Direct calculation of $V(\theta, \phi)$ using the solutions in (5.30, 31) gives

$$V(\theta, \phi) = \cosh 2\chi t - \sinh 2\chi t \cos(\theta + \phi) . \quad (5.58)$$

When $\theta + \phi = 0$, $V(\theta, \phi) = e^{-2xt}$ and, for long times, $V(\theta, \phi)$ becomes increasingly small reflecting the build up of correlation between the two variables for this case. Initially, of course, the two systems are uncorrelated and $V(\theta, \phi) = 1$. As $V(\theta, \phi)$ tends to zero the system becomes correlated in the sense of the EPR paradox. As time proceeds a measurement of X_1^θ yields an increasingly certain value of X_2^ϕ . However one could equally have measured $X_1^{\theta-\pi/2}$. Thus certain values for two noncommuting observables $X_2^\phi, X_2^{\phi+\pi/2}$ may be obtained without in anyway disturbing system 2. This outcome constitutes the centre of the *EPR argument*.

Of course, in reality no measurement enables a perfect inference to be made. To quantify the extent of the apparent paradox, we can define the variances $V_{\text{inf}}(X_2^\phi)$ and $V_{\text{inf}}(X_2^{\phi+\pi/2})$ which determine the error in inferring X_2^ϕ and $X_2^{\phi+\pi/2}$ from direct measurements on X_2^θ and $X_1^{\theta-\pi/2}$. In the case of direct measurements made on $(X_2^\phi, X_2^{\phi+\pi/2})$ quantum mechanics would suggest

$$V(X_2^\phi)V(X_2^{\phi+\pi/2}) \geq 4 .$$

However the variances in the inferred values are not constrained. Thus whenever $V_{\text{inf}}(X_2^\phi)V_{\text{inf}}(X_2^{\phi+\pi/2}) < 4$, we can claim an EPR correlation paradoxically less than expected by direct measurement on the same state. This result seems to contradict the uncertainty principle. That this is not the case is seen as follows. In the standard uncertainty principle the variances are calculated with respect to the same state. However in the inference uncertainty product the variances are not calculated in the same state. That is to say $V_{\text{inf}}(X_2^{\phi+\pi/2})$ is calculated on the conditional state given a result for a measurement of $X_2^{\phi+\pi/2}$, however $V_{\text{inf}}(X_2^\phi)$ is calculated on the different conditional state given a result for the measurement of X_2^ϕ .

Recently Ou et al. [5.4] performed an experimental test of these for the parametric amplifier. Using their quadrature normalization, the inferred variances indicate a paradoxical result if

$$V_{\text{inf}}(X_1^\phi)V_{\text{inf}}(X_1^{\phi+\pi/2}) \leq 2 .$$

The experimental result for the lowest value of the product was 0.7 ± 0.01 .

5.2.4 Wigner Function

The full quantum correlations present in the parametric amplifier may be represented using a quasi-probability distribution. If both modes of the amplifier are initially in the vacuum state no Glauber P function for the total system exists at any time. However, a Wigner function may be obtained. We shall proceed to derive the Wigner function for the parametric amplifier.

We may define a two mode characteristic function by a simple generalization of the single-mode definition. For both modes initially in the vacuum state this may be expressed as

$$\begin{aligned} \chi(\eta_1, \eta_2, t) &= \langle 0 | \exp[\eta_1 a_1^\dagger(t) - \eta_1^* a_1(t)] \exp[\eta_2 a_2^\dagger(t) - \eta_2^* a_2(t)] | 0 \rangle \\ &= \exp[-\frac{1}{2}[\eta_1(t)|^2 - \frac{1}{2}[\eta_2(t)|^2]] . \end{aligned} \quad (5.59)$$

where

$$\eta_1(t) = \eta_1 \cosh \chi t - \eta_2^* \sinh \chi t ,$$

$$\eta_2(t) = \eta_2 \cosh \chi t - \eta_1^* \sinh \chi t .$$

The Wigner function is then given by

$$\begin{aligned} W(\alpha_1, \alpha_2, t) &= \frac{1}{\pi^4} \int d^2 \eta_1 \int d^2 \eta_2 \exp(\eta_1^* \alpha_1 - \eta_1 \alpha_1^*) \exp(\eta_2^* \alpha_2 - \eta_2 \alpha_2^*) \chi(\eta_1, \eta_2, t) \\ &= \frac{4}{\pi^2} \exp(-2|\alpha_1 \cosh \chi t - \alpha_2^* \sinh \chi t|^2 \\ &\quad - 2|\alpha_2 \cosh \chi t - \alpha_1^* \sinh \chi t|^2) . \end{aligned} \quad (5.60)$$

This distribution may be written in terms of the uncoupled c-number variables

$$\gamma_1 = \alpha_1 + \alpha_2^* ,$$

$$\gamma_2 = \alpha_1 - \alpha_2^* .$$

In these new variables the Wigner function is

$$W(\gamma_1, \gamma_2, t) = \frac{1}{4\pi^2} \exp \left[-\frac{1}{2} \left(\frac{|\gamma_1|^2}{e^{2xt}} + \frac{|\gamma_2|^2}{e^{-2xt}} \right) \right] , \quad (5.61)$$

in which form it is particularly easy to see that squeezing occurs in a linear combination of the two modes. The variances in the two quadratures being given by e^{-2xt} and e^{2xt} , respectively. It is interesting to note that even though the state produced contains non-classical correlations the Wigner function always remains positive.

5.2.5 Reduced Density Operator

When a two component system is in a pure state the reduced state of each component system, determined by a partial trace operation, will be a mixed state. An interesting feature of the non-degenerate parametric amplifier is that the reduced state of each mode is a thermal state, if each mode starts from the vacuum.

To demonstrate this result we first show the high degree of correlation between the photon number in each mode. The state of the total system at time t is

$$|\psi(t)\rangle = \exp[\chi t(a_1^\dagger a_2^\dagger - a_1 a_2)]|0\rangle . \quad (5.62)$$

We now make use of the disentangling theorem [5.5]

$$e^{\theta(a_1^\dagger a_2^\dagger - a_1 a_2)} = e^{\Gamma a_1^\dagger a_2^\dagger} e^{-g(a_1^\dagger a_1 + a_2^\dagger a_2 + 1)} e^{-\Gamma a_1 a_2} , \quad (5.63)$$

where

$$\Gamma = \tanh \theta ,$$

$$g = \ln(\cosh \theta) .$$

Thus

$$|\psi(t)\rangle = e^{-g} e^{\Gamma a_1^\dagger a_2^\dagger} |0\rangle = (\cosh \chi t)^{-1} \sum_{n=0}^{\infty} (\tanh \chi t)^n |n, n\rangle , \quad (5.64)$$

where $|n, n\rangle \equiv |n\rangle_1 \otimes |n\rangle_2$. As photons are created in pairs there is perfect correlation between the photon number in each mode. The reduced state of either mode is then easily seen to be

$$\rho_i(t) = \text{Tr}_i\{|\psi(t)\rangle\langle\psi(t)|\} = (\cosh \chi t)^{-2} \sum_{n=0}^{\infty} (\tanh \chi t)^{2n} |n\rangle\langle n| . \quad (5.65)$$

This is a thermal state with mean $\bar{n} = \sinh^2 \chi t$, having strong analogies with the Hawking effect associated with the thermal evaporation of black holes.

Suppose, however, that a photodetector with quantum efficiency μ has counted m photons in mode b . What is the state of mode a conditioned on this result? Such a conditional state for mode a is referred to as the *selected state* as it is selected from an ensemble of systems each with different values for the number of photons counted in mode b . We shall now describe how the conditional state of mode a may be calculated.

In Chap. 3 we saw that the probability to detect m photons from a field with the photon-number distribution $P(n)$ and detector efficiency μ is

$$P_\mu(m) = \sum_{n=m}^{\infty} \binom{n}{m} (1-\mu)^{n-m} \mu^m P_1(n) , \quad (5.66)$$

where $P_1(n)$ is the photon number distribution for the field. This equation may be written as

$$P_\mu(m) \approx \text{Tr}\{\rho Y_\mu^\dagger(m) Y_\mu(m)\} \quad (5.67)$$

and the operator Y on mode b is defined by

$$Y_\mu(m) = \sum_{n=m}^{\infty} \binom{n}{m}^{1/2} (1-\mu)^{(n-m)/2} \mu^{m/2} |n-m\rangle_b \langle n| . \quad (5.68)$$

Note that when $\mu \rightarrow 1$ this operator approaches the projection operator $|0\rangle_b \langle m|$. This is quite different to the projection operator $|m\rangle_b \langle m|$ that a naive application of the von Neumann projection postulate would indicate for photon counting measurements, and reflects the fact that real photon-counting measurements are destructive, i.e. photons are absorbed upon detection. The conditional state of mode a is then given by

$$\rho^{(m)} = (P_\mu(m))^{-1} \text{Tr}_b\{Y_\mu(m) \rho Y_\mu^\dagger(m)\} . \quad (5.69)$$

This equation is a generalisation of the usual projection postulate. In the case of the correlated two mode state in (5.65), the conditional state of mode a becomes

$$\rho^{(m)} = (P_\mu(m))^{-1} \sum_{n=m}^{\infty} \binom{n}{m} \mu^m (1-\mu)^{n-m} |n\rangle\langle n| , \quad (5.70)$$

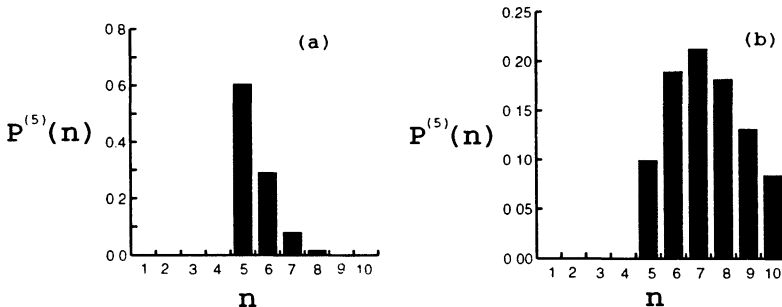


Fig. 5.2. Photon number distribution for mode a given that 5 photons are counted in mode b of a parametric amplifier. (a) $\mu = 0.9$. (b) $\mu = 0.6$

with

$$P_\mu(m) = (1 + \bar{n})^{-1} (\lambda\mu)^m [1 - \lambda(1 - \mu)]^{-(m+1)}, \quad (5.71)$$

where $\lambda = \tanh^2 \chi t$, $\bar{n} = \sinh^2 \chi t$. Equation (5.70) represents a state with *at least* m quanta. In Fig. 5.2 we show the photon number distribution $P^{(m)}(n)$ for this conditional state. As one would expect, when $\mu \rightarrow 1$, this approaches a number state $|m\rangle$. It should be noted, however, that the conditional state computed above refers to a situation in which the counting is done *after* the interaction which produces the correlated state, is turned off. In a cavity configuration, however, it is likely that photon counting is proceeding simultaneously with the process of parametric amplification. In that case one must proceed a little differently, however the overall result is much the same, i.e. mode a is left with at least m quanta. The details of this more complicated calculation will be found in the paper by Holmes et al. [5.6].

5.3 Quantum Limits to Amplification

The non-degenerate parametric amplifier exemplifies many features of general linear amplification. One such feature is the limit placed on the amplifier gain if the output is to be squeezed. To see how this limit arises, and to see how it might be overcome, we write the solutions (5.30, 31) in the form

$$X_{1,\text{OUT}}^\theta = G^{1/2} X_{1,\text{IN}}^\theta + (G - 1)^{1/2} X_{2,\text{IN}}^\theta, \quad (5.72)$$

where $G = \cosh^2 \chi t$ and the quadrature phase operators are defined in (5.53). The subscript IN denotes operators defined at $t = 0$ and the subscripts 1 and 2 refer to the signal and idler modes, respectively. In (5.72) the first term

describes the amplification of the quadrature and the second term the noise added by the amplifier. The variances obey the equation

$$V(X_{1,\text{OUT}}^\theta) = GV(X_{1,\text{IN}}^\theta) + (G - 1)V(X_{2,\text{IN}}^\theta) . \quad (5.73)$$

The maximum gain consistent with any squeezing at the output is

$$G_{\text{MAX}} = \frac{1 + V(X_{2,\text{IN}}^\theta)}{V(X_{1,\text{IN}}^\theta) + V(X_{2,\text{IN}}^\theta)} . \quad (5.74)$$

If the idler mode is in the vacuum state, $V(X_{2,\text{IN}}^\theta) = 1$ then

$$G_{\text{MAX}} = \frac{2}{1 + V(X_{1,\text{IN}}^\theta)} , \quad (5.75)$$

which gives a maximum gain of 2 for a highly squeezed state at the signal input. For higher values of the gain the squeezing at the signal output is lost due to contamination from the amplification of vacuum fluctuation in the idler input.

Greater gains may be achieved while still retaining the squeezing in the output signal if the input to the idler mode, is squeezed ($V(X_{1,\text{IN}}^\theta) < 1$).

If we define the total noise in the signal as the sum of the noise in the two quadratures

$$N = \text{Var}\{X_1^\theta\} + \text{Var}\{X_1^{\theta+\pi/2}\} \quad (5.76)$$

then

$$N_{\text{OUT}} = G(N_{\text{IN}} + A) , \quad (5.77)$$

where

$$\begin{aligned} A &= \left(1 - \frac{1}{G}\right)(\text{Var}\{X_{2,\text{IN}}^\theta\} + \text{Var}\{X_{2,\text{IN}}^{\theta+\pi/2}\}) \\ &\geq 2\left(1 - \frac{1}{G}\right) . \end{aligned} \quad (5.78)$$

This is in agreement with a general theorem for the noise added by a linear amplifier [5.7]. The minimum added noise $A = 2(1 - 1/G)$ occurs when $\text{Var}(X_{2,\text{IN}}^\theta) = \text{Var}(X_{2,\text{IN}}^{\theta+\pi/2}) = 1$, that is, when the idler is in a coherent or vacuum state.

5.4 Amplitude Squeezed State with Poisson Photon Number Statistics

Finally we consider a simple nonlinear optical model which produces an amplitude squeezed state which has Poissonian photon number statistics [5.8, 9]. The model describes a quantised field undergoing a self-interaction via

the Kerr effect. The Kerr effect is a nonlinear process involving the third-order nonlinear polarisability of a nonlinear medium. The field undergoes an intensity dependent phase shift, and thus we regard the medium as having a refractive index proportional to the intensity of the field.

Quantum mechanically the Kerr effect may be described by the effective Hamiltonian

$$\mathcal{H} = \hbar \frac{\chi}{2} (a^\dagger)^2 a^2 , \quad (5.79)$$

where χ is proportional to the third-order nonlinear susceptibility. The Heisenberg equation of motion for the annihilation operator is

$$\frac{da}{dt} = -i\chi a^\dagger a . \quad (5.80)$$

As $a^\dagger a$, the photon number operator, is a constant of motion the photon number statistics is time invariant. The solution is then

$$a(t) = e^{-i\chi t a^\dagger a} a(0) . \quad (5.81)$$

Assume the initial state is a coherent state with real amplitude α . The mean amplitude at a later time is then

$$\langle a(\theta) \rangle = \alpha \exp [-\alpha^2(1 - \cos \theta) - i\alpha^2 \sin \theta] , \quad (5.82)$$

where we have defined $\theta = \chi t$. Typically $\theta \ll 1$ and then

$$\langle a(\theta) \rangle \approx \alpha e^{-i\alpha^2 \theta - \alpha^2 \theta^2/2} . \quad (5.83)$$

This result displays two effects. Firstly, there is a rotation of the mean amplitude by $\alpha^2 \theta$; the expected nonlinear phase shift. Secondly, there is a decay of the amplitude which goes quadratically with time. This decay is due to the fact that the Kerr effect transforms intensity fluctuations in the initial coherent state into phase fluctuations (Fig. 5.3). In effect, the initial coherent state error circle undergoes a rotational shearing while the area remains constant.

Inspection of Fig. 5.3 suggests that, at least for short times, this system is likely to produce a squeezed state with reduced amplitude fluctuations. This is indeed the case. For short times ($\theta \ll 1$) and large intensities ($\alpha^2 \gg 1$) one finds the minimum variance of the in-phase quadrature approaches the value

$$V(X_1)_{\min} = 0.4 . \quad (5.84)$$

This occurs at the value

$$\theta_{\min} \approx \pm \frac{0.55}{\alpha^2} . \quad (5.85)$$

This short time behaviour is evident in Fig. 5.4a. Thus even though the photon statistics is at all times Poissonian, for short times the field is amplitude squeezed.

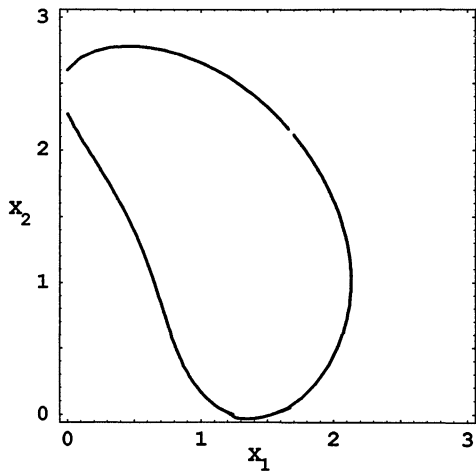


Fig. 5.3. Contour of the Q -function (at height of 0.3) for the state of a single mode field in a Kerr nonlinearity. The initial state was a coherent state with amplitude equal to 2.0. The state shown is at time $\theta = 0.25$

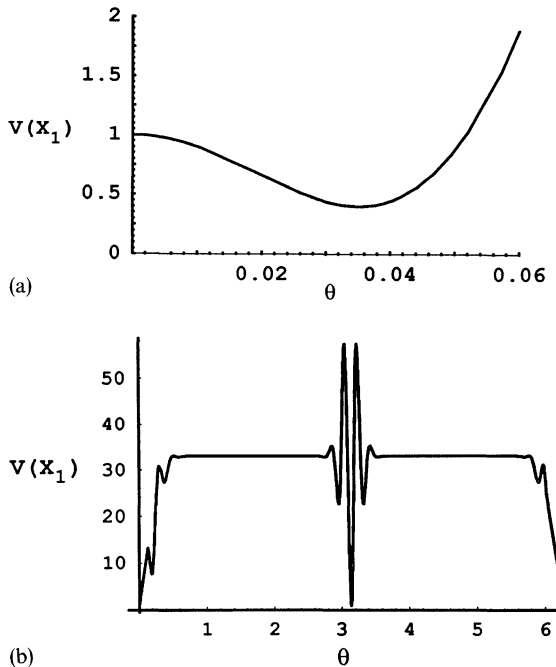


Fig. 5.4. A plot of the variance in the in-phase quadrature for the Kerr interaction, versus the dimensionless interaction time θ , with an initial coherent state of amplitude $\alpha = 4.0$. (a) Short time behaviour. (b) Long time behaviour

We now consider mixing the output of the nonlinear process with a coherent field on a beam splitter of low reflectivity. The output field is now given by

$$a_0 = \sqrt{T} e^{-i\theta a^\dagger a} a + \sqrt{R} \beta , \quad (5.86)$$

where β is the coherent amplitude of the mixing field, and T and R are, respectively, the transmittivity and reflectivity of the beam splitter. We assume $T \rightarrow 1$ with $\sqrt{R}\beta \rightarrow \xi$, that is the mixing field is very strong. In this limit we have

$$a_0 = e^{-i\theta a^\dagger a} a + \xi . \quad (5.87)$$

We now can choose ξ so as to minimise the photon number noise at the output. This requires ξ to be $-\pi/2$ out-of-phase with the coherent excitation of the input. As θ increases, the ratio of the number variance to number mean decreases to a minimum at $\theta = 1/2 \langle n_0 \rangle^{-2/3}$ (for optimal ξ), and then increases. The minimum photon number variance is [5.10]

$$V(n_0) = \langle n_0 \rangle^{1/3} , \quad (5.88)$$

where $\langle n_0 \rangle = \langle n \rangle + |\xi|^2$. This is smaller than the similar result for a squeezed state, which has a minimum value of $\langle n \rangle^{2/3}$.

Were the rotational shearing to continue (as one might expect from a classical model) the variance in the in-phase and out-of-phase quadratures would saturate at the value $2\alpha^2 + 1$. This would be the variance for a number state with the photon number equal to α^2 . That this does not happen is evident in Fig. 5.4b. Indeed, from (5.82) it is clear that for $\theta = 2\pi$ the mean amplitude returns to the initial value. A similar result holds for the variances (Exercise 5.6). This is an example of a quantum recurrence and arises from the discrete nature of the photon number distribution for a quantised field. The details are left for Exercise 5.6. In fact at $\theta = \pi$ the system evolves to a coherent superposition of coherent states:

$$|\psi(\theta = \pi)\rangle = \frac{1}{\sqrt{2}}(e^{i\pi/4}|i\alpha\rangle + e^{-i\pi/4}|-i\alpha\rangle) . \quad (5.89)$$

This phenomenon would be very difficult to observe experimentally as typical values of χ would require absurdly large interaction times, which in practice means extremely large interaction lengths. In Chap. 16 we will show that dissipation also makes the observation of such a coherent superposition state unlikely in a Kerr medium.

Problems

- 5.1** Derive the Wigner and P functions for the reduced density operator of the signal mode for the non-degenerate parametric amplifier.

5.2 Show that, $n_1 - n_2$, the difference in the number of photons in the signal and idler mode is a constant for the parametric amplifier.

5.3 The Hamiltonian for the frequency up-converter is

$$\mathcal{H} = \hbar\omega_1 a_1^\dagger a_1 + \hbar\omega_2 a_2^\dagger a_2 + \hbar\kappa(e^{i\omega t} a_1^\dagger a_2 + e^{-i\omega t} a_1 a_2^\dagger) ,$$

where $\omega = \omega_2 - \omega_1$. Show that $n_1 + n_2$, the sum of the number of photons in the signal and idler modes, is a constant.

5.4 Show that the process of parametric frequency upconversion is noiseless, that is a coherent state remains coherent.

5.5 Take the initial state for the frequency upconverter to be $|N, N\rangle$. Express the density operator at time t as the tensor product of number states. *Hint: Use the disentangling theorem, see (5.63).* What is the reduced density operator for a single mode?

5.6 (a) If the initial state for the Kerr-effect model is a coherent state with real mean amplitude, calculate the variances for the in-phase and out-of-phase quadratures. Show that at $\chi t = \pi$ the field exhibits amplitude squeezing for small values of the amplitude.

(b) Show that at $\chi t = \pi$ the state may be written in the form

$$e^{i\pi/4}|-i\alpha\rangle + e^{-i\pi/4}|i\alpha\rangle .$$

6. Stochastic Methods

In all physical processes there is an associated loss mechanism. In this chapter we shall consider how losses may be included in the quantum mechanical equations of motion. There are several ways in which a quantum theory of damping may be developed. We shall adopt the following approach: We consider the system of interest coupled to a heat bath or reservoir. We first derive an operator master equation for the density operator of the system in the Schrödinger or interaction picture. Equations of motion for the expectation values of system operators may directly be derived from the operator master equation. Using the quasi-probability representations for the density operator discussed in Chap. 4, the operator master equation may be converted to a c-number Fokker–Planck equation. For linear problems a time-dependent solution to the Fokker–Planck equation may be found. In certain nonlinear problems with an appropriate choice of representation the steady-state solution for the quasi-probability distribution may be found from which moments may be calculated.

Using methods familiar in stochastic processes the Fokker–Planck equation may be converted into an equivalent set of stochastic differential equations. These stochastic differential equations of which the Langevin equations are one example are convenient when linearization is necessary. We begin then with a derivation of the master equation. We follow the method of *Haake* [6.1].

6.1 Master Equation

We consider a system described by the Hamiltonian \mathcal{H}_S coupled to a reservoir described by the Hamiltonian \mathcal{H}_R . The reservoir may be considered to be a large number of harmonic oscillators as, for example, the modes of the free electromagnetic field or phonon modes in a solid. In some cases the reservoir may be more appropriately modelled as a set of atomic energy levels. The derivation of the master equation is not dependent on the specific reservoir model. There is a weak interaction between the system and the reservoir given by the Hamiltonian V . Thus the total Hamiltonian is

$$\mathcal{H} = \mathcal{H}_S + \mathcal{H}_R + V \quad (6.1)$$

Let $w(t)$ be the total density operator of the system plus reservoir in the interaction picture. The equation of motion in the interaction picture is

$$\frac{dw(t)}{dt} = -\frac{i}{\hbar} [V(t), w(t)] \quad (6.2)$$

The reduced density operator for the system is defined by

$$\rho(t) = \text{Tr}_R \{w(t)\} \quad (6.3)$$

where Tr_R indicates a trace over reservoir variables. We assume that initially the system and reservoir are uncorrelated so that

$$w(0) = \rho(0) \otimes \rho_R \quad (6.4)$$

where ρ_R is the density operator for the reservoir.

Integrating (6.2) we obtain

$$w(t) = w(0) - \frac{i}{\hbar} \int_0^t dt_1 [V(t_1), w(t_1)] . \quad (6.5)$$

Iterating this solution we find

$$\begin{aligned} w(t) &= w(0) + \sum_{n=1}^{\infty} \left(-\frac{i}{\hbar} \right)^n \int_0^t dt_1 \int_0^{t_1} dt_2 \dots \\ &\times \int_0^{t_{n-1}} dt_n [V(t_1), [V(t_2), \dots [V(t_n), w(0)]]] . \end{aligned} \quad (6.6)$$

Performing the trace over reservoir variables

$$\begin{aligned} \rho(t) &= \rho(0) + \sum_{n=1}^{\infty} \left(-\frac{i}{\hbar} \right)^n \int_0^t dt_1 \int_0^{t_1} dt_2 \dots \int_0^{t_{n-1}} dt_n \\ &\times \text{Tr}_R \{ [V(t_1), [V(t_2), \dots [V(t_n), \rho_R \otimes \rho(0)]]] \} \\ &\equiv (1 + U_1(t) + U_2(t) + \dots) \rho(0) \\ &\equiv U(t) \rho(0) \end{aligned} \quad (6.7)$$

where

$$U_n(t) = \left(-\frac{i}{\hbar} \right)^n \text{Tr}_R \int_0^t dt_1 \int_0^{t_1} dt_2 \cdots \times \int_0^{t_{n-1}} dt_n [V(t_1), [V(t_2), \dots [V(t_n), \rho_R \otimes (\cdot)]]] \dots . \quad (6.8)$$

Thus

$$\begin{aligned} \frac{d\rho}{dt} &= [\dot{U}_1(t) + \dot{U}_2(t) + \dots] U(t)^{-1} \rho(t) \\ &\equiv l(t) \rho(t) \end{aligned} \quad (6.9)$$

where the generator of time development is

$$l(t) = [\dot{U}_1(t) + \dot{U}_2(t) + \dots] U(t)^{-1} . \quad (6.10)$$

We now assume that $V(t)$ is such that

$$\text{Tr}_R(V(t)\rho_R) = 0 . \quad (6.11)$$

This ensures that $U_1(t) = 0$. If the perturbation is weak we may drop terms from $l(t)$ of order higher than two. Thus

$$\begin{aligned} l(t) &= \dot{U}_2(t) \\ &= -\frac{1}{\hbar^2} \int_0^t dt_1 \text{Tr}_R[V(t), [V(t_1), \rho_R \otimes (\cdot)]] . \end{aligned} \quad (6.12)$$

Thus to second order in the perturbation

$$\frac{d\rho}{dt} = -\frac{1}{\hbar^2} \int_0^t dt_1 \text{Tr}_R[V(t), [V(t_1), \rho_R \otimes \rho(t)]] . \quad (6.13)$$

The next-order correction is at least quartic in the coupling and thus we expect (6.13) to be a good approximation.

Let us now consider the case of a damped simple harmonic oscillator. In this case

$$V(t) = \hbar(a^\dagger \Gamma(t) e^{i\omega_0 t} + a \Gamma^\dagger(t) e^{-i\omega_0 t}) \quad (6.14)$$

where

$$\Gamma(t) = \sum_j g_j b_j e^{-i\omega_j t} , \quad (6.15)$$

and

$$[b_j, b_k^\dagger] = \delta_{jk} . \quad (6.16)$$

Substituting (6.14) into (6.13) we find that the following integrals are required

$$I_1 = \int_0^t dt_1 \langle \Gamma(t) \Gamma(t_1) \rangle e^{i\omega_0(t+t_1)} , \quad (6.17)$$

$$I_2 = \int_0^t dt_1 \langle \Gamma^\dagger(t) \Gamma^\dagger(t_1) \rangle e^{-i\omega_0(t+t_1)} , \quad (6.18)$$

$$I_3 = \int_0^t dt_1 \langle \Gamma(t) \Gamma^\dagger(t_1) \rangle e^{i\omega_0(t-t_1)} , \quad (6.19)$$

$$I_4 = \int_0^t dt_1 \langle \Gamma^\dagger(t) \Gamma(t_1) \rangle e^{-i\omega_0(t-t_1)} \quad (6.20)$$

which we now evaluate.

Using the definition of $\Gamma(t)$ we have

$$I_1 = \int_0^t dt_1 \sum_{i,j} g_i g_j \langle b_i b_j \rangle_R e^{-i(\omega_i t + \omega_j t_1)} e^{i\omega_0(t+t_1)} . \quad (6.21)$$

Converting the sum over modes to a frequency-space integral

$$I_1 = \int_0^t dt_1 \int_0^\infty \frac{d\omega_1}{2\pi} \rho(\omega_1) \int_0^\infty \frac{d\omega_2}{2\pi} \rho(\omega_2) g(\omega_1) g(\omega_2) \langle b(\omega_1) b(\omega_2) \rangle_R \times e^{-i(\omega_1 t + \omega_2 t_1) + i\omega_0(t+t_1)} \quad (6.22)$$

where $\rho(\omega)$ is the density of states function.

For a thermal bath the phase dependent correlation function $\langle b(\omega_1) b(\omega_2) \rangle_R = 0$. However, certain specially prepared reservoirs such as squeezed reservoirs may have phase-dependent correlations.

In order to include these we now assume that

$$\langle b(\omega_1) b(\omega_2) \rangle = 2\pi M(\omega_1) \delta(2\omega_0 - \omega_1 - \omega_2) \quad (6.23)$$

which corresponds to a multimode squeezed vacuum state with the carrier frequency equal to the cavity resonance frequency. Thus

$$I_1 = \int_0^t dt_1 \int_0^\infty \frac{d\omega}{2\pi} \rho(\omega) \rho(2\omega_0 - \omega) g(\omega) g(2\omega_0 - \omega) M(\omega) e^{i(\omega_0 - \omega)(t-t_1)} . \quad (6.24)$$

Note that the time integral depends only on $t - t_1$. This suggests the change of variable $\tau = t - t_1$ and thus

$$I_1 = \int_0^t d\tau \int_0^\infty \frac{d\omega}{2\pi} \rho(\omega) \rho(2\omega_0 - \omega) g(\omega) g(2\omega_0 - \omega) M(\omega) e^{i(\omega_0 - \omega)\tau} . \quad (6.25)$$

We now make the first Markov approximation by assuming $\rho(\omega)$, $g(\omega)$ and $M(\omega)$ are slowly varying functions around $\omega = \omega_0$, where ω_0 is very large. Thus it is convenient to make the change of variable $\varepsilon = \omega - \omega_0$ and write

$$I_1 \approx \int_0^\infty d\tau \int_{-\infty}^\infty \frac{d\varepsilon}{2\pi} \rho^2(\varepsilon + \omega_0) g^2(\varepsilon + \omega_0) M(\varepsilon + \omega_0) e^{-i\varepsilon\tau} , \quad (6.26)$$

assuming a symmetry around ω_0 . Since the integral over frequency is assumed to be a rapidly decaying function of time we have extended the upper limit of the time integration to infinity. Interchanging the order of the time and frequency integral this term becomes

$$I_1 \approx \int_{-\infty}^\infty \frac{d\varepsilon}{2\pi} \rho^2(\varepsilon + \omega_0) g^2(\varepsilon + \omega_0) M(\varepsilon + \omega_0) \left[\pi\delta(\varepsilon) - i \text{PV} \left(\frac{1}{\varepsilon} \right) \right] \quad (6.27)$$

where we have used

$$\int_0^\infty d\tau e^{\pm i\varepsilon\tau} = \pi\delta(\varepsilon) \pm i \text{PV} \left(\frac{1}{\varepsilon} \right) \quad (6.28)$$

with PV being the Cauchy principal value part defined by

$$\text{PV} \int_{-a}^b \frac{f(\omega)}{\omega} d\omega = \lim_{\varepsilon \rightarrow 0} \left(\int_{-a}^{-\varepsilon} \frac{f(\omega)}{\omega} d\omega + \int_\varepsilon^b \frac{f(\omega)}{\omega} d\omega \right) . \quad (6.29)$$

If we now define the damping rate γ by

$$\gamma \equiv \rho^2(\omega_0) g^2(\omega_0) \quad (6.30)$$

and a term

$$\bar{\Delta} = \text{PV} \int_{-\infty}^\infty \frac{d\varepsilon}{2\pi} \frac{1}{\varepsilon} \rho^2(\varepsilon + \omega_0) g^2(\varepsilon + \omega_0) M(\varepsilon + \omega_0) \quad (6.31)$$

then

$$I_1 = \frac{\gamma}{2} M(\omega_0) + i\bar{\Delta} . \quad (6.32)$$

Proceeding in a similar way we find

$$I_2 = \frac{\gamma}{2} M^*(\omega_0) - i\bar{\Delta} , \quad (6.33)$$

$$I_3 = \frac{\gamma}{2} (N(\omega_0) + 1) - i\Delta , \quad (6.34)$$

$$I_4 = \frac{\gamma}{2} N(\omega_0) - i\Delta' , \quad (6.35)$$

where the function $N(\omega)$ is defined by

$$\langle b^\dagger(\omega)b(\omega') \rangle = 2\pi N(\omega)\delta(\omega - \omega')$$

and is thus proportional to the intensity spectrum of the reservoir. The term Δ is defined by

$$\Delta = PV \int_{-\infty}^{\infty} \frac{d\varepsilon}{2\pi} \frac{1}{\varepsilon} \rho^2(\omega_0 + \varepsilon) g^2(\omega_0 + \varepsilon) (N(\omega_0 + \varepsilon) + 1) . \quad (6.36)$$

This term represents a small shift in the frequency of the oscillator. In the case where the system is a two-level atom, this term contributes to the Lamb shift which we discuss in Chap. 10. In what follows we ignore the effects of Δ and $\bar{\Delta}$.

Substituting the above results into (6.13) we find that the evolution of the system's density operator in the interaction picture is described by the master equation

$$\begin{aligned} \frac{d\rho}{dt} = & \frac{\gamma}{2} (N + 1)(2a\rho a^\dagger - a^\dagger a\rho - \rho a^\dagger a) + \frac{\gamma}{2} N(2a^\dagger \rho a - a a^\dagger \rho - \rho a a^\dagger) \\ & + \frac{\gamma}{2} M(2a^\dagger \rho a^\dagger - a^\dagger a^\dagger \rho - \rho a^\dagger a^\dagger) + \frac{\gamma}{2} M^*(2a\rho a - a a^\dagger \rho - \rho a a^\dagger) . \end{aligned} \quad (6.37)$$

(For convenience, we have suppressed the functional dependence of $N(\omega_0)$ and $M(\omega_0)$).

If the bath is in thermal equilibrium at temperature T , $M = 0$ and

$$N(\omega_0) = (e^{\hbar\omega_0/kT} - 1)^{-1} \quad (6.38)$$

which is just the mean number of bath quanta at frequency ω_0 . In this case the master equation considerably simplifies. If the bath temperature is zero, $N = 0$, and the master equation simplifies further. In general the positivity of the density operator requires, $|M|^2 \leq N(N + 1)$.

Equations of motion for the expectation values of system operators may be directly derived from the master equation, (6.37). For example, the mean

amplitude of the simple harmonic oscillator is given by

$$\frac{d\langle a \rangle}{dt} = \text{Tr} \left\{ a \frac{d\hat{\rho}}{dt} \right\} = -\frac{\gamma}{2} \langle a \rangle \quad (6.39)$$

which has the solution

$$\langle a(t) \rangle = \langle a(0) \rangle e^{-\gamma t/2}. \quad (6.40)$$

(Note in the Schrödinger picture the mean amplitude evolves as $\langle a(t) \rangle = \langle a(0) \rangle e^{-i\omega t} e^{-\gamma t/2}$). Thus the mean amplitude decays at a rate $\gamma/2$. The mean number of quanta $\langle n \rangle = \langle a^\dagger a \rangle$ obeys the equation

$$\frac{d\langle a^\dagger a \rangle}{dt} = -\gamma \langle a^\dagger a \rangle + \gamma N. \quad (6.41)$$

The solution to this equation is

$$\langle n(t) \rangle = \langle n(0) \rangle e^{-\gamma t} + N(1 - e^{-\gamma t}). \quad (6.42)$$

In the steady state $\langle n(t) \rangle \rightarrow N$ and the mean number of quanta in the oscillator is equal to the mean number of quanta in the reservoir at that temperature. The role of the terms multiplied by M can be seen by evaluating the equation of motion for $\langle a^2 \rangle$,

$$\frac{d}{dt} \langle a^2 \rangle = -\gamma \langle a^2 \rangle + \gamma M. \quad (6.43)$$

Thus these terms lead to a driving force on the second-order phase dependent moments.

The master equation (6.37) applies to a free damped harmonic oscillator in the interaction picture. If the harmonic oscillator is perturbed by an additional interaction \mathcal{H}_I , the master equation in the Schrödinger picture becomes

$$\begin{aligned} \frac{d\rho}{dt} = & -\frac{i}{\hbar} [\mathcal{H}_0 + \mathcal{H}_I, \rho] + \frac{\gamma}{2} (N + 1)(2a\rho a^\dagger - a^\dagger a\rho - \rho a^\dagger a) \\ & + \frac{\gamma}{2} N(2a^\dagger \rho a - a a^\dagger \rho - \rho a a^\dagger) - \frac{\gamma}{2} M(2a^\dagger \rho a^\dagger - (a^\dagger)^2 \rho - \rho (a^\dagger)^2) \\ & - \frac{\gamma}{2} M^*(2a\rho a - a^2 \rho - \rho a^2). \end{aligned} \quad (6.44)$$

In general, the equations of motion for the mean amplitude, mean quantum number etc. are not as easily obtained from (6.44), as they were for the free damped harmonic oscillator. To proceed in such situations, it is desirable to convert the master equation to an equivalent c-number partial differential equation. We now discuss various ways this may be done.

6.2 Equivalent c-Number Equations

6.2.1 Photon Number Representation

The operator master equation may be converted into an equation for the matrix elements of ρ in the number state basis:

$$\begin{aligned} \frac{\partial \rho_{mn}}{\partial t} = & \gamma N [(nm)^{1/2} \rho_{m-1, n-1} - \frac{1}{2}(m+n+2) \rho_{mn}] \\ & + \gamma(N+1) \{ [(m+1)(n+1)]^{1/2} \rho_{m+1, n+1} - \frac{1}{2}(m+n) \rho_{mn} \} \\ & - \frac{\gamma}{2} M \{ 2[m(n+1)]^{1/2} \rho_{m-1, n+1} - \sqrt{(n+1)(n+2)} \rho_{m, n+2} \\ & - \sqrt{m(m-1)} \rho_{m-2, n} \} - \frac{\gamma}{2} M^* \{ 2[n(m+1)]^{1/2} \rho_{m+1, n-1} \\ & - \sqrt{(m+1)(m+2)} \rho_{m+2, n} - \sqrt{n(n-1)} \rho_{m, n-2} \} \end{aligned} \quad (6.45)$$

where $\rho_{m, n} \equiv \langle m | \rho | n \rangle$. This gives an infinite hierarchy of coupled equations for the off-diagonal matrix elements. When $M = 0$ the diagonal elements $\rho_{m, m}$ are coupled only amongst themselves and not coupled to the off-diagonal elements. In this case the diagonal elements satisfy

$$\frac{dP(n)}{dt} = t_+(n-1)P(n-1) + t_-(n+1)P(n+1) - [t_+(n) + t_-(n)]P(n) \quad (6.46)$$

where we have set $P(n) = \langle n | \rho | n \rangle$ and defined the *transition probabilities*

$$t_+(n) \equiv \gamma N(n+1) , \quad (6.47)$$

$$t_-(n) \equiv \gamma(N+1)n . \quad (6.48)$$

In the steady state the detailed balance condition holds:

$$t_-(n)P(n) = t_+(n-1)P(n-1) \quad (6.49)$$

and the steady state solution is found by iteration

$$P_{ss}(n) = P(0) \prod_{k=1}^n \frac{t_+(k-1)}{t_-(k)} . \quad (6.50)$$

Thus the steady state solution for the ordinary damped harmonic oscillator ($M = 0$) is

$$P_{ss}(n) = \frac{1}{1+N} \left(\frac{N}{1+N} \right)^n . \quad (6.51)$$

An optical cavity damped into a reservoir with phase-independent correlation functions has a power law photon number distribution of thermal light.

In the more general case $M \neq 0$, or when there are additional terms in the master equation such as linear driving with the Hamiltonian $\mathcal{H}_0 = \hbar[\varepsilon(t)a^\dagger + \varepsilon^*(t)a]$, the coupling of diagonal and off-diagonal matrix elements makes the photon number representation less convenient for determining $\rho(t)$.

6.2.2 P Representation

An operator master equation may be transformed to a c-number equation using the Glauber–Sudarshan representation for ρ . It is necessary to first establish the rules for converting operators to an equivalent c-number form. We know the relations

$$a|\alpha\rangle = \alpha|\alpha\rangle , \quad (6.52)$$

$$\langle\alpha|a^\dagger = \alpha^*\langle\alpha| . \quad (6.53)$$

To derive other relations it is convenient to use the Bargmann state $\|\alpha\rangle$ defined by

$$\|\alpha\rangle = e^{1/2|\alpha|^2}|\alpha\rangle \quad (6.54)$$

so that

$$\begin{aligned} a^\dagger\|\alpha\rangle &= \sum_n \frac{\alpha^n}{\sqrt{n!}} \sqrt{n+1}|n+1\rangle \\ &= \frac{\partial}{\partial\alpha}\|\alpha\rangle . \end{aligned} \quad (6.55)$$

Similarly

$$\langle\alpha\|\alpha = \frac{\partial}{\partial\alpha^*}\langle\alpha\| . \quad (6.56)$$

Hence, given the P representation

$$\rho = \int d^2\alpha \|\alpha\rangle\langle\alpha\| e^{-|\alpha|^2} P(\alpha) \quad (6.57)$$

we find

$$a^\dagger\rho = \int d^2\alpha \frac{\partial}{\partial\alpha} (\|\alpha\rangle\langle\alpha\|) e^{-|\alpha|^2} P(\alpha) \quad (6.58)$$

and integrating by parts

$$a^\dagger\rho = \int d^2\alpha \|\alpha\rangle\langle\alpha\| e^{-|\alpha|^2} \left(\alpha^* - \frac{\partial}{\partial\alpha} \right) P(\alpha) . \quad (6.59)$$

We can thus make an operator correspondence between a^\dagger and $\alpha^* - \partial/\partial\alpha$. A similar formula holds for a . Summarizing we have the following operator correspondences:

$$\begin{aligned} a\rho &\leftrightarrow \alpha P(\alpha) , \\ a^\dagger \rho &\leftrightarrow \left(\alpha^* - \frac{\partial}{\partial\alpha} \right) P(\alpha) , \\ \rho a &\leftrightarrow \left(\alpha - \frac{\partial}{\partial\alpha^*} \right) P(\alpha) , \\ \rho a^\dagger &\leftrightarrow \alpha^* P(\alpha) . \end{aligned} \tag{6.60}$$

Consider the correspondences for operator products

$$a^\dagger a\rho \rightarrow \left(\alpha^* - \frac{\partial}{\partial\alpha} \right) \alpha P , \tag{6.61a}$$

$$\rho a^\dagger a \rightarrow \left(\alpha - \frac{\partial}{\partial\alpha^*} \right) \alpha^* P . \tag{6.61b}$$

Notice that the order of the operators in (6.61b) reverses, since acting on ρ , they operate from the right, whereas on P , they operate from the left.

Note that α and α^* are not independent variables. In terms of real variables we may write

$$\begin{aligned} \alpha &= x + iy , \\ \alpha^* &= x - iy , \\ \frac{\partial}{\partial\alpha} &= \frac{1}{2} \left(\frac{\partial}{\partial x} - i \frac{\partial}{\partial y} \right) , \\ \frac{\partial}{\partial\alpha^*} &= \frac{1}{2} \left(\frac{\partial}{\partial x} + i \frac{\partial}{\partial y} \right) . \end{aligned} \tag{6.62}$$

To obtain a c-number equation we substitute the P representation for ρ into the master equation and use the operator correspondences. This leads to the equation

$$\frac{\partial P(\alpha)}{\partial t} = \left[\frac{1}{2}\gamma \left(\frac{\partial}{\partial\alpha} \alpha + \frac{\partial}{\partial\alpha^*} \alpha^* \right) + \frac{\gamma}{2} \left(M^* \frac{\partial^2}{\partial\alpha^{*2}} + M \frac{\partial^2}{\partial\alpha^2} \right) + \gamma N \frac{\partial^2}{\partial\alpha\partial\alpha^*} \right] P(\alpha) . \tag{6.63}$$

When $M > N$ this equation has non-positive, definite diffusion, hence the P representation is unable to describe the system in terms of a classical stochastic process. Alternative representations will be discussed later in this chapter. When $M \leq N$ (6.63) has the form of a Fokker–Planck equation. We shall discuss some useful properties of Fokker–Planck equations below.

6.2.3 Properties of Fokker–Planck Equations

A general Fokker–Planck equation in n variables may be written in the form

$$\frac{\partial}{\partial t} P(\mathbf{x}) = \left[-\frac{\partial}{\partial x_j} A_j(\mathbf{x}) + \frac{1}{2} \frac{\partial}{\partial x_i} \frac{\partial}{\partial x_j} D_{ij}(\mathbf{x}) \right] P(\mathbf{x}) . \quad (6.64)$$

The first derivative term determines the mean or deterministic motion and is called the *drift term*, while the second derivative term, provided its coefficient is positive definite, will cause a broadening or diffusion of $P(x, t)$ and is called the *diffusion term*. $\mathbf{A} = (A_j)$ is the *drift vector* and $\mathbf{D} = (D_{ij})$ is the *diffusion matrix*. The different role of the two terms may be seen in the equations of motion for $\langle x_k \rangle$ and $\langle x_k x_l \rangle$.

$$\frac{d\langle x_k \rangle}{dt} = \langle A_k \rangle , \quad (6.65)$$

$$\frac{d\langle x_k x_l \rangle}{dt} = \langle x_k A_l \rangle + \langle x_l A_k \rangle + \frac{1}{2} \langle D_{kl} + D_{lk} \rangle . \quad (6.66)$$

We see that A_k determines the motion of the mean amplitude whereas D_{lk} enters into the equation for correlations.

Thus, for the damped harmonic oscillator described by (6.63)

$$\frac{d\langle \alpha \rangle_p}{dt} = -\frac{\gamma}{2} \langle \alpha \rangle_p , \quad (6.67)$$

$$\frac{d\langle \alpha^* \alpha \rangle_p}{dt} = -\gamma \langle \alpha^* \alpha \rangle_p + \gamma N , \quad (6.68)$$

which are equivalent to (6.39 and 41) derived directly from the master equation (6.37). Note that the expectation values $\langle \rangle_p$ are defined by integrals over $P(\alpha, t)$.

6.2.4 Steady State Solutions – Potential Conditions

For many problems in nonlinear optics it is sufficient to know the steady state solution. That is the solution after all transients have died out. We shall therefore seek a steady state solution to (6.64).

In the steady state we set the time derivatives to zero which gives

$$\frac{\partial}{\partial x_i} \left[-A_i(\mathbf{x})P(\mathbf{x}) + \frac{1}{2} \frac{\partial}{\partial x_j} D_{ij}(\mathbf{x})P(\mathbf{x}) \right] = 0 . \quad (6.69)$$

As a first attempt consider

$$A_i(\mathbf{x})P(\mathbf{x}) = \frac{1}{2} \frac{\partial}{\partial x_j} [D_{ij}(\mathbf{x})P(\mathbf{x})] \quad (6.70)$$

which implies

$$D_{ij} \frac{\partial \ln P}{\partial x_j} = 2A_i(\mathbf{x}) - \frac{\partial D_{ij}}{\partial x_j}(\mathbf{x}) . \quad (6.71)$$

Denoting $P(\mathbf{x}) = \exp[-\phi(\mathbf{x})]$ we wish to solve

$$-\frac{\partial \phi(\mathbf{x})}{\partial x_i} = 2(D^{-1})_{ij} \left[A_j(\mathbf{x}) - \frac{1}{2} \frac{\partial D_{jk}}{\partial x_k} \right] \equiv F_i(\mathbf{x}) . \quad (6.72)$$

If we consider $F_j(\mathbf{x})$ as a generalized force, $\phi(\mathbf{x})$ corresponds to a potential. The system of equations (6.72) can be solved by integration if the so called *potential conditions* are satisfied

$$\frac{-\partial^2 \phi}{\partial x_i \partial x_j} = \frac{\partial F_j}{\partial x_i} = \frac{\partial F_i}{\partial x_j} = \frac{-\partial^2 \phi}{\partial x_j \partial x_i} . \quad (6.73)$$

These conditions say that the function ϕ is well behaved and that the multivariable integral is independent of the path of integration. The potential conditions are always satisfied in the one dimensional case.

Provided the potential conditions are satisfied a steady state solution of the form

$$P(\mathbf{x}) = N \exp[-\phi(\mathbf{x})] \quad (6.74)$$

exists where

$$\phi(\mathbf{x}) = \int_0^x 2[D(\mathbf{x})^{-1}]_{ij} \left[-A_j(\mathbf{x}) + \frac{1}{2} \frac{\partial D_{jk}}{\partial x_k} \right] dx_i .$$

The turning points of the potential ϕ correspond to the values x such that for each $j = 1, \dots, n$

$$\left(A_j(\mathbf{x}) - \frac{1}{2} \frac{\partial D_{jk}(\mathbf{x})}{\partial x_k} \right) = 0 . \quad (6.75)$$

In systems where the diffusion matrix is diagonal and constant ($D_{ij} = W\delta_{ij}$) equations (6.72) become

$$-\frac{\partial \phi(\mathbf{x})}{\partial x_i} = \frac{2A_i(\mathbf{x})}{W} . \quad (6.76)$$

Hence the turning points of the potential ϕ correspond exactly to the deterministic steady state solutions, that is the steady state solutions to the first-order moment equations.

6.2.5 Time Dependent Solution

In the case where the drift term is linear in the variable (x) and the diffusion coefficient is a constant, a solution to the Fokker–Planck equation may be found using the method of *Wang and Uhlenbeck* [6.2]. We consider the Fokker–Planck equation

$$\frac{\partial P}{\partial t} = - \sum a_i \frac{\partial}{\partial x_i} (x_i P) + \frac{1}{2} d_{ij} \frac{\partial^2 P}{\partial x_i \partial x_j} . \quad (6.77)$$

The Greens function solution to this equation given by the initial condition

$$P(x_i, 0) = \delta(x_i - x_i^0)$$

is

$$P(x_i, x_i^0, t) = \frac{1}{\pi^{n/2} [\det \sigma_{ij}(t)]^{1/2}} \exp \left(- \sum_{ij} \sigma_{ij}(t)^{-1} \{ [x_i - x_i^0 \exp(a_i t)] \right. \\ \left. \times [x_j - x_j^0 \exp(a_j t)] \} \right) \quad (6.78)$$

where

$$\sigma_{ij}(t) = \frac{-2d_{ij}}{a_i + a_j} \{1 - \exp[(a_i + a_j)t]\} .$$

The solution for a damped harmonic oscillator initially in a coherent state with $P(\alpha, 0) = \delta^2(\alpha - \alpha_0)$ is

$$P(\alpha, t) = \frac{1}{\pi N(1 - e^{-\gamma t})} \exp \left(\frac{-|\alpha - \alpha_0 e^{-\gamma t/2}|^2}{N(1 - e^{-\gamma t})} \right) . \quad (6.79)$$

This represents an initial coherent state undergoing relaxation with a heat bath. Its coherent amplitude decays away and fluctuations from the heat bath cause its P function to assume a Gaussian form characteristic of thermal noise. The width of the distribution grows with time until the oscillator reaches equilibrium with the heat bath.

From the above solution we may construct solutions for all initial conditions which have a non-singular P representation. It is not, however, possible to construct the solution for the oscillator initially in a squeezed state since no non-singular P function exists for such states. Nor can we find the solution for an oscillator damped into a squeezed bath.

We now consider alternative methods of converting the operator master equation to a c-number equation, which can be used for initial squeezed states or a squeezed bath.

6.2.6 Q Representation

A c-number representation for the Q function is obtained by first normally ordering all operator products. We shall make use of the following theorem [6.3].

If $f(a, a^\dagger)$ is a function which may be expanded in a power series in a and a^\dagger , then

$$[a, f(a, a^\dagger)] = \frac{\partial f}{\partial a^\dagger} , \quad (6.80a)$$

$$[a^\dagger, f(a, a^\dagger)] = -\frac{\partial f}{\partial a} . \quad (6.80b)$$

The proof of these relations is as follows: We assume that we may expand f in antinormal order $f^{(a)}$

$$[a^\dagger, f] = \sum_{r,s} f_{r,s}^{(a)} [a^\dagger, a^r (a^\dagger)^s] . \quad (6.81)$$

Using the following result for the commutators

$$[A, BC] = [A, B]C + B[A, C] \quad (6.82)$$

where A , B and C are noncommuting operators, we may write

$$\begin{aligned} [a^\dagger, f] &= \sum_{r,s} f_{r,s}^{(a)} \{ [a^\dagger, a^r] a^{s\dagger} + a^r [a^\dagger, a^{s\dagger}] \} \\ &= - \sum_{r,s} f_{r,s}^{(a)} r a^{r-1} a^{s\dagger} \end{aligned} \quad (6.83)$$

$$= - \frac{\partial f}{\partial a} . \quad (6.84)$$

The proof of (6.80a) follows in a similar way.

We consider as an example the term

$$\rho a^\dagger a = a^\dagger \rho a - [a^\dagger, \rho] a . \quad (6.85)$$

Using the result above

$$\rho a^\dagger a = a^\dagger \rho a + \frac{\partial \rho}{\partial a} a . \quad (6.86)$$

Taking matrix elements in coherent states yields

$$\begin{aligned}\langle \alpha | \rho a^\dagger a | \alpha \rangle &= \alpha \left\langle \alpha \left| a^\dagger \rho + \frac{\partial \rho}{\partial a} \right| \alpha \right\rangle \\ &= \left(|\alpha|^2 + \alpha \frac{\partial}{\partial \alpha} \right) Q(\alpha).\end{aligned}\quad (6.87)$$

Following this procedure we may convert the master equation for the damped harmonic oscillator into a c-number equation for the Q function

$$\frac{\partial Q}{\partial t} = \frac{\gamma}{2} \left(\frac{\partial}{\partial \alpha} \alpha + \frac{\partial}{\partial \alpha^*} \alpha^* \right) Q + \frac{\gamma}{2} \left[M^* \frac{\partial^2}{\partial \alpha^{*2}} - M \frac{\partial^2}{\partial \alpha^2} + 2(N+1) \frac{\partial^2 Q}{\partial \alpha \partial \alpha^*} \right] Q.\quad (6.88)$$

This differs from the corresponding equation of motion for the P function only through the phase independent diffusion coefficient which is $N+1$ rather than N . This is sufficient to give a positive definite diffusion matrix when the bath is in an ideal squeezed state.

To illustrate the use of the Q function consider a damped oscillator which is initially in the squeezed state $|\alpha_0, r\rangle$. Using the *Wang and Uhlenbeck* solution for an initial δ -function and convoluting this with the Gaussian Q function for an initial squeezed state we arrive at the result

$$Q(\alpha, t) = \frac{1}{2\pi\sqrt{\det \sigma(t)}} \exp[-\frac{1}{2}\mathbf{u}(t)^T \sigma^{-1}(t) \mathbf{u}(t)]\quad (6.89)$$

where

$$\begin{aligned}\mathbf{u}(t) &= \begin{pmatrix} \alpha - \alpha_0 e^{-\gamma t/2} \\ \alpha^* - \alpha_0^* e^{-\gamma t/2} \end{pmatrix} \\ \sigma(t) &= \begin{pmatrix} -\sinh 2r & \cosh 2r + 1 \\ \cosh 2r + 1 & -\sinh 2r \end{pmatrix} \frac{e^{-\gamma t}}{2} + \begin{pmatrix} M & N+1 \\ N+1 & M^* \end{pmatrix} (1 - e^{-\gamma t}).\end{aligned}$$

The variances for the quadrature phase operators X_i for the oscillator are then easily found to be

$$V(X_1) = \frac{1}{4}[(e^{-2r} - 1)e^{-\gamma t} + 2(N + \text{Re}\{M\})(1 - e^{-\gamma t}) + 1],\quad (6.90a)$$

$$V(X_2) = \frac{1}{4}[(e^{2r} + 1)e^{-\gamma t} + 2(N - \text{Re}\{M\})(1 - e^{-\gamma t}) + 1].\quad (6.90b)$$

In Fig. 6.1 we depict the evolution of an initial squeezed state coupled to a zero temperature reservoir ($N = M = 0$). The amplitude of the squeezed state damps to zero and the variances in X_1 and X_2 become equal at the value one corresponding to the vacuum.

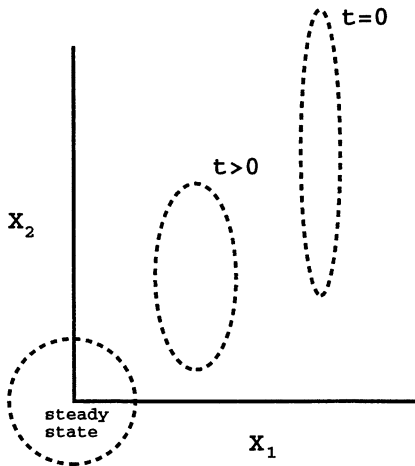


Fig. 6.1. Evolution of the error contour of an initial squeezed state of a simple harmonic oscillator damped into a zero temperature heat bath

6.2.7 Wigner Function

Alternatively one may convert the operator master equation into a c-number equation via the Wigner function. This is best accomplished by deriving an equation for the characteristic function

$$\chi(\beta) = \text{Tr}\{D\rho\} \quad (6.91)$$

where

$$D = e^{\beta a^\dagger - \beta^* a} .$$

An equation of motion for $\chi(\beta)$ may be derived as follows

$$\frac{\partial \chi(\beta)}{\partial t} = \text{Tr} \left\{ D \frac{\partial \rho}{\partial t} \right\} . \quad (6.92)$$

To illustrate the technique we shall derive the equation of motion for the Wigner function of a damped harmonic oscillator.

We require some operator rules to convert to differential operators. Writing D in normal order

$$D = e^{-\beta\beta^*/2} e^{\beta a^\dagger} e^{-\beta^* a} , \quad (6.93)$$

$$\frac{\partial}{\partial \beta} D = -\frac{\beta^*}{2} D + a^\dagger D , \quad (6.94)$$

or

$$a^\dagger D = \left(\frac{\partial}{\partial \beta} + \frac{\beta^*}{2} \right) D . \quad (6.95)$$

Similarly we may show

$$Da = \left(\frac{-\beta}{2} - \frac{\partial}{\partial \beta^*} \right) D . \quad (6.96)$$

Writing D in antinormal order

$$D = e^{\beta\beta^*/2} e^{-\beta^*a} e^{\beta a^\dagger} . \quad (6.97)$$

Thus

$$\frac{\partial}{\partial \beta} D = \frac{\beta^*}{2} D + Da^\dagger \quad (6.98)$$

or

$$Da^\dagger = \left(\frac{\partial}{\partial \beta} - \frac{\beta^*}{2} \right) D \quad (6.99)$$

and similarly

$$aD = \left(\frac{\beta}{2} - \frac{\partial}{\partial \beta^*} \right) D . \quad (6.100)$$

Then using these rules the master equation (6.37) yields the following equation for the characteristic function

$$\begin{aligned} \frac{\partial \chi(\beta)}{\partial t} &= \frac{\gamma}{2} \left(-|\beta|^2 - \beta^* \frac{\partial}{\partial \beta^*} - \beta \frac{\partial}{\partial \beta} \right) \chi(\beta) - \gamma N |\beta|^2 \chi(\beta) \\ &\quad - \frac{\gamma M}{2} (\beta^*)^2 \chi(\beta) - \frac{\gamma M^*}{2} \beta^2 \chi(\beta) . \end{aligned} \quad (6.101)$$

The equation for the Wigner function is obtained by taking the Fourier transform of this equation since

$$W(\alpha) = \int e^{\beta^*\alpha - \beta\alpha^*} \chi(\beta) d^2\beta . \quad (6.102)$$

Thus

$$\begin{aligned} \int e^{\beta^*\alpha - \beta\alpha^*} \beta^* \beta \chi(\beta) d^2\beta &= - \int \frac{\partial}{\partial \alpha} \frac{\partial}{\partial \alpha^*} (e^{\beta^*\alpha - \beta\alpha^*}) \chi(\beta) d^2\beta \\ &= - \frac{\partial^2 W(\alpha)}{\partial \alpha \partial \alpha^*} , \end{aligned} \quad (6.103)$$

and

$$\begin{aligned} \int e^{\beta^* \alpha - \alpha^* \beta} \beta^* \frac{\partial}{\partial \beta^*} \chi(\beta) d^2 \beta &= \frac{\partial}{\partial \alpha} \int (e^{\beta^* \alpha - \alpha^* \beta}) \frac{\partial}{\partial \beta^*} \chi(\beta) d^2 \beta \\ &= - \frac{\partial}{\partial \alpha} \int \chi(\beta) \frac{\partial}{\partial \beta^*} (e^{\beta^* \alpha - \alpha^* \beta}) d^2 \beta \end{aligned} \quad (6.104)$$

$$= - \frac{\partial}{\partial \alpha} [\alpha W(\alpha)] . \quad (6.105)$$

Using these results we may write the equation for the Wigner function as

$$\begin{aligned} \frac{\partial W(\alpha)}{\partial t} &= \frac{\gamma}{2} \left(\frac{\partial}{\partial \alpha} \alpha + \frac{\partial}{\partial \alpha^*} \alpha^* \right) W \\ &\quad + \frac{\gamma}{2} \left[M^* \frac{\partial^2}{\partial \alpha^{*2}} + M \frac{\partial^2}{\partial \alpha^2} + 2 \left(N + \frac{1}{2} \right) \frac{\partial^2}{\partial \alpha \partial \alpha^*} \right] W . \end{aligned} \quad (6.106)$$

A comparison of the three equations (6.63, 88 and 106) for the P , Q and Wigner functions show that they differ only in the coefficient of the diffusion term being γN , $\gamma(N + 1)$ and $\gamma(N + 1/2)$, respectively. However, the additional $+ \gamma$ and $+\gamma/2$ in the equations for the Q and Wigner function are sufficient to ensure that these equations have positive definite diffusion.

6.2.8 Generalized P Representation

In our study of nonlinear problems we shall find systems which either do not give Fokker–Planck equations in the Q and Wigner representations or no steady state solution may readily be found. For some systems a steady state solution in terms of a Glauber–Sudarshan P representation does not exist. For such systems the complex P representation is sometimes useful in deriving a steady state solution to Fokker–Planck equations. The positive P representation is useful when it is desirable to have a Fokker–Planck equation with a positive definite diffusion term, as is necessary in order to deduce the corresponding stochastic differential equations.

Master equations may be converted to a c-number representation using the complex P representation by an analogous set of operator rules used for the diagonal P representation.

The nondiagonal coherent state projection operator is defined as

$$\Lambda(\alpha) = \frac{|\alpha\rangle\langle\beta^*|}{\langle\beta^*|\alpha\rangle} \quad (6.107)$$

where (α) denotes (α, β) . The following identities hold

$$\begin{aligned} a\Lambda(\alpha) &= \alpha\Lambda(\alpha), & a^\dagger\Lambda(\alpha) &= \left(\beta + \frac{\partial}{\partial\alpha}\right)\Lambda(\alpha) , \\ \Lambda(\alpha)a^\dagger &= \Lambda(\alpha)\beta, & \Lambda(\alpha)a &= \left(\frac{\partial}{\partial\beta} + \alpha\right)\Lambda(\alpha) . \end{aligned} \quad (6.108)$$

By substituting the above identities into (4.61) defining the generalized P representation, and using partial integration (providing the boundary terms vanish) these identities can be used to generate operations on the P function depending on the representation.

a) *Complex P representation*

$$\begin{aligned} a\rho &\leftrightarrow \alpha P(\alpha), & a^\dagger\rho &\leftrightarrow \left(\beta - \frac{\partial}{\partial\alpha}\right)P(\alpha) , \\ \rho a^\dagger &\leftrightarrow \beta P(\alpha), & \rho a &\leftrightarrow \left(\alpha - \frac{\partial}{\partial\beta}\right)P(\alpha) . \end{aligned} \quad (6.109)$$

This procedure yields a very similar equation to that for the Glauber–Sudarshan P function. We assume that, by appropriate reordering of the differential operators, we can reduce an operator master equation to the form [where $(\alpha, \beta) = (\alpha) = (\alpha^{(1)}, \alpha^{(2)})$]

$$\begin{aligned} \frac{\partial\rho}{\partial t} &= \int_c \int_{c'} \Lambda(\alpha) \frac{\partial P(\alpha)}{\partial t} d\alpha d\beta \\ &= \int_c \int_{c'} d\alpha^{(1)} d\alpha^{(2)} P(\alpha) \left[A^\mu(\alpha) \frac{\partial}{\partial\alpha^\mu} + \frac{1}{2} D^{\mu\nu}(\alpha) \frac{\partial}{\partial\alpha^\mu} \frac{\partial}{\partial\alpha^\nu} \right] \Lambda(\alpha) . \end{aligned} \quad (6.110)$$

We now integrate by parts and if we can neglect boundary terms, which may be made possible by an appropriate choice of contours, c and c' , at least one solution is obtained by equating the coefficients of $\Lambda(\alpha)$

$$\frac{\partial P(\alpha)}{\partial t} = \left[-\frac{\partial}{\partial\alpha^\mu} A^\mu(\alpha) + \frac{1}{2} \frac{\partial}{\partial\alpha^\mu} \frac{\partial}{\partial\alpha^\nu} D^{\mu\nu}(\alpha) \right] P(\alpha) . \quad (6.111)$$

This equation is sufficient to imply (6.110) but is not a unique equation because the $\Lambda(\alpha)$ are not linearly independent. The Fokker–Planck equation has the same form as that derived using the diagonal P representation with α^* replaced by β .

It should be noted that for the complex P representation, $A^\mu(\alpha)$ and $D^{\mu\nu}(\alpha)$ are always analytic in (α) , hence if $P(\alpha)$ is initially analytic (6.111) preserves this analyticity as time develops.

b) *Positive P Representation*

The operator identities for the positive P representation are the same as (6.109) for the complex P representation. In addition, using the analyticity of $\Lambda(\alpha, \beta)$ and noting that if

$$\alpha = \alpha_x + i\alpha_y, \quad \beta = \beta_x + i\beta_y ,$$

then

$$\frac{\partial}{\partial \alpha} \Lambda(\alpha) = \frac{\partial}{\partial \alpha_x} \Lambda(\alpha) = -i \frac{\partial}{\partial \alpha_y} \Lambda(\alpha)$$

and

$$\frac{\partial}{\partial \beta} \Lambda(\alpha) = \frac{\partial}{\partial \beta_x} \Lambda(\alpha) = -i \frac{\partial}{\partial \beta_y} \Lambda(\alpha) . \quad (6.112)$$

Thus in addition to (6.109) we also have

$$\begin{aligned} a^\dagger \rho &\leftrightarrow \left(\beta - \frac{\partial}{\partial \alpha_x} \right) P(\alpha) \leftrightarrow \left(\beta + i \frac{\partial}{\partial \alpha_y} \right) P(\alpha) , \\ pa &\leftrightarrow \left(\alpha - \frac{\partial}{\partial \beta_x} \right) P(\alpha) \leftrightarrow \left(\alpha + i \frac{\partial}{\partial \beta_y} \right) P(\alpha) . \end{aligned} \quad (6.113)$$

The positive P representation may be used to give a Fokker–Planck equation with a positive definite diffusion matrix. We shall demonstrate this in the following.

We assume that the same equation (6.64) is being considered but with a positive P representation. The symmetric diffusion matrix can always be factorized in the form

$$\mathbf{D}(\alpha) = \mathbf{B}(\alpha) \mathbf{B}^T(\alpha) .$$

We now write

$$\mathbf{A}(\alpha) = A_x(\alpha) + iA_y(\alpha) , \quad (6.114)$$

$$\mathbf{B}(\alpha) = B_x(\alpha) + iB_y(\alpha) , \quad (6.115)$$

where A_x , A_y , B_x , B_y are real. We then find that the master equation yields

$$\begin{aligned} \frac{\partial \rho}{\partial t} &= \iint d^2 \alpha d^2 \beta \Lambda(\alpha) (\partial P(\alpha)/\partial t) \\ &= \iint P(\alpha) [A_x^\mu(\alpha) \partial_\mu^x + A_y^\mu(\alpha) \partial_\mu^y + \frac{1}{2}(B_x^{\mu\sigma} B_x^{\nu\sigma} \partial_\mu^x \partial_\nu^x + B_y^{\mu\sigma} B_y^{\nu\sigma} \partial_\mu^y \partial_\nu^y \\ &\quad + 2B_x^{\mu\sigma} B_y^{\nu\sigma} \partial_\mu^x \partial_\nu^y)] \Lambda(\alpha) d^2 \alpha d^2 \beta . \end{aligned} \quad (6.116)$$

Here we have, for notational simplicity, written $\partial/\partial \alpha_x^\mu = \partial_\mu^x$ etc., and have used the analyticity of $\Lambda(\alpha)$ to make either of the replacements

$$\partial/\partial \alpha^\mu \leftrightarrow \partial_\mu^x \leftrightarrow -i \partial_\mu^y \quad (6.117)$$

in such a way as to yield (6.116). Now, provided partial integration is permissible, we deduce the Fokker–Planck equation:

$$\begin{aligned}\partial P(\alpha)/\partial t = & [-\partial_\mu^x A_x^\mu(\alpha) - \partial_\mu^y A_y^\mu(\alpha) + \frac{1}{2} [\partial_\mu^x \partial_\nu^x B_x^{\mu\sigma}(\alpha) B_x^{\nu\sigma}(\alpha) \\ & + 2 \partial_\mu^x \partial_\nu^y B_x^{\mu\sigma}(\alpha) B_y^{\nu\sigma}(\alpha) + \partial_\mu^y \partial_\nu^y B_y^{\mu\sigma}(\alpha) B_y^{\nu\sigma}(\alpha)] \} P(\alpha) .\end{aligned}\quad (6.118)$$

Again, this is not a unique time-development equation but (6.116) is a consequence of (6.118).

However, the Fokker–Planck equation (6.118) now possesses a positive semidefinite diffusion matrix in a four-dimensional space whose vectors are

$$(\alpha_x^{(1)}, \alpha_x^{(2)}, \alpha_y^{(1)}, \alpha_y^{(2)}) \equiv (\alpha_x, \beta_x, \alpha_y, \beta_y) . \quad (6.119)$$

We find the drift vector is

$$\mathcal{A}(\alpha) \equiv (A_x^{(1)}(\alpha), A_x^{(2)}(\alpha), A_y^{(1)}(\alpha), A_y^{(2)}(\alpha)) \quad (6.120)$$

and the diffusion matrix is

$$\mathcal{D}(\alpha) = \begin{pmatrix} \mathbf{B}_x \mathbf{B}_x^T & \mathbf{B}_x \mathbf{B}_y^T \\ \mathbf{B}_y \mathbf{B}_x^T & \mathbf{B}_y \mathbf{B}_y^T \end{pmatrix}(\alpha) \equiv \mathcal{B}(\alpha) \mathcal{B}^T(\alpha) \quad (6.121)$$

where

$$\mathcal{B}(\alpha) = \begin{pmatrix} \mathbf{B}_x & 0 \\ \mathbf{B}_y & 0 \end{pmatrix}(\alpha) \quad (6.122)$$

and \mathcal{D} is thus explicitly positive semidefinite.

6.3 Stochastic Differential Equations

A Fokker–Planck equation of the form

$$\frac{\partial P}{\partial t} = - \sum_i \frac{\partial}{\partial x_i} A_i(x, t) P + \frac{1}{2} \sum_{ij} \frac{\partial}{\partial x_i} \frac{\partial}{\partial x_j} [\mathbf{B}(x, t) \mathbf{B}^T(x, t)]_{ij} P \quad (6.123)$$

may be written in a completely equivalent form as

$$\frac{dx}{dt} = A(x, t) + B(x) E(t) \quad (6.124)$$

where $E(t)$ are fluctuating forces with zero mean and δ correlated in time

$$\langle E_i(t) E_j(t') \rangle = \delta_{ij} \delta(t - t') . \quad (6.125)$$

We have written (6.124) in the form of a Langevin equation. The relationship between (6.123 and 124) may be derived more rigorously in terms of stochastic differential equations where Ito's rules are used. However, the relation quoted in (6.123 and 124) is sufficient for our use. The reader is referred to the texts of

C.W. Gardiner for a complete discourse on stochastic differential equations and their applications to quantum noise problems.

We shall illustrate the use of the stochastic differential equation for a particle undergoing damping and diffusion in one dimension. This motion is described by the Fokker–Planck equation

$$\frac{\partial P(x)}{\partial t} = \kappa \frac{\partial}{\partial x} [xP(x)] + \frac{D}{2} \frac{\partial^2}{\partial x^2} P(x) \quad (6.126)$$

where κ is the damping coefficient and D is the diffusion coefficient. This equation describes an Ornstein–Uhlenbeck process. It may, for example, describe the Brownian motion of a particle under the random influence of collisions from many particles in thermal motion where the variable x represents the particle's velocity.

The Langevin equation equivalent to the Fokker–Planck Equation (6.126) is

$$\dot{x} = -\kappa x + \sqrt{D} E(t) \quad (6.127)$$

where

$$\langle E(t)E(t') \rangle = \delta(t - t') .$$

The solution to this equation is

$$x(t) = x(0)e^{-\kappa t} + \sqrt{D} \int_0^t e^{-\kappa(t-t')} E(t') dt' . \quad (6.128)$$

If the initial condition is deterministic or Gaussian distributed, then $x(t)$ is clearly Gaussian, with mean and variance

$$\langle x(t) \rangle = \langle x(0) \rangle e^{-\kappa t} , \quad (6.129)$$

$$\text{Var}[x(t)] = \left\langle \left\{ [x(0) - \langle x(0) \rangle] e^{-\kappa t} + \sqrt{D} \int_0^t e^{-\kappa(t-t')} E(t') dt' \right\}^2 \right\rangle . \quad (6.130)$$

Assuming the initial condition is independent of $E(t)$, we may write

$$\begin{aligned} \text{Var}\{x(t)\} &= \text{Var}\{x(0)\} e^{-2\kappa t} + D \int_0^t e^{-2\kappa(t-t')} dt' \\ &= \left[\text{Var}\{x(0)\} - \frac{D}{2\kappa} \right] e^{-2\kappa t} + \frac{D}{2\kappa} . \end{aligned} \quad (6.131)$$

In the steady state

$$\text{Var}\{x(t)\} = \frac{D}{2\kappa} . \quad (6.132)$$

The two time correlation function may be calculated directly, as follows

$$\begin{aligned}
 \langle x(t), x(s) \rangle &= \langle x(t)x(s) \rangle - \langle x(t) \rangle \langle x(s) \rangle \\
 &= \text{Var}\{x(0)\} e^{-\kappa(t+s)} + D \left\langle \int_0^t e^{-\kappa(t-t')} E(t') dt' \int_0^s e^{-\kappa(s-s')} E(s') ds' \right\rangle \\
 &= \text{Var}\{x(0)\} e^{-\kappa(t+s)} + D \int_0^{\min(t,s)} e^{-\kappa(t+s-2t')} dt' \\
 &= \left[\text{Var}\{x(0)\} - \frac{D}{2\kappa} \right] e^{-\kappa(t+s)} + \frac{D}{2\kappa} e^{-\kappa|t-s|}. \tag{6.133}
 \end{aligned}$$

In the stationary state

$$\langle x(t), x(s) \rangle = \frac{D}{2\kappa} e^{-\kappa|t-s|}. \tag{6.134}$$

We shall now consider the equivalent Langevin equation for the Fokker–Planck equation for the damped harmonic oscillator. The Fokker–Planck equation for the P representation is

$$\frac{\partial P}{\partial t} = \frac{\gamma}{2} \left(\frac{\partial}{\partial \alpha} \alpha + \frac{\partial}{\partial \alpha^*} \alpha^* \right) P + \gamma N \frac{\partial^2}{\partial \alpha \partial \alpha^*} P. \tag{6.135}$$

Note that we have set $M = 0$, as the P representation cannot be used with squeezed baths since the diffusion matrix is nonpositive definite. In such cases the Q -function could be used.

Equation (6.135) is an example of an Ornstein–Uhlenbeck process. The diffusion matrix is

$$D = \gamma N \begin{pmatrix} 0 & 1 \\ 1 & 0 \end{pmatrix} \tag{6.136}$$

which may be factored as

$$D = BB^T$$

where

$$B = \left(\frac{\gamma N}{2} \right)^{1/2} \begin{pmatrix} i & 1 \\ -i & 1 \end{pmatrix}. \tag{6.137}$$

Thus the stochastic differential equations become

$$\frac{d}{dt} \begin{pmatrix} \alpha \\ \alpha^* \end{pmatrix} = \begin{pmatrix} -\gamma & 0 \\ 0 & -\gamma \end{pmatrix} \begin{pmatrix} \alpha \\ \alpha^* \end{pmatrix} + \sqrt{\gamma N} \begin{pmatrix} i & 1 \\ -i & 1 \end{pmatrix} \begin{pmatrix} \eta_1(t) \\ \eta_2(t) \end{pmatrix} \tag{6.138}$$

where $\eta_1(t)$ and $\eta_2(t)$ are independent stochastic forces which satisfy

$$\langle \eta_i(t)\eta_j(t') \rangle = \delta_{ij}\delta(t - t') . \quad (6.139)$$

Equations (6.138) may be written

$$\begin{aligned} \frac{d\alpha}{dt} &= -\frac{\gamma}{2}\alpha + \sqrt{\gamma N}\eta(t) , \\ \frac{d\alpha^*}{dt} &= -\frac{\gamma}{2}\alpha + \sqrt{\gamma N}\eta^*(t) \end{aligned} \quad (6.140)$$

where

$$\eta(t) \equiv \frac{1}{\sqrt{2}} [\eta_2(t) + i\eta_1(t)]$$

is a complex stochastic force term which satisfies

$$\langle \eta(t)\eta^*(t') \rangle = \delta(t - t') .$$

An alternative factorisation is

$$B = \left(\frac{\gamma N}{2} \right)^{1/2} \begin{pmatrix} e^{i\pi/4} & e^{-i\pi/4} \\ e^{-i\pi/4} & e^{i\pi/4} \end{pmatrix} . \quad (6.141)$$

In this case

$$\frac{d\alpha}{dt} = -\frac{\gamma}{2}\alpha + \sqrt{\gamma N}\tilde{\eta} \quad (6.142)$$

where

$$\tilde{\eta} = \frac{1}{\sqrt{2}} (\eta_2 e^{i\pi/4} + \eta_1 e^{-i\pi/4}) . \quad (6.143)$$

One easily verifies that $\langle \tilde{\eta}\tilde{\eta}^* \rangle = \delta(t - t')$.

The solutions derived from (6.140) are

$$\langle \alpha(t) \rangle = \langle \alpha(0) \rangle \exp\left(-\frac{\gamma}{2}t\right) , \quad (6.144)$$

$$\langle \alpha^*(t)\alpha(t) \rangle = \langle \alpha^*(0)\alpha(0) \rangle e^{-\gamma t} + N(1 - e^{-\gamma t}) ,$$

$$\langle \alpha^2 \rangle_{ss} = \langle \alpha^{*2} \rangle_{ss} = 0 ,$$

$$\langle \alpha\alpha^* \rangle_{ss} = \langle \alpha^*\alpha \rangle_{ss} = N , \quad (6.145)$$

where ss denotes steady state.

6.3.1 Use of the Positive P Representation

The relationship (6.123 and 124) between the Fokker–Planck equation and the stochastic differential equation only holds if the diffusion matrix

$$\mathcal{D}(\mathbf{x}, t) = \mathcal{B}(\mathbf{x}, t) \mathcal{B}^T(\mathbf{x}, t)$$

is positive semidefinite. In some cases use of the Glauber–Sudarshan P representation will result in Fokker–Planck equations with a non-positive semi-definite diffusion matrix, for example, if the bath is squeezed. In such cases use of the positive P representation will give a Fokker–Planck equation with a positive semi definite diffusion matrix

$$\mathcal{D}(\boldsymbol{\alpha}) = \mathcal{B}(\boldsymbol{\alpha}) \mathcal{B}^T(\boldsymbol{\alpha}) \quad (6.146)$$

where

$$\mathcal{B}(\boldsymbol{\alpha}) = \begin{pmatrix} B_x & 0 \\ B_y & 0 \end{pmatrix}$$

and $\boldsymbol{\alpha} = (\alpha, \beta)$.

The corresponding stochastic differential equations may be written

$$\frac{d}{dt} \begin{pmatrix} \alpha_x \\ \alpha_y \end{pmatrix} = \begin{pmatrix} A_x(\boldsymbol{\alpha}) \\ A_y(\boldsymbol{\alpha}) \end{pmatrix} + \begin{pmatrix} B_x(\boldsymbol{\alpha}) E(t) \\ B_y(\boldsymbol{\alpha}) E(t) \end{pmatrix} \quad (6.147)$$

on recombining real and imaginary parts

$$\frac{d\boldsymbol{\alpha}}{dt} = \mathbf{A}(\boldsymbol{\alpha}) + \mathbf{B}(\boldsymbol{\alpha}) \mathbf{E}(t) . \quad (6.148)$$

Apart from the substitution $\alpha^* \rightarrow \beta$, (6.148) is just the stochastic differential equation which would be obtained by using the Glauber–Sudarshan P representation, and naively converting the Fokker–Planck equation with a non-positive definite diffusion matrix into a stochastic differential equation. In the above derivation the two formal variables (α, α^*) have been replaced by variables in the complex plane (α, β) that are allowed to fluctuate independently. The use of the positive P representation justifies this procedure.

6.4 Linear Processes with Constant Diffusion

For linear processes with constant diffusion coefficients a number of useful results may be proven. These may be derived from the Fokker–Planck equation using the solution (6.78) or the equivalent Langevin equation. We shall quote the results here. The Langevin equations are a useful starting point since for

nonlinear processes approximate results may be obtained by a linearization procedure. We consider a process described by the Langevin equation

$$\frac{dx(t)}{dt} = -Ax(t) + BE(t) \quad (6.149)$$

where A and B are constant matrices. This describes a multivariate Ornstein–Uhlenbeck process. Suppose $AA^T = A^TA$, then we can find an orthogonal matrix S such that

$$\begin{aligned} SS^T &= 1 \\ SAS^T &= SA^TS^T = \text{Diag}\{\lambda_1, \lambda_2 \dots \lambda_n\} . \end{aligned} \quad (6.150)$$

The two time correlation function is given by

$$\langle x(t), x^T(s) \rangle = S^T G(t, s) S$$

where

$$[G(t, s)]_{ij} = \frac{(SBB^TS^T)_{ij}}{\lambda_i + \lambda_j} (e^{-\lambda_i|t-s|} - e^{-\lambda_i t - \lambda_j s}) . \quad (6.151)$$

In the stationary state the second term in the parentheses is zero and the correlation is only a function of the difference, $\tau \equiv t - s$.

Let us define the stationary covariance matrix σ by

$$\sigma = \langle x_{ss}(t), x_{ss}^T(t) \rangle . \quad (6.152)$$

Then by setting $dx(t)/dt = 0$ in (6.149) we find that σ obeys the equation

$$A\sigma + \sigma A^T = BB^T . \quad (6.153)$$

In the case of a two dimensional problem it may be shown that

$$\sigma = \frac{(\text{Det } A)BB^T + [A - (\text{Tr } A)I]BB^T[A - (\text{Tr } A)I]^T}{2(\text{Tr } A)(\text{Det } A)} . \quad (6.154)$$

The two time correlation function in the steady state may be shown to obey the same time development equation as the mean. That is

$$\frac{d}{d\tau} [G_{ss}(\tau)] = -AG_{ss}(\tau) . \quad (6.155)$$

The computation of $G_{ss}(\tau)$, therefore requires the knowledge of $G_{ss}(0) = \sigma$ and the time development equation of the mean.

It is often of more interest to view the noise in the frequency domain. We are thus lead to define the noise spectrum by,

$$S(\omega) = \frac{1}{2\pi} \int_{-\infty}^{\infty} e^{-i\omega\tau} G_{ss}(\tau) d\tau . \quad (6.156)$$

Using (6.155 and 153) we find

$$S(\omega) = \frac{1}{2\pi} (A + i\omega)^{-1} BB^T (A^T - i\omega)^{-1} . \quad (6.157)$$

6.5 Two Time Correlation Functions in Quantum Markov Processes

We shall now demonstrate how two time correlation functions for operators may be derived from the master equation or the equivalent Fokker–Planck equation.

Consider a system coupled to a reservoir. $W(t)$ is the total density operator in the Schrödinger picture and \mathcal{H} is the Hamiltonian, A and B are operators for variables to be measured, then

$$\langle A(t) \rangle = \text{Tr}\{AW(t)\} \quad (6.158)$$

and

$$\langle A(t + \tau)B(t) \rangle = \text{Tr}\{e^{i\mathcal{H}t/\hbar} A e^{i\mathcal{H}\tau/\hbar} B W(t)\} \quad (6.159)$$

while this is exact it is not particularly useful. For a system interacting with a heat bath in the Markov approximation we wish to express everything in terms of the Liouvillian for the reduced system in which heat bath variables have been traced out.

Supposing A and B are operators in the system space, then

$$\langle A(t + \tau)B(t) \rangle = \text{Tr}_s\{A \text{Tr}_R[e^{-i\mathcal{H}\tau/\hbar} B W(t) e^{i\mathcal{H}\tau/\hbar}]\} . \quad (6.160)$$

The equation of motion for the term

$$X(\tau, t) = e^{-i\mathcal{H}\tau/\hbar} B W(t) e^{i\mathcal{H}\tau/\hbar} \quad (6.161)$$

in terms of τ is

$$i\hbar \frac{\partial}{\partial \tau} X(\tau, t) = [\mathcal{H}, X(\tau, t)] . \quad (6.162)$$

Proceeding in exactly the same way as for the derivation of the Markoffian master equation (6.21) which may be written in the form

$$\frac{\partial}{\partial t} \rho(t) = L\rho(t) \quad (6.163)$$

where L is a Liouvillian operator, where $\rho = \text{Tr}_R\{W\}$ is the reduced density operator for the system, we may derive the equation

$$\frac{\partial}{\partial \tau} [\text{Tr}_R\{X(\tau, t)\}] = L\{\text{Tr}_R X(\tau, t)\} \quad (6.164)$$

so that the two time correlation function may be expressed as

$$\langle A(t + \tau)B(t) \rangle = \text{Tr}_s\{A e^{L\tau} B \rho(t)\} . \quad (6.165)$$

6.5.1 Quantum Regression Theorem

In cases where the master equation gives linear equations for the mean, we can develop a quantum regression theorem, similar to that for ordinary Markov processes. This result was first derived by Lax [6.4].

Suppose for a certain set of operators Y_i , the master equation can be shown to yield, for any initial ρ

$$\frac{\partial}{\partial t} \langle Y_i(t) \rangle = \sum G_{ij}(t) \langle Y_j(t) \rangle . \quad (6.166)$$

Then we assert that

$$\frac{\partial}{\partial \tau} \langle Y_i(t + \tau) Y_l(t) \rangle = \sum G_{ij}(\tau) \langle Y_j(t + \tau) Y_l(t) \rangle . \quad (6.167)$$

For

$$\langle Y_i(t + \tau) Y_l(t) \rangle = \text{Tr}_s\{Y_i e^{L\tau} Y_l \rho(t)\} \quad (6.168)$$

the right-hand side is an average of Y_i at time $t + \tau$, with the choice of initial density matrix

$$\rho_{\text{init}} = Y_l \rho(t) . \quad (6.169)$$

Since by hypothesis, any initial ρ is permitted and the equation is linear, we may generate any initial condition whatsoever. Hence, choosing ρ_{init} as defined in (6.170) the hypothesis (6.166) yields the result (6.167) which is the quantum regression theorem.

6.6 Application to Systems with a P Representation

For systems where a P representation exists the following results for normally ordered time correlation functions may be proved

$$G^{(1)}(t, \tau) = \langle a^\dagger(t + \tau) a(t) \rangle = \langle \alpha^*(t + \tau) \alpha(t) \rangle , \quad (6.170)$$

$$\begin{aligned} G^{(2)}(t, \tau) &= \langle a^\dagger(t) a^\dagger(t + \tau) a(t + \tau) a(t) \rangle , \\ &= \langle |\alpha(t + \tau)|^2 |\alpha(t)|^2 \rangle . \end{aligned} \quad (6.171)$$

In these cases the measured correlation functions correspond to the same correlation function for the variables in the P representation. For non-normally ordered correlation functions the result is not as simple.

Exercises

6.1 The photon number distribution for a laser may be shown to obey the master equation

$$\frac{d}{dt} P(n) = \frac{An}{1+n/n_s} P(n-1) - \frac{A(n+1)}{1+(n+1)/n_s} P(n) - \gamma n P(n) + \gamma(n+1)P(n+1) ,$$

where A is related to the gain, n_s is the saturation photon number and γ is the cavity loss rate.

Use detailed balance to show that the steady state solution is

$$P_{ss}(n) = N \frac{\left(\frac{An_s}{\gamma}\right)^n}{(n+n_s)!}$$

where N is a normalisation constant.

6.2 The interaction picture master equation for a damped harmonic oscillator driven by a resonant linear force is

$$\frac{d\rho}{dt} = i\varepsilon[a + a^\dagger, \rho] + \frac{\gamma}{2}(2apa^\dagger - a^\dagger ap - \rho a^\dagger a) .$$

Show that the steady state solution is the coherent state $|2i\varepsilon/\gamma\rangle$.

6.3 A model for phase diffusion of a simple harmonic oscillator is provided by the master equation

$$\frac{d\rho}{dt} = -\Gamma[a^\dagger a, [a^\dagger a, \rho]] .$$

Show that the Q function obeys the Fokker–Planck equation.

$$\frac{\partial Q}{\partial t} = \frac{\Gamma}{2} \left(\frac{\partial}{\partial \alpha} \alpha Q + \frac{\partial}{\partial \alpha^*} \alpha^* Q + 2 \frac{\partial^2}{\partial \alpha \partial \alpha^*} |\alpha|^2 Q - \frac{\partial^2}{\partial \alpha^2} \alpha^2 Q - \frac{\partial^2}{\partial \alpha^{*2}} \alpha^{*2} Q \right) .$$

Thus show that while the mean amplitude decays the energy remains constant. Using intensity and phase variables $\alpha = I^{1/2}e^{i\theta}$ show that the model is simply a diffusion process for the phase.

6.4 Show that in terms of the quadrature operators $X_1 = a + a^\dagger$, $X_2 = -i(a - a^\dagger)$, the master equation (6.37) may be written

$$\begin{aligned} \frac{d\rho}{dt} &= i\frac{\gamma}{8}[X_2, \{X_1, \rho\}] - i\frac{\gamma}{8}[X_1, \{X_2, \rho\}] \\ &\quad - \frac{\gamma}{8}e^{2r}[X_1, [X_1, \rho]] - \frac{\gamma}{8}e^{-2r}[X_2, [X_2, \rho]] \end{aligned}$$

where $\{, \}$ is an anticommutator and we have taken $N = \sinh^2 r$, $M = \sinh r \cosh r$ for an ideal squeezed bath. Show that the first and second terms describe damping in X_1 and X_2 respectively, while the third and fourth terms describe diffusion in X_2 and X_1 , respectively.

7. Input–Output Formulation of Optical Cavities

In preceding chapters we have used a master-equation treatment to calculate the photon statistics inside an optical cavity when the internal field is damped. This approach is based on treating the field external to the cavity, to which the system is coupled, as a heat bath. The heat bath is simply a passive system with which the system gradually comes into equilibrium. In this chapter we will explicitly treat the heat bath as the external cavity field, our object being to determine the effect of the intracavity dynamics on the quantum statistics of the output field. Within this perspective we will also treat the field input to the cavity explicitly. This approach is necessary in the case of squeezed state generation due to interference effects at the interface between the intracavity field and the output field.

An input–output formulation is also required if the input field state is specified as other than simply a vacuum or thermal state. In particular, we will want to discuss the case of an input squeezed state.

7.1 Cavity Modes

We will consider a single cavity mode interacting with an external field. The frequency of the external modes most strongly interacting with the system is very large compared to the strength of the interaction (measured in frequency units) for quantum optical systems. This permits us to use the Rotating Wave Approximation (RWA) coupling which excludes counter rotating terms from the equations of motion. We will also treat the external field as essentially one dimensional, for simplicity. We follow closely the treatment of *Collett* and *Gardiner* [7.1]. The Hamiltonian is given by

$$\mathcal{H} = \mathcal{H}_{\text{SYS}} + \mathcal{H}_{\text{BATH}} + \mathcal{H}_{\text{INT}} , \quad (7.1)$$

where \mathcal{H}_{SYS} is the free Hamiltonian for the intracavity field mode, $\mathcal{H}_{\text{BATH}}$, is the free Hamiltonian for the external field modes and \mathcal{H}_{INT} is the interaction Hamiltonian given by

$$\mathcal{H}_{\text{INT}} = i\hbar \int_{-\infty}^{\infty} d\omega \kappa(\omega) [b(\omega)a^\dagger - ab^\dagger(\omega)] , \quad (7.2)$$

where a is the annihilation operator for the intracavity field, and $b(\omega)$ are the annihilation operators for the external field which satisfy the commutation relations

$$[a, a^\dagger] = 1 , \quad (7.3)$$

$$[b(\omega), b^\dagger(\omega')] = \delta(\omega - \omega') , \quad (7.4)$$

and $\kappa(\omega)$ is coupling constant. In actual fact the physical frequency limits are $(0, \infty)$. However, for high frequency optical systems we may shift the integration to a frequency Ω characteristic of the system (for example, the cavity resonance frequency), and the integration limits are $(-\Omega, \infty)$. As Ω is so large, extending the lower limit to $-\infty$ is a good approximation.

The Heisenberg equation of motion for $b(\omega)$ is

$$\dot{b}(\omega) = -i\omega b(\omega) + \kappa(\omega)a . \quad (7.5)$$

The solution to this equation may be written in two ways depending on whether we choose to solve in terms of initial conditions at time $t_0 < t$ (the *input*) or in terms of the final conditions at times $t_1 > t$ (the *output*). The two solutions are, respectively,

$$b(\omega) = e^{-i\omega(t-t_0)} b_0(\omega) + \kappa(\omega) \int_{t_0}^t e^{-i\omega(t-t')} a(t') dt' , \quad (7.6)$$

where $t_0 < t$ and $b_0(\omega)$ is the value of $b(\omega)$ at $t = t_0$, and

$$b(\omega) = e^{-i\omega(t-t_1)} b_1(\omega) - \kappa(\omega) \int_t^{t_1} e^{-i\omega(t-t')} a(t') dt' , \quad (7.7)$$

where $t < t_1$, and $b_1(\omega)$ is the value of $b(\omega)$ at $t = t_1$. In physical terms $b_0(\omega)$ and $b_1(\omega)$ are usually specified at $-\infty$ and $+\infty$, respectively, however (7.6, 7) hold for any t_0 and t_1 such that $t_0 < t < t_1$.

The system operator obeys the equation

$$\dot{a} = -\frac{i}{\hbar}[a, \mathcal{H}_{\text{sys}}] - \int_{-\infty}^{\infty} d\omega \kappa(\omega) b(\omega) . \quad (7.8)$$

In terms of the solution with initial conditions (7.6) this equation becomes

$$\dot{a} = -\frac{i}{\hbar}[a, \mathcal{H}_{\text{sys}}] - \int_{-\infty}^{\infty} \kappa(\omega) e^{-i\omega(t-t_0)} b_0(\omega) d\omega$$

$$- \int_{-\infty}^{\infty} d\omega \kappa(\omega)^2 \int_{t_0}^t e^{-i\omega(t-t')} a(t') dt' . \quad (7.9)$$

We now assume that $\kappa(\omega)$ is independent of frequency over a band of frequencies about the characteristic frequency Ω . This introduces the first approximation necessary to obtain a Markov process but it is not sufficient in itself to obtain such a result. Thus we set

$$\kappa(\omega)^2 = \gamma/2\pi . \quad (7.10)$$

We also define an *input field* operator by

$$a_{\text{IN}}(t) \equiv \frac{-1}{\sqrt{2\pi}} \int_{-\infty}^{\infty} d\omega e^{-i\omega(t-t_0)} b_0(\omega) , \quad (7.11)$$

where we have used the convention that the leftward propagating field is negative and the rightward propagating field is positive in Fig. 7.1.

Using the relation

$$\int_{-\infty}^{\infty} d\omega e^{-i\omega(t-t')} = 2\pi \delta(t-t') \quad (7.12)$$

the input field may be shown to satisfy

$$[a_{\text{IN}}(t), a_{\text{IN}}^\dagger(t)] = \delta(t-t') . \quad (7.13)$$

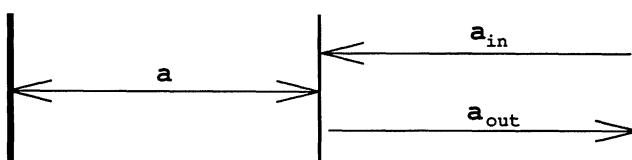


Fig. 7.1. A schematic representation of the cavity field and the input and output fields for a single-sided cavity

Whenever (7.12) is achieved as the limit of an integral over a function which goes smoothly to zero at $\pm \infty$ (for example, a Gaussian) the following result also holds:

$$\int_{t_0}^t f(t') \delta(t - t') dt' = \int_t^{t_1} f(t') \delta(t - t') dt' = \frac{1}{2} f(t) \quad (t_0 < t < t_1) . \quad (7.14)$$

Interchanging the order of time and frequency integration in the last term of (7.9) and using (7.14)

$$\frac{da(t)}{dt} = -\frac{i}{\hbar} [a(t), \mathcal{H}_{\text{SYS}}] - \frac{\gamma}{2} a(t) + \sqrt{\gamma} a_{\text{IN}}(t) . \quad (7.15)$$

Equation (7.15) is a Langevin equation for the damped amplitude $a(t)$ in which the noise term appears explicitly as the input field.

In a similar manner we may substitute the solution in terms of final conditions, (7.7) into (7.9), to obtain the time reversed Langevin equation

$$\frac{da(t)}{dt} = -\frac{i}{\hbar} [a(t), \mathcal{H}_{\text{SYS}}] + \frac{\gamma}{2} a(t) - \sqrt{\gamma} a_{\text{OUT}}(t) , \quad (7.16)$$

where the output field is

$$a_{\text{OUT}}(t) = \frac{1}{\sqrt{2\pi}} \int_{-\infty}^{\infty} d\omega e^{-i\omega(t-t_1)} b_1(\omega) . \quad (7.17)$$

A relation between the external fields and the intracavity field may be obtained by subtracting (7.16) from (7.15)

$$a_{\text{OUT}}(t) + a_{\text{IN}}(t) = \sqrt{\gamma} a(t) . \quad (7.18)$$

Equation (7.18) is a boundary condition relating each of the far-field amplitudes outside the cavity to the internal cavity field. It is easy to see that interference terms between the input and the cavity field may contribute to the observed output field moments.

7.2 Linear Systems

For many systems of interest the Heisenberg equations of motion are linear and may be written in the form

$$\frac{d}{dt} \mathbf{a}(t) = A \mathbf{a}(t) - \frac{\gamma}{2} \mathbf{a}(t) + \sqrt{\gamma} \mathbf{a}_{\text{IN}}(t) , \quad (7.19)$$

where

$$\mathbf{a}(t) = \begin{pmatrix} a(t) \\ a^\dagger(t) \end{pmatrix}, \quad (7.20)$$

$$\mathbf{a}_{\text{IN}}(t) = \begin{pmatrix} a_{\text{IN}}(t) \\ a_{\text{IN}}^\dagger(t) \end{pmatrix}, \quad (7.21)$$

Define the Fourier components of the intracavity field by

$$a(t) = \frac{1}{\sqrt{2\pi}} \int_{-\infty}^{\infty} e^{-i\omega(t-t_0)} a(\omega) d\omega \quad (7.22)$$

and a frequency component vector

$$\mathbf{a}(\omega) = \begin{pmatrix} a(\omega) \\ a^\dagger(\omega) \end{pmatrix} \quad (7.23)$$

where $a^\dagger(\omega)$ is the Fourier transform of $a^\dagger(t)$.

The equations of motion become

$$\left[\mathbf{A} + \left(i\omega - \frac{\gamma}{2} \right) \mathbf{I} \right] \mathbf{a}(\omega) = -\sqrt{\gamma} \mathbf{a}_{\text{IN}}(\omega). \quad (7.24)$$

However, we may use (7.18) to eliminate the internal modes to obtain

$$\mathbf{a}_{\text{OUT}}(\omega) = - \left[\mathbf{A} + \left(i\omega + \frac{\gamma}{2} \right) \mathbf{I} \right] \left[\mathbf{A} + \left(i\omega - \frac{\gamma}{2} \right) \mathbf{I} \right]^{-1} \mathbf{a}_{\text{IN}}(\omega). \quad (7.25)$$

To illustrate the use of this result we shall apply it to the case of an empty one-sided cavity. In this case the only source of loss in the cavity is through the mirror which couples the input and output fields. The system Hamiltonian is

$$\mathcal{H}_{\text{SYS}} = \hbar\omega_0 a^\dagger a.$$

Thus

$$\mathbf{A} = \begin{pmatrix} -i\omega_0 & 0 \\ 0 & i\omega_0 \end{pmatrix}. \quad (7.26)$$

Equation (7.25) then gives

$$\mathbf{a}_{\text{OUT}}(\omega) = \frac{\frac{\gamma}{2} + i(\omega - \omega_0)}{\frac{\gamma}{2} - i(\omega - \omega_0)} \mathbf{a}_{\text{IN}}(\omega). \quad (7.27)$$

Thus there is a frequency dependent phase shift between the output and input. The relationship between the input and the internal field is

$$\mathbf{a}(\omega) = \frac{\sqrt{\gamma}}{\frac{\gamma}{2} - i(\omega - \omega_0)} a_{\text{IN}}(\omega) , \quad (7.28)$$

which leads to a Lorentzian of width $\gamma/2$ for the intensity transmission function.

7.3 Two-Sided Cavity

A two-sided cavity has two partially transparent mirrors with associated loss coefficients γ_1 and γ_2 , as shown in Fig. 7.2. In this case there are two input ports and two output ports. The equation of motion for the internal field is then given by an obvious generalisation as

$$\frac{da(t)}{dt} = -i\omega_0 a(t) - \frac{1}{2}(\gamma_1 + \gamma_2)a(t) + \sqrt{\gamma_1}a_{\text{IN}}(t) + \sqrt{\gamma_2}b_{\text{IN}}(t) . \quad (7.29)$$

The relationship between the internal and input field frequency components for an empty cavity is then

$$\mathbf{a}(\omega) = \frac{\sqrt{\gamma_1} \mathbf{a}_{\text{IN}}(\omega) + \sqrt{\gamma_2} \mathbf{b}_{\text{IN}}(\omega)}{\left(\frac{\gamma_1 + \gamma_2}{2}\right) - i(\omega - \omega_0)} . \quad (7.30)$$

The relationship between the input and output modes may be found using the boundary conditions at each mirror, see (7.18),

$$a_{\text{OUT}}(t) + a_{\text{IN}}(t) = \sqrt{\gamma_1}a(t) , \quad (7.31a)$$

$$b_{\text{OUT}}(t) + b_{\text{IN}}(t) = \sqrt{\gamma_2}a(t) . \quad (7.31b)$$

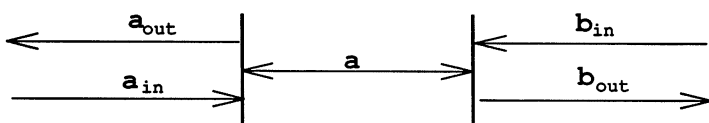


Fig. 7.2. A schematic representation of the cavity field and the input and output fields for a double-sided cavity

We find

$$\mathbf{a}_{\text{OUT}}(\omega) = \frac{\left[\frac{\gamma_1 - \gamma_2}{2} + i(\omega - \omega_0) \right] \mathbf{a}_{\text{IN}}(\omega) + \sqrt{\gamma_1 \gamma_2} \mathbf{b}_{\text{IN}}(\omega)}{\frac{\gamma_1 + \gamma_2}{2} - i(\omega - \omega_0)} . \quad (7.32)$$

For equally reflecting mirrors $\gamma_1 = \gamma_2 = \gamma$ this expression simplifies to

$$\mathbf{a}_{\text{OUT}}(\omega) = \frac{i(\omega - \omega_0) \mathbf{a}_{\text{IN}}(\omega) + \gamma \mathbf{b}_{\text{IN}}(\omega)}{\gamma - i(\omega - \omega_0)} . \quad (7.33)$$

Near to resonance this is approximately a through pass Lorentzian filter

$$\mathbf{a}_{\text{OUT}}(\omega) \approx \frac{\gamma \mathbf{b}_{\text{IN}}(\omega)}{\gamma - i(\omega - \omega_0)} , \quad (7.34)$$

This is only an approximate result, the neglected terms are needed to preserve the commutation relations. Away from resonance there is an increasing amount of backscatter. In the limit $|\omega - \omega_0| \gg \gamma$ the field is completely reflected

$$\mathbf{a}_{\text{OUT}}(\omega) = -\mathbf{a}_{\text{IN}}(\omega) . \quad (7.35)$$

Before going on to consider interactions within the cavity we shall derive some general relations connecting the two time correlation functions inside and outside the cavity.

7.4 Two Time Correlation Functions

Integrating (7.6) over ω , and using (7.12) gives

$$\mathbf{a}_{\text{IN}}(t) = \frac{\sqrt{\gamma}}{2} \mathbf{a}(t) - \frac{1}{\sqrt{2\pi}} \int_{-\infty}^{\infty} d\omega b(\omega, t) . \quad (7.36)$$

Let $c(t)$ be any system operator. Then

$$[c(t), \sqrt{\gamma} \mathbf{a}_{\text{IN}}(t)] = \frac{\gamma}{2} [c(t), \mathbf{a}(t)] . \quad (7.37)$$

Now since $c(t)$ can only be a function of $a_{\text{IN}}(t')$ for earlier times $t' < t$ and the input field operators must commute at different times we have

$$[c(t), \sqrt{\gamma} \mathbf{a}_{\text{IN}}(t')] = 0, \quad t' > t . \quad (7.38)$$

Similarly

$$[c(t), \sqrt{\gamma} \mathbf{a}_{\text{OUT}}(t')] = 0, \quad t' < t . \quad (7.39)$$

From (7.39 and 18) we may show that

$$[c(t), \sqrt{\gamma}a_{\text{IN}}(t')] = \gamma[c(t), a(t)], \quad t' < t . \quad (7.40)$$

Combining (7.37–40) we then have

$$[c(t), \sqrt{\gamma}a_{\text{IN}}(t')] = \gamma\theta(t - t')[c(t), a(t')] , \quad (7.41)$$

where $\theta(t)$ is the step function

$$\theta(t) = \begin{cases} 1 & t > 0, \\ \frac{1}{2} & t = 0, \\ 0 & t < 0 . \end{cases} \quad (7.42)$$

The commutator for the output field may now be calculated to be

$$[a_{\text{OUT}}(t), a_{\text{OUT}}^\dagger(t')] = [a_{\text{IN}}(t), a_{\text{IN}}^\dagger(t')] \quad (7.43)$$

as required.

For the case of a coherent or vacuum input it is now possible to express variances of the output field entirely in terms of those of the internal system. For an input field of this type all moments of the form $\langle a_{\text{IN}}^\dagger(t)a_{\text{IN}}(t') \rangle$, $\langle a(t)a_{\text{IN}}(t') \rangle$, $\langle a^\dagger(t)a_{\text{IN}}(t') \rangle$, $\langle a_{\text{IN}}^\dagger(t)a(t') \rangle$, and $\langle a_{\text{IN}}^\dagger(t)a^\dagger(t') \rangle$ will factorise. Using (7.18) we find

$$\langle a_{\text{OUT}}^\dagger(t)a_{\text{OUT}}(t') \rangle = \gamma\langle a^\dagger(t)a(t') \rangle , \quad (7.44)$$

where

$$\langle U, V \rangle \equiv \langle UV \rangle - \langle U \rangle \langle V \rangle . \quad (7.45)$$

In this case there is a direct relationship between the two time correlation of the output field and the internal field. Consider now the phase dependent two time correlation function

$$\begin{aligned} \langle a_{\text{OUT}}(t), a_{\text{OUT}}(t') \rangle &= \langle a_{\text{IN}}(t) - \sqrt{\gamma}a(t), a_{\text{IN}}(t') - \sqrt{\gamma}a(t') \rangle \\ &= \gamma\langle a(t), a(t') \rangle - \sqrt{\gamma}\langle [a_{\text{IN}}(t'), a(t)] \rangle \\ &= \gamma\langle a(t), a(t') \rangle + \gamma\theta(t' - t)\langle [a(t'), a(t)] \rangle \\ &= \gamma\langle a(\max(t, t')), a(\min(t, t')) \rangle . \end{aligned} \quad (7.46)$$

In this case the two time correlation functions of the output field are related to the time ordered two time correlation functions of the cavity field.

These results mean that the usual spectrum of the output field, as given by the Fourier transform of (7.44), will be identical to the spectrum of the cavity field. The photon statistics of the output field will also be the same as the intracavity field. Where a difference will arise, is in phase-sensitive spectrum such as in squeezing experiments.

7.5 Spectrum of Squeezing

The output field from a cavity is a continuum of frequencies. Just as one can define the intensity of such a field as the Fourier transform of the phase independent moment in (7.44), so we can define the squeezing spectrum as the Fourier transform of an appropriate phase dependent moment. The squeezing spectrum will give the squeezing in the frequency components of an appropriate quadrature phase operator. In an experiment this squeezing is measured by beating the field output from the cavity with a local oscillator field of the reference frequency Ω and the reference phase θ . In effect, Ω is the cavity resonance frequency. We are thus led to define the output quadrature phase operators by

$$a_{\text{OUT}}(t) = \frac{1}{2}[X_1^{\text{OUT}}(t) + iX_2^{\text{OUT}}]e^{i(\theta - \Omega t)}, \quad (7.47)$$

that is

$$X_1^{\text{OUT}}(t) = a_{\text{OUT}}(t)e^{-i(\theta - \Omega t)} + a_{\text{OUT}}^\dagger(t)e^{i(\theta - \Omega t)}, \quad (7.48a)$$

$$X_2^{\text{OUT}}(t) = -i[a_{\text{OUT}}(t)e^{-i(\theta - \Omega t)} - a_{\text{OUT}}^\dagger(t)e^{i(\theta - \Omega t)}], \quad (7.48b)$$

The squeezing spectrum is then defined by the Fourier transform of the normally-ordered two time correlation function $\langle :X_i^{\text{OUT}}(t), X_i^{\text{OUT}}(0):\rangle$,

$$:S_i^{\text{OUT}}(\omega): \equiv \int \langle :X_i^{\text{OUT}}(t), X_i^{\text{OUT}}(0):\rangle e^{-i\omega t} dt. \quad (7.49)$$

Using (7.46 and 48) this becomes

$$:S_i^{\text{OUT}}(\omega): \equiv \gamma \int T \langle :X_i(t), X_i(0):\rangle e^{-i\omega t} dt, \quad (7.50)$$

where T denotes time ordering and $X(t)$ is the intracavity quadrature phase operators defined in an interaction picture at frequency Ω

$$X_1(t) = a(t)e^{-i\theta} + a^\dagger(t)e^{i\theta}, \quad (7.51a)$$

$$X_2(t) = -i[a(t)e^{-i\theta} - a^\dagger(t)e^{i\theta}]. \quad (7.51b)$$

(We have not designated explicitly that $a(t)$ is defined in an interaction picture at frequency Ω but this should be kept in mind in the remainder of this chapter.)

7.6 Parametric Oscillator

We shall now proceed to calculate the squeezing spectrum from the output of a parametric oscillator. Below threshold the equations for the parametric oscillator are linear and hence we can directly apply the linear operator techniques. When the equations are nonlinear such as for the parametric oscillator above threshold, then linearization procedures must be used. One procedure

using the Fokker–Planck equation is described in Chap. 8.

Below threshold the pump mode of the parametric oscillator may be treated classically. It can then be described by the Hamiltonian

$$\mathcal{H} = \hbar\omega a^\dagger a + \frac{i\hbar}{2}(\varepsilon a^{\dagger 2} - \varepsilon^* a^2) + a\Gamma^\dagger + a^\dagger\Gamma , \quad (7.52)$$

where $\varepsilon = \varepsilon_p \chi$ and ε_p is the amplitude of the pump, and χ is proportional to the nonlinear susceptibility of the medium. Γ is the reservoir operator representing cavity losses. We consider here the case of a single ended cavity with loss rate γ_1 .

The Heisenberg equations of motion for $a(t)$ are linear and given by (7.19) where

$$A = \begin{pmatrix} \frac{\gamma_1}{2} & -\varepsilon \\ -\varepsilon^* & \frac{\gamma_1}{2} \end{pmatrix} . \quad (7.53)$$

We can obtain an expression for the Fourier components of the output field from (7.25)

$$a_{\text{OUT}}(\omega) = \frac{1}{\left[\left(\frac{\gamma_1}{2} - i\omega\right)^2 - |\varepsilon|^2\right]} \left\{ \left[\left(\frac{\gamma_1}{2}\right)^2 + \omega^2 + |\varepsilon|^2 \right] \right. \\ \left. \times a_{\text{IN}}(\omega) + \varepsilon\gamma_1 a_{\text{IN}}^\dagger(-\omega) \right\} . \quad (7.54)$$

Defining the quadrature phase operators by

$$2a_{\text{OUT}} = e^{i\theta/2}(X_1^{\text{OUT}} + iX_2^{\text{OUT}}) , \quad (7.55)$$

where θ is the phase of the pump, we find the following correlations:

$$\langle : X_1^{\text{OUT}}(\omega), X_1^{\text{OUT}}(\omega') : \rangle = \frac{2\gamma_1|\varepsilon|}{\left(\frac{\gamma_1}{2} - |\varepsilon|\right)^2 + \omega^2} \delta(\omega + \omega') , \quad (7.56)$$

$$\langle : X_2^{\text{OUT}}(\omega), X_2^{\text{OUT}}(\omega') : \rangle = \frac{-2\gamma_1|\varepsilon|}{\left(\frac{\gamma_1}{2} + |\varepsilon|\right)^2 + \omega^2} \delta(\omega + \omega') , \quad (7.57)$$

where the input field a_{IN} has been taken to be in the vacuum.

The δ function in (7.56, 57) may be removed by integrating over ω' to give the normally ordered spectrum $:S^{\text{OUT}}(\omega):$. The final result for the squeezing spectra

of the quadrature is

$$S_1^{\text{OUT}}(\omega) = 1 + :S_1^{\text{OUT}}(\omega): = 1 + \frac{2\gamma_1|\varepsilon|}{\left(\frac{\gamma_1}{2} - |\varepsilon|\right)^2 + \omega^2}, \quad (7.58)$$

$$S_2^{\text{OUT}}(\omega) = 1 + :S_2^{\text{OUT}}(\omega): = 1 - \frac{2\gamma_1|\varepsilon|}{\left(\frac{\gamma_1}{2} + |\varepsilon|\right)^2 + \omega^2}, \quad (7.59)$$

These spectra are defined in a frame of frequency Ω so that $\omega = 0$ is on cavity resonance.

The maximum squeezing occurs at the threshold for parametric oscillation $|\varepsilon| = \gamma_1/2$ where

$$S_1^{\text{OUT}}(\omega) = 1 + \left(\frac{\gamma_1}{\omega}\right)^2, \quad (7.60)$$

$$S_2^{\text{OUT}}(\omega) = 1 - \frac{\gamma_1^2}{\gamma_1^2 + \omega^2}, \quad (7.61)$$

Thus the squeezing occurs in the X_2 quadrature which is $\pi/2$ out of phase with the pump. The light generated in parametric oscillation is therefore said to be phase squeezed.

In Fig. 7.3 we plot $S_2^{\text{OUT}}(\omega)$ at threshold. We see that at $\omega = 0$, that is the cavity resonance, the fluctuations in the X_2 quadrature tend to zero. The fluctuations in the X_1 quadrature on the other hand diverge at $\omega = 0$. This is characteristic of critical fluctuations which diverge at a critical point. In this case however the critical fluctuations are phase dependent. As the fluctuations in one phase are reduced to zero the fluctuations in the other phase necessarily diverge. This characteristic of good squeezing near critical points is found in other phase dependent nonlinear optical systems [7.2]. This behaviour is in contrast to the threshold for laser oscillation where the critical fluctuations are random in phase.

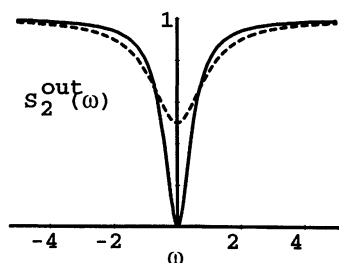


Fig. 7.3. A plot of the spectrum of the squeezed quadrature for a cavity containing a parametric amplifier with a classical pump. Solid: single-sided cavity with $\gamma_1 = \gamma_2$, dashed: double-sided cavity

7.7 Squeezing in the Total Field

The squeezing in the total field may be found by integrating (7.61) over ω . At threshold we find

$$S_2^{\text{TOT}} = \int \left(1 - \frac{\gamma_1^2}{\gamma_1^2 + \omega^2} \right) d\omega = \frac{\gamma_1}{2}. \quad (7.62)$$

The squeezing in the total field is given by the equal time correlation functions

$$\begin{aligned} \langle a, a \rangle_{\text{OUT}} &= \gamma_1 \langle a, a \rangle, \\ \langle a, a^\dagger \rangle_{\text{OUT}} &= \gamma_1 \langle a, a^\dagger \rangle. \end{aligned} \quad (7.63)$$

Hence, the squeezing in the internal field is

$$V(X_2) = \frac{1}{2}. \quad (7.64)$$

Thus the internal field mode is 50% squeezed, in agreement with the calculations of *Milburn* and *Walls* [7.3]. This can be surpassed in the individual frequency components of the output field which have 100% squeezing for $\omega = 0$. It is the squeezing in the individual frequency components of the output field which may be measured by a spectrum analyser following a homodyne detection scheme.

7.8 Fokker–Planck Equation

We shall now give an alternative method for evaluating the squeezing spectrum. This converts the operator master equation to a *c*-number Fokker–Planck equation. This is a useful technique when the operator equations are nonlinear. Standard linearization techniques for the fluctuations may be made in the Fokker–Planck equation. We shall consider applications of this technique to nonlinear systems in Chap. 8.

We shall first demonstrate how time and normally-ordered moments may be calculated directly using the *P* representation. We consider the following time- and normally-ordered moment

$$\begin{aligned} T \langle : X_1(t) X_1(0) : \rangle &= e^{-2i\theta} \langle a(t)a(0) \rangle + e^{2i\theta} \langle a^\dagger(0)a^\dagger(t) \rangle \\ &\quad + \langle a^\dagger(t)a(0) \rangle + \langle a^\dagger(0)a(t) \rangle. \end{aligned} \quad (7.65)$$

The two-time correlation functions may be evaluated using the *P* representation which determines normally-ordered moments. Thus equal time moments of the

c-number variables give the required normally-ordered operator moments. The two time moments imply precisely the time ordering of the internal operators that are required to compute the output moments. This can be seen by noting that the evolution of the system will in general mix a^\dagger and a . Hence $a(t + \tau)$ contains both $a(t)$ and $a^\dagger(t)$, $\tau > 0$. In a normally-ordered two time product $a(t + \tau)$ must therefore stand to the left of $a(t)$, similarly $a^\dagger(t + \tau)$ must stand to the right of $a^\dagger(t)$. Thus

$$\langle \alpha(t + \tau)\alpha(t) \rangle_p = \langle a(t + \tau)a(t) \rangle , \quad (7.66)$$

$$\langle \alpha^*(t + \tau)\alpha^*(t) \rangle_p = \langle a^\dagger(t)a^\dagger(t + \tau) \rangle , \quad (7.67)$$

where the left-hand side of these equations represent averages of *c*-number variables over the P representation. The normally-ordered output correlation matrix defined by

$$:C^{\text{OUT}}(\tau): = \begin{pmatrix} \langle a_{\text{OUT}}(t + \tau), a_{\text{OUT}}(t) \rangle & \langle a_{\text{OUT}}^\dagger(t), a_{\text{OUT}}(t + \tau) \rangle \\ \langle a_{\text{OUT}}^\dagger(t + \tau), a_{\text{OUT}}(t) \rangle & \langle a_{\text{OUT}}^\dagger(t + \tau), a_{\text{OUT}}^\dagger(t) \rangle \end{pmatrix} \quad (7.68)$$

is given by

$$\begin{aligned} :C^{\text{OUT}}(\tau): &= \gamma \begin{pmatrix} \langle \alpha(t + \tau), \alpha(t) \rangle & \langle \alpha(t + \tau), \alpha^*(t) \rangle \\ \langle \alpha^*(t + \tau), \alpha(t) \rangle & \langle \alpha^*(t + \tau), \alpha^*(t) \rangle \end{pmatrix} \\ &\equiv \gamma C_p(\tau) . \end{aligned} \quad (7.69)$$

The two time correlation functions for the output field may be calculated directly from the correlation functions of the stochastic variables describing the internal field using the P representation.

For nonlinear optical processes the Fokker–Planck equation for the P function may have nonlinear drift terms and nonconstant diffusion. In such circumstances we first linearise the equation about the deterministic steady states, to obtain a linear Fokker–Planck equation of the form

$$\frac{\partial P}{\partial t}(\alpha) = \left(\frac{\partial}{\partial \alpha_i} A_i \alpha_i + \frac{1}{2} \frac{\partial^2}{\partial \alpha_i \partial \alpha_j} D_{ij} \right) P(\alpha) , \quad (7.70)$$

where A is the drift matrix, and D is the diffusion matrix. The linearised description is expected to give the correct descriptions away from instabilities in the deterministic equations of motion. For fields exhibiting quantum behaviour, such as squeezing, D is non-positive definite and a Fokker–Planck equation is not defined for the Glauber–Sudarshan P function. In these cases a Fokker–Planck equation is defined for the positive P representation, where α^* is replaced by α^\dagger an independent complex variable as described in Chap. 6.

The spectral matrix $S(\omega)$ is defined as the Fourier transform of $C_p(\tau)$. In a linearised analysis it is given by

$$S(\omega) = \gamma(A + i\omega I)^{-1}D(A^T - i\omega I)^{-1} . \quad (7.71)$$

The squeezing spectrum for each quadrature phase is then given by

$$S_1^{\text{OUT}} := \gamma [e^{-2i\theta} S_{11}(\omega) + e^{2i\theta} S_{22}(\omega) + S_{12}(\omega) + S_{21}(\omega)] , \quad (7.72)$$

$$S_2^{\text{OUT}} := \gamma [-e^{-2i\theta} S_{11}(\omega) - e^{2i\theta} S_{22}(\omega) + S_{12}(\omega) + S_{21}(\omega)] . \quad (7.73)$$

These spectra are defined in a frame of frequency Ω (the cavity-resonance frequency) so that $\omega = 0$ corresponds to the cavity resonance.

It should be noted that in the above derivation there is only one input field and one output field, that is, there is only one source of cavity loss. Thus the above results only apply to a single-ended cavity; one in which losses accrue only at one mirror.

If there are other significant losses from the cavity the γ appearing in (7.59, 60) is not the total loss but only the loss from the mirror through which the output field of interest is transmitted.

The above procedure enables one to calculate the squeezing in the output field from an optical cavity, provided the internal field may be described by the linear Fokker–Planck equation (7.70).

Alternatively the squeezing spectrum for the parametric oscillator may be calculated using the Fokker–Planck equation. The Fokker–Planck equation for the distribution $P(\alpha)$ for the system described by the Hamiltonian (7.52) may be derived using the techniques of Chap. 6.

$$\begin{aligned} \frac{\partial P(\alpha)}{\partial t} = & - \left\{ \left(\varepsilon^* \frac{\partial}{\partial \alpha^*} \alpha + \varepsilon \frac{\partial}{\partial \alpha} \alpha^* \right) + \frac{\gamma_1}{2} \left(\frac{\partial}{\partial \alpha^*} \alpha^* + \frac{\partial}{\partial \alpha} \alpha \right) \right. \\ & \left. + \frac{1}{2} \left[\varepsilon^* \frac{\partial^2}{\partial \alpha^{*2}} + \varepsilon \frac{\partial^2}{\partial \alpha^2} \right] \right\} P(\alpha) . \end{aligned} \quad (7.74)$$

The drift and diffusion matrices are

$$A = \begin{pmatrix} \frac{\gamma_1}{2} & -\varepsilon \\ \frac{\gamma_1}{2} & \varepsilon^* \end{pmatrix}, \quad D = \begin{pmatrix} \varepsilon & 0 \\ 0 & \varepsilon^* \end{pmatrix} . \quad (7.75)$$

Direct application of (7.71–73) yields the squeezing spectra given by (7.58, 59).

Exercises

7.1 Calculate the squeezing spectrum for a degenerate parametric oscillator with losses γ_1 and γ_2 at the end mirrors.

7.2 Calculate the squeezing spectrum for a non-degenerate parametric oscillator. [Hint: Use the quadratures for a two mode system described in (5.49)].

8. Generation and Applications of Squeezed Light

In this chapter we shall describe how the squeezing spectrum may be calculated for intracavity nonlinear optical processes. We shall confine our examples to processes described by an effective Hamiltonian where the medium is treated classically. Thus we are able to extend the treatment of squeezing in the parametric oscillator to the above-threshold regime. In addition, we calculate the squeezing spectrum for second harmonic generation and dispersive bistability. In Chap. 13 we shall consider the effects of spontaneous emission on the generation of squeezed light in four-wave mixing. This requires the medium to be quantised and the treatment is consequently more involved. We shall also consider the case of nondegenerate parametric oscillation where it is possible to achieve intensity fluctuations below the shot-noise level in the difference of the signal and idler intensities.

Two applications will be discussed: squeezed states in the interferometric detection of gravitational radiation and sub-shot-noise phase measurements.

8.1 Parametric Oscillation and Second Harmonic Generation

We consider the interaction of a light mode at frequency ω_1 with its second harmonic at frequency $2\omega_1$. The nonlinear medium is placed within a Fabry–Perot cavity driven coherently either at frequency $2\omega_1$ (parametric oscillation or frequency ω_1 (second harmonic generation)). We shall begin by including driving fields both at frequency ω_1 and $2\omega_1$ so that both situations may be described within the one formalism. We write the Hamiltonian as [8.1]

$$\mathcal{H} = \mathcal{H}_1 + \mathcal{H}_2 ,$$

$$\begin{aligned}\mathcal{H}_1 = & \hbar\omega_1 a_1^\dagger a_1 + 2\hbar\omega_1 a_2^\dagger a_2 + i\frac{\hbar\kappa}{2} (a_1^{\dagger 2} a_2 - a_1^2 a_2^\dagger) + i\hbar(E_1 a_1^\dagger e^{-i\omega_1 t} \\ & - E_1^* a_1 e^{i\omega_1 t}) + i\hbar(E_2 a_2^\dagger e^{-2i\omega_1 t} - E_2^* a_2 e^{2i\omega_1 t}) ,\end{aligned}$$

$$\mathcal{H}_2 = a_1 \Gamma_1^\dagger + a_1^\dagger \Gamma_1 + a_2 \Gamma_2^\dagger + a_2^\dagger \Gamma_2 ,$$

where a_1 and a_2 are the Boson operators for modes of frequency ω_1 and $2\omega_1$, respectively, κ is the coupling constant for the interaction between the two modes and the spatial mode functions are chosen so that κ is real, Γ_1, Γ_2 are heat

bath operators which represent cavity losses for the two modes and E_1 and E_2 are proportional to the coherent driving field amplitudes.

The master equation for the density operator of the two cavity modes after tracing out over the reservoirs is

$$\frac{\partial \rho}{\partial t} = \frac{1}{i\hbar} [\mathcal{H}_1, \rho] + (L_1 + L_2)\rho , \quad (8.2)$$

where

$$L_i\rho = \gamma_i(2a_i\rho a_i^\dagger - a_i^\dagger a_i\rho - \rho a_i^\dagger a_i) ,$$

and γ_i are the cavity damping rates of the modes.

This master equation may be converted to a c-number Fokker–Planck equation in the generalised P representation. The generalised P representation must be used since the c-number equation would have a non-positive definite diffusion matrix if the Glauber–Sudarshan P representation were used. The result is

$$\begin{aligned} \frac{\partial}{\partial t} P(\alpha) = & \left\{ \frac{\partial}{\partial \alpha_1} (\gamma_1 \alpha_1 - E_1 - \kappa \alpha_1^\dagger \alpha_2) + \frac{\partial}{\partial \alpha_1^\dagger} (\gamma_1 \alpha_1^\dagger - E_1^* - \kappa \alpha_1 \alpha_2^\dagger) \right. \\ & + \frac{\partial}{\partial \alpha_2} \left(\gamma_2 \alpha_2 - E_2 + \frac{\kappa}{2} \alpha_1^2 \right) + \frac{\partial}{\partial \alpha_2^\dagger} \left(\gamma_2 \alpha_2^\dagger - E_2^* + \frac{\kappa}{2} \alpha_1^{*2} \right) \\ & \left. + \frac{1}{2} \left[\frac{\partial^2}{\partial \alpha_1^2} (\kappa \alpha_2) + \frac{\partial^2}{\partial \alpha_1^{*2}} (\kappa \alpha_2^\dagger) \right] \right\} P(\alpha) , \end{aligned} \quad (8.3)$$

where $\alpha = [\alpha_1, \alpha_1^\dagger, \alpha_2, \alpha_2^\dagger]$, and we have made the following transformation to the rotating frames of the driving fields

$$\alpha_1 \rightarrow \alpha_1 \exp(-i\omega_1 t), \quad \alpha_2 \rightarrow \alpha_2 \exp(-2i\omega_1 t) .$$

In the generalized P representation α and α^\dagger are independent complex variables and the Fokker–Planck equation has a positive semi-definite diffusion matrix in an eight-dimensional space. This allows us to define equivalent stochastic differential equations using the Ito rules

$$\frac{\partial}{\partial t} \begin{pmatrix} \alpha_1 \\ \alpha_1^\dagger \end{pmatrix} = \begin{pmatrix} E_1 + \kappa \alpha_1^\dagger \alpha_2 - \gamma_1 \alpha_1 \\ E_1^* + \kappa \alpha_1 \alpha_2^\dagger - \gamma_1 \alpha_1^\dagger \end{pmatrix} + \begin{pmatrix} \kappa \alpha_2 & 0 \\ 0 & \kappa \alpha_2^\dagger \end{pmatrix}^{1/2} \begin{pmatrix} \eta_1(t) \\ \eta_1^\dagger(t) \end{pmatrix} , \quad (8.4)$$

$$\frac{\partial}{\partial t} \begin{pmatrix} \alpha_2 \\ \alpha_2^\dagger \end{pmatrix} = \begin{pmatrix} E_2 - \frac{\kappa}{2} \alpha_1^2 - \gamma_2 \alpha_2 \\ E_2^* - \frac{\kappa}{2} \alpha_1^{*2} - \gamma_2 \alpha_2^\dagger \end{pmatrix} , \quad (8.5)$$

where $\eta_1(t), \eta_1^\dagger(t)$ are delta correlated stochastic forces with zero mean, namely

$$\begin{aligned} \langle \eta_1(t) \rangle &= \langle \eta_1^\dagger(t) \rangle = 0 , \\ \langle \eta_1(t) \eta_1^\dagger(t') \rangle &= \delta_{ij} \delta(t - t') . \end{aligned} \quad (8.6)$$

8.1.1 Semi-classical Steady States and Stability Analysis

The semi-classical or mean value equations follow directly from (8.4 and 5) with the replacement of α_i^\dagger by α_i^* .

$$\frac{\partial}{\partial t} \alpha_1 = E_1 + \kappa \alpha_1^* \alpha_2 - \gamma_1 \alpha_1 , \quad (8.7)$$

$$\frac{\partial \alpha_2}{\partial t} = E_2 + \frac{\kappa}{2} \alpha_1^2 - \gamma_2 \alpha_2 . \quad (8.8)$$

We shall investigate the steady states of these equations and their stability. The stability of the steady states may be determined by a linearized analysis for small perturbations around the steady state

$$\alpha_1 = \alpha_1^0 + \delta \alpha_1, \quad \alpha_2 = \alpha_2^0 + \delta \alpha_2 , \quad (8.9)$$

where α_1^0, α_2^0 are the steady-state solutions of (8.7 and 8). The linearized equations for the fluctuations are

$$\frac{\partial}{\partial t} \begin{pmatrix} \delta \alpha_1 \\ \delta \alpha_1^* \\ \delta \alpha_2 \\ \delta \alpha_2^* \end{pmatrix} = \begin{pmatrix} -\gamma_1 & \kappa \alpha_2^0 & \kappa \alpha_1^0 & 0 \\ \kappa \alpha_2^{0*} & -\gamma_1 & 0 & \kappa \alpha_1^0 \\ -\kappa \alpha_1^{0*} & 0 & -\gamma_2 & 0 \\ 0 & -\kappa \alpha_1^{0*} & 0 & -\gamma_2 \end{pmatrix} \begin{pmatrix} \delta \alpha_1 \\ \delta \alpha_1^* \\ \delta \alpha_2 \\ \delta \alpha_2^* \end{pmatrix} . \quad (8.10)$$

The four eigenvalues of these equations are

$$\begin{aligned} \lambda_1, \lambda_2 &= -\frac{1}{2}(-|\kappa \alpha_2^0| + \gamma_1 + \gamma_2) \pm \frac{1}{2}[(-|\kappa \alpha_2^0| + \gamma_1 - \gamma_2)^2 - 4|\kappa \alpha_1^0|^2]^{1/2} , \\ \lambda_3, \lambda_4 &= -\frac{1}{2}(|\kappa \alpha_2^0| + \gamma_1 + \gamma_2) \pm \frac{1}{2}[(|\kappa \alpha_2^0| + \gamma_1 - \gamma_2)^2 - 4|\kappa \alpha_1^0|^2]^{1/2} . \end{aligned} \quad (8.11)$$

We shall consider the cases of parametric oscillation and second harmonic generation separately.

8.1.2 Parametric Oscillation

For parametric oscillation only the mode at frequency $2\omega_1$ is pumped so we set $E_1 = 0$. The stable steady state solutions for the mode amplitudes are

below threshold $E_2 < E_2^c$

$$\alpha_1^0 = 0, \quad \alpha_2^0 = \frac{E_2}{\gamma_2} , \quad (8.12)$$

above threshold $E_2 > E_2^c$

$$\alpha_1^0 = \pm \left[\frac{2}{\kappa} (E_2 - E_2^c) \right]^{1/2}, \quad \alpha_2^0 = \frac{\gamma_1}{\kappa}, \quad (8.13)$$

where $E_2^c = \gamma_1 \gamma_2 / \kappa$, and we have taken E_2 to be positive. Thus the system exhibits behaviour analogous to a second-order phase transition at $E_2 = E_2^c$ where the below-threshold solution $\alpha_1^0 = 0$ becomes unstable and the system moves onto a new stable branch. Above threshold there exist two solutions with equal amplitude and opposite phase. In Fig. 8.1 we plot the amplitude α_1^0 versus E_2 .

8.1.3 Second Harmonic Generation

For second harmonic generation only the cavity mode at frequency ω is pumped so we set $E_2 = 0$. Equations (8.7, 8) then yield the following equation for the steady state amplitude of the second harmonic

$$-2\gamma_2(\kappa\alpha_2^0)^3 + 4\gamma_1\gamma_2(\kappa\alpha_2^0) - 2\gamma_1^2\gamma_2(\kappa\alpha_2^0) = |\kappa E_1|^2. \quad (8.14)$$

This gives a solution for α_2^0 which is negative and the intensity $|\alpha_2^0|^2$ is a monotonically increasing, single valued function of $|E_1|^2$.

However from the stability analysis we find that the eigenvalues

$$\lambda_1, \lambda_2 \rightarrow 0 \pm i\omega, \quad (8.15)$$

where $\omega = [\gamma_2(2\gamma_1 + \gamma_2)]^{1/2}$ when the driving field E_1 reaches the critical value

$$E_1^c = \frac{1}{\kappa}(2\gamma_1 + \gamma_2)[2\gamma_2(\gamma_1 + \gamma_2)]^{1/2}. \quad (8.16)$$

Thus the light modes in the cavity undergo a hard mode transition, where the steady state given by (8.14) becomes unstable and is replaced by periodic limit cycle behaviour. This behaviour is illustrated in Fig. 8.2 which shows the time development of the mode intensities above the instability point.

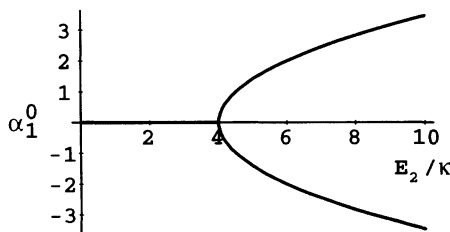


Fig. 8.1. Steady state amplitude of the fundamental mode versus pump field amplitude for parametric oscillation, $\kappa = 1.0$, $E_2^c = 4.0$

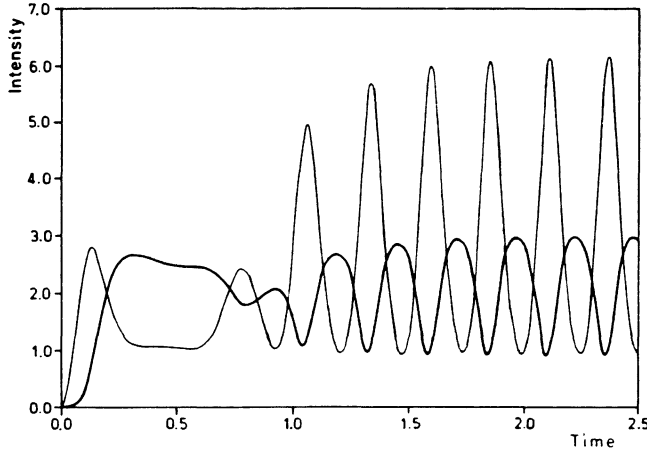


Fig. 8.2. Self pulsing in second harmonic generation: $|\alpha_1|^2$ (light), $|\alpha_2|^2$ (heavy) as functions of time. Numerical solutions of (8.7, 8) with $\kappa = 10.0$, $\gamma_1 = \gamma_2 = 3.4$, $\varepsilon_1 = 20.0$, $\varepsilon_2 = 0.0$ and initial conditions $\alpha_1 = 0.1 + 0.1i$, $\alpha_2 = 0.0$

8.1.4 Squeezing Spectrum

We shall calculate the squeezing spectrum using a linearized fluctuation analysis about the steady state solutions [8.2, 3]. The linearized drift and diffusion matrices for the Fokker–Planck equation (8.3) are

$$A = \begin{pmatrix} \gamma_1 & -\varepsilon_2 & -\varepsilon_1^* & 0 \\ -\varepsilon_2^* & \gamma_1 & 0 & -\varepsilon_1 \\ \varepsilon_1 & 0 & \gamma_2 & 0 \\ 0 & \varepsilon_1^* & 0 & \gamma_2 \end{pmatrix}, \quad (8.17)$$

$$D = \begin{pmatrix} \varepsilon_2 & 0 & 0 & 0 \\ 0 & \varepsilon_2^* & 0 & 0 \\ 0 & 0 & 0 & 0 \\ 0 & 0 & 0 & 0 \end{pmatrix}. \quad (8.18)$$

where $\varepsilon_2 = \kappa\alpha_2^0$, $\varepsilon_1 = \kappa\alpha_1^0$, and we have replaced α_2 in the diffusion matrix by its steady state value. We may then use (7.50) to calculate the spectral matrix $S(\omega)$.

The results for the squeezing in the amplitude and phase quadratures follow from (8.17 and 18). The squeezing in the low frequency mode (ω_1) is

$$S_{1\pm}^{\text{out}}(\omega) = 1 \pm \frac{4\gamma_1|\varepsilon_2|(\gamma_2^2 + \omega^2)}{[\gamma_2(\gamma_1 \mp |\varepsilon_2|) + |\varepsilon_1|^2 - \omega^2]^2 + \omega^2(\gamma_1 \mp |\varepsilon_2| + \gamma_2)^2}, \quad (8.19)$$

where the + and - refer to the unsqueezed and squeezed quadratures, respectively. The squeezing in the high frequency mode ($2\omega_1$) is

$$S_{2\pm}^{\text{out}}(\omega) = 1 \pm \frac{4\gamma_2|\varepsilon_2||\varepsilon_1|^2}{[\gamma_2(\gamma_1 \mp |\varepsilon_2|) + |\varepsilon_1|^2 - \omega^2]^2 + \omega^2(\gamma_1 \mp |\varepsilon_2| + \gamma_2)^2}, \quad (8.20)$$

The above results are general for two driving field ε_1 and ε_2 . We now consider the special cases of parametric oscillation and second harmonic generation.

8.1.5 Parametric Oscillation

For parametric oscillation $\varepsilon_1 = 0$ and below threshold the expression for the squeezing spectrum simplifies considerably. The phase quadrature is squeezed with

$$S_{1-}^{\text{out}}(\omega) = 1 - \frac{4\gamma_1|\varepsilon_2|}{(\gamma_1 + |\varepsilon_2|)^2 + \omega^2}. \quad (8.21)$$

This is a Lorentzian dip below the vacuum level which as threshold is approached $|\varepsilon_2| = \gamma$ gives $S_{1-}^{\text{out}}(0) = 0$. This is the same result as obtained in Chap. 7 where the pump mode was treated classically. However, this treatment also allows us to investigate the above-threshold regime. The squeezing spectrum above threshold becomes double peaked for

$$|\varepsilon_1|^2 > \gamma_2^2 \{ [\gamma_2^2 + (\gamma_2 + 2\gamma_1)^2]^{1/2} - (\gamma_2 + 2\gamma_1) \}. \quad (8.22)$$

The double-peaked squeezing spectrum is plotted in Fig. 8.3. If the high-frequency losses from the cavity are insignificant ($\gamma_2 \ll \gamma_1$), this splitting occurs immediately above threshold, with the greatest squeezing being at $\omega = \pm |\varepsilon_1|$. The value of $S_{1-}^{\text{out}}(|\varepsilon_1|)$ remains close to zero even far above threshold. In Fig. 8.4 we plot the maximum squeezing obtained as a function of $|\varepsilon_1|$ for different values of the ratio of the cavity losses γ_2/γ_1 . Below threshold the squeezing is independent of this ratio but above threshold the squeezing depends crucially on this

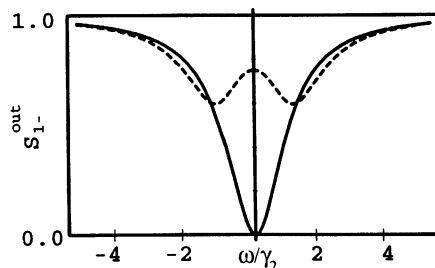


Fig. 8.3. The squeezing spectrum for parametric oscillation with $\gamma_1 = 2\gamma_2$. Solid line: on threshold with $\varepsilon_2 = \gamma_1$. Dashed line: above threshold with $\varepsilon_2 = \gamma_2$

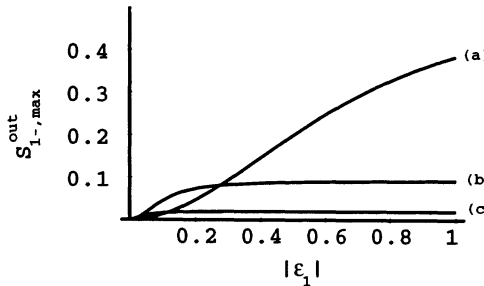


Fig. 8.4. Maximum squeezing above threshold as a function of the amplitude of the fundamental mode $|\epsilon_1|$, for different values of the cavity losses γ_2/γ_1 ; (a) 0.02, (b) 0.1, (c) 1.0

ratio. Above threshold the pump is depleted, and noise from the pump enters the signal field. If the cavity losses at the pump frequency are significant, then uncorrelated vacuum fluctuations will feed through into the signal and degrade the squeezing. Thus a low cavity loss at the pump frequency by comparison with the signal loss is needed to obtain good squeezing above threshold in the parametric oscillator.

We may also consider the squeezing in the pump mode. Below threshold this mode is not squeezed. Above threshold the peak squeezing (at $\omega = 0$) increases to a maximum value of 50% at $|\epsilon_1| = 2\gamma_1\gamma_2$. When $|\epsilon_1| = 2\gamma_1^2 + \frac{1}{2}\gamma_2^2$, we again find a splitting into a double peak.

8.1.6 Experiments

An experiment demonstrating the generation of squeezed light in an optical parametric oscillator below threshold has been performed by Wu et al. [4]. A schematic diagram of the principal elements of the apparatus is shown in Fig. 8.5. The central element is an optical parametric oscillator containing a MgOLiNbO_3 crystal. The oscillator is pumped at $0.53 \mu\text{m}$ with the frequency doubled output of a Nd: YAG laser. Squeezed light is generated at $1.06 \mu\text{m}$ and passes through the end cavity mirror which is perfectly reflecting at $0.53 \mu\text{m}$. In order to provide a local oscillator at $1.06 \mu\text{m}$ part of the output of the original Nd: YAG laser is incident on one port of a balanced homodyne detector. The squeezed light is incident on the other port. The phase of the local oscillator is adjusted to correspond to the maximally squeezed quadrature. The vacuum noise level is determined by blocking the squeezed light so that only the vacuum field is incident on the input port of the homodyne detector.

The phase dependence of the rms noise voltage $V(\theta)$ from the balanced homodyne receiver as a function of local-oscillator phase θ at fixed analysis frequency Ω is exhibited in Fig. 8.6. The flat line gives the vacuum noise level. The maximum dips below this level represent a 61% reduction in noise power relative to the vacuum level. The maximum squeezing at a given pump power is

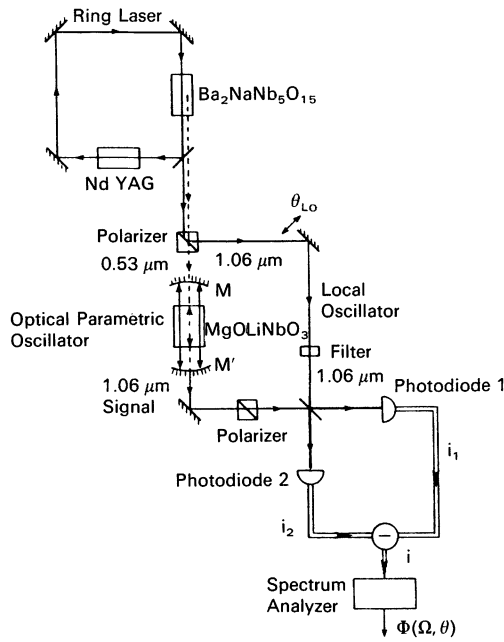


Fig. 8.5. Schematic representation of the experiment of Wu et al. [8.4] to produce squeezed light in parametric oscillation.

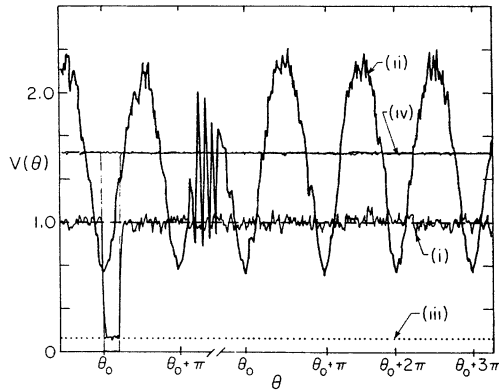


Fig. 8.6. The phase dependence of the squeezed quadrature phase fluctuations as measured by the rms noise voltage from the balanced homodyne detection scheme, as a function of local oscillator phase θ at fixed frequency Ω . The flat line (i) gives the vacuum noise level. Curve (iii) is the amplifier noise level. Curve (iv) gives the level of dc photocurrent

plotted in Fig. 8.7. The experimental data has been adjusted to compensate for linear losses in the cavity and detector inefficiencies. A comparison is made with the theoretical predictions given by (8.21). The best experimental data obtained by the group of Kimble allows one to infer that a field emitted from the cavity

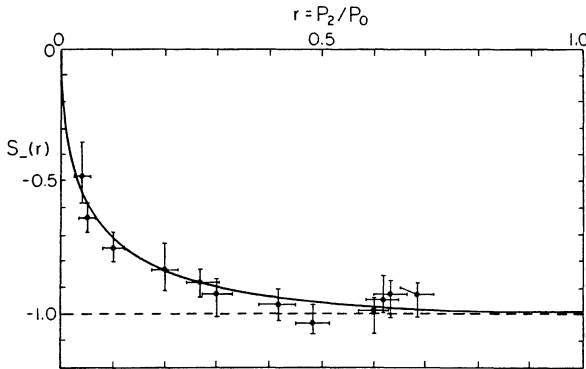


Fig. 8.7. Maximum squeezing at a given pump power for the experiment of *Wu et al.* [8.4] at fixed frequency. The solid line represents the theory

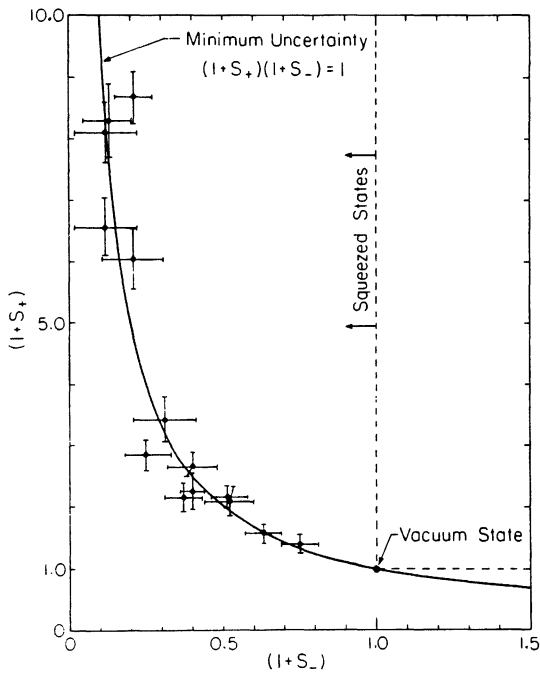


Fig. 8.8. A plot of the squeezed quadrature fluctuations versus the unsqueezed quadrature fluctuations. The hyperbola is the minimum uncertainty state line

has a tenfold squeezing. Detector inefficiencies reduce the amount of squeezing observed to threefold. A plot of the variance in the squeezed quadrature versus the variance in the unsqueezed quadrature is given in Fig. 8.8. A comparison is made with the hyperbola determining the minimum uncertainty state. A remarkable agreement is obtained demonstrating that the light field generated in the optical parametric oscillator is a minimum uncertainty squeezed state.

8.2 Twin Beam Generation and Intensity Correlations

Another second-order process which can produce non-classical states is non-degenerate down conversion. A pump photon with frequency 2ω creates a signal and an idler photon each with frequency ω but different polarisations. Alternatively the signal and idler may be distinguished by having different frequencies ω_1 and ω_2 , respectively, such that $\omega_1 + \omega_2 = 2\omega$. Such a process ensures that the photon numbers in the signal and idler beams are highly correlated. Although the intensity of each beam may fluctuate, the fluctuations on the two beams are identical. This suggests that the intensity difference of the two beams will carry no fluctuations at all. That is to say, the variance of $I_1 - I_2$ can be zero. If the process occurs inside a cavity the correlation between the two photons may be lost as photons escape the cavity. This is true for times short compared to the cavity lifetime. For long times, however, the correlation is restored; if one waits long enough all photons will exit the cavity. Consequently the spectrum of fluctuations in the difference of the intensities in the two beams reduces to zero at zero frequency.

The Hamiltonian describing this process may be written as

$$\mathcal{H}_I = i\hbar\chi(a_0 a_1^\dagger a_2^\dagger - a_0^\dagger a_1 a_2) , \quad (8.23)$$

where a_0 describes the pump field, while a_1 and a_2 describe the signal and idler fields. The pump field is driven by a coherent field external to the cavity with amplitude ε . The damping rates for the three cavity modes a_0 , a_1 and a_2 are κ_0 , κ_1 and κ_2 , respectively.

Following from the Fokker–Planck equation for the positive P representation we establish the c-number stochastic differential equations [8.5]

$$\begin{aligned} \dot{\alpha}_0 &= -\kappa_0\alpha_0 + \varepsilon - \chi\alpha_1\alpha_2 , \\ \dot{\alpha}_1 &= -\kappa_1\alpha_1 + \chi\alpha_0\alpha_2^\dagger + R_1(t) , \\ \dot{\alpha}_2 &= -\kappa_2\alpha_2 + \chi\alpha_0\alpha_1^\dagger + R_2(t) . \end{aligned} \quad (8.24)$$

In our treatment we will assume for simplicity that $\kappa_1 = \kappa_2 = \kappa$, where the only non-zero noise correlation functions are

$$\begin{aligned} \langle R_1(t)R_2(t') \rangle &= \chi\langle\alpha_0\rangle\delta(t - t') , \\ \langle R_1^\dagger(t)R_2^\dagger(t') \rangle &= \chi\langle\alpha_0^\dagger\rangle\delta(t - t') . \end{aligned} \quad (8.25)$$

The semi-classical steady state solutions depend on whether the driving field ε is above or below a critical “threshold” value given by

$$\varepsilon_{\text{thr}} = \frac{\kappa_0\kappa}{\chi} . \quad (8.26)$$

Above threshold one of the eigenvalues of the drift matrix is zero. This is associated with a phase instability. To see this we use an amplitude and phase representation:

$$\alpha_j(t) = r_j[1 + \mu_j(t)]e^{-i(\phi_j + \psi_j(t))} \quad (8.27)$$

where r_j , ϕ_j are the steady state solutions, and $\mu_j(t)$ and $\psi_j(t)$ represent small fluctuations around the steady state. Solving for the steady state below threshold we have

$$r_1 = r_2 = 0, \quad r_0 = \frac{|\varepsilon|}{\kappa_0}, \quad \phi_0 = \phi_p, \quad (8.28)$$

where we have used $\varepsilon = |\varepsilon|e^{i\phi_p}$, with ϕ_p denoting the phase of the coherent pump. Above threshold

$$\begin{aligned} r_0 &= \frac{\kappa}{\chi}, \quad \phi_0 = \phi_p, \\ r_1 = r_2 &= \frac{\sqrt{\kappa_0\kappa}}{\chi}(E - 1)^{1/2}, \quad \phi_1 + \phi_2 = \phi_p, \end{aligned} \quad (8.29)$$

with

$$E = \frac{|\varepsilon|}{|\varepsilon_{\text{thr}}|}. \quad (8.30)$$

Note that in the above threshold solution only the sum of the signal and idler phases is defined. No steady state exists for the phase difference. It is the phase difference variable which is associated with the zero eigenvalue.

We now turn to an analysis of the intensity fluctuations above threshold. The nonlinear dynamics of (8.24) is approximated by a linear dynamics for intensity fluctuations about the steady states above threshold. Define the new variables by

$$\Delta I_j = \alpha_j^\dagger \alpha_j - I_j^{\text{ss}}, \quad (8.31)$$

where I_j^{ss} is the steady state intensity above threshold for each of the three modes. It is more convenient to work with scaled ‘intensity-sum’ and ‘intensity-difference’ variables defined by

$$\Delta I_s = \kappa(\Delta I_1 + \Delta I_2), \quad \Delta I_D = \kappa(\Delta I_1 - \Delta I_2), \quad (8.32)$$

The linear stochastic differential equations are then given by

$$\Delta \dot{I}_0 = -\kappa_0 \Delta I_0 - \Delta I_s, \quad (8.33)$$

$$\Delta \dot{I}_s = 2\kappa\kappa_0(E - 1)\Delta I_0 + F_s(t), \quad (8.34)$$

$$\Delta \dot{I}_D = -2\kappa\Delta I_D + F_D(t), \quad (8.35)$$

where the non zero noise correlations are

$$\langle F_s(t)F_s(t') \rangle = -\langle F_D(t)F_D(t') \rangle = 4 \frac{\kappa_0 \kappa^4}{\chi^2} (E - 1) \delta(t - t') . \quad (8.36)$$

We are now in a position to calculate the spectrum of fluctuations in the intensity difference in the signal and idler modes outside the cavity. The equation for the intensity difference fluctuations may be solved immediately to give

$$\Delta I_0(t) = \Delta I_D(0)e^{-2\kappa t} + \int_0^t dt' e^{-2\kappa(t-t')} F_D(t') . \quad (8.37)$$

Thus the steady state two-time correlation function is found to be

$$\langle I_D(\tau), I_D(0) \rangle = \langle \Delta I_D(\tau) \Delta I_D(0) \rangle = \frac{\kappa_0 \kappa^3}{\chi^2} (E - 1) e^{-2\kappa\tau} \quad (8.38)$$

with $\langle A, B \rangle = \langle AB \rangle - \langle A \rangle \langle B \rangle$.

The spectrum of fluctuations in the intensity difference field outside the cavity is defined by

$$S_D(\omega) = \int d\tau e^{-i\omega\tau} \langle \hat{I}_1(\tau) - \hat{I}_2(\tau), \hat{I}_1(0) - \hat{I}_2(0) \rangle_{ss} , \quad (8.39)$$

where $\hat{I}_j(t)$ are the external intensity operators. However, from Chap. 7, we can relate this operator average to the c-number averages for $\alpha_j(t)$ inside the cavity. The result is

$$\langle \hat{I}_j(\tau), \hat{I}_k(0) \rangle = 2\delta_{jk}\kappa\delta(\tau)\langle I_j(0) \rangle + 4\kappa^2\langle I_j(\tau), I_k(0) \rangle , \quad (8.40)$$

where $I_j \equiv \alpha_j^\dagger(t)\alpha_j(t)$. Finally, we write the result directly in terms of the valuables $\Delta I_D(t)$,

$$S_D(\omega) = S_0 + 4 \int d\tau e^{-i\omega\tau} \langle \Delta I_D(\tau) \Delta I_D(0) \rangle , \quad (8.41)$$

where

$$S_0 = 2\kappa(\langle I_1 \rangle_{ss} + \langle I_2 \rangle_{ss}) = \frac{4\kappa_0 \kappa^3}{\chi^2} (E - 1) . \quad (8.42)$$

The frequency independent term S_0 represents the contribution of the shot-noise from each beam. Thus to quantify the degree of reduction below the shot-noise level we define the ‘normalised’ intensity difference spectrum

$$\bar{S}_D(\omega) \equiv \frac{S_D(\omega)}{S_0} . \quad (8.43)$$

Substituting (8.38 and 42) into (8.41), and integrating we obtain

$$\bar{S}_D(\omega) \equiv \frac{\omega^2}{\omega^2 + 4\kappa^2} . \quad (8.44)$$

This is a simple inverted Lorentzian with a width 2κ . As expected, at zero frequency there is perfect noise suppression in the intensity difference between the signal and idler. This result was first obtained by Reynaud et al. [8.6].

The above results assume no additional cavity losses beyond those corresponding to the (equal) transmittivities at the output mirror. When additional losses are included the correlation between the signal and idler is no longer perfect as one of the pair of photons may be lost otherwise than through the output mirror. In that case there is no longer perfect suppression of quantum noise at zero frequency [8.7]. The result is shown in Fig. 8.9a. Furthermore, the spectrum of intensity difference fluctuations is very sensitive to any asymmetry in the loss for each mode [8.7]. In Fig. 8.9b we depict the effect of introducing different intracavity absorption rates for each mode. This phenomenon could form the basis of a sub-shot-noise absorption spectrometer.

The prediction of noise suppression in the differenced intensity has been confirmed in the experiment of Heidmann et al. [8.8]. They used a type II phase-matched potassium triphosphate, known as KTP, crystal placed inside an optical cavity, thus forming an Optical Parametric Oscillator (OPO).

The damping constant at the pump frequency was much greater than for the signal and idler. Above threshold the OPO emits two cross polarised twin beams at approximately the same frequency. The twin beams are separated by polarising beam splitters and then focussed on two photodiodes which have quantum efficiencies of 90%. The two photo-currents are amplified and then subtracted with a 180° power combiner. The noise on the resulting difference current is then monitored by a spectrum analyser.

A maximum noise reduction of $30\% \pm 5\%$ is observed at a frequency of 8 MHz. The noise reduction is better than 15% from 3 to 13 MHz. The noise reduction is limited due to other losses inside the OPO and various detector inefficiencies.

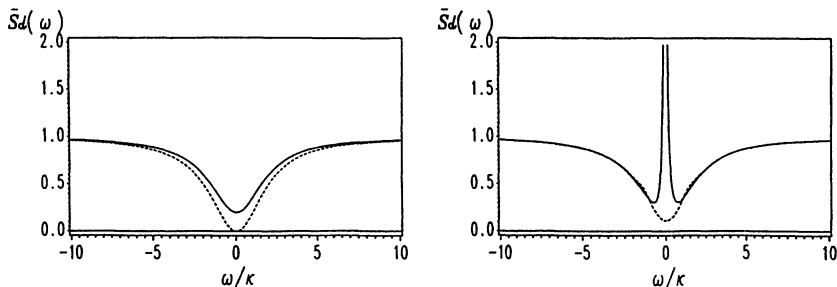


Fig. 8.9. The effect of intracavity absorption on the intensity difference spectrum. (a) A plot of the normalized spectrum when the total cavity losses for each mode are equal to the total loss from the pump mode, and greater than the output loss rate κ (solid line). The dashed line shows the perfect case when the only losses are through the output mirrors. (b) The effect of asymmetrical intracavity absorption. The total loss for the idler is equal to the idler damping rate but the damping rate for the signal is only 80% of the total loss for that mode. $E = 1.05$ solid line, $E = 2.0$, dashed line. [8.7]

In a refinement of this experiment *Debuisschert et al.* [8.9] have reported an improved quantum noise reduction of 69% on the intensity difference.

The bandwidth of squeezing in cavity experiments is restricted to the cavity bandwidth. Single-pass experiments are feasible using the higher intensity possible with pulsed light. Pulsed twin beams of light have been generated by means of an optical parametric amplifier that is pumped by the second harmonic of a mode-locked and *Q*-switched Nd:YAG laser [8.10]. While the noise levels of the individual signal and idler beams exceed their coherent state limits by about 11 dB the correlation is so strong that the noise in the difference current falls below the quantum limit by more than 6 dB (75%).

8.2.1 Second Harmonic Generation

We now consider second harmonic generation setting $E_2 = 0$. For both the second harmonic and fundamental modes the squeezing increases monotonically as $|\varepsilon_2|$ increases from zero to the critical value $|\varepsilon_2| = \gamma_1 + \gamma_2$. The squeezing spectrum splits into two peaks first for the fundamental and then provided $\gamma_2^2 > \frac{1}{2} \gamma_1^2$ for the second harmonic.

Above the critical point the system exhibits self-sustained oscillations. We plot the maximum squeezing as a function of the driving field E_1 for both the fundamental and second harmonic in Fig. 8.10 [8.3].

In both the cases considered the maximum squeezing occurs as an instability point is approached. This is an example of critical quantum fluctuations which are asymmetric in the two quadrature phases. It is clear that in order to approach zero fluctuations in one quadrature the fluctuations in the other must diverge. At the critical point itself, with the critical frequency being $\omega_c^2 = \gamma_2(\gamma_2 + 2\gamma_1)$ (which is, in fact, the initial frequency of the hard mode

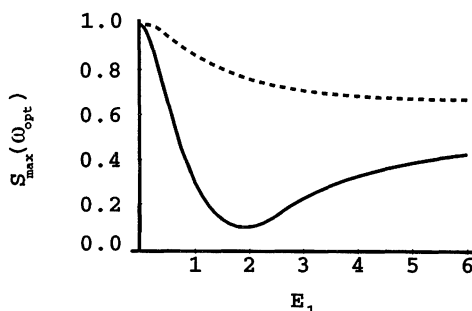


Fig. 8.10. A plot of the maximum squeezing versus driving field amplitude for second harmonic generation. The solid line is the fundamental, the dashed line is the second-harmonic. $\gamma_1 = \gamma_2 = 1.0$

oscillations) we have for the amplitude quadrature of the fundamental.

$$S_{1+}^{\text{OUT}}(\omega_c) = 1 - \frac{\gamma_1}{\gamma_1 + \gamma_2}, \quad (8.45)$$

which gives perfect squeezing for $\gamma_1 \gg \gamma_2$ at $\omega = \pm\sqrt{2\gamma_1\gamma_2}$, and for the amplitude quadrature of the second harmonic

$$S_{2+}^{\text{OUT}}(\omega_c) = 1 - \frac{\gamma_2}{\gamma_1 + \gamma_2}, \quad (8.46)$$

this gives perfect squeezing for $\gamma_2 \gg \gamma_1$ at $\omega = \gamma_2$. The squeezing spectra for the two modes at the critical point is shown in Fig. 8.11. The fluctuations in the phase quadrature must tend to infinity, a characteristic of critical fluctuations. We note that the linearization procedure we have used will break down in the vicinity of the critical point and in practice the systems will operate some distance from the critical point.

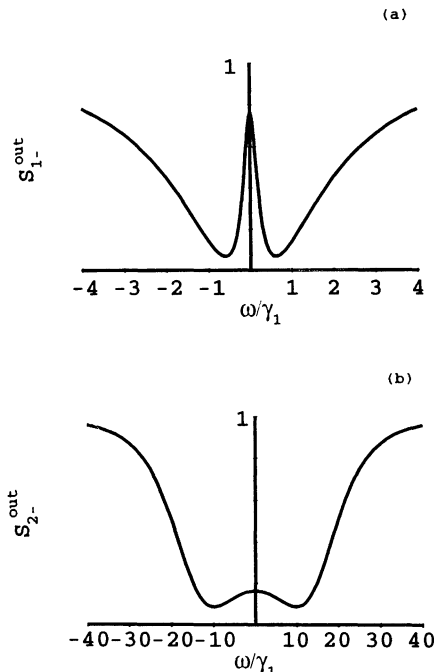


Fig. 8.11. The squeezing spectrum for the fundamental and the second harmonic at the critical point for oscillation. $\gamma_1 = 1.0$, (a) $\gamma_2 = 0.1$, (b) $\gamma_2 = 10.0$

8.2.2 Experiments

There have been two experiments which demonstrated amplitude squeezing in second harmonic generation. Pereira et al. [8.11] used an optical cavity containing a crystal of lithium niobate doped with magnesium oxide ($\text{MgO}: \text{LiNbO}_3$) and driven by the field from a frequency stabilized Nd:YAG laser. Since in second harmonic generation the squeezing occurs in the amplitude quadrature a direct detection scheme may be employed. They looked for squeezing at the fundamental frequency. Sensitivity to phase noise both from the pump laser and from scattering processes in the crystal limited the amount of squeezing observed in this experiment to a 13% reduction relative to the vacuum level.

Sizman et al. [8.12] have reported a 40% reduction in the intensity fluctuations of the second harmonic light generated in a $\text{MgO}: \text{LiNbO}_3$ monolithic cavity pumped by a Nd:YAG laser. The end faces of the crystal have dielectric mirror coatings with a high reflectivity for both fundamental and second harmonic modes. The experimental arrangement is displayed in Fig. 8.12. The second harmonic light is split by a beam splitter and detected by two photodiodes. The noise amplitudes of the sum and difference photocurrents $i_+ = i_1 + i_2$ and $i_- = i_1 - i_2$ are recorded by spectrum analysers. The spatial densities $\Phi_{\pm}(v) = 20 \log_{10} \left(\frac{i_{\pm}(v)}{i_0} \right)$ of the photocurrent fluctuations of i_+ and i_- are compared. The reference current i_0 is chosen to give Φ_{\pm} in dB_m units. In the difference current i_- the intensity fluctuations coming from the second harmonic (SH) mode cancel out, and only the Poissonian fluctuations introduced by the beam splitter are left. In the sum current i_+ the original SH photon statistics are reproduced. Hence Φ_+ is proportional to the spectral density of the intensity fluctuations in the SH mode, whereas Φ_- is proportional to the corresponding Poissonian level. If the SH mode has a sub-Poissonian character, then Φ_+ is smaller than Φ_- . Experimental results are shown in Fig. 8.13 where the cavity detuning is swept. Close to resonance the fluctuations Φ_+ abruptly drop below the shot-noise level Φ_- . The large amounts of excess noise on both

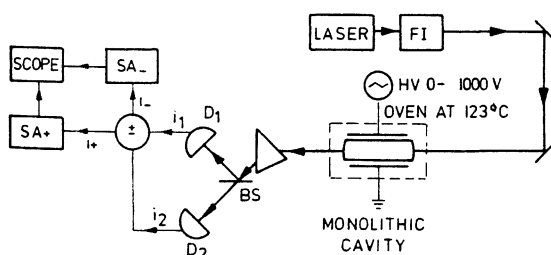


Fig. 8.12. Schematic representation of the experiment of Sizman et al. to produce squeezed light in the second harmonic and the fundamental modes. (FI: Faraday isolator; BS: beam splitter; SA: spectrum analyzer; D: photodiodes; HV: high voltage function generator)

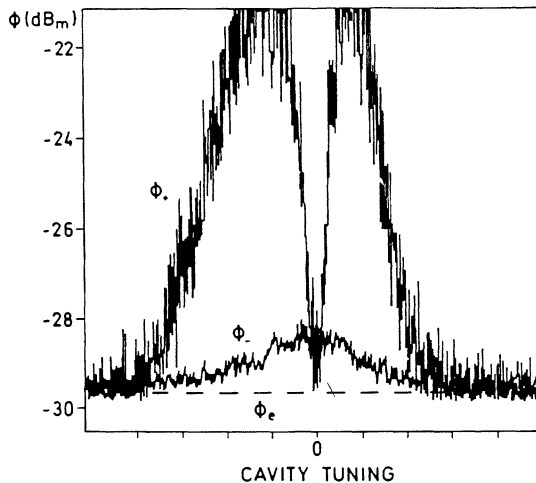


Fig. 8.13. Spectral densities of the differenced photocurrent as a function of detuning. The bottom line ϕ_e indicates the electronic noise level. The displayed full tuning range is 300 MHz

sides of the resonance are phase fluctuations which are transformed into intensity fluctuations due to the slope of the cavity transmission curve.

Second harmonic generation is a convenient way of extending squeezing to shorter wavelengths.

8.2.3 Dispersive Optical Bistability

We shall consider a model for dispersive bistability for a single mode in a cavity. An optical cavity containing a medium with a third-order nonlinear susceptibility is coherently driven. Initially the frequency of the coherent driving field does not match the cavity resonance and the cavity transmission is low. However, since the medium has an intensity dependent refractive index, as the intensity of the coherent driving field is increased the cavity resonance changes until it matches the frequency of the coherent driving field and a high cavity transmission results. The full behaviour may be shown to be bistable.

We shall follow the approach of *Drummond* and *Walls* [8.13] who gave a simple quantum mechanical treatment of this phenomena. The medium is assumed to have a third-order optical nonlinearity which gives rise to a quartic term in the electric field in the Hamiltonian. In the single mode and rotating wave approximations the Hamiltonian is

$$\mathcal{H} = \sum_{j=1}^4 \mathcal{H}_j ,$$

$$\mathcal{H}_1 = \hbar\omega_c a^\dagger a ,$$

$$\begin{aligned}\mathcal{H}_2 &= i\hbar(Ee^{-i\omega_L t}a^\dagger - E^*e^{i\omega_L t}a) , \\ \mathcal{H}_3 &= a\Gamma_c^\dagger + a^\dagger\Gamma_c , \\ \mathcal{H}_4 &= \hbar\chi a^{\dagger 2}a^2 ,\end{aligned}\tag{8.47}$$

where ω_c is the cavity resonance frequency, E is the amplitude, and ω_L the frequency of the coherent driving field. Γ_c denotes the bath operator for the cavity damping, χ is the nonlinear susceptibility. In a reference frame rotating at frequency ω_L , the master equation for the density operator of the cavity field mode is

$$\begin{aligned}\dot{\rho} &= \sum_{i=1}^4 L_i(\rho) , \\ L_1\rho &= -i\delta[a^\dagger a, \rho], \quad L_2\rho = -i\chi[a^{\dagger 2}a^2, \rho] , \\ L_3\rho &= [Ea^\dagger - E^*a, \rho], \quad L_4\rho = \gamma(2a\rho a^\dagger - \rho a^\dagger a - a^\dagger a\rho) ,\end{aligned}\tag{8.48}$$

where γ is the cavity damping rate into the external vacuum field and $\delta = \omega_c - \omega_L$ is the detuning between the coherent driving field and the cavity.

The semiclassical behaviour for the mean field amplitude $\alpha = \langle a \rangle$ may be deduced from the master equation by assuming that all correlation functions factorize:

$$\frac{\partial}{\partial t} \begin{pmatrix} \alpha \\ \alpha^* \end{pmatrix} = \begin{pmatrix} E - (\gamma + i\delta)\alpha - 2i\chi\alpha|\alpha|^2 \\ E^* - (\gamma - i\delta)\alpha^* + 2i\chi\alpha|\alpha|^2 \end{pmatrix} .\tag{8.49}$$

The steady state solution showing the bistable behaviour of α as a function of the driving field E is presented in Fig. 8.14.

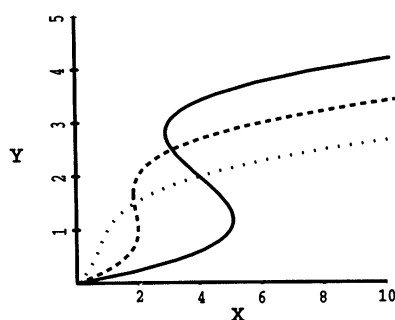


Fig. 8.14. A plot of the scaled output intensity, $Y = |E|^2/\gamma^2$, versus scaled input intensity, $X = |\alpha|^2$, with $\chi/\gamma = 0.5$, $\delta/\gamma = -3.0$ (solid), $= -2.0$ (dash), $= -1.0$ (dot)

To analyse the quantum fluctuations we transform the master equation (8.48) into a Fokker–Planck equation in the generalized P representation

$$\frac{\partial}{\partial t} P(\mathbf{a}) = \left\{ \frac{\partial}{\partial \alpha} [(\gamma + i\delta)\alpha - 2i\chi\alpha^2\alpha^\dagger - E] - i\chi \frac{\partial^2}{\partial \alpha^2} \alpha^2 + \frac{\partial}{\partial \alpha^\dagger} [(\gamma - i\delta)\alpha^\dagger - 2i\chi\alpha^{\dagger 2}\alpha - E^*] + i\chi \frac{\partial^2}{\partial \alpha^{\dagger 2}} \alpha^2 \right\} P(\mathbf{a}), \quad (8.50)$$

where $\mathbf{a} = (\alpha, \alpha^\dagger)$.

The equivalent stochastic differential equations in the Ito calculus are

$$\frac{\partial}{\partial t} \begin{pmatrix} \alpha \\ \alpha^\dagger \end{pmatrix} = \begin{pmatrix} E - (\gamma + i\delta)\alpha - 2i\chi\alpha^2\alpha^\dagger \\ E^* - (\gamma - i\delta)\alpha + 2i\chi\alpha^{\dagger 2}\alpha \end{pmatrix} + \begin{pmatrix} -2i\chi\alpha^2 & 0 \\ 0 & 2i\chi\alpha^{\dagger 2} \end{pmatrix}^{1/2} \begin{pmatrix} \varepsilon_1(t) \\ \varepsilon_2(t) \end{pmatrix}, \quad (8.51)$$

where $\varepsilon_1, \varepsilon_2$ are delta correlated random Gaussian functions so that α, α^\dagger are complex conjugate in the mean. We now linearize these equations about the solutions for the mean amplitude $\langle \mathbf{a} \rangle = \mathbf{a}_0$, $\mathbf{a} = \mathbf{a}_0 + \mathbf{a}_1(t)$. To first order in the fluctuations $\mathbf{a}_1(t)$ obeys the equation

$$\frac{\partial}{\partial t} \mathbf{a}_1(t) = -\mathbf{A} \cdot \mathbf{a}_1(t) + \mathbf{D}^{1/2}(\mathbf{a}_0) \cdot \varepsilon(t), \quad (8.52)$$

where \mathbf{A} is the linearized drift and \mathbf{D} is the diffusion array evaluated at $\mathbf{a} = \mathbf{a}_0$

$$\mathbf{A} = \begin{pmatrix} \gamma + i\delta + 2\varepsilon & \varepsilon e^{i\phi} \\ \varepsilon^* e^{-i\phi} & \gamma - i\delta + 2\varepsilon^* \end{pmatrix}, \quad (8.53)$$

$$\mathbf{D} = \begin{pmatrix} -\varepsilon e^{-i\phi} & 0 \\ 0 & -\varepsilon^* e^{-i\phi} \end{pmatrix}. \quad (8.54)$$

where $\varepsilon = 2i\chi|\alpha|^2$. $e^{i\phi}$ is the phase of the steady-state solution and is of no material consequence in our considerations. The spectral matrix may be obtained directly using (6.157). This gives

$$\begin{aligned} S(\omega) &= \frac{4}{|\lambda(\omega)|^2} \\ &\times \begin{pmatrix} -\varepsilon e^{i\phi} [(\gamma + 2\varepsilon^* - i\delta)^2 + \omega^2 + |\varepsilon|^2] & 2|\varepsilon|^2(\gamma + \varepsilon + \varepsilon^*) \\ 2|\varepsilon|^2(\gamma + \varepsilon + \varepsilon^*) & -\varepsilon^* e^{-i\phi} [(\gamma + 2\varepsilon + i\delta)^2 + \omega^2 + |\varepsilon|^2] \end{pmatrix}, \end{aligned} \quad (8.55)$$

where

$$\lambda(\omega) = (\gamma + 2\varepsilon^* - i\delta + i\omega)(\gamma + 2\varepsilon + i\delta + i\omega) + |\varepsilon|^2.$$

The spectrum of squeezing may then be calculated from (7.72) with the phase $e^{i\theta}$ chosen to maximise the squeezing. The situation is complicated by the fact that the best choice of phase varies with ω , while in any practical situation, only one

choice of phase can be made at a time. If we want to optimize the squeezing at some particular frequency ω_0 , the appropriate choice of phase in (7.48, 51) is

$$e^{2i\theta} = \frac{S_{22}^*(\omega_0)}{|S_{22}(\omega_0)|} = e^{i\phi} \frac{\varepsilon[(\gamma + 2\varepsilon^* - i\delta)^2 + \omega_0^2 + |\varepsilon|^2]}{|\varepsilon[(\gamma + 2\varepsilon^* - i\delta)^2 + \omega_0^2 + |\varepsilon|^2]|}. \quad (8.56)$$

The squeezing spectrum in the output field where the phase θ has been chosen to give maximum squeezing at frequency ω_0 is

$$S_{\pm}^{\text{OUT}}(\omega) = 1 + 4\gamma|\varepsilon| \times \left(\frac{2\gamma|\varepsilon| \mp \frac{(\gamma^2 + \omega^2 - \Delta^2)(\gamma^2 + \omega_0^2 - \Delta^2) + 4\gamma^2(\Delta^2 + |\varepsilon|^2)}{[(\gamma^2 + \omega_0^2 - \Delta^2)^2 + 4\gamma^2(\Delta^2 + |\varepsilon|^2)]^{1/2}}}{(\gamma^2 + \omega^2 - \Delta^2)^2 + 4\gamma^2\Delta^2} \right), \quad (8.57)$$

where

$$\Delta^2 = (3|\varepsilon| + \delta)(|\varepsilon| + \delta) = (2|\varepsilon| + \delta)^2 - |\varepsilon|^2. \quad (8.58)$$

To find any points of perfect squeezing we can utilize the fact that perfect squeezing in one quadrature must be associated with an infinite uncertainty in the other, and hence can only occur at a critical point. At a critical point the fluctuations diverge to infinity, resulting in divergence in the fluctuation spectrum for some frequency ω . It is readily seen from (8.57) that the critical points occur at

$$\gamma \pm i\Delta \pm i\omega = 0. \quad (8.59)$$

The accessible ones are with $\omega = 0$ and

$$\gamma^2 = -\Delta^2 = -(3|\varepsilon| + \delta)(|\varepsilon| + \delta). \quad (8.60)$$

These values of the driving field $|\varepsilon|$ correspond to the turning points of dispersive optical bistability.

Setting $\omega_0 = 0$ (to optimize the squeezing for $\omega = 0$) and taking a critical combination of the driving and detuning, as given by (8.60), gives

$$S_{+}^{\text{OUT}}(\omega) = 1 - \frac{4\gamma^2}{4\gamma^2 + \omega^2}, \quad (8.61)$$

which reaches zero, (perfect squeezing) at $\omega = 0$. The spectrum of the squeezed quadrature at the critical point is thus a simple Lorentzian of width 2γ . The spectrum of the other quadrature is

$$S_{-}^{\text{OUT}}(\omega) = 1 + \frac{4\gamma^2}{4\gamma^2 + \omega^2} \frac{4|\varepsilon|^2 + \omega^2}{\omega^2}, \quad (8.62)$$

which diverges at $\omega = 0$. Thus, again, we have a case of critical quantum fluctuations which are asymmetric in the two quadratures.

To gain an overview of the general behaviour of the output squeezing, it is convenient to choose the phase of the quadrature operators so that the peak of the squeezing spectrum is maximized. Three regions of operation can be distinguished. For $\Delta^2 < -\gamma^2$, there is no stable solution, and the linearized analysis used here cannot be applied. For $-\gamma^2 < \delta^2 < \gamma^2$, the output squeezing spectrum has a single peak at $\omega = 0$, of height

$$S_{\pm}^{\text{OUT}}(0) = 1 - \frac{4\gamma|\varepsilon|}{2\gamma|\varepsilon|^2 \pm [(\gamma^2 + \Delta^2)^2 + 4\gamma^2|\varepsilon|^2]^{1/2}}. \quad (8.63)$$

Finally, for $\Delta^2 > \gamma^2$, the spectrum splits into two peaks at $\omega^2 = \Delta^2 - \gamma^2$ with the height

$$S_{\pm}^{\text{OUT}}((\Delta^2 - \gamma^2)^{1/2}) = 1 - \frac{2|\varepsilon|}{|\varepsilon| \pm (|\varepsilon|^2 + \Delta^2)^{1/2}}. \quad (8.64)$$

The squeezing spectra for several values of the parameters are plotted in Fig. 8.15. The squeezing of the internal cavity mode may be calculated from the integration of the squeezing spectrum over all ω

$$\langle :X_{\pm}, X_{\pm}: \rangle = \frac{1}{2\pi} \int d(\omega) \langle S_{\pm}(\omega) \rangle. \quad (8.65)$$

The integral of the right-hand side is a maximum for $\omega_0^2 = \Delta^2 + \gamma^2$ which corresponds to the optimum choice of phase θ for the integral quadratures. Then the best internal squeezing is

$$\langle X_{\pm}, X_{\pm} \rangle = 1 + |\varepsilon| \frac{[|\varepsilon| \pm (\gamma^2 + \Delta^2 + |\varepsilon|^2)^{1/2}]}{\gamma^2 + \Delta^2}. \quad (8.66)$$

Even at the critical points the maximum internal squeezing is only 50%.

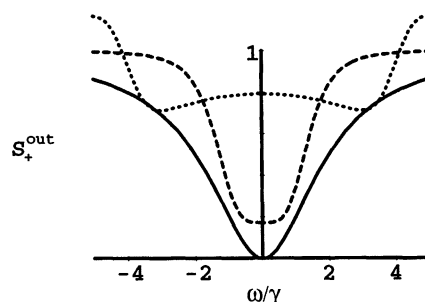


Fig. 8.15. Output squeezing spectrum for dispersive optical bistability. $\gamma = \varepsilon = 1.0$, Solid: $\delta^2 = -1.0$, Dot: $\delta^2 = 4$ Dash: $\delta^2 = 1$

8.3 Applications of Squeezed Light

8.3.1 Interferometric Detection of Gravitational Radiation

Interest in the practical generation of squeezed states of light became significant when *Caves* [8.14] suggested in 1981 that such light might be used to achieve better sensitivity in the interferometric detection of gravitational radiation. The result of *Caves* indicated that while squeezed light would not increase the maximum sensitivity of the device, it would enable maximum sensitivity to be achieved at lower laser power. Later analyses [8.15–18] demonstrated that by an optimum choice of the phase of the squeezing it is possible to increase the maximum sensitivity of the interferometer. This result was established by a full nonlinear quantum theory of the entire interferometer, including the action of the light pressure on the end mirrors. We shall demonstrate this following the treatment of *Pace et al.* [8.18].

A schematic illustration of a laser interferometer for the detection of gravitational radiation is shown in Fig. 8.16. To understand how the device works we need to recall some properties of gravitational radiation. A gravitational wave induces weak tidal forces, in a plane perpendicular to the direction of propagation. A gravitational wave passing normal to a circular arrangement of masses would periodically force the circle into an ellipse [8.19]. In the case of the interferometer depicted in Fig. 8.16, the end mirrors of the two cavities are constrained by a weak harmonic potential, and lie on a circular arc separated by 90° . Thus, when a gravitational wave passes orthogonal to the plane of the interferometer, one cavity will be shortened as the other cavity is lengthened. If the intensity difference of the light leaving each arm

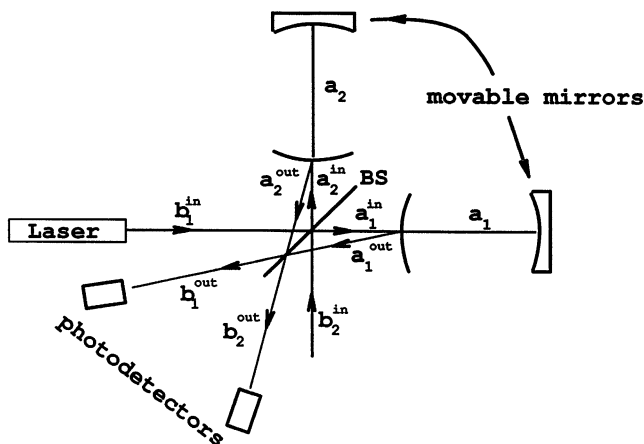


Fig. 8.16. Schematic representation of a laser interferometer for the detection of gravitational radiation

of the interferometer is monitored, the asymmetric detuning of each cavity caused by the moving end mirrors causes this intensity to be modulated at the frequency of the gravitational wave.

While this scheme sounds very promising it suffers from a big problem. Even though gravitational radiation reaching terrestrial detectors is highly classical (many quanta of excitation) it interacts very weakly with the end mirrors. The relative change in the length of each cavity is then so small that it is easily lost amid a multitude of noise sources, which must somehow be reduced if any systematic effect is to be observed. To begin with, it is necessary to isolate the end mirrors from external vibrations and seismic forces. Then one must ensure that the random thermal motion of the end mirrors is negligible. Ultimately as each end mirror is essentially an oscillator, there is the zero-point motion to take account of. Quite apart from the intrinsic noise in the motion of the end mirrors, noise due to the light also limits the sensitivity of the device. The light noise can be separated into two contributions. Firstly the measurement we ultimately perform is an intensity measurement which is limited by shot-noise. In the case of shot-noise, however, the signal-to-noise ratio scales as the square root of the input power, thus one might attempt to avoid this noise source by simply raising the input power. Unfortunately, increasing the input power increases the contribution from another source – radiation pressure. Individual photons reflecting from the end mirrors cause a random force large enough to mask the very small movements due to gravitational radiation.

In the light of the above discussion it would seem that trying to detect gravitational radiation in this manner will be hopeless. However, as we now show, a careful study reveals that while the task is difficult it is achievable and made more so by the careful use of squeezed light. In this calculation we treat each end mirror as a damped simple harmonic oscillator subject to zero-point fluctuations and the classical driving force of the gravitational wave. Thus we assume the thermal motion has been eliminated. We also include the radiation pressure force and associated fluctuations in the cavity fields.

To begin we first determine how the intracavity fields determine the intensity difference signal. Denote the intracavities fields by the annihilation operators a_i ($i = 1, 2$) and the input and output fields for each cavity are represented by a_i^{in} and a_i^{out} , respectively. Let b_i^{in} and b_i^{out} denote the input and output fields for each arm of the interferometer. The central beam-splitter (BS in Fig. 8.16) connects the cavity inputs and outputs to the interferometer inputs and outputs by

$$a_1^{\text{in}} = \frac{1}{\sqrt{2}}(b_1^{\text{in}} + i b_2^{\text{in}}) , \quad (8.67)$$

$$a_2^{\text{in}} = \frac{1}{\sqrt{2}}(b_1^{\text{in}} - i b_2^{\text{in}}) , \quad (8.68)$$

$$b_1^{\text{out}} = \frac{1}{\sqrt{2}}(a_1^{\text{out}} + ia_2^{\text{out}} e^{i\phi}) , \quad (8.69)$$

$$b_2^{\text{out}} = \frac{1}{\sqrt{2}}(a_1^{\text{out}} - ia_2^{\text{out}} e^{i\phi}) , \quad (8.70)$$

where ϕ is a controlled phase shift inserted in arm 2 of the interferometer to enable the dc contribution to the output intensity difference to be eliminated.

The measured signal is then represented by the operator

$$\begin{aligned} I_{-}(t) &= (b_1^{\text{out}})^{\dagger} b_1^{\text{out}} - (b_2^{\text{out}})^{\dagger} b_2^{\text{out}} \\ &= -i[(a_2^{\text{out}})^{\dagger} a_1^{\text{out}} e^{-i\phi} - \text{h.c.}] . \end{aligned} \quad (8.71)$$

Now the relationship between the cavity fields and the respective input and output fields is given by

$$a_i^{\text{out}} = \sqrt{\gamma} a_i - a_i^{\text{in}} \quad (i = 1, 2), \quad (8.72)$$

where we assume the damping rate for each cavity, γ , is the same.

We now assume that arm one of the interferometer is driven by a classical coherent source with amplitude $E/\sqrt{\gamma}$ in units such that the intensity of the input is measured in photons/second. The scaling $\gamma^{-1/2}$ is introduced, for convenience. Then from (8.67 and 68), each cavity is driven with the same amplitude $\varepsilon/\sqrt{\gamma}$, where $\varepsilon = E/\sqrt{2}$. That is

$$\langle a_1^{\text{in}} \rangle = \langle a_2^{\text{in}} \rangle = \frac{\varepsilon}{\sqrt{\gamma}} . \quad (8.73)$$

As we show below, it is possible to operate the device in such a way that in the absence of gravitational radiation, a stable deterministic steady state amplitude α_0 is established in each cavity. This steady state is then randomly modulated by fluctuations in the cavity fields and deterministically modulated by the moving end mirrors of each cavity. Both these effects are of similar magnitude. It thus becomes possible to linearise the output fields around the stationary states. With this in mind we now define the fluctuation operators δa_i and δa_i^{in} for each cavity ($i = 1, 2$)

$$\delta a_i = a_i - \alpha_0 , \quad (8.74)$$

$$\delta a_i^{\text{in}} = a_i^{\text{in}} - \frac{\varepsilon}{\sqrt{\gamma}} . \quad (8.75)$$

Using these definitions, together with (8.67–70), in (8.71), the output signal is then described by the operator

$$I_{-}(t) = \frac{\gamma \alpha_0}{2} [\delta y_1(t) - \delta y_2(t)] - \frac{\sqrt{\gamma \alpha_0}}{2} [\delta y_1^{\text{in}}(t) - \delta y_2^{\text{in}}(t)] , \quad (8.76)$$

where

$$\delta y_i(t) \equiv -i(\delta a_i - \delta a_i^\dagger) , \quad (8.77)$$

$$\delta y_i^{\text{in}}(t) \equiv -i[\delta a_i^{\text{in}} - (\delta a_i^{\text{in}})^\dagger] . \quad (8.78)$$

We have chosen the arbitrary phase reference so that the input amplitude, and thus the steady state amplitude α_0 , is real.

Equation (8.76) indicates that the signal is carried by the phase quadrature not the amplitude quadrature. Thus we must determine $y_i(t)$.

We turn now to a description of the intracavity dynamics. The end mirror is treated as a quantised simple harmonic oscillator with position and momentum operators (Q, P). The radiation pressure force is proportional to the intracavity photon number. The total Hamiltonian for the system may then be written [8.18]

$$\mathcal{H} = \hbar\Delta a^\dagger a + \frac{P^2}{2M} + \frac{M\Omega^2}{2} Q^2 - \hbar\frac{\omega_0}{L} a^\dagger a Q + F(t)Q , \quad (8.79)$$

where M is the mass of the end mirror, Ω is the oscillator frequency of the end mirror, L is the cavity length, Δ is the cavity detuning, and $F(t)$ is the driving force on the end mirror due to the gravitational wave. If we assume the acceleration produced by the gravitational wave is

$$g(t) = g \cos(\omega_g t) , \quad (8.80)$$

the force $F(t)$ may be written as

$$F(t) = -MhL\omega_g^2 S(t) \quad (8.81)$$

where h is defined to be the maximum fractional change in the cavity length, L , produced by the gravitational wave in the absence of all other forces, and $s(t) = \cos(\omega_g t)$.

It is convenient to define the dimensionless position q and the momentum variables p for the mirror, which are the analogue of the quadrature phase operators for the field,

$$q = \left(\frac{2\hbar}{M\Omega} \right)^{-1/2} Q , \quad (8.82)$$

$$p = (2\hbar M \Omega)^{-1/2} P . \quad (8.83)$$

The commutation relations for these new variables is $[q, p] = i/2$. Thus in the ground state, the variance in q and p are both equal to $1/4$.

The quantum stochastic differential equations for this system may now be written

$$\frac{da}{dt} = \varepsilon - i(\Delta + 2\kappa q)a - \frac{\gamma}{2}a + \sqrt{\gamma}a^{\text{in}} , \quad (8.84)$$

$$\frac{dq}{dt} = \Omega p - \frac{\Gamma}{2}q + \sqrt{\Gamma}q^{\text{in}} , \quad (8.85)$$

$$\frac{dp}{dt} = -\Omega q - \kappa a^\dagger a - ks(t) - \frac{\Gamma}{2} p + \sqrt{\Gamma} p^{\text{in}} , \quad (8.86)$$

where

$$\kappa \equiv \frac{-\omega_0}{L} \left(\frac{\hbar}{2M\Omega} \right)^{1/2} , \quad (8.87)$$

$$k = -hL\omega_g^2 \left(\frac{M}{2\hbar\Omega} \right)^{1/2} , \quad (8.88)$$

and $\gamma/2$ is the damping rate for the intracavity field, while $\Gamma/2$ is the damping rate for the end mirrors. Note that the form of the stochastic equation for the mirror is that for a zero-temperature, under-damped oscillator and will thus only be valid provided $\Gamma \ll \Omega$.

Let us first consider the corresponding deterministic semi-classical equations

$$\dot{\alpha} = \varepsilon - i(\Delta + 2\kappa q)\alpha - \frac{\gamma}{2}\alpha , \quad (8.89)$$

$$\dot{q} = \Omega p - \frac{\Gamma}{2}q , \quad (8.90)$$

$$\dot{p} = -\Omega q - \kappa|\alpha|^2 - ks(t) - \frac{\Gamma}{2}p . \quad (8.91)$$

These equations represent a pair of nonlinearly coupled harmonically driven oscillators, and as such are candidates for unstable, chaotic behaviour. However, the amplitude of the driving, k , is so small that one expects the system to remain very close to the steady state in the absence of driving. The first step is thus to determine the steady state values, α_0 , q_0 and p_0 . If we choose Δ such that $\Delta = -2\kappa q_0$ (so the cavity is always on resonance), then

$$\alpha_0 = \frac{2\varepsilon}{\gamma} . \quad (8.92)$$

Of course, this steady state itself may be unstable. To check this we linearise the undriven dynamics around the steady state. Define the variables

$$\delta x(t) = \text{Re}\{\alpha(t) - \alpha_0\} , \quad (8.93)$$

$$\delta y(t) = \text{Im}\{\alpha(t) - \alpha_0\} , \quad (8.94)$$

$$\delta q(t) = q(t) - q_0 , \quad (8.95)$$

$$\delta p(t) = p(t) - p_0 . \quad (8.96)$$

Then

$$\frac{d}{dt} \begin{pmatrix} \delta x \\ \delta y \\ \delta q \\ \delta p \end{pmatrix} = \begin{pmatrix} -\frac{\gamma}{2} & 0 & 0 & 0 \\ 0 & -\frac{\gamma}{2} & -\mu & 0 \\ 0 & 0 & -\frac{\Gamma}{2} & \Omega \\ -\mu & 0 & -\Omega & -\frac{\Gamma}{2} \end{pmatrix} \begin{pmatrix} \delta x \\ \delta y \\ \delta q \\ \delta p \end{pmatrix}, \quad (8.97)$$

where $\mu = 4\kappa\alpha_0$ and we have assumed ε and thus α_0 are real. The eigenvalues of the linear dynamics are then found to be $(-\gamma/2, -\gamma/2, -\Gamma/2 + i\Omega, -\Gamma/2 - i\Omega)$, so clearly the steady state is stable in the absence of the gravitational wave.

We shall point out the interesting features of (8.97). First we note that the quadrature carrying the coherent excitation (δx) is totally isolated from all other variables. Thus $\delta x(t) = \delta x(0)e^{-\gamma t/2}$. However, as fluctuations evolve from the steady state $\delta x(0) = 0$, one can completely neglect the variables $\delta x(t)$ for the deterministic part of the motion. Secondly we note the mirror position fluctuations δq feed directly into the field variable $\delta y(t)$ and thus directly determine the output intensity difference signal by (8.76). Finally, we note the fluctuations of the in-phase field variable δx drive the fluctuating momentum of the mirror. This is, of course, the radiation pressure contribution. However, for the deterministic part of the dynamics $\delta x(t) = 0$, as discussed above, so the mirror dynamics is especially simple – a damped harmonic oscillator. In the presence of the gravitational wave the deterministic dynamics for the end mirrors is then

$$\begin{pmatrix} \delta \dot{q} \\ \delta \dot{p} \end{pmatrix} = \begin{pmatrix} -\frac{\Gamma}{2} & \Omega \\ -\Omega & -\frac{\Gamma}{2} \end{pmatrix} \begin{pmatrix} \delta q \\ \delta p \end{pmatrix} - \begin{pmatrix} 0 \\ ks(t) \end{pmatrix}, \quad (8.98)$$

with the initial conditions $\delta q(0) = \delta p(0)$ the solution for $\delta q(t)$ is

$$\delta q(t) = R \cos(\omega_g t + \phi), \quad (8.99)$$

with

$$R = \frac{k\Omega}{\left| \frac{\Gamma}{2} + i(\omega_g - \Omega) \right| \left| \frac{\Gamma}{2} + i(\omega_g + \Omega) \right|}, \quad (8.100)$$

$$\phi = \arctan \left(\frac{-\Gamma\omega_g}{\frac{\Gamma^2}{4} + \Omega^2 - \omega_g^2} \right). \quad (8.101)$$

Substituting this solution into the equation for $\delta y(t)$ and solving, again with $\delta y(0) = 0$, we find

$$\delta y(t) = \frac{-4\kappa\alpha_0 R}{\left| \frac{\gamma}{2} + i\omega_g \right|} \cos(\omega_g t + \theta + \phi) , \quad (8.102)$$

where

$$\theta = \arctan\left(\frac{\alpha\omega_g}{\gamma}\right) . \quad (8.103)$$

We have neglected an initial decaying transient. Apart from the phase shifts θ and ϕ , the out-of-phase field quadrature follows the displacements of the end mirror induced by the gravitational wave.

Due to the tidal nature of the gravitational wave if one cavity end mirror experiences a force $F(t)$, the other experiences $-F(t)$. Thus $\delta y_1(t) = -\delta y_2(t)$ and the mean signal is

$$\langle I_{-}(t) \rangle = -\frac{16\kappa IR \cos(\omega_g t + \phi + \theta)}{\left| \frac{\gamma}{2} + i\omega_g \right|} , \quad (8.104)$$

where the output intensity I is defined by

$$I = |\langle a_i^{\text{out}} \rangle|^2 = \frac{\gamma\alpha_0^2}{4} . \quad (8.105)$$

Using the definitions in (8.100, 87 and 88) we find

$$\langle I_{-}(t) \rangle = \frac{-8hI\omega_0\omega_g^2 \cos(\omega_g t + \theta + \phi)}{\left| \frac{\gamma}{2} + i\omega_g \right| \left| \left| \frac{\Gamma}{2} + i(\omega_g - \Omega) \right| \left| \frac{\Gamma}{2} + i(\omega_g + \Omega) \right| \right|} \quad (8.106)$$

and the signal is directly proportional to the mirror displacement h .

Before we consider a noise analysis of the interferometer it is instructive to look at the frequency components of variable $\delta y(t)$ by

$$\delta y(\omega) = \int_{-\infty}^{\infty} dt e^{i\omega t} \delta y(t) . \quad (8.107)$$

As $\delta y(t)$ is real we have that $\delta y(t) = \delta y^*(-\omega)$. This relationship enables us to write

$$\delta y(t) = \int_0^{\infty} d\omega [\delta y(\omega) e^{-i\omega t} + \delta y(\omega)^* e^{i\omega t}] , \quad (8.108)$$

thus distinguishing positive and negative frequency components. Inspection of (8.104) immediately gives that

$$\delta y(\omega) = \frac{-2\kappa\alpha_0 R e^{-i(\theta+\phi)}}{\left| \frac{\gamma}{2} + i\omega_g \right|} \delta(\omega - \omega_g) . \quad (8.109)$$

Thus

$$|\langle I_-(\omega) \rangle| = hS(\omega_g)\delta(\omega - \omega_g) , \quad (8.110)$$

where

$$S(\omega_g) = \frac{8hI\omega_0\omega_g^2}{\left| \frac{\gamma}{2} + i\omega_g \right| \left| \frac{\Gamma}{2} + i(\omega_g - \omega) \right| \left| \frac{\Gamma}{2} + i(\omega_g + \Omega) \right|} . \quad (8.111)$$

We now analyse the noise response of the interferometer. As the gravitational wave provides an entirely classical driving of the mirrors it can only effect the deterministic part of the dynamics, which we have already described above. To analyse the noise component we must consider the fluctuation *operators* δx , δy , δq and δp defined by $\delta x = x(t) - x_s(t)$, where x_s is the semi-classical solution. In this way the deterministic contribution is removed.

The quantum stochastic differential equations are then

$$\frac{d}{dt} \delta x(t) = -\frac{\gamma}{2} \delta x(t) + \sqrt{\gamma} \delta x^{in}(t) , \quad (8.112)$$

$$\frac{d}{dt} \delta y(t) = -\frac{\gamma}{2} \delta y(t) - \mu \delta q(t) + \sqrt{\gamma} \delta y^{in}(t) , \quad (8.113)$$

$$\frac{d}{dt} q(t) = -\frac{\Gamma}{2} q(t) + \Omega p(t) + \sqrt{\Gamma} q^{in}(t) , \quad (8.114)$$

$$\frac{d}{dt} p(t) = -\frac{\Gamma}{2} p(t) - \Omega q(t) - \mu x(t) + \sqrt{\Gamma} p^{in}(t) , \quad (8.115)$$

with the only non-zero noise correlations being

$$\langle \delta x^{in}(t) \delta x^{in}(t') \rangle = \langle \delta y^{in}(t) \delta y^{in}(t') \rangle = \delta(t - t') , \quad (8.116)$$

$$\langle \delta x^{in}(t) \delta y^{in}(t') \rangle = \langle \delta y^{in}(t) \delta x^{in}(t') \rangle^* = i\delta(t - t') , \quad (8.117)$$

$$\langle q^{in}(t) q^{in}(t') \rangle = \langle p^{in}(t) p^{in}(t') \rangle = \delta(t - t') , \quad (8.118)$$

$$\langle q^{in}(t) p^{in}(t') \rangle = \langle p^{in}(t) q^{in}(t') \rangle^* = i\delta(t - t') , \quad (8.119)$$

From an experimental perspective the noise response in the frequency domain is more useful. Thus we define

$$\delta y(\omega) = \int_{-\infty}^{\infty} dt e^{i\omega t} \delta y(t) \quad (8.120)$$

and similar expressions for the other variables. As $\delta y(t)$ is Hermitian we have $\delta y(\omega) = \delta y(-\omega)^\dagger$. The two time correlation functions for the variables are then determined by

$$\langle \delta y(t) \delta y(0) \rangle = \int_{-\infty}^{\infty} d\omega e^{-i\omega t} \langle \delta y(\omega) \delta y^\dagger(\omega) \rangle \quad (8.121)$$

and similar expressions for the other quantities. Thus our objective is to calculate the signal variance

$$V_{I_-}(\omega) = \langle I_-(\omega) I_-^\dagger(\omega) \rangle . \quad (8.122)$$

In order to reproduce the δ -correlated noise terms of (8.116–119), the correlation function in the frequency domain must be

$$\langle \delta x^{\text{in}}(\omega) \delta x^{\text{in}}(\omega')^\dagger \rangle = \langle \delta y^{\text{in}}(\omega) \delta y^{\text{in}}(\omega') \rangle = \delta(\omega - \omega') , \quad (8.123)$$

$$\langle \delta x^{\text{in}}(\omega) \delta y^{\text{in}}(\omega')^\dagger \rangle = \langle \delta y^{\text{in}}(\omega) \delta x^{\text{in}}(\omega')^\dagger \rangle^* = i\delta(\omega - \omega') , \quad (8.124)$$

$$\langle q^{\text{in}}(\omega) q^{\text{in}}(\omega')^\dagger \rangle = \langle p^{\text{in}}(\omega) p^{\text{in}}(\omega')^\dagger \rangle = \delta(\omega - \omega') , \quad (8.125)$$

$$\langle q^{\text{in}}(\omega) p^{\text{in}}(\omega')^\dagger \rangle = \langle p^{\text{in}}(\omega) q^{\text{in}}(\omega')^\dagger \rangle^* = i\delta(\omega - \omega') , \quad (8.126)$$

We now directly transform the equations of motion and solve the resulting algebraic equations for the frequency components. The result for the crucial field variable is

$$\delta y(\omega) = A \delta x^{\text{in}}(\omega) + B \delta y^{\text{in}}(\omega) + C q^{\text{in}}(\omega) + D p^{\text{in}}(\omega) , \quad (8.127)$$

where

$$A = \frac{\mu^2 \Omega \sqrt{\gamma}}{\Lambda(\omega) \left(\frac{\gamma}{2} - i\omega \right)^2} ,$$

$$B = \frac{\sqrt{\gamma}}{\frac{\lambda}{2} - i\omega} ,$$

$$C = \frac{-\mu\sqrt{\Gamma}\left(\frac{\Gamma}{2} - i\omega\right)}{\Lambda(\omega)\left(\frac{\gamma}{2} - i\omega\right)},$$

$$D = \frac{-\mu\sqrt{\Gamma\Omega}}{\Lambda(\omega)\left(\frac{\gamma}{2} - i\omega\right)}, \quad (8.128)$$

$$\Lambda(\omega) = \left(\frac{\Gamma}{2} - i\omega\right)^2 + \Omega^2. \quad (8.129)$$

Thus

$$\begin{aligned} \langle y(\omega)y^\dagger(\omega) \rangle &= |A|^2 \langle \delta x^{\text{in}}(\omega)\delta x^{\text{in}}(\omega)^\dagger \rangle + |B|^2 \langle \delta y^{\text{in}}(\omega)\delta y^{\text{in}}(\omega)^\dagger \rangle \\ &\quad + |C|^2 \langle q^{\text{in}}(\omega)q^{\text{in}}(\omega)^\dagger \rangle + |D|^2 \langle p^{\text{in}}(\omega)p^{\text{in}}(\omega') \rangle \\ &\quad + (AB^*\langle \delta x^{\text{in}}(\omega)\delta y^{\text{in}}(\omega)^\dagger \rangle + \text{c.c.}) \\ &\quad + (CD^*\langle q^{\text{in}}(\omega)p^{\text{in}}(\omega)^\dagger \rangle + \text{c.c.}) . \end{aligned} \quad (8.130)$$

It is now constructive to consider the physical interpretation of each term. The first term proportional to the in-phase field amplitude is the error in the output intensity due to radiation pressure fluctuations. The second term is the error due to the out-of-phase amplitude of the field, i.e. the intrinsic phase fluctuations. The second and third terms are the fluctuations in mirror position and momentum due to intrinsic mirror fluctuations and radiation pressure. The fourth term represents correlations between the amplitude and the phase of the field due to radiation pressure modulating the length of the cavity. In a similar way the final term is the correlation between the position and momentum of the mirror as the radiation pressure changes the momentum which is coupled back to the position under free evolution.

Define the normalised variance by

$$N(\omega) = \frac{V_{I_-}(\omega)}{2I}, \quad (8.131)$$

where I is the output intensity from each cavity. This quantity is given by

$$N(\omega) = 1 + \frac{16\kappa^2 I\Gamma\left(\frac{\Gamma^2}{4} + \Omega^2 + \omega^2\right)}{|\Lambda(\omega)|^2\left|\frac{\gamma}{2} - i\omega\right|^2} + \frac{(16\kappa^2 I)^2\Omega^2}{|\Lambda(\omega)|^2\left|\frac{\gamma}{2} - i\omega\right|^4}. \quad (8.132)$$

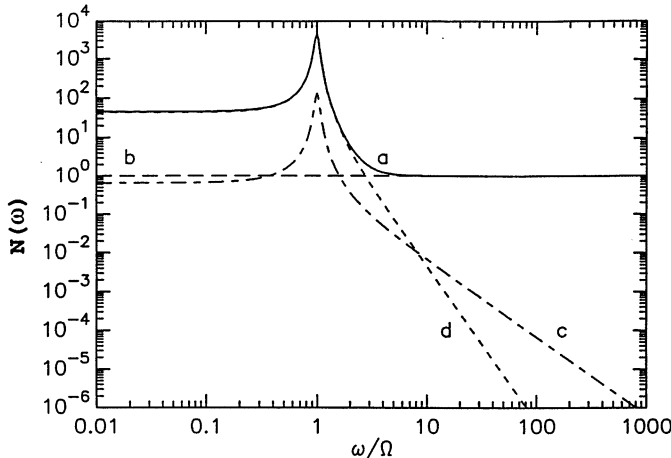


Fig. 8.17. The normalized variance for the fluctuations in the intensity difference versus frequency. The solid line (a) represents the total noise, (b) represents the photon counting noise, (c) represents the mirror noise and (d) represents the radiation pressure noise. The interferometer parameters used are given in Table 8.1

Table 8.1. The values of the experimental parameters used in the graphs

Quantity	Symbol	Value
Mass of mirror	M	10 kg
Mirror characteristic angular frequency	Ω	$20\pi \text{ rad s}^{-1}$
Mirror damping	γ_b	$2\pi \text{ rad s}^{-1}$
Length of cavity	L	4 m
Reflectivity	R	0.98
Laser power	P	10 W
Laser angular frequency	ω_0	$3.66 \times 10^5 \text{ rad s}^{-1}$
Gravity-wave-angular frequency	ω_g	$2000\pi \text{ rad s}^{-1}$

The first term in (8.132) is the shot-noise of the incident light on the detector, the second term arises from the intrinsic (zero-point) fluctuations in the positions of the end mirrors, while the last term represents the radiation pressure noise.

In Fig. 8.17 we display the total noise $N(\omega)$ as a function of frequency (a) (solid line) together with the contributions to the noise from: (b) photon-counting noise (dashed line); (c) mirror noise (dash-dot line); (d) radiation-pressure noise (dotted line). Typical interferometer parameters, summarised in Table 8.1 were used.

From signal processing theory, a measurement at frequency ω_g of duration τ entails an error Δh in the displacement h given by

$$\Delta h^2 = \frac{2S(\omega_g)}{\tau V_{I-}(\omega_g)} . \quad (8.133)$$

We may now substitute the expressions for the signal frequency components $S(\omega_g)$ and the noise at this frequency to obtain an error which depends on the input intensity I (or equivalently the input power $P = 2\hbar\omega_0 I$). The error may then be minimised with respect to I to give minimum detectable displacement h_{\min} . In the limit $\omega_g^2 \gg \Gamma^2 + \Omega^2$, the appropriate limit for practical interferometers we find

$$h_{\min}^2 = \frac{\hbar}{32M\omega_g^2 L^2 \tau \Omega} (2\Omega + \Gamma) . \quad (8.134)$$

The first term in this expression is due to the light fluctuations whereas the second term is due to the intrinsic quantum noise in the end mirrors. If we neglect the mirror-noise contribution we find the ‘standard quantum limit’

$$h_{SQL} = \frac{1}{L} \left(\frac{\hbar}{16M\omega_g^2 \tau} \right)^{1/2} . \quad (8.135)$$

In Fig. 8.18 we plot the Δh as a function of input power (8.133), for a measurement time of 1 s, and typical values for the other parameters. Clearly the optimum sensitivity is achieved at rather high input powers.

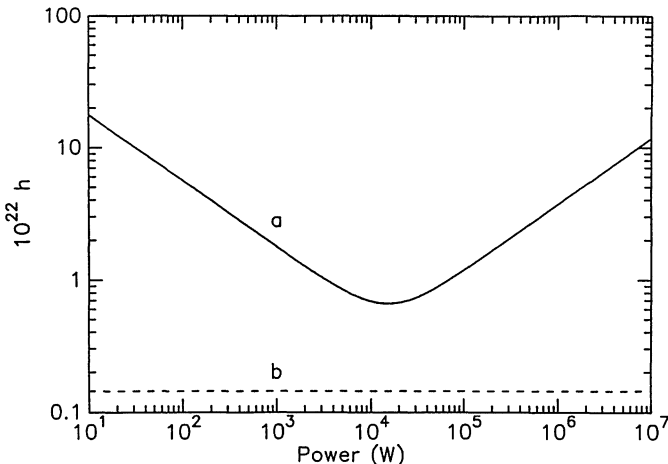


Fig. 8.18. The error in the fractional length change versus input power for a measurement time of one second. Parameters are as in Table 8.1

Can one do better than this, either in achieving the standard quantum limit at lower powers or perhaps even beating the standard quantum limit? As we now show both these results can be achieved by a careful use of squeezed states.

To see now how this might work return to (8.130) and the physical interpretation of each term. Firstly, we note that one might reduce radiation pressure fluctuations (the first term) by using input squeezed light with reduced amplitude fluctuations. Unfortunately, this would increase the overall intensity fluctuations at the detector, i.e. it would increase the photon counting noise. However, as these two terms scale differently with intensity it is possible to apply such a scheme to enable the standard quantum limit to be achieved at lower input power. This is indeed the conclusion of *Caves* [8.14] in a calculation which focussed entirely on these terms. However, one can actually do better by using squeezed states to induce correlations between the in-phase and out-of-phase quadratures of the field. In fact, if one chooses the phase of the squeezing (with respect to the input laser) carefully the fifth term in (8.130) can be made negative with a consequent improvement in the overall sensitivity of the device.

We will not present the details of this calculation [8.18], but summarise the results with reference to Fig. 8.19. Firstly, if we simply squeeze the fluctuations in \hat{x}^{in} without changing the vacuum correlations between \hat{x}^{in} and \hat{y}^{in} , the standard quantum limit (8.135) is the optimum sensitivity regardless of the degree of squeezing and it is achieved for the input power

$$P_{\text{ss}} = e^{-2r} P_o , \quad (8.136)$$

where r is the squeeze parameter, and P_o is the optimum laser power for the system with no squeezing.

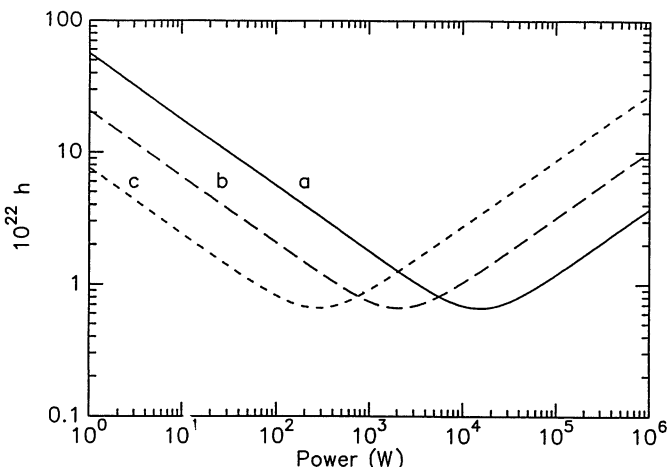


Fig. 8.19. The minimum possible detectable gravitational wave amplitude h as a function of power using amplitude squeezed light at the input and for three different squeeze parameters; (a) $r = 0$; (b) $r = 1$; (c) $r = 2$

However, if one now optimises the phase of the squeezing thereby introducing correlations between $\delta\hat{x}^{\text{in}}$ and $\delta\hat{y}^{\text{in}}$ we find the optimum sensitivity is achieved with the *same* input power P_o as the unsqueezed state, but the optimum sensitivity in the appropriate limit is

$$h_{\min}^2 \approx \frac{\hbar}{32M\omega_g^2 L^2 \tau \Omega} (2e^{-2|r|}\Omega + \Gamma) . \quad (8.137)$$

Clearly this may be made much smaller than the standard quantum limit. For highly squeezed input light the sensitivity is ultimately limited by the intrinsic quantum fluctuations in the positions of the end mirrors. The optimum phase of squeezing is $\pi/4$ which is the angle at which maximum correlation between \hat{x}^{in} and \hat{y}^{in} occurs, i.e., the error ellipse has the same projection onto the in-phase and out-of-phase directions. The exact results are shown in Fig. 8.20 for the same parameters, as employed in Fig. 8.19. Shown is the minimum-possible value of h detectable as a function of power at the optimum phase of squeezing, for three different values of the squeeze parameter. Also exhibited is the noise floor due to the intrinsic quantum fluctuations of the mirror positions.

In summary, the experimentalist can apply a squeezed input to a gravitational wave interferometer in two ways. Either the maximum sensitivity of the device can be greatly increased but achieved at a rather high input power, or the standard quantum limit can be achieved at input powers less threatening to the life of the optical components of the interferometer.

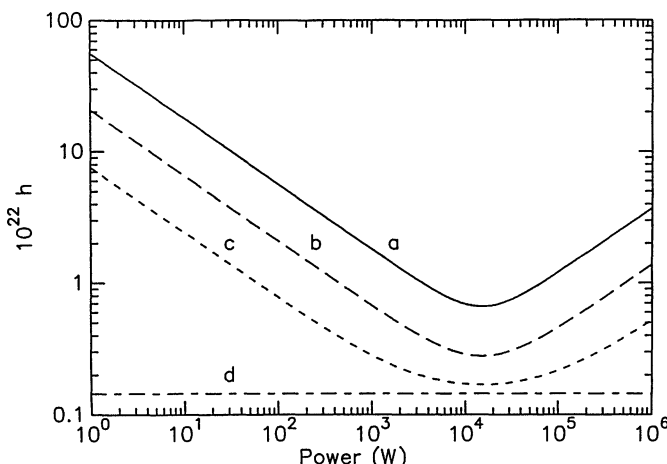


Fig. 8.20. The minimum possible detectable amplitude h as a function of input power when the phase of the input squeezed light is optimized, for three different values of the squeeze parameter (a) $r = 0$; (b) $r = 1$; (c) $r = 2$. Also shown is the mirror noise contribution (d)

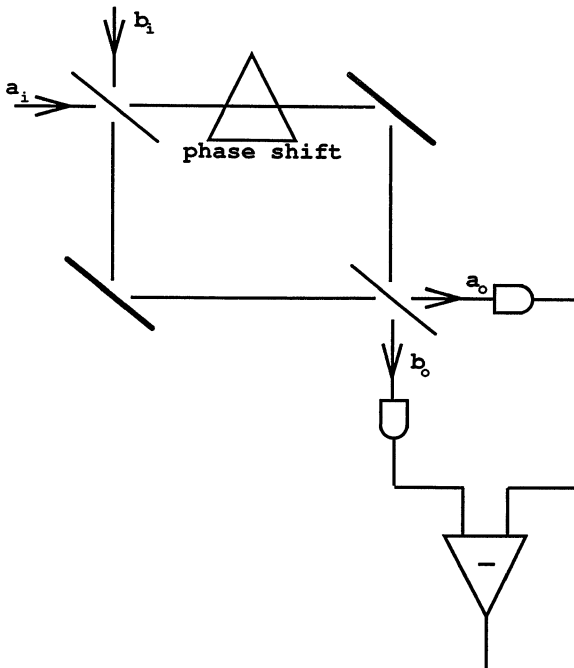


Fig. 8.21. Schematic representation of an experiment designed to measure a phase shift below the shot-noise limit

8.3.2 Sub-Shot-Noise Phase Measurements

The second major application of squeezed light is to the detection of very small phase shifts. A Mach-Zehnder interferometer (Fig. 8.21) can be used to determine a phase shift introduced in one arm.

Assuming 50:50 beam splitters the relationship between the input and output field operators is

$$a_o = e^{i\theta/2} \left(\cos \frac{\theta}{2} a_i + \sin \frac{\theta}{2} b_i \right), \quad (8.138)$$

$$b_o = e^{i\theta/2} \left(\cos \frac{\theta}{2} b_i + \sin \frac{\theta}{2} a_i \right), \quad (8.139)$$

where θ is the phase difference between the two arms. The two output fields are directed onto two photo-detectors and the resulting currents combined with a 180° power combiner. This realises a measurement of the photon number

difference

$$\begin{aligned} c_o^\dagger c_o &= a_o^\dagger a_o - b_o^\dagger b_o \\ &= \cos\theta(a_i^\dagger a_i - b_i^\dagger b_i) - i \sin\theta(a_i b_i^\dagger - a_i^\dagger b_i) . \end{aligned} \quad (8.140)$$

In standard interferometry the input a_i is a stabilised cw laser while b_i is the vacuum state. However, as we shall show, smaller phase changes may be detected if b_i is prepared in a squeezed vacuum state.

Assuming a_i is in the coherent state $|\alpha\rangle$ while b_i is in the squeezed state $|0, r\rangle$, the mean and variance of the photon number difference at the output is

$$\langle c_-^\dagger c_- \rangle = \cos\theta(|\alpha|^2 - \sinh^2 r) \quad (8.141)$$

$$\begin{aligned} V(c_-^\dagger c_-) &= \cos^2\theta(|\alpha|^2 + \sinh^2 r \cosh 2r) + \sin^2\theta[|\alpha|^2(1 - 2\sinh^2 r) \\ &\quad - \frac{1}{2}(\alpha^2 + \alpha^{*2})\sinh 2r + \sinh^2 r] . \end{aligned} \quad (8.142)$$

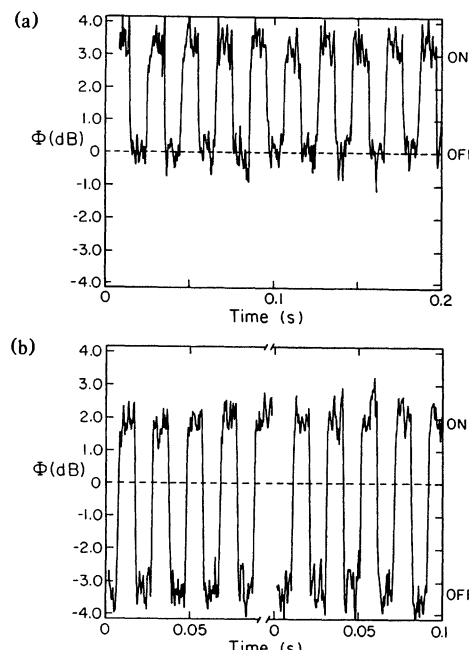


Fig. 8.22. A comparison of the level of fluctuations in the differenced-photocurrent for a Mach-Zehnder interferometer versus time as the phase difference is varied at a frequency of 1.6 MHz. Curve in (a) is for the case of vacuum state input, curve (b) uses squeezed state input. The dashed line gives the vacuum level with no phase modulation [8.20]

If we now set $\theta = \pi/2 + \delta\theta$, then when phase shift $\delta\theta$ is zero, the mean signal is zero. That is we operate on a null fringe. The Signal-to-Noise Ratio (SNR) is defined by

$$\text{SNR} = \frac{\langle c_-^\dagger c_- \rangle}{\sqrt{V(c_-^\dagger c_-)}} . \quad (8.143)$$

In the standard scheme $r = 0$ and

$$\text{SNR} = \bar{n}^{1/2} \sin \delta\theta \quad (8.144)$$

where $\bar{n} = |\alpha|^2$. The smallest detectable phase shift is defined to be that phase for which $\text{SNR} = 1$. Thus the minimum detectable phase shift for coherent state interferometry is

$$\delta\theta_{\min} = \bar{n}^{-1/2} . \quad (8.145)$$

However, if b_i is prepared in a squeezed vacuum state with squeezing in phase with the amplitude α we find for moderate squeezing ($|\alpha|^2 \gg \sinh^2 r$)

$$\text{SNR}_{\text{ss}} = \bar{n}^{1/2} e^r \sin \delta\theta \quad (8.146)$$

and thus the minimum detectable phase change is

$$\delta\theta_{\min} = \bar{n}^{1/2} e^r . \quad (8.147)$$

The minimum detectable phase change may thus be much smaller than for coherent state interferometry, provided we choose $r < 0$ i.e. *phase squeezing*.

Such an enhancement has been reported by *Xiao* et al. [8.20] in an experiment on the measurement of phase modulation in a Mach Zehnder interferometer. They reported on an increase in the signal-to-noise ratio of 3 dB relative to the shot-noise limit when squeezed light from an optical parametric oscillator is injected into a port of the interferometer. A comparison of the fluctuations in the difference current for the cases of squeezed and a vacuum input is shown in Fig. 8.22. A similar experiment was performed by *Grangier* et al. [8.21] employing a polarization interferometer which is equivalent to a Mach–Zehnder scheme. In their experiment an enhancement factor of 2 dB was achieved.

Exercises

- 8.1** Calculate the squeezing spectrum for parametric oscillation in a cavity with losses γ'_1 at the other mirror at frequency ω_1 , in addition to the output losses γ_1 .

8.2 Calculate the spectrum of fluctuations in the difference current $I_1 - I_2$ if an intracavity loss is present at the idler frequency.

8.3 Analyse the problem of two-photon absorption inside an optical cavity. Take as an effective Hamiltonian

$$\mathcal{H} = a^2 \Gamma^\dagger + a^{\dagger 2} \Gamma$$

where Γ is a reservoir operator. Determine the squeezing spectrum.

9. Nonlinear Quantum Dissipative Systems

In the preceding chapter we derived linearised solutions to the quantum fluctuations occurring in some nonlinear systems in optical cavities. In these solutions the quantum noise has been treated as a small perturbation to the solutions of the corresponding nonlinear classical problem. It is not possible, in general, to find exact solutions to the nonlinear quantum equations which arise in nonlinear optical interactions. It has, however, been possible to find solutions to some specific systems. These solutions provide a test of the region of validity of the linearised solutions especially in the region of an instability. Furthermore they allow us to consider the situation where the quantum noise is large and may no longer be treated as a perturbation. In this case, manifestly quantum mechanical states may be produced in a nonlinear dissipative system.

We shall give solutions to the nonlinear quantum equations for two of the problems considered in Chap. 8, namely, the parametric oscillator and dispersive optical bistability.

9.1 Optical Parametric Oscillator: Complex P Function

We shall first solve for the steady state of the parametric oscillator using the complex P function. Then, we show, using the positive P function, that the steady state subharmonic field is in a superposition state. We go on to calculate the tunnelling time between the two states in the superposition.

We consider the degenerate parametric oscillator described in Chap. 8, following the treatment of *Drummond et al.* [9.1]. The Hamiltonian is

$$\mathcal{H} = \sum_{i=0}^3 \mathcal{H}_i \quad (9.1)$$

where

$$\mathcal{H}_0 = \hbar\omega a_1^\dagger a_1 + 2\hbar\omega a_2^\dagger a_2 , \quad (9.2)$$

$$\mathcal{H}_1 = i\hbar \frac{\kappa}{2} (a_1^{\dagger 2} a_2 - a_1^2 a_2^\dagger) , \quad (9.3)$$

$$\mathcal{H}_2 = i\hbar(\varepsilon_2 a_2^\dagger e^{-2i\omega t} - \varepsilon_2^* a_2 e^{2i\omega t}) , \quad (9.4)$$

$$\mathcal{H}_3 = a_1 \Gamma_1^\dagger + a_2 \Gamma_2^\dagger + \text{h.c.} \quad (9.5)$$

where a_1 and a_2 are the boson operators for two cavity modes of frequency ω and 2ω , respectively. κ is the coupling constant for the nonlinear coupling between the modes. The cavity is driven externally by a coherent driving field with frequency 2ω and amplitude ε_2 . Γ_1, Γ_2 are the bath operators describing the cavity damping of the two modes.

We recall from Chap. 8 that there are two stable steady state solutions depending on whether the driving field amplitude is above or below the threshold amplitude $\varepsilon_2^c = \gamma_1 \gamma_2 / \kappa$. In particular, the steady states for the low frequency mode α_1 are

$$\begin{aligned} \alpha_1^0 &= 0, \quad \varepsilon_2 < \varepsilon_2^c , \\ \alpha_1^0 &= \pm \left[\frac{2}{\kappa} (\varepsilon_2 - \varepsilon_2^c) \right]^{1/2}, \quad \varepsilon_2 \geq \varepsilon_2^c . \end{aligned} \quad (9.6)$$

The master equation for the density operator of the two modes is

$$\begin{aligned} \frac{\partial}{\partial t} \rho &= \frac{1}{i\hbar} [\mathcal{H}_0 + \mathcal{H}_1 + \mathcal{H}_2, \rho] + \gamma_1 (2a_1 \rho a_1^\dagger - a_1^\dagger a_1 \rho - \rho a_1^\dagger a_1) \\ &\quad + \gamma_2 (2a_2 \rho a_2^\dagger - a_2^\dagger a_2 \rho - \rho a_2^\dagger a_2) \end{aligned} \quad (9.7)$$

where the irreversible part of the master equation follows from (6.44) for a zero-temperature bath. γ_1, γ_2 are the cavity damping rates.

This equation may be converted to a c-number Fokker–Planck equation using the generalized P representation discussed in Chap. 6. Using the operator-algebra rules described in Chap. 6, we arrive at the Fokker–Planck equation

$$\begin{aligned} \frac{\partial}{\partial t} P(\mathbf{a}) &= \left\{ \frac{\partial}{\partial \alpha_1} (\gamma_1 \alpha_1 - \kappa \beta_1 \alpha_2) + \frac{\partial}{\partial \beta_1} (\gamma_1 \beta_1 - \kappa \alpha_1 \beta_2) \right. \\ &\quad + \frac{\partial}{\partial \alpha_2} \left(\gamma_2 \alpha_2 - \varepsilon_2 + \frac{\kappa}{2} \alpha_1^2 \right) + \frac{\partial}{\partial \beta_2} \left(\gamma_2 \beta_2 - \varepsilon_2^* + \frac{\kappa}{2} \beta_1^2 \right) \\ &\quad \left. + \frac{1}{2} \left[\frac{\partial^2}{\partial \alpha_1^2} (\kappa \alpha_2) + \frac{\partial^2}{\partial \beta_1^2} (\kappa \beta_2) \right] \right\} P(\mathbf{a}) \end{aligned} \quad (9.8)$$

where $(\mathbf{a}) = [\alpha_1, \beta_1, \alpha_2, \beta_2]$.

An attempt to find the steady state solution of this equation by means of a potential solution fails since the potential conditions (6.73) are not satisfied.

We proceed by adiabatically eliminating the high-frequency mode. This may be accomplished best in the Langevin equations equivalent to (9.8).

$$\begin{aligned} \frac{\partial}{\partial t} \begin{pmatrix} \alpha_1 \\ \beta_1 \end{pmatrix} &= \begin{pmatrix} \kappa\beta_1\alpha_2 - \gamma_1\alpha_1 + \sqrt{\kappa\alpha_2}[\eta_1(t)] \\ \kappa\alpha_1\beta_2 - \gamma_1\beta_1 + \sqrt{\kappa\beta_2}[\tilde{\eta}_1(t)] \end{pmatrix} \\ \frac{\partial}{\partial t} \begin{pmatrix} \alpha_2 \\ \beta_2 \end{pmatrix} &= \begin{pmatrix} \varepsilon_2 - \frac{\kappa}{2}\alpha_1^2 - \gamma_2\alpha_2 \\ \varepsilon_2^* - \frac{\kappa}{2}\beta_2^2 - \gamma_2\beta_2 \end{pmatrix} \end{aligned} \quad (9.9)$$

where $\eta_1(t), \tilde{\eta}_1(t)$ are delta correlated stochastic forces with zero mean

$$\langle \eta_1(t) \rangle = \langle \tilde{\eta}_1(t) \rangle = \langle \eta_1(t)\eta_1(t') \rangle = \langle \tilde{\eta}_1(t)\tilde{\eta}_1(t') \rangle = 0 , \quad (9.10)$$

$$\langle \eta_1(t)\tilde{\eta}_1(t) \rangle = \delta(t - t') . \quad (9.11)$$

Under the conditions $\gamma_2 \gg \gamma_1$ we can adiabatically eliminate α_2 and β_2 which gives the resultant Langevin equation for α_1 and β_1

$$\frac{\partial}{\partial t} \begin{pmatrix} \alpha_1 \\ \beta_1 \end{pmatrix} = \left(\begin{pmatrix} \frac{\kappa}{\gamma_2} \left(\varepsilon_2 - \frac{\kappa}{2}\alpha_1^2 \right) \beta_1 - \gamma_1\alpha_1 \\ \frac{\kappa}{\gamma_2} \left(\varepsilon_2^* - \frac{\kappa}{2}\beta_1^2 \right) \alpha_1 - \gamma_1\beta_1 \end{pmatrix} + \left(\begin{pmatrix} \frac{\kappa}{\gamma_2} \left(\varepsilon_2 - \frac{\kappa}{2}\alpha_1^2 \right) \\ \frac{\kappa}{\gamma_2} \left(\varepsilon_2^* - \frac{\kappa}{2}\beta_1^2 \right) \end{pmatrix}^{1/2} \begin{pmatrix} \eta_1(t) \\ \tilde{\eta}_1(t) \end{pmatrix} \right) \right) . \quad (9.12)$$

The Fokker–Planck equation corresponding to these equations is

$$\begin{aligned} \frac{\partial}{\partial t} P(\alpha_1, \beta_1) &= \left\{ \frac{\partial}{\partial \alpha_1} \left[\gamma_1\alpha_1 - \frac{\kappa}{\gamma_2} \left(\varepsilon_2 - \frac{\kappa}{2}\alpha_1^2 \right) \beta_1 \right] \right. \\ &\quad + \frac{\partial}{\partial \beta_1} \left[\gamma_1\beta_1 - \frac{\kappa}{\gamma_2} \left(\varepsilon_2^* - \frac{\kappa}{2}\beta_1^2 \right) \alpha_1 \right] \\ &\quad \left. + \frac{1}{2} \left[\frac{\partial^2}{\partial \alpha_1^2} \frac{\kappa}{\gamma_2} \left(\varepsilon_2 - \frac{\kappa}{2}\alpha_1^2 \right) + \frac{\partial}{\partial \beta_1^2} \frac{\kappa}{\gamma_2} \left(\varepsilon_2^* - \frac{\kappa}{2}\beta_1^2 \right) \right] \right\} P(\alpha_1, \beta_1) . \end{aligned} \quad (9.13)$$

We set $\frac{\partial}{\partial t} P(\alpha_1, \beta_1) = 0$ and attempt to find a potential solution as given by (6.72). It is found as

$$F_1 = -2 \left(\beta_1 - \frac{2\gamma_2 \left(\gamma_1 - \frac{\kappa^2}{2\gamma_2} \right) \alpha_1}{2\kappa\varepsilon_2 - \kappa^2\alpha_1^2} \right) \quad (9.14)$$

$$F_2 = -2 \left(\alpha_1 - \frac{2\gamma_2 \left(\gamma_1 - \frac{\kappa^2}{2\gamma_2} \right) \beta_1}{2\kappa\varepsilon_2^* - \kappa^2\beta_1^2} \right) \quad (9.15)$$

It follows that the potential conditions

$$\frac{\partial F_1}{\partial \alpha_1} = \frac{\partial F_2}{\partial \beta_1} \quad (9.16)$$

are satisfied.

The potential is obtained on integrating (9.14, 15)

$$P(a) = N \exp \left[2\alpha_1 \beta_1 + \frac{2\bar{\gamma}_1 \gamma_2}{\kappa^2} \ln(c^2 - \kappa^2 \alpha_1^2) + 2 \left(\frac{\bar{\gamma}_1 \gamma_2}{\kappa^2} \right)^* \ln(c^{*2} - \kappa^2 \beta_1^2) \right] \quad (9.17)$$

where

$$c = \sqrt{2\kappa\varepsilon_2}, \quad \bar{\gamma}_1 = \gamma_1 - \frac{\kappa^2}{2\gamma_2}.$$

It is clear that this function diverges for the usual integration domain of the complex plane with $\beta_1 = \alpha_1^*$. The observable moments may, however, be obtained by use of the complex P representation. The calculations are described in Appendix 9.A.

The semi-classical solution for the intensity exhibits a threshold behaviour at $\varepsilon_2 = \varepsilon_2^c = \gamma_1 \gamma_2 / \kappa$. This is compared in Fig. 9.1 with the mean intensity $I = \langle \beta_1 \alpha_1 \rangle$ calculated from the solution (9.17), as shown in the Appendix 9.A. For comparison, the mean intensity when thermal fluctuations are dominant (Exercise 9.4) is also plotted. The mean intensity with thermal fluctuations displays the rounding of the transition familiar from classical fluctuation theory. The quantum calculation shows a feature never observed in a classical system where the mean intensity actually drops below the semi-classical intensity. This deviation from the semi-classical behaviour is most significant for small threshold photon numbers. As the parameter $\gamma_1 \gamma_2 / \kappa^2$ is increased the quantum mean approaches the semi-classical value.

The variance of fluctuations in the quadratures $X_1 = a_1 + a_1^\dagger$ and $X_2 = (a_1 - a_1^\dagger)/i$ is given by

$$\Delta X_1^2 = [\langle (\alpha_1 + \beta_1)^2 \rangle - \langle \alpha_1 + \beta_1 \rangle^2] + 1, \quad (9.18)$$

$$\Delta X_2^2 = -[\langle (\alpha_1 - \beta_1)^2 \rangle - \langle \alpha_1 - \beta_1 \rangle^2] + 1. \quad (9.19)$$

The variance in the quadratures is plotted in Fig. 9.2a versus the scaled driving field λ . The variance in the phase quadrature X_2 reaches a minimum at threshold. This minimum approaches $\frac{1}{2}$ as the threshold intensity is increased. The value of one half in the variance of the intracavity field corresponds to zero fluctuations found at the resonance frequency in the external field. The fluctuations in the amplitude quadrature X_1 increase dramatically as the threshold is approached. However, unlike the calculation where the pump is treated classically the fluctuations do not diverge. This is because (9.17) is an exact solution to the nonlinear interaction including pump depletion.

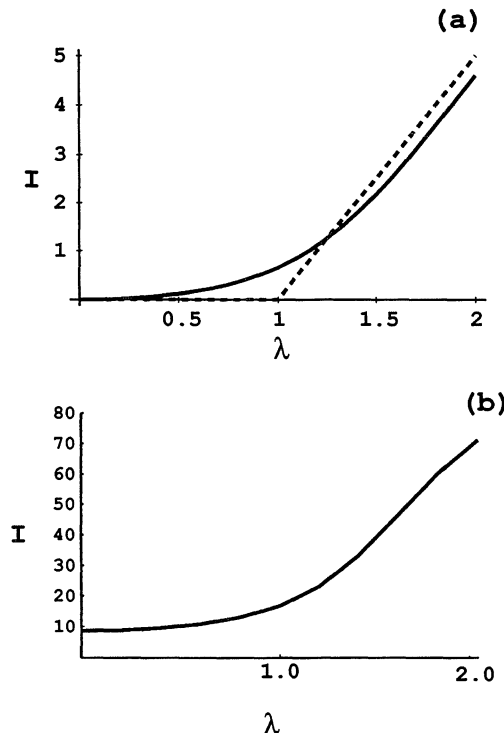


Fig. 9.1. A plot of the mean intensity for the degenerate parametric oscillator versus the scaled driving field λ . (a) The case of zero thermal fluctuations. The dashed curve represents the semi-classical intensity, the solid curve is the exact quantum result. In both cases $\mu^2 = 2\varepsilon_2^s/\kappa = 5.0$. Note that above threshold the exact quantum result is less than the semi-classical prediction. (b) The case of dominant thermal fluctuations. The mean thermal photon number is 10.0 and $\mu^2 = 2\varepsilon_2^s/\kappa = 100.0$

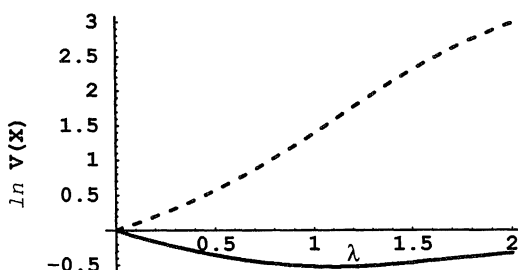


Fig. 9.2. The log variance of the squeezed (solid) and unsqueezed (dashed) quadrature in a degenerate parametric amplifier versus the scaled driving field with $\mu^2 = 2\varepsilon_2^s/\kappa = 5.0$

As the threshold value increases and therefore the number of pump photons required to reach threshold increases, the fluctuations become larger. In the limit $\gamma_1\gamma_2/\kappa^2 \rightarrow \infty$ the fluctuations diverge, as this corresponds to the classical pump (infinite energy). The variance in the amplitude quadrature above threshold continues to increase as the distribution is then double-peaked at the two stable output amplitudes.

The above solution demonstrates the usefulness of the complex P representation. Although the solution obtained for the steady state distribution has no interpretation in terms of a probability distribution, the moments calculated by integrating the distribution on a suitable manifold correspond to the physical moments. We have demonstrated how exact moments of a quantized intracavity field undergoing a nonlinear interaction may be calculated. To calculate the moments of the external field however, we must resort to linearization techniques.

9.2 Optical Parametric Oscillator: Positive P Function

As an alternative to the foregoing description we may consider the use of the positive P representation, following the treatment of *Wolinsky and Carmichael* [9.3]. We can obtain an analytic solution for the steady state positive P function. This solution is a function of two phase space variables; one variable is the *classical field* amplitude, the other is a *non-classical variable* needed to represent superpositions of coherent states. A three-dimensional plot of the positive P function allows one to distinguish between the limiting regions of essentially classical behaviour and predominantly quantum behaviour.

We begin with the Langevin equations for the low frequency mode

$$\frac{d\alpha}{d\tau} = -\alpha - \beta(\lambda - \alpha^2) + g(\lambda - \alpha^2)^{1/2} \eta_1 , \quad (9.20)$$

$$\frac{d\beta}{d\tau} = -\beta - \alpha(\lambda - \beta^2) + g(\lambda - \beta^2)^{1/2} \eta_2 , \quad (9.21)$$

where τ is measured in cavity lifetimes (γ_1^{-1}),

$$g = \frac{\kappa}{(2\gamma_1\gamma_2)^{1/2}} \equiv \frac{1}{\mu} , \quad (9.22)$$

and λ is a dimensionless measure of the pump field amplitude scaled to give the threshold condition $\lambda = 1$, and we have scaled the c-number variables by

$$\alpha = g\alpha_1, \quad \beta = g\beta_1 . \quad (9.23)$$

Equations (9.20, 21) describe trajectories in a four-dimensional phase space. The region of phase space satisfying the conjugacy condition $\beta = \alpha^*$ is called the *classical subspace*. Two extra non-classical dimensions are required by the quantum noise. If we neglect the fluctuating forces η_1 and η_2 (9.20, 21) have the stable steady state solution $\alpha = \beta = 0$ below threshold ($\lambda < 1$), and $\alpha = \beta = \pm(\lambda - 1)^{1/2}$ above threshold ($\lambda > 1$). In the full phase space there are additional steady states which do not satisfy the conjugacy condition: two steady states $\alpha = \beta = \pm i(1 - \lambda)^{1/2}$ below threshold and two steady states $\alpha = -\beta = \pm(\lambda + 1)^{1/2}$ both below and above threshold.

The variables α and β are restricted to a bounded manifold $\alpha = x, \beta = y$ with x and y both real and $|x|, |y| \leq \sqrt{\lambda}$. We denote this manifold by $\Lambda(x, y)$. Trajectories are confined within this manifold by reflecting boundary conditions. If a trajectory starts within this manifold, then it is clear from (9.20 and 21) that the drift and noise terms remain real, so a trajectory will remain on the real plane. Furthermore, at the boundary, the trajectory must follow the deterministic flow inwards, as the transverse noise component vanishes. If the initial quantum state is the vacuum state, the entire subsequent evolution will be confined to this manifold.

The manifold $\Lambda(x, y)$ is alternatively denoted by $\Lambda(u, v)$ with $u = \frac{1}{2}(x + y)$, $v = \frac{1}{2}(x - y)$. The line $v = 0$ is a one-dimensional classical subspace, the subspace preserving $\alpha = \beta$. The variable v denotes a transverse, non-classical dimension used by the noise to construct manifestly non-classical states.

We may now construct a pictorial representation of these states which dramatically distinguishes between the quantum and classical regimes.

With $\alpha = x, \beta = y$ both real, the solution to the Fokker–Planck equation (9.13) is of the form given by (9.17). With $|x|, |y| \leq \sqrt{\lambda}$

$$P_{\text{ss}}(x, y) = N[(\lambda - x^2)(\lambda - y^2)]^{1/g^2 - 1} e^{2xy/g^2}. \quad (9.24)$$

For weak noise ($g \ll 1$), $P_{\text{ss}}(x, y)$ is illustrated in Fig. 9.3. Below threshold ($\lambda < 1$) $P_{\text{ss}}(u, v)$ may be written

$$P_{\text{ss}}(u, v) = \frac{(1 - \lambda^2)^{1/2}}{\pi \lambda g/2} \exp \left(\frac{-(1 - \lambda)u^2 + (1 + \lambda)v^2}{\frac{\lambda g^2}{2}} \right). \quad (9.25)$$

The normally-ordered field quadrature variances are determined by the quantities

$$\langle : \Delta X_1^2 : \rangle = V \left(\frac{\alpha + \beta}{2} \right), \quad (9.26)$$

$$\langle : \Delta X_2^2 : \rangle = V \left(\frac{\alpha - \beta}{2} \right) \quad (9.27)$$

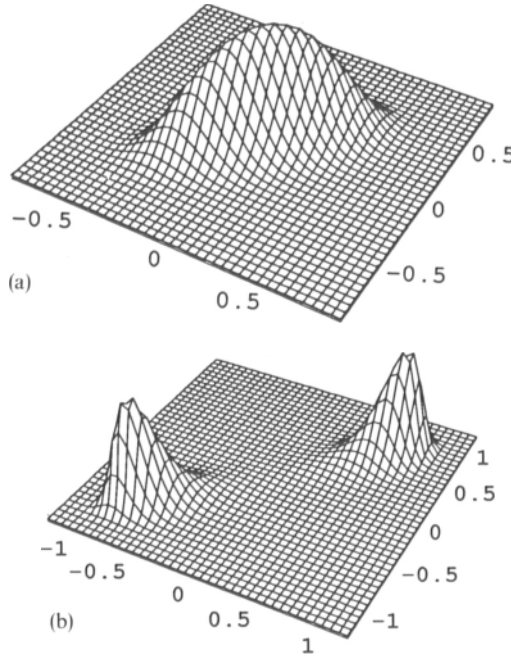


Fig. 9.3. A plot of the complex P representation of the steady state of the degenerate parametric amplifier, below and above threshold: (a) $\lambda = 0.8$ (b) $\lambda = 1.5$. In both cases $g = (2\epsilon_2^c/\kappa)^{-1/2} = 0.25$

where $V(z)$ refers to the variance over the stationary distribution function. As $u = (\alpha + \beta)/2$ and $v = i(\alpha - \beta)/2$, on the manifold $\Lambda(u, v)$, the quadrature variances are given by

$$\langle : \Delta X_1^2 : \rangle = V(u)/g^2 , \quad (9.28)$$

$$\langle : \Delta X_2^2 : \rangle = -V(v)/g^2 . \quad (9.29)$$

The variances $g^{-2}\langle \Delta u^2 \rangle$ and $-g^{-2}\langle \Delta v^2 \rangle$ correspond to the normally ordered variances of the unsqueezed and squeezed quadratures, respectively, of the subharmonic field.

The threshold distribution ($g \ll 1, \lambda = 1$) is given by

$$P_{ss}(u, v) = \left[4\sqrt{\pi} g^{3/2} \Gamma\left(\frac{1}{4}\right) \right] e^{-(u^4 + 4v^2)/g^2} . \quad (9.30)$$

Above threshold the distribution splits into two peaks. We note that in the low-noise regime $P_{ss}(x, y)$ is a slightly broadened version of the classical steady state with only a small excursion into the nonclassical space.

Figure 9.4 shows $P_{ss}(x, y)$ for the same values of λ as Fig. 9.3 but for the noise strength $g = 1$. The quantum noise has become sufficiently strong to explore

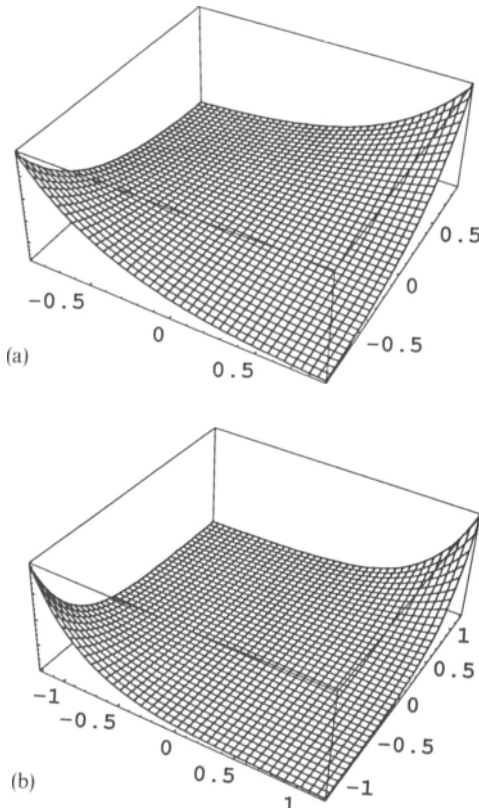


Fig. 9.4. As in Fig. 9.3 but with quantum noise parameter $g = 1.0$. (a) $\lambda = 0.8$ (b) $\lambda = 1.5$

thoroughly the non-classical dimension of the phase space. $P_{ss}(x, y)$ is strongly influenced by the boundary $\Lambda(x, y)$.

As the noise strength g is increased beyond 1, the characteristic threshold behaviour of the parametric oscillator disappears and squeezing is significantly reduced (Fig. 9.5). In the large- g limit the stochastic trajectories are all driven to the boundary of $\Lambda(x, y)$, and then along this boundary to the corners, where both noise terms in (9.20, 21) vanish. $P_{ss}(x, y)$ approaches a sum of δ functions

$$\begin{aligned} P_{ss}(x, y) = & \frac{1}{2}(1 + e^{4\lambda/g^2})^{-1} [\delta(x - \sqrt{\lambda}) \delta(y - \sqrt{\lambda}) \\ & + \delta(x + \sqrt{\lambda}) \delta(y + \sqrt{\lambda})] + \frac{1}{2}(1 + e^{4\lambda/g^2})^{-1} \\ & \times [\delta(x - \sqrt{\lambda}) \delta(y + \sqrt{\lambda}) + \delta(x + \sqrt{\lambda}) \delta(y - \sqrt{\lambda})]. \end{aligned} \quad (9.31)$$

The two δ functions that set $x = -y = \pm \sqrt{\lambda}$ represent off-diagonal or interference terms $e^{-2\sqrt{\lambda}/g} |\sqrt{\lambda}/g\rangle \langle -\sqrt{\lambda}/g|$. Figure 9.6a–c illustrates the behaviour of $P_{ss}(x, y)$ as a function of λ in the strong-noise limit. When $4\lambda/g^2 \ll 1$ all

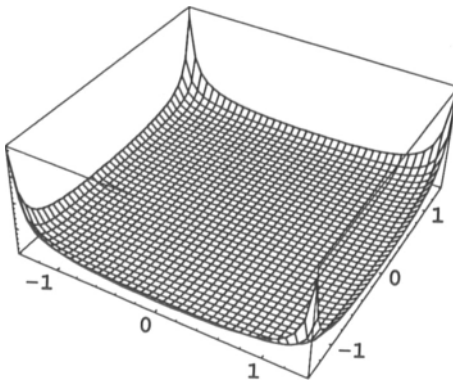


Fig. 9.5. As in Fig. 9.3 but with $\lambda = 1.5$ and $g = 10.0$

δ functions carry equal weight and the state of the subharmonic field is the coherent state superposition $\frac{1}{2}(|\sqrt{\lambda}/g\rangle + |-\sqrt{\lambda}/g\rangle)$. As λ increases, this superposition state is replaced by a classical mixture of coherent states $|\sqrt{\lambda}/g\rangle$ and $|-\sqrt{\lambda}/g\rangle$ for $4\lambda/g^2 \gg 1$. This is a consequence of the competition between the creation of quantum coherence by the parametric process and the destruction of this coherence by dissipation. It will be shown in Chap. 16, that the decay of quantum coherence in a damped superposition state proceeds at a rate proportional to the phase space separation of the states.

This example has illustrated how quantum dissipative systems can exhibit manifestly quantum behaviour in the limit of large quantum noise. This is outside the realm of linear noise theory where classical states are only slightly perturbed.

9.3 Quantum Tunnelling Time

We proceed to calculate the quantum tunnelling time between the two stable states. We shall follow the procedure of *Drummond and Kinsler* [9.4]. In order to calculate the quantum tunnelling rate, we shall transform the variables α and β to give constant diffusion, or additive stochastic noise.

$$u = \sin^{-1} \left(\frac{g\alpha}{\sqrt{\lambda}} \right) + \sin^{-1} \left(\frac{g\beta}{\sqrt{\lambda}} \right), \quad (9.32)$$

$$v = \sin^{-1} \left(\frac{g\alpha}{\sqrt{\lambda}} \right) - \sin^{-1} \left(\frac{g\beta}{\sqrt{\lambda}} \right). \quad (9.33)$$

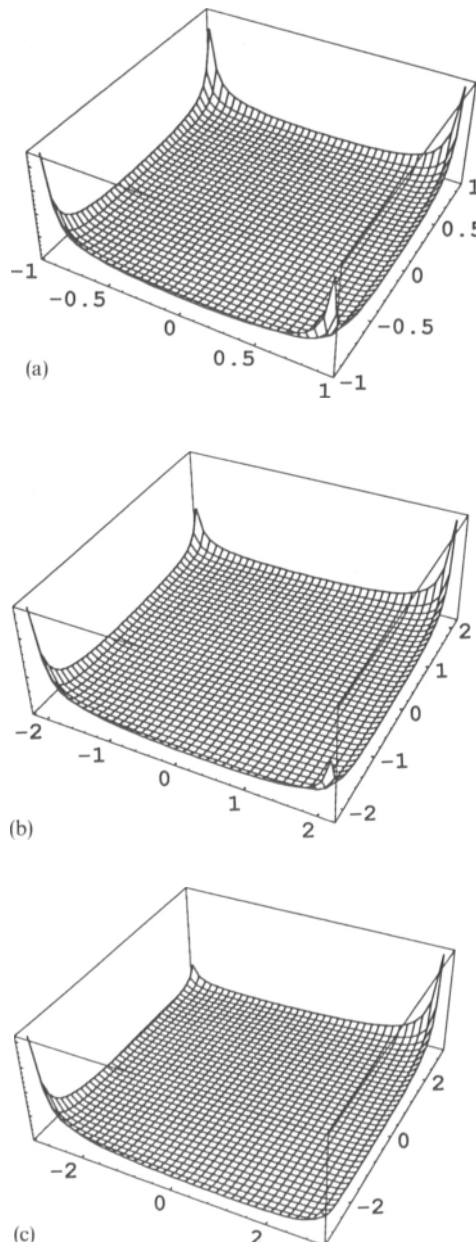


Fig. 9.6. As in Fig. 9.3 but demonstrating the dependence on λ with $g = 5.0$. (a) $\lambda = 1.0$ (b) $\lambda = 5.0$ (c) $\lambda = 10.0$

These new variables are constrained to have a range such that $|u| + |v| \leq \pi$. Referring back to the variables α and β , it can be seen that the u axis represents the classical subspace of the phase space where $\alpha = \beta$. Thus the variable v is a non-classical dimension which allows for the creation of quantum features. The stochastic equations corresponding to these variables are

$$du = \left\{ \lambda \sin(u) - \sigma \left[\tan\left(\frac{u+v}{2}\right) + \tan\left(\frac{u-v}{2}\right) \right] \right\} d\tau + \sqrt{2} g dW_u , \quad (9.34)$$

$$dv = \left\{ -\lambda \sin(v) - \sigma \left[\tan\left(\frac{u+v}{2}\right) - \tan\left(\frac{u-v}{2}\right) \right] \right\} d\tau + \sqrt{2} g dW_v . \quad (9.35)$$

Here $\sigma = 1 - g^2/2$, dW_u , dW_v are Wiener processes.

These Ito equations have a corresponding Fokker–Planck equation and a probability distribution in the limit as $\tau \rightarrow \infty$ of

$$P(u, v) = N \exp[-V(u, v)/g^2] \quad (9.36)$$

where the potential $V(u, v)$ is

$$V(u, v) = -2\sigma \ln |\cos u + \cos v| + \lambda \cos u - \lambda \cos v . \quad (9.37)$$

Above threshold the potential has two minima corresponding to the stable states of the oscillator. These minima have equal intensities and amplitudes of opposite sign, and are at classical locations with $\alpha = \alpha^*$

$$(u_0, v_0) = (\pm 2 \sin^{-1}[(\lambda - \sigma)^{1/2}/\sqrt{\lambda}], 0) \quad (9.38)$$

or

$$g\alpha_0 = \pm (\lambda - 1 + g^2)^{1/2} . \quad (9.39)$$

There is also a saddle point at $(u_s, v_s) = (0, 0)$.

Along the u axis the second derivative of the potential in the v direction is always positive. The classical subspace ($v = 0$) is therefore at a minimum of the potential with respect to variations in the non-classical variable v . This valley along the u axis between the two potential wells is the most probable path for a stochastic trajectory in switching from one well to the other. The switching rate between them will be dominated by the rate due to trajectories along this route. Using an extension of Kramer's method, developed by Landauer and Swanson [9.5], the mean time taken for the oscillator to switch from one state to the other in the limit of $g^2 \ll 1$ is

$$T_p = \frac{\pi}{\gamma_1} \left(\frac{\lambda + \sigma}{\lambda(\lambda - \sigma)^2} \right)^{1/2} \exp \left\{ \frac{2}{g^2} \left[\lambda - \sigma - \sigma \ln \left(\frac{\lambda}{\sigma} \right) \right] \right\} . \quad (9.40)$$

The switching time is increased as the pump amplitude λ is increased or the nonlinearity g^2 is reduced.

Previous attempts to compute the tunnelling time for this problem have used the Wigner function [9.6]. Unfortunately the time-evolution equation for the Wigner function contains third-order derivative terms and is thus not a Fokker–Planck equation. In the case of linear fluctuations around a steady state truncating the evolution equation at second-order derivatives is often a good approximation. However, it is not clear that this procedure will give quantum tunnelling times correctly.

In the limit of large damping in the fundamental mode the truncated Wigner function of the sub-harmonic mode obeys with $\tau = \gamma_1 t$

$$\begin{aligned} \frac{d}{d\tau} W(\beta, t) = & \left\{ \frac{\partial}{\partial \beta} [\beta - \beta^*(\lambda - g^2 \beta^2)] + \frac{\partial}{\partial \beta^*} [\beta^* - \beta(\lambda - g^2 \beta^{*2})] \right. \\ & \left. + \frac{\partial^2}{\partial \beta \partial \beta^*} (1 + 2g^2 \beta \beta^*) \right\} W(\beta, \tau) . \end{aligned} \quad (9.41)$$

This truncated Wigner function equation does not have potential solutions, however an approximate potential solution can be obtained that is valid near threshold. Here, the noise contribution $2g^2 \beta \beta^*$ is small and is neglected leaving only subharmonic noise. Writing $\beta = x + ip$, the solution in the near threshold approximation is

$$W_{NT} = N_{NT} \exp[-V_{NT}(x, p)] \quad (9.42)$$

where

$$V_{NT}(x, p) = \frac{2}{g^2} [g^2 x^2 + g^2 p^2 + \frac{1}{2}(g^2 x^2 + g^2 p^2)^2 - \lambda(g^2 x^2 - g^2 p^2)] \quad (9.43)$$

and N_{NT} is the normalisation constant.

Above threshold this potential has two minima, at $gx = \pm(\lambda - 1)^{1/2}$. In the limit of large-threshold photon numbers, these minima are very close to those obtained in (9.39). The tunneling time has been calculated from the Wigner distribution by Graham [9.7], with the result

$$T_w = \frac{\pi}{\gamma_1} \left(\frac{\lambda + 1}{\lambda(\lambda - 1)^2} \right)^{1/2} \exp \left[\frac{1}{g} (\lambda - 1)^2 \right] . \quad (9.44)$$

This result is compared with the expression derived using the P function in Fig. 9.7 which shows the variation in the logarithm of the tunnelling rate with the pump amplitude λ . The Wigner function result predicts a slower switching time above threshold. The difference in the two predictions can be many orders of magnitude. The calculations from the exact positive P Fokker–Planck equation represent a true quantum tunnelling rate. Whereas the truncation of the Wigner function equation involves dropping higher order derivatives dependent on the interaction strength g . Thus nonlinear terms in the quantum noise are neglected and the only quantum noise terms included are due to the vacuum fluctuations from the cavity losses. These give a diffusion term in the truncated

Wigner Fokker–Planck equation which is identical to classical thermal noise, with an occupation number of half a photon per mode. Also indicated in Fig. 9.7 are the tunnelling times computed by direct numerical simulation of the stochastic differential equations resulting from either the positive P representation

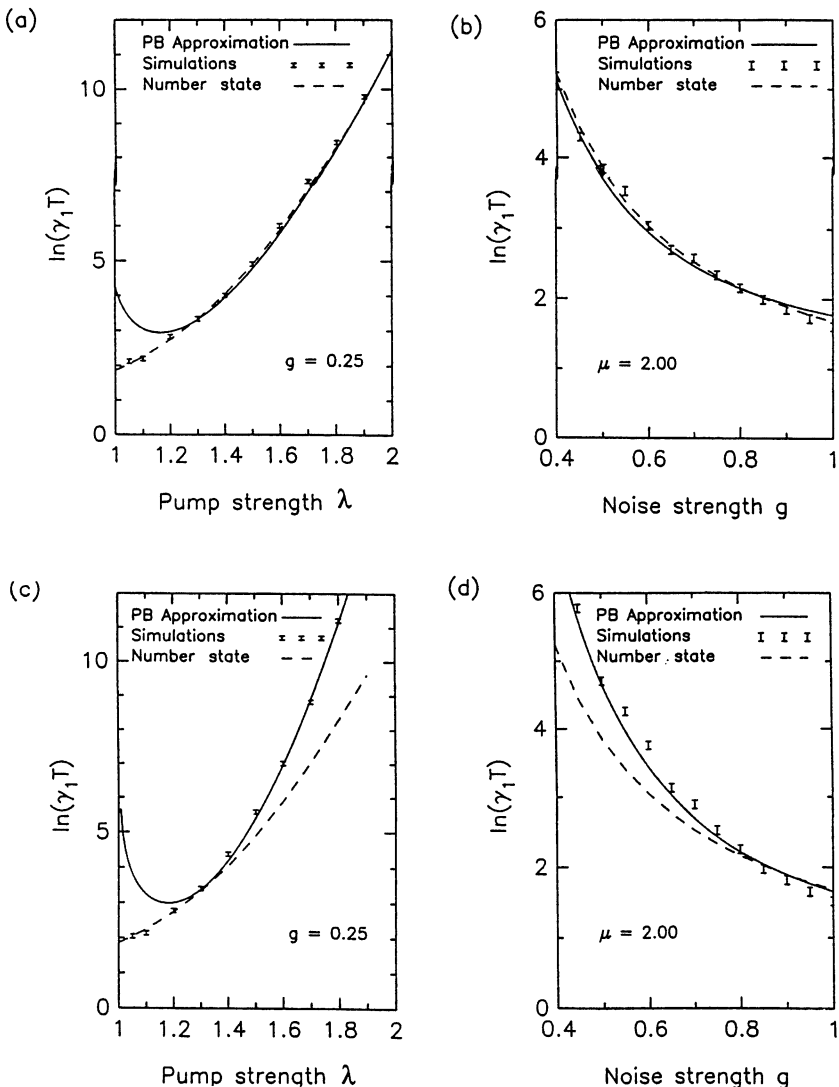


Fig. 9.7. A plot of the log of the tunnelling time for the degenerate parametric amplifier above threshold, versus pump strength or noise strength. In (a) and (b) we show the results computed by the positive P Representation (PB approximation) while in (c) and (d) we give the results for the truncated Wigner function model. In all cases we contrast the results obtained by potential methods with the results obtained by direct simulation of the corresponding stochastic differential equations and number state solution of the master equation (dashed line) [9.4]

(Fig. 9.7a, b) or the Wigner representation (Fig. 9.7c, d) and by directly solving the master equation in the number basis.

The differences between the two rates obtained reflect the difference between classical thermal activation and true quantum tunnelling. Classical thermal-activation rates are slower than quantum tunnelling rates far above threshold where the former are large since the thermal trajectory must go over the barrier. A quantum process, on the other hand, can short cut this by tunnelling.

9.4 Dispersive Optical Bistability

We consider a single mode model for dispersive optical bistability. An optical cavity is driven off resonance with a coherent field. The intracavity medium has an intensity dependent refractive index. As the intensity of the driving field is increased the cavity is tuned to resonance and becomes highly transmissive.

We shall model the intracavity medium as a Kerr type $\chi^{(3)}$ nonlinear susceptibility treated in the rotating wave approximation. The Hamiltonian and Fokker–Planck equation are given by (8.47 and 50), respectively. The Fokker–Planck equation is

$$\frac{\partial P}{\partial t} = \left[\frac{\partial}{\partial \alpha} (\kappa\alpha + 2i\chi\alpha^2\beta - E_0) - i\chi \frac{\partial^2}{\partial \alpha^2} \alpha^2 + \frac{\partial}{\partial \beta} (\kappa^*\beta - 2i\chi\beta^2\alpha - E_0) + i\chi \frac{\partial^2}{\partial \beta^2} \beta^2 \right] P(\alpha, \beta) \quad (9.45)$$

where we choose the phase of the driving field such that E_0 is real and $\kappa = \gamma + i\delta$. We shall seek a steady state solution using the potential conditions (6.72). The calculation of F gives

$$F_1 = -\left(\frac{i}{\chi}\right)\left(\frac{\bar{\kappa}}{\alpha} + 2\chi\beta - \frac{E_0}{\alpha^2}\right), \quad F_2 = \left(\frac{i}{\chi^*}\right)\left(\frac{\bar{\kappa}^*}{\alpha} - 2\chi^*\beta - \frac{E_0}{\beta^2}\right), \quad (9.46)$$

where we have defined $\bar{\kappa} = \kappa - 2i\chi$. The cross derivatives

$$\partial_\alpha F_2 = \partial_\beta F_1 = 2 \quad (9.47)$$

so that the potential conditions are satisfied.

The steady state distribution is given by

$$\begin{aligned} P_{ss}(\alpha, \beta) &= \exp \left[\int^\alpha F_p(\alpha') d\alpha'_p \right] \\ &= \exp \left\{ \int^\alpha \left[\frac{1}{i\chi} \left(\frac{\bar{\kappa}}{\alpha_1} + 2i\chi\beta_1 - \frac{E_0}{\alpha_1^2} \right) d\alpha_1 - \frac{1}{i\chi} \left(\frac{\bar{\kappa}^*}{\beta_1} - 2i\chi\alpha_1 - \frac{E_0}{\beta_1^2} \right) d\beta_1 \right] \right\} \end{aligned}$$

$$= \alpha^{c-2} \beta^{d-2} \exp \left[\left(\frac{E_0}{i\chi} \right) \left(\frac{1}{\alpha} + \frac{1}{\beta} \right) + 4\alpha\beta \right] \quad (9.48)$$

where $c = \frac{\kappa}{i\chi}$, $d = \left(\frac{\kappa}{i\chi} \right)^*$.

It can be seen immediately that the usual integration domain of the complex plane with $\alpha^* = \beta$ is not possible since the potential diverges for $\alpha\beta \rightarrow \infty$. However, the moments may be calculated using the complex P representation. The calculations are described in Appendix 9.A. The results for the mean amplitude $\langle a \rangle$ and correlation function $g^{(2)}(0)$ are plotted in Fig. 9.8 where they are compared with the semi-classical value for the amplitude α_{ss} .

It is seen that, whereas the semi-classical equation predicts a bistability or hysteresis, the exact steady state equation which includes quantum fluctuations does not exhibit bistability or hysteresis. The extent to which bistability is observed in practice will depend on the fluctuations, which in turn determine the time for random switching from one branch to the other. The driving field must be ramped in time intervals shorter than this random switching time in order for bistability to be observed.

The variance of the fluctuations as displayed by $g^{(2)}(0)$ show an increase as the fluctuations are enhanced near the transition point. The dip in the steady state mean at the transition point is due to out-of-phase fluctuations between the upper and lower branches.

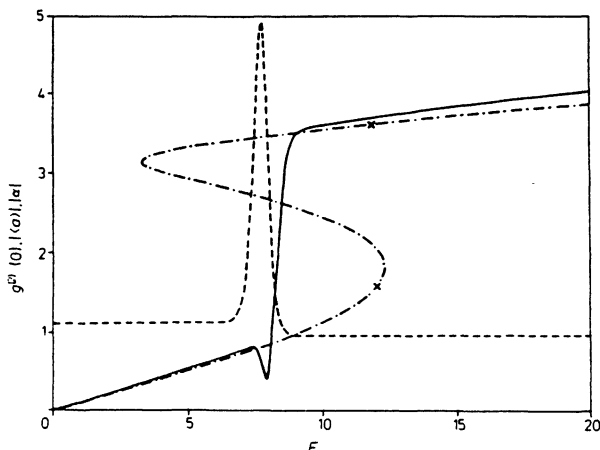


Fig. 9.8. The steady state amplitude, and second-order correlation function for optical bistability versus the pump amplitude. The chain curve gives the semi-classical steady state amplitude. The full curve gives the exact steady state amplitude. The broken curve presents the second-order correlation function $g^{(2)}(0)$. The detuning is chosen so that $\Delta\omega \chi < 0$ with $\Lambda\omega = -10$ and $\chi = 0.5$

9.5 Comment on the Use of the Q and Wigner Representations

We will compare the above solution we have obtained with the generalised P representation with the equation obtained using the Q and Wigner representations. With the Q representation we obtain the following equation

$$\frac{\partial Q}{\partial t}(\alpha^*, \alpha) = \left[\frac{\partial}{\partial \alpha} (-\varepsilon + \bar{\kappa}\alpha + 2i\chi\alpha^2\alpha^*) + i\chi \frac{\partial^2}{\partial \alpha^2} \alpha^2 + \kappa \frac{\partial^2}{\partial \alpha \partial \alpha^*} + \text{c.c.} \right] Q(\alpha^*, \alpha) \quad (9.49)$$

where $\bar{\kappa} = \kappa - 4i\chi + i\Delta\omega$.

This equation has a non-positive definite diffusion matrix. Furthermore, it does not satisfy the potential conditions, hence its steady-state solution is not readily obtained.

The equation for the Wigner function may be shown to be as in,

$$\begin{aligned} \frac{\partial W(\alpha^*, \alpha)}{\partial t} = & \left(\varepsilon \frac{\partial}{\partial \alpha} + \kappa \frac{\partial}{\partial \alpha} + \frac{\kappa}{2} \frac{\partial^2}{\partial \alpha^* \partial \alpha} - 2i\chi \frac{\partial}{\partial \alpha} - i\chi \frac{1}{2} \frac{\partial^2}{\partial \alpha^{*2}} \alpha \right. \\ & \left. + 2i\chi \frac{\partial^3}{\partial \alpha^3} \alpha^* \alpha^2 + \text{c.c.} \right) W(\alpha^*, \alpha) . \end{aligned} \quad (9.50)$$

This equation is not of a Fokker–Planck form since it contains third-order derivatives. Again a steady-state solution is not readily obtainable. It is clear that for this problem the use of the complex P representation is preferable to the other two representations.

Exercises

9.1 Derive the Fokker–Planck equation for $P(\alpha_1, \alpha_2, t)$ for the non-degenerate parametric oscillation after adiabatically eliminating the pump mode. Solve for the potential solution and derive the moments.

9.2 Derive the evolution equations for the Q and Wigner functions for the degenerate parametric oscillator described by (9.1).

9.3 Derive the equation of motion for the Q function for optical bistability. Show that with zero detuning and zero driving the solution for an initial coherent state is

$$\begin{aligned} Q(\alpha, t) = & \exp(-|\alpha|^2) \sum_{q,p=0}^{\infty} (q!p!)^{-1} (\alpha \alpha_0^*)^q (\alpha^* \alpha_0)^p f(t)^{(p+q)/2} \\ & \times \exp \left\{ -|\alpha_0|^2 \frac{[f(t) + i\delta]}{(1 + i\delta)} \right\} \end{aligned}$$

where

$$\delta = (p - q)/\kappa, \quad f(t) = \exp[-\kappa v - i\nu(p - q)], \quad v = 2\mu t, \quad \kappa = \frac{\gamma}{2\mu}.$$

9.4 Calculate the steady state distribution $P(\alpha)$ and the mean intensity $\langle \alpha^* \alpha \rangle$ for the parametric oscillator for the case where the thermal fluctuations dominate the quantum fluctuations.

9.A Appendix

9.A.1 Evaluation of Moments for the Complex P function for Parametric Oscillation (9.17)

It is necessary to integrate on a suitable manifold, chosen so that the distribution (9.17) and all its derivatives vanish at the boundary of integration. If we expand the term $\exp(2\alpha_1 \beta_1)$ in (9.17) in a power series, the expression for the moment

$$I_{nn'} = \int \int \beta^n \alpha^{n'} P(\alpha) d\alpha d\beta . \quad (9.A.1)$$

can be written as

$$I_{nn'} = N(2|c|)^{2(j_2 - 2)} \sum_{m=0}^{\infty} \frac{2^{m+2}}{m!} \left(\frac{-c}{\kappa}\right)^{m+n-1} \left(\frac{-c^*}{\kappa}\right)^{m+n'+1} \\ \times \int \int z_1^{j_1-1} (1-z_1)^{j_2-j_1-1} (1-2z_1)^{m+n} (1-2z_2)^{m+n'} \\ \times z_2^{j_1-1} (1-z_2)^{j_2} dz_1 dz_2 \quad (9.A.2)$$

where

$$j_1 = \frac{2\gamma_1 \gamma_2}{\kappa^2}, \quad j_2 = \frac{4\gamma_1 \gamma_2}{\kappa^2}, \quad z_1 = \frac{1}{2} \left(1 + \frac{\kappa \alpha_1}{c}\right), \quad z_2 = \frac{1}{2} \left(1 + \frac{\kappa \beta_2}{c^*}\right).$$

These integrals are identical to those defining the Gauss' hypergeometric functions. The integration path encircles each pole and traverses the Riemann sheets so that the initial and final values of the integrand are equal, allowing partial integration operations to be defined. The result is [9.8].

$$I_{nn'} = N' \sum_{m=0}^{\infty} \frac{2^m}{m!} \left(\frac{-c}{\kappa}\right)^{m+n} \left(\frac{-c^*}{\kappa}\right)^{m+n'} \\ \times {}_2F_1(- (m+n), j_1, j_2, 2) {}_2F_1(- (m+n), j_1, j_2, 2) \quad (9.A.3)$$

where ${}_2F_1$ are hypergeometric functions.

9.A.2 Evaluation of the Moments for the Complex P Function for Optical Bistability (9.48)

The normalization integral is

$$I(c, d) = \int_c \int \sum \frac{2^n}{n!} x^{-c-n} y^{-d-n} \exp \left[\frac{E_0}{\chi} (x + y) \right] dx dy \quad (9.A.4)$$

where we have made the variable change $x = 1/\alpha$, $y = 1/\beta$, and C is the integration path. $\alpha^* = \beta$ since the potential diverges for $|\alpha|^2 \rightarrow \infty$. This means no Glauber–Sudarshan P function exists in the steady state (except as a generalised function). Hence, we shall use the complex P function where the paths of integration for α and β are line integrals on the individual (α, β) complex planes.

The integrand is now in a recognisable form as corresponding to a sum of gamma function integrals. It is therefore appropriate to define each path of integration to be a Hankel path of integration, from $(-\infty)$ on the real axis around the origin in an anticlockwise direction and back to $(-\infty)$. With this definition of the integration domain, the following gamma function identity holds [9.9]:

$$[\Gamma(c + n)]^{-1} = \left(\frac{t^{1-c-n}}{2\pi i} \right) \int_c x^{-c-n} \exp(xt) dx . \quad (9.A.5)$$

Hence, applying this result to both x and y integrations, one obtains with $\tilde{\chi} = i\chi$

$$I(c, d) = -4\pi^2 \sum_{n=0}^{\infty} \frac{2^n (E_0/\tilde{\chi})^{c+d+2(n-1)}}{n! \Gamma(c+n) \Gamma(d+n)} . \quad (9.A.6)$$

The series is a transcendental function which can be written in terms of the generalised Gauss hypergeometric series. That is, there is a hypergeometric series called ${}_0F_2$ which is defined as [9.10]

$${}_0F_2(c, d, z) = \sum_{n=0}^{\infty} \frac{z^n \Gamma(c) \Gamma(d)}{\Gamma(c+n) \Gamma(d+n) n!} . \quad (9.A.7)$$

From now on, for simplicity, we will write just $F()$, instead of ${}_0F_2()$. Now the normalisation integral can therefore be rewritten in the form

$$I(c, d) = \left(\frac{-4\pi^2 |E_0/\tilde{\chi}|^{c+d-2}}{\Gamma(c) \Gamma(d)} \right) F(c, d, 2|E_0/\tilde{\chi}|^2) . \quad (9.A.8)$$

The moments of the distribution function divided by the normalisation factor give all the observable one-time correlation functions. Luckily the moments have exactly the same function form as the normalisation factor [with the

replacement of (c, d) by $(c + i, d + j)$] so that no new integrals need to be calculated. The i th-order correlation function is

$$G^{(i)} = \langle (a^\dagger)^i (a)^i \rangle = \left(\frac{|E_0/\tilde{\chi}|^{2i} \Gamma(c) \Gamma(d) F(i+c, i+d, 2|E_0/\tilde{\chi}|^2)}{\Gamma(i+c) \Gamma(i+d) F(c, d, 2|E_0/\tilde{\chi}|^2)} \right). \quad (9.A.9)$$

This is the general expression for the i th-order correlation function of a nonlinear dispersive cavity with a coherent driving field and zero-temperature heat baths.

The results for the mean amplitude $\langle a \rangle$ and correlation function $g^2(0)$ are

$$\langle a \rangle = \frac{1}{c} \frac{|E_0/\tilde{\chi}| F(1+c, d, 2|E_0/\tilde{\chi}|^2)}{F(c, d, 2|E_0/\tilde{\chi}|^2)}, \quad (9.A.10)$$

$$g^{(2)}(0) = \left(\frac{cd F(c, d, 2|E_0/\tilde{\chi}|^2) F(c+2, d+2, 2|E_0/\tilde{\chi}|^2)}{(c+1)(d+1)[F(c+1, d+1, 2|E_0/\tilde{\chi}|^2)]^2} \right). \quad (9.A.11)$$

10. Interaction of Radiation with Atoms

The preceding chapters have been concerned with the properties of the free radiation field. We shall now consider the interaction of the radiation field with atoms. In order to give a quantized theory of the interaction it will first be necessary to quantize the electron wave field of the atoms. We shall follow the approach of *Haken* who quantizes the electron wave field in an analogous fashion to the light field [10.1]. For a more rigorous derivation the reader is referred to the book by *Power* [10.2].

10.1 Quantization of the Electron Wave Field

A general wave function $\Psi(x)$ for the electron field may be expanded in terms of a complete set of wave functions obeying the Schrödinger equation

$$\mathcal{H}_0 \Psi_j(x) = \left(-\frac{\hbar^2}{2m} \nabla^2 + V \right) \Psi_j(x) = E_j \Psi_j(x) , \quad (10.1)$$

where V is the Coulomb potential due to the nucleus and inner core electrons. The interaction between the electrons is neglected. Thus

$$\Psi(x) = \sum_j a_j \Psi_j(x) . \quad (10.2)$$

By analogy with the quantization of the light field the expansion coefficients a_j will become operators in the quantized electron field, and $\Psi(x)$ becomes a field operator. The Hermitian conjugate of $\Psi(x)$ is

$$\Psi^\dagger(x) = \sum_j a_j^\dagger \Psi_j^*(x) . \quad (10.3)$$

The functions $\Psi_i^*(x)$ obey the orthonormality relations

$$\int \Psi_i^*(x) \Psi_j(x) d^3x = \delta_{ij} . \quad (10.4)$$

The energy in this representation is

$$\hat{\mathcal{H}}_0 = \int \Psi^\dagger \mathcal{H}_0 \Psi d^3x . \quad (10.5)$$

From (10.2) and using the orthogonality of the eigenfunctions

$$\hat{\mathcal{H}}_0 = \sum_j E_j a_j^\dagger a_j . \quad (10.6)$$

We see that $a_j^\dagger a_j$ may be interpreted as the number operator for the occupation number of electrons in energy level j . We may introduce a vacuum state defined by

$$a_j |0\rangle = 0 . \quad (10.7)$$

A state with one electron in the j th energy level is described by $a_j^\dagger |0\rangle$. Since the Pauli exclusion principle excludes the possibility of two or more electrons in the same state, the state formed by two applications of the creation operator on the vacuum cannot exist. Thus

$$a_j^\dagger a_j^\dagger |0\rangle = 0 . \quad (10.8)$$

In fact, $(a_j^\dagger a_j^\dagger)|\phi\rangle = 0$ for any arbitrary state $|\phi\rangle$. This may be expressed as a requirement on the operator

$$(a_j^\dagger)^2 = 0 . \quad (10.9)$$

The electron operators obey a different set of commutation relations than the photon operators. A consistent formalism results from the following set of (anti) commutation relations.

$$a_j^\dagger a_k + a_k a_j^\dagger = \delta_{jk}, \quad a_j^\dagger a_k^\dagger + a_k^\dagger a_j^\dagger = 0, \quad a_j a_k + a_k a_j = 0 . \quad (10.10)$$

These give the following anti-commutation relations for the electron field operators

$$\begin{aligned} \Psi(\mathbf{x})\Psi^\dagger(\mathbf{x}') + \Psi^\dagger(\mathbf{x}')\Psi(\mathbf{x}) &= \delta(\mathbf{x} - \mathbf{x}') , \\ \Psi(\mathbf{x})\Psi(\mathbf{x}') + \Psi(\mathbf{x}')\Psi(\mathbf{x}) &= 0 . \end{aligned} \quad (10.11)$$

This formalism is eminently suitable for the treatment of many body problems. For example, an atomic system with n electrons occupying the quantum states $j_1 \dots j_n$ is described by

$$|(\{j\})\rangle = a_{j_1}^\dagger a_{j_2}^\dagger \dots a_{j_n}^\dagger |0\rangle . \quad (10.12)$$

In quantum optics we shall mainly be concerned with single-electron states.

One particle expectation values of an operator O , can be represented by

$$\langle (\{j\}) | \int \Psi^\dagger(\mathbf{x}) O(\mathbf{x}) \Psi(\mathbf{x}) d^3x | (\{j\}) \rangle = \langle (\{j\}) | \sum_{jl} a_j^\dagger a_l \int \Psi_j^* O(\mathbf{x}) \Psi_l d^3x | (\{j\}) \rangle . \quad (10.13)$$

10.2 Interaction Between the Radiation Field and the Electron Wave Field

The Hamiltonian describing the interaction between the electromagnetic field and an electron (neglecting the electron spin) is

$$\mathcal{H} = \frac{1}{2m}(\mathbf{p} - e\mathbf{A})^2 + eV(\mathbf{x}) + \mathcal{H}_{\text{field}} \quad (10.14)$$

where $V(\mathbf{x})$ is the Coulomb potential, \mathbf{p} is the momentum of the electron, and \mathbf{A} is the vector potential of the electromagnetic field. $\mathcal{H}_{\text{field}}$ is the Hamiltonian of the free field. When the electron wave field is quantized the representation of the Hamiltonian is

$$\hat{\mathcal{H}} = \hat{\mathcal{H}}_{\text{el}} + \hat{\mathcal{H}}_{\text{I}} + \hat{\mathcal{H}}_{\text{field}} , \quad (10.15)$$

where

$$\hat{\mathcal{H}}_{\text{el}} = \int \Psi^\dagger(\mathbf{x}) \left[-\frac{\hbar^2}{2m} \nabla^2 + eV(\mathbf{x}) \right] \Psi(\mathbf{x}) d^3x$$

refers to the free motion of the electrons, and $\hat{\mathcal{H}}_{\text{I}}$ describes the interaction of the electrons with the light field. This may be written in two parts as

$$\begin{aligned} \hat{\mathcal{H}}_{\text{I},1} &= \int \Psi^\dagger(\mathbf{x}) \left(-\frac{e}{m} \mathbf{A} \cdot \mathbf{p} \right) \Psi(\mathbf{x}) d^3x , \\ \hat{\mathcal{H}}_{\text{I},2} &= \int \Psi^\dagger(\mathbf{x}) \left(-\frac{e^2}{2m} \mathbf{A}^2 \right) \Psi(\mathbf{x}) d^3x . \end{aligned} \quad (10.16)$$

The \mathbf{A}^2 term makes a negligible contribution to one photon processes. Even for two photon processes the contribution from the \mathbf{A}^2 term is small and we shall neglect it. Expanding the electron field operators $\Psi(\mathbf{x})$ as a superpositions of the unperturbed wave functions $\phi_j(\mathbf{x})$

$$\Psi(\mathbf{x}) = \sum_j a_j \phi_j(\mathbf{x}) \quad (10.17)$$

and using (2.6) for the vector potential $\mathbf{A}(\mathbf{x}, t)$ of the radiation field we may express the Hamiltonian as

$$\begin{aligned} \hat{\mathcal{H}}_{\text{el}} &= \sum_j E_j a_j^\dagger a_j , \\ \hat{\mathcal{H}}_{\text{I},1} &= \hbar \sum_{j,k,\lambda} a_j^\dagger a_k (g_{\lambda j k} b_\lambda + g_{\lambda j k}^* b_\lambda^\dagger) . \end{aligned} \quad (10.18)$$

where b_λ is the annihilation operator for the field mode λ .

The coefficients g are given by

$$g_{\lambda jk} = -\frac{e}{m} \sqrt{\frac{1}{2\hbar\omega_\lambda\epsilon_0}} \int \phi_j^*(\mathbf{x}) [u_\lambda(\mathbf{x}) \mathbf{p}] \phi_k(\mathbf{x}) d^3x$$

where u_λ is a field mode function and the sum over λ is a sum over all field wave vectors and polarizations.

We may simplify this expression for g by making the electric dipole approximation. The spatial behaviour of the vector mode function $u_\lambda(\mathbf{x})$ is assumed to vary more slowly than the electronic wave functions, hence we may take $u_\lambda(\mathbf{x})$ outside the integral and replace it by $u_\lambda(\mathbf{x}_0)$ where \mathbf{x}_0 is the position of the atom. That this approximation is justified in the optical region may be seen as follows. For a plane wave mode function

$$u_k(\mathbf{x}) = \frac{1}{\sqrt{V}} e^{ik \cdot x} . \quad (10.19)$$

In the optical region the wavelength of the photon is much greater than the linear dimension of the atom $\bar{\lambda}_{\text{photon}} = 1/|\mathbf{k}| \gg r_{\text{atom}}$, since $\bar{\lambda}_{\text{photon}} \sim 10^3$ Ångstroms and $r_{\text{atom}} \sim 1$ Ångstrom.

Thus, to a first approximation, we may replace

$$\begin{aligned} e^{ik \cdot x} &= e^{ik \cdot (x_0 + \delta x)} = e^{ik \cdot x_0} \left(1 + ik \cdot \delta x - \frac{(k \cdot \delta x)^2}{2} \right) \\ &\approx e^{ik \cdot x_0} . \end{aligned} \quad (10.20)$$

The matrix element $e \int \phi_j^* \mathbf{p} \phi_l d^3x$ may be written as the dipole matrix element

$$im v_{jl} \int \phi_j^* \mathbf{e} \mathbf{x} \phi_l d^3x$$

where m denotes the mass and

$$v_{jl} = \frac{1}{\hbar} (E_j - E_l) ,$$

This may be shown as follows:

$$\begin{aligned} \int \phi_j^* \mathbf{p} \phi_l d^3x &= \frac{im}{\hbar} \int \phi_j^* [\mathcal{H}_{\text{el}}, \mathbf{x}] \phi_l d^3x \\ &= \frac{im}{\hbar} (E_j - E_l) \int \phi_j^* \mathbf{x} \phi_l d^3x \\ &= im v_{jl} \int \phi_j^* \mathbf{x} \phi_l d^3x . \end{aligned} \quad (10.21)$$

The total Hamiltonian is therefore given by

$$\mathcal{H}_{\text{TOT}} = \mathcal{H}_{\text{el}} + \mathcal{H}_{\text{I}} + \mathcal{H}_{\text{field}} , \quad (10.22)$$

where

$$\mathcal{H}_{\text{field}} = \sum_k \hbar \omega_k b_k^\dagger b_k ,$$

$$\mathcal{H}_{\text{el}} = \sum_j E_j a_j^\dagger a_j$$

and

$$\mathcal{H}_I = \hbar \sum_{jk\lambda} a_j^\dagger a_k g_{jk} (b_\lambda + b_\lambda^\dagger) ,$$

where the phase of $u_\lambda(x_0)$ is chosen so that g_{jk} is real.

The total Hamiltonian refers to a single atom but may be easily generalized to N atoms by summing over N atoms, for example $\sum_{\mu=1}^N (a_j^\dagger a_l)_\mu$. The wave function for the total system obeys the Schrödinger equation

$$(\mathcal{H}_0 + \mathcal{H}_I)\Phi = i\hbar \frac{d\Phi}{dt} , \quad (10.23)$$

where \mathcal{H}_0 refers to the free Hamiltonian of the light field and the electrons. It is often convenient to transform out this free part of the Hamiltonian. We therefore make the following transformation to the interaction picture:

$$\Phi = U\Phi_I , \quad (10.24)$$

where

$$U = e^{-\frac{i\mathcal{H}_0 t}{\hbar}} .$$

Then Φ_I obeys the equation

$$\hat{\mathcal{H}}_I \Phi_I = i\hbar \frac{d\Phi_I}{dt} \quad (10.25)$$

where

$$\hat{\mathcal{H}}_I = U^\dagger \mathcal{H}_I U .$$

Transforming the Hamiltonian (10.22) into the interaction picture we use the relation between the operators in the Schrödinger and interaction picture

$$\hat{a}_j = a_j e^{-iE_j t/\hbar} , \quad \hat{b}_k = b_k e^{-i\omega_k t} , \quad (10.26)$$

we obtain

$$\hat{\mathcal{H}}_I = \hbar \sum_{j,k,\lambda} g_{jk} (b_\lambda^\dagger e^{i\omega_\lambda t} + b_\lambda e^{-i\omega_\lambda t}) a_j^\dagger e^{iE_j t/\hbar} a_k e^{-iE_k t/\hbar} . \quad (10.27)$$

We see that terms of the form

$$e^{i(\omega_\lambda + v_{jk})t}$$

and

$$e^{-i(\omega_\lambda - v_{jk})t}$$

occur. When $\omega_\lambda \approx v_{jk}$ the first of these terms is rapidly oscillating in time as $e^{2i\omega_\lambda t}$. We may neglect these terms with respect to the near resonant terms. This is known as the rotating wave approximation. The terms which are rapidly oscillating correspond to highly non-energy-conserving processes such as the excitation of the atom along with the emission of a photon.

Thus for a two-level atom the interaction Hamiltonian in the interaction representation is

$$\hat{\mathcal{H}}_I = \hbar \sum_{\lambda} a_1 a_2^\dagger b g_\lambda e^{-i(\omega_\lambda - v_{21})t} + \text{h.c.} , \quad (10.28)$$

where

$$g_\lambda = -i \sqrt{\frac{1}{2\hbar\epsilon_0\omega_\lambda}} v_{21} u_\lambda(x_0) d_{12} ,$$

with

$$d_{12} = \int \phi_2^*(x) \mathbf{e} \cdot \mathbf{x} \phi_1(x) d^3x .$$

is the dipole moment for the transition $1 \rightarrow 2$, and x_0 is the coordinate of the centre of the atom.

It is often convenient to use the analogy between a two-level atom and a spin $\frac{1}{2}$ particle in a magnetic field and apply the Pauli spin operators instead of the Fermi operators for the atomic levels.

The Pauli spin operators (multiplied by one-half for convenience) are

$$\sigma_x = \frac{1}{2} \begin{pmatrix} 0 & 1 \\ 1 & 0 \end{pmatrix}, \quad \sigma_y = \frac{1}{2} \begin{pmatrix} 0 & -i \\ i & 0 \end{pmatrix}, \quad \sigma_z = \frac{1}{2} \begin{pmatrix} 1 & 0 \\ 0 & -1 \end{pmatrix} . \quad (10.29)$$

We may define raising and lowering operators

$$\sigma^+ = \sigma_x + i\sigma_y, \quad \sigma^- = \sigma_x - i\sigma_y . \quad (10.30)$$

These have the following properties

$$[\sigma^+, \sigma^-] = 2\sigma_z, \quad [\sigma^\pm, \sigma_z] = \mp\sigma^\pm, \quad \sigma^+\sigma^- + \sigma^-\sigma^+ = 1 . \quad (10.31)$$

We may show that the two-level atomic system described by the Fermi operators a_1, a_2 may be described by pseudo-spin operators with the correspondence

pseudo-spin operators	electron operators
σ^+	$a_2^\dagger a_1$
σ^-	$a_1^\dagger a_2$
σ_z	$\frac{1}{2}(a_2^\dagger a_2 - a_1^\dagger a_1)$.

The pseudo-spin operators obey the same commutation relations as the electron operators. (Use the commutation relations for the electron operators and the fact that

$$a_1^\dagger a_1 + a_2^\dagger a_2 = 1 \quad (10.32)$$

in the two-level system). We note that this analogy is only formal.

Thus the Hamiltonian for a two-level atom may be written as

$$\mathcal{H}_0 = \hbar\omega_0 \sigma_z . \quad (10.33)$$

Denoting the lower and upper levels as $|1\rangle$ and $|2\rangle$, respectively, we see that

$$\mathcal{H}_0 |1\rangle = -\frac{\hbar\omega_0}{2} |1\rangle, \quad \mathcal{H}_0 |2\rangle = +\frac{\hbar\omega_0}{2} |2\rangle . \quad (10.34)$$

The action of the raising and lowering operators on the energy states is

$$\sigma^+ |1\rangle = |2\rangle, \quad \sigma^- |2\rangle = |1\rangle . \quad (10.35)$$

The probability of being in the upper state is

$$\rho_{22} = \langle \sigma^+ \sigma^- \rangle . \quad (10.36)$$

The probability of being in the lower state is

$$\rho_{11} = \langle \sigma^- \sigma^+ \rangle . \quad (10.37)$$

The atomic inversion is given by

$$\rho_{22} - \rho_{11} = 2\langle \sigma_z \rangle , \quad (10.38)$$

while the atomic coherences are given by

$$\rho_{21} = \langle \sigma^- \rangle, \quad \rho_{12} = \langle \sigma^+ \rangle . \quad (10.39)$$

In terms of the pseudo-spin operators the Hamiltonian describing the interaction of the radiation field with a two-level atom in the electric dipole and rotating wave approximation is

$$\begin{aligned} \mathcal{H} &= \mathcal{H}_0 + \mathcal{H}_1 , \\ \mathcal{H}_0 &= \hbar \sum_k \omega_k b_k^\dagger b_k + \hbar\omega_0 \sigma_z , \\ \mathcal{H}_1 &= \hbar \sum_\lambda (g_\lambda b_\lambda \sigma^+ + g_\lambda^* b_\lambda^\dagger \sigma^-) . \end{aligned} \quad (10.40)$$

10.3 Interaction of a Two-Level Atom with a Single Mode Field

In the case of a single field mode on resonance with the atomic transition we may write the Hamiltonian as

$$\mathcal{H} = \mathcal{H}_0 + \mathcal{H}_1, \quad \mathcal{H}_0 = \hbar\omega b^\dagger b + \hbar\omega\sigma_z, \quad \mathcal{H}_1 = \hbar g(b\sigma^+ + b^\dagger\sigma^-) \quad (10.41)$$

where we have taken the coupling constant g to be real. This is the simplest form of the atom–field interaction and is known as the *Jaynes–Cummings* [10.3] model. We shall demonstrate how the Schrödinger equation for this system may readily be solved in a special case. It is seen that \mathcal{H}_0 and \mathcal{H}_1 commute

$$[\mathcal{H}_0, \mathcal{H}_1] = 0. \quad (10.42)$$

This indicates that the eigenstates of \mathcal{H} may be written as linear combinations of the degenerate eigenstates of \mathcal{H}_0 . The eigenstates of the free Hamiltonian are $|n, 2\rangle, |n + 1, 1\rangle$ where $|n\rangle$ are field states and $|2\rangle$ and $|1\rangle$ are atomic states. For the interaction Hamiltonian in the rotating wave approximation (10.40) these two states are sufficient to form a basis. We shall then express the eigenstates of \mathcal{H}_1 as a linear combination of these basis states.

The Schrödinger equation in the interaction picture is

$$\mathcal{H}_1 \begin{pmatrix} |n, 2\rangle \\ |n + 1, 1\rangle \end{pmatrix} = \hbar \begin{pmatrix} 0 & \Omega \\ \Omega & 0 \end{pmatrix} \begin{pmatrix} |n, 2\rangle \\ |n + 1, 1\rangle \end{pmatrix}, \quad (10.43)$$

where $\Omega = g\sqrt{n + 1}$. The eigenvalues of this system are $\pm\Omega\hbar$, with corresponding eigenstates

$$\begin{aligned} |\phi^+\rangle &= \frac{1}{\sqrt{2}}(|n, 2\rangle + |n + 1, 1\rangle), \\ |\phi^-\rangle &= \frac{1}{\sqrt{2}}(|n, 2\rangle - |n + 1, 1\rangle). \end{aligned} \quad (10.44)$$

Given that the atom is initially in the excited state and the field has exactly n photons we may calculate the probability for finding the atom in the excited state and the field with n photons at time t

$$P_2(t) = |\langle n, 2|e^{-i\mathcal{H}_1 t/\hbar}|n, 2\rangle|^2. \quad (10.45)$$

We may evaluate this expression exactly with the eigenstates given by (10.44) and the orthonormality properties of the eigenstates. This yields

$$P_2(t) = \cos^2 \Omega t. \quad (10.46)$$

This is the well known Rabi nutation of the atom with Ω being the Rabi frequency. We now consider the interaction of a two-level atom with a light field in a coherent state. This leads to some interesting quantum recurrence phenomena.

10.4 Quantum Collapses and Revivals

The behaviour of a two-level atom interacting with a coherent field may be derived from (10.46) with (2.37), which expands a coherent state in terms of the number states. Thus, if the atom is initially in the excited state, the probability for the atom to be found in the excited state at time t regardless of the state of the field is given by the following Poissonian weighted sum

$$P_2(t) = \frac{1}{2} \left(1 + \sum \frac{e^{-\bar{n}} \bar{n}^n}{n!} \cos 2g\sqrt{n+1}t \right). \quad (10.47)$$

Due to the Poisson distribution of the photon number there is a spread in the Rabi frequencies $\Delta n \sim \bar{n}^{1/2}$. As a result the Rabi nutation will collapse after some oscillations due to the destructive interference between the various cosine functions. An approximate evaluation of the sum valid for times $t < \bar{n}^{1/2}/g$ yields [10.4]

$$P_2(t) = \frac{1}{2} \left[1 + \cos 2g(\bar{n} + 1)^{1/2}t \exp \left(-\frac{g^2 t^2 \bar{n}}{2(\bar{n} + 1)} \right) \right]. \quad (10.48)$$

Thus the Rabi oscillations occur under a Gaussian envelope. The characteristic time for the oscillation collapse for $\bar{n} \gg 1$ is

$$t_{\text{collapse}} \sim \frac{1}{g}, \quad (10.49)$$

and the number of observed oscillations before the collapse occurs is $\sim \bar{n}^{1/2}$. A more accurate evaluation shows a partial revival of the initial oscillations after a time

$$t_{\text{revival}} \sim \frac{2\pi}{g} \bar{n}^{1/2}. \quad (10.50)$$

Thus a quasi periodic burst of Rabi oscillations occurs after approximately \bar{n} Rabi periods.

The existence of periodic revivals is due to the discreteness of the sum over number states. This discrete character ensures that after some finite time all the oscillating terms almost come back in phase with each other, and restore the coherent oscillations. The rephasing is not perfect as the frequencies are irrational and thus incommensurate. Thus the revivals may be considered as a pure quantum effect resulting from the discreteness of the harmonic oscillator spectrum.

Evidence for the collapses and revivals has been seen by Rempe et al. [10.5] in experiments on micromasers where the conditions for the interaction of a single mode of a microwave field with two Rydberg levels of an atom has been achieved.

10.5 Spontaneous Decay of a Two-Level Atom

The Hamiltonian (10.40) describes the interaction of a two-level atom with all modes of the radiation field in the electric dipole and rotating wave approximation. We may write this Hamiltonian in the form

$$\mathcal{H} = \frac{1}{2}\hbar\omega_0\sigma_z + \mathcal{H}_{\text{bath}} + \hbar(\sigma_+\Gamma + \sigma_-\Gamma^\dagger) \quad (10.51)$$

where Γ, Γ^\dagger are both operators defined by $\Gamma = \sum g_j b_j$ and $\mathcal{H}_{\text{bath}} = \sum \hbar\omega_k b_k^\dagger b_k$. The master equation technique developed in Chap. 6 is immediately applicable to this problem. The modes of the radiation field may be considered as a reservoir since the continuum of field modes will be little affected by the emission of a single photon into them.

The master equation for the reduced density operator of the atom in the interaction picture is

$$\begin{aligned} \frac{d\rho^I}{dt} &= \frac{\gamma}{2}(1 + \bar{n})(2\sigma^- \rho^I \sigma^+ - \sigma^+ \sigma^- \rho^I - \rho^I \sigma^+ \sigma^-) \\ &\quad + \frac{\gamma\bar{n}}{2}(2\sigma^+ \rho^I \sigma^- - \sigma^- \sigma^+ \rho^I - \rho^I \sigma^- \sigma^+) . \end{aligned} \quad (10.52)$$

We have neglected the term which gives rise to a small frequency shift $\Delta\omega$. This term gives a contribution to the Lamb shift. The above equation describes an atom interacting with a thermal field at temperature T . For spontaneous emission $\bar{n} = 0$. We shall derive equations for the expectation values of atomic operators in the case $\bar{n} = 0$. In the Schrödinger picture

$$\frac{d\rho^S}{dt} = \frac{d\rho^I}{dt} - i\omega_0[\sigma_z, \rho] . \quad (10.53)$$

The atomic coherence $\rho_{12} = \langle \sigma^- \rangle$ obeys the equation

$$\frac{d}{dt}\langle \sigma^- \rangle = \left(-i\omega_0 - \frac{\gamma}{2}\right)\langle \sigma^- \rangle , \quad (10.54)$$

which has the solution

$$\langle \sigma^-(t) \rangle = \exp\left[\left(-i\omega_0 - \frac{\gamma}{2}\right)t\right]\langle \sigma^-(0) \rangle . \quad (10.55)$$

The probability of the atom being in the upper state $P_2(t) = \rho_{22}(t)$ is $\langle \sigma_+(t)\sigma_-(t) \rangle$. This obeys the equation

$$\frac{d}{dt}P_2(t) = -\gamma P_2(t) , \quad (10.56)$$

which has the solution

$$P_2(t) = e^{-\gamma t}P_2(0) . \quad (10.57)$$

That is, the probability of an initially excited atom remaining in the excited state decays exponentially, as predicted by Wigner–Weisskopf exponential decay theory. For purely radiative decay the decay time, T_1 , of the inversion and the decay time, T_2 , of the polarization obey the simple relation $T_2 = 2T_1$.

The two-time correlation function $\langle \sigma^+(t)\sigma^-(t') \rangle$ may be calculated using (10.54 and 56) and the quantum regression theorem

$$\begin{aligned}\langle \sigma^+(t)\sigma^-(t') \rangle &= \exp\left[\left(i\omega_0 - \frac{\gamma}{2}\right)(t-t')\right]\langle \sigma^+(t')\sigma^-(t') \rangle \\ &= \exp\left[i\omega_0(t-t') - \frac{\gamma}{2}(t+t')\right]\langle \sigma^+(0)\sigma^-(0) \rangle .\end{aligned}\quad (10.58)$$

This two-time correlation function may be used to find the spectrum of the emitted light. The spectrum is defined in terms of the probability for photo-detection by a monochromatic detector a distance r from the source during an interval T . For an optical frequency field and an ideal detector (photoefficiency being one) we have the result [10.6].

$$S(\omega, r, T) = \frac{1}{2\pi} \int_{r/c}^{T+r/c} dt_1 \int_{r/c}^{T+r/c} dt_2 e^{i\omega(t_2-t_1)} G^{(1)}(rt_1, rt_2) , \quad (10.59)$$

where

$$G^{(1)}(rt_1, rt_2) = \langle E^{(-)}(r, t_1)E^{(+)}(r, t_2) \rangle .$$

The spectrum is expressed in terms of the correlation functions of the electric field operators, whereas the solutions of the master equation yielded the correlation functions of the atomic operators. Fortunately a connection may be made between the two. The outwardly propagating field at position r and time t is given for times $t \gg 1/\omega_0$ by [10.7].

$$E^{(+)}(r, t) = E_{\text{IN}}^{(+)}(r, t) - \frac{\omega_0^2}{4\pi\epsilon_0 c^2 r} \left(\boldsymbol{\mu} \times \frac{\mathbf{r}}{r} \right) \times \frac{\mathbf{r}}{r} \sigma_- \left(t - \frac{\mathbf{r}}{c} \right) , \quad (10.60)$$

where $E_{\text{IN}}^{(+)}(r, t)$ is the inwardly propagating field. This is the retarded field generated by a point dipole with the classical dipole moment replaced by the atomic lowering operator σ_- . It is another example of the relation between input, output and source previously discussed in Chap. 7.

Using (10.60) the first-order correlation functions for the field may be written in terms of the first-order correlation function for the atoms as

$$G^{(1)}(rt, rt') = \langle E^{(-)}(r, t)E^{(+)}(r, t') \rangle = I_0(r)\langle \sigma_+(\hat{t})\sigma_-(\hat{t}') \rangle , \quad (10.61)$$

where $\hat{t} = t - r/c$ and

$$I_0(r) = \left| \frac{\omega_0^2}{4\pi\epsilon_0 c^2 r} \left(\boldsymbol{\mu} \times \frac{\mathbf{r}}{r} \right) \times \frac{\mathbf{r}}{r} \right|^2 .$$

Then using (10.58) we have

$$G^{(1)}(\mathbf{r}t, \mathbf{r}t') = I_0(\mathbf{r}) \exp \left[i\omega_0(t - t') - \frac{\gamma}{2}(t + t') \right]. \quad (10.62)$$

The spectrum from (10.59) is

$$S(\omega, \mathbf{r}, T) = \frac{I_0(\mathbf{r})}{2\pi} \int_0^T dt \int_0^T dt' \exp \left[-i(\omega - \omega_0)(t - t') - \frac{\gamma}{2}(t + t') \right], \quad (10.63)$$

where we have neglected r/c with respect to t and T . This gives for the spectrum after counting the time T

$$S(\omega, \mathbf{r}, T) = \frac{I_0(\mathbf{r})}{2\pi} \frac{[1 + e^{-\gamma T} - 2e^{-\gamma T} \cos(\omega - \omega_0)T]}{(\omega - \omega_0)^2 + \left(\frac{\gamma}{2}\right)^2} \quad (10.64)$$

In the limit $T \rightarrow \infty$ (counting times long compared to atomic decay rate) this reduces to

$$2\pi S(\omega, \mathbf{r}, \infty) = \frac{I_0(\mathbf{r})}{(\omega - \omega_0)^2 + \left(\frac{\gamma}{2}\right)^2} \quad (10.65)$$

which is the familiar Lorentzian lineshape of the Wigner–Weisskopf theory with the half width equal to $\gamma/2$.

10.6 Decay of a Two-Level Atom in a Squeezed Vacuum

It is instructive to consider how the atomic decay is modified if the vacuum is squeezed. Of course, the atom is no longer interacting with a vacuum but with a field having phase sensitive correlation functions.

We shall assume that the atom is interacting with a broad band squeezed vacuum, the squeezing being centred about the resonance frequency of the atom. The bandwidth of the squeezing is assumed to be broad compared with the natural linewidth of the atom, so that the squeezed vacuum appears as δ -correlated squeezed white noise to the atom. We follow the description given by Gardiner [10.8] and begin with the Hamiltonian (10.51), where the correlation functions for the bath operators are

$$\begin{aligned} \langle \Gamma^\dagger(t)\Gamma(t') \rangle &= \gamma N \delta(t - t'), \\ \langle \Gamma(t)\Gamma^\dagger(t') \rangle &= \gamma(N + 1) \delta(t - t'), \end{aligned} \quad (10.66)$$

$$\begin{aligned} \langle \Gamma(t)\Gamma(t') \rangle &= \gamma M e^{-2i\omega_A t} \delta(t - t'), \\ \langle \Gamma^\dagger(t)\Gamma^\dagger(t') \rangle &= \gamma M^* e^{2i\omega_A t} \delta(t - t'). \end{aligned} \quad (10.67)$$

This generalizes the correlation functions for interaction with a thermal field ($M = 0$) to include phase dependent correlation functions. N and M are parameters that describe the squeezing and obey the relationship

$$|M|^2 \leq N(N + 1) , \quad (10.68)$$

with the equality holding for a minimum uncertainty squeezed state. We define the variances in the quadrature phases of the squeezed field at the site of the atom are

$$V(X_\theta) = \langle X_\theta^2 \rangle - \langle X_\theta \rangle^2 = 2[N + |M| \cos(2\theta - \phi) + \frac{1}{2}] \quad (10.69)$$

where $M = |M|e^{i\phi}$, where ϕ is the phase of the squeezed field. We choose this phase to be equal to zero. For a highly squeezed minimum uncertainty state from (10.68) we find

$$|M| = N + \frac{1}{2} - \frac{1}{8N} + \dots . \quad (10.70)$$

The variances in the inphase quadrature $\theta = 0$ and out of phase quadrature $\theta = +\pi/2$ are

$$\begin{aligned} V(X_0) &= 2(N + |M| + \frac{1}{2}) \approx 4N , \\ V(X_{\pi/2}) &= 2(N - |M| + \frac{1}{2}) \approx \frac{1}{4N} . \end{aligned} \quad (10.71)$$

The master equation for the atom interacting with a squeezed vacuum may be derived in the same manner as (6.37) for a harmonic oscillator was derived.

In a frame rotating at the atomic frequency the master equation for the atomic density operator is

$$\begin{aligned} \dot{\rho} &= \frac{1}{2}\gamma(N + 1)(2\sigma_- \rho \sigma_+ - \sigma_+ \sigma_- \rho - \rho \sigma_+ \sigma_-) \\ &\quad + \frac{1}{2}\gamma N(2\sigma_+ \rho \sigma_- - \sigma_- \sigma_+ \rho - \rho \sigma_- \sigma_+) \\ &\quad - \gamma M \sigma_+ \rho \sigma_+ - \gamma M^* \sigma_- \rho \sigma_- . \end{aligned} \quad (10.72)$$

This may be compared with the master-equation (10.52) describing the interaction of a two-level atom with a thermal field. We see that we have additional phase-dependent terms with the coefficient M . The expectation values of the atomic operators are

$$\langle \dot{\sigma}_x \rangle = -\gamma_x \langle \sigma_x \rangle, \quad \langle \dot{\sigma}_y \rangle = -\gamma_y \langle \sigma_y \rangle, \quad \langle \dot{\sigma}_z \rangle = -\gamma_z \left(\langle \sigma_z \rangle + \frac{1}{2N + 1} \right), \quad (10.73)$$

with

$$\gamma_x = \gamma(N + |M| + \frac{1}{2}), \quad \gamma_y = \gamma(N - |M| + \frac{1}{2}), \quad \gamma_z = \gamma_x + \gamma_y ,$$

where x and y polarization quadratures have been defined with

$$\langle \sigma_x \rangle = (\langle \sigma_- \rangle + \langle \sigma_+ \rangle), \quad \langle \sigma_y \rangle = -i(\langle \sigma_- \rangle - \langle \sigma_+ \rangle) . \quad (10.74)$$

The polarization $\langle \sigma_y \rangle$ and $\langle \sigma_x \rangle$ are in phase with the maximally squeezed quadrature and corresponding out-of-phase quadrature of the squeezed

vacuum, respectively. The damping rates γ_x and γ_y for the polarization quadratures are proportional to the variances of the maximally squeezed and maximally unsqueezed quadrature phases of the squeezed vacuum field.

These two components of the atomic dipole now decay with different rates. The atomic decay is now a *phased* rather than a phase-independent process. For large squeezing the decay rates γ_x and γ_z will be large while γ_y will be small. (Thus the $\langle \sigma_x \rangle$ and $\langle \sigma_z \rangle$ components of the Bloch vector may come to a steady state on a time scale short compared with $1/\gamma_y$. This will result in a narrow component in the spectrum resulting from the $\langle \sigma_x \rangle$ decay and a broad component from the $\langle \sigma_y \rangle$ decay.)

Experimentally, the task of providing an environment for the atom consisting only of squeezed vacuum modes presents some difficulty. The best prospect appears by situating the atom inside a micro cavity, which supports only a few modes of the electromagnetic field. It is only then necessary to squeeze these modes of the field with which the atom is coupled.

10.7 Phase Decay in a Two-Level System

When a two-level atom decays into a broad band squeezed state the population and polarisation decay at different rates as we showed above. Another physical process which leads to a similar result is phase decay induced by atomic collisions. The collisions between a single two-level atom and other atoms or molecules does not change the population of the two-level atom but does cause a phase randomisation of the atomic dipole. We model this process by considering the inversion σ_z to be coupled to a high temperature heat bath. This is described by the Hamiltonian

$$\mathcal{H} = \sigma_z \Gamma_p , \quad (10.75)$$

where Γ_p is the bath operator describing the collisions.

The master equation in the interaction picture now becomes

$$\frac{d\rho}{dt} = \frac{\gamma}{2} (2\sigma^- \rho \sigma^+ - \sigma^+ \sigma^- \rho - \rho \sigma^+ \sigma^-) - \gamma_p [\sigma_z, [\sigma_z, \rho]] . \quad (10.76)$$

The expectation values for σ_x , σ_y and σ_z obey

$$\begin{aligned} \frac{d}{dt} \langle \sigma_z \rangle &= -\gamma (\langle \sigma_z \rangle + \frac{1}{2}) , \\ \frac{d}{dt} \langle \sigma_x \rangle &= -\left(\frac{\gamma}{2} + \gamma_p\right) \langle \sigma_x \rangle , \\ \frac{d}{dt} \langle \sigma_y \rangle &= -\left(\frac{\gamma}{2} + \gamma_p\right) \langle \sigma_y \rangle . \end{aligned} \quad (10.77)$$

The equation of motion for the inversion is unchanged, however, the polarization decay rate is increased above the spontaneous emission result. In the presence of collisions the decay time of the polarization T_2 is less than $2T_1$.

Exercises

10.1 Derive (10.47).

10.2 Derive (10.48).

Hint: Expand $(n + 1)^{1/2}$ around \bar{n}

$$(n + 1)^{1/2} \approx (\bar{n} + 1)^{1/2} + \frac{1}{2(\bar{n} + 1)^{1/2}}(n - \bar{n}) .$$

10.3 The Hamiltonian for a single two-level atom interacting with a single-mode field at a different frequency from the atomic frequency in the interaction picture is

$$\mathcal{H}_1 = \hbar\Delta\sigma_z + \hbar g(b\sigma^+ + b^\dagger\sigma^-) ,$$

see (10.41), where $\Delta = \omega_A - \omega_F$ is the frequency difference between the field and the atom. Find the generalisation of (10.44) for the eigenstate of this system.

10.4 Show that the transformation $\sigma_z\rho\sigma_z$ changes the phase of the off-diagonal (coherence) terms by π . See (10.75).

11. Resonance Fluorescence

In the present chapter we shall study resonance fluorescence from a two-level atom. It represents a classic problem in quantum optics as many of the quantum mechanical features we have discussed, for example, photon antibunching and squeezing are present in this system. This problem was considered as early as the 1930's by E. Wigner and V. Weisskopf who treat the light scattering by perturbation techniques, including only elastic scattering. With the advent of the laser, higher incident intensities were possible, which gave rise to nonlinear interactions and inelastic scattering.

In Fig. 11.1 we show a schematic picture of the interaction of the light field with a two-level atom. For low incident light intensities (Fig. 11.1a) the interaction is linear and the scattering is clearly elastic $\omega_s = \omega_L$. For higher incident light intensities nonlinear interactions may play a role as in Fig. 11.1b where two laser photons are involved with $2\omega_L = \omega_s + \omega'_s$, however, ω_s, ω'_s are not necessarily equal to ω_L . The master equation formalism we have developed in Chaps. 6 and 7 is ideally suited to treat this problem.

11.1 Master Equation

We consider a two-level atom driven with a single coherent mode of the radiation field. We shall treat this coherent driving field classically. The atom may decay by spontaneous emission into all the vacuum modes of the electromagnetic field.

The system may be described by the Hamiltonian

$$\begin{aligned}\mathcal{H} &= \mathcal{H}_0 + \mathcal{H}_{\text{Driving}} + \mathcal{H}_{\text{Damping}} , \\ \mathcal{H}_0 &= \hbar\omega_0\sigma_z + \hbar\sum_k b_k^\dagger b_k , \\ \mathcal{H}_{\text{Driving}} &= \hbar\left(g\frac{\varepsilon^*}{2}\sigma^- e^{i\omega t} + g^*\frac{\varepsilon}{2}\sigma^+ e^{-i\omega t}\right) , \\ \mathcal{H}_{\text{Damping}} &= \hbar\sum_k (g_k b_k^\dagger \sigma_- + g_k^* b_k \sigma_+) ,\end{aligned}\tag{11.1}$$

where ε is the amplitude of the coherent driving field, $\sigma_+, \sigma_-, \sigma_z$ are the pseudo spin operators for the atom. b_k, b_k^\dagger are the photon creation and annihilation

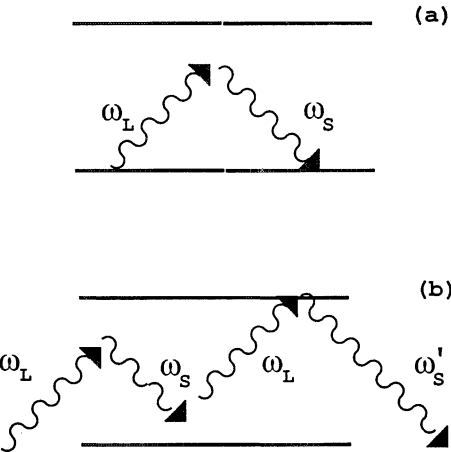


Fig. 11.1. Schematic representation of elastic (a) and inelastic (b) scattering of laser light with frequency ω_L . The length of the arrows is proportional to the frequency of the light

operators for all modes of the radiation field for the highly populated mode. g is the dipole matrix element of the atomic transition. We have allowed for a detuning, $\Delta\omega = \omega_0 - \omega$, between the incident field and the atomic transition. As in the case of pure spontaneous emission the modes of the radiation field may be treated as a reservoir at zero temperature. The master equation for the reduced density operator of the atom is identical to that for spontaneous emission plus a coherent part corresponding to the coherent driving term:

$$\frac{\partial\rho}{\partial t} = \left(\frac{\partial\rho}{\partial t} \right)_{coh} + \left(\frac{\partial\rho}{\partial t} \right)_{incoh}. \quad (11.2)$$

In the interaction picture this becomes

$$\frac{\partial\rho}{\partial t} = -i\Delta\omega [\sigma_z, \rho] - i\frac{\Omega}{2} [\sigma_+ + \sigma_-, \rho] + \frac{\gamma}{2} (2\sigma_- \rho \sigma_+ - \rho \sigma_+ \sigma_- - \sigma_+ \sigma_- \rho), \quad (11.3)$$

where γ is the natural linewidth of the atom, and we have chosen the phase of ε such that the Rabi frequency $\Omega = \varepsilon g^*/\hbar$ is real.

From the master equation we may derive the equations of motion for the expectation values $\langle\sigma_+(t)\rangle$, $\langle\sigma_-(t)\rangle$ and $\langle\sigma_z(t)\rangle$. These are

$$\frac{d}{dt} \langle\sigma_+\rangle = -\left(\frac{\gamma}{2} - i\Delta\omega\right) \langle\sigma_+\rangle - i\Omega \langle\sigma_z\rangle, \quad (11.4)$$

$$\frac{d}{dt} \langle\sigma_-\rangle = -\left(\frac{\gamma}{2} + i\Delta\omega\right) \langle\sigma_-\rangle + i\Omega \langle\sigma_z\rangle, \quad (11.5)$$

$$\frac{d}{dt} \langle\sigma_z\rangle = -\gamma \left(\langle\sigma_z\rangle + \frac{1}{2} \right) - i\frac{\Omega}{2} (\langle\sigma_+\rangle - \langle\sigma_-\rangle). \quad (11.6)$$

These equations have the same form as those derived using semi-classical radiation theory where the atoms are quantized with phenomenological damping constants introduced to simulate atomic decay and the radiation field is treated classically. They are known as the optical Bloch equations and play a central role in the interaction of radiation with atoms. The inhomogeneous equations (11.4–6) may be written as a set of homogeneous equations:

$$\frac{d}{dt}(\langle \sigma(t) \rangle - \langle \sigma \rangle_s) = A(\langle \sigma(t) - \langle \sigma \rangle_{ss} \rangle), \quad (11.7)$$

where

$$A = \begin{pmatrix} -\left(\frac{\gamma}{2} - i\Delta\omega\right) & 0 & -i\Omega \\ 0 & -\left(\frac{\gamma}{2} + i\Delta\omega\right) & i\Omega \\ -\frac{i\Omega}{2} & \frac{i\Omega}{2} & -\gamma \end{pmatrix}.$$

The steady state solutions are

$$\langle \sigma_z \rangle_{ss} = -\frac{1}{2} \frac{1 + \delta^2}{1 + \delta^2 + Z^2}, \quad (11.8)$$

$$\langle \sigma_+ \rangle_{ss} = \frac{i}{\sqrt{2}} \frac{Z(1 + i\delta)}{1 + \delta^2 + Z^2}, \quad (11.9)$$

where we have defined

$$Z = \frac{\sqrt{2}\Omega}{\gamma}, \quad \delta = \frac{2\Delta\omega}{\gamma}. \quad (11.10)$$

Equations (11.7–9) represent the steady state solutions in the interaction picture. In the Schrödinger picture the solutions are $\sigma_{\pm}^{Schr}(t) = \sigma_{\pm} e^{\pm i\omega t}$. We shall derive the time-dependent solutions for the special case of resonance ($\delta = 0$). For the atom initially in the ground state we have

$$\langle \sigma_z(t) \rangle = \frac{\Omega^2}{\gamma^2 + 2\Omega^2} \left[1 - e^{-3\gamma t/4} \left(\cosh \kappa t + \frac{3\gamma}{4\kappa} \sinh \kappa t \right) \right] - \frac{1}{2}, \quad (11.11)$$

$$\langle \sigma_+(t) \rangle = i\Omega \frac{\gamma}{\gamma^2 + 2\Omega^2} \left\{ 1 - e^{-3\gamma t/4} \left[\cosh \kappa t + \left(\frac{\kappa}{\gamma} + \frac{3\gamma}{16\kappa} \right) \sinh \kappa t \right] \right\}, \quad (11.12)$$

$$\langle \sigma_-(t) \rangle = \langle \sigma_+(t) \rangle^*, \quad (11.13)$$

where

$$\kappa = \left[\left(\frac{\gamma}{4} \right)^2 - \Omega^2 \right]^{1/2}.$$

In these solutions we see the dynamics separating into an initial transient regime followed by a saturation steady state.

There is a threshold at $\Omega = \gamma/4$ below which the solutions are monotonic functions of time and above which they exhibit oscillations. The solutions for $\Omega \gg \gamma/4$ are

$$\langle \sigma_z(t) \rangle = -\frac{1}{2} e^{-3\gamma t/4} \cos \Omega t , \quad (11.14)$$

$$\langle \sigma_+(t) \rangle = \frac{i}{2} e^{-3\gamma t/4} \sin \Omega t . \quad (11.15)$$

The probability for the atom to be in the excited state $P_+(t) = \langle \sigma_z(t) \rangle + 1/2$ is (Fig. 11.2)

$$P_+(t) = \frac{1}{2} (1 - e^{-3\gamma t/4} \cos \Omega t) . \quad (11.16)$$

The steady state probability for the atom to be in the excited state for an arbitrary strength driving field is

$$P_+^{ss} = \frac{\Omega^2}{\gamma^2 + 2\Omega^2} . \quad (11.17)$$

For weak coupling the atom settles close to its lower level, and we expect the behaviour of a classical electron oscillator. For very intense illumination the atom becomes saturated with equal probability of being found in the upper and lower levels, respectively,

$$\lim_{\Omega \rightarrow \infty} P_+^{ss} = \frac{1}{2} . \quad (11.18)$$

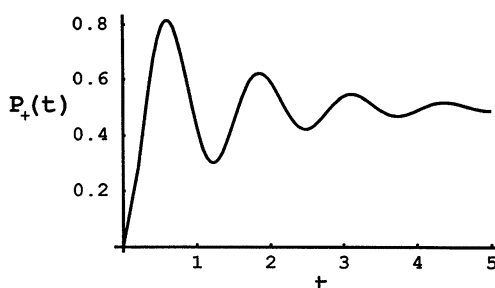


Fig. 11.2. Probability to find a damped, driven two-level atom in the excited state as a function of time, see (11.16). The atomic damping rate is $\gamma = 1.0$ and the Rabi frequency is $\Omega = 5.0$

Thus the atom spends one half of its time in the upper state where spontaneous emission plays a significant role. Quantum fluctuations may therefore be expected to become important with intense illumination, while remaining of no consequence for weak scattering.

To illustrate the role that fluctuations play, we shall calculate the mean of the scattered field. The correlation properties of the scattered field may be calculated using the relation (10.60) connecting the scattered field with the atomic operator

$$E^{(+)}(\mathbf{r}, t) = E_{\text{in}}^{(+)}(\mathbf{r}, t) - \Psi(\mathbf{r})\sigma_-(\hat{t}) , \quad (11.19)$$

where $\hat{t} = t - r/c$, and $E^{(+)}$ is the outward propagating part of the field. Thus in the Schrödinger picture

$$\langle E^{(+)}(\mathbf{r}, t) \rangle = -\Psi(\mathbf{r})\langle \sigma^-(\hat{t}) \rangle e^{-i\omega_0 t} . \quad (11.20)$$

Substituting (11.12) for $\langle \sigma^-(t) \rangle$ we find for strong driving fields ($\Omega \gg \gamma/4$)

$$\begin{aligned} \langle E^{(+)}(\mathbf{r}, t) \rangle &= \Psi(\mathbf{r}) \frac{-i\Omega\gamma}{\gamma^2 + 2\Omega^2} \left\{ e^{-i\omega_0 \hat{t}} - \frac{1}{2} e^{-3\gamma\hat{t}/4} [e^{-i(\omega_0 + \Omega)\hat{t}} \right. \\ &\quad \left. + e^{-i(\omega_0 + \Omega)\hat{t}}] \right\} . \end{aligned} \quad (11.21)$$

Thus in the transient regime the mean field oscillates with frequency components at ω_0 and $\omega_0 \pm \Omega$, whereas in the steady state the only oscillation frequency is ω_0 . We shall see, however, that the steady state spectrum contains components at ω_0 , and $\omega_0 \pm \Omega$. This is because the spectrum is calculated from the two-time correlation function which does not factorize for resonance fluorescence

$$\langle E^{(-)}(\mathbf{r}, t)E^{(+)}(\mathbf{r}, t') \rangle \neq \langle E^{(-)}(\mathbf{r}, t) \rangle \langle E^{(+)}(\mathbf{r}, t') \rangle . \quad (11.22)$$

This correlation function factorizes for a coherent field, for example, in a laser well above threshold. It does not factorize in resonance fluorescence because of the strong fluctuations present.

11.2 Spectrum of the Fluorescent Light

The definition of the spectrum used in Chap. 10 cannot be directly applied to the case of steady state resonance fluorescence. This is because such a field persists indefinitely into the past and future. However, averaging over a finite observation time T and taking the limit $T \rightarrow \infty$ a sensible result is obtained. The expression is

$$S(\omega) = \frac{1}{2\pi} \int_{-\infty}^{\infty} e^{-i\omega\tau} \langle E^{(-)}(t)E^{(+)}(t + \tau) \rangle_{ss} dt . \quad (11.23)$$

Using (11.19) relating $E^{(+)}(t)$ and $\sigma^-(\hat{t})$ we may write the steady-state spectrum as

$$S(\omega) = \frac{I_0(r)}{2\pi} \int_{-\infty}^{\infty} e^{-i\omega\tau} \langle \sigma_+(\hat{t})\sigma_-(\hat{t} + \tau) \rangle_{ss} d\tau , \quad (11.24)$$

where $I_0(r) = \Psi^2(r)$.

We shall consider only the stationary, two-time correlation functions for the atomic operator

$$G(t) = \begin{pmatrix} \langle \sigma^+(\tau), \sigma^+(0) \rangle_{ss} & \langle \sigma^+(\tau), \sigma^-(0) \rangle_{ss} & \langle \sigma^+(\tau), \sigma_z(0) \rangle_{ss} \\ \langle \sigma^-(\tau), \sigma^+(0) \rangle_{ss} & \langle \sigma^-(\tau), \sigma^-(0) \rangle_{ss} & \langle \sigma^-(\tau), \sigma_z(0) \rangle_{ss} \\ \langle \sigma_z(\tau), \sigma^+(0) \rangle_{ss} & \langle \sigma_z(\tau), \sigma^-(0) \rangle_{ss} & \langle \sigma_z(\tau), \sigma_z(0) \rangle_{ss} \end{pmatrix} , \quad (11.25)$$

where

$$\langle a, b \rangle = \langle ab \rangle - \langle a \rangle \langle b \rangle .$$

From the quantum regression theorem $G(\tau)$ obeys the same equation as $(\langle \sigma(\tau) \rangle - \langle \sigma \rangle_{ss})$:

$$\frac{dG(\tau)}{dt} = AG(\tau) , \quad (11.26)$$

where A is defined in (11.7)

This matrix equation can be integrated and the complete solution derived. The initial condition is simplified using the algebra of the σ matrices

$$\langle \sigma_+ \sigma_- \rangle_{ss} = \langle \sigma_z \rangle_{ss} + \frac{1}{2}, \quad \langle \sigma_z \sigma_- \rangle_{ss} = -\frac{1}{2} \langle \sigma_- \rangle_{ss}, \quad \langle \sigma_-^2 \rangle_{ss} = 0 , \quad (11.27)$$

where the stationary values have been given by (11.8–10).

We shall present the result for the case of resonance ($\Delta\omega = 0$). The first-order correlation function for the radiation field is (in the Schrödinger picture)

$$\begin{aligned} G_{ss}^{(1)}(\tau) = I_0(r) \frac{\Omega^2}{\gamma^2 + 2\Omega^2} & \left(\frac{\gamma^2}{\gamma^2 + 2\Omega^2} e^{-i\omega_0\tau} + \exp \left[-\left(\frac{\gamma}{2} + i\omega_0 \right) \tau \right] \right. \\ & - \lambda_+ \exp \left\{ - \left[\left(\frac{3\gamma}{4} - \kappa \right) + i\omega_0 \right] \tau \right\} \\ & \left. + \lambda_- \exp \left\{ - \left[\left(\frac{3\gamma}{4} + \kappa \right) + i\omega_0 \right] \tau \right\} \right) , \end{aligned} \quad (11.28)$$

where

$$\lambda_{\pm} = \frac{1}{4} \left(\frac{-\frac{\gamma}{4\kappa} (10\Omega^2 - \gamma^2) \pm (\gamma^2 - 2\Omega^2)}{\gamma^2 + 2\Omega^2} \right) .$$

Remembering that the steady state spectrum is given by the Fourier transform of this expression we can identify four separate contributions to the spectrum. The first term corresponds to elastic scattering, whereas the second term corresponds to inelastic scattering described by a Lorentzian peaked about ω_0 with the linewidth $\gamma/2$. The last two terms contribute to this central peak for $\Omega < \gamma/4$. However, for $\Omega > \gamma/4$ they give rise to two sidebands with width $3\gamma/4$.

We shall consider the spectrum resulting from this expression for $G^{(1)}(\tau)$. For low intensities of the incident light only the first term in (11.28) remains, and this gives rise to the δ -function spectrum

$$S(\omega, \mathbf{r}) = I_0(\mathbf{r}) \frac{\gamma^2}{\gamma^2 + 2\Omega^2} \delta(\omega - \omega_0). \quad (11.29)$$

It corresponds to the elastic scattering considered by E. Wigner and V. Weisskopf.

As the intensity of the incident light is increased but with $\Omega < \gamma/4$ the δ -function spectrum broadens. For $\Omega > \gamma/4$ the spectrum splits into three peaks. We consider the case of a strong driving field $\Omega \gg \gamma/4$, in which the correlation function (11.28) reduces to

$$\begin{aligned} G_s^{(1)}(\tau) = & \frac{I_0(\mathbf{r})}{2} \left(\frac{\gamma^2}{\gamma^2 + 2\Omega^2} e^{-i\omega_0\tau} + \frac{1}{2} \exp \left[-\left(\frac{\gamma}{2} + i\omega_0 \right) \tau \right] \right. \\ & + \frac{1}{4} \exp \left\{ -\left[\frac{3\gamma}{4} + i(\omega_0 + \Omega) \right] \tau \right\} \\ & \left. + \frac{1}{4} \exp \left\{ -\left[\frac{3\gamma}{4} + i(\omega_0 - \Omega) \right] \tau \right\} \right). \end{aligned} \quad (11.30)$$

The corresponding spectrum is

$$\begin{aligned} S(\omega, \mathbf{r}) = & \frac{I_0(\mathbf{r})}{2\pi} \left(\frac{\pi\gamma^2}{\gamma^2 + 2\Omega^2} \delta(\omega - \omega_0) + \frac{1}{2} \frac{\frac{1}{2}\gamma}{(\frac{1}{2}\gamma)^2 + (\omega - \omega_0)^2} \right. \\ & + \frac{1}{4} \frac{\frac{3}{4}\gamma}{(\frac{3}{4}\gamma)^2 + [\omega - (\omega_0 + \Omega)]^2} + \left. \frac{1}{4} \frac{\frac{3}{4}\gamma}{(\frac{3}{4}\gamma)^2 + [\omega - (\omega_0 - \Omega)]^2} \right). \end{aligned} \quad (11.31)$$

For intense driving fields $\Omega > \gamma/4$ the contribution from the elastic scattering is negligible and we have a spectrum consisting of three Lorentzians, a central peak at $\omega = \omega_0$ with width $\gamma/2$, and two sidebands at $\omega = \omega_0 \pm \Omega$ with width $3\gamma/4$.

This spectrum was first predicted theoretically by *Mollow* [11.1] and has since been derived by a number of different methods. It has been verified by the experiments of *Ezekiel* et al [11.2] and *Walther* [11.3]. These experiments used a beam of Na atoms optically pumped to give a two-level system. The atomic beam was irradiated at right angles by a highly stabilized dye laser. The fluorescent radiation was detected in a direction at right angles to

the plane formed by the laser and atomic beams. This minimized any Doppler broadening. A comparison of the experimentally observed spectrum with the theoretical predictions is shown in Fig. 11.3.

The total fluorescent intensity is given by

$$I = I_{\text{IN}} \times (\text{probability of being in the upper state}) , \quad (11.32)$$

where I_{IN} is the incident intensity.

On resonance

$$I = I_{\text{IN}}(\langle \sigma_z \rangle + \frac{1}{2}) = I_{\text{IN}}\langle \sigma_+ \sigma_- \rangle = I_{\text{IN}} \frac{1}{2} \frac{Z^2}{1 + Z^2} , \quad (11.33)$$

$$\text{where } Z = \frac{\Omega}{\gamma}$$

The total fluorescent intensity may be separated into coherent and incoherent parts

$$\begin{aligned} I &= I^{\text{COH}} + I^{\text{INCOH}} \\ &= I_{\text{IN}} [\langle \sigma_+ \rangle \langle \sigma_- \rangle + (\langle \sigma_+ \sigma_- \rangle - \langle \sigma_+ \rangle \langle \sigma_- \rangle)] \\ &= I_{\text{IN}} \left[\frac{1}{2} \left(\frac{Z}{1 + Z^2} \right)^2 + \frac{1}{2} \left(\frac{Z^2}{1 + Z^2} \right)^2 \right] . \end{aligned} \quad (11.34)$$

It is clear that the coherent component dominates at low intensities, $Z \ll 1$, but the coherent component dominates at high intensities, $Z \gg 1$.

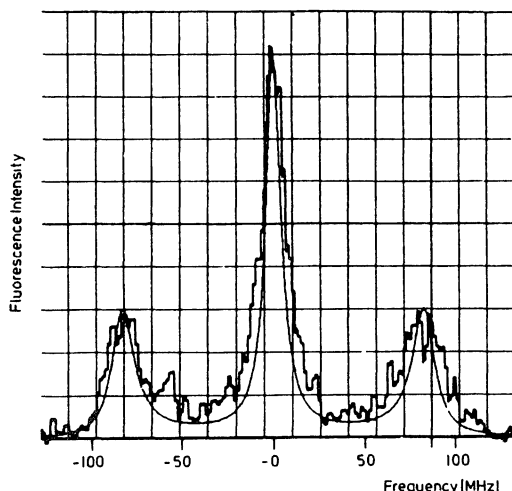


Fig. 11.3. A comparison of the theoretical and experimental spectra from a strongly-driven hyperfine transition of Na, as reported by Grove et al. [11.2]. [Reproduced in: Cresser et al. 1982, in "Dissipative Systems in Quantum Optics", ed. R. Bonafacio (Springer 1982).]

11.3 Photon Correlations

The measurement of the spectrum of the fluorescent light gives information on the first-order correlation function of the light. Photon correlation or measurements of the second-order correlation function will provide further information on the statistics of the light field. The second-order correlation function is defined by

$$G^{(2)}(\mathbf{r}t, \mathbf{r}t + \tau) = \langle E^{(-)}(\mathbf{r}, t)E^{(-)}(\mathbf{r}, t + \tau)E^{(+)}(\mathbf{r}, t + \tau)E^{(+)}(\mathbf{r}, t) \rangle . \quad (11.35)$$

This may be expressed in terms of atomic operators using (11.19):

$$G^{(2)}(\hat{\mathbf{r}}t, \hat{\mathbf{r}}t + \tau) = I_0^2(\mathbf{r})\langle \sigma_+(\hat{t})\sigma_+(\hat{t} + \tau)\sigma_-(\hat{t} + \tau)\sigma_-(\hat{t}) \rangle . \quad (11.36)$$

With the operator relation

$$\sigma_+\sigma_- = \sigma_z + \frac{1}{2} \quad (11.37)$$

we may write the steady-state two-time correlation function

$$\begin{aligned} & \langle \sigma_+(t)(\sigma_+(t + \tau)\sigma_-(t + \tau) - \langle \sigma_+(t)\sigma_-(t) \rangle_{ss})\sigma_-(t) \rangle_{ss} \\ &= \langle \sigma_+(t)(\sigma_z(t + \tau) - \langle \sigma_z(t) \rangle_{ss})\sigma_-(t) \rangle_{ss} \end{aligned} \quad (11.38)$$

which may be calculated using the quantum regression theorem from the equation for $\langle \sigma_z(t) \rangle$.

The solution for the steady-state correlation function is

$$\begin{aligned} & \langle \sigma_+(t)\sigma_+(t + \tau)\sigma_-(t + \tau)\sigma_-(t) \rangle_{ss} \\ &= \left(\frac{\Omega^2}{\gamma^2 + 2\Omega^2} \right)^2 \left[1 - e^{-3\gamma\tau/4} \left(\cosh \kappa\tau + \frac{3\gamma}{4\kappa} \sinh \kappa\tau \right) \right] . \end{aligned} \quad (11.39)$$

The normalized second-order correlation function is

$$g^{(2)}(\tau) = \frac{G_{ss}^{(2)}(\tau)}{|G_{ss}^{(1)}(0)|^2} = 1 - e^{-3\gamma\tau/4} \left(\cosh \kappa\tau + \frac{3\gamma}{4\kappa} \sinh \kappa\tau \right) . \quad (11.40)$$

This has the value $g^{(2)}(0) = 0$ at $\tau = 0$. That is, the fluorescent light exhibits photon antibunching – a result first predicted by Carmichael and Walls [11.4].

For low incident light intensities ($\Omega < \gamma/4$) $g^{(2)}(\tau)$ is a monotonic function of time. In the weak field limit ($\Omega \ll \gamma/4$) it becomes

$$g^{(2)}(\tau) = (1 - e^{-\gamma\tau/2})^2 \quad (11.41)$$

whereas for $\Omega \gg \lambda/4$ it becomes

$$g^{(2)}(\tau) = 1 - e^{-3\gamma\tau/4} \cos \Omega\tau . \quad (11.42)$$

This behaviour is shown in Fig. 11.4. Now $g^{(2)}(\tau)$ may be expressed as a photon number correlation function

$$g^{(2)}(\tau) = \frac{\langle :n(t)n(t+\tau):\rangle}{\langle n(t)\rangle^2}. \quad (11.43)$$

Thus, it is a correlation of the photon number at time t with the photon number at a time τ later. For chaotic light $g^{(2)}(0) = 2$, that is, the correlation at $\tau = 0$ is twice the random background correlation indicating the tendency of the photons to bunch together (Chap. 3). In resonance fluorescence we find $g^{(2)}(0) = 0$, indicating a tendency of the photons to be separated, or an anti-bunching effect.

The interpretation of this result is simple. It is due to the quantum nature of the scattering. The detection of the first photon serves to prepare the atom in its ground state. Knowing that any subsequent emission must begin with an excited atom, a delay corresponding to the time taken for the atom to be re-excited is naturally expected. We ask therefore what is the probability for finding an initially unexcited atom in its upper state? The answer is given by (11.11)

$$P_+(\tau) = \frac{\Omega^2}{\gamma^2 + 2\Omega^2} \left[1 - e^{-3\gamma\tau/4} \left(\cosh \kappa\tau + \frac{3\gamma}{4\kappa} \sinh \kappa\tau \right) \right]. \quad (11.44)$$

which is just the expression for $G_{ss}^{(2)}(\tau)$.

These theoretical predictions show that a light field which exhibits photon anti-bunching may be produced in resonance fluorescence from a single two-level atom. Such a light field cannot be explained by a classical treatment of the radiation field. The observation of photon anti-bunching would be direct evidence for the quantum nature of the electromagnetic field. Note, however, that the source of this field is a *single* two-level atom – clearly a quantum mechanical source. If one had an ensemble of N atoms the antibunching would disappear for N large. In fact, for a large number of atoms as the source

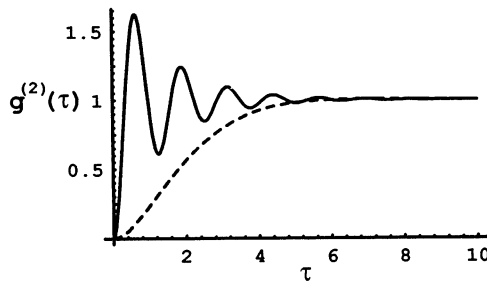


Fig. 11.4. A plot of the second-order intensity correlation function $g^{(2)}(\tau)$ (11.39) versus time τ . The solid line corresponds to the Rabi frequency $\Omega = 5.0$, while the dashed line corresponds to $\Omega = 0.5$. In both cases $\gamma = 1.0$.

we would observe fluorescent light from a large number of independent scattering centres and hence from the central limit theorem we have the result for Gaussian statistics

$$g^{(2)}(\tau) = 1 + | | g^{(1)}(\tau) |^2 . \quad (11.45)$$

Since $g^{(1)}(0) = 1$, we find in the limit of many atoms $g^{(2)}(0) \rightarrow 2$. Thus, in devising an experiment to look for photon anti-bunching in resonance fluorescence, one must attempt to observe the fluorescence light from a single atom. The first experiments were performed by *Kimble* et al. [11.5] and *Leuchs* et al. [11.6], with an atomic beam. The experimental set up was similar to that used to measure the spectrum. The intensity of the atomic beam was, however, maintained very low so that on average only one atom is in the scattering volume (defined by the detector) at a time. We shall give an order-of-magnitude estimate of the number of fluorescent photons. In a typical experiment each atom remains in the laser beam 10^{-6} s (atomic velocity: $\approx 10^3$ m/s, diameter of laser beam: 10^{-3} m). If there is to be only one atom in the beam at a time, we can have at most 10^6 atoms/s. The lifetime of the excited state (Na atoms) is $\approx 10^{-8}$ s. Since the saturated atom spends one half of its time in the excited state the average number of emissions per atom is ≈ 50 . It gives 5×10^7 fluorescent photons/s (in 4π solid angles). This order of photon flux was sufficient to perform the experiment using photon counting techniques. Since the lifetime of the excited state for Na atoms is 17 nanoseconds, correlators working with a correlation time of ≈ 2 nanoseconds were necessary. This was accomplished using time-to-amplitude convertors.

The experimental results obtained showed a $g^{(2)}(\tau)$ with a positive slope at $\tau = 0$, thus clearly indicating the presence of photon antibunching. A further modification to the theory was necessary before an accurate fit to the experimental data could be made. While it was possible to get the mean number of atoms in the scattering volume to equal unity, there would be number fluctuations about this value due to the thermal nature of the atomic beam.

The experimentally observed $g^{(2)}(\tau)$ may thus be obtained from the single atom $g_A^{(2)}(\tau)$ by averaging over the number fluctuations of the atoms (assumed Poissonian). This gives [11.7]

$$g^{(2)}(\tau) = 1 + \frac{1}{\bar{N}} g_A^{(2)}(\tau). \quad (11.46)$$

The formula is valid for the case where a large number of coherence areas are observed, and the background noise has been neglected. We see that the contribution of the single atom correlation function $g_A^{(2)}(\tau)$ is reduced by $1/\bar{N}$. This reflects the Poissonian statistics of the scattering atoms. Hence, the $g_A^{(2)}(\tau)$ may only be inferred from the fluorescent light observed. In Figs. 11.5 we show the experimental data obtained by *Kimble* et al. [11.5]. The data is fitted to the theoretical calculations which have compensated for the effect of atomic number fluctuations. From these results

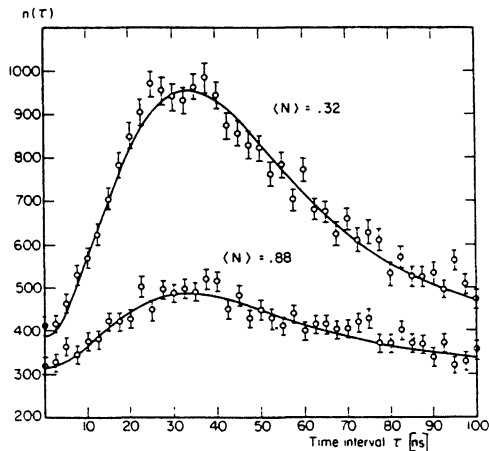


Fig. 11.5. Experimental indication of photon anti-bunching in resonance fluorescence, as obtained by Kimble et al. [11.5]. The quantity $n(\tau)$ is the expected number of pulse pairs with time separation τ , for N atoms. The solid line represents the theoretical prediction. The Rabi frequency to line width ratio is 1.75

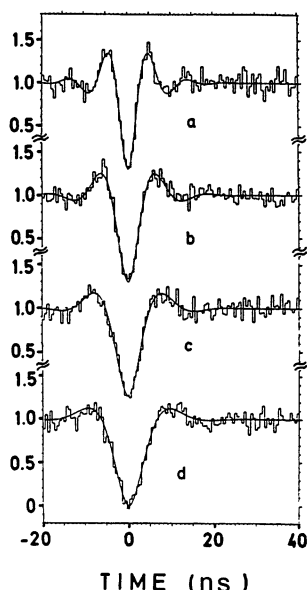


Fig. 11.6. Experimental results for the second-order intensity correlation function of a single ion in a trap, as obtained by Diedrich and Walther [11.8]. The solid line represents the theoretical prediction. From Dr. H. Walther Phys. Rev. Letts. **58** 203 (1987)

one may deduce that the light emitted from a coherently driven two-level atom is anti-bunched.

More recently the modern technology of radio-frequency ion traps has made it possible to trap a single ion for periods of several minutes. *Diedrich* and *Walther* [11.8] used a Paul radio-frequency trap to store a single atomic ion for periods of about ten minutes. This single ion was excited by coherent radiation and the photon correlations of the fluorescent light were measured. The measured values of $g^{(2)}(\tau)$ taken in this experiment are displayed in Fig. 11.6. The experimental results are fitted with the theoretical prediction given by (11.40). In this experiment with a single atom source there are not atomic number fluctuations and a value of $g^{(2)}(0)$ close to zero was obtained. Thus, in addition to photon antibunching, the photon statistics of the fluorescent light is sub-Poissonian.

The theoretical prediction and experimental observation of photon antibunching in resonance fluorescence is one of the major triumphs of quantum optics providing, as it does, direct evidence for the quantum nature of light. It was the precursor for much of the present work on non-classical radiation.

11.4 Squeezing Spectrum

The squeezing spectrum of the fluorescent light may be calculated from (11.26) for the two-time atomic correlation function [11.9].

We define a slowly varying electric field operator with phase θ :

$$\begin{aligned} E_\theta(\mathbf{x}, t) &= \frac{1}{2} [E^{(+)}(\mathbf{x}, t) \exp(-i\omega_L t + i\theta) + E^{(-)}(\mathbf{x}, t) \exp(i\omega_L t - i\theta)] \\ &= E_1(\mathbf{x}, t) \cos \theta + E_2(\mathbf{x}, t) \sin \theta , \end{aligned} \quad (11.47)$$

where $E_1(\mathbf{x}, t) = E^{(+)} + E^{(-)}$ and $E_2(\mathbf{x}, t) = -i(E^{(+)} - E^{(-)})$ are the quadrature phases of the fluorescent field in-phase and out-of-phase with the coherent driving field.

The normally-ordered squeezing spectrum of the fluorescent field is defined by

$$:\mathbf{S}(\omega): = \frac{1}{2\pi} \int_{-\infty}^{\infty} d\tau \langle :E_\theta(t), E_\theta(t+\tau):\rangle e^{i\omega\tau} . \quad (11.48)$$

Using (11.19) the two-time field correlation function may be written in terms of atomic correlation functions, i.e.

$$\begin{aligned} \langle :E_\theta(t), E_\theta(t+\tau):\rangle &= \gamma [e^{-2i\theta} \langle \sigma_-(\tau), \sigma_-(0) \rangle + e^{2i\theta} \langle \sigma_+(\tau), \sigma_+(0) \rangle \\ &\quad + \langle \sigma_+(\tau), \sigma_-(0) \rangle + \langle \sigma_+(0), \sigma_-(\tau) \rangle] , \end{aligned} \quad (11.49)$$

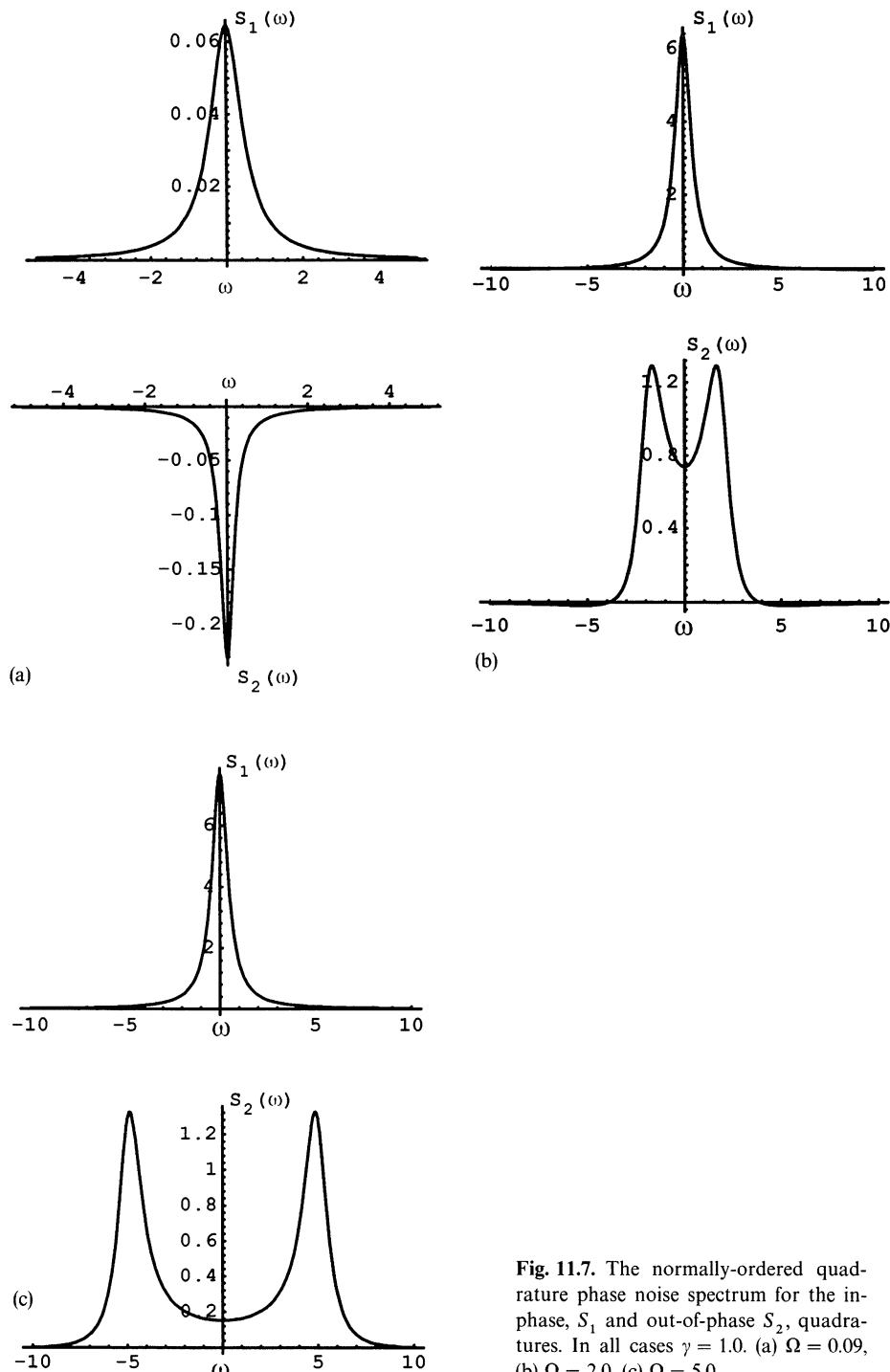


Fig. 11.7. The normally-ordered quadrature phase noise spectrum for the in-phase, S_1 and out-of-phase S_2 , quadratures. In all cases $\gamma = 1.0$. (a) $\Omega = 0.09$, (b) $\Omega = 2.0$, (c) $\Omega = 5.0$

where we have renormalised the correlation functions to the total outgoing flux. γ is the radiative decay rate of the two-level atom. The steady state solutions for these atomic correlation functions are found from (11.26):

$$\begin{aligned} \langle \sigma_{\pm}(t), \sigma_{-}(0) \rangle &= \langle \sigma_{-}(t), \sigma_{\mp}(0) \rangle \\ &= \frac{1}{4} \frac{2\Omega^2}{\gamma^2 + 2\Omega^2} \left[\exp\left(-\frac{1}{2}\gamma t\right) \right. \\ &\quad \left. \pm \frac{\gamma}{4\kappa} \frac{10\Omega^2 - \gamma^2}{\gamma^2 + 2\Omega^2} \exp\left(-\frac{3}{4}\gamma t\right) \sinh \kappa t \right. \\ &\quad \left. \pm \frac{2\Omega^2 - \gamma^2}{\gamma^2 + 2\Omega^2} \exp\left(-\frac{3}{4}\gamma t\right) \cosh \kappa t \right]. \end{aligned} \quad (11.50)$$

Substituting into (11.48) for the squeezing spectrum we find for the in-phase quadrature

$$:S_1(\omega): = \frac{8\Omega^2}{\gamma^2 + \Omega^2} \frac{(\gamma/2)^2}{(\gamma/2)^2 + \omega^2} \quad (11.51)$$

which does not show any squeezing. For the out-of-phase quadrature

$$:S_2(\omega): = \gamma^2 \frac{2\Omega^2}{\gamma^2 + 2\Omega^2} \frac{4\Omega^2 - \gamma^2 - \omega^2}{[(\gamma/2)^2 + \Omega^2 - \omega^2]^2 + (3\gamma/2)^2 \omega^2} \quad (11.52)$$

which may exhibit squeezing for $\Omega^2 < \frac{1}{4}\gamma^2$. The squeezing spectrum is plotted for several parameter values in Fig. 11.7. Maximum squeezing of approximately 28% occurs near $\omega = 0$ for $\Omega \approx 0.09\gamma$. With the onset of saturation the maximum squeezing shifts from the frequency component at $\omega = 0$ to the wings of the spectrum.

Well above saturation $:S_1(\omega):$ gives rise to the central component and $:S_2(\omega):$ to the sidebands of the Mollow fluorescent triplet, as is seen in the plots in Fig. 11.7 for $\Omega^2 = 4\gamma^2$.

To date there has been no experimental measurement of the squeezing spectrum in resonance fluorescence.

Exercises

11.1 The effect of collisional dephasing of the dipole may be modelled by adding the term $-\Gamma_p[\sigma_z, [\sigma_z, \rho]]$ to the atomic master equator. What is the corresponding effect on

- (a) $g^{(2)}(\tau)$, and
- (b) the fluorescent spectrum.

11.2 Derive the optical Bloch equations for a coherently driven two-level atom damped by a squeezed vacuum, see (10.73). Find the steady-state solutions for $\langle\sigma_x\rangle$, $\langle\sigma_y\rangle$ and $\langle\sigma_z\rangle$.

11.3 Derive the spectrum of resonance fluorescence for a two-level atom interacting with a squeezed bath. [Hint: use the optical Bloch equations derived in exercise 11.2 and the quantum regression theorem.]

12. Quantum Theory of the Laser

The quantum theory of the laser was developed in the 1960s principally by the schools associated with H. Haken, W. E. Lamb and M. Lax, see [12.1–4]. Haken and Lax independently developed sophisticated techniques to convert operator master equations into *c*-number Fokker–Planck equations or equivalent Langevin equations. We shall describe and use these techniques in Chap. 13, where we study the effect of spontaneous emission on the quantum noise properties of four wave mixing.

In this chapter we shall follow the approach of *Scully and Lamb* [12.3] to compute photon statistics and the linewidth of the laser. In the *Scully–Lamb* treatment the pumping is modelled by the injection of a sequence of inverted atoms into the laser cavity. In a usual laser, with a thermal pumping mechanism, a Poisson distributed sequence of inverted atoms is assumed. Introduction of a Bernoulli distribution enables a more general class of pumping mechanisms to be considered, including the case of the regularly pumped laser. Diode lasers with more regular pumping than usual lasers have recently been shown to give rise to sub-shot-noise photocurrent fluctuations.

12.1 Master Equation

A single mode cavity field is excited by a sequence of atoms injected into the cavity. Let t_i be the arrival time of the atom i in the cavity and τ the time spent by each atom in the cavity. The change in the density operator for the field due to the interaction with the i th atom may be represented by

$$\rho(t_i + \tau) = \mathcal{P}(\tau) \rho(t_i) . \quad (12.1)$$

The explicit form of $\mathcal{P}(\tau)$ depends on the particular atomic system used in the excitation process. The model we will employ is indicated in Fig. 12.1.

Of the four levels, only levels $|1\rangle$ and $|2\rangle$ are coupled to the intracavity field, which thus are referred to as the lasing levels. Each of these levels may then decay. Level $|1\rangle$ decays to level $|3\rangle$ at a rate γ_1 while level $|2\rangle$ decays to level $|4\rangle$ at a rate γ_2 . We will assume that these decay rates are very much greater than the spontaneous decay rate of level $|2\rangle$ to level $|1\rangle$, and thus we neglect spontaneous emission in the lasing levels. Each atom is prepared in the excited

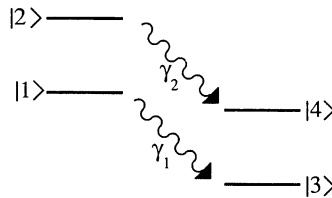


Fig. 12.1. Schematic representation of the four-level atomic model of a laser. Only levels 1 and 2 are coupled to the laser field

state $|2\rangle$ prior to interaction with the cavity field. In the usual laser system the lifetimes γ_1^{-1} and γ_2^{-1} are much shorter than the time τ spent by each atom in the cavity. This means that each atom rapidly attains a steady state in passing through the cavity and the pump operation $\mathcal{P}(\tau)$ is effectively independent of the time τ . The effect of a single atom on the state of the field may then be written as

$$\rho' = \mathcal{P}\rho , \quad (12.2)$$

where we have dropped the time dependence in ρ for simplicity, the prime serving to indicate the state of the field after the passage of a single atom through the cavity. We may represent the initial state of the field quite generally as

$$\rho = \sum_{n,m=0}^{\infty} \rho_{n,m}(0) |n\rangle \langle m| . \quad (12.3)$$

In appendix [12.A] we solve the master equation for the system over the time τ under the assumptions discussed above. The result is

$$\rho' = \sum_{n,m=0}^{\infty} \rho_{n,m}(0) (A_{nm}|n\rangle \langle m| + B_{nm}|n+1\rangle \langle m+1|) , \quad (12.4)$$

where the explicit expressions for A_{nm} , B_{nm} are given in the appendix.

We now assume that each atom contributes independently to the field. (This assumption remains valid even if there is more than one atom in the cavity at any time, provided that they are sufficiently dilute.) Thus, if k atoms are passed through the cavity from time 0 to time t the field density operator at time t is given by

$$\rho(t) = \mathcal{P}^k \rho(0) . \quad (12.5)$$

More generally, however, not all atoms entering the cavity are prepared in the excited state. Let the probability for an excited atom to enter the cavity between t and $t + \Delta t$ be $r\Delta t$, r being the average injection rate. This defines a Poisson excitation process. Thus the field at time $t + \Delta t$ is made up of a mixture of states

corresponding to atomic excitation and no atomic excitation, thus

$$\rho(t + \Delta t) = r\Delta t \mathcal{P}\rho(t) + (1 - r\Delta t)\rho(t) . \quad (12.6)$$

In the limit $\Delta t \rightarrow 0$ we have

$$\frac{d\rho(t)}{dt} = r\mathcal{U}\rho(t) \quad (12.7)$$

where

$$\mathcal{U} = \mathcal{P} - 1 . \quad (12.8)$$

We must now include the decay of the cavity field through the end mirrors. This is modelled in the usual way by coupling the field to a zero temperature heat bath. Thus the total master equation for the field density operator is

$$\frac{d\rho}{dt} = r\mathcal{U}\rho + \frac{\kappa}{2}(2a\rho a^\dagger - a^\dagger a\rho - \rho a^\dagger a) , \quad (12.9)$$

where κ is the cavity decay rate. This is the usual *Scully–Lamb* laser master equation.

In the special case that $\gamma_1 = \gamma_2 = \gamma$ the matrix elements of \mathcal{U} in the number basis are greatly simplified. In this case the master equation in the number basis may be written as

$$\begin{aligned} \frac{d\rho_{nm}}{dt} = & G \left(\frac{\sqrt{nm}}{1 + (n + m)/2n_s} \rho_{n-1,m-1} \right. \\ & - \frac{(m + n + 2)/2 + (m - n)^2/8n_s}{1 + (n + m + 2)/2n_s} \rho_{nm} \Big) \\ & + \frac{\kappa}{2} [2\sqrt{(n + 1)(m + 1)} \rho_{n+1,m+1} - (n + m)\rho_{nm}] , \end{aligned} \quad (12.10)$$

where

$$G = \frac{r}{2n_s} \quad (12.11)$$

and

$$n_s = \frac{\gamma^2}{4g^2} . \quad (12.12)$$

We have neglected terms $\propto n_s^{-2}$ in the denominators of the first two coefficients.

12.2 Photon Statistics

The photon number distribution obeys the equation

$$\frac{dp_n}{dt} = -G \left(\frac{n+1}{1+(n+1)/n_s} p_n - \frac{n}{1+(n/n_s)} p_{n-1} \right) + \kappa(n+1) p_{n+1} - \kappa n p_n . \quad (12.13)$$

The gain coefficient G is defined by

$$G = \frac{r\gamma_1}{2\gamma_+ n_s} , \quad (12.14)$$

where $\gamma_+ = (\gamma_1 + \gamma_2)/2$.

If we expand the denominators in (12.13) to first-order an approximate equation for the mean photon number may be obtained, namely

$$\frac{d\bar{n}}{dt} = (G - \kappa)\bar{n} - \frac{G}{n_s} (\bar{n}^2 + 2\bar{n} + 1) + G . \quad (12.15)$$

If $G > \kappa$ there will be an initial exponential increase in the mean photon number. Thus $G = \kappa$ is the threshold condition for the laser.

The steady state photon number distribution may be deduced directly from (12.13), using the condition of detailed balance. It may be written in the form

$$p_n^{ss} = \mathcal{N} \frac{(Gn_s/\kappa)^{n+n_s}}{(n+n_s)!} , \quad (12.16)$$

where \mathcal{N} is a normalisation constant. Below threshold ($G < \kappa$) this distribution may be approximated by a chaotic (thermal) distribution with the mean $\bar{n} = G/(\kappa - G)$ (Exercise 12.1). Above threshold ($G > \kappa$) the mean and variance are given, to a good approximation, by (Exercise 12.2),

$$\bar{n} = n_s \left(\frac{G}{\kappa} - 1 \right) , \quad (12.17)$$

$$V(n) = \bar{n} + n_s . \quad (12.18)$$

Well above threshold $\bar{n} \gg n_s$ and thus $V(n) \approx \bar{n}$, indicating an approach to Poisson statistics. In Fig. 12.2 we show the exact photon number distribution for below and above threshold. The transition from power law to the Poisson distribution is quite evident.

Photon counting experiments by *Arecchi* [12.5], *Johnson* et al. [12.6], and *Morgan* and *Mandel* [12.7], demonstrated that the photon statistics of a laser well above threshold, approaches a Poisson distribution. In Fig. 12.3 we present the results of photon counting measurements by *Arecchi* on both thermal and laser light. A comparison of the experimental data with the thermal and Poisson distributions is also shown.

12.2.1 Spectrum of Intensity Fluctuations

Equations (12.17, 18) give the photon number fluctuations for the internal cavity mode. This quantity, however, is not directly observable. We must now determine how the photon number fluctuations inside the cavity determine the intensity fluctuations in the many mode field to which it is coupled through the output mirrors. This is an application of the general input/output theory described in Chap. 7.

A single photoelectron detector placed at the output of the cavity measures a photocurrent given by

$$\overline{i(t)} = e\xi \langle b_{\text{out}}^\dagger(t)b_{\text{out}}(t) \rangle , \quad (12.19)$$

where e is the electronic charge, and $\xi = 2\varepsilon_0 c A / \hbar\omega$ with A the area of the detector surface. (We will assume unit quantum efficiency and unit amplification, for simplicity.) The output field $b_{\text{out}}(t)$ is related to the internal field and the input field by

$$b_{\text{out}}(t) = \sqrt{\kappa} a(t) - b_{\text{in}}(t) . \quad (12.20)$$

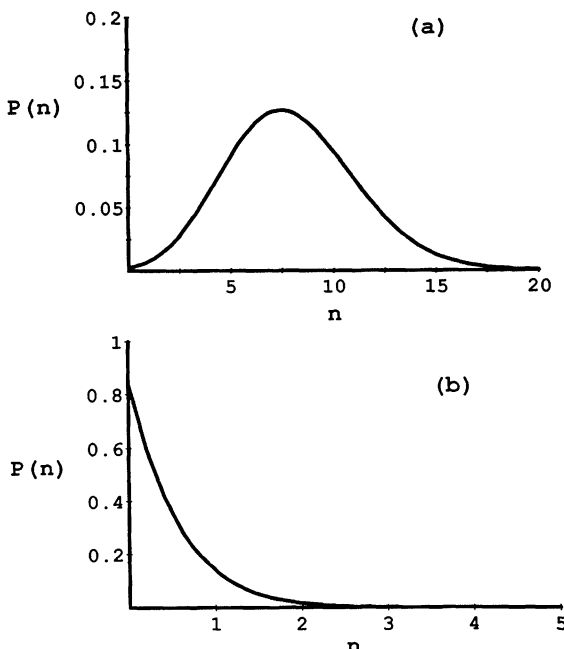


Fig. 12.2. The steady state photon number distribution of a laser operating above and below threshold. In (a) $G/\kappa = 5.0$, in (b) $G/\kappa = 0.25$. In both cases $n_s = 2$

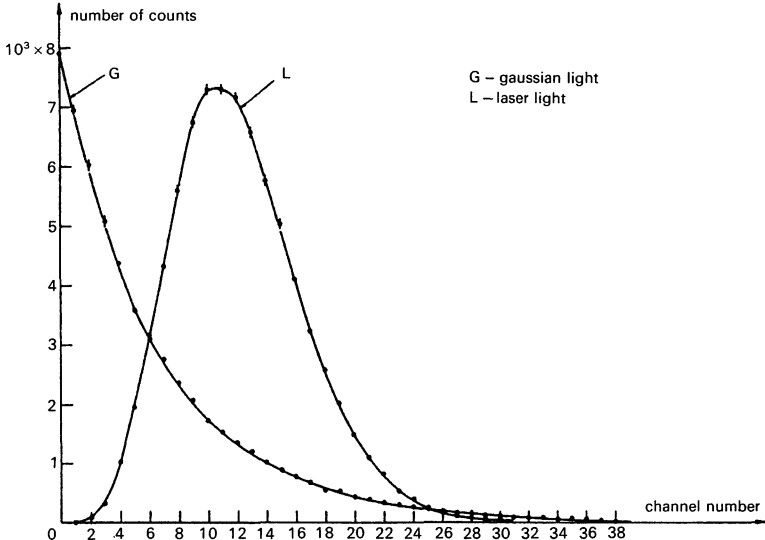


Fig. 12.3. Experimental results for the steady state photon number distribution for a thermal (i.e. Gaussian) light source and a laser operator above threshold. The laser exhibits Poissonian photon number statistics [12.5]

We will assume the input field to be in the vacuum state. In that case

$$\overline{i(t)} = e\xi\kappa\bar{n} , \quad (12.21)$$

where \bar{n} is the mean photon number inside the cavity.

To determine the noise properties of the output field, the appropriate detector quantity is $\overline{i(0)i(\tau)}$. The theory of photo-electron detection (Chap. 3) enables this to be related to the intensity fluctuations by

$$\overline{i(0)i(\tau)} = e^2\xi^2 [1 + \delta(\tau)] \langle b_{\text{out}}^\dagger(0) b_{\text{out}}(0) \rangle + e^2\xi^2 \langle :I(0), I(\tau): \rangle \quad (12.22)$$

where $: :$ denotes normal and time ordering and

$$I(\tau) = [b_{\text{out}}(\tau) + b_{\text{out}}^\dagger(\tau)]^2 . \quad (12.23)$$

The first two terms in (12.22) represent a dc term and a δ -correlated shot-noise term. The last term carries information on a possible reduction in intensity fluctuations. We now define the normalised power spectrum

$$P(\omega) = \frac{2}{e^2\xi^2} \int_0^\infty d\tau \cos(\omega\tau) \overline{i(0)i(\tau)} . \quad (12.24)$$

Using (12.20) one may show that

$$\langle :I(0), I(\tau):\rangle = \kappa^2 (\langle a^\dagger(0) a^\dagger(\tau) a(\tau) a(0)\rangle - \langle a^\dagger(0) a(0)\rangle^2) . \quad (12.25)$$

Thus

$$\overline{\frac{i(0)i(\tau)}{e^2\zeta^2}} = \kappa\bar{n}(1 - \kappa\bar{n}) + \kappa\bar{n}\delta(\tau) + \kappa^2 g(\tau) \quad (12.26)$$

where

$$g(\tau) = \langle a^\dagger(0) a^\dagger(\tau) a(\tau) a(0)\rangle . \quad (12.27)$$

We are only interested in the steady state fluctuations of the output field. In which case we can show that $g(\tau) = \bar{n}^2$ and thus

$$P(\omega) = \kappa\bar{n} . \quad (12.28)$$

This flat photocurrent spectrum is the shot-noise limit of the laser.

12.3 Laser Linewidth

Well above threshold the laser produces Poisson photon statistics. A coherent state has the same photon statistics, and this suggests that well above threshold the laser might be producing a coherent state. This is not the case. While the intensity of the laser is stabilised with a Poissonian distribution the phase of the laser undergoes a diffusion process. The effect of this phase diffusion is to cause a decay in the mean amplitude of the laser field, as the phase becomes uniformly distributed over 2π . The rate of amplitude decay Γ is thus a direct measure of the phase diffusion rate.

We will only discuss the case $\gamma_1 = \gamma_2 = \gamma$. The mean amplitude is defined by

$$\langle a(t)\rangle = \sum_{n=0}^{\infty} n^{1/2} \rho_{n,n-1}(t) . \quad (12.29)$$

Using (12.10) we find

$$\frac{d\langle a\rangle}{dt} = -\frac{G}{2} \sum_{n=0}^{\infty} \frac{(1/4n_s) - 1}{1 + (2n + 1)/2n_s} \sqrt{n} \rho_{n,n-1} . \quad (12.30)$$

Assuming the laser operates well above threshold we can replace n by \bar{n} in the denominator of each coefficient. Then as $\bar{n} \gg n_s$

$$\frac{d\langle a\rangle}{dt} = -\frac{G}{8\bar{n}} \langle a\rangle . \quad (12.31)$$

Thus the phase diffusion rate is inversely proportional to the intensity of the laser. All second-order phase dependent correlation functions will decay at a similar rate. In particular, the two-time correlation function

$$F(\tau) = \langle a^\dagger(\tau)a(0) \rangle \quad (12.32)$$

will decay at the rate $\Gamma = G/8\bar{n}$, i.e.

$$F(\tau) = \bar{n}e^{-\Gamma\tau}. \quad (12.33)$$

The Fourier transform of this function defines the laser spectrum

$$S(\omega) = \frac{\bar{n}}{\omega^2 + \Gamma^2}, \quad (12.34)$$

and thus the laser linewidth is simply

$$\Gamma = \frac{G}{8\bar{n}}. \quad (12.35)$$

It must be emphasised, however, that these results only apply well above threshold.

12.4 Regularly Pumped Laser

The Poissonian photon statistics of a laser reflect the contributions from the random pumping mechanism and spontaneous emission, which lead to an irregular photo-emission sequence. By suppressing the pump fluctuations, sub-Poissonian photon statistics and thus sub-shot-noise photo-current fluctuations, are possible. This has been demonstrated in recent experiments by *Machida et al.* [12.8] and also *Richardson and Shelby* [12.9] with semiconductor lasers. The pump amplitude fluctuations were reduced by high impedance suppression of the electron injection rate.

We shall demonstrate how the *Scully–Lamb* laser theory can readily be modified to incorporate regular pumping. Regular pumped lasers have been considered theoretically by a number of researchers [12.10–14]. We shall follow the approach of *Golubov and Sokolov* [12.10], with some modifications.

Consider a time interval Δt short compared to the time scale on which the field is changing due to damping through the end mirrors. However, the time Δt is very long compared to the time interval between successive pumping atoms entering the cavity. Divide the interval Δt into N steps of length τ . The probability for an excited atom to enter the cavity at time $t_j = j\tau$ is defined to be p . The fundamental probabilities of interest are then the probability of r excited

atoms to enter the cavity at any of the N time steps, over the interval Δt . These probabilities are

$$P_r(\Delta t) = \frac{\Delta t(\Delta t - \tau)(\Delta t - 2\tau) \dots (\Delta t - r\tau)}{\tau^r r!} \left(\frac{p}{1-p} \right)^r \times \exp \left[\frac{\Delta t}{\tau} \ln(1-p) \right]. \quad (12.36)$$

To first order in Δt this is

$$P_r(t) = (-1)^{r+1} \left(\frac{p}{1-p} \right)^r \frac{\Delta t}{r\tau}. \quad (12.37)$$

Between each atom entering the cavity the field evolves freely according to

$$\mathcal{T}(\tau) = e^{-i\omega_a \tau a^\dagger a} \rho e^{+i\omega_a \tau a^\dagger a}. \quad (12.38)$$

The change in the state of the field due to the passage of a single atom is given by (12.4). It is a simple matter to prove that the operation describing the effect of the pump atoms \mathcal{P} commutes with the free evolution operator \mathcal{T} (if this is not the case a simple master equation for the field state cannot be obtained in general). Thus the change in the state of the field over a time Δt is

$$\rho(t + \Delta t) = \mathcal{T}(\Delta t) \left[\sum_{n=0}^N P_n(\Delta t) \mathcal{P}^n \rho(t) \right] \quad (12.39)$$

(i.e., we can factor out the free evolution between each time step). We henceforth assume we are working in the interaction picture and drop the free evolution term. As we assume $\tau \ll \Delta t$ we extend the upper limit on the sum to ∞ , then

$$\begin{aligned} \rho(t + \Delta t) &= \rho(t) + \frac{\Delta t}{\tau} \ln(1-p) \rho(t) \\ &\quad + \frac{\Delta t}{\tau} \left[\frac{p}{1-p} \mathcal{P} - \frac{1}{2} \left(\frac{p}{1-p} \right)^2 \mathcal{P}^2 + \dots \right] \rho(t). \end{aligned} \quad (12.40)$$

From which we obtain

$$\frac{d\rho}{dt} = \frac{1}{\tau} \ln(1-p) \rho(t) + \frac{1}{\tau} \ln \left(1 + \frac{p}{1-p} \mathcal{P} \right) \rho(t) \quad (12.41)$$

$$= R \ln(1 + p \mathcal{U}) \rho(t), \quad (12.42)$$

where $R = \tau^{-1}$ is the pumping rate for a perfectly regular process ($p = 1$) and

$$\mathcal{U} = \mathcal{P} - 1. \quad (12.43)$$

We can define an average injection rate $r = pR$, then

$$\frac{d\rho}{dt} = \frac{r}{p} \ln(1 + p\mathcal{U}) \rho(t). \quad (12.44)$$

In this form we can take the Poisson limit defined by $p \rightarrow 0$, $R \rightarrow \infty$, such that $pR = \text{constant} = r$. In this limit the equation reduces to that for a normal laser.

The difficulty in discussing the regularly pumped laser is the logarithm term in (12.42). As \mathcal{U} represents the change in the state of the field due to a single atom we might expect \mathcal{U} to be in some sense small. With this in mind we expand the logarithm to second order. Unfortunately this leads to a rather pathological master equation. However, the procedure does give accurate results for the first- and second-order moments of the photon number.

The photon number distribution now obeys the equation

$$\begin{aligned} \frac{dp_n}{dt} &= \kappa[-np_n + (n+1)p_{n+1}] + r(-a_{n+1}P_n + a_np_{n-1}) \\ &+ \frac{pr}{2}[-a_{n+1}^2 p_n + a_n(a_n + a_{n+1})p_{n-1} - a_n a_{n-1} p_{n-2}], \end{aligned} \quad (12.45)$$

where

$$a_n = \frac{Gn}{r(1 + (n/n_s))}. \quad (12.46)$$

To obtain the stationary state variances is a rather more difficult process than for the Poisson pumped case. The mean photon number above threshold is not changed, however the variance is given by

$$V(n) = \bar{n} \left(1 - \frac{p\gamma_1}{2(\gamma_1 + \gamma_2)} \right) + n_s. \quad (12.47)$$

We consider some special cases of this result for regular pumping, $p = 1$. Far above threshold $\bar{n} \gg n_s$ so we may neglect the last term in (12.47). When the decay rates are equal, the photon number variance is

$$V(n) = \frac{3\bar{n}}{4} \quad (\gamma_1 = \gamma_2). \quad (12.48)$$

In this case spontaneous emission from level $|2\rangle$ is contributing to the noise. This effect may be reduced by increasing the decay rate of the lower level with respect to the upper level, $\gamma_1 \gg \gamma_2$. In this case

$$V(n) = \frac{\bar{n}}{2} \quad (\gamma_1 \gg \gamma_2). \quad (12.49)$$

Thus the width of the photon number distribution inside the cavity is reduced by half.

We now consider intensity fluctuations of the light emerging from the cavity. We may obtain a solution for the normally ordered two-time correlation function $g(\tau)$, from the master equation (12.45) assuming a Gaussian steady state distribution. The result is

$$g(\tau) = \bar{n}^2 + [V(n) - \bar{n}] e^{-\delta\tau}, \quad (12.50)$$

where

$$\delta = \kappa \frac{\bar{n}/n_s}{1 + (\bar{n}/n_s)}. \quad (12.51)$$

Substituting (12.47 and 50) into (12.26) the spectrum of the photocurrent fluctuations is given by

$$P(\omega) = \kappa \bar{n} \left(1 + \frac{2\kappa Q \delta}{\omega^2 + \delta^2} \right), \quad (12.52)$$

where

$$Q = \frac{V(n) - \bar{n}}{\bar{n}} \quad (12.53)$$

$$= -\frac{p\gamma_1}{2(\gamma_1 + \gamma_2)} + \frac{n_s}{\bar{n}}. \quad (12.54)$$

The Q parameter measures the deviation of the intracavity field from Poisson statistics. In the limit of regular pumping ($p = 1$) and far above threshold

$$P(\omega) = \kappa \bar{n} \left(1 - \frac{\gamma_1 \kappa^2}{(\gamma_1 + \gamma_2)(\kappa^2 + \omega^2)} \right). \quad (12.55)$$

Thus at cavity resonance ($\omega = 0$),

$$\begin{aligned} P(0) &= \kappa \bar{n} (1 + 2Q) \\ &= \kappa \bar{n} \frac{\gamma_1}{\gamma_1 + \gamma_2}. \end{aligned} \quad (12.56)$$

The first term in the first equation represents the shot-noise contribution. A negative value of Q leads to a reduction below the shot-noise limit. If the decay rates are equal ($\gamma_1 = \gamma_2$), spontaneous emission is not suppressed and

$$P(0) = \frac{\kappa \bar{n}}{2}, \quad (12.57)$$

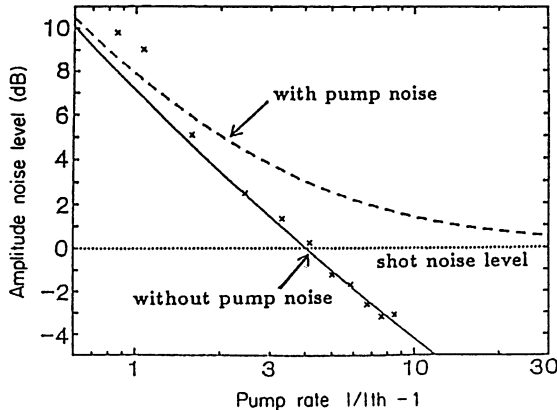


Fig. 12.4. The normalised amplitude noise level versus the pump rate for a laser with pump noise (dashed) and with pump noise suppressed (solid) [12.11]

which represents a 50% reduction below the shot-noise level. However, in the limit $\gamma_1 \gg \gamma_2$, Q approaches -0.5 far above threshold and

$$P(\omega) = \kappa\bar{n} \left(1 - \frac{\kappa^2}{\kappa^2 + \omega^2} \right). \quad (12.58)$$

Then at cavity resonance, the fluctuation spectrum is zero. This may be compared with the light inside the cavity where the photon number fluctuations were only reduced by one half. This result has the same interpretation as the limit to the intracavity squeezing in a parametric oscillator; there is a destructive interference from the vacuum fluctuations reflected from the cavity mirror and the reduced noise light emerging from the cavity. This results in no fluctuations in the output light on resonance.

In Fig. 12.4 we show the results of the experiment by *Machida et al.* [12.8] for a regularly pumped semiconductor laser.

12.A Appendix: Derivation of the Single-Atom Increment

Consider a single multilevel atom (Fig. 12.1) prepared in the state $|2\rangle$. Level $|1\rangle$ is damped at the rate γ_1 to level $|3\rangle$ and level $|2\rangle$ is damped at the rate γ_2 to level $|4\rangle$. Only levels $|1\rangle$ and $|2\rangle$ interact with the cavity field. The master equation

describing the dynamics of this system is

$$\begin{aligned} \frac{d\rho}{dt} = & ig[a^\dagger\sigma_-^{12} + a\sigma_+^{12}, \rho] \\ & + \frac{\gamma_1}{2}(2\sigma_-^{13}\rho\sigma_+^{13} - \sigma_+^{13}\sigma_-^{13}\rho - \rho\sigma_+^{13}\sigma_-^{13}) \\ & + \frac{\gamma_2}{2}(2\sigma_-^{24}\rho\sigma_+^{24} - \sigma_+^{24}\sigma_-^{24}\rho - \rho\sigma_+^{24}\sigma_-^{24}) \end{aligned} \quad (12.59)$$

(we ignore spontaneous emission on the lasing levels $|1\rangle, |2\rangle$). We will present a complete operator solution to the master equation over the time τ and then consider the limit $\gamma_i\tau \gg 1$.

Define the operation

$$\mathcal{J}\rho = \gamma_1\sigma_+^{13}\rho\sigma_+^{13} + \gamma_2\sigma_-^{24}\rho\sigma_-^{24} \quad (12.60)$$

and the rate operator

$$R = \gamma_1\sigma_+^{13}\sigma_-^{13} + \gamma_2\sigma_+^{24}\sigma_-^{24} \quad (12.61)$$

$$= \gamma_1|1\rangle\langle 1| + \gamma_2|2\rangle\langle 2| . \quad (12.62)$$

The solution to the master equation may then be written formally

$$\begin{aligned} \rho(t) = & \mathcal{S}(t)\rho(0) + \int_0^t dt_1 \mathcal{S}(t-t_1)\mathcal{J}\mathcal{S}(t_1)\rho(0) \\ & + \int_0^t dt_1 \int_0^{t_1} dt_2 \mathcal{S}(t-t_1)\mathcal{J}\mathcal{S}(t_1-t_2)\mathcal{J}\mathcal{S}(t_2)\rho(0) \\ & + \dots , \end{aligned} \quad (12.63)$$

where

$$\mathcal{S}(t)\rho = \mathcal{B}(t)\rho\mathcal{B}^\dagger(t) , \quad (12.64)$$

with

$$\mathcal{B}(t) = \exp[-ig(a^\dagger\sigma_-^{12} + a\sigma_+^{12}) - \gamma_1 t|1\rangle\langle 1| - \gamma_2 t|2\rangle\langle 2|] . \quad (12.65)$$

For

$$\rho(0) = |2\rangle\langle 2| \otimes \rho_F(0) \quad (12.66)$$

$$= \sum_{n,m=0}^{\infty} \rho_{nm}(0)|n,2\rangle\langle m,2|, \quad (12.67)$$

with

$$|n, 2\rangle = |n\rangle_F \otimes |2\rangle . \quad (12.68)$$

Note that after the action of \mathcal{J} the atom is in a mixture of the states $|3\rangle$ and $|4\rangle$ and is then decoupled from the field. All further action of $\mathcal{S}(t)$ is just the identity, and \mathcal{J} destroys the state. The series thus truncates at first order.

Now one may use the eigenstates of the free Hamiltonian (Chap. 10)

$$|n, +\rangle = \frac{1}{\sqrt{2}}(|n, 2\rangle + |n+1, 1\rangle) , \quad (12.69)$$

$$|n, -\rangle = \frac{1}{\sqrt{2}}(|n, 2\rangle - |n+1, 1\rangle) , \quad (12.70)$$

to show that

$$\begin{aligned} \mathcal{S}(t)(|n, 2\rangle \langle m, 2|) &= (c_n^+(t)|n, +\rangle + c_n^-(t)|n, -\rangle) \\ &\times (\langle m, +|c_m^+(t)^* + \langle m, -|c_m^-(t)^*) \end{aligned} \quad (12.71)$$

where

$$\begin{aligned} c_n^+(t) &= \frac{-i \exp\left(-\frac{\gamma_+ t}{2}\right)}{2\sqrt{2\Delta\Omega(n)}} \left\{ \left[-i\Omega(n)(1-\Delta) + \frac{\gamma_-}{2} \right] e^{i\Delta\Omega(n)t} \right. \\ &\quad \left. + \left[i\Omega(n)(1+\Delta) - \frac{\gamma_-}{2} \right] e^{-i\Delta\Omega(n)t} \right\} \end{aligned} \quad (12.72)$$

and

$$\begin{aligned} c_n^-(t) &= \frac{-i \exp\left(-\frac{\gamma_+ t}{2}\right)}{2\sqrt{2\Delta\Omega(n)}} \left\{ \left[i\Omega(n)(1+\Delta) + \frac{\gamma_-}{2} \right] e^{i\Delta\Omega(n)t} \right. \\ &\quad \left. + \left[-i\Omega(n)(1-\Delta) - \frac{\gamma_-}{2} \right] e^{-i\Delta\Omega(n)t} \right\} \end{aligned} \quad (12.73)$$

where

$$\gamma_{\pm} = \frac{1}{2}(\gamma_1 \pm \gamma_2) , \quad (12.74)$$

$$\Delta = \left(1 - \frac{\gamma_-^2}{4\Omega(n)^2}\right)^{1/2} , \quad (12.75)$$

$$\Omega(n) = g\sqrt{n+1} . \quad (12.76)$$

We now assume $\gamma_{1,2}t \gg 1$. The first term in (12.63) may be ignored as it simply decays to zero.

We are interested in the state of the field alone which is obtained by tracing out over the atomic states. We use

$$\begin{aligned} \text{Tr}_A(\mathcal{J}\mathcal{S}(t)|n,2\rangle\langle m,2|) &= \frac{\gamma_2}{2}|n\rangle\langle m|[c_n^+(t) + c_n^-(t)][c_m^+(t)^* + c_m^-(t)^*] \\ &\quad + \frac{\gamma_1}{2}|n+1\rangle\langle m+1|[c_n^+(t) - c_n^-(t)] \\ &\quad \times [c_m^+(t)^* - c_m^-(t)^*] . \end{aligned} \quad (12.77)$$

Thus we obtain in the steady state, the single atom increment

$$\rho' = \sum_{n,m=0}^{\infty} \rho_{nm}(0)(A_{nm}|n\rangle\langle m| + B_{nm}|n+1\rangle\langle m+1|), \quad (12.78)$$

where

$$A_{nm} = \frac{\gamma_2}{2} \int_0^{\infty} dt [c_n^+(t) + c_n^-(t)][c_m^+(t)^* + c_m^-(t)^*], \quad (12.79)$$

$$B_{nm} = \frac{\gamma_1}{2} \int_0^{\infty} dt [c_n^+(t) - c_n^-(t)][c_m^+(t)^* - c_m^-(t)^*]. \quad (12.80)$$

Note that $\text{Tr}(\rho) = 1$ requires that $A_{nn} + B_{nn} = 1$. We quote only the results for the diagonal matrix elements,

$$A_{nn} = \left(\frac{\gamma_2}{2\gamma_+} \right) \frac{4\Omega(n)^2 + 2\gamma_1\gamma_+}{4\Omega(n)^2 + \gamma_1\gamma_2} \quad (12.81)$$

and

$$B_{nn} = 1 - A_{nn} = \left(\frac{\gamma_2}{2\gamma_+} \right) \frac{4\Omega(n)^2}{4\Omega(n)^2 + \gamma_1\gamma_2} . \quad (12.82)$$

To compute the change in the state we write

$$\rho' = (1 + \mathcal{U})\rho = \mathcal{P}\rho . \quad (12.83)$$

The diagonal matrix elements of $\mathcal{U}\rho$ are then found to be

$$\langle n|\mathcal{U}\rho|n\rangle = -a_{n+1}p_n + a_np_{n+1} , \quad (12.84)$$

where

$$a_{n+1} = A_{nn} - 1 . \quad (12.85)$$

Exercises

12.1 Show that below threshold ($G < \kappa$) the master equation may be approximated by

$$\frac{d\rho}{dt} = \frac{G}{2} (2a^\dagger \rho a - aa^\dagger \rho - \rho aa^\dagger) + \kappa(2a\rho a^\dagger - a^\dagger a \rho - \rho a^\dagger a) .$$

Thus demonstrate that the steady state density operator is

$$\rho^{ss} = \left(1 - \frac{G}{\kappa}\right) \sum_{n=0}^{\infty} \left(\frac{G}{\kappa}\right)^n |n\rangle \langle n| \quad (12.86)$$

which is equivalent to a chaotic state.

12.2 Show that well above threshold the laser master equation may be approximated by

$$\begin{aligned} \frac{d\rho}{dt} = Gn_s(2n^{-1/2}a^\dagger \rho an^{-1/2} - an^{-1}a^\dagger \rho - \rho an^{-1}a^\dagger) \\ + \kappa(2a\rho a^\dagger - a^\dagger \rho a - \rho a^\dagger a) \end{aligned}$$

where $n = a^\dagger a$. Show that the steady-state solution is

$$\rho^{ss} = \exp\left(-\frac{Gn_s}{\kappa}\right) \sum_{n=0}^{\infty} \frac{(Gn_s/\kappa)^n}{n!} |n\rangle \langle n| . \quad (12.87)$$

12.3 Show that the contours of the Q -function for the laser steady states in Exercises 12.1, 2 are: (a) Circles centred on the origin for below threshold, (b) annuli centered at the radius $r = (Gn_s/\kappa)^{1/2}$, for the above threshold state. Thus in both cases the phase of the field is random.

13. Intracavity Atomic Systems

In Chap. 9 we discussed the interaction of light with various nonlinear media. There we used a nonlinear polarizability model in which the underlying atomic dynamics did not appear explicitly. In this chapter we consider the light/atom interaction explicitly and consider two examples; optical bistability and squeezed light generation in four wave mixing. The main objective is to determine the dependence of the nonlinear coupling and noise terms on the atomic parameters.

We begin with a discussion of optical bistability, in which a single mode intracavity field interacts with a collection of two-level atoms. We will make extensive use of the generalised P representation, extended to take account of atomic variables. This technique is very powerful and may be used for a wide range of light/atom systems. We will describe the technique in the context of optical bistability. With the techniques in hand we go on to describe the more complicated process of four wave mixing.

13.1 Optical Bistability

We shall follow the treatment of *Drummond* and *Walls* [13.1] who adopted the method of *Haken* [13.2], developed for the laser, to treat the problem of optical bistability. In the electric dipole and rotating wave approximation the Hamiltonian describing the interaction of an ensemble of N two-level atoms with a single mode of the radiation field is

$$\mathcal{H} = \sum_{j=1}^5 \mathcal{H}_j , \quad (13.1)$$

$$\mathcal{H}_1 = \hbar\omega_c a^\dagger a + \frac{1}{2}\hbar\omega_0 \sum_{\mu=1}^N \sigma_\mu^z , \quad (13.2)$$

$$\mathcal{H}_2 = i\hbar \sum_{\mu=1}^N (ga^\dagger \sigma_\mu^- e^{-ik \cdot r_\mu} - h.c.) , \quad (13.3)$$

$$\mathcal{H}_3 = i\hbar(a^\dagger \mathcal{E} e^{-i\omega_l t} - h.c.) , \quad (13.4)$$

$$\mathcal{H}_4 = \sum_{\mu=1}^N (\Gamma \sigma_\mu^+ + \Gamma^\dagger \sigma_\mu^- + \Gamma_p \sigma_\mu^z) , \quad (13.5)$$

$$\mathcal{H}_5 = \Gamma_c a^\dagger + \Gamma_c^\dagger a , \quad (13.6)$$

where h.c. means the Hermitian conjugate. The term \mathcal{H}_1 is the free Hamiltonian for the field and the atoms, \mathcal{H}_2 describes the field/atom interaction, \mathcal{H}_3 represents the driving of the cavity mode at frequency ω_c by a classical laser field at frequency ω_L . The terms \mathcal{H}_4 and \mathcal{H}_5 represent damping. In \mathcal{H}_4 the dipole and inversion are coupled to reservoir operators to model dipole decay due to spontaneous emission and dephasing due to collisions. The term \mathcal{H}_5 models damping of the intracavity field. The atomic transition frequency is ω_0 .

The master equation for the density operator, ρ of the atom/field system follows in the usual way by projecting out reservoir operators and using the Markov and Born approximation. The result is

$$\frac{d\rho}{dt} = \frac{-i}{\hbar} [\mathcal{H}_1 + \mathcal{H}_2 + \mathcal{H}_3, \rho] + \mathcal{L}_4[\rho] + \mathcal{L}_5[\rho] , \quad (13.7)$$

where the nonunitary terms are

$$\begin{aligned} \mathcal{L}_4[\rho] = & \sum_{\mu=1}^N \left(\frac{\gamma_{||}}{2} ([\sigma_\mu^- \rho, \sigma_\mu^+] + [\sigma_\mu^-, \rho \sigma_\mu^+]) \right. \\ & \left. + \frac{\gamma_p}{4} ([\sigma_\mu^z \rho, \sigma_\mu^z] + [\sigma_\mu^z, \rho \sigma_\mu^z]) \right) \end{aligned} \quad (13.8)$$

$$\mathcal{L}_5[\rho] = \kappa([a\rho, a^\dagger] + [a, \rho a^\dagger] + 2\bar{n}[[a, \rho], a^\dagger]) . \quad (13.9)$$

The cavity damping rate is κ and \bar{n} is the mean thermal photon number in the external field. The spontaneous emission rate is $\gamma_{||}$ and γ_p is the rate of collision induced dipole decay. The atomic reservoirs are assumed to be at low temperature so that we can define the transverse atomic decay rate γ_\perp as

$$\gamma_\perp = \gamma_p + \frac{\gamma_{||}}{2} . \quad (13.10)$$

It is convenient to define a ratio which gives the relative degree of radiative and collisional decay

$$f = \frac{\gamma_{||}}{2\gamma_\perp} . \quad (13.11)$$

Collisional broadening corresponds to the limit $f \rightarrow 0$ while $f \rightarrow 1$ gives the natural linewidth limit.

We begin by converting (13.7) to a c-number equivalent Fokker–Planck equation. Define the collective atomic operators by

$$S = \sum_{\mu=1}^N \sigma_{\mu}^- e^{-ik \cdot r_{\mu}} , \quad (13.12)$$

$$S^\dagger = \sum_{\mu=1}^N \sigma_{\mu}^+ e^{ik \cdot r_{\mu}} , \quad (13.13)$$

$$D = \sum_{\mu=1}^N \sigma_{\mu}^z . \quad (13.14)$$

We next define the normally order characteristic function by

$$\chi(\lambda) = \text{Tr}\{\rho \Xi(\lambda)\} , \quad (13.15)$$

where

$$\Xi(\lambda) = e^{i\lambda_5 S^\dagger} e^{i\lambda_4 D} e^{i\lambda_3 S} e^{i\lambda_2 a^\dagger} e^{i\lambda_1 a} , \quad (13.16)$$

with $\lambda = (\lambda_1, \lambda_2, \lambda_3, \lambda_4, \lambda_5)$. The positive P representation for the atom/field state is then defined as the Fourier transform of the characteristic function

$$P(\alpha) = \frac{1}{(2\pi)^5} \int \chi(\lambda) e^{-i\lambda \cdot \alpha} d\lambda , \quad (13.17)$$

where $\alpha = (\alpha, \beta, v, D, u)$.

To obtain an equation of motion for $P(\alpha)$ we first derive an equation of motion for the characteristic function. The details will be left as an exercise, however it is instructive to work through one term in some detail. Consider the term arising from the atom/field interaction, denoted with a subscript I. Then

$$\left(\frac{\partial \chi}{\partial t} \right)_I = g \langle [\Xi, a^\dagger S] \rangle - g \langle [\Xi, a S^\dagger] \rangle . \quad (13.18)$$

To proceed we make use of the commutation relations for the atomic variables

$$[S^\dagger, S] = D , \quad (13.19)$$

$$[D, S^\dagger] = 2S^\dagger , \quad (13.20)$$

$$[D, S] = -2S . \quad (13.21)$$

(A word of caution: These are not the same as the atomic operator commutation relations used in Chap. 10, but are derived with the atomic operators mapped to the corresponding Pauli matrix). For example, we find

$$\begin{aligned} \langle [\Xi, a^\dagger S] \rangle &= \left(\lambda_1 \frac{\partial}{\partial \lambda_3} - (1 - e^{2i\lambda_4}) \frac{\partial^2}{\partial \lambda_2 \partial \lambda_3} \right. \\ &\quad \left. - i\lambda_5 \frac{\partial^2}{\partial \lambda_2 \partial \lambda_4} + \lambda_5^2 \frac{\partial^2}{\partial \lambda_2 \partial \lambda_5} \right) \chi(\lambda) . \end{aligned} \quad (13.22)$$

Using this result in equation (13.17) and integrating by parts the contribution to the equation for P is

$$\begin{aligned} \left(\frac{\partial P}{\partial t} \right)_1 = g & \left(- \frac{\partial}{\partial \alpha} v + (1 - e^{-2\partial/\partial D}) \beta v \right. \\ & \left. + \frac{\partial^2}{\partial u^2} \beta u - \frac{\partial}{\partial u} \beta D \right) P - \text{c.c.} , \end{aligned} \quad (13.23)$$

where c.c. stands for the complex conjugate.

A problem is immediately apparent; this term contains infinite order derivatives and thus the resulting equation of motion for P is not a Fokker–Planck equation. However a careful analysis shows that the exponential term may be truncated to second order in an asymptotic expansion in N^{-1} . As $N \gg 1$ this is a reasonable approximation. The result after truncating is

$$\begin{aligned} \frac{\partial P}{\partial t} = & \{ - \partial_\alpha [\mathcal{E}(t) - \tilde{\kappa}\alpha + gv] - \partial_v (g\alpha D - \gamma v) \\ & - \frac{1}{2} \partial_D [-\gamma_{||}(D + N) - 2g(u\alpha + v\beta)] \\ & + \frac{1}{2} \partial_v^2 2g\alpha v + \frac{1}{2} \partial_{vu}^2 (D + N) \gamma_p \\ & + \frac{1}{2} \partial_D^2 [2\gamma_{||}(D + N) - 4g(u\alpha + v\beta)] + \kappa \bar{n} \partial_{\alpha\beta}^2 + \text{c.c.} \} P , \end{aligned} \quad (13.24)$$

where we have abbreviated the derivatives as

$$\partial_\alpha = \frac{\partial}{\partial \alpha} , \quad (13.25)$$

and so on, and

$$\tilde{\kappa} = \kappa + i\omega_c , \quad (13.26)$$

$$\gamma = \gamma_{\perp} + i\omega_0 , \quad (13.27)$$

$$\mathcal{E}(t) = \mathcal{E} e^{-i\omega_L t} . \quad (13.28)$$

The corresponding stochastic differential equations in a frame rotating at frequency ω_L are

$$\dot{\alpha} = \mathcal{E} - k\alpha + gv + \Gamma_\alpha , \quad (13.29)$$

$$\dot{\beta} = \mathcal{E}^* - k\beta + gu + \Gamma_\beta , \quad (13.30)$$

$$\dot{v} = -\gamma_1 v + g\alpha D + \Gamma_v , \quad (13.31)$$

$$\dot{u} = -\gamma_1^* u + g\beta D + \Gamma_u , \quad (13.32)$$

$$\dot{D} = -\gamma_{||}(D + N) - 2g(\alpha u + \beta v) + \Gamma_D , \quad (13.33)$$

where

$$k = \kappa(1 + i\phi) , \quad (13.34)$$

$$\phi = \frac{\omega_c - \omega_L}{\kappa} , \quad (13.35)$$

$$\gamma_1 = \gamma_{\perp}(1 + i\Delta_1) , \quad (13.36)$$

$$\Delta_1 = \frac{\omega_0 - \omega_L}{\gamma_{\perp}} . \quad (13.37)$$

The noise correlation functions are

$$\langle \Gamma_v(t)\Gamma_v(t') \rangle = 2g\alpha v\delta(t - t') , \quad (13.38)$$

$$\langle \Gamma_u(t)\Gamma_u(t') \rangle = 2g\beta u\delta(t - t') , \quad (13.39)$$

$$\langle \Gamma_D(t)\Gamma_D(t') \rangle = [2\gamma_{||}(D + N) - 4g(u\alpha + v\beta)]\delta(t - t') , \quad (13.40)$$

$$\langle \Gamma_v(t)\Gamma_u(t') \rangle = \gamma_p(D + N)\delta(t - t') , \quad (13.41)$$

$$\langle \Gamma_{\alpha}(t)\Gamma_{\beta}(t') \rangle = 2\kappa\bar{n}\delta(t - t') . \quad (13.42)$$

To proceed we assume $\gamma_{\perp} \gg \kappa$, that is the atoms are assumed to decay much faster than the field variables. This enables the atomic variables to be adiabatically eliminated. It involves finding the steady states for the atomic variables, with the field variables occurring in the atomic equations held constant. The next step is to approximate the correlation functions of the atomic variables by substituting the deterministic steady state of the atomic variables. This means we are using a first-order approximation for the atomic variables to evaluate the diffusion coefficients in the atomic variable equations. Once again the validity of this approximation rests on the condition $N \gg 1$. Effectively we are ignoring quantum fluctuations which are of order $1/N$ or smaller. The resulting solutions for the atomic variables are then substituted into the field equations to give

$$\dot{\alpha} = \mathcal{E} - k\alpha - \frac{g^2\alpha N}{\gamma_1\Pi(\beta\alpha)} + \Gamma(t) , \quad (13.43)$$

and a similar equation for β with complex conjugation and the replacement $\alpha \rightarrow \beta$. The correlation functions are

$$\langle \Gamma(t)\Gamma(t') \rangle = -d\delta(t - t') , \quad (13.44)$$

$$\langle \Gamma^{\dagger}(t)\Gamma(t') \rangle = \bar{\Gamma}\delta(t - t') , \quad (13.45)$$

where

$$d = \frac{2Cx^2\kappa}{(1 + X + \Delta_1^2)^3} \left[(1 - i\Delta_1)^3 f + i\Delta_1 X (1 - f) (1 - i\Delta_1) + \frac{X^2}{2} \right], \quad (13.46)$$

$$\bar{\Gamma} = \frac{2Cx^2\kappa}{(1 + X + \Delta_1^2)^3} \left\{ (1 + \Delta_1^2)(1 - f) + X[2 + \Delta_1^2(1 - f)] + \frac{X^2}{2} \right\} + 2\kappa\bar{n} \quad (13.47)$$

and

$$\Pi(\beta\alpha) = 1 + \frac{\beta\alpha}{(1 + \Delta_1^2)n_0}, \quad (13.48)$$

$$n_0 = \frac{\gamma_{\perp}\gamma_{||}}{4|g|^2}, \quad (13.49)$$

$$C = \frac{g^2 N}{2\kappa\gamma_{\perp}}, \quad (13.50)$$

$$x = \frac{\alpha}{\sqrt{n_0}}; \quad X = \frac{\alpha\beta}{n_0}. \quad (13.51)$$

The corresponding drift vector and diffusion matrices are

$$A(\alpha, \beta) = \begin{pmatrix} \kappa\alpha \left(1 + i\phi + \frac{2C(1 - i\Delta_1)}{1 + X + \Delta_1^2} \right) - \mathcal{E} \\ \kappa\beta \left(1 - i\phi + \frac{2C(1 + i\Delta_1)}{1 + X + \Delta_1^2} \right) - \mathcal{E}^* \end{pmatrix}, \quad (13.52)$$

$$D(\alpha, \beta) = \begin{pmatrix} -d(\alpha, \beta) & \Gamma(\alpha, \beta) \\ \Gamma(\alpha, \beta) & -d^*(\alpha, \beta) \end{pmatrix}. \quad (13.53)$$

The semiclassical steady state equation for the field is

$$\mathcal{E} = \left[\kappa(1 + i\phi) + \frac{g^2 N}{\gamma_{\perp}(1 + i\Delta_1)\Pi^{ss}} \right] \alpha^{ss}, \quad (13.54)$$

where ss means that this variable is evaluated in the steady state. The input intensity and the cavity intensity are thus related by

$$I_p = I \left[\left(1 + \frac{2C}{(1 + \Delta_1^2)\Pi(I)} \right)^2 + \left(\phi - \frac{2C\Delta_1}{(1 + \Delta_1^2)\Pi(I)} \right)^2 \right], \quad (13.55)$$

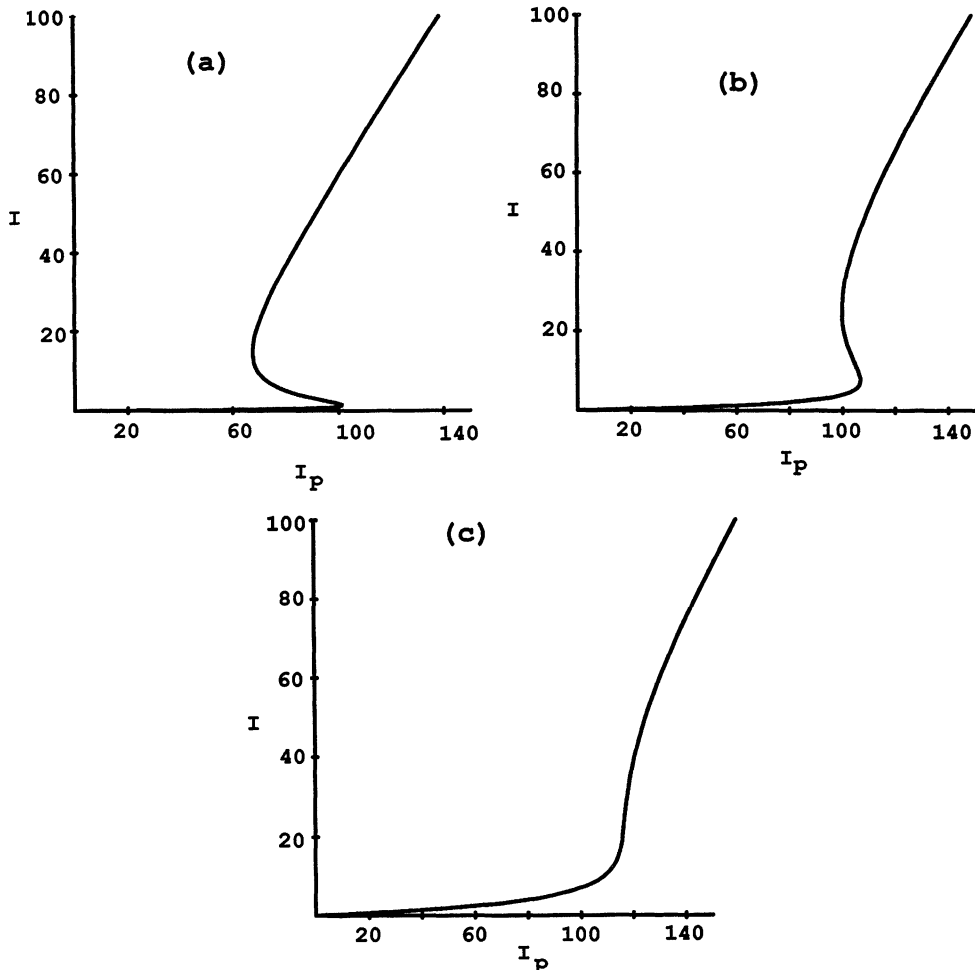


Fig. 13.1. The bistable output intensity as a function of the input intensity for various values of detuning (a) $\Delta = 0$, (b) $\Delta = 2$, (c) $\Delta = 3$. In all cases $C = 9$ and $\phi = 0$

where the scaled pump intensity I_p is given by

$$I_p = \frac{|\mathcal{E}|^2}{\kappa^2 n_0} \quad (13.56)$$

and

$$\Pi(I) = 1 + \frac{I}{1 + \Delta_1^2} . \quad (13.57)$$

The phase θ_0 of the steady state cavity field is shifted from the phase of the external driving field \mathcal{E} (which, for convenience, we take as real)

$$\tan \theta_0 = -\frac{\phi - 2\Delta_1 C/(1 + \Delta_1^2) \Pi(I)}{1 + 2C/(1 + \Delta_1^2) \Pi(I)}. \quad (13.58)$$

Equation (13.55) is the bistable state equation. In general, for a given value of the driving field, the intracavity intensity (and thus the transmitted intensity), can have three solutions. In Fig. 13.1 we demonstrate this bistable behaviour for various parameters. It can be shown that for a high- Q cavity, all the positive slope branches are stable while the negative slope regions are unstable. Thus, the turning points of the state equation are the boundaries of stability, which enables the condition for two stable branches to coexist to be easily determined. This is left as an exercise for the reader.

In Chap. 9 we presented a phenomenological model for dispersive bistability. We may obtain this limit directly from (13.52). Expanding the nonlinear drift equation to first order in $|\alpha|^2$, including nonlinear dispersion, but neglecting nonlinear absorption, we find

$$A(\alpha, \beta) = \left(\bar{k}\alpha + 2\chi\alpha^2\beta - \mathcal{E} \right) + O\left(\frac{|\alpha|^4}{\Delta_1^4 n_0^2}\right), \quad (13.59)$$

where

$$\bar{k} = \kappa \left(1 + i\phi + \frac{2C}{1 + i\Delta_1} \right), \quad (13.60)$$

$$\chi = \frac{iC\Delta_1\kappa}{(1 + \Delta_1^2)^2 n_0} + O\left(\frac{1}{\Delta_1^4}\right). \quad (13.61)$$

The drift vector is identical to that obtained for the nonlinear polarizability model in Chap. 9. The diffusion matrix in this limit is

$$D(\alpha, \beta) = \begin{pmatrix} -2\chi f\alpha^2 & \kappa\bar{n} \\ \kappa\bar{n} & -2\chi^* f\beta^2 \end{pmatrix}. \quad (13.62)$$

In the limit $\bar{n} = 0, f = 1$ this is the same as that obtained for the bistability model of Chap. 9.

13.2 Nondegenerate Four Wave Mixing

We now consider the quantum theory of four wave mixing, in which three cavity field modes interact with a system of N two-level atoms. The theory is an extension of the theory of optical bistability discussed in the previous section. We shall follow the treatment of *Reid and Walls* [13.3].

The Hamiltonian is

$$\mathcal{H} = \sum_{j=1}^5 \mathcal{H}_j , \quad (13.63)$$

$$\mathcal{H}_1 = \hbar \sum_{i=1}^3 \omega_c a_i^\dagger a_i + \frac{1}{2} \hbar \omega_0 \sum_{\mu=1}^N \sigma_\mu^z , \quad (13.64)$$

$$\mathcal{H}_2 = i\hbar \sum_{\mu=1}^N \sigma_\mu^- \sum_{i=1}^3 g a_i^\dagger e^{-ik_i \cdot r_\mu} - \text{h.c.} , \quad (13.65)$$

$$\mathcal{H}_3 = i\hbar (a_1^\dagger \mathcal{E} e^{-i\omega_L t} - \text{h.c.}) , \quad (13.66)$$

$$\mathcal{H}_4 = \sum_{\mu=1}^N (\Gamma \sigma_\mu^+ + \Gamma^\dagger \sigma_\mu^- + \Gamma_p \sigma_\mu^z) , \quad (13.67)$$

$$\mathcal{H}_5 = \Gamma_c a^\dagger + \Gamma_c^\dagger a . \quad (13.68)$$

The operator a_1 is the annihilation operator for the pump mode at frequency ω_1 , while a_2 and a_3 are annihilation operators for cavity modes at frequencies ω_1 and ω_2 which represent the side-band cavity modes, either side of the pump frequency, coupled by the nonlinearity. That is to say, $2\omega_1 = \omega_2 + \omega_3$ (and $\mathbf{k}_1 = \mathbf{k}_2 + \mathbf{k}_3$). We write the two side band frequencies as

$$\omega_2 = \omega_1 - \varepsilon , \quad (13.69)$$

$$\omega_3 = \omega_1 + \varepsilon , \quad (13.70)$$

Note that the cavity field at frequency ω_1 is driven by a coherent input at frequency ω_L . We will assume that the cavity detuning $\omega_1 - \omega_L$ is much smaller than the frequency separation of adjacent cavity modes, ε , so that only the mode at frequency ω_1 is effectively pumped.

We now proceed in a way similar to the previous treatment of optical bistability in the last section. The problem is simplified by assuming that the pump mode a_1 will be much stronger than the modes a_2, a_3 . We are thus interested in a limit where the strong pump mode is treated correctly to all orders, describing the saturation of the medium, while weak fields are retained to first order only. One may derive an equation of motion for the distribution function $P(\alpha)$ neglecting terms involving summations such as $\exp(i\Delta k \cdot r_\mu)$ over all the atoms. These terms are small compared to the phase or frequency matched terms for which $\Delta k = 2k_1 - k_2 - k_3 = 0$.

The atomic polarisation v may be expected to oscillate at the three dominant frequencies $\omega_L, \omega_L \pm \varepsilon$. Thus we expand the polarisation and total field as

$$\alpha = \alpha_1 e^{-i\omega_L t} + \alpha_2 e^{-i(\omega_L - \varepsilon)t} + \alpha_3 e^{-i(\omega_L + \varepsilon)t} , \quad (13.71)$$

$$v = v_1 e^{-i\omega_L t} + v_2 e^{-i(\omega_L - \varepsilon)t} + v_3 e^{-i(\omega_L + \varepsilon)t} , \quad (13.72)$$

Inspection of the equation for the inversion (equation [13.33]) shows that D will oscillate at the frequencies $0, \pm \varepsilon$ thus,

$$D = D_1 + D_2 e^{-i\epsilon t} + D_3 e^{i\epsilon t}. \quad (13.73)$$

The c-number Langevin equations for the nine variables $((\alpha_i), (v_i), (D_i))$ are then readily obtained by substituting (13.71, 72) into (13.29–33), for the single mode case and matching terms of the same frequency, retaining terms in $\alpha_2, \alpha_3, v_2, v_3, D_2, D_3$ to first order only. Finally we assume the high- Q limit $\kappa \ll \gamma_{\perp}, \gamma_{||}$ and adiabatically eliminate the atomic variables. The resulting field equations are

$$\dot{\alpha}_1 = \mathcal{E} - \kappa(1 + i\phi)\alpha_1 - \frac{2C\kappa\alpha_1}{(1 + i\Delta_1)\Pi(I)} + F_{\alpha_1}(t), \quad (13.74)$$

$$\dot{\alpha}_2 = -\kappa\gamma(\delta)\alpha_2 + \kappa\chi(\delta)\beta_3 e^{2i\theta_0} + F_{\alpha_2}(t), \quad (13.75)$$

$$\dot{\alpha}_3 = -\kappa\gamma(-\delta)\alpha_3 + \kappa\chi(-\delta)\beta_2 e^{2i\theta_0} + F_{\alpha_3}(t), \quad (13.76)$$

and similar equations for the dagged variables. The parameter Π is defined by

$$\Pi(I) = 1 + \frac{I}{1 + \Delta_1^2}, \quad (13.77)$$

with $I = |\alpha_1^{ss}|^2/n_0$, which is the steady state intracavity pump intensity in units of n_0 . The phase θ_0 is given by (13.58). Other parameters are

$$\phi = (\omega_1 - \omega_L)/\kappa, \quad (13.78)$$

$$\gamma_j = \gamma_{\perp}(1 + i\Delta_j), \quad (13.79)$$

$$\gamma = \gamma_{||}(1 - i\delta), \quad (13.80)$$

$$\Delta_1 = (\omega_0 - \omega_L)/\gamma_{\perp}, \quad (13.81)$$

$$\Delta_2 = \Delta_1 + 2\delta f, \quad (13.82)$$

$$\Delta_3 = \Delta_1 - 2\delta f, \quad (13.83)$$

$$\delta = \varepsilon/\gamma_{||}. \quad (13.84)$$

A schematic representation of the various frequency parameters is given in Fig. 13.2. The nonzero noise correlation functions are

$$\langle F_{\alpha_2}(t)F_{\alpha_3}(t') \rangle = \kappa R e^{2i\theta_0}\delta(t - t'), \quad (13.85)$$

$$\langle F_{\beta_2}(t)F_{\beta_3}(t') \rangle = \kappa R^* e^{-2i\theta_0}\delta(t - t'), \quad (13.86)$$

$$\langle F_{\alpha_2}(t)F_{\beta_2}(t') \rangle = \langle F_{\alpha_3}(t)F_{\beta_3}(t') \rangle = \kappa \Lambda \delta(t - t'). \quad (13.87)$$

The explicit expressions for the coupling constants $\gamma(\delta), \chi(\delta), R, \Lambda$ are quite complicated and we do not give them here. They may be found in the original paper by *Reid* and *Walls*.

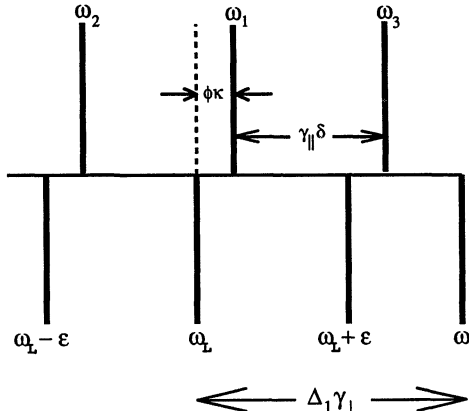


Fig. 13.2. A schematic representation of the frequency parameters for four wave mixing

To discuss the physical content of these equations we write

$$\gamma(\delta) = \gamma_R(\delta) + i\gamma_I(\delta) , \quad (13.88)$$

$$\chi(\delta) = \chi_R(\delta) + i\chi_I(\delta) . \quad (13.89)$$

The function $\gamma_R(\delta)$ is the loss/gain coefficient of the mode α_2 , while $\gamma_I(\delta)$ represents the dispersive response of this mode. The function $\chi(\delta)$ is the semiclassical coupling constant, giving rise to the generation of the field α_2 in the presence of the pump mode α_1 and a weak field α_3 . What we are especially interested in here is the squeezing spectrum of the transmitted field.

Squeezing is observed by homodyne detection of a linear superposition of the output fields at frequencies $\omega_L \pm \epsilon$. These output side-band modes are represented by the field operators $a_{2,\text{out}}, a_{3,\text{out}}$. The homodyne detection is performed with a local oscillator with a complex amplitude $\mathcal{E}_{\text{LO}} = \mathcal{E} e^{i\theta_{\text{LO}}}$ where θ_{LO} is the phase-shift of the local oscillator with respect to the external driving field at frequency ω_L . The spectral components of the output fields are determined by the linearised drift and diffusion matrices for the internal field amplitudes (Chap. 7). The linearisation is defined with respect to the steady state solutions of the deterministic part of the stochastic differential equations for these fields. The steady state solution for the pump mode is given by the optical bistability state equation (13.54). The steady state solution for the side-band fields are

$$\alpha_2^{\text{ss}} = (\beta_2)^{\text{ss}} = \alpha_3^{\text{ss}} = (\beta_3)^{\text{ss}} = 0 . \quad (13.90)$$

The stability of these solutions may be determined in the usual way, by calculating the eigenvalues of the linearised drift matrix. For the degenerate situation $\delta = 0$, the stability criteria reduce to $\gamma_R(0) > 0$ and $|\gamma(0)| > |\chi(0)|$. The

first of these conditions is always satisfied, indicating that the medium is absorbing at the pump frequency. However, the second condition indicates that as the degenerate coupling coefficient increases unstable regions become possible.

The spectral matrix for the field is defined by

$$S_{ij}(\omega, \delta) = \int_{-\infty}^{\infty} e^{i\omega t} \langle \beta_i(t) \beta_j(0) \rangle dt , \quad (i, j = 1, \dots, 4) \quad (13.91)$$

where $\beta = (\alpha_2, \alpha_2^+, \alpha_3, \alpha_3^+)$. For simplicity, we only give the results for $\omega = 0$, i.e., at the local oscillator frequency,

$$S_{12}(\delta) = \frac{\Lambda(|\gamma(-\delta)|^2 + |\chi(\delta)|^2) + (R\gamma^*(-\delta)\chi^*(\delta) + c.c.)}{\kappa|\gamma(\delta)\gamma^*(-\delta) - \chi(\delta)\chi^*(-\delta)|^2} \quad (13.92)$$

$$= S_{21}(\delta) , \quad (13.93)$$

$$S_{34}(\delta) = S_{12}(-\delta) = S_{43}(\delta) , \quad (13.94)$$

$$S_{13}(\delta) = e^{2i\theta_0} \bar{S}_{13} = S_{31}(\delta) , \quad (13.95)$$

$$\begin{aligned} \bar{S}_{13}(\delta) &= \frac{\Lambda(\gamma^*(-\delta)\chi(-\delta) + \gamma^*(\delta)\chi(\delta))}{\kappa|\gamma(\delta)\gamma^*(-\delta) - \chi(\delta)\chi^*(-\delta)|^2} \\ &\quad + \frac{R\gamma^*(\delta)\gamma(-\delta) + R^*\chi(\delta)\chi(-\delta)}{\kappa|\gamma(\delta)\gamma^*(-\delta) - \chi(\delta)\chi^*(-\delta)|^2} . \end{aligned} \quad (13.96)$$

The elements $S_{12}(\delta)$ and $S_{34}(\delta)$ determine the intensity fluctuations in the detected field, while $S_{13}(\delta)$ determines the phase dependent properties (i.e., squeezing) of the detected field.

The quadrature phase fluctuation spectrum of the observed field at $\omega = 0$ is

$$V(\theta) = 2\kappa[S_{12}(\delta) + S_{34}(\delta) + e^{-2i\theta}\bar{S}_{13}(\delta) + e^{2i\theta}\bar{S}_{13}^*(\delta)] + 1 , \quad (13.97)$$

where $\theta = \theta_{LO} - \theta_0$, and we have assumed the optimal situation of single-port cavity. Squeezing occurs if $V(\theta) < 1$.

It is now possible to give a physical interpretation of the function Λ . Consider decoupling the side-bands so that $\chi(\delta) = R = 0$. The observed quadrature phase fluctuations contain an incoherent component $S_{12}(\delta)$, which we shall refer to as the transmitted intensity. When the side-bands are decoupled we find for C sufficiently small,

$$S_{21}(\delta) \approx \frac{\Lambda}{\kappa} , \quad (13.98)$$

thus Λ may be interpreted as the transmitted fluorescent spectrum for the atoms when the side-bands are not coupled into the dynamics. In this limit $V(\theta)$ is independent of θ . In order to observe squeezing we must find a parameter regime where the nonlinear phase-sensitive coupling $\chi(\delta)$ and R dominate the absorption term $\gamma_R(\delta)$ and the fluorescence term Λ . The problem, however, is that

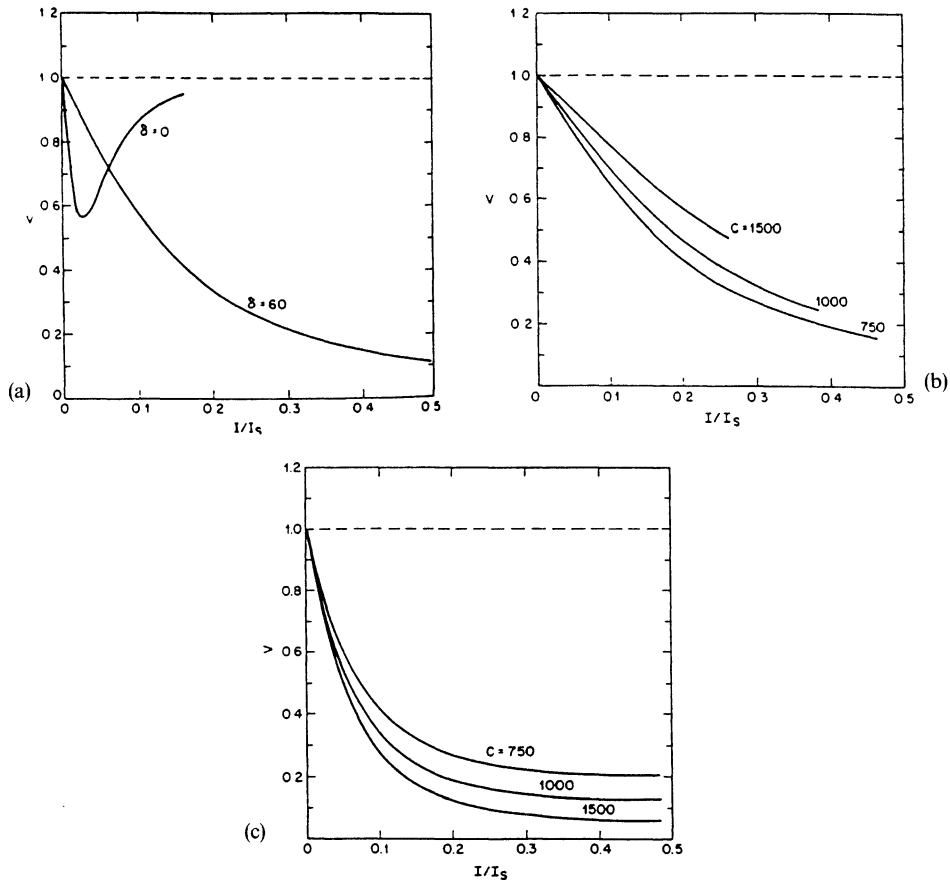


Fig. 13.3. The variance V for the minimum noise quadrature at resonance ($\omega = 0$), versus the normalised pump intensity. (a) $C = 1000$, $\Delta = -300$, $\delta = 0$ (degenerate case), $\delta = 60$. (b) $\Delta = -250$, $\delta = 60$, (c) $\Delta = -600$, $\delta = 60$. From JOSA B 4 1453 (1987)

attempts to increase $\chi(\delta)$ and R will also increase Λ as the atomic system becomes saturated. This problem is particularly acute in the degenerate case where $\delta = 0$ and squeezing can only be obtained for high atomic detunings ($\Delta_1 > 10^3$) and thus high values for C ($2C > \Delta_1$) and high intensities ($I > \Delta_1$), to attain sufficient $\chi(0)$.

Nondegenerate operation, however, offers the possibility of moving away from the fluorescence peak of Λ . What really matters then is the relative size of Λ and χ . Thus one may hope to totally saturate the atoms, achieving a high χ , yet avoid the dephasing associated with spontaneous emission by increasing δ . As a consequence squeezing becomes possible at much more reasonable detunings and a wider range of parameters generally.

In Figs 13.3a–c we show the squeezing function $V(0)$ plotted versus the pump intensity normalised to the saturation intensity, $I_s = (1 + \Delta_1^2)I_{so}$ where I_{so}

is the line-center saturation intensity for different values of atomic detuning, side-band detuning δ , and atomic cooperativity C . The results shown are, in fact, for a ring cavity. In Fig. 13.3a the major advantage of non-degenerate operation is clearly evident.

Values of Δ greater than 400 result in squeezing that increases with increasing values of C (Fig. 13.3c). In this region the reduced variance is simply limited by the nonlinear gain, and the absorptive loss is negligible because of the large detuning. The variance flattens at $I/I_s > 0.2$ because the nonlinear gain begins to saturate. This region thus represents the best squeezing, but it is difficult to achieve due to pump intensity limitations.

13.3 Experimental Results

The first [13.4] observation of squeezed states of light was made by Slusher and coworkers in 1985, using the atomic system described in the previous section.

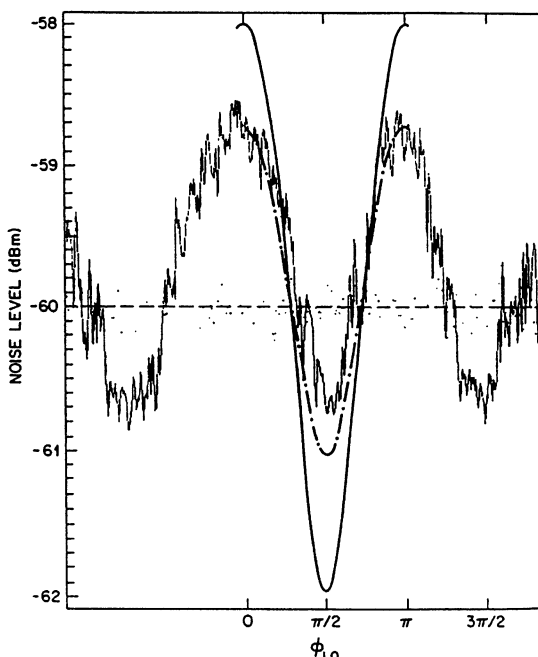


Fig. 13.4. The measured quadrature phase noise level compared with the theoretical prediction, as a function of local oscillator phase ϕ_{LO} , $\Delta = -400$, $\delta = 60$, $C = 1000$, $I/I_s = 0.056$. The solid curve is the theoretical prediction for these parameters. The dashed curve represents the theoretical prediction when account is taken of the detection inefficiencies and amplifier noise. From JOSA B 4 1453 (1987)

The atomic system was a beam of sodium atoms. The pump frequency was chosen at 1.5 GHz to the high frequency side of the D₂ Na resonance. In fact, the pump field did not drive a cavity mode, but was passed directly through the atomic beam at a slight angle to the cavity defining the side-band modes and reflected back through the atomic beam in the opposite direction. However, it was tuned to a frequency that is exactly centred between the two cavity side-band modes. This modification does not significantly alter the theoretical treatment given in the previous section. The side-band modes were at ± 595 MHz from the pump laser frequency. The squeezed light was detected using balanced homodyne detection, with the local oscillator being a 3 mW portion of the pump field.

A comparison of the experimental results and the theory is presented in Fig. 13.4 [13.5]. The dashed line is the average signal produced with the squeezing cavity blocked, and thus forms the shot-noise limit. The smooth solid curve in Fig. 13.4 is the predicted result for the parameters of this experiment. When the measured efficiency and amplifier noise are included to convert the theoretical predictions to the expected observed signal, the dashed curve, there is reasonable agreement between theory and experiment. The noise minima reach 0.7 dB or 15% below vacuum level, instead of the predicted 1.05 dB. Thus experimentally the results at small I/I_s (< 0.1) and large Δ (> 300) agree well with the predictions of the theory.

Exercises

13.1 A laser may be modelled by the master equation in (13.7) by setting $\mathcal{E} = 0$ and replacing the atomic damping term by

$$\begin{aligned}\mathcal{L}_4(\rho) = & \sum_{\mu=1}^N \frac{\gamma_{||}}{2} ([\sigma_\mu^-, \rho \sigma_\mu^+] + [\sigma_\mu^- \rho, \sigma_\mu^+]) \\ & + \frac{\omega_{12}}{2} ([\sigma_\mu^+, \rho \sigma_\mu^-] + [\sigma_\mu^+ \rho, \sigma_\mu^-]) \\ & + \frac{\gamma_p}{4} ([\sigma_\mu^z, \rho \sigma_\mu^z] + [\sigma_\mu^z \rho, \sigma_\mu^z]) ,\end{aligned}\tag{13.99}$$

where ω_{12} is the incoherent atomic pump rate.

(a) Using the characteristic function method derive the following Fokker–Planck equation for the P representation,

$$\begin{aligned} \frac{\partial P}{\partial t} = & (\{ -\partial_\alpha(-\tilde{\kappa}\alpha + gv) - \partial_v(g\alpha D - \gamma_\perp v) \\ & - \frac{1}{2}\partial_D[-\gamma_{||}(D - D_0) - 2g(u\alpha + v\beta)] \\ & + \frac{1}{2}\partial_v^2 2g\alpha v + \frac{1}{2}\partial_{vu}^2(N\omega_{12} + (D + N))\gamma_p \\ & + \frac{1}{2}\partial_D^2[\omega_{12}(N - D) + \gamma_{||}(N + D) - 2g(u\alpha + v\beta)] \\ & + 2\kappa\bar{n}\partial_{\alpha\beta}^2\} + \text{c.c.})P , \end{aligned} \quad (13.100)$$

where

$$D_0 = N \frac{\omega_{12} - \gamma_{||}}{\omega_{12} + \gamma_{||}} \quad (13.101)$$

- (b) By considering the deterministic equations of motion show that D_0 is the steady state atomic inversion and thus laser action requires $D_0 > 0$.
(c) Show that the steady state field amplitude obeys the equation

$$x \left(1 - \frac{C_1}{1 + |x|^2} \right) = 0 , \quad (13.102)$$

where $x = \alpha/\sqrt{n_0}$ and $C_1 = 2g^2 D_0 / \kappa\gamma_\perp$.

- (d) Define $I = |x|^2$ as the cavity intensity. Show that the stable stationary solutions are

$$I = \begin{cases} 0 & \text{if } C_1 < 1 \\ C_1 - 1 & \text{if } C_1 > 1 \end{cases} . \quad (13.103)$$

14. Bells Inequalities in Quantum Optics

The early days of quantum mechanics were characterised by debates over the applicability of established classical concepts, such as position and momentum, to the new formulation of mechanics. The issues became quite distinct in the protracted exchange between A. Einstein and N. Bohr, culminating in the paper of *Einstein, Podolsky and Rosen* (EPR) in 1935 [14.1]. Bohr, in his response to this paper, [14.2] expanded upon his concept of complementarity and showed that the EPR argument did not establish the incompleteness of quantum mechanics, as EPR had claimed, but rather highlighted the inapplicability of classical modes of description in the quantum domain. A. Einstein, however, did not accept this position and the two sides of the debate remained unreconciled, while most physicists generally believed that N. Bohr's argument carried the day.

Thus the matter rested until 1964 when J.S. Bell opened up the possibility of directly testing the consequences of the EPR premises. We will discuss the EPR argument and the analysis of Bell in the context of correlated photon states.

14.1 The Einstein–Podolsky–Rosen (EPR) Argument

The essential step in the EPR argument is to introduce correlated pure states of two particles (or photons) of the form

$$|\Psi\rangle = \sum_n |a_n\rangle_1 \otimes |b_n\rangle_2 , \quad (14.1)$$

where $\{|a_n\rangle_1\}$ and $\{|b_n\rangle_2\}$ are ortho-normal eigenstates for some operators \hat{A}_1 and \hat{B}_2 of particles 1 and 2, respectively. The correlations between the particles persist even if in the course of the experiment the particles become spatially separated after the interaction responsible for the correlated state.

Now suppose one were to measure the operator \hat{A}_1 on particle one long after the interaction between the particles has ended, and the two particles are far apart. If the result is some eigenvalue a_n , particle 1 must thence-forth be considered to be in the state $|a_n\rangle_1$, while particle 2 must be in the state $|b_n\rangle_2$. As the state of particle 2 is now an eigenstate of \hat{B}_2 we can predict with probability

one that the physical quantity represented by \hat{B}_2 if measured will give the result b_n . Thus we can predict the value of this physical quantity for particle 2 without in any way interacting with it.

Suppose, however, that instead of measuring \hat{A}_1 on particle 1 we measured some other quantity, \hat{C}_1 , with eigenstates $|c_n\rangle_1$. We then rewrite the state in (14.1) as

$$|\Psi\rangle = \sum_n |c_n\rangle_1 \otimes |d_n\rangle_2 , \quad (14.2)$$

where $|d_n\rangle_2$ is an eigenstate of some other operator \hat{D}_2 for particle 2. If the result c_n is obtained for the measurement on particle 1, particle 2 must be in the state $|d_n\rangle_2$ for which a measurement of \hat{D}_2 must give the result d_n . Thus depending on what we choose to measure on particle 1 the state of particle 2 after the measurement, can be an eigenstate of two quite different operators. This is another example of the measurement ambiguity discussed in the previous chapter. However, the EPR argument now raises one very important question. Is it possible that the two operators on particle 2, \hat{B}_2 and \hat{D}_2 , do not commute? If this were the case the EPR argument establishes that, depending on what is measured on particle 1, we can predict with certainty the values of physical quantities, represented by noncommuting operators without in anyway interacting with this particle. By explicit construction *Einstein, Podolsky and Rosen* showed that this is indeed possible.

EPR claimed that “if without in anyway disturbing a system, we can predict with certainty (i.e., with probability equal to unity), the value of a physical quantity, then there exists an element of physical reality corresponding to that quantity”.

Assuming that the wave function does contain a complete description of the two-particle system it would seem that the argument of EPR establishes that it is possible to assign two different states ($|b_n\rangle_2$ and $|d_n\rangle_2$) to the same reality. However, in the language of EPR, two physical quantities represented by operators which do not commute cannot have simultaneous reality. The conclusion of EPR was that the quantum mechanical description of physical reality given by the wave function is not complete.

14.2 Bell Inequalities and the Aspect Experiment

Were one to adopt the conclusion of EPR it would seem necessary to search for a more complete physical theory than quantum mechanics. To obtain such a theory, quantum mechanics should be supplemented by additional, perhaps inaccessible, variables. As *Bell* [14.3] showed, attempting to complete the theory in this way and maintain the locality condition (that measurements on particle 1 carried out when the particles are spatially separated should have no effect on

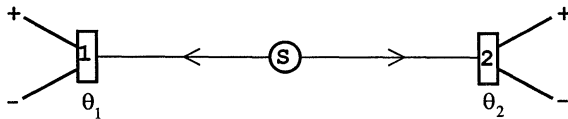


Fig. 14.1. Schematic representation of the experiment of Aspect et al. [14.5] to test quantum mechanics against the Bell inequality. S is a source of two polarised photons. 1 and 2 label polarisation analysers, with orthogonal output channels labelled + and -. The polarisation analysers are set at angles θ_1, θ_2

particle 2) leads to statistical predictions which differ from those of standard quantum theory.

To elucidate *Bell's* argument we consider a system in which correlated photon polarisation states are produced. Such a system is the $(J = 0) \rightarrow (J = 1) \rightarrow (J = 0)$ cascade two-photon transition in calcium-40 (Fig. 14.1). The two photons are emitted in opposite directions (by conservation of momentum) with correlated polarisation states. Each photon passes through separate polarisation analysers, emerging in either the horizontal (+) channel, or the vertical channel (−) of each analyser. Initially let us assume that the horizontal polarisation is chosen to be orthogonal to the plane of the experiment and that both analysers are so aligned. However, we are free to rotate the polarisers in the plane orthogonal to the propagation direction of the photons. We follow the treatment of *Reid and Walls* [14.4].

Let $a_{\pm}(b_{\pm})$ be the annihilation operator for the horizontally (+) or vertically (−) polarised mode for the field travelling to analyser 1 (labelled 1) or analyser 2 (labelled 2). The state of the two photons may be written as

$$|\psi\rangle = \frac{1}{\sqrt{2}}(a_+^\dagger b_+^\dagger + a_-^\dagger b_-^\dagger)|0\rangle , \quad (14.3)$$

where $|0\rangle$ is the vacuum state. Using the notation $|n_1, n_2, n_3, n_4\rangle$ to denote n_1 photons in mode a_+ , n_2 photons in mode a_- , n_3 photons in mode b_+ and n_4 photons in mode b_- , the state may be expressed as

$$|\psi\rangle = \frac{1}{\sqrt{2}}(|1, 0, 1, 0\rangle + |0, 1, 0, 1\rangle) . \quad (14.4)$$

If the photon in analyser 1 is detected in the (+) channel, the state of the photon directed towards 2 must be polarised in the horizontal direction. This correlation is thus precisely of the kind required for the EPR experiment.

We are free to measure the polarisation in any direction by rotating the analysers through the angles θ_1 and θ_2 for detector 1 and 2, respectively. The detected modes in this case are orthogonal transformations of the modes

a_{\pm} and b_{\pm} ;

$$c_+ = a_+ \cos \theta_1 + a_- \sin \theta_1 , \quad (14.5a)$$

$$c_- = -a_+ \sin \theta_1 + a_- \cos \theta_1 , \quad (14.5b)$$

$$d_+ = b_+ \cos \theta_2 + b_- \sin \theta_2 , \quad (14.5c)$$

$$d_- = -b_+ \sin \theta_2 + b_- \cos \theta_2 . \quad (14.5d)$$

The detectors placed after the polarisers measure the intensities $\langle I_1^{\pm} \rangle$ and $\langle I_2^{\pm} \rangle$, while the correlators measure $\langle I_1^+ I_2^+ \rangle$, etc. In fact, for the two-photon state $\langle I_i^{\pm} \rangle = P_i^{\pm}$, is the probability for one count in the + or - channel of detector i . Of course, these moments depend on θ_1 and θ_2 . Let us further suppose that in a complete theory these functions also depend on the variable λ which remains hidden from direct determination and for which only a statistical description is available. This variable is distributed according to some density $\rho(\lambda)$. In general, we may then write

$$\langle I_1^{\pm} I_2^{\pm} \rangle_{\theta_1 \theta_2} = \int \rho(\lambda) I_1^{\pm}(\lambda, \theta_1, \theta_2) I_2^{\pm}(\lambda, \theta_1, \theta_2) d\lambda , \quad (14.6)$$

where I_1^+ denotes the expected intensity at detector 1 given a value for λ , namely

$$I_1^+(\lambda, \theta_1, \theta_2) = \int I_1^+ \rho(I_1^+ | \lambda, \theta_1, \theta_2) dI_1^+ . \quad (14.7)$$

It is reasonable to assume, as in EPR, that for a given value of λ the results at 1 cannot depend on the angle θ_2 chosen at 2, (and conversely). This is the “locality assumption”, it is formally represented by

$$I_1^{\pm}(\lambda, \theta_1, \theta_2) = I_1^{\pm}(\lambda, \theta_1) , \quad (14.8a)$$

$$I_2^{\pm}(\lambda, \theta_1, \theta_2) = I_2^{\pm}(\lambda, \theta_2) . \quad (14.8b)$$

Consider the following correlation functions:

$$E(\theta_1, \theta_2) = \frac{\langle (I_1^+ - I_1^-)(I_2^+ - I_2^-) \rangle}{\langle (I_1^+ + I_1^-)(I_2^+ + I_2^-) \rangle} . \quad (14.9)$$

In terms of the detected mode operators this may be written in the form

$$E(\theta_1, \theta_2) = \frac{\langle : (c_+^\dagger c_+ - c_-^\dagger c_-) (d_+^\dagger d_+ - d_-^\dagger d_-) : \rangle}{\langle : (c_+^\dagger c_+ + c_-^\dagger c_-) (d_+^\dagger d_+ + d_-^\dagger d_-) : \rangle} \quad (14.10)$$

where $: :$ denotes normal ordering.

Assuming a local hidden variable theory we may write

$$E(\theta_1, \theta_2) = N^{-1} \int f(\lambda) S_1(\lambda, \theta_1) S_2(\lambda, \theta_2) d\lambda , \quad (14.11)$$

where

$$S_1(\lambda, \theta_1) = \frac{I_1^+(\lambda, \theta_1) - I_1^-(\lambda, \theta_1)}{I_1(\lambda)} , \quad (14.12)$$

$$S_2(\lambda, \theta_2) = \frac{I_2^+(\lambda, \theta_2) - I_2^-(\lambda, \theta_2)}{I_2(\lambda)} , \quad (14.13)$$

$$f(\lambda) = \rho(\lambda)I_1(\lambda)I_2(\lambda) \quad (14.14)$$

with

$$I_1(\lambda) = I_1^+(\lambda, \theta_1) + I_1^-(\lambda, \theta_2) , \quad (14.15a)$$

$$I_2(\lambda) = I_2^+(\lambda, \theta_2) + I_2^-(\lambda, \theta_1) . \quad (14.15b)$$

The latter equations correspond to the intensity of light measured at 1 or 2 with the polarisers removed. The normalisation N is

$$N = \int f(\lambda) d\lambda . \quad (14.16)$$

The functions $|S_1(\lambda, \theta_1)|$ and $|S_2(\lambda, \theta_2)|$ are bounded by unity:

$$|S_1(\lambda, \theta_1)| \leq 1 , \quad (14.17a)$$

$$|S_2(\lambda, \theta_2)| \leq 1 . \quad (14.17b)$$

To obtain a testable statistical quantity we need to consider how $E(\theta_1, \theta_2)$ changes as the orientation of the polarisers are changed. With this in mind, consider $E(\theta_1, \theta_2) - E(\theta_1, \theta'_2)$. This quantity may be expressed as

$$\begin{aligned} E(\theta_1, \theta_2) - E(\theta_1, \theta'_2) &= N^{-1} \int d\lambda f(\lambda) S_1(\lambda, \theta_1) S_2(\lambda, \theta_2) [1 \pm S_1(\lambda, \theta'_1) S_2(\lambda, \theta'_2)] \\ &\quad - N^{-1} \int d\lambda f(\lambda) S_1(\lambda, \theta_1) S_2(\lambda, \theta'_2) \\ &\quad \times [1 \pm S_1(\lambda, \theta'_1) S_2(\lambda, \theta_2)] . \end{aligned} \quad (14.18)$$

Then using (14.17a and b)

$$\begin{aligned} |E(\theta_1, \theta_2) - E(\theta_1, \theta'_2)| &\leq N^{-1} \int d\lambda f(\lambda) [1 \pm S_1(\lambda, \theta'_1) S_2(\lambda, \theta'_2)] \\ &\quad + N^{-1} \int d\lambda f(\lambda) [1 \pm S_1(\lambda, \theta'_1) S_2(\lambda, \theta_2)] \\ &= 2 \pm [E(\theta'_1, \theta'_2) + E(\theta'_1, \theta_2)] . \end{aligned}$$

Finally, we obtain the Bell inequality

$$|B| \leq 2 , \quad (14.19)$$

where

$$B = E(\theta_1, \theta_2) - E(\theta_1, \theta'_2) + E(\theta'_1, \theta'_2) + E(\theta'_1, \theta_2) .$$

This particular Bell inequality is known as the Clauser–Horne–Shimony–Holt (CHSH) inequality.

As we shall see, there are states of the field which violate the inequality equation (14.19) [for example, the state given in (14.4)]. We note firstly, however, that if the state of the field can be represented by a positive, normalisable Glauber–Sudarshan P -representation no violation of this inequality is possible. Let $\mathbf{a} = (\alpha_+, \alpha_-, \beta_+, \beta_-)$ be the c-number corresponding to the modes a_{\pm}, b_{\pm} . If we define the following ‘transformation’ variables for the modes c_{\pm}, d_{\pm} ,

$$\begin{aligned}\gamma_+ &= \alpha_+ \cos \theta_1 + \alpha_- \sin \theta_1, & \delta_+ &= \beta_+ \cos \theta_2 + \beta_- \sin \theta_2, \\ \gamma_- &= -\alpha_+ \sin \theta_1 + \alpha_- \cos \theta_1, & \delta_- &= -\beta_+ \sin \theta_2 + \beta_- \cos \theta_2,\end{aligned}\quad (14.20)$$

the correlation function $E(\theta_1, \theta_2)$ becomes

$$E(\theta_1, \theta_2) = N^{-1} \int P(\mathbf{a}) (|\gamma_+|^2 - |\gamma_-|^2) (|\delta_+|^2 - |\delta_-|^2) d^2 \mathbf{a} \quad (14.21)$$

with

$$N = \int P(\mathbf{a}) (|\gamma_+|^2 + |\gamma_-|^2) (|\delta_+|^2 + |\delta_-|^2) d^2 \mathbf{a}.$$

Recalling that the transformations in (14.20) are orthogonal we note that

$$|\gamma_+|^2 + |\gamma_-|^2 = |\alpha_+|^2 + |\alpha_-|^2 \quad \text{and} \quad |\delta_+|^2 + |\delta_-|^2 = |\beta_+|^2 + |\beta_-|^2$$

the normalisation may be written

$$N = \int P(\mathbf{a}) (|\alpha_+|^2 + |\alpha_-|^2) (|\beta_+|^2 + |\beta_-|^2) d^2 \mathbf{a}, \quad (14.22)$$

where the integrand does not depend on θ_1 or θ_2 . Then

$$E(\theta_1, \theta_2) = N^{-1} \int P(\mathbf{a}) (|\alpha_+|^2 + |\alpha_-|^2) (|\beta_+|^2 + |\beta_-|^2) S(\gamma) S(\delta), \quad (14.23)$$

where

$$S(\gamma) = \frac{|\gamma_+|^2 - |\gamma_-|^2}{|\alpha_+|^2 + |\alpha_-|^2} \quad (14.24)$$

and

$$S(\delta) = \frac{|\delta_+|^2 - |\delta_-|^2}{|\beta_+|^2 + |\beta_-|^2}. \quad (14.25)$$

As $S(\gamma)$ is a function of θ_1 and not θ_2 while $S(\delta)$ is a function of θ_2 and not θ_1 , the Glauber–Sudarshan representation is local. It then follows immediately that provided $P(\mathbf{a})$ is positive and normalisable, the Bell inequality in (14.19) must hold.

The correlation function $E(\theta_1, \theta_2)$ may be evaluated directly for the state in (14.4) using the normally-ordered moment in (14.9). One finds

$$E(\theta_1, \theta_2) = \cos 2\psi, \quad (14.26)$$

where

$$\psi \equiv \theta_1 - \theta_2 .$$

If we choose

$$\psi = \theta_2 - \theta_1 = \theta'_1 - \theta_2 = \theta'_1 - \theta'_2 = \frac{1}{3}(\theta_1 - \theta'_2) ,$$

one finds

$$B = 3 \cos 2\psi - \cos 6\psi . \quad (14.27)$$

When $\psi = 22.5^\circ$, $B = 2\sqrt{2}$ showing a clear violation of the Bell inequality $|B| \leq 2$.

This violation has convincingly been demonstrated in the experiment of Aspect [14.5]. In this experiment the polarisation analysers were essentially beam splitters with polarisation-dependent transmittivity. Ideally, one would like to have the transmittivity (T^+) for the modes a_+ and b_+ equal to one, and the reflectivity (R^-) for the modes a_- and b_- also equal to one. However, in the experiment the measured values were $T_1^+ = R_1^- = 0.950$, $T_1^- = R_1^+ = 0.007$ and $T_2^+ = T_2^- = 0.930$, $T_2^- = R_2^+ = 0.007$.

The expression for $E(\theta_1, \theta_2)$ is then modified:

$$E(\theta_1, \theta_2) = F \frac{(T_1^+ - T_1^-)(T_2^+ - T_2^-)}{(T_1^+ + T_1^-)(T_2^+ + T_2^-)} \cos 2\psi , \quad (14.28)$$

where F is a geometrical factor accounting for finite solid angles of detection. In this experiment $F = 0.984$, and quantum mechanics would give for $\psi = 22.5^\circ$, $B = 2.7$.

The observed value was 2.697 ± 0.015 , in quite good agreement with quantum theory and a clear violation of the Bell inequality. In Fig. 14.2 is shown

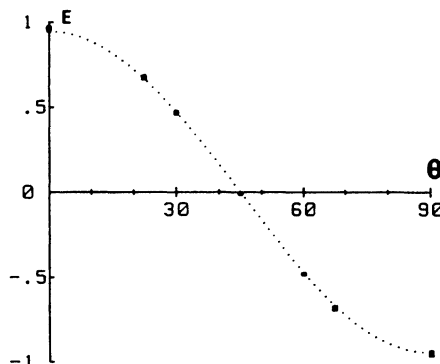


Fig. 14.2. Correlation of polarisations as a function of the relative angle of the polarisation analysers. The indicated errors are ± 2 standard deviations. The dotted curve is the quantum-mechanical prediction for the experiment. For ideal polarisers the curves would reach the values ± 1 . (From Aspect et al. Phys. Rev. Letts. **49**, 92 (1982))

a plot of the theoretical and experimental results as a function of ψ . The agreement with quantum mechanics is better than 1%. It would appear in the light of this experiment that realistic local theories for completing quantum mechanics are untenable.

14.3 Violations of Bell's Inequalities Using a Parametric Amplifier Source

The Bell inequality presented in (14.19) is only one of a large class of inequalities violated by quantum mechanics. Another inequality has recently been tested by *Ou and Mandel* [14.6] based on an experiment first suggested by *Reid and Walls* [14.4]. It has now been realised in a number of configurations [14.7, 8]. We shall discuss the *Ou and Mandel* experiment presented schematically in Fig. 14.3. A parametric down converter produces two beams of linearly polarized signal and idler photons. Phase matching conditions give a relative angle of 4° between the propagation direction of the two beams. The idler photons pass through a 90° polarization rotator. The signal and idler beams are then incident from opposite sides onto a beam splitter. After the beam splitter, the two beams now consisting of mixed signal and idler photons pass through linear polarizers set at adjustable angles θ_1 and θ_2 before falling on two photodetectors. The coincidence counting rate of the two detectors is then measured with a time-to-digital

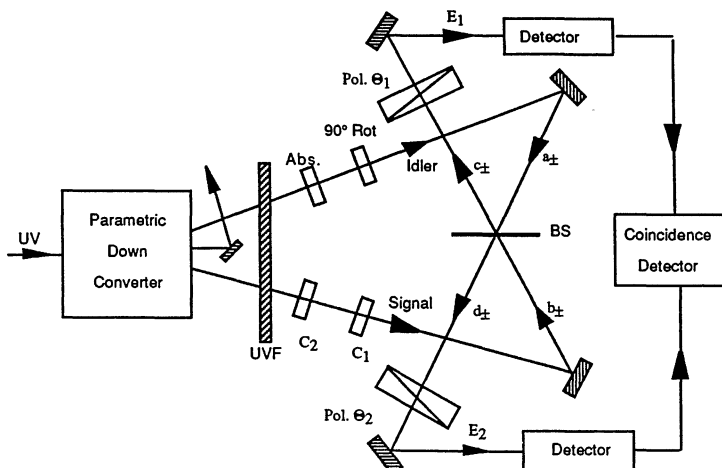


Fig. 14.3. Schematic representation of the experiment of *Ou and Mandel* to test the CHSH inequality using parametric down conversion [14.9]

converter. This provides a measure of the joint probability of detecting two photons for various settings θ_1 and θ_2 of the two polarizers.

In this experiment the polarisation analysers used have only a single output channel. However, we can still derive a Bell inequality violated by quantum mechanics. If we define the correlation function $P(\theta_1, \theta_2)$ by

$$P(\theta_1, \theta_2) = \langle I_1 I_2 \rangle_{\theta_1, \theta_2} \quad (14.29)$$

the following Bell inequality may be derived as

$$\begin{aligned} S &= P(\theta_1, \theta_2) - P(\theta_1, \theta'_2) + P(\theta'_1, \theta'_2) + P(\theta'_1, \theta_2) \\ &\quad - P(\theta_1, -) - P(-, \theta_2) \leq 0 , \end{aligned} \quad (14.30)$$

where

$$P(\theta_1, -) = \langle I_1 I_2 \rangle_{\theta_1} , \quad (14.31)$$

$$P(-, \theta_2) = \langle I_1 I_2 \rangle_{\theta_2} \quad (14.32)$$

are the intensity correlation functions with one or the other polariser removed. The inequality in (14.30) is known as the Clauser–Horne inequality. Just as in the case of the CHSH inequality (14.19) this inequality is satisfied for states of the field which can be represented by a positive, normalisable Glauber–Sudarshan P -representation [14.4]. It may, however, be violated for certain quantum fields.

We follow closely the treatment given by *Tan and Walls* [14.9]. We now proceed to calculate $P(\theta_1, \theta_2)$ and S for the experiment of *Ou and Mandel* [14.6]. We include the possibility of placing an attenuator in the idler beam. Let a_+ and a_- denote the annihilation operators for the x and y polarized modes in the idler beam, and let b_+ and b_- denote the operators for the corresponding modes in the signal beam. The outgoing modes from the beam splitter are described by the operators c_\pm and d_\pm , and obey the following relationships:

$$\begin{aligned} c_+ &= \sqrt{T_+} b_+ + i\sqrt{R_+} a_+ , \\ c_- &= \sqrt{T_-} b_- - i\sqrt{R_-} a_- , \\ d_+ &= \sqrt{T_+} a_+ + i\sqrt{R_+} b_+ , \\ d_- &= \sqrt{T_-} a_- - i\sqrt{R_-} b_- , \end{aligned} \quad (14.33)$$

where T_\pm and R_\pm are the intensity transmission and reflection coefficients for the x and y polarizations. The phase relationships arise from the Fresnel formula. Since the signal beam is polarized in the x direction, and the idler beam is polarized in the y direction, the modes associated with the operators a_+ and b_+ are the annihilation operators for the output modes of the parametric

down converter. When an attenuator with the intensity transmission coefficient η is placed in the idler beam, the operators a_- in the above equations is replaced by

$$\sqrt{\eta}a_- + \sqrt{1-\eta}v , \quad (14.34)$$

where the vacuum mode operator v is included to give the correct level of fluctuations in the attenuated beam. Photodetectors 1 and 2 respond to the fields $E_1^{(+)}$ and $E_2^{(+)}$, respectively, where

$$\begin{aligned} E_1^{(+)} &= c_+ \cos \theta_1 + c_- \sin \theta_1 , \\ E_2^{(+)} &= d_+ \cos \theta_2 + d_- \sin \theta_2 , \end{aligned} \quad (14.35)$$

The joint two-photon detection probability (for perfect detector efficiency) is

$$P(\theta_1, \theta_2) = \langle \psi | E_1^{(-)} E_2^{(-)} E_2^{(+)} E_1^{(+)} | \psi \rangle . \quad (14.36)$$

For low conversion efficiencies the output of the parametric down converter is a pair of photons, one in each of the signal and idler modes a_- and b_+ . Thus $|\psi\rangle = |1,1\rangle$, this yields

$$P(\theta_1, \theta_2) = \eta(\sqrt{R_+ R_-} \sin \theta_1 \cos \theta_2 + \sqrt{T_+ T_-} \cos \theta_1 \sin \theta_2)^2 . \quad (14.37)$$

Taking a 50/50 beam splitter ($R_+ = R_- = T_+ = T_- = \frac{1}{2}$),

$$P(\theta_1, \theta_2) = \frac{1}{4}\eta \sin^2(\theta_1 + \theta_2) . \quad (14.38)$$

Removing one polarizer, we must calculate

$$P(-, \theta_2) = \langle \psi | : (c_+^\dagger c_+ + c_-^\dagger c_-) E_2^{(-)} E_2^{(+)} : | \psi \rangle , \quad (14.39)$$

where $: :$ represents normal ordering. For the input state $|1,1\rangle$ we find

$$P(-, \theta_2) = \frac{1}{4}\eta , \quad (14.40)$$

and similarly

$$P(\theta_1, -) = \frac{1}{4}\eta , \quad (14.41)$$

for a 50/50 beam splitter.

Substituting (14.38, 14.40 and 14.41) into the Clauser–Horne–Bell inequality (14.2) gives

$$S = \frac{1}{4}\eta [\sin^2(\theta_1 + \theta_2) - \sin^2(\theta_1 + \theta'_2) + \sin^2(\theta'_1 + \theta'_2) + \sin^2(\theta'_1 + \theta_2) - 2] .$$

Choosing the angles such that $\theta_1 = \pi/8$, $\theta_2 = \pi/4$, $\theta'_1 = 3\pi/8$ and $\theta'_2 = 0$,

$$S = \frac{1}{4}\eta(\sqrt{2} - 1) > 0 , \quad (14.42)$$

which violates the inequality.

In a classical wave analysis of the parametric down converter, we represent the signal and idler fields incident on the beam splitter by the complex numbers E_s and E_i . The beam splitter combines these fields to produce E_1 and E_2 at the detectors, where

$$\begin{aligned} E_1 &= \cos \theta_1 \sqrt{T_+} E_s - i \sin \theta_1 \sqrt{R_-} E_i , \\ E_2 &= i \cos \theta_2 \sqrt{R_+} E_s + \sin \theta_2 \sqrt{T_-} E_i . \end{aligned} \quad (14.43)$$

The joint detection probability $P(\theta_1, \theta_2)$ is proportional to the intensity correlation $\langle |E_1|^2 |E_2|^2 \rangle$. Using the above forms for E_1 and E_2 , and assuming that the difference in the phases of the signal and idler fields is random, we find that for a 50/50 beam splitter

$$\begin{aligned} P(\theta_1, \theta_2) &\propto \langle I_s I_i \rangle \sin^2(\theta_1 + \theta_2) \\ &\quad + \langle I_s^2 \rangle \cos^2 \theta_1 \cos^2 \theta_2 + \langle I_i^2 \rangle \sin^2 \theta_1 \sin^2 \theta_2 , \end{aligned} \quad (14.44)$$

where we have written I_s for $|E_s|^2$ and for I_i for $|E_i|^2$. With the attenuator in the idler beam, $I_i = \eta I_s$, and if we assume that the intensity fluctuations are such that $\langle I^2 \rangle \propto \langle I \rangle^2$ and $\langle I_i I_s \rangle \propto \langle I_i \rangle \langle I_s \rangle$, then

$$P(\theta_1, \theta_2) \propto \eta \sin^2(\theta_1 + \theta_2) + \cos^2 \theta_1 \cos^2 \theta_2 + \eta^2 \sin^2 \theta_1 \sin^2 \theta_2 . \quad (14.45)$$

In order to compare the quantum and classical result we consider $P(\theta, \pi/4)$ with $R_+ = R_- = T_+ = T_- = \frac{1}{2}$. Then

$$P(\theta, \pi/4) = \frac{\eta}{8}(1 + \sin 2\theta) , \quad (14.46)$$

which exhibits a sinusoidal modulation with respect to the angle 2θ . The visibility of the resulting modulation is unity. However, the classical result gives

$$P(\theta, \pi/4) \propto \frac{\eta}{2}(1 + \sin 2\theta) + \frac{1}{2} \cos^2 \theta + \frac{\eta^2}{2} \sin^2 \theta , \quad (14.47)$$

which in the absence of the absorber ($\eta = 1$) gives

$$P(\theta, \pi/4) \propto (1 + \frac{1}{2} \sin 2\theta) . \quad (14.48)$$

In the classical case the modulation is not 100%, in fact the visibility is only one half.

In the experiment of *Ou* and *Mandel* the value of S was found to be positive with an accuracy of six standard deviations, in clear violation of the Bell inequality (14.30). The experiment also distinguished between the different quantum and classical predictions for the phase dependence of $P(\theta, \pi/4)$. These results are shown in Fig. 14.4. The solid and dashed-dotted lines correspond to the quantum and classical wave predictions, respectively, with constants of

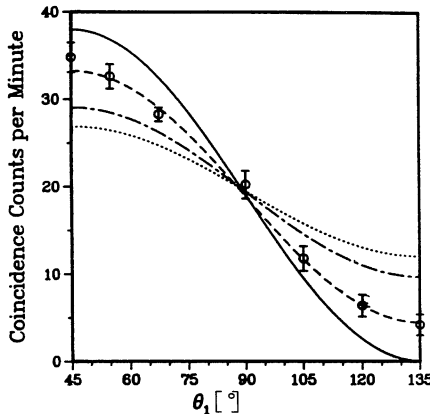


Fig. 14.4. The coincidence counting rate as a function of polariser angle θ_1 with θ_2 fixed at 45° . The solid curve is the quantum prediction based on (14.46), and the dash-dot curve is the classical prediction based on (14.48). The dashed and dotted curves are the quantum and classical predictions, respectively, including a detector inefficiency of 0.76.

proportionality adjusted to fit. Clearly, $P(\theta, \pi/4)$ does exhibit the phase dependence predicted by quantum mechanics. The observed visibility obtained from a best fit was 0.76; greater than the classical prediction of 0.5.

Instead of the correlated two-photon state discussed above we can also use the output state of a parametric down converter. We assume that the pump field in this device may be treated classically. The solutions for the output modes of the device are

$$a_- = a_0 \cosh \kappa + b_0^\dagger \sinh \kappa , \quad (14.49)$$

$$b_+ = b_0 \cosh \kappa + a_0^\dagger \sinh \kappa , \quad (14.50)$$

where κ is proportional to the second-order nonlinear susceptibility of the crystal, and a_0, b_0 are the input modes. We assume that the input state is a vacuum. With a 50:50 beam splitter $\eta = 1$ and with $\theta'_2 = 0, \theta_1 = \psi, \theta_2 = 2\psi, \theta'_1 = 3\psi$ the quantity S which occurs in the Bell inequality (14.30) is given by (Exercise 14.2)

$$S = \frac{1}{4} \sinh^2 \kappa \{ F(\psi) + 2 \sinh^2 \kappa [F(\psi) + 2G(\psi)] \} , \quad (14.51)$$

where

$$F(\psi) = 2 \sin^2 3\psi - \sin^2 \psi + \sin^2 5\psi - 2 ,$$

$$G(\psi) = \sin^2 \psi \sin^2 2\psi + \sin^2 3\psi \sin^2 2\psi - \sin^2 3\psi - \sin^2 2\psi .$$

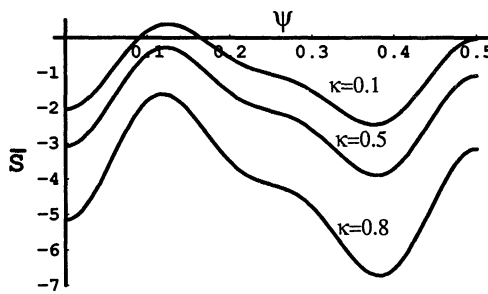


Fig. 14.5. The correlation function in (14.51) normalised by $\sinh^2 \kappa$, versus ψ for various values of κ . The violation of the classical inequality is evident for small κ .

When $\kappa \ll 1$ this may be approximated by

$$S \approx \frac{1}{4} \kappa^2 F(\psi) . \quad (14.52)$$

For purposes of comparison the two-photon state, with the same choice of angles would give

$$S = \frac{1}{4} F(\psi) . \quad (14.53)$$

Up to a scale constant in this limit the parametric down converter gives the same result as for a correlated photon pair.

In the limit $\kappa \gg 1$ we find

$$S \propto F(\psi) - 2G(\psi) . \quad (14.54)$$

As the function on the right-hand side is always nonpositive no violation of the Clauser–Horne inequality is possible. In Fig. 14.5 we plot S normalised by the intensity $I = \sinh^2 \kappa$ versus ψ for various values of κ . We see that the maximum violation for $\kappa \ll 1$ occurs when $\theta = \pi/8$ (solid curve).

We note that the form of the intensity correlation function for the parametric down-converter in the limit of $\kappa \gg 1$ coincides with that of the classical analysis (14.44).

14.4 One-Photon Interference

In all the schemes discussed above the states which lead to a violation of the Bell inequalities are correlated two-photon states. We now consider a scheme which demonstrates the non-local nature of quantum mechanics, which does not rely on two-photon states. This experiment illustrates on the nonlocal behaviour of a single photon.

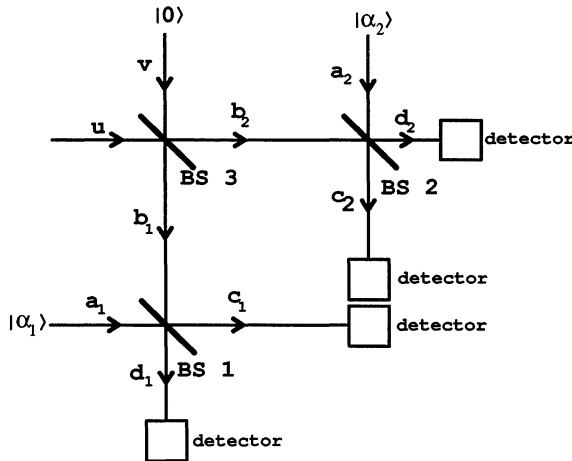


Fig. 14.6. Schematic representation of an experiment with a single photon state to demonstrate non-locality [14.10]

The scheme is illustrated in Fig. 14.6. A field is split at a 50:50 beam splitter, and each of the two output fields directed to homodyne detectors. Each of the homodyne detectors mix the output field from the first beam splitter with a coherent local oscillator of amplitude $\alpha_k = \alpha e^{i\theta_k}$, and the final intensities at the two output channels of each of the homodyne detectors are measured using photodetectors. We follow closely the treatment of Tan et al. [14.10].

Referring to Fig. 14.6 we see that the homodyne detector k may be regarded as making a measurement of b_k with a local parameter θ_k . This parameter is analogous to the angle of the polarisation analysers in the two-photon schemes. We wish to determine the probabilities with which the individual photodetectors respond, and the coincidence probabilities for pairs of photodetectors, one in each homodyne detector.

The transformation between the mode operators shown in Fig. 6 are given by

$$\begin{pmatrix} c_k \\ d_k \end{pmatrix} = \frac{1}{\sqrt{2}} \begin{pmatrix} 1 & i \\ i & 1 \end{pmatrix} \begin{pmatrix} a_k \\ b_k \end{pmatrix},$$

$$\begin{pmatrix} b_1 \\ b_2 \end{pmatrix} = \frac{1}{\sqrt{2}} \begin{pmatrix} 1 & i \\ i & 1 \end{pmatrix} \begin{pmatrix} v \\ u \end{pmatrix}. \quad (14.55)$$

Thus the modes input into the detectors may be expressed in terms of the input mode operators by

$$\begin{pmatrix} c_1 \\ d_1 \\ c_2 \\ d_2 \end{pmatrix} = \begin{pmatrix} \frac{1}{\sqrt{2}} & \frac{i}{2} & 0 & -\frac{1}{2} \\ \frac{i}{\sqrt{2}} & \frac{1}{2} & 0 & \frac{i}{2} \\ 0 & -\frac{1}{2} & \frac{1}{\sqrt{2}} & \frac{i}{2} \\ 0 & \frac{i}{2} & \frac{i}{\sqrt{2}} & \frac{1}{2} \end{pmatrix} \begin{pmatrix} a_1 \\ v \\ a_2 \\ u \end{pmatrix}. \quad (14.56)$$

This enables us to calculate the coincidence probabilities between the detectors directly in terms of the input field.

We begin by considering vacuum inputs to the modes u and v . The local oscillators are assumed to be in coherent states $|\alpha e^{i\theta_1}\rangle$, $|\alpha e^{i\theta_2}\rangle$. The intensities at all detectors are found to be equal

$$\langle I_{c_1} \rangle = \langle I_{c_2} \rangle = \langle I_{d_1} \rangle = \langle I_{d_2} \rangle = \frac{1}{2}\alpha^2. \quad (14.57)$$

The two-photon coincidence rates due to rare chance coincidences between the local oscillators are also equal between the pairs of detectors

$$\langle I_{c_1} I_{c_2} \rangle = \langle I_{d_1} I_{d_2} \rangle = \langle I_{c_1} I_{d_2} \rangle = \langle I_{d_1} I_{c_2} \rangle = \frac{1}{4}\alpha^4. \quad (14.58)$$

We now consider the input of a single photon in mode u while the mode v is the vacuum. The state of the two-mode field (b_1 and b_2) after the first beam-splitter is then an entangled state of a one-photon state and the vacuum

$$|\psi\rangle = \frac{1}{\sqrt{2}}(i|1\rangle|0\rangle + |0\rangle|1\rangle) \quad (14.59)$$

which is precisely the same state as one gets (except for a phase factor) for a one-photon state incident on the two slits in Young's interference experiment.

The photon count probabilities at the individual detectors are now

$$\langle I_{c_1} \rangle = \langle I_{c_2} \rangle = \langle I_{d_1} \rangle = \langle I_{d_2} \rangle = \frac{1}{2}\alpha^2 + \frac{1}{4}. \quad (14.60)$$

Thus the intensities at each detector are increased by $\frac{1}{4}$, being the probability that the one-photon input is detected by any given detector. The coincidence count probabilities between the pairs of detectors differ, now depending on which is considered. We find

$$\langle I_{c_1} I_{c_2} \rangle = \langle I_{d_1} I_{d_2} \rangle = \frac{1}{4}\{\alpha^4 + \alpha^2[1 + \sin(\theta_1 - \theta_2)]\} \quad (14.61)$$

and

$$\langle I_{c_1} I_{d_2} \rangle = \langle I_{d_1} I_{c_2} \rangle = \frac{1}{4}\{\alpha^4 + \alpha^2[1 - \sin(\theta_1 - \theta_2)]\}. \quad (14.62)$$

The coincidence probabilities depend on the phase difference between the local oscillators $\theta_1 - \theta_2$. If this is set to $-\pi/2$, we get the minimum possible

coincidence probability of $\frac{1}{4}\alpha^4$ between detector pairs (c_1, c_2) and (d_1, d_2) and the maximum coincidence probability of $\frac{1}{4}\alpha^4 + \frac{1}{2}\alpha^2$ between the pairs (c_1, d_2) and (d_1, c_2) . We shall be most interested in the situation where α is small compared to one.

Let us first try to interpret these results from a naïve particle viewpoint. The great enhancement of the single count probability over that with vacuum inputs is easily understood by the above argument. On the other hand, a coincidence between two detectors is expected to be a rare event since there is only one incident photon, and a coincidence can only occur if an additional photon is generated by the (weak) local oscillator of the homodyne detector which the photon does *not* reach. Since these two photons are detected at two spatially separated detectors and have apparently arisen from independent sources, we would not expect any correlation between the paths of these photons within each homodyne detector. Nevertheless, the quantum mechanical analysis reveals that such a correlation is present. In fact, this correlation is so great that for the choice of phases given above, no additional coincidence (above the vacuum level) occur for particular detector pairs, whereas there is a relatively large coincidence probability (proportional to the local oscillator intensity) for the other pairs.

Non-local intensity correlation and their dependence on the local oscillator phases are not unexpected from a classical wave description of light. A classical analogue to the single photon input is a wave of low amplitude and unspecified phase. We may formally obtain the results for the classical wave theory from the quantum-mechanical calculation by substituting the wave amplitude $\beta e^{\pm i\phi}$ for b and b^\dagger , respectively, and averaging over the random phase ϕ . It is easy to check that the predicted average intensities and intensity correlations are given by

$$\langle I_{c_1} \rangle = \langle I_{c_2} \rangle = \langle I_{d_1} \rangle = \langle I_{d_2} \rangle = \frac{1}{2}\alpha^2 + \frac{1}{4}\beta^2 , \quad (14.63)$$

$$\langle I_{c_1} I_{c_2} \rangle = \langle I_{d_1} I_{d_2} \rangle = \frac{1}{4}\{\alpha^4 + \alpha^2\beta^2[1 + \sin(\theta_1 - \theta_2)] + \frac{1}{4}\beta^4\} , \quad (14.64)$$

$$\langle I_{c_1} I_{d_2} \rangle = \langle I_{d_1} I_{c_2} \rangle = \frac{1}{4}\{\alpha^4 + \alpha^2\beta^2[1 - \sin(\theta_1 - \theta_2)] + \frac{1}{4}\beta^4\} . \quad (14.65)$$

If we consider the coincidence probabilities as a function of $(\theta_1 - \theta_2)$, we see that they can vary between $\frac{1}{4}(\alpha^4 + \frac{1}{4}\beta^4)$ to $\frac{1}{4}(\alpha^4 + 2\alpha^2\beta^2 + \frac{1}{4}\beta^4)$. This corresponds to a “visibility” of

$$v = \frac{\rho}{\rho^2 + \rho + \frac{1}{4}} \quad (14.66)$$

where $\rho = (\alpha/\beta)^2$. The visibility attains a maximum value of $\frac{1}{2}$ when $\rho = \frac{1}{2}$. By contrast, the visibility as calculated from the quantum-mechanical result is

$$v = \frac{1}{\alpha^2 + 1} . \quad (14.67)$$

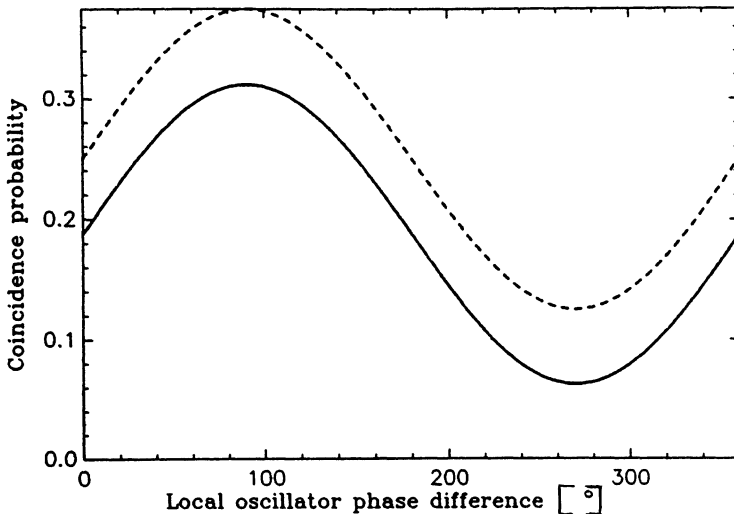


Fig. 14.7. Coincidence probability for the single photon non-locality experiment. The solid line is the quantum mechanical model, the dashed line is the prediction for a classical wave model [14.10]

This can be made arbitrarily close to unity by choosing a sufficiently small value of α . Figure 14.7 shows the coincidence probabilities $\langle I_{c_1} I_{c_2} \rangle = \langle I_{d_1} I_{d_2} \rangle$ as a function of the local oscillator phase difference for the quantum mechanical and classical results with $\beta = 1$ and $\alpha = 1/\sqrt{2}$. This gives the same single count probability of $\frac{1}{2}$ in each detector, and the local oscillator amplitudes are optimized for maximum visibility in the classical result. However, the quantum mechanical visibility is considerably larger than that expected classically. This is clearly seen in Fig. 14.8 where the visibility v is plotted as a function of the coherent local oscillator amplitude α for the quantum mechanical single state and the classical wave mode with $\beta = 1$.

We thus see that by measuring the coincidence probability in a pair of detectors, it is possible to distinguish between the classical and quantum mechanical models. If the detector efficiencies are less than unity, coincidences will be missed, but this does not affect the measurement of the visibility of the effect.

Preparation of a single photon state may be achieved experimentally by using the signal beam of a parametric amplifier while monitoring photons in the idler beam [14.11]. *Hong and Mandel* [14.12] described an experiment in which a nearly pure single photon state was produced using this method. If the pump for the parametric amplifier is derived by frequency doubling a coherent beam, this provides a convenient source for the local oscillator required in the experiment under discussion.

In order to rigorously rule out classical explanations for the quantum mechanical result, it is necessary to show that Bell's inequality may be violated.

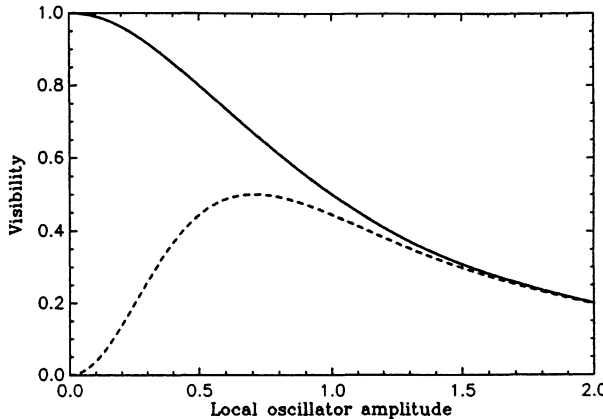


Fig. 14.8 Variation of visibility with the amplitude of the local oscillator for the quantum model (solid line) and a classical wave model (dashed line) [14.10]

An intensity correlation coefficient is used which involves all four photo-detectors

$$E(\theta_1 - \theta_2) = \frac{\langle (I_{d_1} - I_{c_1})(I_{d_2} - I_{c_2}) \rangle}{\langle (I_{d_1} + I_{c_1})(I_{d_2} + I_{c_2}) \rangle}. \quad (14.68)$$

Evaluating this in terms of the statistics of the input mode u , where v is the vacuum yields

$$E(\theta_1 - \theta_2) = -\frac{\alpha^2 \{ \langle u^\dagger u \rangle \sin(\theta_2 - \theta_1) + |\langle u^2 \rangle| \sin(\theta_2 + \theta_1 - \xi) \}}{\alpha^4 + \langle u^\dagger u \rangle \alpha^2 + \frac{1}{4} \langle u^\dagger u^2 \rangle} \quad (14.69)$$

where $\langle u^2 \rangle = R \exp(i\xi)$. When a single photon input is considered for u , this reduces to

$$E(\theta_1, \theta_2) = \frac{1}{\alpha^2 + 1} \sin(\theta_1 - \theta_2). \quad (14.70)$$

If the coefficient of $\sin(\theta_1 - \theta_2)$ is greater than $1/\sqrt{2}$ it is well-known that this functional form for the correlation allows a violation of Bell's inequalities. This is clearly possible if α is made sufficiently small. It has been shown [14.13] that such a violation of Bell's inequalities is not possible if u is in a coherent state, no matter how small the input amplitude may be.

In conclusion, some of the most striking features of non-locality in quantum mechanics may be demonstrated using phase-sensitive measurements on the field produced by a single photon. These effects may not be explained classically using a particle, wave or hidden-variable theory involving local causality.

Exercises

14.1 Derive (14.26) for the correlation function $E(\theta_1, \theta_2)$. Show that with the choice $\psi = \theta_2 - \theta_1 = \theta'_1 - \theta_2 = \theta'_1 - \theta'_2 = \frac{1}{3}(\theta_1 - \theta'_2)$ one obtains (14.27) for B.

14.2 Derive (14.51) for the Bell parameter S for the parametric amplifier.

14.3 The state going from the beam splitter in the one-photon interference experiment is the linear superposition state

$$|\psi\rangle = \frac{1}{\sqrt{2}}(i|1\rangle|0\rangle + |0\rangle|1\rangle).$$

Compute the intensity correlations were this state replaced by the mixed state

$$\rho = \frac{1}{2}(|1\rangle_u\langle 1| \otimes |0\rangle_v\langle 0| + |0\rangle_u\langle 0| \otimes |1\rangle_v\langle 1|)$$

and show that no violation of the Bell inequality can occur.

15. Quantum Nondemolition Measurements

Current attempts to detect gravitational radiation have to take into account the quantum uncertainties in the measurement process. Considering that the detectors are macroscopic objects in some cases as large as a 10-ton bar, the fact that quantum fluctuations in the detector must be taken into account seems surprising. However, as discussed in Chap. 8, gravitational waves interact so weakly with terrestrial detectors that a displacement of the order of 10^{-19} cm is expected. To illustrate how the measurement process may introduce uncertainties which obscure the signal we consider the simple example of a free mass. A measurement of the position of a free mass with a precision $\Delta x_i \approx 10^{-19}$ cm will disturb the momentum by an amount given by the uncertainty principles as $\Delta p \geq \hbar(2\Delta x_i)^{-1}$. The period of the gravitational waves is expected to be about 10^{-3} s, hence a second measurement of the position should be made after this time. During this period, however, the position uncertainty will grow under free evolution by an amount $\Delta x^2(\tau) = \Delta x^2(0) + [\Delta p^2(0)\tau^2/m^2]$. The following inequality then holds

$$\Delta x^2(\tau) \geq 2\Delta x(0)\Delta p(0) \frac{\tau}{m} . \quad (15.1)$$

Using the uncertainty principle we then find $\Delta x^2(\tau) \geq \hbar\tau/m$. Taking the detector mass equal to 10 tons, we find $\Delta x \geq 5 \times 10^{-19}$ cm. That is, the uncertainty introduced by the first measurement has made it impossible for a second measurement to determine with certainty whether a gravitational wave has acted or not. This is the standard quantum limit.

It is instructive to consider measurements of momentum instead of position. The first measurement of momentum causes an uncertainty in position. This however does not feed back to disturb the momentum as the momentum is a constant of motion for a free mass. Hence, subsequent determination of the momentum may be made with great predictability. The momentum of a free mass is an example of a quantum nondemolition (QND) variable. The concept of quantum nondemolition measurements has been introduced over the past few years to allow the detection, in principle, of very weak forces below the level of quantum noise in the detector. In the next section we will give a brief review of the concept of a quantum nondemolition measurement.

We mention here another way in which the standard quantum limit might be overcome. Quantum nondemolition measurements generally presume that

nothing at all is known about the state of the system to be measured. The standard quantum limit for a free mass, for example, was derived by assuming no correlation between position and momentum. If however we are permitted to prepare the state of the system to be measured, the accuracy of a measurement can be improved without resort to a QND scheme. For example, in the case of a free particle the position variance at time τ is given by

$$\Delta x^2(\tau) = \Delta x^2(0) + \frac{\Delta p^2(0)\tau^2}{m^2} + \langle \Delta x(0)\Delta p(0) + \Delta p(0)\Delta x(0) \rangle \frac{\tau}{m} \quad (15.2)$$

where the possibility of nonzero correlation between position and momentum has been included. In fact, this correlation may be negative if the initial state of the particle is chosen to be a ‘contractive state’. If this is the case it is clear that at a later time τ it is possible that $\Delta x^2(\tau) < \hbar\tau/m$, thus allowing a greater accuracy than the standard quantum limit.

15.1 Concept of a QND Measurement

The basic requirement of a QND measurement is the availability of a variable which may be measured repeatedly giving predictable results in the absence of a gravitational wave [15.1]. Clearly this requires that the act of measurement itself does not degrade the predictability of subsequent measurements. Then in a sufficiently long sequence of measurements the output becomes predictable.

This requirement is satisfied if for an observable $A^1(t)$ (in the interaction picture)

$$[A^1(t), A^1(t')] = 0 . \quad (15.3)$$

The condition ensures that if the system is in an eigenstate of $A^1(t_0)$ it remains in this eigenstate for all subsequent times although the eigenvalues may change. Such observables are called *QND observables*. Clearly constants of motion will be QND observables. Thus for a free particle, energy and momentum are QND observables while the position is not as

$$x(t + \tau) = x(t) + p \frac{\tau}{m} \quad (15.4)$$

and

$$[x(t), x(t + \tau)] = \frac{i\hbar\tau}{m} . \quad (15.5)$$

For a harmonic oscillator of unit mass

$$[x(t), x(t + \tau)] = \frac{i\hbar}{\omega} \sin \omega\tau . \quad (15.6)$$

and

$$[p(t), p(t + \tau)] = i\hbar\omega \sin \omega\tau , \quad (15.7)$$

thus position and momentum are not QND observables for the harmonic oscillator.

There are, however, QND observables for the harmonic oscillator. We define the explicitly time dependent quadrature phase amplitudes for the oscillator as follows.

$$X_1(t) = a e^{i\omega t} + a^\dagger e^{-i\omega t} \quad (15.8)$$

and

$$X_2(t) = -i(a e^{i\omega t} - a^\dagger e^{-i\omega t}) . \quad (15.9)$$

In the Heisenberg picture the quadrature phase operators are given by

$$X_1 = a + a^\dagger , \quad (15.10)$$

$$X_2 = -i(a - a^\dagger) , \quad (15.11)$$

which clearly shows that the quadrature phase operators are constants of the motion. In terms of the position and momentum the quadrature phase operators are

$$X_1(t) = \left(\frac{2\omega}{\hbar}\right)^{1/2} [x(t) \cos \omega t - \frac{p(t)}{\omega} \sin \omega t] \quad (15.12)$$

and

$$X_2(t) = \left(\frac{2\omega}{\hbar}\right)^{1/2} [x(t) \sin \omega t + \frac{p(t)}{\omega} \cos \omega t] . \quad (15.13)$$

Thus the X_1 and X_2 axes rotate with respect to the position and momentum axes of phase space, at frequency ω .

The behaviour of X_1 and X_2 are most easily discussed with reference to an amplitude and phase diagram. In such a diagram the state of the system is represented by a set of points centred on the mean and contained within an error ellipse determined by the variance of the quadrature phases. Alternatively the error box may be regarded as a contour of the Wigner function. In Fig. 15.1 an error ellipse for the oscillator is shown. The error ellipse is stationary with respect to the X_1 and X_2 axes but rotates with respect to the x and p axes. This clearly illustrates how uncertainties in momentum feed back into position.

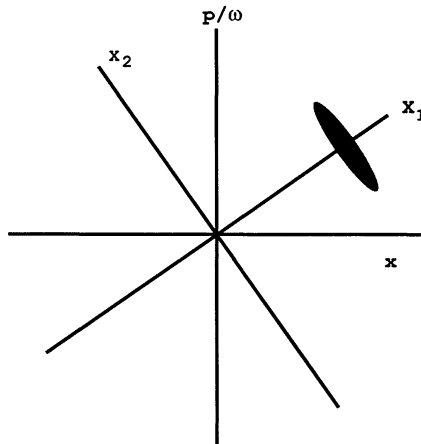


Fig. 15.1. Error box in the phase plane for a harmonic oscillator. The error box rotates with respect to the x and p/ω axes but is stationary with respect to the x_1 , x_2 axes

15.2 Back Action Evasion

Having first determined the QND variables of the detector it is necessary to couple the detector to a readout system or meter. It is essential that the coupling to the meter does not feed back fluctuations into the QND variable of the detector. In order to avoid this it is sufficient if the QND variable A commutes with the Hamiltonian coupling the detector and the meter, H_{DM} , that is

$$[A, H_{\text{DM}}] = 0 \quad (15.14)$$

This is known as the *back action evasion criterion*.

In this chapter we are primarily concerned with QND measurements on optical systems. This requires a slight change in nomenclature. We will refer to the field with respect to which the QND variable is defined as the ‘signal’ rather than the detector, and the field upon which measurements are ultimately made as the ‘probe’ rather than the meter.

15.3 Criteria for a QND Measurement

We need to clearly define the objectives of a quantum nondemolition measurement in an optical context. These objectives may differ depending on the situation of the measurement. For example, in a transmission with a series of receivers, the goal may be to tap information from the signal, without degrading

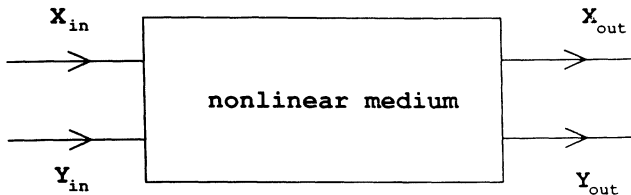


Fig. 15.2. General scheme for a QND measurement in an optical context

the signal transmitted to the next receiver. In a system used to measure the magnitude of an external force the goal of the measurement may be state preparation. That is an initial measurement prepares the system in a known quantum state. The presence of the perturbing force will be detected by a subsequent measurement on the system. In order to evaluate the merits of a measurement scheme we shall define a set of criteria which we would like to be satisfied in a good measurement. We begin by considering the general measurement scheme depicted in Fig. 15.2 where an observable X_{in} of the input signal is determined by a measurement of an observable Y_{out} of the output probe. The measurement may be characterised by the following criteria [15.2]:

1. *How good is the measurement scheme?* This is determined by the level of correlation between the probe field measured by a detector and the signal field incident on the apparatus. The appropriate correlation function is

$$C_{X^{in} Y^{out}}^2 = \frac{|\langle X^{in} Y^{out} \rangle_s - \langle X^{in} \rangle \langle Y^{out} \rangle|^2}{V_{X^{in}} V_{Y^{out}}} \quad (15.15)$$

where $V(A) = \langle A^2 \rangle - \langle A \rangle^2$ is the variance in a measurement of A and $\langle AB \rangle_s = \langle AB + BA \rangle / 2$. For a perfect measurement device the phase quadrature of the probe output is equal to the amplitude quadrature of the signal input multiplied by the QND gain, plus the input probe phase quadrature. In this case the correlation coefficient defined above is unity, for large gain.

2. *How much does the scheme degrade the signal?* The quantity of interest here is the correlation between the signal input field and the signal output field:

$$C_{X^{in} X^{out}}^2 = \frac{|\langle X^{in} X^{out} \rangle_s - \langle X^{in} \rangle \langle X^{out} \rangle|^2}{V_{X^{in}} V_{X^{out}}} \quad (15.16)$$

This is a measure of the back action evasion, that is the ability of the scheme to isolate quantum noise introduced by the measurement process from the observable of interest. For an ideal QND scheme we require this correlation to be unity. Thus, for a perfect QND scheme we have $C_{X^{in} Y^{out}}^2 + C_{X^{in} X^{out}}^2 = 2$.

3. *How good is the scheme as a state preparation device?* If we have a perfect measurement device that does not degrade the signal at all, we satisfy the two

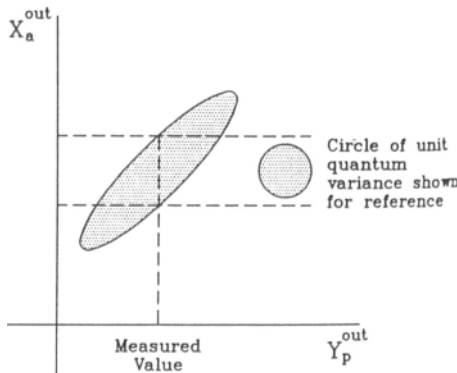


Fig. 15.3. Illustration of a situation in which a value of the probe output has been measured, but when mapped onto the error ellipse, does not permit an inference of the signal to better than the quantum limit

previous criteria exactly, then we must be able to completely predict the state of the signal output. However, once we leave this ideal case the predictability of the signal output is no longer fully determined by correlations with the signal input. The extreme example is that of a destructive measurement: independently of how well the input is measured the output is always the vacuum. On the other hand, the correlation between the signal and probe output fields is not a good indicator of the quality of state preparation. Figure 15.3 shows a situation in which both output fields are well correlated, but a probe measurement does not allow inference of the signal output field to be better than the quantum limit. This situation arises when the interaction within the QND medium introduces significant correlated noise to both output fields.

Given that we have made a perfect measurement of some physical quantity X with the result x , what is the state of the system after such a measurement conditioned on the result x ? In standard quantum mechanics the conditional state is generally assumed to be an eigenstate of X with an eigenvalue equal to the measured result, at least for perfect measurements. In the case of the QND measurement scheme above we then expect the state of the signal mode conditioned on the results of the probe measurements should in some limit be an eigenstate of X^{out} . Of course, the variance of X^{out} in such a state is zero. Thus as a measure of how well the scheme prepares eigenstates at the output we need to consider the conditional variance $V(X^{\text{out}}|Y^{\text{out}})$. This quantity is calculated as follows:

The probability to obtain the result Y^{out} for a probe measurement is given by

$$P(Y^{\text{out}}) = \text{Tr}\{\rho^{\text{out}}|Y^{\text{out}}\rangle\langle Y^{\text{out}}|\} \quad (15.17)$$

(assuming perfect readout of the probe state). The conditional state of the signal mode based on this result is

$$\rho^{\text{out}} = \frac{\text{Tr}_{\text{probe}}\{\rho^{\text{out}}|Y^{\text{out}}\rangle\langle Y^{\text{out}}|\}}{P(Y^{\text{out}})} . \quad (15.18)$$

Using this result we see that the conditional distribution for X^{out} is

$$\begin{aligned} P(X^{\text{out}}|Y^{\text{out}}) &= \text{Tr}_{\text{signal}}\{\rho_{\text{signal}}^{\text{out}}|X^{\text{out}}\rangle\langle X^{\text{out}}|\} \\ &= \frac{P(X^{\text{out}}, Y^{\text{out}})}{P(Y^{\text{out}})} \end{aligned}$$

where

$$P(X^{\text{out}}, Y^{\text{out}}) = \text{Tr}\{\rho^{\text{out}}|X^{\text{out}}\rangle\langle X^{\text{out}}|\otimes|Y^{\text{out}}\rangle\langle Y^{\text{out}}|\} . \quad (15.19)$$

In many cases of interest $P(X^{\text{out}}, Y^{\text{out}})$ is a bivariate Gaussian. In that case one may show

$$V(X^{\text{out}}|Y^{\text{out}}) = V(X^{\text{out}})(1 - C_{X^{\text{out}}Y^{\text{out}}}^2) . \quad (15.20)$$

Thus, the condition for a perfect state reduction in the conditional state is

$$C_{X^{\text{out}}Y^{\text{out}}}^2 = 1 . \quad (15.21)$$

We shall now analyse some possible measurement schemes and see how well they approach the conditions for an ideal measurement.

15.4 The Beam Splitter

We consider first a beam splitter deflecting part of the incident signal field onto a homodyne detector, as shown in Fig. 15.4. This will serve as a standard of comparison for other measurement schemes. There is obviously little point in constructing complicated schemes involving cavities containing nonlinear media if they cannot improve on the performance of a beam splitter. We consider the case where the signal and probe fields are single mode with annihilation operators a and b , respectively. The amplitude and phase quadratures of the signal and probe fields are defined as

$$X_a = a + a^\dagger , \quad (15.22)$$

$$X_\phi = -i(a - a^\dagger) , \quad (15.23)$$

$$Y_a = b + b^\dagger , \quad (15.24)$$

$$Y_\phi = -i(b + b^\dagger) . \quad (15.25)$$

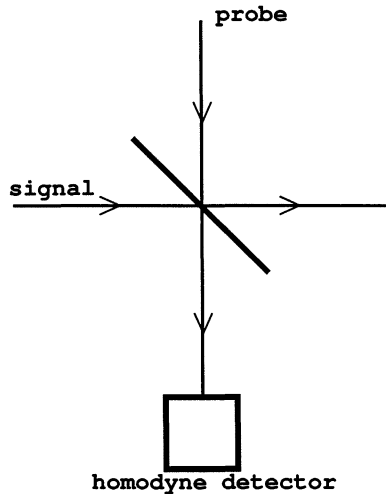


Fig. 15.4. An optical measurement scheme for the quadrature phase based on a beam splitter

(This notation assumes that the coherent amplitude of each field is real). Note that according to the uncertainty principle

$$\Delta X_a \Delta X_\phi \geq 1 \quad (15.26)$$

where ΔX_a and ΔX_ϕ are the square root of the variances. A precise measurement of the amplitude quadrature must therefore be at the expense of uncertainty in the phase. A good back action evading scheme must be able to feed all the quantum noise induced by the act of measurement into the phase quadrature of the signal.

In the beam splitter the phase change on reflection gives a coupling between the amplitude quadrature of the signal and the phase quadrature of the probe. We consider making a measurement on the phase quadrature of the probe in order to determine the amplitude quadrature of the signal. The input quadrature fields can be related to the output quadrature fields using the transformation at the beam splitter:

$$\begin{pmatrix} X_a^{\text{out}} \\ Y_\phi^{\text{out}} \end{pmatrix} = \begin{pmatrix} \sqrt{1 - \eta^2} & -\eta \\ \eta & \sqrt{1 - \eta^2} \end{pmatrix} \begin{pmatrix} X_a^{\text{in}} \\ Y_\phi^{\text{in}} \end{pmatrix} \quad (15.27)$$

where η is real and represents the mirror amplitude reflectivity, and there is a $\pi/2$ phase change upon reflection.

The first criterion for a good QND measurement scheme is that it must be a good back action evading device. In other words, it must be able to isolate the signal field from quantum noise introduced by the measurement. How well the

beam splitter achieves this is represented by the correlation between the input and the output signal fields,

$$C_{X_a^{in} Y_\phi^{out}}^2 = \frac{(1 - \eta^2) V_{X_a^{in}}}{(1 - \eta^2) V_{X_a^{in}} + \eta^2 V_{Y_\phi^{in}}} \quad (15.28)$$

where $V_{X_a^{in}}$ denotes the variance of the signal input, and $V_{Y_\phi^{in}}$ is the corresponding variance for the probe. These quantities are a measure of the quantum or classical noise present in the input fields at the appropriate quadrature phase. For a beam splitter with 50% reflectivity, the correlation between the signal input and output is given by the ratio of the signal noise to the total noise introduced to the system through both input ports.

The second criterion reflects how well the scheme acts as a measurement device. The readout measurement is made on the probe output field, so the level of correlation between this quantity and the signal field incident on the device determines how well a measurement can be made. The appropriate correlation function is

$$C_{X_a^{in} Y_\phi^{out}}^2 = \frac{\eta^2 V_{X_a^{in}}}{\eta^2 V_{X_a^{in}} + (1 - \eta^2) V_{Y_\phi^{in}}} \quad (15.29)$$

Again, for a 50% beam splitter, the correlation is given by the ratio of the incident signal noise to the total noise introduced.

The third criteria is that the measurement must prepare the output observable in a well known state. This is given by the variance in the output state after the measurement has been performed. Using

$$C_{X_a^{out} Y_\phi^{out}}^2 = \frac{\eta^2 (1 - \eta^2) (V_{X_a^{in}} - V_{Y_\phi^{in}})^2}{[(1 - \eta^2) V_{X_a^{in}} + \eta^2 V_{Y_\phi^{in}}] [(\eta^2 V_{X_a^{in}} + (1 - \eta^2) V_{Y_\phi^{in}}]} \quad (15.30)$$

and

$$V_{X_a^{out}} = (1 - \eta^2) V_{X_a^{in}} + \eta^2 V_{Y_\phi^{in}}, \quad (15.31)$$

and the linearity predictor for the beam splitter, the conditional variance is given by

$$V(X_a^{out} | Y_\phi^{out}) = \frac{V_{X_a^{in}} V_{Y_\phi^{in}}}{\eta^2 V_{X_a^{in}} + (1 - \eta^2) V_{Y_\phi^{in}}} \quad (15.32)$$

We would like this variance to be zero. If both signal and probe inputs are in the vacuum or coherent states with unit quantum variance in both quadratures, then

$$C_{X_a^{in} Y_\phi^{out}}^2 = \eta^2 ,$$

$$C_{X_a^{in} X_a^{out}}^2 = 1 - \eta^2 ,$$

$$C_{X_a^{out} Y_\phi^{out}}^2 = 0$$

$$V(X_a^{out} | Y_\phi^{out}) = 1 .$$

As expected, the correlation between the signal input field and the signal output field is the intensity transmission coefficient of the mirror. To reduce the amount of noise added to the signal variable we would like to split off only a small portion of the light field. However, this reduces the correlation between the signal input field and the probe field upon which the readout is made, which is given by the intensity reflection coefficient. It is not possible therefore to simultaneously satisfy the first two criteria for a good QND scheme. Since the signal and probe fields are completely uncorrelated, a measurement of the probe does not reduce the signal output variable at all. The result is that you cannot use a beam splitter to prepare the state of the output signal with probe fluctuations at the vacuum level. Clearly the performance of the beam splitter improves if the input probe has squeezed fluctuations (Exercise 15.5).

Note that for the beam splitter $C_{X_a^{in}Y_\phi^{out}}^2 + C_{X_a^{in}Y_a^{out}}^2 = 1$, a typical result for a non-back-action evasion scheme, and significantly less than the maximum result of 2 for this quantity achieved in an ideal scheme. The quality of a QND scheme can thus be measured by the extent to which this quantity exceeds unity and approaches the upper limit of 2.

15.5 Ideal Quadrature QND Measurements

We now consider another scheme to make perfect QND measurements of the quadrature phase of a single mode field. We shall assume that the amplitude quadratures of each mode are coupled. That is, the interaction Hamiltonian has the form

$$\mathcal{H} = \hbar\chi X_a Y_a \quad (15.33)$$

where χ is the coupling strength and X_a , Y_a are defined by (15.22, 24). Clearly X_a is a QND variable of the signal which satisfies the back action evading condition (15.12). The input and output quadratures are related by

$$X_a^{out} = X_a^{in} ,$$

$$Y_\phi^{out} = G X_a^{in} + Y_\phi^{in} ,$$

where $G = \chi t$ is known as the QND gain (t being the interaction time).

A measurement on the phase quadrature of the probe will be used to determine the amplitude quadrature of the input signal. To begin we calculate the correlation coefficients which define the measurement. Clearly $C_{X_a^{in}X_a^{out}} = 1$, the signal is completely unaffected by the measurement. The correlation between

the input signal and the phase of the output probe is

$$C_{X_a^{in} Y_\phi^{out}} = \frac{G^2 V_{X_a^{in}}}{G^2 V_{X_a^{in}} + V_{Y_\phi^{in}}} \quad (15.34)$$

where we have taken $\langle Y_\phi^{in} \rangle = 0$. For a large QND gain $G^2 \gg 1$,

$$C_{X_a^{in} Y_\phi^{out}} \rightarrow 1 . \quad (15.35)$$

The conditional variance $V(X_a^{out} | Y_\phi^{out})$ which determines the value of the scheme as a state preparation device is given by

$$\begin{aligned} V(X_a^{out} | Y_\phi^{out}) &= V_{X_a^{in}} \left(1 - \frac{G^2 V_{X_a^{in}}}{G^2 V_{X_a^{in}} + V_{Y_\phi^{in}}} \right) \\ &\approx \frac{V_{Y_\phi^{in}}}{G^2} \\ &\rightarrow 0 \quad \text{for } G^2 \gg 1 . \end{aligned}$$

Again in the limit of high QND gain this device operates as a good state preparation device.

Another measure of the performance of the measurement is the signal-to-noise ratio of the probe output

$$\begin{aligned} \frac{\text{signal}}{\text{noise}} &= \frac{\langle Y_\phi^{out} \rangle^2}{V_{Y_\phi^{out}}} \\ &= \frac{G^2 \langle X_a^{in} \rangle^2}{G^2 V_{X_a^{in}} + V_{Y_\phi^{in}}} \\ &\rightarrow \frac{\langle X_a^{in} \rangle^2}{V_{X_a^{in}}} \quad \text{for } G^2 \gg 1 . \end{aligned}$$

In the limit of large QND gain the signal-to-noise ratio of the output probe is equal to that of the signal input.

15.6 Experimental Realisation

It is possible to achieve a QND coupling of the form in (15.33) by considering two degenerate modes a and b with frequency ω and orthogonal polarisation, which undergo parametric amplification [15.3]. The two polarisation modes initially undergo a mixing interaction using polarisation rotators, after which a mixture of the signal and probe fields will propagate along each of the ordinary and orthogonal extraordinary axis of a KTP crystal pumped by a pulsed intense classical field. After this amplification step the fields then pass

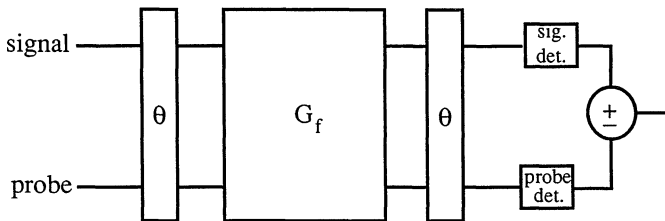


Fig. 15.5. Schematic representation of a perfect QND scheme based on a parametric interaction

through a second polarisation rotator adjusted to give the same mixing angle as the first. In order to ensure that the device operates as an ideal QND scheme the mixing angle of the rotators must be carefully adjusted. The situation is depicted in Fig. 15.5.

The transformation performed by the polarisation rotators is given by

$$a(\theta) = a \cos \theta + ib \sin \theta , \quad (15.36)$$

$$b(\theta) = b \cos \theta + ia \sin \theta , \quad (15.37)$$

with θ being the mixing angle. The transformation in the parametric amplification process is

$$a(r) = a \cosh r + ib^\dagger \sinh r , \quad (15.38)$$

$$b(r) = b \cosh r + ia^\dagger \sinh r , \quad (15.39)$$

where r is related to the parametric gain G_f by $G_f = e^r$. Using these transformations for the system in Fig. 15.5, we find that the transformations for the signal and probe quadratures are

$$X_a^{\text{out}} = X_a^{\text{in}} , \quad (15.40)$$

$$X_\phi^{\text{out}} = X_\phi^{\text{in}} + (G_f - G_f^{-1}) Y_\phi^{\text{in}} , \quad (15.41)$$

$$Y_a^{\text{out}} = Y_a^{\text{in}} - (G_f - G_f^{-1}) X_a^{\text{in}} , \quad (15.42)$$

$$Y_\phi^{\text{out}} = Y_\phi^{\text{in}} , \quad (15.43)$$

where we have taken the polarisation mixing angle to be

$$\theta = \arccos \left(\frac{G_f + 1}{\sqrt{2(G_f^2 + 1)}} \right) . \quad (15.44)$$

Clearly this represents an ideal QND scheme.

In the experiment of *La Porta* et al. [15.3], the incident signal was in a coherent state while the probe was in the vacuum state at input. The measured gain was $G_f = 1.33$ thus giving $\theta = 8^\circ$. The output quadratures are measured by

phase sensitive homodyne detection using polarisation beam splitters. To demonstrate that the experiment is operating as a back action evading measurement, three quantities were measured. Firstly the variances of each quadrature of the signal and probe were measured, with the gain both on and off. The probe shows a large noise in only one quadrature when the paramp was on. This is a reflection of the gain term appearing in the amplitude quadrature of the probe. The phase quadrature noise was at the shot-noise level. Secondly, the signal variances alone were measured showing a similar effect. Finally the variance of the quantities

$$X_{\pm} = (G_f - G_f^{-1})X_a^{\text{out}} \pm Y_a^{\text{out}} \quad (15.45)$$

was measured. For the chosen input states one easily verifies that

$$V(X_+) = 1 , \quad (15.46)$$

$$V(X_-) = 4(G_f - G_f^{-1})^2 . \quad (15.47)$$

These quantities were measured by adjusting the relative gain of the photocurrent amplifiers to weight the X_a^{out} quadrature as indicated. This ensures that any correlation between X_a^{out} and Y_a^{out} will give maximum cancellation of the noise from each quadrature separately in the variances for X_{\pm} . The results of this experiment are shown in Fig. 15.6. The results of all experiments taken together clearly indicate that the scheme is operating as a back action evasion device.

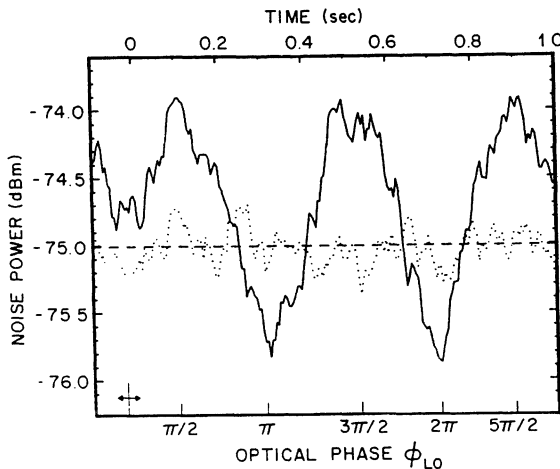


Fig. 15.6. The combination of the amplified signal and probe quadrature at output versus the phase of the local oscillator. The variance of X_- occurs at integer multiples of π . The dotted line corresponds to the case of the paramp off, and is identical to randomly added shot-noise levels of the signal and probe. The noise reduction is 0.6 dB below the combined shot-noise level. From Arthur La Porta: Phys. Rev. Lett. **62**, 28 (1989)

Recently, QND experiments have been performed [15.5] with two-photon transitions in three-level atoms, where the signal amplitude is strongly correlated with the probe phase. The measurement correlation between the signal in and the probe out is $C_{X_a^{\text{in}} Y_{\phi}^{\text{out}}}^2 = 0.45$ and the back action evasion correlation between signal in and signal out is $C_{X_a^{\text{in}} X_a^{\text{out}}}^2 = 0.9$. The overall performance measure of this device as a QND optical tap is then determined by $C_{X_a^{\text{in}} Y_{\phi}^{\text{out}}}^2 + C_{X_a^{\text{in}} X_a^{\text{out}}}^2 = 1.35$, which exceeds the beam splitter limit of one, but is still well below the optimal value of 2.

15.7 A Photon Number QND Scheme

We turn now to a scheme to measure the photon number in the signal field. Conventional photon counting techniques absorb quanta. The scheme considered is a true nondemolition measurement of photons in that no photons are absorbed from the signal field [15.4].

Consider the coupled signal/probe system described by the interaction Hamiltonian

$$\mathcal{H}_1 = \hbar\chi a^\dagger ab^\dagger b \quad (15.48)$$

where a refers to the signal mode, and b to the probe. Such a coupling can occur in a four wave mixing process in which case χ is proportional to the third-order nonlinear susceptibility.

Clearly, $a^\dagger a$ is a constant of the motion and is thus a QND variable for the signal. The solution of the Heisenberg equations of motion gives

$$a(t) = e^{-i\chi b^\dagger b t} a(0), \quad (15.49)$$

$$b(t) = e^{-i\chi a^\dagger a t} b(0). \quad (15.50)$$

These equations describe a mutual intensity-dependent phase shift for the signal and probe fields. If we can measure this phase shift on the probe, information on the signal photon number may be obtained. The probe phase shift may, in fact, be determined by homodyne detection of a probe quadrature.

Using (15.24 and 25) the phase quadrature for the probe field becomes

$$Y_{\phi}^{\text{out}} = \cos(\kappa a^\dagger a) Y_{\phi}^{\text{in}} - \sin(\kappa a^\dagger a) Y_a^{\text{in}} \quad (15.51)$$

where $\kappa = \chi t$. It would appear from this equation that the signal operator that we actually measure is not simply $a^\dagger a$ but a nonlinear function of $a^\dagger a$. However in any practical scheme κ is so small that we may approximate the trigonometric functions by the lowest order in κ . Thus, we use

$$Y_{\phi}^{\text{out}} = Y_{\phi}^{\text{in}} - \kappa a^\dagger a Y_a^{\text{in}}. \quad (15.52)$$

What quantity plays the role of the QND gain in this scheme? To answer this question we need to evaluate the correlation functions which provide criteria for the quality of the QND measurement. The first of these functions is

$$\begin{aligned} C_{a^\dagger a Y_\phi^{\text{out}}}^2 &= \frac{|\langle a^\dagger a Y_\phi^{\text{out}} \rangle - \langle a^\dagger a \rangle \langle Y_\phi^{\text{out}} \rangle|^2}{V(a^\dagger a) V(Y_\phi^{\text{out}})} \\ &= \frac{\kappa^2 \langle Y_a^{\text{in}} \rangle^2 V(a^\dagger a)}{V(Y_\phi^{\text{in}}) + 2\kappa F_1 + \kappa^2 F_2} \end{aligned}$$

where

$$F_1 = \langle a^\dagger a \rangle \langle Y_a^{\text{in}}, Y_\phi^{\text{in}} \rangle_s,$$

$$F_2 = V(a^\dagger a) \langle Y_\phi^{\text{in}} \rangle^2 + V(Y_\phi^{\text{in}}) (V(a^\dagger a) + \langle a^\dagger a \rangle^2)$$

and the symmetrised correlation function is defined by

$$\langle A, B \rangle_s = \frac{1}{2} \langle AB + BA \rangle - \langle A \rangle \langle B \rangle . \quad (15.53)$$

If we now assume $\langle Y_a^{\text{in}} \rangle^2 \gg V(Y_a^{\text{in}}), V(Y_\phi^{\text{in}})$ (that is the coherent amplitude of the probe is much greater than the fluctuations in either quadrature), we find,

$$C_{a^\dagger a Y_\phi^{\text{out}}}^2 \rightarrow 1 \quad (15.54)$$

when $\langle Y_a^{\text{in}} \rangle$ is large. It would thus appear that the coherent amplitude of the probe plays the role of the QND gain. This result is easily understood in terms of a complex amplitude diagram for the probe. If the vector representing the input state of the probe is very long a small rotation due to the signal makes a large change in the projection of the coherence vector onto the phase quadrature direction. In a similar way the signal-to-noise ratio of the output quadrature reduces to the signal-to-noise ratio for $a^\dagger a$ in the limit of $\langle Y_\phi^{\text{in}} \rangle \gg 1$. One easily verifies that the conditional variance of $a^\dagger a$ at the output approaches zero in the same limit. This last result indicates that the conditional state of the signal output will have sub-Poissonian statistics.

If κ is not small, we cannot simply approximate the coupling between the signal and probe as being linear in the signal photon number. A measurement of the probe quadrature phase still provides information on the signal photon number, however, due to the multivalued nature of the trigonometric functions, the signal is reduced to a superposition of number states in the case that the initial photon number distribution of the signal is sufficiently broad [15.4].

Exercises

15.1 Consider a signal beam and a probe beam coupled via a four wave mixing interaction;

$$\mathcal{H}_1 = \hbar\chi a^\dagger ab^\dagger b \quad (15.55)$$

Calculate the QND correlation coefficients between the amplitude quadrature of the signal $X_a = a^\dagger + a$ and the phase quadrature of the probe, $Y_\phi = -i(b - b^\dagger)$.

15.2 Consider a QND measurement in an optical cavity. Generalise the QND correlations to the frequency domain. For example, the stationary spectral covariance between signal X and probe Y is defined as

$$C_{XY}(\omega) = \int dt e^{-i\omega t} \frac{1}{2} \langle X(t) Y(t + \tau) + Y(t + \tau) X(t) \rangle \quad (15.56)$$

Using the input/output formulation developed in Chap. 7, calculate the spectral QND correlations between the signal amplitude and the probe phase in the input and output fields for the intracavity interaction

$$\mathcal{H}_I = \hbar \frac{\chi}{2} X_a Y_\phi . \quad (15.57)$$

15.3 Consider the four wave mixing process with the Hamiltonian

$$\mathcal{H}_1 = \hbar\chi a^\dagger ab^\dagger b \quad (15.58)$$

taking place inside a cavity. Calculate the QND spectral correlations between the amplitude quadrature X_a of the signal and the phase quadrature Y_ϕ of the probe, in the input and output fields.

15.4 Consider a degenerate parametric amplifier inside a resonant two-sided optical cavity with mirrors with loss rates γ_1, γ_2 . Treat the left-hand input as the signal and the right-hand input as the probe. Calculate the QND spectral correlations between the phase quadratures of the signal and the probe.

15.5 Calculate the QND correlations for a beam splitter with a squeezed input probe.

16. Quantum Coherence and Measurement Theory

The feature of quantum mechanics which most distinguishes it from classical mechanics is the coherent superposition of distinct physical states. Many of the less intuitive aspects of the quantum theory can be traced to this feature. Does the superposition principle operate on macroscopic scales? The famous Schrödinger cat argument highlights problems of interpretation where macroscopic superposition states is allowed. In this chapter we discuss schemes to produce and detect superposition states in an optical context. As we shall show such states are very fragile in the presence of dissipation and rapidly collapse to a classical mixture exhibiting no unusual interference features.

The superposition principle is also the source of the ‘problem of measurement’ in quantum mechanics. We do not seek to present a solution to this problem here. Rather we show how the effect of the environment on superposition states enables a consistent description of the measurement process to be given, which avoids some of the problems inherent in previous approaches.

16.1 Quantum Coherence

The well known two slit experiment demonstrates the observational consequences of the coherent superposition of states, namely the possibility of interference patterns. In analogy with the classical theory of wave interference the visibility of the interference pattern in the probability distributions for various measurements can be used as a measure of quantum coherence. (There is a possibility of confusion here which should be cleared up. In the interference of waves we are usually concerned with the interference of two or more field modes. In this chapter, however, we are concerned with the superposition of different states of a single mode.)

The essential point in understanding quantum coherence is the physical distinction between the coherent superposition state

$$|\psi\rangle = \sum_j c_j |\phi_j\rangle \quad (16.1)$$

and the classical mixture

$$\rho_m = \sum_j |c_j|^2 |\phi_j\rangle\langle\phi_j| . \quad (16.2)$$

The density operator corresponding to the pure state in (13.1) is

$$\rho_p = \rho_m + \sum_{i \neq j} c_i c_j^* |\phi_i\rangle \langle \phi_j| . \quad (16.3)$$

How is one to distinguish these states in practice? Let X be the operator corresponding to some physical quantity with eigenvalues x . The probability distribution for X in the state $|\psi\rangle$ is given by

$$P_p(x) = P_m(x) + \sum_{i \neq j} c_i c_j^* \langle x | \phi_i \rangle \langle \phi_j | x \rangle , \quad (16.4)$$

where $P_m(x)$ is the probability distribution for the state ρ_m given by

$$P_m(x) = \sum_i |c_i|^2 |\langle x | \phi_i \rangle|^2 = \sum_i |c_i|^2 P_{\phi_i}(x) . \quad (16.5)$$

Measurements of X will distinguish the states ρ_m and ρ_p provided the second term in (16.4) is nonzero. We are thus led to define the quantum coherence with respect to the measurement of X by the coherence function

$$\mathcal{C}(x) = \sum_{i \neq j} c_i c_j^* \langle x | \phi_i \rangle \langle \phi_j | x \rangle . \quad (16.6)$$

How does one choose an operator X such that the resulting probability distribution will exhibit interference fringes? Clearly one cannot choose operators which are diagonal in the basis $\{|\phi_i\rangle\}$ as then the coherence function vanishes. The simplest example of an operator which distinguishes these states is the projector

$$P = |\psi\rangle \langle \psi| \quad (16.7)$$

with eigenvalues $p \in \{0, 1\}$. Then

$$P_p(p) = \delta_{1,p} \quad (16.8)$$

while

$$P_m(p) = \begin{cases} \sum_j |c_j|^4 & \text{if } p = 1 \\ 1 - \sum_j |c_j|^4 & \text{if } p = 0 . \end{cases} \quad (16.9)$$

The coherence function is

$$\mathcal{C}(p) = (-1)^p \left(\sum_j |c_j|^4 - 1 \right) . \quad (16.10)$$

In practice, however, there may be no way to measure the operator P .

In quantum optics one either measures photon number (by photon counting) or quadrature phase (by balanced homodyne detection). As an example consider the superposition of two number states

$$|\psi\rangle = \frac{1}{\sqrt{2}}(|n_1\rangle + |n_2\rangle), \quad (16.11)$$

and the corresponding mixed state

$$\rho_m = \frac{1}{2}(|n_1\rangle\langle n_1| + |n_2\rangle\langle n_2|). \quad (16.12)$$

A measurement of the photon number will not distinguish these states. However, as the quadrature phase does not commute with the number operator, quadrature phase measurements should distinguish the states.

Define the quadrature operator

$$X_\theta = (ae^{-i\theta} + a^\dagger e^{i\theta}) \quad (16.13)$$

with the eigenstates $|x_\theta\rangle$. Using the result

$$\langle x_\theta | n \rangle = (2\pi)^{-1/4} (2^n n!)^{-1/2} H_n \left(\frac{x_\theta}{\sqrt{2}} \right) e^{-x_\theta^2/4 - in\theta} \quad (16.14)$$

one finds

$$P_m(x_\theta) = \frac{1}{2}[P^{(1)}(x_\theta) + P^{(2)}(x_\theta)] \quad (16.15)$$

and

$$\mathcal{C}(x_\theta) = (2\pi)^{-1/2} e^{-x_\theta^2/2} (2^{n_1+n_2} n_1! n_2!)^{-1/2} \mathfrak{h}(x_\theta) \quad (16.16)$$

$$\mathfrak{h}(x_\theta) = H_{n_1} \left(\frac{x_\theta}{\sqrt{2}} \right) H_{n_2} \left(\frac{x_\theta}{\sqrt{2}} \right) \cos(n_1 - n_2)\theta \quad (16.17)$$

where

$$P^{(i)}(x_\theta) = (2\pi)^{-1/2} (2_i^n n_i!)^{-1} H_{n_i} \left(\frac{x_\theta}{\sqrt{2}} \right)^2 e^{-x_\theta^2/2}. \quad (16.18)$$

Thus a superposition of number states will exhibit interference fringes for some quadrature phase angle θ . In Fig. 16.1 we plot $P_p(x_\theta)$ versus x_θ for $\theta = 0$. It is surprising that, depending on whether $n_1 - n_2$ is even or odd, certain phase angles do not give interference. However, it is quite clear that the superposition of two number states will exhibit phase dependent noise despite the fact that number states themselves have phase independent noise.

As a second example consider the superposition of two coherent states

$$|\psi\rangle = \mathcal{N}(|\alpha_1\rangle + |\alpha_2\rangle), \quad (16.19)$$

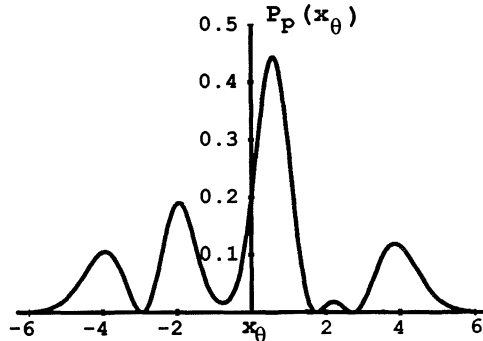


Fig. 16.1. A plot of the probability density for the quadrature phase with phase angle at zero, for a superposition of two number states with $n_1 = 0, n_2 = 5.0$

where

$$\mathcal{N} = \frac{1}{\sqrt{2}} \left[1 + \frac{1}{2} e^{-(|\alpha_1|^2 + |\alpha_2|^2)/2} (e^{\alpha_1^* \alpha_2} + e^{\alpha_1 \alpha_2^*}) \right]^{-1/2} \quad (16.20)$$

and

$$\rho_m = \frac{1}{2} (|\alpha_1\rangle\langle\alpha_1| + |\alpha_2\rangle\langle\alpha_2|) . \quad (16.21)$$

In this case measurements of either quadrature phase or photon number should exhibit interference fringes as neither of the corresponding operators commutes with a coherent state projector. However, as we shall see there is an optimal quadrature phase angle which leads to maximum interference.

In the case of photon number one finds

$$P_p(n) = \mathcal{N}^2 [P^{(1)}(n) + P^{(2)}(n) + \mathcal{C}(n)] \quad (16.22)$$

where

$$\mathcal{C}(n) = \frac{1}{n!} \exp \left[-\frac{1}{2} (|\alpha_1|^2 + |\alpha_2|^2) \right] [(\alpha_1 \alpha_2^*)^n + (\alpha_1^* \alpha_2)^n] \quad (16.23)$$

and

$$P^{(i)}(n) = \frac{1}{n!} |\alpha_i|^{2n} e^{-|\alpha_i|^2} . \quad (16.24)$$

If we write $\alpha_i = |\alpha_i| e^{i\phi}$ then

$$\mathcal{C}(n) = 2 [P^{(1)}(n) P^{(2)}(n)]^{1/2} \cos n(\phi_1 - \phi_2) \quad (16.25)$$

and we see that the degree of interference depends on the phase angle between the amplitudes of the superposed states. For simplicity, let us take $|\alpha_1| = |\alpha_2| = |\alpha|$. Then

$$P_p(n) = 2\mathcal{N}^2 \frac{1}{n!} |\alpha|^{2n} e^{-|\alpha|^2} [1 + \cos n(\phi_1 - \phi_2)] . \quad (16.26)$$

When $\phi_1 - \phi_2 = \pi$, $P_p(n)$ is zero for n odd. Thus a superposition of coherent states π out of phase but of equal amplitude will contain only even photon number; a similar situation to that of a squeezed vacuum state.

In the case of quadrature phase measurements one finds

$$P^{(i)}(x_\theta) = (2\pi)^{-1/2} \exp \left(-|\alpha_i|^2 + \frac{x_\theta^2}{2} - \frac{(x_\theta - \alpha_i e^{-i\theta})^2}{2} - \frac{(x_\theta - \alpha_i^* e^{i\theta})^2}{2} \right) \quad (16.27)$$

and thus

$$\mathcal{C}(x_\theta) = 2[P^1(x_\theta)P^2(x_\theta)]^{1/2} \cos \Phi(\alpha_1, \alpha_2, x_\theta) \quad (16.28)$$

where

$$\Phi = \text{Im} \left\{ \frac{(\alpha_1^*)^2}{2} e^{2i\theta} + \frac{\alpha_2^2}{2} e^{-2i\theta} + \alpha_1 x_\theta e^{-i\theta} + \alpha_2^* x_\theta e^{i\theta} \right\} . \quad (16.29)$$

To gain some insight into these equations we take $|\alpha_1| = |\alpha_2| = |\alpha|$ and choose

$$\theta = \phi_+ = (\phi_1 + \phi_2)/2 . \quad (16.30)$$

This phase angle bisects the angle between the two coherent states (Fig. 16.2). We then have

$$P^{(1)}(x) = P^{(2)}(x) = (2\pi)^{-1/2} \exp[-(x - 2|\alpha| \cos \phi_-)^2/2] \quad (16.31)$$

and

$$\mathcal{C}(x) = 2P^{(1)}(x) \cos[2|\alpha| \sin \phi_- (x - |\alpha| \cos \phi_-)] \quad (16.32)$$

with $\phi_- = (\phi_1 - \phi_2)/2$ and we have put $x = x_{\phi^+}$. Thus

$$P_p(x) = 2\mathcal{N}^2 P^{(i)}(x) \{1 + \cos[2|\alpha| \sin \phi_- (x - |\alpha| \cos \phi_-)]\} . \quad (16.33)$$

This is a gaussian centred at $2|\alpha| \cos \phi_-$ modulated by an interference envelope (Fig. 16.3)

The above result has a simple geometric interpretation. Referring to Fig. 16.2 we see that projecting the two coherent states onto the x_{ϕ^+} axis gives a maximum overlap centred on the mean value $\langle X_{\phi^+} \rangle = 2|\alpha| \cos \phi_-$. We conclude that whenever the coherent states are projected onto a quadrature such that they overlap exactly, the interference will be maximum. Conversely, we expect that if we project the coherent states onto a quadrature with $\theta = \phi_+ \pm \pi/2$,

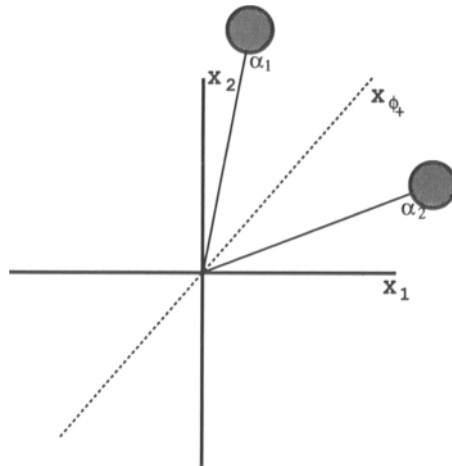


Fig. 16.2. Phase-space representation of the superposition of two coherent states. The dashed line represents the direction of the quadrature phase angle which exhibits maximum interference

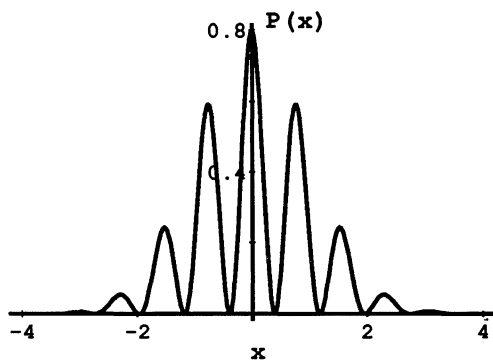


Fig. 16.3. The probability density for the quadrature phase at phase angle $\theta = \phi_+ = \pi/2$ for a superposition of two coherent states with $\phi_- = \pi/2$. This is the quadrature direction that bisects the angle between the two coherent amplitudes, and which exhibits maximum interference ($\alpha = 4.0$)

there will be minimum overlap and thus the least interference. (Exercise 16.1) In the next section we consider schemes to generate such coherent superpositions of coherent states in nonlinear optics.

We now need to analyse the effect of dissipation on the interference features discussed above. With this in mind we write the coherence function in terms of the complex valued functions $C(x)$

$$\mathcal{C}(x) = C(x) + C(x)^* . \quad (16.34)$$

where for a general superposition state

$$C(x) = \sum_{i < j} c_i c_j^* \langle x | \phi_i \rangle \langle \phi_j | x \rangle . \quad (16.35)$$

A convenient measure for the degree of quantum coherence is the quantum visibility defined by

$$\mathcal{V}(x) = \frac{|C(x)|}{[P^{(1)}(x)P^{(2)}(x)]^{1/2}} . \quad (16.36)$$

In all the cases investigated above $\mathcal{V}(x)$ is unity for all values of x and the states considered thus have maximum quantum coherence. However, when dissipation is present this is no longer the case.

16.2 The Effect of Fluctuations

In this section we show that quantum coherence associated with superposition states is extremely fragile in the presence of nonunitary effects such as damping. Such effects cause a decay of quantum coherence at a rate which is proportional to a parameter which measures the separation of the superposed states. For macroscopic separations this decay can be very rapid. Early work on this subject was done by Joos and Zeh [16.1] and Calderia and Leggett [16.2]. We follow the treatment of Milburn and Walls [16.3].

We first consider the effects of dissipation. The master equation for a damped harmonic oscillator in the interaction picture is

$$\frac{d\rho}{dt} = \frac{\gamma}{2} (2a\rho a^\dagger - a^\dagger a\rho - \rho a^\dagger a) \quad (16.37)$$

where γ is the damping constant and the reservoir is taken to be at zero temperature. We will solve this equation for an initial superposition of coherent states using the normally ordered characteristic function,

$$X(\lambda, t) = \text{Tr} [\rho(t) e^{\lambda a^\dagger} e^{-\lambda^* a}] . \quad (16.38)$$

Using (16.36) the equation of motion for $X(\lambda, t)$ is

$$\frac{\partial X}{\partial t} = -\frac{\gamma}{2} \left(\lambda^* \frac{\partial X}{\partial \lambda} + \text{c.c.} \right) \quad (16.39)$$

where c.c. means complex conjugate. The solution to this equation is

$$X_0(\lambda e^{-\gamma t/2}, \lambda^* e^{-\gamma t/2}) \quad (16.40)$$

where

$$X_0(\lambda) = X(\lambda, 0) . \quad (16.41)$$

For the initial state given in (16.19), a superposition of coherent states, we find

$$X_0(\lambda) = \mathcal{N}^2 \sum_{i,j=1}^2 e^{(\lambda\alpha_i^* - c.c.)} \langle \alpha_i | \alpha_j \rangle . \quad (16.42)$$

Thus

$$X(\lambda, t) = \mathcal{N}^2 \sum_{i,j=1}^2 \langle \alpha_i | \alpha_j \rangle \exp[(\lambda\alpha_i^* - c.c.)e^{-\gamma t/2}] . \quad (16.43)$$

The corresponding solution for the density operator is

$$\rho(t) = \mathcal{N}^2 \sum_{i,j=1}^2 \langle \alpha_i | \alpha_j \rangle^{(1-e^{-\gamma t})} |\alpha_i e^{-\gamma t/2}\rangle \langle \alpha_j e^{-\gamma t/2}| . \quad (16.44)$$

Due to the coefficient with $i \neq j$ in this expansion the contribution of the off-diagonal terms to the coherence function will be small. Thus the superposition is reduced to a near mixture of coherent states.

The visibility for any measurement is easily found to be

$$\mathcal{V}(x) = |\langle \alpha_1 | \alpha_2 \rangle|^{(1-e^{-\gamma t})} \quad (16.45)$$

where $x = x_\theta$ for quadrature phase or $x = n$ for number measurements. For short times this is given approximately by

$$\mathcal{V}(x) \approx \exp\left(-\frac{\gamma t}{2} |\alpha_1 - \alpha_2|^2\right) . \quad (16.46)$$

Thus the rate at which coherence decays is proportional to the square of the distance between the superposed coherent amplitudes. In the last section we considered the case $\alpha_1 = -\alpha_2$ which gave good interference fringes centered on the origin for the appropriate quadrature. However, we now see that such fringes must decay rapidly causing the quadrature phase statistics to be indistinguishable from a classical mixture of coherent states. A word of caution is required here. Even though the visibility decays in the same way for all measurements in this case, for certain measurements there may be no interference in the first place. For example, if we take a superposition of two coherent states with amplitudes α and $-\alpha$ (with α real), the measurements of the real quadrature $X = a^\dagger + a$, will not show interference. In this case there is no decay of the cross term in the probability density as it merely represents the overlap of two distinct gaussians, not interference.

This result is not confined to amplitude damping. For example, for the phase diffusion model discussed in Exercise 6.3 the master equation is

$$\frac{d\rho}{dt} = \frac{\gamma}{2} [2a^\dagger a \rho a^\dagger a - (a^\dagger a)^2 \rho - \rho (a^\dagger a)^2] . \quad (16.47)$$

The solution for the matrix elements in the number basis is

$$\langle n | \rho(t) | m \rangle = \exp \left[-\frac{\gamma t}{2} (n - m)^2 \right] \langle n | \rho(0) | m \rangle . \quad (16.48)$$

If $\rho(0)$ is a superposition of number states $|n_1\rangle$ and $|n_2\rangle$ the visibility of the quadrature phase statistics is given by

$$\mathcal{V}(x) = \exp \left[-\frac{\gamma t}{2} (n_1 - n_2)^2 \right] \quad (16.49)$$

which shows a rapid decay when $n_1 - n_2$ is large.

These examples are special; the visibility in each case decays in the same way for all measurements which give interference fringes. This is because the superposed states are eigenstates or near eigenstates of the operator appearing in the irreversible part of the evolution equation. This is an important point to which we shall return in the next section. In other cases the visibility is more complicated. For example, consider the effect of phase diffusion on the quadrature phase statistics of a superposition of two coherent states with $\alpha_1 = -\alpha_2 = q_0$ where q_0 is real. If we choose $\theta = \pi/2$ (that is, we project onto the imaginary axis in the complex amplitude diagram) we find that for short times

$$\mathcal{V}(x_{\pi/2}) \approx 1 - \gamma t (2q_0 x_{\pi/2})^2 . \quad (16.50)$$

As expected, the coherence decays from unity at a rate which is proportional to the square of the separation of the superposed states. In Fig. 16.4 we plot the exact visibility for the quadrature phase with a superposition of coherent states subject to phase diffusion at $\gamma t = 0.1$.

A similar result may be derived for quadrature-phase measurements on a superposition of number states undergoing damping. To show this we use the complex P -representation for the projector $|n_i\rangle\langle n_j|$

$$|n_i\rangle\langle n_j| = \oint_{c_1} d\alpha \oint_{c_2} d\beta P_{ij}(\alpha, \beta) \frac{|\alpha\rangle\langle\beta^*|}{\langle\beta^*|\alpha\rangle} \quad (16.51)$$

where

$$P_{ij}(\alpha, \beta) = -\frac{1}{4\pi^2} e^{\alpha\beta} (n_i! n_j!)^{1/2} \alpha^{-(n_i+1)} \beta^{-(n_j+1)} \quad (16.52)$$

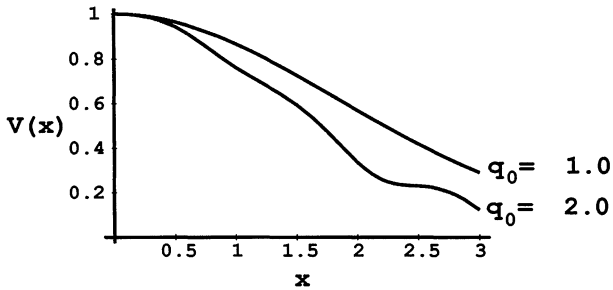


Fig. 16.4. A plot of the visibility for quadrature phase measurements on an oscillator prepared in a coherent superposition of coherent states which is subject to phase diffusion

and c_1, c_2 are contours encircling the origin. Thus under time evolution $|n_i\rangle\langle n_j|$ evolves to

$$(|n_i\rangle\langle n_j|)_t = \oint_{c_1} d\alpha \oint_{c_2} d\beta P_{ij}(\alpha, \beta) \langle \beta^* | \alpha \rangle^{(1 - e^{-\gamma t})} \times \frac{|\alpha e^{-\gamma t/2}\rangle\langle \beta^* e^{-\gamma t/2}|}{\langle \beta^* | \alpha \rangle}. \quad (16.53)$$

Using this result one may show

$$\begin{aligned} C(x_\theta, t) &= (2\pi)^{-1/2} 2^{-(n_1 + n_2)/2} (n_1! n_2!)^{-1/2} (-1)^{n_1 + n_2} \\ &\times \exp \left[-\frac{x_\theta^2}{2} - i(n_1 - n_2)\theta \right] e^{-\gamma t(n_1 + n_2)/2} \\ &\times \sum_{p=0}^{\min(n_1, n_2)} 2^p e^{\gamma t p} p! \binom{n_1}{p} \binom{n_2}{p} H_{n_1 + n_2 - 2p} \left(\frac{x_\theta}{2} \right). \end{aligned} \quad (16.54)$$

The dominant term in the sum occurs for $p = \min(n_1, n_2)$. For example, if $n_1 > n_2$ the time dependence of the dominant term is proportional to $\exp[-\gamma t(n_1 - n_2)/2]$. The coherence decays at a rate which is proportional to the separation of the states.

16.3 Quantum Measurement Theory

The object of any physical theory is to provide an explanation for the results of measurements. It is usually the case that measurements are made by coupling a macroscopic device to the system of interest which may be of any size. If the system is very small then some element of amplification is required. Can this

process, considered purely as a physical interaction between systems, be described entirely within the framework of quantum mechanics? Would such a description, if given, accord with our intuitive understanding of real measuring devices? How is the measured system effected by the measurement? These are questions which are generally included under the heading of *the measurement problem*.

To understand why there might be a problem we will consider a simple model for the interaction between a measured system S and a measuring device M . Let us first ignore the macroscopic nature of M and simply treat it as a single quantum system with one degree of freedom. As we shall see such an assumption does not lead to an adequate description of the measurement process. The macroscopic nature of M is essential for a complete description.

Let $\{|m_i\rangle\}$ denote a set of eigenstates of some meter quantity and let $\{|s_i\rangle\}$ denote the eigenstates which diagonalise the system operator we are seeking to measure. Suppose the initial state of the system is $|m_0\rangle \otimes |s_i\rangle$, and further suppose that under unitary evolution this state evolves to

$$|\psi_i(t)\rangle = |m_i\rangle \otimes |s_i\rangle . \quad (16.55)$$

Then, for a general system state

$$|\psi\rangle = \sum_i c_i |s_i\rangle \otimes |m_0\rangle \quad (16.56)$$

the state at time t will be

$$|\psi(t)\rangle = \sum_i c_i |m_i\rangle \otimes |s_i\rangle . \quad (16.57)$$

We regard m_i as the value read-out from the meter scale. If an observer finds the meter in a state $|m_j\rangle$ (with probability $|c_j|^2$) the system is subsequently (i.e., conditionally) described by the state $|s_j\rangle$. It is clear that in effect we have measured some physical quantity S , which is diagonal in the basis $\{|s_i\rangle\}$,

$$S = \sum_i a_i |s_i\rangle \langle s_i| . \quad (16.58)$$

Suppose one only knows that a measurement has taken place but we do not select a particular result. The state of the system must then be described by the reduced density operator obtained by tracing out over the meter states

$$\rho_s = \sum_i |c_i|^2 |s_i\rangle \langle s_i| . \quad (16.59)$$

Thus as a result of the measurement the density operator of the system is diagonal in the basis which diagonalises the measured operator. Alternatively the basis in which ρ_s is diagonal determines the system operator which has been measured. This is the standard description of the measurement process. Unfortunately, it is inadequate as we now explain.

The description given above assumed we read out a meter quantity which is diagonal in the basis $\{|m_i\rangle\}$. Suppose, however, we decide to read out another meter quantity diagonal in the basis $\{|\tilde{m}_i\rangle\}$. We can then express the meter states $|m_i\rangle$ in the alternative basis $\{|\tilde{m}_i\rangle\}$, i.e.,

$$|m_i\rangle = \sum_j \langle \tilde{m}_j | m_i \rangle |\tilde{m}_j\rangle . \quad (16.60)$$

The state of the combined system after the interaction is then

$$\begin{aligned} |\psi(t)\rangle &= \sum_i c_i |m_i\rangle \otimes |s_i\rangle \\ &= \sum_j d_j |\tilde{m}_j\rangle \otimes |r_j\rangle \end{aligned} \quad (16.61)$$

where

$$d_j |r_j\rangle = \sum_i c_i \langle \tilde{m}_j | m_i \rangle |s_i\rangle . \quad (16.62)$$

Although the system meter coupling has not altered there is now some ambiguity as to what system operator has been measured; is it

$$S = \sum_i a_i |s_i\rangle \langle s_i| \quad (16.63)$$

or

$$R = \sum_i b_i |r_i\rangle \langle r_i| ? \quad (16.64)$$

This ambiguity can only be removed if we say that the meter is so constructed that the only physical property that we readout is the one which is diagonal in the basis $\{|m_i\rangle\}$. What is the property of the meter which determines such a preferred or *pointer* basis?

We can answer this question by admitting that a true measuring device must be macroscopic and thus contain many degrees of freedom. Hence, in addition to the read-out variable, we must consider the meter as composed of many other degrees of freedom possibly coupled to the read-out variable. These other degrees of freedom cannot be determined in any realistic scheme and thus may be treated as a reservoir. In order to model this situation we now divide the measurement scheme into system + meter + reservoir. The system and meter are directly coupled and the meter is coupled to the reservoir (Fig. 16.5). As Zurek has shown [16.4], it is the coupling between the meter and the reservoir which determines the pointer basis.

In order that the special correlation between the system and the meter given by (16.54) be preserved in the presence of the coupling to the reservoir, described

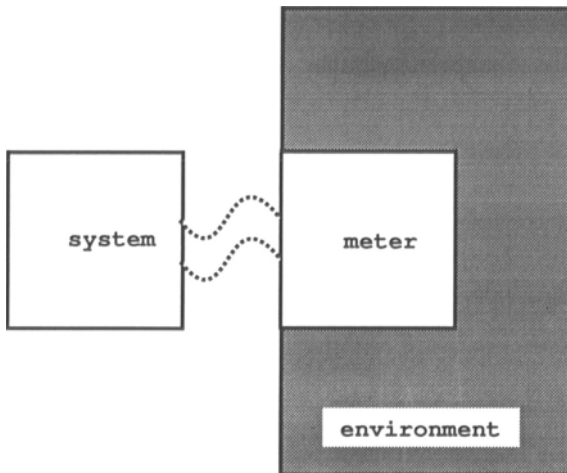


Fig. 16.5. Schematic representation of the subdivision of a generic measurement scheme

by some Hamiltonian \mathcal{H}_{ME} , we require that the pointer basis $\{|m_i\rangle\}$ be a complete set of eigenstates for a pointer quantity M which commutes with \mathcal{H}_{ME} . This ensures that fluctuations from the reservoir do not find there way back to the measured system quantity S . In many situations it may not be possible to find an operator which satisfies this condition exactly. However, an approximate pointer basis may exist in as much as the diagonal elements of the density operator in such a basis relax on a very long time scale while the off-diagonal elements decay on a much shorter time scale.

Thus it is the meter-reservoir interaction which determines the pointer observable M and thus the corresponding pointer basis appropriate to the measurement. The to-be-measured quantity is only defined in the course of the meter-reservoir interaction; a situation consistent with Bohr's general description of measurement in quantum mechanics.

The meter cannot be observed in a superposition of pointer-basis states as its state vector is being continually collapsed. It is the monitoring of the meter by the reservoir which results in the apparent state reduction of the system and the meter is so constructed to ensure that this occurs. The correlations between the corresponding system and pointer-basis states are preserved in the final mixed state density operator

$$\sum_{i,j} c_i c_j^* |m_i\rangle \langle m_j| \otimes |s_i\rangle \langle s_j| \rightarrow \sum_i |b_i|^2 |\tilde{m}_i\rangle \langle \tilde{m}_i| \otimes |r_i^p\rangle \langle r_i^p| \quad (16.65)$$

where $\{|r_i^p\rangle\}$ are the system states determined by the pointer basis, referred to as the *relative states*.

There is a close connection between the concept of a quantum nondemolition measurement and the concept of a pointer basis. The condition that an operator $Q(t)$ be a QND variable is that (in the interaction picture)

$$[Q(t), Q(t')] = 0 . \quad (16.66)$$

Applying this idea to the measurement description above it is clear that the pointer observable P , which determines the pointer basis, must be a QND variable of the meter. This ensures that an initial eigenstate of P evolves entirely within the pointer basis set.

In the theory of QND measurements we also require the variable Q to maintain its QND property in the presence of couplings to other systems, the reservoir in our example, which represent further stages of the meter device. This will be true provided the back action evasion criterion is satisfied

$$[Q(t), \mathcal{H}_{\text{ME}}] = 0 \quad (16.67)$$

where \mathcal{H}_{ME} represents the interaction Hamiltonian between the system of the QND variable and other systems to which it is coupled (the reservoir in our case). This property is precisely the property that the pointer observable must satisfy. We may thus view the pointer observable as a QND variable of the meter which is coupled to the environment by a back action evasion coupling.

16.4 Examples of Pointer Observables

In Sect. 16.2 we considered a number of models which lead to the density operator becoming diagonal in a preferred basis. For example, if the meter is a harmonic oscillator coupled to the bath by

$$\mathcal{H}_{\text{ME}} = aa^\dagger \Gamma_E , \quad (16.68)$$

so that it evolves according to the master equation (13.46), the state of the meter becomes diagonal in the number basis. The pointer observable is $a^\dagger a$ and (16.67) represents an ideal back action evasion coupling.

As another example suppose that the amplitude of an oscillator is coupled to the environment by

$$\mathcal{H}_{\text{ME}} = a\Gamma^\dagger + a^\dagger\Gamma . \quad (16.69)$$

This is not a back-action evasion coupling. However, the meter state tends to become diagonal in the coherent state basis which are eigenstates of the operator a . Unfortunately the diagonal elements of the density operator in this basis are also changed. However, as we saw in (16.43) for short times the diagonal elements do not change much, yet coherence between states separated by large coherent amplitudes decays quite rapidly. In this case we can say that the coherent states are an approximate pointer basis.

16.5 Model of a Measurement

We are now able to consider a full model of a quantum limited measurement including the interaction of the meter with the environment. The model we discuss was first given by Walls et al. [16.5]. The quantum system and meter are taken to be harmonic oscillators with annihilation operators a and b , respectively. The coupling between the system and the meter is taken to be quadratic in the system amplitude and the interaction Hamiltonian is

$$\mathcal{H}_{\text{SM}} = \frac{\hbar}{2} a^\dagger a (bE^* + b^\dagger E) . \quad (16.70)$$

Such a system may represent a four wave mixing interaction in quantum optics, where one field is taken as classical of amplitude E . The measured system operator is, as we shall see, $a^\dagger a$ (or some function thereof).

We assume that mode b is coupled to the environment by amplitude coupling

$$\mathcal{H}_{\text{ME}} = b\Gamma^\dagger + b^\dagger\Gamma . \quad (16.71)$$

This will determine a particular pointer basis. There are good physical reasons why this is a suitable choice for \mathcal{H}_{ME} . First, if the oscillators are realised as field modes this coupling represents the usual system-bath interaction of a linear loss mechanism. In particular it could represent the interaction of a field mode with a photo-electron counter. Perhaps the most important reason for choosing \mathcal{H}_{ME} in this form, however, is that it leads to the coherent state pointer basis. As coherent states have a well defined semi-classical limit this is a desirable basis for a real (i.e., classical) measuring device. We now solve for the complete dynamics of the system and meter coupled to the bath.

The density operator for the system and meter after tracing out the reservoir obeys the master equation

$$\frac{d\rho}{dt} = -\frac{i}{2}[(Eb^\dagger + E^*b)a^\dagger a, \rho] + \frac{\gamma}{2}(2b\rho b^\dagger + b^\dagger b\rho - \rho b^\dagger b) . \quad (16.72)$$

We have assumed that the environment is at zero temperature. Initially the state of the system is arbitrary while the meter is in the ground state

$$\rho(0) = \sum_{n,m=0}^{\infty} (\rho_{nm}|n\rangle\langle m|)_S \otimes (|0\rangle\langle 0|)_M \quad (16.73)$$

where we have expanded the system state in energy eigenstates and $\rho_{nm} = \langle n|\rho_s(0)|m\rangle$. Equation (16.72) may be solved by the characteristic function.

The solution is

$$\rho(t) = \sum_{n,m=0}^{\infty} \exp\left[\frac{|E|^2}{\gamma^2}(n-m)^2(1 - \gamma t/2 - e^{-\gamma t/2})\right] \\ \times (|n\rangle\langle m|)_S \otimes \left(\frac{|\alpha_n(t)\rangle\langle\alpha_m(t)|}{\langle\alpha_m(t)|\alpha_n(t)\rangle}\right)_M \quad (16.74)$$

where $|\alpha_n(t)\rangle$ is a meter coherent state with

$$\alpha_n(t) = \frac{En}{\gamma} (1 - e^{-\gamma t/2}) \quad (16.75)$$

In the long-time limit we have

$$\rho \rightarrow \sum_n P(n) (|n\rangle\langle n|)_S \otimes (|\alpha_n\rangle\langle\alpha_n|)_M \quad (16.76)$$

where $P(n)$ is the initial number distribution for the system. This is a mixture of number states in the system, perfectly correlated with a mixture of coherent states in the meter. It is thus of the general form of (16.65). The coherent states $|\alpha_n\rangle$ are the pointer basis states and the number states the corresponding relative states. The amplitude of the coherent states can be made arbitrarily large by increasing the strength of the system meter coupling E . Hence this model includes amplification in a natural way. The large- E limit is the appropriate limit for an accurate measurement [16.5]. In fact, the states $|\alpha_n\rangle$ for different values of n become approximately orthogonal as the coupling strength is increased.

We have assumed in this analysis that the environment is at zero temperature. For photoelectric detection this is a good assumption at optical frequencies. Were the environment not taken at zero temperature there would be an additional thermal spread in the diagonal part of the meter states.

This model contains all the features of the measurement process discussed in Sect. 16.3. The correlations between the system and the meter are created by unitary evolution. The (almost complete) reduction of the meter states to the pointer basis (the coherent states) occurs as a result of nonunitary dissipative evolution, which causes the off-diagonal elements of the meter state in the pointer basis to decay. It is clear that the model represents the measurement of some function of the system number operator $a^\dagger a$. To determine what this function is, we must reconsider the interpretation of the environment as a photo-electron counter. If we assume that every meter quanta lost to the environment is actually counted in the detector, a full analysis shows that, in fact, the model describes the measurement of the square of the number operator. This analysis may be found in the paper by Walls et al. [16.5].

From (16.74) we can calculate the reduced state of the system by tracing out over the meter states. The resulting state has an exponential decay of

off-diagonal elements in the number basis which goes as t^2 for short times. Such a dependence indicates that for short times a Markovian evolution equation does not describe the evolution of the system state. However, if the rate of photon counting, γ , is very large, then this short time behaviour is rapidly superceded by an exponential linear dependence. If we differentiate the resulting long time solution with respect to time we find the effective master equation for the system state is

$$\frac{d\rho_S}{dt} = -\frac{|E|^2}{2\gamma} [a^\dagger a, [a^\dagger a, \rho_S]] . \quad (16.77)$$

This equation may also be obtained by writing down the master equation for both modes a and b , and adiabatically eliminating mode b . In this strong measurement limit we see that as far as the system is concerned the effect of the measurement of photon number is to induce a diffusion in the oscillator phase. In some sense the phase is the conjugate variable to the photon number so this result is consistent with the uncertainty principle.

Exercises

16.1. Consider the superposition of two coherent states

$$|\psi\rangle = \mathcal{N}(|\alpha_0\rangle + |-\alpha_0\rangle) \quad (16.78)$$

where α_0 is real. Show that the probability distribution for $X_1 = a + a^\dagger$ is a double peaked Gaussian ($\alpha_0 \gg 1$), while the distribution for $X_2 = -i(a - a^\dagger)$ exhibits interference fringes.

16.2. The superposition of two squeezed vacuum states with orthogonal squeezing is given by

$$|\psi\rangle = \mathcal{N}(|0, r\rangle + |0, -r\rangle) . \quad (16.79)$$

Calculate the photon number distribution and show that only even photon numbers occur. Demonstrate also that the quadrature phase distributions exhibit interference fringes.

16.3. Consider the Hamiltonian

$$\mathcal{H} = \hbar\omega a^\dagger a + \hbar\chi(a^\dagger a)^2 . \quad (16.80)$$

Show that this Hamiltonian can generate a superposition of two coherent states or two squeezed states of the type discussed in the preceding questions.

16.4. The spin coherent states are defined by

$$|j; \gamma\rangle = \exp\left[-\frac{\theta}{2}(J_+ e^{-i\phi} - J_- e^{i\phi})\right] |j, j\rangle \quad (16.81)$$

where $\gamma = e^{i\phi} \tan(\theta/2)$ and $|j, j\rangle$ is a J_z eigenstate with eigenvalue j . Consider the superposition state

$$|\psi\rangle = \mathcal{N}(|j; \gamma_0\rangle + |j; -\gamma_0\rangle) \quad (16.82)$$

with γ_0 real. Calculate the probability distributions for J_x, J_y, J_z and show that the J_y distribution exhibits interference effects. Give a geometrical interpretation of this result.

16.5. Consider the two-mode squeezed vacuum state

$$|\psi\rangle = (\cosh r)^{-1} \sum_{n=0}^{\infty} (\tanh r)^n |n\rangle_1 \otimes |n\rangle_2 \quad (16.83)$$

and the mixed state with the same diagonal distribution

$$\rho = (\cosh r)^{-2} \sum_{n=0}^{\infty} (\tanh r)^{2n} |n\rangle_1 \langle n| \otimes |n\rangle_2 \langle n|. \quad (16.84)$$

Show that these states may be distinguished by the probability distributions for the two mode operators $a_{\pm}^\dagger a_{\pm}$ where

$$a_{\pm} = \frac{1}{\sqrt{2}}(a_1 \pm a_2). \quad (16.85)$$

17. Atomic Optics

The wave-particle duality of matter is a well established consequence of quantum theory. Interferometers with de Broglie waves have been demonstrated for electrons and neutrons. More recently such interference experiments have been demonstrated for atoms. Interferometric effects of neutral atoms were first observed in diffraction from optical standing waves [17.1]. This was followed by demonstrations of optical interferometers which explicitly used beam splitting and recombining mechanisms. The simplest configuration is a Young's double slit experiment shown in Fig. 17.1 which was demonstrated by *Carnal and Mlynek* [17.2]. The source of atoms in this experiment was a thermal beam of metastable helium atoms. The temperature of the source could be set to $T = 295$ K corresponding to a mean de Broglie wavelength of $\lambda_{\text{DB}} = 0.56$ Å or to $T = 83$ K corresponding to $\lambda_{\text{DB}} = 1.03$ Å. The interference pattern of the detected atoms is shown in Fig. 17.2. Other experiments have separated the atomic paths using gratings [17.3] or a splitting due to a coherent transition between two internal states [17.4–6]. Laser cooling of the atoms may be employed to increase the de Broglie wavelength of the atoms [17.4, 7]. In a cold atom interferometer the passage time of the atom is long. This greatly increases the phase sensitivity to a perturbation of potential energy.

Atomic interferometers have the advantage of a greater mass than electron or neutron interferometers and hence a greater sensitivity to changes in the gravitational potential. Atoms also have internal degrees of freedom which may be probed with light fields giving, for example, position information. This may be used to demonstrate certain quantum mechanical phenomena such as loss of interference when which path information is available. We shall give a description of a Feynman light microscope which gives path information in a Young's double slit experiment with atoms. Experiments and theory on atomic diffraction by a classical standing wave are discussed. We then consider the optical Stern-Gerlach effect where an atomic beam passed through a standing light wave is split into two beams depending on the atomic state. This phenomenon may be used to obtain a QND measurement of the atomic inversion.

We next consider atoms interacting with a quantum standing light wave. The momentum distribution of the scattered atoms is shown to be dependent on the photon statistics of the light field. This may be used to give a QND measurement of the photon number in a cavity field mode.

The interaction of the atom with the light field imparts a phase shift to the light field depending on the position of the standing wave which the atom passes

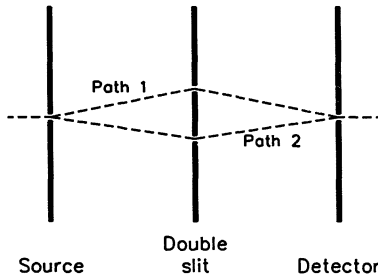


Fig. 17.1. Sketch of a double slit interferometer

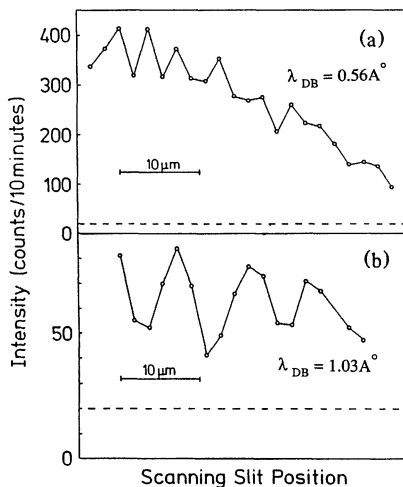


Fig. 17.2. Measured atomic intensity profiles in the detector plane as a function of the lateral detector position x . The profile is probed with a $2\text{ }\mu\text{m}$ wide single slit [17.2]. Atomic wavelength (a) $\lambda_{DB} = 0.56\text{ \AA}$, (b) $\lambda_{DB} = 1.03\text{ \AA}$

through. Thus, a phase-sensitive measurement of the field will give atomic position information.

17.1 Young's Interference with Path Detectors

Young's double slit experiment perhaps provides the simplest example in which the coherent addition of quantum-mechanical amplitudes leads to interference. When a path detector is introduced in order to monitor which slit the particle passes through, the principle of complementarity states that the interference is

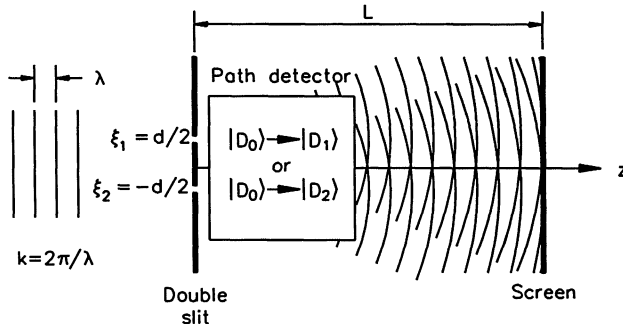


Fig. 17.3. Young's interference experiment with path detectors

necessarily destroyed. Detection of path information necessarily involves an interaction which couples the particles to the detectors. A path detector may be realised in atomic interferometry using the interaction with a light field.

Consider a Young's interference experiment for atoms of mass m together with a path detector (Fig. 17.3). We suppose that the atoms are propagating along the z direction with a well defined longitudinal momentum $p_z = \hbar k$ which is large compared to the transverse momentum changes during the course of the experiment. This allows us to work in the paraxial approximation throughout. The screen with the double slit is taken to be in the plane $z = 0$ with the narrow slits spaced d apart at the positions $x = \xi_1 = \frac{1}{2}d$ and $x = \xi_2 = -\frac{1}{2}d$. Starting with a plane atomic wave and assuming infinitesimally wide slits, the state immediately after passing through the double slit (at time t_1) is a coherent superposition of eigenstates

$$|\psi(t_1^+)\rangle = \frac{1}{\sqrt{2}}(|\xi_1\rangle + |\xi_2\rangle) . \quad (17.1)$$

If we first suppose that no path detector is present, the atom propagates freely to the screen (located in the plane $z = L$) under the unitary time evolution $U(t_2, t_1)$ for free motion with the Hamiltonian $\mathcal{H} = p^2/2m$. Thus when the atom hits the screen

$$\begin{aligned} |\psi(t_2)\rangle &= \frac{1}{\sqrt{2}} U(t_2, t_1) (|\xi_1\rangle + |\xi_2\rangle) \\ &= \frac{1}{\sqrt{2}} \int_{-\infty}^{\infty} [\psi_1(x) + \psi_2(x)] |x\rangle dx \end{aligned} \quad (17.2)$$

where

$$\psi_l(x) = \langle x | U(t_1, t_2) | \xi_l \rangle \propto \exp\left(i \frac{m(x - \xi_l)^2}{2\hbar(t_2 - t_1)}\right)$$

is the probability amplitude for detecting the atom at x on the screen given that the atom passed through slit l . We shall not be concerned with the normalisation constant in this discussion.

Under the assumption that the longitudinal momentum remains approximately constant at p_z throughout the interaction, the time of passage between double slit and screen is mL/p_z . We can then write

$$\psi_l(x) \propto \exp\left(\frac{ik(x - \xi_l)^2}{2L}\right). \quad (17.3)$$

From (17.2), the probability density for detecting an atom at the position x on the screen is

$$|\langle x | \psi(t_2) \rangle|^2 = \frac{1}{2} [|\psi_1(x)|^2 + |\psi_2(x)|^2 + 2\Re(\psi_1^*(x)\psi_2(x))] . \quad (17.4)$$

Substituting the expression for ψ_1 and ψ_2 for the situation of infinitesimally wide slits, yields

$$|\langle x | \psi(t_2) \rangle|^2 \propto 1 + \cos\left(\frac{k dx}{L}\right) \quad (17.5)$$

which is the familiar two-slit interference pattern with unit visibility.

We now include the effect of the path detector. We shall treat the path detector also as a quantum mechanical system which is initially in a pure state $|D_0\rangle$. As a result of the interaction between the atom and the path detector, by the time the atom hits the screen, the detector has evolved either into state $|D_1\rangle$ or into state $|D_2\rangle$ depending on the path taken by the atom. The joint state of the system and the path detector at time t_2 is thus given by

$$|\psi(t_2)\rangle = \frac{1}{\sqrt{2}} \int_{-\infty}^{\infty} [\psi_1(x)|D_1\rangle + \psi_2(x)|D_2\rangle] |x\rangle dx . \quad (17.6)$$

This is an entangled state of the system and the path detector. If we again ask for the probability density that the atom be found at position x on the screen, we need to compute

$$\begin{aligned} P(x) &= |\langle x | \psi(t_2) \rangle|^2 = \text{Tr} \{ |\psi(t_2)\rangle \langle \psi(t_2)| |x\rangle \langle x| \} \\ &= \frac{1}{2} \{ |\psi_1(x)|^2 + |\psi_2(x)|^2 + 2\Re[\psi_1^*(x)\psi_2(x)\langle D_1|D_2\rangle] \} . \end{aligned} \quad (17.7)$$

The interference term has the additional factor $\langle D_1|D_2\rangle$ which causes the visibility to be reduced by $|\langle D_1|D_2\rangle|$. If the detector states $|D_1\rangle$ and $|D_2\rangle$ are

orthogonal, it becomes possible to distinguish them with certainty and the interference disappears. On the other hand, if the detection process is less efficient, the overlap between $|D_1\rangle$ and $|D_2\rangle$ is larger and partial interference remains.

As an example of a path detector we shall consider the Feynman light microscope.

17.1.1 The Feynman Light Microscope

In the Young's double slit experiment in Fig. 17.4 a light field travelling along the x direction is used to indicate the path by scattering off the atom. We shall consider only elastic scattering and use the S -matrix approach for the problem. Following Cohen-Tannoudji et al. [17.8], we denote by $S(\mathbf{K}_i, \mathbf{K}_f, \mathbf{k})$ the amplitude of the elementary process where a photon of initial momentum $\hbar\mathbf{K}_i$ scatters off an atom of momentum $\hbar\mathbf{k}$ to yield a final photon momentum of $\hbar\mathbf{K}_f$ and an atomic momentum of $\hbar(\mathbf{k} - \mathbf{K}_f + \mathbf{K}_i)$. If we neglect the Doppler effect, this amplitude is independent of the atomic momentum $\hbar\mathbf{k}$ and we may write $S(\mathbf{K}_i, \mathbf{K}_f)$. The magnitude $|S(\mathbf{K}_i, \mathbf{K}_f)|$ depends on the projection of the polarisation vector of the outgoing photon on the polarisation vector of the incoming photon if the atomic dipole moment is aligned with the incoming polarisation. If we denote the polar and azimuthal angles of \mathbf{K}_f relative to \mathbf{K}_i by (θ, ϕ) , the angular dependence of this amplitude is

$$|S(\mathbf{K}_i, \mathbf{K}_f)| \propto \sqrt{1 + \cos^2 \theta} \delta(|\mathbf{K}_i| - |\mathbf{K}_f|) \quad \text{for circular polarization ,} \quad (17.8)$$

$$|S(\mathbf{K}_i, \mathbf{K}_f)| \propto \sqrt{1 + \sin^2 \theta \cos^2 \phi} \delta(|\mathbf{K}_i| - |\mathbf{K}_f|) \quad \text{for linear polarization ,} \quad (17.9)$$

where the delta-function restricts our attention to elastic scattering. In order to assign the phase to the scattering amplitude, we consider scattering off an atom in a position eigenstate

$$|\mathbf{x}\rangle \propto \int d^3k \exp(-i\mathbf{k} \cdot \mathbf{x}) |k\rangle . \quad (17.10)$$

For an initial joint state $|\mathbf{x}\rangle|\mathbf{K}_i\rangle$ of atom and photon, the outgoing state is proportional to

$$\int d^3\mathbf{K}_f S(\mathbf{K}_i, \mathbf{K}_f) \exp[i(\mathbf{K}_i - \mathbf{K}_f) \cdot \mathbf{x}] |\mathbf{x}\rangle |\mathbf{K}_f\rangle . \quad (17.11)$$

Thus, if we choose $S(\mathbf{K}_i, \mathbf{K}_f)$ as purely real, this corresponds to the assumption that all the plane wave components of the scattered field are in phase at the location of the atom.

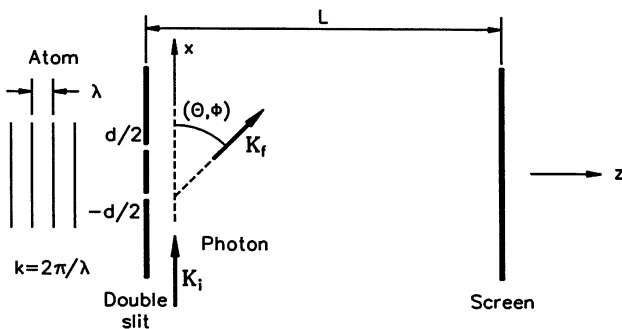


Fig. 17.4. Path detectors using the Feynman light microscope

In this configuration, the state of the outgoing photon plays the role of the path detector. If the two slits are located at $x = \xi_1 = d/2$ and $x = \xi_2 = -d/2$, the state $|D_l\rangle$ of the outgoing photon which couples with the path though the slit at ξ_l is

$$|D_l\rangle \propto \exp(iK\xi_l) \int_0^{2\pi} d\phi \int_0^\pi d\theta S(K_i, K_f) \exp(-iK\xi_l \cos \theta) K^2 \sin \theta |K_f\rangle \quad (17.12)$$

where $K = |K_i| = |K_f|$. The inner product of these two states, for either circular or linear polarisation, is

$$\langle D_1 | D_2 \rangle = V(Kd) \exp(-iKd) \quad (17.13)$$

where

$$V(u) = \frac{3}{2} \left(\frac{\cos u}{u^2} + \frac{\sin u}{u} - \frac{\sin u}{u^3} \right).$$

The modulus of this quantity $v = |V(kd)|$ gives the visibility of the interference pattern, in agreement with the result of Sleator et al. [17.9]. A graph of $V(u)$ is shown in Fig. 17.5. The total interference pattern is given by (17.7)

$$P(x) \propto 1 + \Re[\exp(-iKd) V(Kd) \exp(iKdx/L)]. \quad (17.14)$$

For small slit separation d of much less than $\lambda/2$ the visibility is close to unity since the atomic position cannot be localised by the optical probe to better than about a wavelength. As the slit separation is increased, localisation becomes possible and the visibility is reduced. Physically, this arises from the convolution of the interference pattern with the momentum transferred to the atom by the photon. This can be seen from the following simple argument. The spacing between the fringe maxima corresponds to a transverse momentum change of

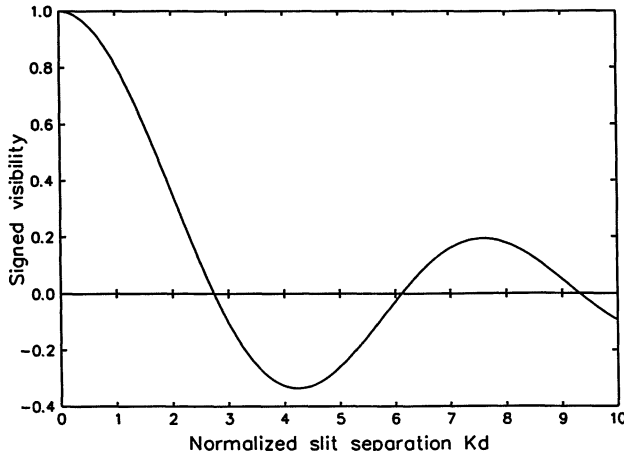


Fig. 17.5. Fringe visibility versus slit separation

the atom of h/d . If the momentum kick ($p = h/\lambda$) imparted by the photon is greater than the fringe spacing ($h/\lambda > h/d$), that is $d > \lambda$, then the fringes will be washed out.

17.2 Atomic Diffraction by a Standing Light Wave

We shall consider the deflection of a beam of two-level atoms by a classical standing wave light field in a cavity. The atomic beam is normally incident on the standing wave and experiences an exchange of momentum with the photons in the light wave. We shall assume that the frequency of the light field is well detuned from the atomic resonance so that we may neglect spontaneous emission.

The Hamiltonian describing the interaction is

$$\mathcal{H} = \hbar\omega_0\sigma_z + \frac{\mathbf{p}^2}{2m} + \hbar\Omega(\sigma_- e^{-i\omega t} + \sigma_+ e^{i\omega t}) \cos kx , \quad (17.15)$$

where \mathbf{p} is the centre of mass momentum of the atom along the transverse (x direction), m is the atomic mass, σ_z and σ_{\pm} are the pseudo spin operators for the atom, ω_0 and ω are the atomic and field frequencies, $k = \omega/c$ is the wave number of the standing wave, and $\Omega = \mu\epsilon_0/\hbar$ the Rabi frequency with μ being the dipole moment and ϵ_0 the maximum field amplitude. We shall assume that the interaction time is sufficiently small that the transverse kinetic energy absorbed by the atom during the interaction can be neglected. This is known as

the Raman–Nath regime and requires $t < 2\pi/\omega_r$, where the recoil energy is $\hbar\omega_r = (2r\hbar k)^2/2m$ where r is an integer. This is equivalent to neglecting the term $p^2/2m$ in the Hamiltonian.

Transforming to the interaction picture with $\mathcal{H}_0 = \hbar\omega\sigma_z$ the Hamiltonian may be written in the form

$$\mathcal{H} = \hbar\delta\omega\sigma_z + 2\hbar\Omega\sigma_x \cos kx , \quad (17.16)$$

where $\delta\omega = \omega_a - \omega$ and $2\sigma_x = \sigma_+ + \sigma_-$. This Hamiltonian may be diagonalised and written in the form

$$\mathcal{H} = V(x)[\cos\theta(x)\sigma_z + \sin\theta(x)\sigma_x] \quad (17.17)$$

where

$$V(x) = \hbar\sqrt{(\delta\omega)^2 + (2\Omega\cos kx)^2} ,$$

$$\cos\theta(x) = \frac{\delta\omega}{\sqrt{(\delta\omega)^2 + (2\Omega\cos kx)^2}} ,$$

$$\sin\theta(x) = \frac{2\Omega\cos kx}{\sqrt{(\delta\omega)^2 + (2\Omega\cos kx)^2}} .$$

In the limit of large detuning ($\delta\omega \gg 2\Omega\cos kx$),

$$\cos\theta \approx 1, \quad \text{and } \sin\theta \approx 0 ,$$

so that

$$V(x) \approx \hbar\delta\omega\left(1 + \frac{2\Omega^2\cos^2 kx}{\delta\omega^2}\right) . \quad (17.18)$$

This leads to the effective Hamiltonian

$$\mathcal{H}_{\text{eff}} = \hbar\delta\omega\sigma_z + \left(\frac{2\hbar\Omega^2\cos^2 kx}{\delta\omega}\right)\sigma_z . \quad (17.19)$$

The atomic state vector in the coordinate representation may be written as

$$\langle x|\psi(t)\rangle = a(x, t)|a\rangle + b(x, t)|b\rangle , \quad (17.20)$$

where $|a\rangle$ and $|b\rangle$ are the upper and lower atomic states, and $a(x, t)$ ($b(x, t)$) are the probability amplitudes for the atom to be in the upper (lower) state at the transverse coordinate x at time t .

We assume that the atoms are initially in their ground state with a Gaussian wavefunction

$$a(\xi, 0) = 0 ,$$

$$b(\xi, 0) = (\pi\sigma^2)^{-1/4} \exp\left(-\frac{\xi^2}{2\sigma^2}\right) , \quad (17.21)$$

where $\xi = kx$ and σ is proportional to the r.m.s. transverse position spread of the input beam. This may be written as

$$b(\xi, 0) = \left(\frac{2\sigma_n^2}{\pi} \right)^{1/4} \exp[-(\sigma_n \xi)^2], \quad (17.22)$$

where σ_n is the r.m.s. transverse momentum spread of the input beam scaled to the photon momentum $\hbar k$ ($\eta = p/\hbar k$). The Schrödinger equation in the large detuning limit is

$$\frac{\partial}{\partial \tau} \begin{pmatrix} a \\ b \end{pmatrix} = \begin{pmatrix} -i\Delta - \frac{i \cos^2 \xi}{2\Delta} & 0 \\ 0 & i\Delta + \frac{i \cos^2 \xi}{2\Delta} \end{pmatrix} \begin{pmatrix} a \\ b \end{pmatrix} \quad (17.23)$$

where $\tau = \Omega t$ and $\Delta = \delta\omega/2\Omega$. We shall assume that the atom interacts with a field of constant amplitude for a time τ . The Rabi frequency is Ω .

The solution for $b(\xi, \tau)$ may be written in the form [17.10]

$$b(\xi, \tau) = \exp \left[i \left(\Delta + \frac{1}{4\Delta} \right) \tau \right] \sum_{n=-\infty}^{\infty} i^n J_n \left(\frac{\tau}{4\Delta} \right) \exp(2in\xi) b(\xi, 0). \quad (17.24)$$

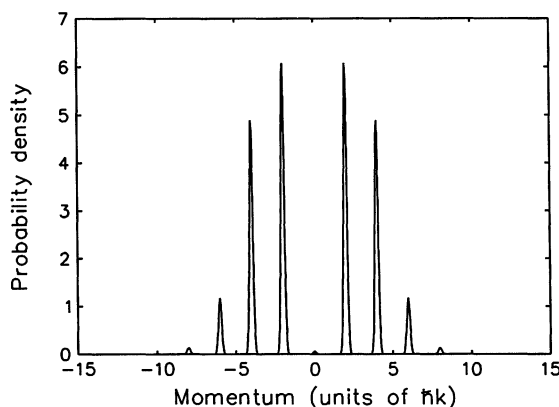


Fig. 17.6. Output momentum distribution for atoms scattered from a standing optical wave in the Kapitza-Dirac regime in the large detuning limit. Initial RMS momentum uncertainty is $\sigma_n = 0.1$ (units of $\hbar k$) and the normalised interaction time $\tau/\Delta = 10$

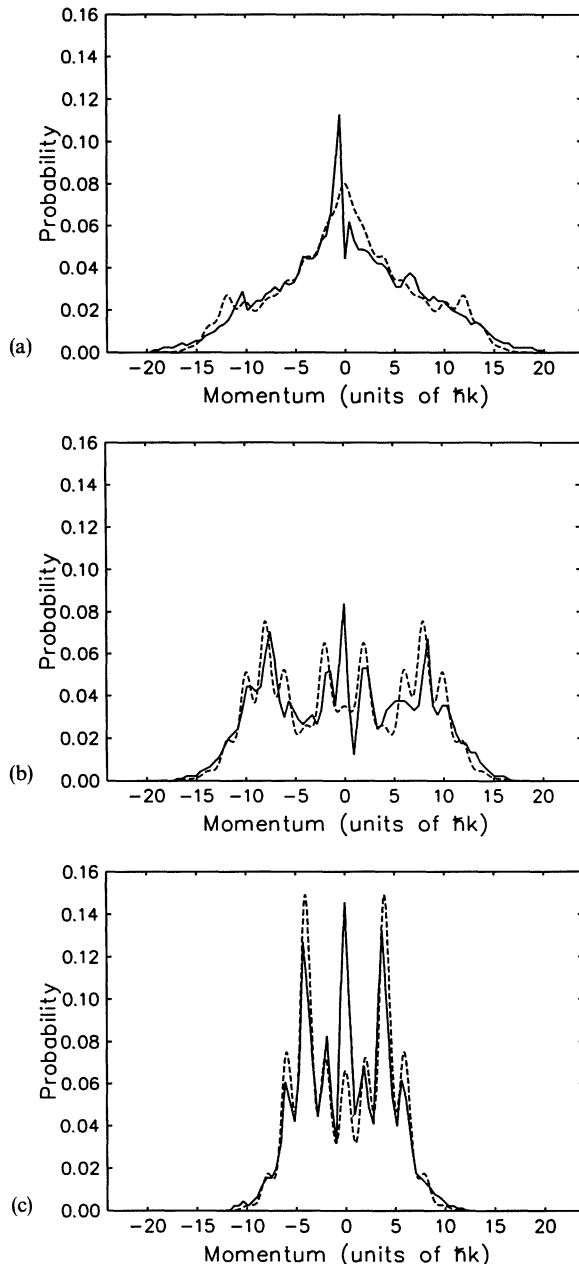


Fig. 17.7. Output momentum distribution for atoms scattered from a standing optical wave. Comparison of experimental data [17.9] (—) and theoretical predictions [17.12] (---) for (a) $\Delta = 0$, (b) $\Delta = 0.6$, (c) $\Delta = 1.2$

Taking the Fourier transform of this relationship shows the effect in momentum space is a convolution

$$\begin{aligned}\tilde{b}(\eta, \tau) &= \exp\left[i\left(\Delta + \frac{1}{4\Delta}\right)\tau\right] \sum_{n=-\infty}^{\infty} i^n J_n\left(\frac{\tau}{4\Delta}\right) \delta(\eta - 2n) * \tilde{b}(\eta, 0) \\ &= \exp\left[i\left(\Delta + \frac{1}{4\Delta}\right)\tau\right] \sum_{n=-\infty}^{\infty} i^n J_n\left(\frac{\tau}{4\Delta}\right) \tilde{b}(\eta - 2n, 0)\end{aligned}\quad (17.25)$$

where \tilde{b} denotes the Fourier transform of b .

The scattered ground state wavefunction is a superposition of Gaussian modulated plane waves with momenta $p = 2n\hbar k$. The momentum transferred from the field to the atom is in even multiples of $\hbar k$ corresponding to the absorption of a photon from the $(+k)$ component, followed by induced emission into the $(-k)$ component of the standing wave. The final output momentum probability distribution is composed of a comb of images of the initial momentum distribution. In order to resolve these peaks it is necessary to have a narrow initial momentum spread such that $\Delta p \ll 2\hbar k$ or $\sigma_\eta \ll 1$. The output momentum distribution is shown in Fig. 17.6 for $\sigma_\eta = 0.1$, where the propagation time after the interaction is assumed short so that further spreading has been neglected. The above result holds for large atomic detuning. For smaller atomic detunings spontaneous emission becomes important. Since the recoil imparted to an atom by a spontaneously emitted photon occurs in a random direction, exchanges of momentum in non-integral multiples of $\hbar k$ may occur and the diffractive peaks will be smeared out. That is, as the laser is tuned closer to the atomic resonance one moves from the diffractive to the diffusive regime. The transition from the diffractive to the diffusive regime has been demonstrated in an experiment by *Gould et al.* [17.11]. A fit to their data using a calculation which includes spontaneous emission has been given by *Tan and Walls* [17.12] and is shown in Fig. 17.7.

17.3 Optical Stern–Gerlach Effect

In the previous section, we discussed the diffraction of atoms in their ground state from a standing wave light field. In order to resolve the diffraction peaks in the momentum distribution it was necessary that the initial atomic spatial wave packet be larger than a wavelength. In this regime, the momentum transfer is symmetrical about $\Delta p = 0$ and is the same for input atoms in either the ground or excited states. As the spatial extent of the input wave packet is reduced to a fraction of the optical wavelength, the momentum transfer becomes asymmetrical and dependent upon the initial atomic state. Figure 17.8 shows the outgoing probability density of the atomic momentum for an initial atomic beam width $\sigma = 0.3$. The solid curve is for atoms in the ground state while the dotted curve is for the excited state.

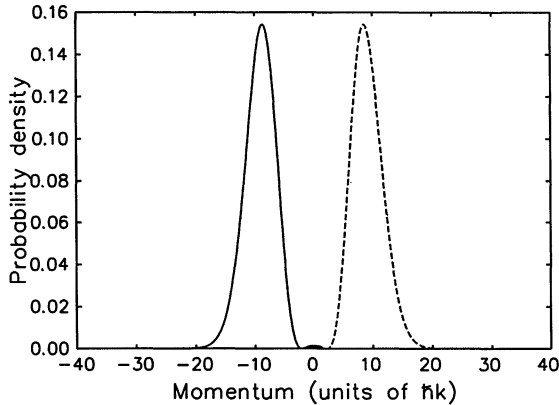


Fig. 17.8. Output momentum distribution for atoms scattered from a standing optical wave in the Stern-Gerlach regime. Initial rms momentum uncertainty is $\sigma_\eta = 2.4$ (units of $\hbar k$). The atomic beam is incident midway between a node and an antinode and the normalised interaction time $\tau/\Delta = 20$. (a) solid curve, ground state atoms, (b) dotted curve, excited state atoms

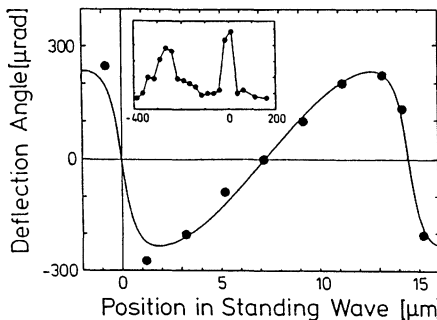


Fig. 17.9. Deflection of an atomic beam by a standing wave as a function of the atomic beam position in the standing wave. The detuning from resonance was $\Delta/2\pi = 160$ MHz. Position 0 on the horizontal scale was arbitrarily chosen to be at a node. Inset: Atomic intensity profile at the detector for the atomic beam at a position of $-11 \mu\text{m}$ in the standing wave. The peak at zero angle is due to undeflected atoms [17.13]

In the limit when the spatial extent of the input wave packet is very small compared to the optical wavelength, an input beam is split into two beams depending on its atomic state. This is called the optical Stern-Gerlach limit in which the atom interacts with only a small part of the light wave ($\Delta x^{\text{IN}} \ll 1/k$) and the individual photon exchanges are not resolvable ($\Delta p \gg \hbar k$). In the large-detuning limit the momentum transfer, which can be many times the photon momentum, depends on the intensity gradient of the optical field. An experimental demonstration of the optical Stern-Gerlach effect has been given by Sleator et al. [17.13] using a beam of metastable He atoms (Fig. 17.9).

We shall demonstrate how the standing wave optical field encodes information about the atomic state in the centre of mass momenta of the outgoing atoms. A non-destructive determination of the atomic state may be useful in conjunction with micromaser experiments in which the photon statistics within the micromaser cavities are indirectly measured via their effects on the states of the Rydberg atoms which pass through them. The ability to spatially separate atoms according to their state without destroying them also makes it possible to consider their subsequent coherent recombination in an atomic interferometer.

In order to measure their atomic state we shall require that the momentum transfer be well correlated with the initial atomic state and that the process of splitting the input beam should not cause this atomic state to change. We shall demonstrate how one may make a QND measurement of the atomic inversion. We consider the case where the standing wave field is far detuned from the atomic resonance. In this case we may use the effective Hamiltonian given by (17.19).

The inversion of the atom, σ_z , we take as the signal observable and the centre of mass momentum p of the atom as the probe. It is evident that the Hamiltonian is back action evading for σ_z which is a constant of the motion. We shall follow the treatment given by *Tan and Walls* [17.14].

Consider a beam of atoms in a mixture of excited and ground states. The interaction with the standing light wave will impart some momentum to these atoms causing a deflection. The mean momentum transfer will have opposite signs for the two states. The mean momentum transfer compared to the standard deviation of the momentum transfer will determine how well the atomic beam can be separated into two beams of either excited or ground state atoms.

The probability amplitudes $a(\xi, \tau)$ and $b(\xi, \tau)$ for the atom to be in the excited and ground states at time τ are given in the large detuning limit by the solution of (17.23).

After passage through the field, the mean momentum transfer to this beam is given by

$$\langle \eta^{\text{OUT}} \rangle = \int_{-\infty}^{\infty} a(\xi, \tau)^* \left(\frac{-i\partial}{\partial \xi} \right) a(\xi, \tau) d\xi + \int_{-\infty}^{\infty} b(\xi, \tau)^* \left(\frac{-i\partial}{\partial \xi} \right) b(\xi, \tau) d\xi \quad (17.26)$$

where $\eta = p/\hbar k$ is a normalised momentum. Similarly the mean squared momentum transfer is

$$\begin{aligned} \sigma_{\eta}^2 = \langle \eta^{\text{OUT}2} \rangle &= \int_{-\infty}^{\infty} a^*(\xi, \tau) \left(\frac{-\partial^2}{\partial \xi^2} \right) a(\xi, \tau) d\xi \\ &\quad + \int b^*(\xi, \tau) \left(\frac{-\partial^2}{\partial \xi^2} \right) b(\xi, \tau) d\xi . \end{aligned} \quad (17.27)$$

In the large detuning limit we find for a Gaussian beam with width σ centred at ξ_0

$$\langle \eta_{\pm}^{\text{OUT}} \rangle = \pm \frac{\tau}{2\Delta} e^{-\sigma^2} \sin(2\xi_0) \quad (17.28)$$

$$\langle \eta_{\pm}^{\text{OUT}^2} \rangle = \sigma_{\eta}^2 = \frac{1}{2\sigma^2} + \frac{\tau^2}{8\Delta^2} [1 - 2e^{-2\sigma^2} \sin^2(2\xi_0) - e^{-4\sigma^2} \cos(4\xi_0)] \quad (17.29)$$

where the $+$ sign is for initial state $|e\rangle$ and the $-$ sign for initial state $|g\rangle$. In Fig. 17.10 we plot these quantities as a function of the width of the atomic beam σ for $\tau/\Delta = 20$. The mean momentum transfer depends on the gradient of the intensity of the light field where the atom crosses and so the atomic beam must be narrow in order for the momentum transfer to be well defined. As the width of the atomic beam increases, different portions of the beam are deflected differently, reducing the mean momentum transfer. The variance of the output momentum arises from two effects: The term involving $(2\sigma^2)^{-1}$ represents the original momentum uncertainty of the input beam, which increases rapidly as σ is reduced. If, however, σ is increased so that it covers a significant portion of an optical wavelength, the variation in momentum imparted to different parts of the beam again increases the variance. Consequently there is a minimum in the standard deviation, as seen in Fig. 17.10. The condition for a good measurement

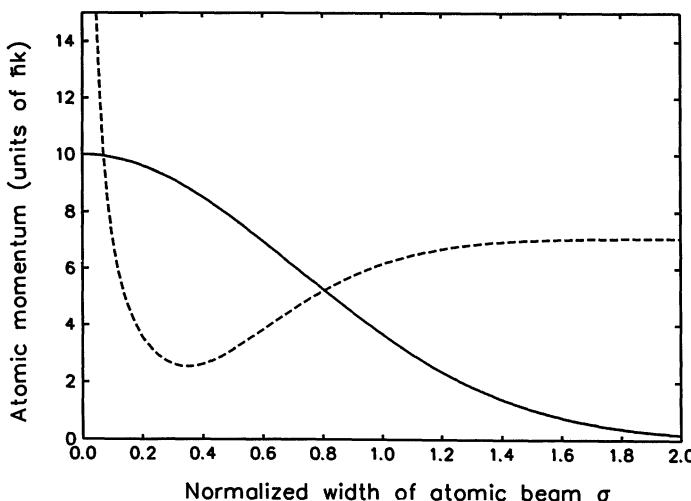


Fig. 17.10. Mean (solid curve) and standard deviation (dashed curve) of the atomic momentum plotted against the normalised width of the atomic beam. The atomic beam is incident midway between a node and an antinode and the normalised interaction time $\tau/\Delta = 20$

is that the mean momentum transfer to the beam prepared in an eigenstate is larger than the spread of the outgoing momentum. From Fig. 17.10 it is clear that there is an optimal width of the input beam which gives the best quality of measurement. This optimum width depends on the interaction time since the mean momentum transfer rises with τ/Δ , and for larger interaction times this will exceed the intrinsic momentum uncertainty for a narrower initial beam. We may use the QND correlation coefficient introduced in Chap. 15 to evaluate the quality of the measurement. In this case the signal is the atomic inversion σ_z and the probe is the centre-of-mass momentum η of the atom.

These correlation coefficients depend on expectation values which have to be taken over some initial state. We choose the state which is a statistical mixture of ground and excited states with equal probability. In the large detuning limit the measurement correlation may be written as

$$\begin{aligned} C_{A_s^{\text{IN}} A_p^{\text{OUT}}}^2 &= \frac{|\langle \eta^{\text{OUT}} \sigma_z^{\text{IN}} \rangle|^2}{\langle \eta^{\text{OUT}^2} \rangle \langle \sigma_z^{\text{IN}^2} \rangle} \\ &= \frac{\frac{1}{2}[\langle \eta_+^{\text{OUT}} \rangle(\frac{1}{2}) - \langle \eta_-^{\text{OUT}} \rangle(-\frac{1}{2})]^2}{\frac{1}{2}(\langle \eta_+^{\text{OUT}^2} \rangle + \langle \eta_-^{\text{OUT}^2} \rangle) \frac{1}{2}[(\frac{1}{2})^2 + (-\frac{1}{2})^2]} , \end{aligned} \quad (17.30)$$

from (17.28 and 29) this may be written as

$$C_{A_s^{\text{IN}} A_p^{\text{OUT}}}^2 = \frac{2\sigma^2 \tau^2 e^{-2\sigma^2} \sin^2(2\xi_0)}{4\Delta^2 + \sigma^2 \tau^2 [1 - e^{-4\sigma^2} \cos(4\xi_0)]} . \quad (17.31)$$

The state preparation correlation $C_{A_s^{\text{IN}} A_p^{\text{OUT}}}^2$ has an identical expression. In the large detuning limit an atom prepared in an eigenstate of σ_z remains in an eigenstate of σ_z . Consequently, the non-demolition correlation

$$C_{A_s^{\text{IN}} A_s^{\text{OUT}}}^2 = 1 . \quad (17.32)$$

In Fig. 17.11 we plot $C_{A_s^{\text{IN}} A_p^{\text{OUT}}}^2$ as a function of the width of the atomic beam σ for a range of different interaction times $\tau/\Delta = 2, 5, 10, 20, 50$.

The position of the beam centre is $\xi_0 = \pi/4$ corresponding to the point midway between a node and antinode where the intensity gradient is greatest. We see that for sufficiently large interaction times and an atomic beam of optimal width the measurement correlation may approach unity. Thus the deflection of an atomic beam by a standing wave field may be used to give a good QND measurement of the atomic inversion σ_z in the detuning limit. For smaller detuning a QND measurement of an operator $d\mathbf{x}\sigma_x + d\mathbf{y}\sigma_y + d\mathbf{z}\sigma_z$ can be made. For example, for zero detuning the appropriate QND observable is the atomic polarisation σ_x .

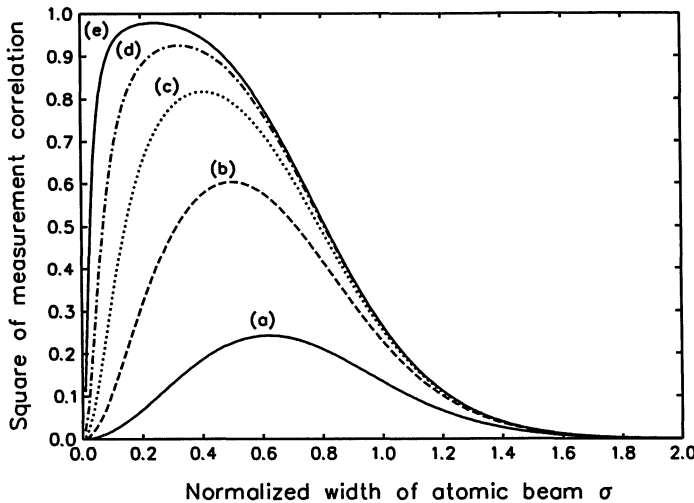


Fig. 17.11. Measurement correlation coefficient squared plotted against the normalised width of the atomic beam for τ/Δ = (a) 2, (b) 5, (c) 10, (d) 20, (e) 50

17.4 Quantum Non-Demolition Measurement of the Photon Number by Atomic Beam Deflection

If we consider atoms passing through a quantised standing wave field the outgoing momentum distribution of the atoms is sensitive to the photon statistics for a small photon number. We shall show that by measuring the momentum distribution of a sequence of atoms passing through a cavity field a quantum non-demolition (QND) measurement of the photon number can be made.

With a quantised single mode cavity field the Hamiltonian (17.15) describing the interaction is modified to

$$\mathcal{H} = \hbar\omega a^\dagger a + \hbar\omega_0 \sigma_z + \hbar(g\sigma_- a^\dagger + g^*\sigma_+ a) \cos kx , \quad (17.33)$$

where the field is described by the boson annihilation operator a , and g is the dipole coupling constant. We shall once again consider the case of large detuning where spontaneous emission can be neglected and the upper atomic level adiabatically eliminated. The effective Hamiltonian (17.19) is modified to

$$\mathcal{H}_{\text{eff}} = \hbar\delta\omega\sigma_z + \frac{2\hbar g^2}{\delta\omega} \sigma_z a^\dagger a \cos^2 kx , \quad (17.34)$$

where we have replaced Ω^2 by $|g|^2 a^\dagger a$. A derivation of this effective Hamiltonian is given in Appendix 17.A.

We see from this Hamiltonian that the photon number $a^\dagger a$ is a QND observable. It may be determined by either measuring the atomic phase [17.15] or the outgoing momentum [17.16]. We shall calculate the outgoing momentum distribution which is the probe observable in this QND measurement.

Consider the atom to be in the ground state with an initial Gaussian position distribution given by (17.21). Then, if the field has n photons initially the state of the atom after the interaction is given by (17.24) with $\Omega = |g| \sqrt{n}$. In terms of the original variables

$$b_n(\xi, t) = \exp \left[i \left(\frac{1}{2} \delta\omega + \frac{|g|^2 n}{2\delta\omega} \right) t \right] \sum_{r=-\infty}^{\infty} i^r J_r \left(\frac{|g|^2 nt}{2\delta\omega} \right) \exp(2ir\xi) b(\xi, 0) , \quad (17.35)$$

or in the momentum representation,

$$\tilde{b}_n(\eta, t) = \exp \left[i \left(\frac{1}{2} \delta\omega + \frac{|g|^2 n}{2\delta\omega} \right) t \right] \sum_{r=-\infty}^{\infty} i^r J_r \left(\frac{|g|^2 nt}{2\delta\omega} \right) \tilde{b}(\eta - 2r, 0) . \quad (17.36)$$

Since the photon number of the field is unchanged by the interaction, the joint state of atom and field is $\int \tilde{b}_n(\eta, t) |n\rangle |\eta\rangle d\eta$.

Now let us suppose that the initial state of the field is given by the superposition of number states $\sum c_n |n\rangle$. The final joint state is then presented by

$$|\psi\rangle = \sum_{n=0}^{\infty} \int c_n \tilde{b}_n(\eta, t) |n\rangle |\eta\rangle d\eta . \quad (17.37)$$

We now wish to measure the probability that the final atomic momentum is $p = \eta\hbar k$ without regard for the field state. This involves calculating the following trace

$$\begin{aligned} P(\eta) &= \text{Tr} \{ |\psi\rangle \langle \psi| |\eta\rangle \langle \eta| \} = \sum_{n=0}^{\infty} |c_n|^2 b_n(\eta, t)|^2 \\ &= \sum_{n=0}^{\infty} |c_n|^2 \left| \sum_{r=-\infty}^{\infty} i^r J_r \left(\frac{|g|^2 nt}{2\delta\omega} \right) \tilde{b}(\eta - 2r, 0) \right|^2 . \end{aligned} \quad (17.38)$$

If the original momentum uncertainty is so small that $\tilde{b}(\eta)$ is non-zero only when $|\eta| < 1$,

$$P(\eta) = \sum_{r=-\infty}^{\infty} \left(\sum_{n=0}^{\infty} |c_n|^2 \left| J_r \left(\frac{|g|^2 nt}{2\delta\omega} \right) \right|^2 \right) |\tilde{b}(\eta - 2r, 0)|^2 , \quad (17.39)$$

which consists of copies of the input beam shifted in momentum by even multiples of $\hbar k$. The amplitudes of these copies are related to the photon number statistics of the light field $P(n) = |c_n|^2$.

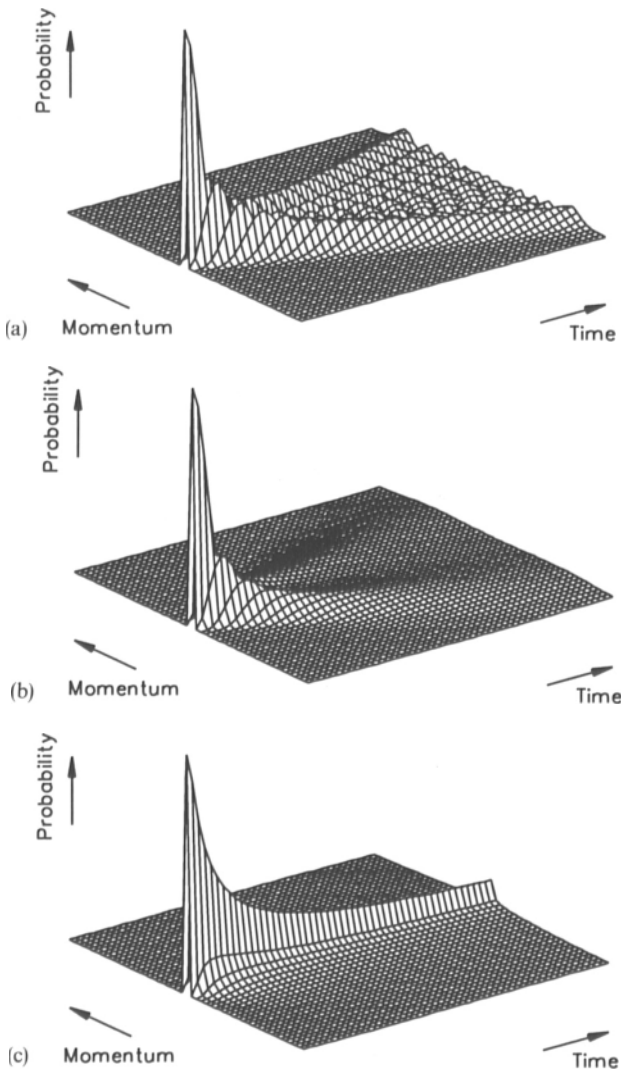


Fig. 17.12. Output momentum distribution for atoms scattered from a standing wave field in (a) a number state $N = 10$, (b) a coherent state $\bar{n} = 10$, (c) a thermal state $\bar{n} = 10$. The interaction time ranges from $t = 0$ to $|g|^2 t / (2\delta\omega) = 2$. The successive points along the momentum axis are separated by twice the photon momentum

The output momentum distribution $P(\eta)$ is plotted in Fig. 17.12 for the cavity field in (a) a number state $N = 10$, (b) a coherent state $\bar{n} = 10$, (c) a thermal state $\bar{n} = 10$. We see that for a number state the momentum distribution consists of a series of peaks corresponding to exchanges of $2n\hbar k$ units of momentum. For a coherent state the distribution is split into two principle peaks. For a thermal state the spread of momentum is much smaller. For a more intense coherent

field $\Delta n/\bar{n} \sim 1/\sqrt{\bar{n}}$ is small and the momentum distribution corresponds closely to that derived for a classical field in Sect. 17.2.

We see from (17.39) that the momentum distribution depends on the photon statistics $P(n)$ of the cavity field. This may be exploited to obtain a quantum non-demolition (QND) measurement of the photon number by measuring the momentum distribution of the scattered atoms. This is equivalent to the position distribution in the far field. Each atomic position measurement gives some information about the field photon statistics and reduces the density operator of the field. If the cavity lifetime is long compared to the time between atomic injections, (17.39) can be inverted and sufficiently repeated measurements will eventually completely determine the photon statistics. If the cavity is not significantly coupled to any external reservoir, continual probing of the cavity by successive atoms will eventually result in the complete collapse of the field state to that of a number state. We shall illustrate this phenomenon by simulating repeated atomic measurements and examining the residual density of states.

For simplicity, we consider a monokinetic atomic beam in which the longitudinal velocity spread is small compared to the mean velocity. The first atom which passes through the cavity acquires an output momentum p_0 which gives us some information on the field statistics. The diagonal elements of the field density matrix $P(n)$ are then altered by the back projection of the measurement

$$P(n|p_0) = MP(p_0|n)P(n) \quad (17.40)$$

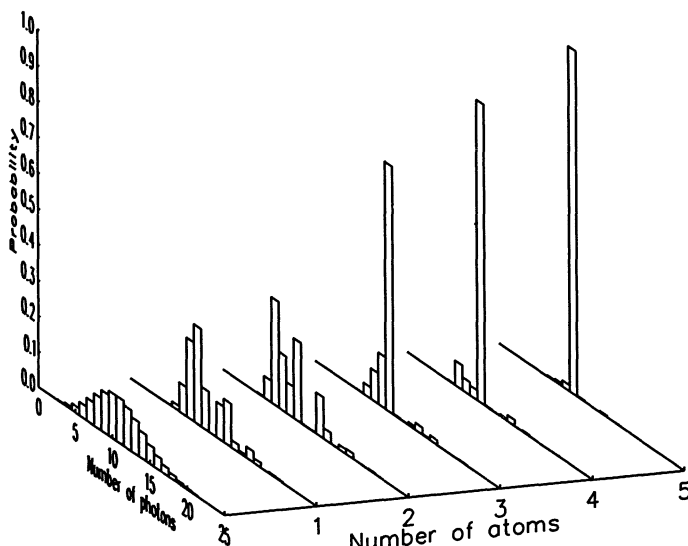


Fig. 17.13. Simulation of the collapse of the field density of the states to a single photon number after measuring five atoms. The interaction is chosen so that $|g|^2 t/(2\delta\omega) = 1$. The momentum of the five atoms leaving the standing wave were $12\hbar k, 8\hbar k, -16\hbar k, 8\hbar k, 16\hbar k$

where M is a normalisation constant. The next atom passing through acquires a momentum p_1 and the field density matrix is further reduced. A simulation of a sequence of five atoms and their effect on the field photon distribution $P(n)$ is shown in Fig. 17.13. The number of times that each value of the exit momentum is chosen is completely determined by the initial photon statistics. Note the photon measurement of each individual atom extracts partial information from the field, and it is only the cumulative information contained in the full measurement sequence which contracts the field to a well defined number state.

17.5 Measurement of Atomic Position

We shall describe a technique for localising the atom's position better than the wavelength of light. The atom is passed through a standing wave in an optical cavity. We consider the situation where the standing wave is far off the atomic resonance. Via its interaction with the standing wave the atom imparts a phase shift to the field. The magnitude of the phase shift depends on the atom's position relative to the nodes and antinodes of the standing wave. By making a phase sensitive measurement of the optical field, position information on the atom is obtained. The initial atomic wave packet needs to be localised better than the wavelength of the light or else one is not able to determine which portion of the periodic standing wave the atom passes through, unless the atom is passed through a second cavity containing light of a non-commensurate wavelength.

The atom is modelled as an ideal two level system interacting with a single mode of the cavity field. The system is similar to that described in Sect. 17.4. The atomic transition frequency is highly detuned from the cavity frequency hence spontaneous emission can be neglected. The transverse motion of the atom during its passage through the standing wave is assumed to be negligible (the Raman–Nath approximation). We follow the treatment of *Storey et al.* [17.17].

In a frame rotating at the cavity frequency ω , the potential experienced by the atom as it passes through the standing wave is given by the effective potential (17.34) valid for large detuning. Before the interaction with the atom, the field is assumed to be in a coherent state $|\alpha\rangle$. The atom is assumed to enter the cavity in its ground state with a transverse spread in position given by $\kappa(x)$. In order to observe diffraction and interference effects, the atomic distribution must be phase coherent across its width. The atom must therefore enter the cavity in a pure state

$$|\psi(0)\rangle_{\text{atom}} = \int dx \kappa(x) |x, g\rangle , \quad (17.41)$$

where the ket specifies the position and internal state of the atom.

The initial state of the system is just the direct product of the initial field and atomic states

$$\Psi(0) = |\alpha\rangle \otimes |\psi(0)\rangle_{\text{atom}} . \quad (17.42)$$

After an interaction time t , the combined atom-field state (in a frame rotating at frequency ω) is calculated by operating on the initial state with the evolution operator $U(t) = \exp(-iVt/\hbar)$

$$|\psi(t)\rangle = \int dx \kappa(x) e^{-iVt/\hbar} |\alpha\rangle \otimes |x, g\rangle . \quad (17.43)$$

The evolution operator includes the factor $\exp[i\eta(x)a^\dagger a]$ where $\eta(x) = (|g|^2 t/\delta\omega) \cos^2(kx)$ when evaluated over the atomic ket $|x, g\rangle$. This operator changes the phase of the field by the amount $\eta(x)$ which depends on the position of the atom

$$e^{i\eta a^\dagger a} |\alpha\rangle = |\alpha e^{i\eta}\rangle . \quad (17.44)$$

If the atom passes through a node of the standing wave, no interaction occurs and the field is unchanged. However, if the atom passes through an antinode of the standing wave, the phase of the field is altered by the amount $|g|^2 t/\delta\omega$. Thus, information about the position of the atom is recorded in the field, leaving the system in an entangled state of the atom and field, i.e.,

$$|\psi(t)\rangle = e^{\frac{-i\delta\omega t}{2}} \int dx \kappa(x) |\alpha e^{[i|g|^2 t/\delta\omega] \cos^2(kx)}\rangle \otimes |x, g\rangle . \quad (17.45)$$

The position of the atom relative to the nodes and antinodes of the standing wave can be deduced by measuring a phase sensitive quantity such as the quadrature phase $X_\theta = ae^{-i\theta} + a^\dagger e^{i\theta}$. A quadrature phase measurement is directly realised using balanced homodyne detection described in Chap. 8.

If the atom is in a pure state before the interaction, determining the phase of the field does not simply provide an indirect classical measurement of the atom's position, the field measurement collapses the atomic wave function, producing a quantum localisation. A quantum mechanical treatment of the measurement process allows us to calculate the wave function of the atom after the field measurement. The measurement determines not only the probability of finding the atom at position x , but also the phase across the atomic wavefront.

Suppose the field quadrature operator X_θ is measured, giving the result χ_θ . The state of the atom after the field measurement is found by projecting the system onto the eigenstate $|\chi_\theta\rangle$ of the quadrature operator X_θ

$$|\psi(t)\rangle_{\text{atom}} = N \int dx \kappa(x) \langle \chi_\theta | \alpha e^{[i|g|^2 t/\delta\omega] \cos^2(kx)} \rangle |x, g\rangle , \quad (17.46)$$

where N is a normalisation factor. The probability amplitude distribution of the atom after the measurement is simply

$$\psi_{\text{atom}}(x, t) = N \kappa(x) \langle \chi_\theta | \alpha e^{[i|g|^2 t/\delta\omega] \cos^2(kx)} \rangle . \quad (17.47)$$

The position probability distribution $P(x|\chi_\theta)$ of the atom given that the value $X_\theta = \chi_\theta$ has been measured for the field is then

$$P(x|\chi_\theta) = |\chi_{\text{atom}}(x, t)|^2 . \quad (17.48)$$

$P(x|\chi_\theta)$ satisfies the classical relation for conditional probabilities

$$P(x|\chi_\theta) = |N|^2 P(x) P(\chi_\theta|x) , \quad (17.49)$$

where

$$P(x) = |\kappa(x)|^2$$

is the overall probability of finding the atom at position x regardless of the field measurement, and

$$P(\chi_\theta|x) = |\langle \chi_\theta | \alpha e^{[i|g|^2 t / \delta\omega] \cos^2(kx)} \rangle|^2 , \quad (17.50)$$

is the probability of measuring the value χ_θ for the field quadrature X_θ given that the atom is at position x . If the atom's position distribution is not phase coherent as it enters the cavity, the classical relation can still be used to obtain information about the position of the atom from the field measurement. In this case the process may be described as an indirect classical position measurement rather than a quantum localisation. The atom leaves the cavity with a statistical position distribution and no interference effect may be observed. Evaluation of (17.50) requires an expression for a quadrature phase eigenstate. $|\chi_\theta\rangle$ may be defined as a squeezed state in the limit in infinite squeezing.

$$|\chi_\theta\rangle = (2\pi)^{-1/4} \exp[-\frac{1}{2}(a^\dagger e^{i\theta} - \chi_\theta)^2 + \frac{1}{4}\chi_\theta^2] |0\rangle , \quad (17.51)$$

which satisfies the normalisation condition

$$\langle \chi_\theta | \chi'_\theta \rangle = \delta(\chi_\theta - \chi'_\theta) . \quad (17.52)$$

Using (17.51) in (17.46) gives for the state of the atom after the field measurement $X_\theta = \chi_\theta$

$$|\psi(t)\rangle_{\text{atom}} = N \int dx \kappa(x) \frac{1}{\sqrt[4]{2\pi}} e^{-\left[\frac{(x_1 - X_\theta)^2}{2} + i\alpha_2(x_1 - X_\theta)\right]} |x, g\rangle , \quad (17.53)$$

where

$$\alpha_1 + i\alpha_2 \equiv \alpha \exp \left\{ i \left[\left(\frac{|g|^2 t}{\delta\omega} \right) \cos^2 kx - \theta \right] \right\} ,$$

and N is a normalisation factor.

The localisation scheme depends on measuring the phase of the field. The phase change induced by the atom depends on the vacuum light shift $(\hbar|g|^2 t / \delta\omega) \cos^2 kx$ of the atomic ground state, and is independent of the number of photons in the cavity. However, the resolution with which a phase change can be detected depends on the amplitude of the field. The position resolution of the scheme is found to be proportional to $1/|\alpha|$ (Exercise 17.3).

17.5.1 Atomic Focussing and Contractive States

The measurement of the position of an atom described above may be used to prepare an atom in a contractive state discussed in Chap. 16.

A standing light wave acts as an atomic lens which focuses an atom passing close to an antinode. Unless a field measurement is made, the atom leaves the cavity in a mixed state. A field measurement projects the atom into a (pure) contractive state. If the field measurement is such that the atom is localised near an antinode, the phase induced across the atomic wavefront is approximately parabolic and the atom is focused. In Fig. 17.14 we show the time evolution of the probability distribution of an atom prepared in a contractive state using the position localisation scheme. The distribution contracts until it reaches a waist beyond which it spreads out again. In Fig. 17.15 we depict the time evolution of the position uncertainty of the atom. This is compared with the theoretical maximum focussing achieved using Yuens twisted coherent state (Chap. 16) with the same momentum uncertainty and initial position uncertainty. The deviation from the maximally focussed state is seen to be small. In Fig. 17.16 we plot the Wigner function for the contractive state produced by the position localisation scheme. The focal length of the atomic lens produced by the standing wave field may be shown (Exercise 17.4) to be inversely proportional to the intensity of the field.

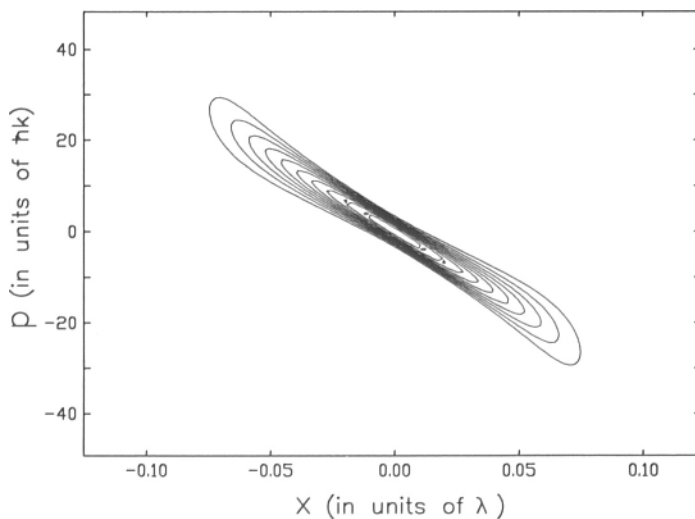


Fig. 17.14. Time evolution of the probability of an atom prepared in a contractive state using the position localisation scheme. The contour levels are spaced logarithmically

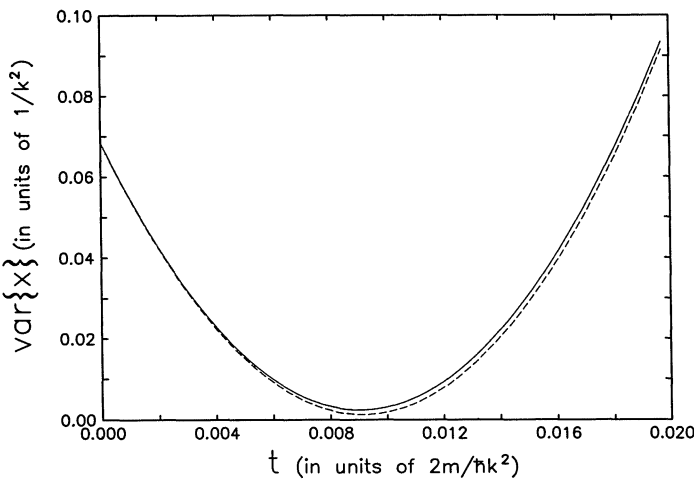


Fig. 17.15. Time evolution of the position uncertainty of an atom (solid line). This is compared with the theoretical maximum focussing (dashed line) achievable with the same momentum uncertainty and initial position uncertainty

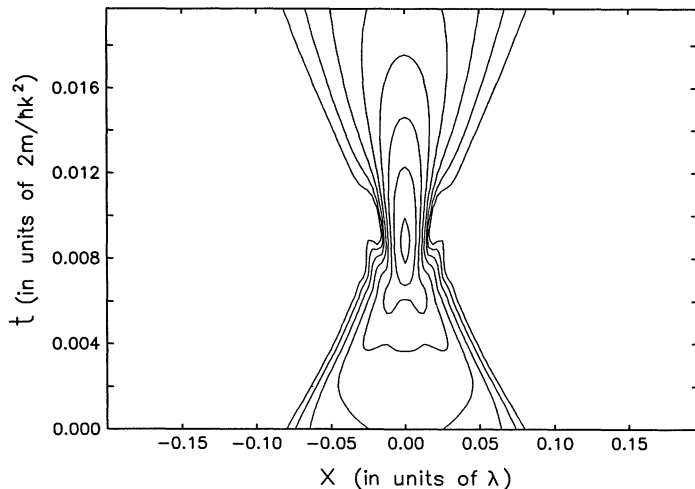


Fig. 17.16. The Wigner distribution for the atomic state after the field measurement which prepares it in a contractive state

Both focussing and deflection of atomic beams by standing light waves have been observed. However, a field measurement is required if the atom is to be prepared in a pure contractive state.

Exercises

17.1 Derive (17.28 and 17.29) for $\langle \eta \rangle$ and σ_η^2 .

17.2 Derive (17.31) for $C_{A_s^{\text{IN}} A_p^{\text{OUT}}}^2$

17.3 Show that the resolution of the position measurement described in Sect. 17.5 is

$$\delta x \sim \frac{1}{|\alpha| \pi k} .$$

where $|\alpha|$ is the amplitude and k the wave number of the light field.

17.4 Show that the focal length of the lens created by a standing wave of intensity I and wave number k is

$$f \sim \frac{1}{2\pi I k} .$$

17.A Appendix

Derivation of the Hamiltonian (17.34)

$$\mathcal{H} = \hbar\omega a^\dagger a + \hbar\omega_0 \sigma_z + \hbar \cos kx (g^* \sigma_- a^\dagger + g \sigma_+ a) \quad (17.54)$$

write $|\psi\rangle = a|e\rangle|n-1\rangle + b|g\rangle|n\rangle$.

In the Schrödinger picture we have

$$i\hbar \frac{\partial a}{\partial t} = [\hbar\omega(n-1) + \frac{1}{2}\hbar\omega_0]a + \hbar g\sqrt{n} \cos kx b , \quad (17.55)$$

$$i\hbar \frac{\partial b}{\partial t} = (\hbar\omega n - \frac{1}{2}\hbar\omega_0)b + \hbar g^*\sqrt{n} \cos kx a . \quad (17.56)$$

Transforming to the interaction picture with $\mathcal{H}_0 = \hbar\omega a^\dagger a + \hbar\omega_0 \sigma_z$

$$a_2 = a e^{+i[(n-1)\omega + 1/2\omega_0]t} \quad (17.57)$$

$$b_2 = b e^{i(n\omega - 1/2\omega_0)t} \quad (17.58)$$

these equations become

$$\frac{\partial a_2}{\partial t} = -ig\sqrt{n} \cos kx e^{i(\omega_0 - \omega)t} b_2 , \quad (17.59)$$

$$\frac{\partial b_2}{\partial t} = -ig^*\sqrt{n} \cos kx e^{-i(\omega_0 - \omega)t} a_2 . \quad (17.60)$$

In order to remove the time dependence in (17.59) we need the component of $a_2 \sim e^{i(\omega_0 - \omega)t}$. This may be derived by the following adiabatic elimination procedure.

Integrating (17.59)

$$a_2(t) = \int_{-\infty}^t -ig \cos kx e^{i(\omega_0 - \omega)\tau} \sqrt{n} b_2(\tau) d\tau . \quad (17.61)$$

Integrating by parts

$$\begin{aligned} a_2(t) &= \left[\frac{-ig \cos kx}{i(\omega_0 - \omega)} e^{i(\omega_0 - \omega)\tau} \sqrt{n} b_2(\tau) \right] \\ &\quad - \int_{-\infty}^t d\tau \sqrt{n} \left(\frac{\partial b_2}{\partial \tau} \right) \left(\frac{-ig \cos kx}{i(\omega_0 - \omega)} e^{i(\omega_0 - \omega)\tau} \right) . \end{aligned} \quad (17.62)$$

Now $\partial b_2 / \partial \tau$ is very small in the large detuning limit and hence we may neglect the second term, thus

$$a_2(t) \approx \frac{-\sqrt{n} g \cos kx}{\omega_0 - \omega} e^{i(\omega_0 - \omega)t} b_2(\tau) . \quad (17.63)$$

Hence

$$\frac{\partial b_2}{\partial t} = \frac{i n |g|^2 \cos^2 kx}{(\omega_0 - \omega)} b_2 \quad (17.64)$$

which is consistent with the effective Hamiltonian (17.34).

References

Chapter 2

- 2.1 E.A. Power: *Introductory Quantum Electrodynamics* (Longmans, London 1964)
- 2.2 R.J. Glauber: Phys. Rev. B **1**, 2766 (1963)
- 2.3 W.H. Louisell: *Statistical Properties of Radiation* (Wiley, New York 1973)
- 2.4 D.F. Walls: Nature **324**, 210 (1986)
- 2.5 C.M. Caves: Phys. Rev. D **23**, 1693 (1981)
- 2.6 H.P. Yuen: Phys. Rev. A **13**, 2226 (1976)
- 2.7 R. Loudon: *Quantum Theory of Light* (Oxford Univ. Press, Oxford 1973)
- 2.8 W. Schleich, J.A. Wheeler: Nature **326**, 574 (1987)
- 2.9 C.M. Caves, B.L. Schumaker: Phys. Rev. A **31**, 3068 (1985)
- 2.10 L. Susskind, J. Glogower: Physics **1**, 49 (1964).
- 2.11 D.T. Pegg, S.M. Barnett: Phys. Rev. A **39**, 1665 (1989)
- 2.12 J.H. Shapiro, S.R. Shepard: Phys. Rev. A **43**, 3795 (1990)
- 2.13 M.J.W. Hall: Quantum Optics **3**, 7 (1991)

Further Reading

- Glauber, R.J.: In *Quantum Optics and Electronics*, ed. by C. de Witt, C. Blandin, C. Cohen Tannoudji
Gordon and Breach, New York 1965)
- Klauder, J.R., Sudarshan, E.C.G.: *Fundamentals of Quantum Optics* (Benjamin, New York 1968)
- Loudon, R.: *Quantum Theory of Light* (Oxford Univ. Press, Oxford 1973)
- Louisell, W.H.: *Quantum Statistical Properties of Radiation* (Wiley, New York 1973)
- Meystre, P., M. Sargent, III: *Elements of Quantum Optics*, 2nd edn. (Springer, Berlin, Heidelberg 1991)
- Nussenneig, H.M.: *Introduction to Quantum Optics* (Gordon and Breach, New York 1974)

Chapter 3

- 3.1 R.J. Glauber: Phys. Rev. **130**, 2529 (1963)
- 3.2 M. Born, E. Wolf: *Principles of Optics*, 3rd edn. (Pergamon, London 1965)
- 3.3 P.A.M. Dirac: *The Principles of Quantum Mechanics*, 3rd edn. (Clarendon, London 1947)
- 3.4 G.I. Taylor: Proc. Cam. Phil. Soc. Math. Phys. Sci. **15**, 114 (1909)
- 3.5 P. Grangier, G. Roger, A. Aspect: Europhys. Lett. **1**, 173 (1986)
- 3.6 R.F. Pfleegor, L. Mandel: Phys. Rev. **159**, 1084 (1967)
- 3.7 R. Hanbury-Brown, R.W. Twiss: Nature **177**, 27 (1956)
- 3.8 F.T. Arecchi, E. Gatti, A. Sona: Phys. Rev. Lett. **20**, 27 (1966); F.T. Arecchi, Phys. Lett. **16**, 32 (1966)
- 3.9 E.R. Pike: In *Quantum Optics*, ed. by R.J. Glauber (Academic, New York 1970)
- 3.10 W. Demtroeder: *Laser Spectroscopy*, 2nd edn. (Springer, Berlin, Heidelberg 1993)
- 3.11 D. Mettzer, L. Mandel: IEEE J. QE-6, 661 (1970)
- 3.12 H.P. Yuen, J.H. Shapiro: IEEE Trans. IT **26**, 78 (1980)

- 3.13 L. Mandel: *Progress in Optics* **2**, 183 (North-Holland, Amsterdam 1963)
- 3.14 L. Mandel: Phys. Rev. Lett. **49**, 136 (1982)
- 3.15 P.L. Kelley, W.H. Kleiner: Phys. Rev. **136**, 316 (1964)
- 3.16 M.O. Scully, W.E. Lamb: Phys. Rev. **179**, 368 (1969)
- 3.17 H.J. Carmichael: J. Opt. Soc. Am. B **4**, 1588 (1987)

Further Reading

- Meystre, P., M. Sargent III: *Elements of Quantum Optics*, 2nd edn. (Springer, Berlin, Heidelberg 1991)
 Perina, J.: *Coherence of Light* (van Nostrand Reinhold, London 1972).

Chapter 4

- 4.1 R.J. Glauber: Phys. Rev. **131**, 2766 (1963)
- 4.2 E.C.G. Sudarshan: Phys. Rev. Lett. **10**, 277 (1963)
- 4.3 J.R. Klauder, E.C.G. Sudarshan: *Fundamentals of Quantum Optics* (Benjamin, New York 1968)
- 4.4 E.P. Wigner: Phys. Rev. **40**, 749 (1932)
- 4.5 P.D. Drummond, C.W. Gardiner: J. Phys. A **13**, 2353 (1980)
- 4.6 S.L. Braunstein, C.M. Caves and G.J. Milburn: Phys. Rev. A **43**, 1153 (1991)

Chapter 5

- 5.1 B.R. Mollow, R.J. Glauber: Phys. Rev. **160**, 1097 (1967); ibid. **162**, 1256 (1967)
- 5.2 B.L. Schumaker, C.M. Caves: Phys. Rev. A **31**, 3093 (1985)
- 5.3 M.D. Reid, P.D. Drummond: Phys. Rev. Lett. A **41**, 3930 (1990)
- 5.4 Z.Y. Ou, L. Mandel: Phys. Rev. Lett. **61**, 50 (1988)
- 5.5 M.J. Collett: Phys. Rev. A **38**, 2233 (1988)
- 5.6 C.A. Holmes, G.J. Milburn, D.F. Walls: Phys. Rev. A **39**, 2493 (1989)
- 5.7 C.M. Caves: Phys. Rev. D **26**, 1817 (1982)
- 5.8 G.J. Milburn: Phys. Rev. A **33**, 674 (1985)
- 5.9 B. Yurke, D. Stoler: Phys. Rev. Lett. **57**, 13 (1985)
- 5.10 M. Kitagawa, Y. Yamamoto: Phys. Rev. A **34**, 345 (1986)

Chapter 6

- 6.1 F. Haake: (private communication)
- 6.2 W.H. Louisell: *Quantum Statistical Properties of Radiation* (Wiley, New York 1973)
- 6.3 M.C. Wang, G.E. Uhlenbeck: Rev. Mod. Phys. **17**, 323 (1945)
- 6.4 M. Lax: In *Brandeis University Summer Institute Lectures*, ed. by M. Chretien, E.P. Gross, S. Deser (Gordon and Breach, New York 1966) Vol. 2

Further Reading

- Agarwal, G.S.: *Quantum Statistical Theories of Spontaneous Emission and their Relation to Other Approaches*, Springer Tracts Mod. Phys., Vol. 70 (Springer, Berlin, Heidelberg 1974).
 Gardiner, C.W.: *Handbook of Stochastic Processes* (Springer, Berlin, Heidelberg 1985).
 Gardiner, C.W.: *Quantum Noise* (Springer, Berlin, Heidelberg 1991).
 Risken, H.: *The Fokker Planck Equation* (Springer, Berlin, Heidelberg 1984).

Chapter 7

- 7.1 M.J. Collett, C.W. Gardiner: Phys. Rev. A **30**, 1386 (1984)
 7.2 M.J. Collett, D.F. Walls: Phys. Rev. A **32** 2887 (1985)
 7.3 G.J. Milburn, D.F. Walls: Optics Commun. **39**, 401 (1981)

Further Reading

- Gardiner, C.W.: *Quantum Noise* (Springer, Berlin, Heidelberg 1991)
 Reynaud, S.: A. Heidman: Optics Comm. **71**, 209 (1989)
 Yurke, B.: Phys. Rev. A **32**, 300 (1985)

Chapter 8

- 8.1 P.D. Drummond, K.J. McNeil, D.F. Walls: Optica Acta **28**, 211 (1981)
 8.2 M.J. Collett, C.W. Gardiner: Phys. Rev. **30**, 1386 (1984)
 8.3 M.J. Collett, D.F. Walls: Phys. Rev. A **32**, 2887 (1985)
 8.4 L.A. Wu, M. Xiao, H.J. Kimble: J. Opt. Soc. Am. B **4**, 1465 (1987)
 8.5 A.S. Lane, M.D. Reid, D.F. Walls: Phys. Rev. A **38**, 788 (1988)
 8.6 S. Reynaud, C. Fabre, E. Giacobino: J. Opt. Soc. Am. B **4**, 1520 (1987)
 8.7 A.S. Labne, M.O. Reid, D.F. Walls: Phys. Rev. Lett. **60**, 1940 (1988)
 8.8 A. Heidmann, R.J. Horowicz, S. Reynaud, E. Giacobino, C. Fabre: Phys. Rev. Lett. **59**, 2555 (1987)
 8.9 T. Debuisschert, S. Reynaud, A. Heidman, E. Giacobino, C. Fabre: Quantum Optics **1**, 3 (1989)
 8.10 O. Aytür, P. Kumar: Phys. Rev. Lett. **65**, 1551 (1990)
 8.11 S.F. Pereira, M. Xiao, H.J. Kimble, J.L. Hall: Phys. Rev. A **38**, 4931 (1989)
 8.12 A. Sizman, R.J. Horowicz, G. Wagner, G. Leuchs: Opt. Commun. **80**, 138 (1990)
 8.13 P.D. Drummond, D.F. Walls: J. Phys. A **13**, 725 (1980)
 8.14 C.M. Caves: Phys. Rev. Lett. **45**, 75 (1980)
 8.15 W.G. Unruh: In *Quantum Optics, Experimental Gravitation and Measurement Theory*, ed. by P. Meystre, M.O. Scully (Plenum, New York 1983) p. 647
 8.16 R.S. Bondurant, J.H. Shapiro: Phys. Rev. D **30**, 2548 (1984)
 8.17 M.T. Jaekel, S. Reynaud: Europhys. Lett. **13**, 301 (1990)
 8.18 A.F. Pace, M.J. Collett, D.F. Walls: Phys. Rev. A **47**, 3173 (1993)
 8.20 C.W. Misner, K.S. Thorne, J.A. Wheeler: *Gravitation* (Freeman, San Francisco 1973)
 8.21 M. Xiao, L.A. Wu, H.J. Kimble: Phys. Rev. Lett. **59**, 278 (1987)
 8.22 P. Grangier, R.E. Slusher, B. Yurke, A. La Porta: Phys. Rev. Lett. **59**, 2153 (1987)

Further Reading

- Giacobino, E., C. Fabre (guest eds.): Quantum Noise Reduction in Optical Systems – Experiments. Appl. Phys. B **55**, No. 3 (1992).
 Kimble, H.J., D.F. Walls (guest eds.): Special Issue on Squeezed States of the Electromagnetic Field. J. Opt. Soc. Am. B **4**, No. 10 (1987).
 Loudon, R., P.L. Knight (guest eds.): Speical Issue on Squeezed Light. J. Mod. Opt. **34**, No. 6/7 (1987).

Chapter 9

- 9.1 P.D. Drummond, K.J. McNeil, D.F. Walls: Optica Acta **28**, 211 (1981)
 9.2 G.J. Milburn, D.F. Walls: Optics Commun. **39**, 401 (1981)

- 9.3 M. Wolinsky, H.J. Carmichael: Phys. Rev. Lett. **60**, 1836 (1988)
- 9.4 P. Kinsler, P.D. Drummond: Phys. Rev. A **43**, 6194 (1991)
- 9.5 R. Landauer, S. Swanson: Phys. Rev. **121**, 1668 (1961)
- 9.6 P.D. Drummond, D.F. Walls: J. Phys. A**13** 725 (1980)
- 9.7 R. Graham: *Quantum Statistics in Optics and Solid State Physics*, Springer Tracts Mod. Phys., Vol. 66 (Springer, Berlin, Heidelberg 1973)
- 9.8 T.M. MacRobert: *Function of a Complex Variable* (Macmillan, London 1938)
- 9.9 M. Abramowitz, I.A. Stegun: *Handbook of Mathematical Function* (Dover, New York 1965)
- 9.10 I.S. Gradshteyn, I.M. Ryzhik: *Tables of Series, Products and Integrals*, (Deutsch, Frankfurt/M 1981).

Further Reading

Gibbs, H.: *Optical Bistability*, Academic Press (1985).
 Lugiato, L.A. in *Progress in Optics*, p. 69, Ed. E. Wolf, North-Holland (1984).

Chapter 10

- 10.1 H. Haken: *Waves, Photons and Atoms* (North-Holland, Amsterdam 1981) Vols. 1 and 2
- 10.2 E.A. Power: *Introductory Quantum Electrodynamics* (Longmans, London 1964)
- 10.3 E.T. Jaynes, F.W. Cummings: Proc IEEE **51**, 89 (1963)
- 10.4 S. Haroche: In *New Trends in Atomic Physics*, ed. by G. Grynberg, R. Stora, Les Houches Session XXXVIII (Elsevier, Amsterdam 1984)
- 10.5 G. Rempe, H. Walther, N. Klein: Phys. Rev. Lett. **58**, 353 (1987)
- 10.6 R.J. Glauber: Phys. Rev. **131**, 2766 (1963)
- 10.7 G.S. Agarwal: *Quantum Statistical Theories of Spontaneous Emission and their Relation to Other Approaches*, Springer Tracts Mod. Phys., Vol. 70 (Springer, Berlin, Heidelberg 1974)
- 10.8 C.W. Gardiner: Phys. Rev. Lett. **56**, 1917 (1986)

Further Reading

Allen, L., J.H. Eberly: *Optical Resonance and Two-Level Atoms* (Wiley, New York 1975).
 Cohen Tannoudji, C., J. Dupont Roc, G. Grynberg: *Photon and Atoms, Introduction to Quantum Electrodynamics*, (Wiley, New York 1989).

Chapter 11

- 11.1 B.R. Mollow: Phys. Rev. **188**, 1969 (1969)
- 11.2 R.E. Grove, F.Y. Wu, S. Ezekiel: Phys. Rev. Lett. **35**, 1426 (1975)
- 11.3 W. Hartig, W. Rasmussen, R. Schieder, H. Walther: Z. Physik. A **278** 205 (1976)
- 11.4 H.J. Carmichael, D.F. Walls: J. Phys. B **9**, L43 (1976), J. Phys. B **9**, 1199 (1976)
- 11.5 H.J. Kimble, M. Dagenais, L. Mandel: Phys. Rev. Lett. **39**, 691 (1977); Phys. Rev. A **18**, 201 (1978)
- 11.6 F.M. Rateike, G. Leuchs, H. Walther: See results in J.D. Cresser, J. Häger, G. Leuchs, F.M. Rateike and H. Walther in *Dissipative Systems in Quantum Optics*, edited by R. Bonifacio, Springer 1982
- 11.7 H.J. Carmichael, P. Drummond, P. Meystre, D.F. Walls: J. Phys. A **11**, L121 (1978)
- 11.8 F. Diedrich, H. Walther: Phys. Rev. Lett. **58**, 203 (1987)
- 11.9 M.J. Collett, D.F. Walls, P. Zoller: Optics Commun. **52**, 145 (1984)

Further Reading

- Cohen-Tannoudji, C: In *Frontiers in Laser Spectroscopy*, ed. by R. Balcan, S. Haroche, S. Liberman (North-Holland, Amsterdam 1977)
- Mollow, B.R.: *Progress in Optics* **19**, (North-Holland, Amsterdam 1987)

Chapter 12

- 12.1 H. Haken: *Laser Theory*, Reproduction from *Handbuch der Physik* (Springer, Berlin, Heidelberg 1984)
- 12.2 M. Sargent III, M.O. Scully, W.E. Lamb: *Laser Physics* (Addison Wesley 1974)
- 12.3 M.O. Scully, W.E. Lamb: Phys. Rev. **159**, 208 (1967)
- 12.4 M. Lax, W.H. Louisell: Phys. Rev. **185**, 568 (1969)
- 12.5 F.T. Arecchi: Phys. Rev. Lett. **15**, 912 (1965)
- 12.6 E.A. Johnson, R. Jones, T.P. McLean, E.R. Pike: Phys. Rev. Lett. **16**, 589 (1966)
- 12.7 B.L. Morgan, L. Mandel: Phys. Rev. Lett. **16**, 1012 (1966)
- 12.8 S. Machida, Y. Yamamoto, Y. Itaya: Phys. Rev. Lett. **58**, 1000 (1987)
- 12.9 W. Richardson, R.E. Shelby: Phys. Rev. Lett. **64**, 400 (1990)
- 12.10 Y.M. Golubov, I.V. Sokolov: Sov. Phys. JETP **60**, 234 (1984)
- 12.11 Y. Yamamoto, S. Machida, O. Nilsson: Phys. Rev. A **34**, 4025 (1986)
- 12.12 F. Haake, S.M. Tan, D.F. Walls: Phys. Rev. A **40**, 7121 (1989)
- 12.13 J. Bergou, L. Davidovich, M. Orszag, C. Berkert, M. Hillery, M.O. Scully: Opt. Commun. **72**, 82 (1989)
- 12.14 M. Marte, P. Zoller: Quantum Optics **2**, 229 (1990)

Chapter 13

- 13.1 P.D. Drummond, D.F. Walls: Phys. Rev. A **23**, 2563 (1981)
- 13.2 H. Haken: *Encyclopedia of Physics*, Vol. XXV/2c (Springer, Berlin, Heidelberg 1970); and *Laser Theory* (Springer, Berlin, Heidelberg 1984)
- 13.3 M.D. Reid, D.F. Walls, Phys. Rev. A **34**, 4929 (1986)
- 13.4 R.E. Slusher, L.W. Hollberg, B. Yurke, J.C. Mertz, J.F. Valley: Phys. Rev. Lett. **55**, 2409 (1985)
- 13.5 R.E. Slusher, B. Yurke, P. Grangier, A. LaPorta, D.F. Walls, M. Reid: J. Opt. Soc. Am. B **4**, 1453 (1987)

Chapter 14

- 14.1 A. Einstein, B. Podolsky, N. Rosen: Phys. Rev. **47**, 777 (1935)
- 14.2 N. Bohr: Phys. Rev. **48**, 696 (1935)
- 14.3 J.S. Bell: Physics **1**, 105 (1964); Rev. Mod. Phys. **38**, 447 (1966)
- 14.4 M.D. Reid, D.F. Walls: Phys. Rev. A **34**, 1260 (1986)
- 14.5 A. Aspect, P. Grangier, G. Roger: Phys. Rev. Lett. **49**, 91 (1982). A. Aspect, J. Dalibard, G. Roger: Phys. Rev. Lett. **49**, 1804 (1982)
- 14.6 Z.Y. Ou, L. Mandel: Phys. Rev. Lett. **61**, 50 (1988)
- 14.7 Y.H. Shih, C. Alley: Phys. Rev. Lett. **61**, 2921 (1988)
- 14.8 P.G. Kwiat, W.A. Vareka, C.K. Hong, H. Nathel, R.Y. Chiao: Phys. Rev. A **41**, 2910 (1990)
- 14.9 S.M. Tan, D.F. Walls: Optics Commun. **71**, 235 (1989)
- 14.10 S.M. Tan, D.F. Walls, M.J. Collet: Phys. Rev. Lett. **66**, 252 (1991)
- 14.11 C.A. Holmes, G.J. Milburn, D.F. Walls: Phys. Rev. Lett. A **39**, 2493 (1989)
- 14.12 C.K. Hong, L. Mandel: Phys. Rev. Lett. **56**, 58 (1986)
- 14.13 S.M. Tan, M.J. Holland, D.F. Walls: Opt. Commun. **77**, 285 (1990)

Chapter 15

- 15.1 C.M. Caves, K.S. Thorne, R.W.P. Drever, V.P. Sandberg, M. Zimmerman: Rev. Mod. Phys. **52**, 341 (1980)
- 15.2 M.J. Holland, M.J. Collett, D.F. Walls, M.D. Levenson: Phys. Rev. A **42**, 2995 (1990)
- 15.3 A. La Porta, R.E. Slusher, B. Yurke: Phys. Rev. Lett. **62**, 28 (1989)
- 15.4 G.J. Milburn, D.F. Walls: Phys. Rev A **28**, 2065 (1983)
- 15.5 J. Ph. Poizat, P. Grangier: Phys. Rev. Lett. (1992)

Chapter 16

- 16.1 E. Joos, H.D. Zeh: Z. Physik B **59**, 223 (1985)
- 16.2 A. Caldeira, A.J. Leggett: Physica A **121**, 587 (1983)
- 16.3 D.F. Walls, G.J. Milburn: Phys. Rev. A **31**, 2403 (1985)
- 16.4 W.H. Zurek: Phys. Rev. D **24**, 1516 (1981); ibid D **26**, 1862 (1982); Physics Today **44**, 36 (October 1 1991)
- 16.5 D.F. Walls, M.J. Collett, G.J. Milburn: Phys. Rev. D **32**, 3208 (1985)

Chapter 17

- 17.1 P.L. Gould, G.A. Ruff, D.E. Pritchard: Phys. Rev. Lett. **56**, 827 (1986)
- 17.2 O. Carnal, J. Mlynek: Phys. Rev. Lett. **66**, 2689 (1991)
- 17.3 D.W. Keith, C.R. Ekstrom, Q.A. Turchette, D.E. Pritchard: Phys. Rev. Lett. **66**, 2693 (1991)
- 17.4 M. Kasevich, S. Chu: Phys. Rev. Lett. **67**, 181 (1991)
- 17.5 F. Riehle, Th. Kisters, A. Witte, J. Helmcke, Ch. J. Börde: Phys. Rev. Lett. **67**, 177 (1991)
- 17.6 Ch. Miniatura, F. Perales, G. Vassilev, J. Reinhardt, J. Robert, J. Baudon: J. Physique **1**, 425 (1991)
- 17.7 F. Shimizu, K. Shimizu, H. Takuma: Phys. Rev. A **46**, 17 (1992)
- 17.8 C. Cohen-Tannoudji, F. Bardou, A. Aspect: In *Laser Spectroscopy*, ed. by M. Ducloy et al. (World Scientific, Singapore 1992)
- 17.9 T. Sleator, O. Carnal, A. Faulstich, J. Mlynek: In *Quantum Measurement in Optics*, ed. by P. Tombesi, D.F. Walls (Plenum, New York 1992)
- 17.10 E.M. Wright, P. Meystre: Optics Commun. **75**, 388 (1990)
- 17.11 P.L. Gould, P.J. Martin, G.A. Ruff, R.E. Stoner, J.L. Picque, D.E. Pritchard: Phys. Rev. A **43**, 585 (1991)
- 17.12 S.M. Tan, D.F. Walls: Appl. Phys B **54**, 434 (1992)
- 17.13 T. Sleator, T. Pfau, V. Balykin, O. Carnal, J. Mlynek: Phys. Rev. Lett. **68**, 1996 (1992)
- 17.14 S.M. Tan, D.F. Walls: Phys. Rev. A
- 17.15 M. Brune, S. Haroche, V. Lefèvre, J.M. Raimond, N. Zagury: Phys. Rev. Lett. **65**, 976 (1990)
- 17.16 M.J. Holland, D.F. Walls, P. Zoller: Phys. Rev. Lett. **67**, 1716 (1991)
- 17.17 E.P. Storey, M.J. Collett, D.F. Walls: Phys. Rev. Lett. **68**, 472 (1992)

Subject Index

- adiabatic elimination 179, 249, 254
antibunching, photon 2
 laser 3
 resonance fluorescence 221
 second-order correlation function 42
 sub-Poissonian statistics 42
atomic decay rate, transverse 246
atomic operators, collective 247
atomic optics 5
- back action evasion 284
Bargmann state 99
beam splitter 287
Bell inequality 4, 265
 CHSH form 266
 parametric down conversion 268
bistability, dispersive (linear) 153
 squeezing spectrum 156
bistability, dispersive (nonlinear) 191
 Fokker-Planck equation 191
bistability, optical 245
 atomic model 245
 noise correlation 249
Brownian motion 112
bunching, photon 2
 second-order correlation function 40, 42
 sub-Poissonian statistics 42
- Cauchy-Schwarz inequality 32, 78
cavity, boundary condition 121
cavity, laser 229
cavity, two-sided 126
chaotic field, see thermal field
characteristic function 62
 optical bistability 247
 P representation 62
 Q representation 65
 quantum coherence 303
 Wigner representation 63, 106
CHSH inequality 266
Clauser-Horne inequality 269
coherence, first order optical 34
 Young's interference experiment 35
- coherence function 298
coherence, optical 29
coherence, quantum 303
 visibility 303
coherent field 38
coherent state 12, 108
 completeness 14
 displacement operator 12
 number state expansion 12
 Poissonian statistics 13, 58
 second-order correlation function 42, 58
coherent state, two photon 18
coincidence probability 275
collisional broadening limit 246
complementarity 5, 261, 316
contractive state 282, 337
correlated state 261
correlated state, polarization 263
correlation function 31
 general inequalities 31
 phase information 44
correlation function, first order 30
correlation function, higher order 30
correlation function, phase dependent 44
correlation function, photon number 222
correlation function, QND 285
correlation function, second-order 39
 antibunching 42
 bunching 40
 coherent state 42
 number state 42
 resonance fluorescence 222
 thermal field 58
correlation function, two-time 53
 Brownian motion 113
 input-output formalism 127
 master equation 91
 Ornstein-Uhlenbeck process 116
 parametric oscillator 133
 phase diffusion 236
 photon counting 53
 regularly pumped laser 237
 resonance fluorescence 217, 225
 two-level atom 207

- correlation, intensity 39
 Hanbury-Brown Twiss experiment 1, 30, 39
 parametric amplifier 75
- covariance matrix 61
 covariance matrix, stationary 116
- density operator, reduced 92
 detailed balance 98
 harmonic oscillator 98
 laser 232
 duality, wave-particle 315
- efficiency, quantum 52
 Einstein-Podolsky-Rosen paradox, see EPR paradox
- electric dipole approximation 200, 245
 electromagnetic field 7
 commutation relations 10
 Hamiltonian 10
 quantisation 7
 vacuum state 10
- entangled state 275, 318
 EPR paradox 4, 261
 parametric amplifier 81
- error ellipse 16
 coherent state 16
 Wigner function 63
- Fock state, see number state
 Fokker-Planck equation 101
 degenerate parametric oscillator 178
 dispersive bistability 155, 191
 Green's function 103
 potential condition 101
 stochastic differential equation 111
- four-wave mixing 3, 245, 252
 degenerate operation 257
 noise correlation 254
 phase matching 253
 QND 294
 side-band modes 253
 squeezing spectrum 256
- gain, QND 290, 295
 gravitational radiation 281
- Hanbury-Brown Twiss experiment 1, 30, 37
 harmonic oscillator 11
 electromagnetic field 11
 harmonic oscillator, damped 115
 harmonic oscillator, master equation 93
 Fokker-Planck equation 100, 110
 transition probabilities 98
- heat bath, see reservoir
- hidden variable theory 264
 homodyne detection 45
 four-wave mixing 255
 parametric oscillator 132
- input-output formalism 121
 boundary condition 124
 laser fluctuations 233
 parametric oscillator 129
 photon counting distribution 51
 squeezing spectrum 129
 two-time correlation function 127
- intensity fluctuations, laser 234, 239
 interaction picture 201
 interferometer, gravity wave 158
 semiclassical behaviour 162
 signal variance 166
 total noise 167
- interferometer, Mach-Zehnder 172
 interferometer, polarization 174
 interferometry, matter 5, 315, 327
 interferometry, optical 1
 squeezed light 3
- Jaynes Cummings model 204
- Kapitza-Dirac regime 323
 Kerr effect 87, 191
 KTP crystal 291
- Langevin equation 112
 Brownian motion 112
 constant diffusion process 115
 damped harmonic oscillator 113
 four-wave mixing 254
 input-output formalism 124
- laser 2, 229
 diode 229
 gain 232
 phase diffusion 235
 Scully-Lamb form 231
 sub-Poissonian statistics 3
 threshold 232
- laser cooling 5, 315
 laser, fluctuations 229
 intensity 234
 photon number 233, 238
 pump 236
 sub-shot noise 229
- laser, quantum theory 229
 laser, regularly pumped 239
 laser, semiconductor 236, 240
- lens, atomic 337

- linewidth, laser 236
 Liouvillian operator 117
- Markov approximation, first 95, 123
 master equation 91
 gravitational wave interferometer 161, 165
 optical bistability 155, 246
 parametric oscillator 138
 resonance fluorescence 213
 Scully-Lamb laser 231
 two-level atom 206
 two-time correlation function 117
- Maxwell's equations 8
 measurement limit, strong 313
 measurement theory, quantum 306
 micro-cavity 210
 microscope, Feynman light 315
 minimum uncertainty state 16
 parametric oscillator 145
 squeezed state 15
 mixture, classical 297
- noise spectrum 116
 normal ordering 51, 54
 P representation 118
 number state 10, 57
- observable, QND 282
 optical Bloch equations 215
 oscillation threshold 216
 optical tap 284, 294
 Ornstein-Uhlenbeck process 112
 Brownian motion 112
 constant diffusion process 116
 damped harmonic oscillator 115
- P* representation 58, 61
 Bell inequality 266
 chaotic state 59
 coherent state 59
 harmonic oscillator 99
 normal ordering 118
 quadrature variance 61
- P* representation, complex 68
 coherent state 69
 dispersive bistability 192, 195
 harmonic oscillator 109
 number state 69
 parametric oscillator 132, 180, 194
 squeezed state 70
- P* representation, generalised 68, 138
 bistability 155
 harmonic oscillator 108
 parametric oscillator 138, 178
- P* representation, positive 71, 115
 Fokker-Planck equation 72
 harmonic oscillator 110
 optical bistability 247
 parametric oscillator 182
 twin beams 146
- parametric amplifier, QND 291
 parametric amplifier, degenerate 73
 parametric amplifier, nondegenerate 77
 selected state 84
 thermal reduced state 83
 two-mode squeezing 80
- parametric down conversion 3, 73
 Bell inequality 268
 parametric oscillator (linear) 3, 129, 137
 critical fluctuations 131
 Fokker-Planck equation 132, 134
 linearistation 129, 132, 139
 minimum uncertainty state 145
 output correlation matrix 133
 squeezing spectrum 129, 142
 threshold 129, 131
- parametric oscillator (nonlinear) 177
 quadrature variance 183
 semiclassical solution 180
 threshold distribution 184
- Paul trap 225
 Pauli spin operators 202
 phase decay, collisionally induced 210, 246
 phase diffusion, laser 235
 linewidth 236
 two-time correlation function 236
- phase instability 147
 phase matching 253
 phase operator, Pegg-Barnett 25
 phase operator, Susskind-Glogower 23
 photo-detection 29, 39, 233
 photon counting 299
 photon counting, classical 46
 depletion effects 50
 ergodic hypothesis 49
 generating function 48
 photon counting, conditional 84
 parametric amplifier 84
 photon counting distribution 52
 photon counting, nonclassical 70
 number state 71
 squeezed state 71
- photon counting, quantum mechanical 51
 photon number, QND 294
 Planck distribution 58
 pointer basis 308
 Poissonian pumping 230
 polarization rotator 291

- projection postulate, von Neumann 84
 pump depletion 180
- Q* function 65
 coherent state 66
 harmonic oscillator 104
 number state 66
 squeezed state 66
- QND measurement 4, 315, 329, 330
 pointer basis 310
 sub-Poissonian statistics 295
 two photon transition 294
- QND measurement, ideal 290
- Q* parameter 239
- quadrature phase measurement 44
 quadrature phase operator 16
- quantisation, electromagnetic field 7
 quantisation, electron field 197
- quantum nondemolition measurement, see
 QND measurement
- quantum recurrence phenomena 205
 Kerr effect 89
- quantum regression theorem 118
 resonance fluorescence 221
- R* representation 66
 Rabi frequency 204
 radiation pressure 159
 Raman-Nath regime 322, 334
 recoil energy 322
 refractive index, nonlinear 153
 relative states 309
 reservoir 91
 collisional process 210
 spectrum 96
 spontaneous emission 214
 two-level atom 206
- reservoir, squeezed 94, 208
 correlation function 208
 two-level atom 208
- reservoir, thermal 96
- resonance fluorescence 2, 213
 elastic scattering 219
 inelastic scattering 219
 quantum features 221
 spectrum 217
- rotating wave approximation 121, 202, 245
 Rydberg atom 205, 327
- Schrödinger cat 297
 second harmonic generation 137
 critical behaviour 140, 150
 self pulsing 141
- squeezing spectrum 151
 steady-state solution 140
 shot-noise limit 54
 laser 235, 239
- signal-to-noise ratio 291, 295
 spectroscopy, photon correlation 40
 spontaneous emission 206
 master equation 206
 Wigner-Weisskopf theory 207
- squeezed state 15
 photon number distribution 21
 super-Poissonian statistics 43
- squeezed state, multimode 22
 squeezed state, two-mode 22
 parametric amplifier 80
 squeezing generator 23
- squeezing 3, 137
 four-wave mixing 255
 input-output formalism 129
 nonlinear susceptibility 154
 parametric oscillator 129
- squeezing, generator 16
 parametric amplifier 74, 80
- squeezing spectrum 129
 dispersive bistability 156
 parametric oscillator 129, 142
 resonance fluorescence 225
 second harmonic generation 151
 twin beams 148
- stability analysis 139
- standard quantum limit 169
 gravity wave 281
- state preparation 285, 329
- statistics, photon 41
 laser 232
 micromaser cavity 327
 regularly pumped laser 238
- statistics, photon counting 53
 statistics, Poissonian 2, 13
 coherent state 13, 58
 Kerr effect 86
 laser 232
- statistics, sub-Poissonian 3
 antibunching 42
 bunching 42
 laser 3, 236
 QND 295
 resonance fluorescence 225
- statistics, super-Poissonian 42
 squeezed state 43
- Stern-Gerlach effect, optical 32, 315
- stochastic differential equation 111
 Fokker-Planck equation 111
 gravity wave interferometer 161, 165

- Ito equation 111
- Langevin equation 111
- optical bistability 248
- parametric oscillator 138
- superposition, coherent 297
- superposition, macroscopic 4, 297
- superposition principle 297
- superposition state 177, 186
- susceptibility, nonlinear 154
- switching time 179

- thermal field 58
 - laser 232
 - second-order correlation function 58
- transition probability 98
- tunnelling time 177, 186
- twin beams 146
 - critical behaviour 146
 - pulsed 150
 - semiclassical steady-state 146
 - squeezing spectrum 148
- two-level atom 202
 - master equation 206

- uncertainty principle 16, 288, 313
 - gravity waves 281

- vector potential 8, 199
- visibility 32, 34, 318, 320
 - Bell inequality 271
 - one-photon interference 276
 - quantum coherence 303

- wavelength, de Broglie 315
- Wigner function 63
 - coherent state 64
 - covariance matrix 63
 - harmonic oscillator 106
 - number state 64
 - parametric amplifier 75, 82
 - squeezed state 64
- Wigner-Weisskopf theory 207
 - resonance fluorescence 213, 219

- Young's interference experiment 1, 32
 - coherent superposition 297
 - correlation function 34
 - experiments 37
 - quantum explanation of 37
 - visibility 34
 - with atoms 315